



Metal specificities and catalytic activities of the two superoxide dismutases of *Staphylococcus aureus*

Anna Barwinska-Sendra

**Thesis submitted for the degree of Doctor of Philosophy
Institute for Cell and Molecular Biosciences**

September 2017

Abstract

The superoxide dismutase (SOD) metalloenzymes play a major role in the cellular oxidative stress defence systems of microorganisms including that of an important pathogenic bacterium *Staphylococcus aureus*. *Staphylococcus aureus*, unlike other staphylococci, possesses two isozymes of the Fe/Mn-dependent SOD superfamily, designated SodA and SodM, both of which are predicted to utilise manganese as their essential metal cofactor. The two SODs are critical for the resistance to reactive oxygen species (ROS) and contribute to the pathogenicity of *S. aureus*. The immune system can utilise a Mn-restriction as one of its defence mechanism against pathogens, suggesting a possibility that one of the *S. aureus* SODs can use another metal in order to overcome this host-imposed Mn-starvation.

To clarify the metal requirements of the two *S. aureus* SODs, the recombinant Fe- and Mn-metalated isoforms of *S. aureus* SodA and SodM were produced. All four forms were characterised as catalytically active, regardless of utilised metal. The relative activity analysis showed that SodA exhibits a strong metal preference of Mn over Fe, whereas SodM presented highly cambialistic properties, i.e. it was equally active with either Mn or Fe.

Crystal structures of all four forms of the *S. aureus* SOD proteins were solved and showed a high level of identity. Structure-based mutagenesis led to the successful swapping of catalytic properties between the two proteins, yielding a Mn-specific SodM and a cambialistic SodA, with no significant change to an overall enzyme architecture. HF-EPR analysis gave insight into the mechanism of metal-specific catalysis of the two enzymes.

Phylogenetic analyses suggested the cambialistic SodM originated from a gene duplication of a single, likely Mn-specific SOD, in the common ancestor of all analysed *S. aureus* isolates. The evolution of SodM to work with both metals could have provided an important adaptation for resisting manganese-starvation during infection. Characterisation of SodM purified directly from *S. aureus*, as well as studies in an animal model of infection, provided evidence consistent with the hypothesis that the cambialistic SodM contributes to resisting host-imposed metal starvation during *S. aureus* infection.

Declaration

I certify that this thesis contains my own work, except where acknowledged, and that no part of this work has been submitted in support of an application for other qualifications at this or any other institution.

The collaborative work presented in this thesis includes:

- Initial metal profiling and metalloproteomics were performed by Dr Kevin Waldron and Dr Emma Tarrant, Newcastle University, UK;
- Diffraction data collection and deposition of crystal structures in PDB were performed by Dr Arnaud Baslé, Newcastle University, UK;
- Collection of the SEC-MALS data was performed by Dr Owen Davies, Newcastle University, UK;
- EPR experiments were performed by Dr Sun Un, CEA, Saclay, Paris, France;
- Growth in calprotectin and animal studies were performed by Yuritzi Garcia and Dr Thomas Kehl-Fie University of Illinois, Urbana-Champaign, USA.

Anna Barwinska-Sendra

Acknowledgements

First and foremost, I would like to thank my supervisor, Dr Kevin Waldron for the mentorship, and invaluable support throughout this PhD project. Thanks to his guidance, advice, and most of all enthusiastic encouragement, it has been a great and enjoyable learning experience. He has set an example of an outstanding scientist and it was a great privilege to learn from him.

I would also like to thank Professor Chris Dennison, Newcastle University, and Dr Julie Morrissey, University of Leicester, the members of my supervisory team, for their scientific advice and support. My assessors, Professor Colin Harwood and Dr Julian Rutherford for insightful discussions and constructive feedback.

Special thanks to all past and present members of Waldron Lab, Dr Jack Stevenson, Dr Emma Tarrant, Dr Gus Pelicioli-Riboldi, Safa Alsharif, and Louisa Stewart; for all their help, support, positive attitude, and friendship, that altogether created a great work environment.

I would like to acknowledge the members of the Institute for Cell and Molecular Bioscience, Newcastle University, for their support and technical advice. Dr Paula Salgado and her group for useful discussion and much appreciated scientific support and friendship. Dr Arnaud Baslé for collecting crystallographic data and for his input in solving the structures, as well as time and effort he spent to introduce me to the field of protein crystallography. Professor Rick Lewis and the Newcastle Structural Biology Lab for the opportunity to use their facility and for providing valuable professional support. Dr Owen Davies for collecting SEC-MALS data presented in this thesis.

I would like to extend my acknowledgements to Dr Sun Un, CEA, Saclay, France for hosting me in his lab, introducing me to EPR, and performing experiments presented in Chapter 5 of this thesis. Dr Thomas Khel-Fie and Yuritz Garcia, University of Illinois, Urbana-Champaign, USA for collaborative work using animal models, that is presented in Chapter 6 of this thesis. Their valuable contribution to this project is greatly appreciated.

This PhD project was funded by BBSRC as part of Newcastle-Liverpool-Durham Doctoral Training Partnership.

Table of contents

List of figures	x
List of tables	xiv
List of equations	xv
List of abbreviations	xvi
CHAPTER 1. INTRODUCTION	1
1.1. <i>Staphylococcus aureus</i>, an opportunistic mammalian pathogen	1
1.1.1. Commensalism and pathogenicity of <i>S. aureus</i>	3
1.1.2. Antibiotic resistance (MRSA, VRSA)	5
1.1.2.1. Healthcare-associated MRSA (HA-MRSA)	8
1.1.2.2. Community-associated MRSA (CA-MRSA)	8
1.1.2.3. Livestock-associated MRSA (LA-MRSA)	9
1.1.3. Pathogenesis	9
1.1.3.1. Virulence factors of <i>S. aureus</i>	10
1.2. The response of <i>S. aureus</i> to environmental stimuli	12
1.2.1. General environmental stress	12
1.2.2. Oxidative and nitrosative stress	14
1.3. Nutritional immunity	19
1.3.1. Metal acquisition and homeostasis (“battle for metals”)	21
1.3.1.1. Fe limitation and Fe acquisition	22
1.3.1.2. Mn limitation and Mn acquisition	23
1.3.1.3. Zn limitation and Zn acquisition	24
1.4. Superoxide dismutases (SODs)	25
1.4.1. Classification and properties of SODs	26
1.4.2. Evolution of bacterial Fe-dependent and Mn-dependent specificity of SODs	28
1.4.3. Structure of Fe/Mn SOD enzymes	29
1.4.4. Proposed molecular mechanism of catalysis by MnSOD and FeSOD	31
1.4.5. Metal selectivity and metal specificity of Mn/Fe-SODs; electronic structure and ‘redox tuning’ model of metal specificity	32
1.4.6. Structure-based mutational analyses of Fe/Mn-SODs	34
1.4.7. <i>S. aureus</i> SODs	35
1.5. Aims and objectives of the thesis	38
CHAPTER 2. MATERIALS AND METHODS	40
2.1. Bacterial strains and maintenance	40
2.1.1. Growth media and supplementation of bacterial culture	41

2.2.	DNA manipulations	43
2.2.1.	Isolation of genomic and plasmid DNA	43
2.2.2.	Agarose gel electrophoresis, staining and visualisation	45
2.2.3.	Oligonucleotides	45
2.2.4.	Polymerase chain reaction (PCR)	47
2.2.5.	Molecular cloning	48
2.2.6.	Gene synthesis	50
2.2.7.	Preparation of pS10t-StrepII/FLAG constructs for constitutive SOD expression in <i>S. aureus</i> SH1000	51
2.3.	Preparation of competent cells	52
2.3.1.	Chemically competent <i>E. coli</i>	52
2.3.2.	Electrocompetent <i>S. aureus</i>	52
2.4.	Transformations of bacterial cells with plasmid DNA	52
2.4.1.	<i>Escherichia coli</i>	52
2.4.2.	<i>Staphylococcus aureus</i>	53
2.5.	Phage transductions	53
2.5.1.	Preparation of <i>E. coli</i> BL21(DE3) SOD deletion mutant strains using P1 phage transduction	53
2.5.2.	Preparation of <i>S. aureus</i> SH1000 deletion mutant strains using ϕ 11 transduction	54
2.6.	Complementation of <i>EcSODs</i>' mutant strains with <i>SaSODs</i>	54
2.7.	Purification of proteins	55
2.7.1.	Small-scale protein expression testing	55
2.7.2.	Large scale over-expression of recombinant proteins in <i>E. coli</i> BL21(DE3) and BL21(DE3) sod-deficient strains	56
2.7.3.	Protein extraction from <i>Escherichia coli</i> cells	56
2.7.4.	Gradient anion exchange chromatography of soluble cell lysate (AEC)	56
2.7.5.	Size-exclusion chromatography	57
2.7.6.	Size-exclusion chromatography - multi-angle light scattering (SEC-MALS)	58
2.7.7.	Protein extraction from <i>Staphylococcus aureus</i> cells	58
2.7.8.	Affinity chromatography	58
2.8.	Polyacrylamide gel electrophoresis (PAGE), staining and visualisation	59
2.8.1.	Sodium dodecyl sulphate-polyacrylamide gel electrophoresis (SDS-PAGE)	59
2.8.2.	Non-denaturing- polyacrylamide gel electrophoresis (Native-PAGE)	60
2.9.	SOD activity assays	60
2.9.1.	In-gel assay	60
2.9.2.	Peroxide inhibition assay	61
2.9.3.	Liquid assay	61

2.10. Western blotting	62
2.11. Inductively coupled plasma mass-spectrometry (ICP-MS)	63
2.11.1. Elemental analysis of purified, recombinant and native proteins	63
2.11.2. <i>S. aureus</i> SH1000 whole cell metal content analysis	64
2.12. In vitro refolding	64
2.12.1. Preparation of metal-free dialysis tubing	64
2.12.2. Optimisation of unfolding and refolding protocols	64
2.12.3. Preparation of apo-proteins	65
2.12.4. Metal cofactor exchange	65
2.13. Determination of protein concentration	66
2.14. Protein mass spectrometry	67
2.15. X-ray crystallography	68
2.15.1. Initial screens and optimisation	68
2.15.2. Data collection	68
2.15.3. Structure determination, refinement and validation	69
2.16. Tryptophan fluorescence measurements	69
2.17. Circular dichroism spectroscopy	70
2.18. UV-Vis spectroscopy	70
2.19. High-field high frequency Electron Paramagnetic Resonance (HF-EPR)	71
2.19.1. Sample preparation	71
2.19.2. Hydrogen/Deuterium exchange	71
2.19.3. Experimental procedures	72
2.20. Bioinformatics and phylogenetics	72
2.20.1. Database searches and identification of SOD homologues	72
2.20.2. Multiple sequence alignments and phylogenetic analyses	72
 CHAPTER 3. SaSodA is Mn-specific, whereas SaSodM is cambialistic	 74
3.1 Introduction	74
3.2 Results and discussion	75
3.2.1 <i>Staphylococcus aureus</i> possesses two SOD proteins detected as three bands of activity	75
3.2.2 Bioinformatics and phylogenetic analyses of the origin of SaSODs	76
3.2.3 Purification of recombinant proteins SaSodA and SaSodM	83
3.2.4 Quantification of purified recombinant SODs	84
3.2.5 Recombinant SODs acquire Fe in heterologous host	85

3.2.6	Purified SODs are free of contaminating native <i>E. coli</i> SODs	86
3.2.7	Evaluation of the secondary structure and thermal stability of SOD proteins by CD spectroscopy	87
3.2.8	Metal content of the SaSODs can be manipulated by metal supplementation of bacterial host culture	91
3.2.9	<i>In vitro</i> metal exchange yields Mn-loaded SODs	94
3.2.10	CD spectroscopy and tryptophan fluorescence assays demonstrate Mn-SODs have similar properties as Fe-SODs	95
3.2.11	All four forms of SaSODs are catalytically active	99
3.2.12	Direct metal competition and EDTA effect on the metalation of SaSODs	100
3.2.13	<i>In vitro</i> substitution with non-physiological metal cofactors yields inactive proteins	102
3.2.14	<i>In vitro</i> interaction of SodA and SodM (heterodimer formation)	104
3.3	Conclusions	108
	 CHAPTER 4. Identification of residues determining cambialism of SaSodM	 110
4.1.	Introduction	110
4.2.	Results and discussion	111
4.2.1.	Crystallisation and determination of the structure of SaSODs	111
4.2.1.1.	Data collection and structure solution	111
4.2.2.	Crystal structures of Fe and Mn containing SaSodA and SaSodM are nearly identical	116
4.2.2.1.	Structure analysis	116
4.2.3.	Identification of candidate residues potentially determining the distinct properties of SaSodA and SaSodM	121
4.2.4.	<i>BsSodA</i> is a manganese dependent protein and exhibits similar enzymatic activity profile as <i>SaSodA</i>	123
4.2.5.	Mutated versions of <i>SaSodA</i> and <i>SaSodM</i> purify from heterologous host exclusively with iron cofactor, which can be exchanged <i>in vitro</i> for manganese	125
4.2.6.	Mutations introduced to the secondary sphere of SaSODs alter their relative activity	128
4.2.6.1.	<i>SaSodA</i> isoforms do not yield a cambialistic SodM-like protein, though the G159L; L160F mutation significantly improves catalytic activity with Fe	128
4.2.6.2.	Mutations within <i>SaSodM</i> sequence result in a non-cambialistic, highly Mn-specific protein, analogous to <i>SaSodA</i>	130
4.2.7.	Crystal structure of [I19F; L159G; F160L] <i>SaSodM</i> triple mutant demonstrates only subtle structural changes in protein backbone	132
4.3.	Conclusions	138
	 CHAPTER 5. Biophysical characterisation of the cambialistic and non-cambialistic SaSODs	 139
5.1.	Introduction	139

5.2. Results and discussion	141
5.2.1. SaSodM reversibly changes oligomeric state from dimeric holo-enzyme to monomeric apo-enzyme, when stripped of metal cofactor	141
5.2.2. Tryptophan fluorescence spectroscopy indicate changes in chemical stability of SodM upon introduction of point mutations	146
5.2.3. Circular dichroism spectroscopy demonstrates that mutant isoforms of SaSODs have similar properties to the wild type proteins	148
5.2.4. UV-vis spectroscopy reveals strong propensity of SodA to autooxidation	150
5.2.5. Mn-specific SodA and cambialistic SodM of <i>S. aureus</i> can be distinguished by the zero field interaction of Mn in magnetic field (94 GHz)	152
5.2.6. ENDOR and ELDOR-NMR provide an insight into positions of protons involved in SOD catalysis	156
5.2.7. Density Functional Theory (DFT) modelling together with hyperfine measurements and crystal structures provides an overview of the electronic structure of Mn(II) centre	159
5.3. Conclusions	161
 CHAPTER 6. Role of cambialism of SodM <i>in vivo</i>	 163
6.1. Introduction	163
6.2. Results and discussion	164
6.2.1. Superoxide induces growth phenotypes in SH1000 strains deficient in SOD activity or Mn uptake	166
6.2.2. Manganese-dependence of SH1000 $\Delta sodA\Delta mntA$ and SH1000 $\Delta sodM\Delta mntA$ growth.	168
6.2.3. Whole-cell metal content and specific SOD activity of SH1000 strains.	172
6.2.4. SodM contributes to <i>S. aureus</i> pathogenicity during infection in the presence of calprotectin	174
6.2.5. What is the metal content of <i>S. aureus</i> SODs <i>in vivo</i> ?	176
6.2.6. Complementation with tagged isoforms of cambialistic SodM rescues the phenotype of <i>E. coli</i> strain lacking SODs	178
6.2.7. Manipulation of protein metal content by external supply	180
6.2.8. Manipulation of protein metal content by external supply with non-native metal cofactor	187
6.2.9. <i>S. aureus</i> $\Delta sodM$ strain expressing non-cambialistic isoform of SodM is more sensitive than wild type to Mn starvation.	189
6.3. Conclusions	190
 CHAPTER 7. General discussion	 192
Appendix	198
References	201

List of figures

Figure 1.1 Phylogenetic relationships among Staphylococcus species (Lamers et al., 2010).....	3
Figure 1.2 Disease manifestation of <i>S. aureus</i> infection (taken from Wertheim et al., 2005).	5
Figure 1.3 MRSA invasive isolates in EU/EEA identified in 2015 (ECDC, 2015).....	7
Figure 1.4 Selected cell wall associated and secreted virulence factors of <i>S. aureus</i>	11
Figure 1.5 Phagocytosis of <i>S. aureus</i>	15
Figure 1.6 <i>S. aureus</i> evasion of oxidative killing within phagolysosome.....	16
Figure 1.7 Crystal structure of Mn-bound calprotectin.	21
Figure 1.8 Structural models of the representatives of Fe/Mn-SOD, CuZn-SOD and Ni-SOD.	27
Figure 1.9 Manganese and iron superoxide dismutases of <i>E. coli</i>	30
Figure 1.10 Model of redox potential tuning (Miller, 2012).	34
Figure 1.11 The quantile-normalized data of <i>sodA</i> and <i>sodM</i> expression profiles of <i>S. aureus</i> HG001.....	36
Figure 2.1 SOD assay Kit-WST reaction.....	61
Figure 2.2 A representative inhibition curve (standard 4-parameter logistic model used for the sigmoidal fit).....	62
Figure 2.3 Anomalous Scattering Factors of Mn, Fe and Zn as a function of energy generated with http://skuld.bmsc.washington.edu/scatter/AS_form.html	69
Figure 3.1 In-gel assay of SOD activity of <i>Staphylococcus aureus</i> cell extracts.....	76
Figure 3.2 Bayesian phylogenetic tree of Mn/Fe-SOD homologues.	80
Figure 3.3 Multiple sequence alignment of representative Mn/Fe-SODs (continued on the following page).....	81
Figure 3.4 Protein purification: anion exchange chromatography.	83
Figure 3.5 Protein purification: size exclusion chromatography (SEC).	84
Figure 3.6 Elemental analysis of purified SaSOD proteins.....	86
Figure 3.7 In-gel SOD activity assay shows absence of contamination of purified SaSODs by EcSODs.	87
Figure 3.8 CD spectra of SaSodA and SaSodM.....	88
Figure 3.9 SaSODs' thermal denaturation monitored by CD spectroscopy.	89
Figure 3.10 Tryptophan residues contributing to the fluorescence emission spectra of SaSODs.....	90
Figure 3.11 Tryptophan fluorescence spectroscopy of as-purified (Fe-loaded) forms of SaSODs.	91
Figure 3.12 Manipulation of the metal content of recombinant SaSOD proteins expressed in LB and M9.	93
Figure 3.13 Peroxide treatment of bacterial cultures increases Mn content of SaSODs overexpressed in LB.	94
Figure 3.14 ICP-MS elemental analysis of metalated proteins.....	95
Figure 3.15 CD spectroscopy of Mn-loaded SaSODs.	96
Figure 3.16 Mn-loaded SaSODs' thermal denaturation monitored by CD spectroscopy.....	97
Figure 3.17 Tryptophan fluorescence spectroscopy of refolded (Mn-loaded) forms of SaSODs..	98

Figure 3.18 SOD activity assay.....	100
Figure 3.19 Fractional metal content of SaSOD proteins incubated with another permitted metal cofactor.....	102
Figure 3.20 ICP-MS analysis of proteins after forced mis-metalation through <i>in vitro</i> refolding.....	103
Figure 3.21 Analysis of the oligomeric state of SaSODs in solution by SEC-MALS.....	105
Figure 3.22 <i>In vitro</i> SodA/SodM heterodimer formation by refolding in presence of Mn.....	106
Figure 3.23 <i>In vitro</i> SodA/SodM heterodimer formation in varying temperature conditions.....	107
Figure 3.24 SEC-MALS analysis of Mn-loaded heterodimer.....	107
Figure 4.1 Fe-SodM X-ray data collection.....	113
Figure 4.2 Anomalous difference maps of native proteins.....	115
Figure 4.3 Crystal structures of SaSodA and SaSodM.....	116
Figure 4.4 The Root-Mean-Square-deviation (RMSD) within the backbone of SaSodA and SaSodM.....	117
Figure 4.5 A qualitative protein electrostatic potential mapped on molecular surface.....	118
Figure 4.6 Electrostatic potential at the surface of substrate access funnel.....	119
Figure 4.7 Active sites of SaSodA and SaSodM.....	120
Figure 4.8 Superimposed metal site geometry.....	121
Figure 4.9 Identification of residues potentially determining the distinct properties of SaSodA and SaSodM.....	122
Figure 4.10 <i>Bacillus subtilis</i> SodA.....	123
Figure 4.11 Metal analysis and enzymatic activity of recombinant BsSodA.....	124
Figure 4.12 Purification and elemental analysis of mutated recombinant proteins SaSodA and SaSodM expressed in <i>E. coli</i> and subjected to <i>in vitro</i> metal cofactor exchange.....	127
Figure 4.13 SOD activity in-gel assays across all recombinant SaSodA versions, showing semi-quantitative differences between the activities of the proteins.....	129
Figure 4.14 SOD activity in-gel assays of recombinant SaSodM versions.....	131
Figure 4.15 Crystal structure of Mn-SodM triple mutant.....	135
Figure 4.16 Comparison of the active site coordination and estimated hydrogen bond network within ~10 Å radius of metal ion.....	137
Figure 4.17 Activity assay of the SodA [G159T] and the SodM [L159T] mutants.....	137
Figure 5.1 Production and initial characterisation of apo-SaSODs.....	142
Figure 5.2 SEC-MALS analysis of apo-SaSODs and apo-(Mn)SaSODs.....	144
Figure 5.3 Tryptophan fluorescence emission changes upon metal binding to apo-SaSodA.....	145
Figure 5.4 Tryptophan fluorescence emission spectroscopy of Mn-loaded SaSodA, SaSodM and SodM L159G proteins in 8 M urea.....	148
Figure 5.5 The circular dichroism spectroscopy of Fe-loaded, native and mutated SaSodA and SaSodM proteins.....	150
Figure 5.6 Optical absorption spectra of metalated isoforms of wild type SaSODs.....	151
Figure 5.7 Optical absorption spectra of metalated isoforms of wild type SaSODs upon reduction with dithionite.....	152

Figure 5.8 The models of the Mn-SodA active site structure.....	153
Figure 5.9 A 5K 94 GHz Mn(II) field-swept echo EPR spectra of SaSOD proteins.....	154
Figure 5.10 Correlation of Mn-dependent activity of SaSODs and their magnetic zero-field interaction.....	155
Figure 5.11 A 5 K 94 GHz Mn(II) field-swept echo HF-EPR spectra of Mn(II) SaSODs and Mn-substituted FeSOD of <i>E. coli</i>	157
Figure 5.12 The 5K 94 GHz ELDOR-NMR spectra of Mn(II)-SaSODs and Mn-substituted Fe-SOD.	158
Figure 5.13 The 5 K, 94 GHz Davies ¹ H ENDOR spectra of Mn-SodA, Mn-substituted FeSOD and Mn-SodM.....	158
Figure 5.14 Comparison of the structure of the Mn(II) active site in Mn(Mn)SOD and the DFT GO, N- and O-protonated CD model structures.....	160
Figure 6.1 Growth analysis of <i>S. aureus</i> SH1000 and Newman wild type and mutant strains in rich growth medium TSB and minimal medium TM.	167
Figure 6.2 A 5-hour growth rate change in TM upon Mn supplementation.	170
Figure 6.3 Manganese dependent growth of SH1000 wild type, SOD mutant strains ($\Delta sodA$, $\Delta sodM$, $\Delta sodA\Delta sodM$), a putative manganese transporter ($\Delta mntA$, $\Delta sodA\Delta mntA$, $\Delta sodM\Delta mntA$) deletion strains.	170
Figure 6.4 Effects of calprotectin (CP) on the growth of <i>S. aureus</i> Newman wild type and SOD mutant strains in response to oxidative stress.	171
Figure 6.5 Whole cell metal content of SH1000 wild type, SOD mutant strains ($\Delta sodA$, $\Delta sodM$, $\Delta sodA\Delta sodM$), and a putative manganese transporter ($\Delta mntA$, $\Delta sodA\Delta mntA$, $\Delta sodM\Delta mntA$) deletion strains.....	172
Figure 6.6 A total SOD activity of SH1000 wild type, SOD mutant strains ($\Delta sodA$, $\Delta sodM$, $\Delta sodA\Delta sodM$), and a putative manganese transporter ($\Delta mntA$, $\Delta sodA\Delta mntA$, $\Delta sodM\Delta mntA$) deletion strains.....	173
Figure 6.7 Fractional contribution of SaSODs to total activity during Mn starvation (Garcia et al., 2017).....	174
Figure 6.8 SodM contributes to resisting Mn starvation during infection (Garcia et al., 2017; Fig.5).	175
Figure 6.9 A 2D-LC profiles of soluble <i>S. aureus</i> extracts with two identified manganese pools (Dr Kevin Waldron).	177
Figure 6.10 A 2D-LC Mn and Fe profiles of SH1000 strains (Dr Emma Tarrant).....	178
Figure 6.11 A representative SOD activity assay of recombinant and the StrepII-tagged isoform of Fe-SodM.	179
Figure 6.12 Complementation of <i>E. coli</i> <i>sod</i> mutant phenotype in rich medium liquid culture....	180
Figure 6.13 Immunoblotting of extracts of SH1000 cells.	181
Figure 6.14 Activity assay of complemented SH1000 SOD mutants.	182
Figure 6.15 Change of growth of <i>S. aureus</i> <i>sodM</i> mutant strains complemented <i>in trans</i> with StrapII-tagged <i>sodM</i> and <i>sodM</i> L159G mutant.	183

Figure 6.16 The representative chromatograms of size exclusion step following the StrepTrap purification.....	183
Figure 6.17 Metal analysis of StrepTrap and size exclusion purified proteins from <i>S. aureus</i> cells exposed to external metal supply in culture.	185
Figure 6.18 Change of growth of <i>S. aureus</i> Newman $\Delta sodM$ expressing wild type SodM, grown under oxidative stress and metal content of subsequent protein preparations.....	187
Figure 6.19 Elemental and catalytic analysis of proteins subjected to mis-metalation in <i>S. aureus</i> culture.....	188
Figure 6.20 Non-cambialistic SodM presents reduced growth rate upon Mn-starvation and oxidative stress.....	190
Figure 8.1 All the potential bonded and non-bonded contacts identified at the dimer interface of SaSODs.	200

List of tables

Table 1.1 Ionic radii and midpoint potentials of 3+/2+ couples of Mn and Fe complexes (Sheng et al., 2014).	33
Table 2.1 Bacterial strains used through this study.	40
Table 2.2 Composition of <i>E. coli</i> bacterial growth media and supplements used.	42
Table 2.3 Composition of <i>S. aureus</i> bacterial growth media.	43
Table 2.4 Plasmids used in this project.....	44
Table 2.5 Oligonucleotides used in this project.	47
Table 2.6 Polymerase chain reaction conditions.	47
Table 2.7 QuikChange reaction conditions.	50
Table 2.8 Amino acid analysis output.	67
Table 2.9 EPR experiments' acquisition parameters.....	72
Table 3.1 A correction factors calculated for standard protein assays based on amino acid analysis outcome.	85
Table 3.2 Average metal content of preparations of as-purified recombinant SODs.	86
Table 3.3 An average metal content of Mn-refolded SaSOD proteins.	95
Table 3.4 Comparison of the overall secondary structure contents of SaSODs quantified from far-UV CD spectra.	96
Table 3.5 Overview of the chemical stability of SaSODs evaluated by Trp fluorescence.....	99
Table 4.1 Protein crystallisation final conditions.	112
Table 4.2 Phase problem search models.....	112
Table 4.3 Summary of data collection statistics of the wild type Fe and Mn-loaded SaSODs....	114
Table 4.4 Summary of refinement statistics of the determined crystal structures of wild type SaSODs.	115
Table 4.5 Metal content and specific activity of BsSodA.	125
Table 4.6 A specific SOD activity assay of SodA isozymes.	30
Table 4.7 A specific SOD activity assay of SodM isozymes.....	132
Table 4.8 Data collection and refinement statistics of Mn-SodM triple mutant.....	134
Table 4.9 Bond distances and bond angles of the metal coordination sphere in single chain A.	135
Table 5.1 Summary of the maxima of the tryptophan fluorescence emission spectra of all studied native and mutated versions of SaSodA and SaSodM.	147
Table 5.2 Comparison of the secondary structure contents of SaSODs.....	149
Table 5.3 The Mn(II) zero-field parameters and specific SOD activity of SaSODs.....	155
Table 6.1 Fractional metal content of a purified preparation of Strep-tagged SodM and SodM L159G, purified from <i>S. aureus</i> Δ sodM culture.	185
Table 8.1 Summary of initial screening conditions resulting in positive hits of SodA and SodM crystals.....	198
Table 8.2 Dimer interface and surface description.	199

Table 8.3 Bond distances between active site metal and coordinating ligands.....200

List of equations

Equation 1.1 Four-electron reduction of dioxygen. 15
Equation 1.2 Fenton chemistry..... 16
Equation 1.3 Superoxide dismutase reaction with superoxide anion.26
Equation 2.1 A standard 4-parameter logistic model used for the sigmoidal fit of the inhibition curve.
..... 62
Equation 2.2 Mean residue ellipticity..... 70

List of abbreviations

AEC	Anion-exchange chromatography
amp	Ampicillin
au	Arbitrary units
cam	Chloramphenicol
CD	Circular dichroism
CDS	Coding sequence
CP	Calprotectin
CV	Column volume
ϵ	Extinction coefficient ($M^{-1}cm^{-1}$)
EDTA	Ethylenediaminetetraacetic acid
ELDOR	Electron-electron double resonance-detected NMR
ENDOR	Electron nuclear double resonance
EPR	Electron paramagnetic resonance
ery	Erythromycin
ICP-MS	Inductively-coupled plasma mass spectrometry
IPTG	Isopropyl β -D-1-thiogalactopyranoside
kan	Kanamycin
λ	Wavelength
LB	Lysogeny broth
MES	2-(N-morpholino)ethanesulfonic acid
MRSA	Methicillin resistant <i>Staphylococcus aureus</i>
MV	Methyl viologen
MW	Molecular weight
MWCO	Molecular weight cut off
NHE	Normal hydrogen electrode
OD	Optical density
PCR	Polymerase chain reaction
PQ	Paraquat
ROS	Reactive oxygen species
rpm	Revolutions per minute
SD	Standard deviation
SDS	Sodium dodecyl sulphate
SEC	Size-exclusion chromatography
SOD	Superoxide dismutase
spec	Spectomycin

tet	Tetracycline
TM	Tris minimal medium
Tris	Tris(hydroxymethyl)aminomethane
TSB	Tryptic soy broth
UV-Vis	Ultraviolet-visible

Chapter 1. Introduction

1.1. *Staphylococcus aureus*, an opportunistic mammalian pathogen

Staphylococci are Gram-positive bacteria, which belong to the phylum Firmicutes. They are spherical, non-motile, non-spore forming bacteria, which reproduce by binary fission in multiple planes, forming the characteristic “bunch of grapes” clusters of cells (Schleifer & Bell, 2015). Bacteria belonging to genus *Staphylococcus* are mesophilic, facultative anaerobes, able to grow by aerobic respiration or by fermentation, which are associated with mammalian and avian hosts (Kloos, 1980).

Staphylococcus genus consists of a multitude of species of great importance, from both a human health and economic perspective. The current phylogeny of genus *Staphylococcus* (Lamers et al., 2012) suggest classification of around 60 known taxa into 15 cluster groups, based on multiple loci data (16S rRNA, *dnaJ*, *rpoB*, and *tuf* gene fragments), which phenotypically combine into six major staphylococcal species groups (Figure 1.1). According to this phylogenetic model, the basal divergence of staphylococci into two major clades separates the only species possessing cytochrome C oxidase (*S. sciuri* group), which are novobiocin-resistant, from the clade of oxidase-negative species. Subsequent divergence within the oxidase-negative clade separated the *S. auricularis* from the remaining staphylococcal lineages. The next lineage to diverge from other staphylococci was the novobiocin-susceptible, and coagulase-negative Simulans-Carnosus species group. Following the split of these three early-diverging lineages, the remaining *Staphylococcus* species evolved into three large species groups: the Saprophyticus species group, the Hyicus-Intermedius species group, and the Epidermidis-Aureus species group, which contains the taxa of greatest clinical significance. The Epidermidis-Aureus group consists of 5 clusters, the coagulase-negatives (CoNS) *S. epidermidis*, *S. warneri*, *S. lugdunensis* and *S. haemolyticus* clusters, and the coagulase-positive *S. aureus* cluster group.

The *Staphylococcus aureus* cluster group consists of *S. aureus* subspecies *aureus*, which is a major human pathogen in the Epidermidis-Aureus species group, and *S. aureus* subspecies *anaerobius*, associated predominantly with abscess disease of sheep (La Fuente et al., 1985; Elbir et al., 2013; Peake et al., 2006). The species name “*aureus*” originated from Latin and refers to the fact that the bacteria grow into colonies which (often) have a golden (yellow) colour when cultured on solid media, due to production of staphyloxanthin, whilst CoNS form pale, translucent colonies (Howard & Kloos, 1987).

S. aureus was first isolated in 1880 from a surgical wound infection by Alexander Ogston (Ogston, 1881). The first complete *S. aureus* genome sequences of strains N315 and Mu50 were published in 2001 (Kuroda et al., 2001). To date there are 8266 genome assemblies (NCBI Genome Database 2017-09-16) available for *S. aureus* isolates. The genome of *S. aureus*

consists of a relatively small, chromosome, ranging from 2.3Mbp to 2.8Mbp (Kuroda et al., 2001), with characteristically low (~32%) G+C content, and in the case of many isolates also plasmids (Holden & Lindsay, 2008).

Comparative analysis of the available genome sequences of *S. aureus* strains was shown to present significant diversity between isolates. The majority of the *S. aureus* chromosome (approximately 75%) is highly similar between isolates, while the remaining ~25% of genes are accessory and highly variable (Fitzgerald et al., 2001; Lindsay & Holden, 2004). The conserved genes (core genome) primarily encode proteins essential for central metabolism and cell maintenance, and some virulence factors (Fitzgerald et al., 2001). The accessory genes tend to be non-essential and mainly encode resistance genes, toxins, virulence and host-adaptation factors, contributing to the colonisation of strain-specific niches (Fitzgerald et al., 2001; Lindsay & Holden, 2004). A substantial portion (~10-20%) of these genes is encoded on mobile genetic elements (MGEs) that can be transferred horizontally between bacteria within and across lineages. The major types of MGE are bacteriophage, *S. aureus* pathogenicity islands (SaPI), staphylococcal cassette chromosomes (SCC), plasmids and transposons (Lindsay & Holden, 2004; Lindsay et al., 2006; Holden & Lindsay, 2008; Lindsey, 2010). The population of *S. aureus* is structured in lineages, called clonal complexes (CC), grouping isolates of closely related genetic makeup (Waldron & Lindsay, 2006; Lindsay, 2010; Feil et al., 2003).

Approximately 40% of the proposed coding sequence in *S. aureus* currently has no annotated function. The occurrence of single nucleotide polymorphisms (SNPs), variation in repeats, diversity within operons and the horizontal gene transfer by MGEs, drive the dynamics of the population of pathogenic *S. aureus*, evolving towards higher survival, adaptability and infectivity (Lindsay & Holden, 2004) .

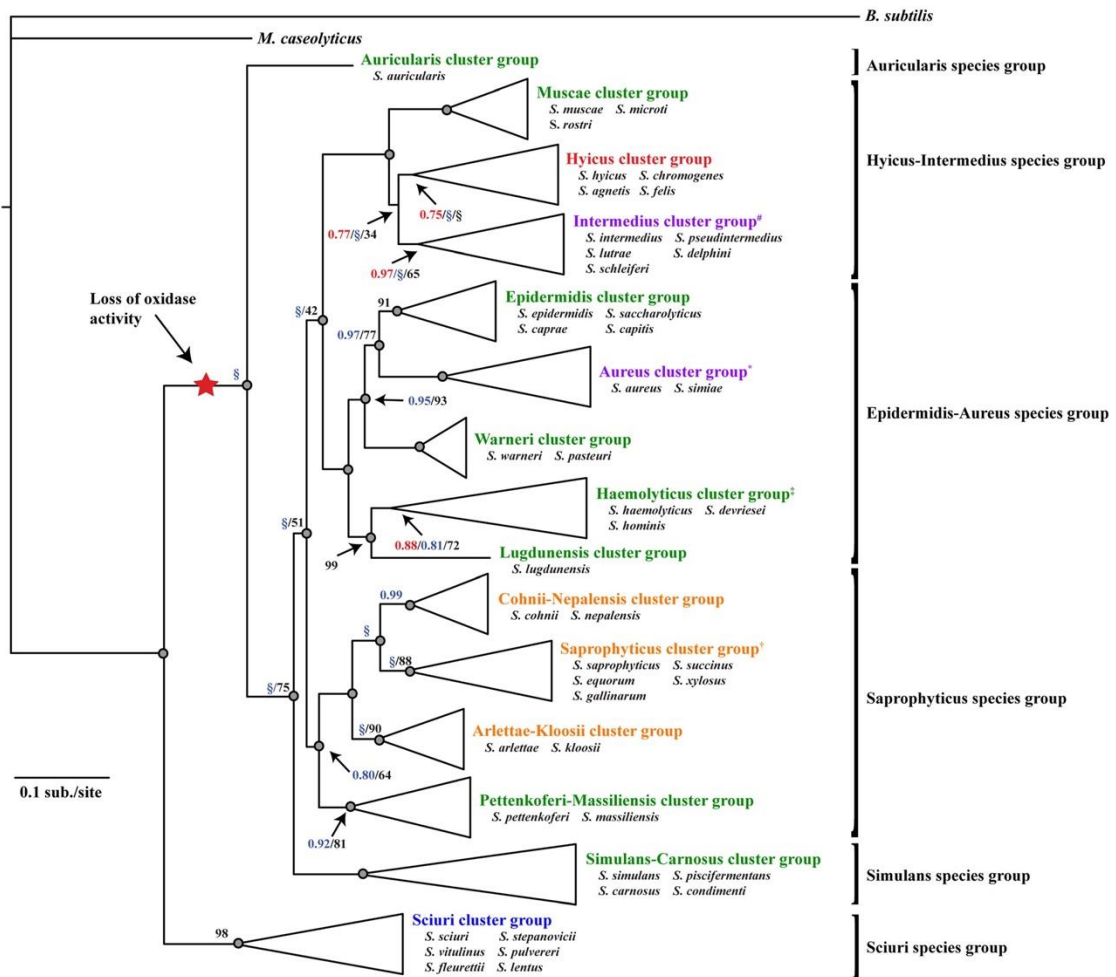


Figure 1.1 Phylogenetic relationships among *Staphylococcus* species (Lamers et al., 2010).

The phylogram represents staphylococcal groupings into six species groups and 15 cluster groups. The cluster groups coloured in **blue** represent species that are novobiocin resistant, coagulase negative, and oxidase positive; **green**, species that are novobiocin susceptible, coagulase negative, and oxidase negative; **orange**, species that are novobiocin resistant, coagulase negative, and oxidase negative; **purple**, species that are novobiocin susceptible, coagulase positive, and oxidase negative; and **red**, species that are novobiocin susceptible, coagulase variable, and oxidase negative.

Colour scheme exceptions are: #*S. schleiferi schleiferi* is coagulase negative; **S. simiae* is coagulase negative; †*S. hominis novobiosepticus* is novobiocin resistant; and ‡*S. equorum linens* is novobiocin susceptible. Figure taken directly from Lamers et al., 2012.

1.1.1. Commensalism and pathogenicity of *S. aureus* (*S. aureus* infection and disease)

Coagulase-negative staphylococci are part of natural, commensal microflora of many species of animals, colonising predominantly skin and mucous membranes of mammals and birds. Humans typically carry 10-20 different strains of CoNS species (Feng et al., 2008). *Staphylococcus aureus*, a coagulase-positive and catalase-positive bacterium, is persistently carried by 20-25%, and intermittently carried by 55-60% of the human population (Wertheim et al., 2004), with approximately 20% of the population that were never colonised. It primarily colonises anterior nares from where it is usually transferred onto skin and often inhabits the axilla and the perineum

areas. In healthy humans *S. aureus* can be occasionally found in the gastro-intestinal (Bhalla et al., 2007; Acton et al., 2009) and the vaginal tracts. The vertical transmission of *S. aureus* from mothers to newborns upon vaginal delivery has been observed, resulting in the colonisation of a small percentage (<5%) of newborns at birth (Burgeois-Nicolaos et al., 2010).

Transmission of *S. aureus* occurs through direct skin-to-skin contact, or from environmental exposure to recently contaminated objects, mostly in hospital settings (Miller & Diep, 2008). It has been suggested that nasal carriers of *S. aureus* have an increased risk of acquiring an invasive infection with this pathogen via autoinfection (Eiff et al., 2001; Peacock et al., 2001; Wertheim et al., 2005), however, it is not an imperative for bacteraemia (Marshall & McBryde, 2014). Commensal colonisation with *S. aureus* has been suggested to have a protective impact on the innate immunity of the host, as the carriers have been shown to have a greater *S. aureus* bacteraemia survival rate than non-carriers (Wertheim et al., 2004). The constant exposure of the persistent carriers to *S. aureus* antigens, stimulating mild immune responses, may potentially develop a form of immune tolerance and suppression of pro-inflammatory responses, allowing persistent colonisation as opposed to pro-inflammatory response and bacterial clearance in non-carriers (Brown et al., 2014).

The clinical significance of *S. aureus* arose from the ability of this bacterium to cause a wide variety of skin and soft tissue infections as well as bloodstream infections and pneumonia in animal hosts, including humans (Diekema et al., 2001). When *S. aureus* crosses the barrier of the human body, through a break in skin or mucous membranes, it can become a highly successful and invasive pathogen. It spreads through the blood stream infecting a variety of tissues and causing a range of infections. These disease manifestations can vary depending on the site of infection and the susceptibility of the host, from local, minor skin infections like boils or impetigo, to more invasive and systemic reactions such as sepsis, infective endocarditis, and deep tissue abscesses in multiple organs (Wertheim et al., 2005; Gordon & Lowy, 2008). The *S. aureus* infections of hosts with undeveloped or compromised immunity and in post-surgical hosts (Weems, 2001; Chu et al., 2005; Valente et al., 2005) most often lead to a systemic response, which are likely to develop into life threatening conditions.

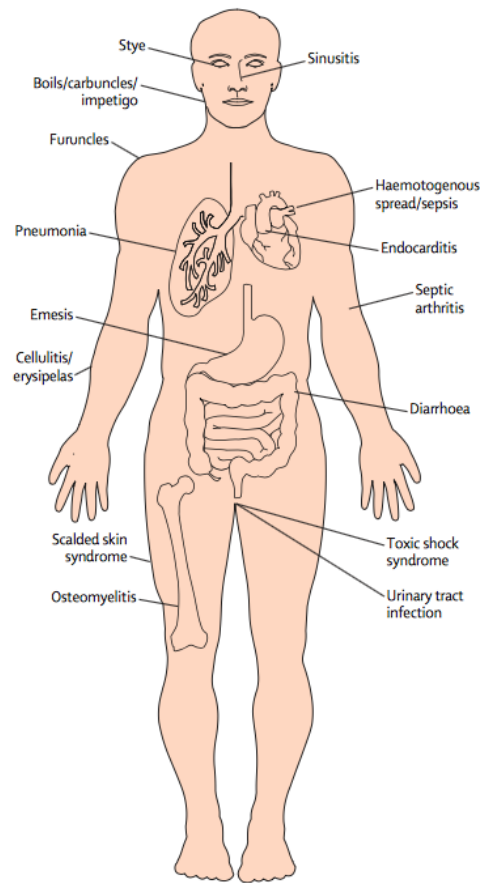


Figure 1.2 Disease manifestation of *S. aureus* infection (taken from Wertheim et al., 2005).

A representative range of diseases caused by *S. aureus* infection and their location in the human body. Figure taken directly from Wertheim et al., 2005.

1.1.2. Antibiotic resistance (MRSA, VRSA)

Numerous treatments and preventative measures have been developed (Lowy, 1998) in response to constant adaptation of this important pathogen (Stefani et al., 2012). Treatment for *S. aureus* infection generally involves targeting the final stages of cell wall synthesis, by the use of β -lactam antibiotics and glycopeptides (vancomycin); penicillin or its derivatives such as methicillin, nafcillin, oxacillin, or ceftaroline and several lipoglycopeptide antibiotics, including telavancin, dalbavacin or oritavanacin. The interference with cell membrane homeostasis by daptomycin or targeting the ribosomal RNA and disrupting protein biosynthesis by macrolides (erythromycin), lincosamides (clindamycin), streptogramins, and tetracyclines, are also used in controlling *S. aureus* infections. Antibiotics targeting DNA replication and inhibiting RNA polymerase are also applied to fight *S. aureus* infections (Maltezou & Giamarellou, 2006; Foster, 2017).

The extensive use of antibiotics to treat *S. aureus* infections has led to the selection of antibiotic resistant strains (Liu et al., 2011; Foster, 2017). The development of resistance to many antibiotics by *S. aureus* has evolved through acquisition of point mutations in genes encoding antibiotic targets or by the horizontal gene transfer of MGEs, resulting in the acquisition of new genes conferring resistance (Jensen & Lyon 2009; Azarian et al., 2016). These horizontally-transferred determinants may have originated in antibiotic producing species to protect them from potentially inhibitory molecules, or in their competitors. Many of the genes that were horizontally acquired by *S. aureus* are carried by plasmid-associated transposons, which by the means of conjugation or phage-mediated transduction between strains, confer transmissible drug resistance (Ray et al., 2016).

Methicillin resistance is conferred by the *mec* gene (*mecA*, *mecB*, *mecC*), which encodes a novel penicillin binding protein (PBP2A), conferring resistance to all β -lactam antibiotics. Compared to the *S. aureus* endogenous penicillin-binding protein, PBP2A presents a decreased binding affinity to β -lactams, rendering the action of β -lactam antibiotics ineffective (Hartman & Tomasz, 1984). The *mecA* or *mecC* gene, alongside its regulatory genes, is carried on a stable MGE known as the staphylococcal chromosomal cassette (*SCCmec*), which can be horizontally transferred between staphylococcal strains (Ito et al., 2003; Wielders et al., 2001; Scharn et al., 2013). After accurate excision and integration mediated by the site-specific recombinase genes encoded by SCC, *SCCmec* is integrated into the staphylococcal chromosome, leading to acquisition of β -lactam antibiotic resistance, and thus allowing for the evolution of methicillin-susceptible *S. aureus* (MSSA) into MRSA.

The Centre for Disease Control and Prevention (CDC) classified MRSA as a significant threat, causing annually over 80,000 invasive infections and 11,000 related deaths in the USA, as estimated in a 2013 report (CDC, 2013). The European Centre for Disease Prevention and Control (ECDC) reported on the decline of MRSA percentages in the EU/EEA from 18.8% in 2011 to 16.8% in 2015, however, substantial variations in the occurrence of MRSA were observed across European countries (ECDC, 2015; Figure 1.3). The World Health Organisation (WHO) declared in 2014 that the reported antibiotic resistant cases of staphylococcal infections (MRSA) exceed 20% in all WHO regions (African Region, Region of the Americas, Eastern Mediterranean, European, South-East Asia and West Pacific Regions), and even 80% in some reports. According to WHO *Staphylococcus aureus*, methicillin-resistant, vancomycin-intermediate and resistant strains are considered to be high priority pathogens, and a serious threat to global health.

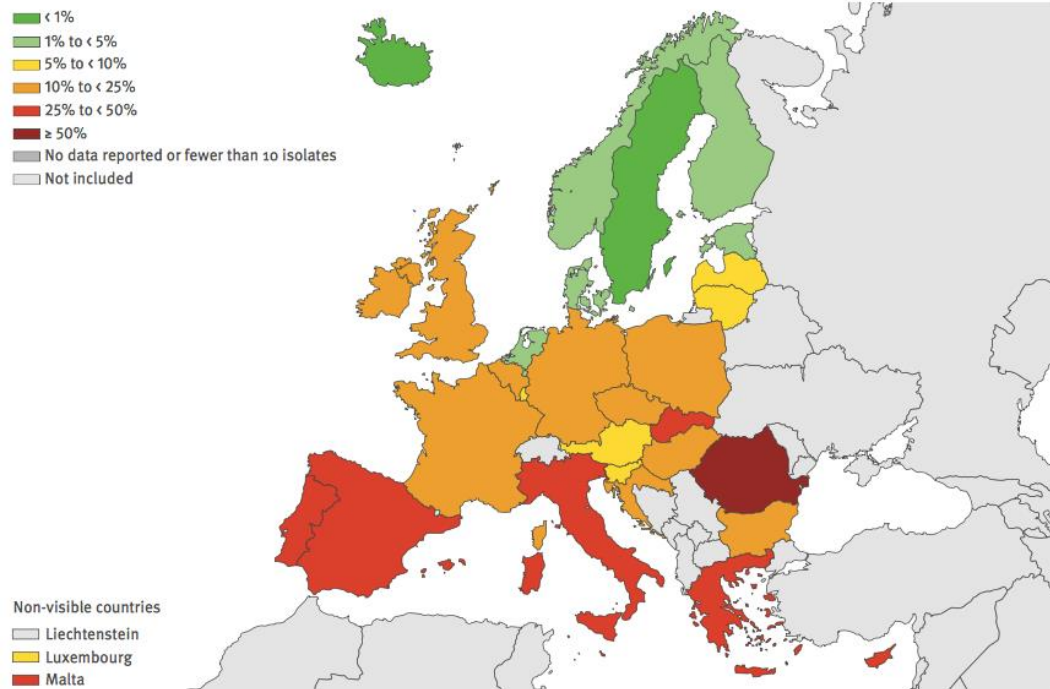


Figure 1.3 MRSA invasive isolates in EU/EEA identified in 2015 (ECDC, 2015).

Number of MRSA isolates identified in EEA territory according to Annual report of the European Antimicrobial Resistance Surveillance network (EARS-Net) 2015.

Vancomycin has been regarded as the drug of choice for treatment of MRSA, however, due to an increase in the use of vancomycin for the treatment of other conditions, such as pseudomembranous colitis due to *Clostridium difficile* and CoNS staphylococcal infections in hospitalised patients, *S. aureus* has also developed resistance to this antibiotic. The first *S. aureus* strain with partial susceptibility to vancomycin was isolated in Japan in 1997 from a surgical wound infection (Hiramatsu et al., 1997). Since then, there has been an increase in the number of cases with both vancomycin-intermediate (VISA) and vancomycin-resistant *S. aureus* (VRSA). Fully vancomycin-resistant *S. aureus* were observed only a few years after emergence of VISA strains, in 2002 (Chang et al., 2003; Sievert et al., 2008). Vancomycin resistance, conferred by *vanA*, has derived from the plasmid-borne transposon Tn 1546, likely acquired from other co-infecting, vancomycin-resistant species such as enterococci, (Gardete & Tomasz, 2014). VRSA strains are not yet widespread amongst the population, allowing for vancomycin to be still used as a drug of last resort. VRSA is often found to be also methicillin-resistant, and thus represent a potential future challenge for clinical *S. aureus* infection control.

MGEs such as plasmids, gene cassettes and transposon elements have been shown to play important roles in co-selection of antibiotic and metal resistance (Baker-Austin et al., 2006; Henriques et al., 2016; Pal et al., 2015; Pal et al., 2016; Li et al. 2017). Co-selection of antibiotic and metal resistance in bacteria is important primarily because it can maintain and promote antibiotic resistance in bacterial populations even in the absence of antibiotics.

Co-resistance, due to the co-occurrence of two resistance genes on a single MGE, or cross-resistance, when a single mechanism facilitates resistance to different drugs, have been demonstrated, as the mechanisms for co-selection of metal and antibiotic resistance. The association of Cd, Zn and methicillin resistance has been reported in the case of MRSA (Cavaco et al., 2010; Cavaco et al., 2011). The unrestricted use and release of metals to the environment is thus suggested to have potential to promote antibiotic resistance in bacteria of clinical importance.

A novel, horizontally-transferred copper resistance mechanism (*copXL*), which is associated with the *SCCmec*, has recently been identified in the highly virulent, community acquired methicillin resistant *Staphylococcus aureus* USA300. The CopXL system comprise the CopX, a copper P₁-ATPase efflux transporter and CopL, a novel lipoprotein, which play a key role in copper efflux, and thus confer high resistance to copper toxicity. This has been proposed to contribute to survival of USA300 in the macrophages, which utilise copper toxicity as one of the mechanisms against invading pathogens (Purves et al., 2018).

Methicillin-resistant *Staphylococcus aureus* (MRSA) are important pathogens associated with three types of environment: healthcare, community and livestock (Lindsay, 2010).

1.1.2.1. Healthcare-associated MRSA (HA-MRSA)

The MRSA strains are well known as the cause of the majority of nosocomial *S. aureus* infections (Lindsay & Holden, 2004). Surgical procedures and the use of devices such as catheters allow the bacteria to easily cross the barrier of the host's body and establish a surgery site infection. Strains associated with health care often possess resistance to multiple drugs. This characteristic has been suggested to arise from acquisition of the *mecA* gene (Ito et al., 2003) as well as mutations conferring resistance to fluoroquinolone (Knight et al., 2012; Holden et al., 2013).

Due to the decreasing number of effective strategies for treatment of MRSA infections, hospitals are implementing approaches aiming to reduce the transmissibility of *S. aureus* between patients. The general efforts are made to improve hospital and staff hygiene as well as providing visitors with access to sanitisers to limit the spread of increasing antibiotic resistance. The natural "self-sterilising" properties of copper surfaces have also been explored by implementing copper-coated door handles, copper-coated surgical trolleys and other copper-coated utensils that are easily contaminated in the healthcare settings, to reduce surface contamination-mediated transmission of nosocomial disease (Casey et al., 2010; Inkinen et al., 2016).

1.1.2.2. Community-associated MRSA (CA-MRSA)

CA-MRSA refers to strains which are acquired outside of the hospital environment, and are of great concern because they infect previously healthy hosts (Witte, 2009; Otto, 2010; Carleton et al., 2004). Strains associated with the community evolved independently of nosocomial strains

(Okuma et al., 2002; Ito et al., 2003). CA-MRSA associated cases are particularly prevalent in the USA and Asia, with the usual clinical manifestation as severe skin and soft tissue infection, but they can also lead to invasive life-threatening conditions, such as necrotising pneumonia and septicaemia (Witte, 2009).

CA-MRSA strains are often characterised by an expanded profile of virulence factors (Baba et al., 2002). One of these is the pore forming Panton-Valentine leukocidin (PVL) toxin, which is linked with necrotising pneumonia in young hosts and is found in most CA-MRSAs (Lindsay, 2008; Feil et al., 2003; Lindsay et al., 2006; Witte, 2009, Otto, 2013). Phenol soluble modulins (PSMs), causing lysis of neutrophils after phagocytosis; lysis of red and white blood cells, stimulating inflammatory responses and contributing to biofilm development, are produced more abundantly by CA-MRSA compared with HA-MRSA strains (Wang et al., 2007; Cheung et al., 2014).

1.1.2.3. Livestock-associated MRSA (LA-MRSA)

Apart from HA-MRSA and CA-MRSA, livestock-associated MRSA (LA-MRSA) strains are persistent in food-producing animals and humans who live and work at these animal farms (Wulf & Voss, 2008). Geographically they are found predominantly in mainland Europe, Asia and North America, where they are associated mostly with pig and cattle farming, but equine and poultry hosts have also been described (Butaye et al., 2016). LA-MRSA acquired resistance to β -lactams independently of the other methicillin-resistant strains. LA-MRSA strains also possess a tetracycline resistance gene that is carried on a plasmids and/or transposon (Benito et al., 2014). It has been demonstrated that MRSA likely spreads in farm settings between animal species (both food-producing and pets) and people residing on farm (farmers, vets; Pletinckx et al., 2013; Wendlandt et al., 2013).

According to the European Food Safety Authority's (EFSA), (EFSA, 2009; EFSA & ECDC, 2017), MRSA has been regarded as an important foodborne microorganism, which may pose potential hazards to both food-handling and occupational staff in the food industry, causing a broad range of staphylococcal food poisoning (SFP). LA-MRSA may transmit between humans with limited efficiency, and the cases of LA-MRSA carriers with zoonotic pneumonia, endocarditis, and necrotising fasciitis have been reported (Graveland et al., 2011; van Cleef, Monnet, et al., 2011; van Cleef, Graveland, et al., 2011; Wassenberg et al., 2011; van Rijen et al., 2014).

1.1.3. Pathogenesis

Anterior nares and the skin (including perineum and pharynx) are main sites of *S. aureus* carriage, which often remains asymptomatic. *S. aureus* infection occurs when the bacteria successfully colonise, breach the physical barrier of the body, invades the host and successfully

evades the host's defence systems. *S. aureus* presents an ability to colonise a wide range of ecological niches, and has the potential to fight the innate immune system and infect almost all host tissues. High adaptability of the population of *S. aureus* is achieved by the combination of the variation of the accessory genomes, the range of different virulence factors produced, and the complex regulatory systems that control gene expression (Lindsay & Holden, 2004). The interaction of these bacterial factors with the host's immunity, age, physiological condition, as well as environmental factors (limited nutrients, limited oxygen, fluctuating osmolarity, pH changes, oxidative stress, nitrosative stress) is critical in colonisation and establishment of the infection (Peacock et al., 2003; Tuchscherer et al., 2010; Gordon & Lowy, 2008).

1.1.3.1. Virulence factors of *S. aureus*

Mobile genetic elements carry more than 50% of virulence factors in *S. aureus*, and by facilitating the exchange of virulence determinants and antibiotic resistance among isolates, possibly contributing to evolution of more virulent and resistant strains (Lindsay & Holden 2006; Lindsay 2010; Malachowa & DeLeo 2010; Stefani et al., 2012).

Virulence factors improve the ability of *S. aureus* to infect a host, from influencing the initial adherence of bacteria to the invaded cell surface and colonisation, through the complex interaction with the host and the defence against the innate immune system (Figure 1.4). In *S. aureus* they include cell-surface factors (teichoic acids, capsules, polysaccharide intracellular adhesion, pigments (staphyloxanthin), microbial surface components recognizing adhesive matrix molecules (MSCRAMMs), surface factors promoting resistance to oxidative killing, (Foster & Höök, 1998), and secreted factors, such as systemic toxins (superantigens (SAGs); exfoliative toxins (ETs), (Xu & McCormick, 2012); cytotoxins (α -toxin, β -toxin, γ -toxin, leucocidins (PVL), δ -toxin, phenol soluble modulins (PSMs), ϵ -toxin); and extracellular enzymes (lipases, nucleases, hyaluronidase); (Makris, 2004).

The interaction of *S. aureus* with phagocytic cells is important in *S. aureus* infection. *S. aureus* can inhibit the recruitment of immune cells to the site of infection, by secreting the chemotaxis inhibiting protein (CHIPS) and staphylococcal extracellular adherence protein (Eap), which inhibits phagosomal enzymes aiming to degrade the CHIPS (de Haas et al., 2004; Stapels et al., 2014).

Bacterial cells possess structural elements that can contribute to defence against phagocytosis. Components associated with the bacterial cell surface, such as staphylococcal protein A (SpA), clumping factors (ClfA, ClfB), fibronectin binding protein (FnBPA, FnBPB), and collagen binding protein (Cna), are members of the MSCRAMMs family, mediating adherence of bacteria to the host cell surface and facilitating abscess formation (Foster & Höök, 1998, O'Riordan & Lee, 2004; Cue et al., 2012). Some strains of *S. aureus* produce capsular polysaccharides, which enhance the adherence to host cells and contribute to the inhibition of the

phagocytosis. Increased virulence amongst capsulated in comparison to non-capsulated strains has been observed (Thakker et al., 1998). Capsular polysaccharides can facilitate formation of the biofilm, an aggregated mass of bacteria covered in a secreted polysaccharide that protects them from environmental stress and antibacterial compounds. The production of a biofilm allows *S. aureus* to colonise medical devices leading to nosocomial prosthetic device infection (Lentino, 2003)

The enzymes (coagulase, hyaluronidase, staphylokinase, lipase) and numerous toxins are secreted to the extracellular environment to break down host cell membranes, lyse host cells to acquire essential nutrients, and ultimately to kill host immune cells and enable the spread of the infection (Archer, 1998; Dinges et al., 2000; Burlak et al., 2007). The cytotoxins and haemolysins damage host's cells and contribute to high level inflammation, and abscess formation (Berube & Wardenburg, 2013; Huseby et al., 2007; DuMont & Torres, 2014; Cheung et al., 2014; Merriman et al., 2015). Production of some of the toxins is associated with a particular disease, for example the exfoliative toxin which breaks down the skin causing Scalded Skin Syndrome (Ladhani et al., 1999). Toxic Shock Syndrome is associated with a superantigen (TSST-1), causing uncontrolled T-cell proliferation and cytokine release, resulting in deep tissue penetration and damage (Brosnahan & Schlievert, 2011).

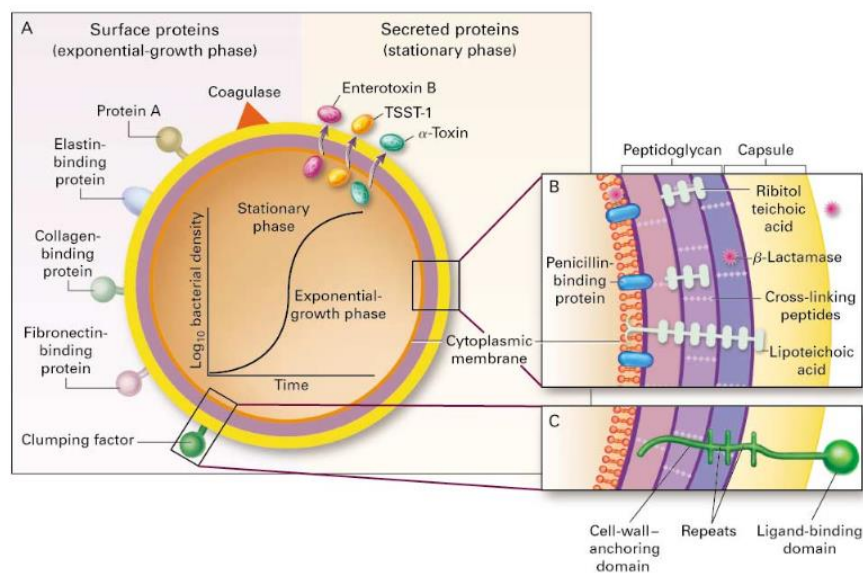


Figure 1.4 Selected cell wall associated and secreted virulence factors of *S. aureus*.

(A) Cell surface and secreted proteins expressed differentially during bacterial growth. Following initiation of infection, predominantly division and adhesion proteins are being produced, and followed by density-sensing mechanism driven production of toxins and exoprotein in post exponential phase, leading to spreading of infection (Harris et al., 2002). (B) and (C) show cross sections of the cell envelope. (C) Many of the surface proteins share a structural organisation resembling clumping factor, including repeated segments of amino acids (figure taken from Lowy, 2008).

1.2. The response of *S. aureus* to environmental stimuli

To ensure the appropriate expression of *S. aureus* virulence factors during infection, these genes are under the control of numerous regulators which often operate together for a coordinated systematic response to the host environment (Cheung et al., 2004; Bronner et al., 2004; Mashruwala & Boyd, 2017).

The *S. aureus* virulence factors are regulated by the two-component regulatory systems (TCRS; Cheung et al., 2004; Gao & Stock, 2009), such as the quorum sensing system and global regulator accessory gene regulator (Agr), SaeRS, SrrAB, ArlSR systems, which respond to environmental signals during the infection. TCRS typically consist of two proteins: a histidine kinase (HK) and a response regulator (RR). The HK can be either cytosolic or membrane-associated and the RR is typically a cytosolic DNA binding protein. A phosphorylation cascade between the HK and RR results in conformational changes in the RR protein, altered affinity towards target DNA sequences, modified gene expression, and an appropriate physiological response. Additionally, the DNA-binding protein families, such as staphylococcal accessory regulator A (Cheung et al., 2008; SarA) and its homologues (SarR, Rot, SarS, SarZ, MgrA), also modulate bacterial adaptation to varying conditions during the infection (Hecker et al., 2003).

S. aureus also uses transcriptional and translational regulators responding to changes in environmental conditions to control the expression of required uptake/resistance systems and metabolic pathways. The ability of pathogenic *S. aureus* to invade and survive in the hostile habitat of host tissue, and evade the innate immune system requires the efficient utilisation of local environmental nutrients, such as metals (Xiong et al., 2000), and rapid multi-signal response to environmental changes. The environmental sensing through specific detection, transmission and response allows *S. aureus* to adapt to a range of environmental stimuli including changes in carbon source, temperature, pH, osmolarity, oxygen and metal ion availability, and together contribute to virulence and resistance of this pathogen (Chan & Foster, 1998; Hecker et al., 2003; Fuchs et al., 2013). Identification of the specific stimuli and the mechanisms of their interaction with receptors could potentially provide a valuable therapeutic target for interference with gene expression pathways necessary for virulence.

1.2.1 General environmental stress

The growth and survival of bacteria is dependent on the ability of cells to adapt to environmental changes. *S. aureus* can asymptotically colonise the nasopharynx (main reservoir: anterior part of the nasal cavity (vestibulum nasi) lined by a stratified, keratinised, non-ciliated squamous epithelium), intact skin; as well as persist outside the host in dust, soil, water and other environments (dissemination of bacteria). To survive within the airways of the host for prolonged time *S. aureus* is involved in constant competition for epithelial attachment sites or limited nutrients, and when adhered needs to outcompete interfering nasopharyngeal microbiota (*Corynebacterium* spp., *Propionibacterium* spp., *Staphylococcus* spp.; Huttenhower et al., 2012),

presenting different susceptibilities to host defence molecules (induction of host inflammation in the nasal epithelium, by the release of pro-inflammatory molecules) and producing antimicrobial molecules (release of antimicrobial molecules by commensal bacteria), as well as host-defence lipids, peptides and proteins produced by epithelial and immune cells (Krismer et al., 2017; Schaubert & Gallo, 2009).

S. aureus promotes binding to nasal epithelial ligands (loricrin, cytokeratin 10 and involucrin) by expressing surface proteins (while down-regulating expression of virulence factors and toxins), such as clumping factor B (ClfB) or iron-regulated surface determinant A (IsdA); (Brown et al., 2014). Further, surface positive charge and expression of aureolysin, staphylokinase, multiple resistance and pH regulation protein F (MrpF) contribute to resisting effects of antimicrobial peptides and lysozyme produced by the host (Herbert et al, 2007; Brown et al., 2014). To overcome challenging condition of the limitation of nutrients in vestibulum nasi (metal ions are bound with very high affinity to the nasal host proteins lactoferrin and calprotectin, which is secreted by primary nasal epithelia in response to *S. aureus* proteases (Kato et al., 2017; see section 1.3), *S. aureus* expresses siderophores, high-affinity manganese and zinc transporters and produces the nicotinamide-like metallophore staphylopine, which facilitates nickel, cobalt, zinc, copper and iron acquisition (see section 1.3).

During both transmission of *S. aureus* occurring by skin-to-skin contact and anterior nares colonisation, bacteria encounter further stresses of desiccation, exposure low pH, the presence of free fatty acids (Kohler et al., 2009), the production of antimicrobials by the resident commensal flora (Schauber & Gallo, 2009), leading to oxidative stress and subsequent damage to lipids, proteins and DNA. Carotenoid pigments (staphyloxanthin, synthesised from enzymes encode by *ctrOPQMN* operon is the main pigment of *S. aureus*; Liu et al., 2005), catalase (KatA) and alkyl hydroperoxide reductase (AhpC) have been shown to contribute to desiccation tolerance of *S. aureus* (Cosgrove et al., 2007).

Changes of the pH, equivalent to physiological differences between skin, abscess and blood environment, were shown to induce responses from the Sae-controlled regulon. Microarray data for mild acid conditions shows modulation of the transcription profiles of the extracellular virulence factors and genes involved in transport of sugar and peptides in these conditions. The acid shock effect, forcing rapid adaptation, seemed to induce changes in transcription of pentose phosphate pathway genes, and of *kata* and *soda* involved in the oxidative stress response, which are implied to also play roles in virulence of *S. aureus* (Voyich et al., 2005).

Most *S. aureus* surface proteins that mediate adhesion to the epithelium are regulated by the agr quorum sensing system (Le & Otto, 2015). Haemoglobin, which is present in nasal fluids at high concentrations, was shown to inhibit the agr system, thereby inducing the expression of *S. aureus* adhesins and promoting nasal colonisation (Pynnonen et al., 2011).

Response to environmental changes involves rapid and complex regulation of the gene expression. In *Bacillus subtilis* the σ^B -dependent general stress response regulon consists of over 200 genes, that confer a multiple, general, and preventive resistance to stress and energy

depletion (Price et al., 2001; Hecker et al., 2009). The expression of the genes within the regulon is controlled by the σ^B regulators (RSB) that interact with the RNA polymerase core unit to initiate the transcription of the regulated genes.

In *S. aureus* the alternative sigma factor, σ^B , plays an important role in modulation of the environmental stress response (thermal, osmotic, alkaline pH; Horsburgh et al., 2002a; Chan et al., 1998; Pane-Farre et al., 2006) and was suggested to contribute to the survival and virulence of this pathogen. In *S. aureus*, in stationary phase or growth under particular stress conditions, the regulatory cascade begins with dephosphorylation of RsbV (anti-anti sigma factor) by RsbU, followed by the interaction of RsbV with RsbW (kinase), allowing σ^B to associate with RNA polymerase to activate transcription of numerous genes (Kullik & Giachino, 1997; Horsburgh et al., 2002a; (Senn et al., 2005). σ^B of *S. aureus* was demonstrated to influence the expression of a variety of virulence and resistance related genes, including virulence factors (Horsburgh et al., 2002a) and regulatory elements (Bischoff et al., 2004). Moreover, it affects methicillin and glycopeptide resistance (Bischoff & Berger-Bächi, 2001), biofilm production (Rachid et al., 2000), and internalisation into endothelial cells (Haslinger-Löffler et al., 2005).

Invasive staphylococcal infection leads to the formation of abscesses within the colonised organs (Cheng et al., 2009). Abscess formation is a mechanism used by the host to contain, starve and ultimately eliminate the pathogen. An abscess is an environment where bacteria routinely encounter reduced oxygen concentration. In *S. aureus*, the SrrAB regulator senses the changes in oxygen availability and modulates expression of genes responsible for aerobic or fermentative energy metabolism (Bischoff et al., 2004; Ulrich et al., 2007). The ability to switch between aerobic and anaerobic metabolism enables the survival of staphylococci in neutrophils, and thus plays an important role in virulence (Bae et al., 2004; Richardson et al., 2006; Prajsnar et al., 2012).

1.2.2 Oxidative and nitrosative stress

The interplay between bacterial, environmental and host factors contribute a key role in *S. aureus* colonisation and infection. Local invasion of epithelium (trauma, surgery) enables entry of pathogenic microorganisms into the underlying tissue and initiates a response of the innate immune system. Formation of local abscess lesions constitutes the initial point of infection and allow the bacterium to avoid host defence strategies. *S. aureus* is able to escape innate immune response using repertoire of mechanisms (see section 1.2.1; Herbert et al, 2007; Brown et al., 2014). Non-professional phagocytes are responsible for most of the initial killing of *S. aureus*, and the ability to avoid or survive phagocytic attack is thus very important for the pathogen (Figure 1.5).

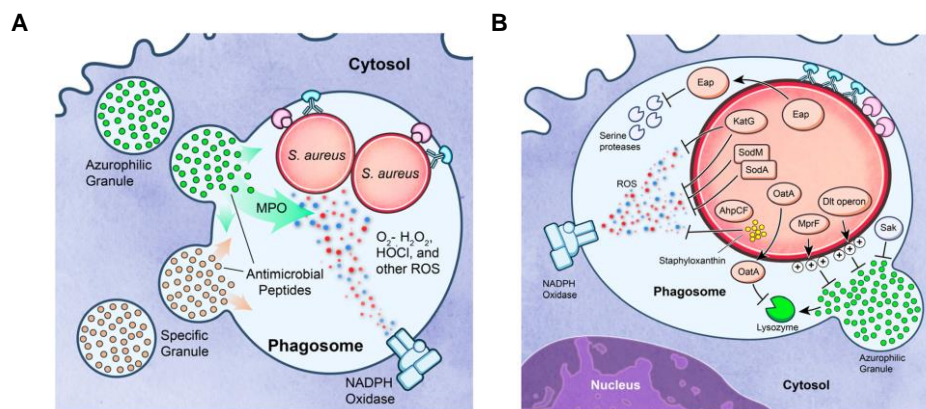


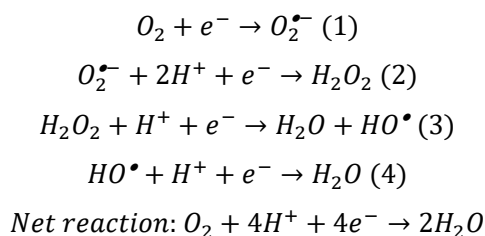
Figure 1.5 Phagocytosis of *S. aureus*.

(A) Bacteria are exposed to oxygen-dependent and oxygen-independent factors within the phagosome. (B) *S. aureus* produces several secreted and surface-bound molecules to avoid neutrophil killing (MPO, myeloperoxidase; adapted from McGuinness et al., 2016).

The ability of *S. aureus* to survive and persist in various host tissues, including professional phagocytes (Prajnsnar et al., 2012), is crucial to the establishment of the disease. Neutrophils can use both oxygen-dependent (reactive oxygen species) and oxygen-independent strategies, such as antimicrobial peptides and proteins (degranulation), to kill invading pathogens (Figure 1.5; McGuinness et al., 2016).

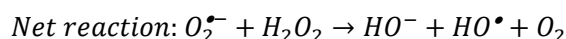
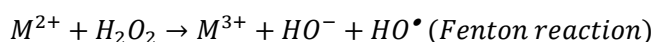
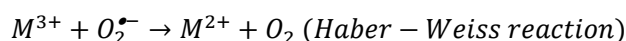
The innate immune system responds to bacterial infection by producing antimicrobial agents, such as reactive oxygen and reactive nitrogen species (ROS and RNS). Environment of phagolysosome exposes *S. aureus* to elevated concentration of ROS, resulting in oxidation and chlorination of bacterial proteins (see Figure 1.6). Successful pathogens, including *S. aureus*, possess the ability to alleviate both endogenous and exogenous oxidative stress as well as nitrosative stress, implementing appropriate protection, detoxification, and repair mechanisms that are controlled by a network of regulators.

Endogenous oxidative stress arises when the concentration of reactive oxygen intermediates increases inside the cell to a level exceeding defence capacity of the cell. ROS (Equation 1.1: superoxide anion (1), hydrogen peroxide (2), hydroxyl radical (3)) can be generated as by-products of cellular metabolism (aerobic respiration, auto-oxidation, or redox reactions), due to the one-, two-, and three-electron reduction of dioxygen, upon interaction with flavoproteins.



Equation 1.1 Four-electron reduction of dioxygen.

While superoxide cannot generally cross biological membranes, it becomes membrane permeable if protonated to hydroperoxyl and can dismutate spontaneously to generate hydrogen peroxide and oxygen. H_2O_2 can also cross biological membranes and may be further reduced through metal-catalysed Fenton chemistry to generate the highly reactive hydroxyl radical (Equation 1.2). Superoxide anion can disrupt Fe-S clusters in proteins, elevate reactive iron levels, cause mismetallation of mononuclear Fe enzymes, or it can be converted to other reactive species to attack the invading pathogen (see Figure 1.6). Fenton chemistry (Equation 1.2) leads to endogenous generation of highly-reactive ROS (hydroxyl radical), upon iron (Imlay, 2003), copper or cadmium - catalysed reduction of hydrogen peroxide (Macomber & Imlay, 2009).



Equation 1.2 Fenton chemistry.

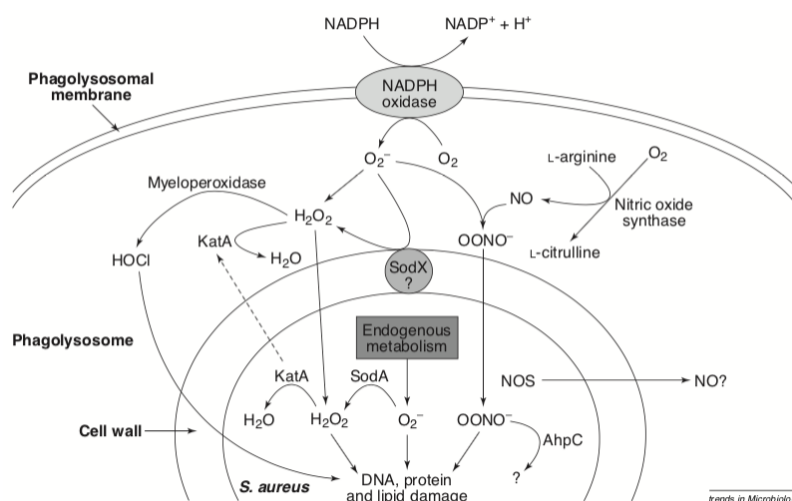


Figure 1.6 *S. aureus* evasion of oxidative killing within phagolysosome.

NADPH oxidase, myeloperoxidase and nitric oxide synthase (NOS), generate superoxide anion, hypochlorous acid and nitric oxide, respectively. The secondary derivatives (hydrogen peroxide and peroxynitrite) are produced from interaction of ROS with other molecules. *S. aureus* defence system against ROS include: catalase (KatA, inactivating external hydrogen peroxide), Alkyl hydroperoxide reductase (AhpC, activity against reactive nitrogen species), superoxide dismutases (SODs, acting against endogenously generated superoxide and involved in resistance against acidification of the phagolysosome by the action of the host myeloperoxidase). ROS can cause damage to proteins, lipids and DNA (Clements & Foster, 1999).

The two important antimicrobial systems of the host innate immune cells, utilising ROS and RNS during bacterial infections, are the NADPH phagocyte oxidase (PHOX) and inducible nitric oxide synthase (iNOS) pathways (Nathan & Shiloh, 2000; Fang, 2004; Gaupp et al., 2012). During the oxidative burst following phagocytosis, PHOX, which is localised in membranes of mammalian macrophages, monocytes and neutrophils, catalyses production of superoxide ($O_2^{\bullet-}$),

which is further converted to hydrogen peroxide (H_2O_2), and hydroxyl radical ($HO\bullet$), (Equation 1.1).

Other secondary oxygen derivatives, such as chloramines and hypochlorous acid ($HOCl$), generated by the myeloperoxidase (MPO) system also contribute to bacterial killing (Winterbourn & Kettle, 2013). The nitric oxide radical ($NO\bullet$) is produced by the iNOS in response to bacterial infection. The toxic intermediates produced through the subsequent reactions include nitrogen dioxide radical ($NO_2\bullet$) and nitrate anion (NO_3^-), (Nathan & Shiloh 2000). Both PHOX and iNOS are dependent on dioxygen and NADPH for their catalytic activities. Although independently regulated, they may function together and produce a range of intermediates or reactive chemical derivatives (Fang, 2004; Gaupp et al., 2012). The reaction between $NO\bullet$ and $O_2\bullet$ produces peroxyxynitrite anion ($ONOO^-$) and peroxyxynitrous acid ($ONOOH$), (Fang, 2004).

ROS are mainly produced in neutrophils whereas greater amount of RNS are found in macrophages (Nathan and Shiloh, 2000). Generic toxicity of the reactive products can target respiratory chain components, protein backbone (irreversible carbonylation and formation of aggregates; (Davies, 2005; Imlay, 2003), reduced organic cofactors ($FADH_2$, NADH), redox-active metabolites, such as thiols (Weber et al., 2004), metal centres (Fe-S clusters), or nucleic acids and cell membranes, which results in bacterial killing (Lushchak 2001; Keyer et al., 1995; Keyer & Imlay, 1996). Superoxide and hydrogen peroxide primarily oxidise the solvent-exposed iron-sulphur clusters (Fe-S) in proteins, leading to the inactivation of enzymes due to the release of Fe (e.g. isopropylmalate isomerase, 6-phosphogluconate dehydratase, fumarases A and B, aconitase, serine dehydratase), (Flint et al., 1993; Jang & Imlay, 2007; Imlay, 2008). Released Fe can further interact with hydrogen peroxide through Fenton chemistry mechanism and produce hydroxyl radical, which induces DNA damage. Like in the case of Fe, Cu and Zn can also be involved in generation of ROS (Baker et al., 2010; Grosseohme et al., 2011; Botella et al., 2011). Macrophages have been shown to increase the concentration of Cu in phagosomes using ATP7A-dependent copper transport (White et al., 2009; Shittisak et al., 2007) in response to infection, leading to the damage of Fe-S clusters via mismetalation, which disrupts Fe-homeostasis, and in turn leads to Fenton chemistry. It has also been shown that *S. aureus* cultured in human blood expressed increased levels of Cu export systems (Malachowa et al., 2011).

The excess metal may also affect the transcriptional regulators that control the oxidative stress response. Sensing and regulation of the staphylococcal response to oxidative stress is complex. Determination of transcriptional changes in response of *S. aureus* to oxidative stress induced by hydrogen peroxide revealed the induction of genes involved in virulence, DNA repair, and anaerobic metabolism (Chang et al., 2006). Proteomic analysis of *S. aureus* treated with different inducers of oxidative stress (methyl viologen, diamide and hydrogen peroxide) showed only limited overlap of the response to the three stimuli (Wolf et al., 2008; Fuchs et al., 2013), suggesting induction of different signalling and response pathways. Exposure to hydrogen peroxide resulted mostly in the increased expression of DNA protection and repair enzymes.

Treatment with diamide, a thiol specific oxidant, lead to accumulation of misfolded and aggregated proteins inside the cell, and affected systems involved in repair and degradation of proteins. Superoxide stress induced group of proteins responsible for various biological functions, such as proteins involved in signal transduction, biosynthesis of amino acids and cofactors; (Wolf et al., 2008; Fuchs et al., 2013).

Transcriptional regulators involved in the sensing of oxidative stress include: Fur, PerR, MgrA, SarZ, and SarA. The PerR is a transcriptional repressor that controls expression of the genes (*kata*, *ahpCF*, *trxB*, *mrgA*, *ftn*) involved in detoxification of ROS and repair mechanisms in *S. aureus* (Horsburgh et al., 2001a). Ferric uptake regulator (Fur) is a positive effector of *kata* transcription. The redox-responsive and metabolite-responsive regulators, such as Rex, CcpA, CodY, RpiR, are also involved in regulation of the oxidative stress response, as they react to changes in a central metabolism of the cell (Majcherczyk et al., 2010; Zhu et al., 2011; Seidl et al., 2009; Pagels et al., 2010).

In order to protect cells from metabolic damage and survive inside the phagosome, bacteria must effectively eliminate these highly reactive species (Clements & Foster, 1999; Figure 1.6). The main detoxification systems involve superoxide dismutase (SODs) enzymes, catalase (KatA; Horsburgh et al., 2001b), alkyl hydroperoxide reductase (AhpC; Cosgrove et al., 2007), flavohemoglobin (Hmp; Richardson et al., 2006), thioredoxin, thioredoxin reductase; (Ballal & Manna, 2009a).

SODs are responsible for detoxification of superoxide anion, producing hydrogen peroxide and oxygen. Peroxide, the reactive product of this reaction, is further converted through the action of catalases and peroxiredoxins to water and oxygen. *S. aureus* possess two SODs, SodA and SodM, that are essential for endogenous stress resistance (Clements et al., 1999; Valderas & Hart, 2001; Valderas et al., 2002) and contribute to *S. aureus* virulence (Karavolos et al., 2003). These enzymes will be discussed in detail in further sections of this chapter,

In the *Staphylococcus* genus, all species possess activity of catalase apart from *S. saccharolyticus* and *S. aureus* subspecies *anaerobius* (Sanz et al., 2000). The role of catalase in a direct influence on *S. aureus* virulence has not been conclusively demonstrated. In a murine skin abscess model of infection, *S. aureus* Δ *kata* strain showed no decrease in numbers of bacteria recovered from the lesion relative to WT (Horsburgh et al., 2001b). In addition to catalase, *S. aureus* possess several peroxiredoxins that are induced in a presence of hydrogen peroxide stress. Peroxiredoxins, such as Tpx, Ohr-like protein or AhpC, detoxify alkyl hydroxyperoxides to alcohols in a NADH- or NADPH-dependent manner (Wolf et al., 2008; Chen et al., 2009). In *S. aureus*, catalase activity accounts for most of the resistance against peroxide stress, whereas the alkyl hydroperoxide reductase possesses activity against lower levels of peroxide relative to catalase but responds to a broader spectrum of ROS (Wolf et al., 2008). Catalase and AhpC are both required for resistance to peroxide stress and nasal colonisation in *S. aureus* (Cosgrove et al., 2007).

Low-molecular-weight (LMW) thiols play an important protective role in either promoting the degradation of ROS and RNS, or in reversing oxidative and nitrosative protein damage. Bacillithiol (BSH) is a LMW thiol, analogous to glutathione in eukaryotes and other bacteria, which acts as cellular redox buffer, neutralising reactive oxygen and nitrogen species, and thus, together with thioredoxin system (thioredoxin/thioredoxin reductase) contribute to the fitness of *S. aureus* during infection (Posada et al., 2014). Thioredoxin's transcription is increased in response to various stressors, such as H₂O₂, diamide, copper toxicity (Wolf et al., 2008), (Baker et al., 2010).

Production of a carotenoid pigment, staphyloxanthin, has also been shown to play a protective role on bacterial cells, by enhancing resistance to phagocytosis and oxidative stress (Liu et al., 2005).

1.3. Nutritional immunity

During infection, the host utilises multiple strategies aiming to eliminate the invading pathogen, one of which is creating an environment devoid of available iron (Weinberg, 1978; Hammer & Skaar, 2011), manganese, and zinc (Corbin et al., 2008), in a process known as nutritional immunity. These essential transition metals determine a variety of bacterial processes, from growth to successful pathogenesis (Corbin et al., 2008; Waldron & Robinson, 2009). Limitation of these metals results in increased susceptibility of the pathogen to various stresses, such as superoxide generated by phagocytes in bacterial abscesses during oxidative burst (Kehl-Fie et al., 2011).

The majority of iron in mammals is associated with the tetrapyrrole ring of haem, and most of haem-iron is bound by haemoglobin. Compartmentalisation of iron represents the first physical barrier of nutritional immunity, limiting availability of Fe to bacteria. Additional host proteins, such as hemopexin and haptoglobin, are involved in complexing of haem and haemoglobin, during erythrocyte lysis, to prevent pathogen's access to haem-bound iron. The Fe-binding glycoproteins, lactoferrin and transferrin, provide another way of restricting pathogen's access to Fe, by sequestering any non-haem iron present in the serum.

Iron availability can be reduced by immune signals such as interferon-gamma, which on one hand activates macrophages but it also down-regulates the expression of the transferrin receptors, and therefore reduces iron availability for intracellular pathogens (Ryu et al., 2000). In addition, interleukin-6 increases the levels of hepcidin; a liver-secreted hormone controlling iron homeostasis; in serum during inflammation and infection (Nemeth et al., 2003; Nemeth et al., 2004). This contributes to a reduction in iron release from the major iron storage cells; enterocytes, hepatocytes and macrophages, and therefore further decreases serum iron levels available for invading bacteria (Vyoral & Petrák, 2005). This functional iron deficiency can lead to the condition called anaemia of chronic inflammation if the source of the inflammation persists and is not eliminated.

In addition to Fe, nutritional immunity enables the host to starve the invading pathogen of Mn and Zn. The Nramp proteins (natural resistance- associated macrophage proteins), which are expressed in mammalian macrophages and neutrophils, are important for controlling bacterial replication by trafficking metal ions between intracellular compartments (Soe-Lin et al., 2008; Cellier et al., 2007; Wessling-Resnick, 2015; Canonne-Hergaux, 2002). Professional phagocytes can recruit Nramp1 to the phagosome to pump the Mn (and Fe) out from the phagolysosomal space, so that pathogens cannot utilise this metal. Activated dendritic cells alter the expression of Zn importers (ZIP) and Zn exporters (ZnT), resulting in reduced cytoplasmic levels of zinc. ZIP8 is expressed by macrophages, dendritic cells, and T cells, and results in decreased lysosomal zinc concentrations (Kehl-Fie & Skaar, 2010).

In addition to using the efflux mechanism, phagocytes utilise the host protein called calprotectin, which effectively chelates Mn and Zn at the site of infection. Calprotectin is a heterodimer of the two Ca-binding EF-hand proteins, S100A8/S100A9 (Gagnon et al., 2015). It possesses two transition metal binding sites (Figure 1.7; S1, S2), both of which can bind Zn (Kehl-Fie et al., 2011) and Ni (Nakashige et al., 2017), but only one can bind Mn with nanomolar affinity (Kehl-Fie et al., 2011), and Fe with subpicomolar affinity (Nakashige et al., 2015). Calprotectin is produced in abundance by neutrophils; it may account for as much as 45% of total protein content of their cytosol (Yui et al., 2003). Efficient metal sequestration by calprotectin is achieved by the local concentration reaching 1 mg/ml within the abscess (Clohessy and Golden, 1995), (Yui et al., 2003), in contrast with 1 µg/ml concentration observed in a healthy human serum (Berntzen et al., 1991). Calprotectin has been shown to inhibit the growth of *S. aureus* by chelating Mn and Zn (Corbin et al., 2008; Damo et al., 2013). It has been proposed that calprotectin enhances the level of endogenous superoxide, and thus sensitivity of *S. aureus* to oxidative stress, through inhibition of manganese-dependent superoxide defence systems (Kehl-Fie et al., 2011). Inactivation of manganese-dependent superoxide dismutase by calprotectin thus increases susceptibility of *S. aureus* to neutrophil-mediated killing and reduces virulence in a systemic model of infection (Kehl-Fie et al., 2011).

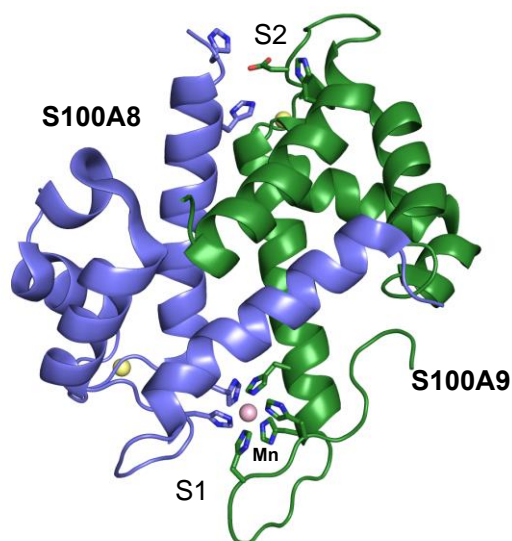


Figure 1.7 Crystal structure of Mn-bound calprotectin.

Ribbon representation of Mn-bound S100A8 (blue) and S100A9 (green) heterodimer. The Zn-specific (S2) and Mn/Zn (S1) binding sites are indicated. Ca ions are shown as yellow spheres, and the Mn ion is shown in purple. The binding site residues represented as sticks. Figure prepared using 4XJK crystal structure (Gagnon et al., 2015) with Pymol (Schrödinger, LLC).

1.3.1. Metal acquisition and homeostasis (“battle for metals”)

Despite the restricted access to micronutrients, *S. aureus* can succeed in establishing infection, often leading to life-threatening disease (Cassat & Skaar, 2011). This pathogen possesses the ability to sense the intracellular concentration of various transition metals and modulate expression of genes encoding metal acquisition systems, efflux pumps, and sequestration proteins, using metalloregulators belonging to ferric uptake regulator (FUR) (Masse & Gottesman, 2002), and diphtheria toxin regulator (DtxR) families (Merchant & Spatafora, 2014). The FURs encoded in the *S. aureus* genome include Fur (regulation of Fe uptake), PerR (regulation of Fe storage and antioxidant proteins) and Zur (Zn homeostasis); (Horsburgh et al., 2001; Horsburgh et al., 2001; Lindsay & S. J. Foster, 2001). *S. aureus* homologue of DtxR, MntR, controls Mn homeostasis (Horsburgh et al., 2002). Regulation of transition metal ion homeostasis plays an important role in acquiring cofactors for redox-active enzymes and avoiding accumulation of toxic levels of metals that could lead to generation of oxidative stress (Wakeman & Skaar, 2012).

The FUR regulators are homologues (share common ancestry) and utilise a similar regulatory mechanism which involves metal-induced conformational rearrangements, that affect the affinity to DNA (Masse & Gottesman, 2002). The Fur typically functions as an Fe-dependent transcriptional repressor, primarily governing transcription of Fe-acquisition systems in *S. aureus* (Horsburgh et al., 2001). Under Fe-replete conditions, Fur-Fe complex binds to a palindromic repeat, known as the Fur box, within the promoter/operator region of the regulated gene and inhibits the transcription of Fe uptake systems. In contrast, apo-Fur has low affinity for DNA and is displaced from the promoter during Fe-deficiency, allowing access by RNA polymerase and

initiation of transcription of Fe-uptake systems (Xiong et al., 2000). As mentioned earlier (section 1.2.2), the Fur positively regulates expression of catalase (Horsburgh et al., 2001), and controls the “iron-sparing response” by down-regulating iron-utilising enzymes during iron starvation. Fur also regulates its own expression (Friedman et al., 2006).

PerR acts as a Mn-, and Fe-dependent transcriptional repressor of the expression of genes involved in Fe storage (*ftn*, *mrgA*) and the oxidative stress response (*katA*, *ahpCF*, *trxB*, *bcp*; Horsburgh et al., 2001). PerR senses the environmental concentration of peroxide, and can regulate transcription of metal uptake and oxidative stress response genes, based on the relative abundance of Mn and Fe (Lee & Helmann, 2006). In the presence of Fe, the PerR regulon is derepressed. Moreover, PerR is auto-regulated and regulates the expression of Fur in a Mn-dependent manner (Horsburgh et al., 2001).

Regulation of Mn-uptake systems is governed by MntR and PerR in a Mn-dependent manner. In Mn-deplete conditions expression of the high affinity metal transporters is upregulated (Kehl-Fie et al., 2013). MntR acts as a bifunctional, Mn-dependent regulator, which can repress transcription of *mntABC* operon but it does not repress *mntH* transcription in Mn-replete conditions. Deletion of *mntR* leads to constitutive transcription of the *mntABC* irrespective of manganese levels. In contrast, *mntH* transcription is reduced in the absence of MntR (Horsburgh et al., 2002).

Similarly, the PerR-Mn complex also inhibits transcription of the *mntABC* operon (Horsburgh et al., 2001). Modulation of Fur by PerR occurs in Mn-dependent manner, highlighting the link between metalloregulators and peroxide sensing regulator, and the cross talk between metal homeostasis and the oxidative stress response, aiming to coordinate Fe accumulation with the endogenous production of peroxide and Mn supply, to control the capacity of Fe to act as a Fenton reaction catalyst (Horsburgh et al., 2001).

Zur is the third known FUR homologue that is encoded in *S. aureus* genome. Zur has been identified as putative Zn-dependent regulator of genes *znuC*, *znuB*, encoding the ATP-binding and membrane permease components of an ABC transporter, respectively, which confer putative high affinity Zn uptake (Lindsay & Foster, 2001; Robinson & Pohl, 2013).

1.3.1.2 Fe limitation and Fe acquisition

S. aureus senses the limited concentration of the environmental Fe, withheld by the host during infection, and in response it produces the high affinity Fe-specific chelators for the sequestration of Fe from serum (Morrissey et al., 2000), or modulates the expression of proteins responsible for the direct Fe acquisition from the iron-containing host proteins, haemoglobin and transferrin (Hammer & Skaar, 2011).

A major source for iron acquisition by *S. aureus* is by the secretion of siderophores. *S. aureus* can acquire Fe from host's transferrin or low affinity chelates in the serum by outcompeting their Fe binding affinity. The siderophores, staphyloferrin A and staphyloferrin B are

secreted from the bacterial cell to chelate Fe from the serum (Beasley et al., 2011; Beasley & Heinrichs, 2010). The Fe-staphyloferrin complexes are further bound by specific cell surface lipoprotein receptors and transported back inside the bacterial cell through the Sir (HtsABC and SirABC) and FhuC (ATPase) uptake system (Speziali et al., 2006; Beasley et al., 2011). Xenosiderophores (hydroxamate-type siderophores) produced by other microorganisms, as well as catecholamine, are alternative sources of Fe for the endogenously produced siderophores in *S. aureus* (Morrissey et al., 2000; Beasley et al., 2011). They are acquired by the means of specific uptake systems, FhuABC and SstABCD, respectively (Beasley et al., 2011; Mariotti et al., 2013). *S. aureus* lipoprotein Fhu (ferric-hydroxamate uptake) D2 was proposed to be promising component of a protein-based vaccine against *S. aureus* (Mariotti et al., 2013; Mishra et al., 2012).

S. aureus encodes a multicomponent system for the high affinity acquisition of Fe directly from haemoglobin, namely iron regulated surface determinant (Isd; Mazmanian et al., 2003; Skaar & Schneewind, 2004). Upon the pathogen's haemolysin-mediated damage of erythrocytes and subsequent haemoglobin degradation, haem is detected, captured by the cell-wall anchored proteins, and transported through the bacterial cell wall to the cytoplasm by a set of four membrane-localised permeases. While inside bacterial cell, haem is degraded by the monooxygenases, with a release of the Fe (Hammer & Skaar, 2011). Fe-acquisition from haem, by the Isd-complex has been suggested to play a role in the pathogenesis of *S. aureus*, and the haemoglobin receptor, IsdB, was shown to be essential for the full virulence of *S. aureus* and abscess formation, in renal model of infection (Cheng et al., 2009; Kim et al., 2010). However, contrasting results were observed in a sepsis model of systemic infection (Hurd et al., 2012). The IsdB has been targeted as potential vaccine antigen (Kuklin et al., 2006).

Due to reactive, redox nature of Fe, and its insolubility in physiological pH, the metal acquired by *S. aureus* is either instantly utilised as a cofactor for metalloproteins or is chelated and stored, bound by ferritin (FtnA), or the ferritin-like, DNA protection during starvation-like protein (MrgA). Transcription of the genes encoding the iron storage protein (*ftnA*), and Fe-chelator/DNA binding protein (*mrgA*) is regulated by the peroxide sensing protein (PerR) and Fur. It indicates the overlapping role of Fe homeostasis and the oxidative stress response systems (Morrissey et al., 2004), aiming to reduce formation of deleterious hydroxyl radical formed by Fenton chemistry.

1.3.1.3 Mn limitation and Mn acquisition

Unlike Fe, Mn is soluble in physiological pH and has a higher reduction potential (Jenkinson & Jakubovics, 2001). Therefore, it is less likely to cause deleterious redox reactions in the cytoplasm. It can, however, facilitate ROS detoxification in an enzymatic and non-enzymatic manner (Horsburgh et al., 2002). In the non-enzymatic reactions Mn can function as an antioxidant agent in form of a free metal or when complexed to lactate, maleate or

orthophosphate (Horsburgh et al., 2002). Mn plays a role in many physiological processes, including metabolism, catabolism, signal transduction, and oxidative stress response (Horsburgh et al., 2002; Yocum & Pecoraro, 1999).

During bacterial infection, the immune system of the host can reduce the concentration of Mn available to the pathogen by use Mn-specific chelator, calprotectin (section 1.3; (Yui et al., 2003; Corbin et al., 2008). To overcome the host-imposed limitations of this essential micronutrient, *S. aureus* expresses uptake systems, to supply Mn to the cell (Lisher, 2013). Currently, there are no known LMW chelators of Mn in *S. aureus*, such as the siderophores for Fe, and the physiological requirement for Mn seems to be managed mainly by the direct Mn uptake systems. There are two known transporters for Mn in *S. aureus*, encoded by *mntABC* and *mntH*. The MntABC consists of ATPase (MntA), membrane permease (MntB), and a solute-binding protein (MntC). The MntH is a proton-dependent Mn transporter, belonging to the natural resistance-associated macrophage protein (Nramp) family (Horsburgh et al., 2002; section 1.3). Regulation of these uptake systems is governed by MntR and PerR in Mn-dependent manner (Horsburgh et al., 2002).

The importance of MntABC for *S. aureus* physiology and pathogenicity has been presented upon treatment of bacterial culture with calprotectin. An increase in the expression of *S. aureus* Mn uptake systems (Kehl-Fie et al., 2013) has been observed in response to metal chelation by calprotectin. The strains devoid of *mntA* and *mntB* were more sensitive to calprotectin, than the wild type, indicating the importance of this metal uptake systems for the growth of *S. aureus* during the host induced metal starvation. The *mntA* and *mntH* deletion strains presented a decreased pathogenicity in infected mice, in comparison to the wild type strain (Horsburgh et al., 2001); and the *S. aureus* strains devoid of *mntA*, *mntH* or *mntR* had reduced survival in the *in vitro* human endothelial cell cultures (Ando et al., 2003). Furthermore, the manganese-binding protein (MntC) of MntABC system was used as a component of currently tested multi-antigen vaccine for the prevention of the *S. aureus* infections (Gribenko et al., 2013), (Begier et al., 2017). The significance of the MntABC during the infection may be due to its role in Mn-dependent resistance to oxidative stress, as the increased sensitivity to superoxide stress is observed upon disruption of elements of this system (Horsburgh et al., 2002; Kehl-Fie et al., 2013; Handke et al., 2013).

1.3.1.4 Zn limitation and Zn acquisition

Zn is a redox-inert metal, which acts as a Lewis acid catalyst and a structural component of numerous proteins. Zinc is utilised by enzymes involved in bacterial gene expression, general cellular metabolism, and as a cofactor of virulence factors. An estimated 5% of bacterial proteome is represented by zinc enzymes, further signifying an important role played by this metal (Andreini et al., 2006). Although zinc is not a redox metal, its intracellular concentration is

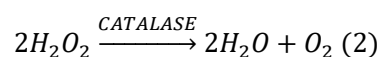
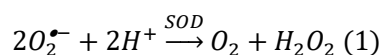
carefully regulated, as the excess of this highly competitive ion (Irving-Williams series Mn < Fe < Co < Ni < Cu > Zn; flexibility of proteins can influence steric selection between metals, and the relative affinities of metals for proteins depend greatly on ligand field stabilization energies of the metals; Irving & Williams, 1953; Johnson & Nelson, 1995), could potentially lead to preferential displacement of the cognate metal in the active site, and inactivation of the protein (zinc forms more stable complex than native Ni or Co in *Clostridium acetobutylicum* glyoxylase, G1x1 (Suttisansanee et al., 2011); zinc also replaces magnesium in β -galactosidase (Fernandes et al., 2002), tyrosine kinase (Sun & Budde, 1999), alkaline phosphatase (Hung & Chang, 2001)).

The complementary action of Zn sensors, which inhibit Zn uptake and activate efflux, respectively (Zur; (Lindsay & Foster, 2001), and CzrA (Pennella et al., 2006)), comprise the characterised Zn homeostasis system of *S. aureus*. Resistance to both zinc and cobalt is conferred by the chromosomally encoded zinc efflux *czrAB* operon (Kuroda et al., 1999), which encodes a metal-regulated transcriptional repressor (CzrA, also known as ZntR; (Singh et al., 1999)) and a cation diffusion facilitator, CDF antiporter (CzrB, also known as ZntA). Binding of Zn or Co to CzrA, alleviates repression of the transcription of *czrAB* operon and efflux of metals occurs through CzrB (Kuroda et al., 1999).

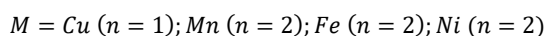
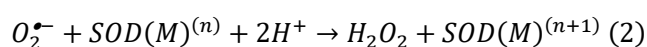
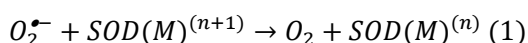
The Zur regulator controls a putative ABC-type Zn uptake system, that is encoded in the *S. aureus* genome, in the *mreAB zur* locus (*znuCBA*), (putative operon; Lindsay & Foster, 2001). The elements of this system, were identified through sequencing in *S. aureus*, based on homology to other Zn transporters. In the *in vitro* characterisation, *znuC* and *znuB* (*znuABC*) were suggested to be involved in high-affinity ion uptake. Zur was shown to repress expression of the entire operon in a Zn-dependent manner (Lindsay & Foster, 2001).

1.4. Superoxide dismutases (SODs)

Successful establishment of infection by pathogenic bacteria arises from their ability to overcome host-imposed limitation of essential nutrients (section 1.3), concomitant with capacity to withstand the innate immune response, such as the oxidative burst of phagocytes (section 1.2.2). Bacterial defence systems against superoxide and other reduced forms of oxygen comprise numerous mechanisms, including enzymatic activities such as superoxide dismutase, which detoxify the damaging reactive oxygen species. SODs catalyse disproportionation of superoxide anion, both the by-product of oxidative metabolism and the superoxide released by immune cells, to oxygen and hydrogen peroxide, which further (by the action of catalase) is decomposed to water and oxygen.



Superoxide is a small anion highly soluble in water, which in solution is tightly solvated by water molecules (Tachikawa, 2014; Martins-Costa et al., 2012). It is a strong, but selective oxidant, which predominantly targets Fe-S clusters, leading to the release of Fe from the complexes, with subsequent Fenton chemistry reactions (Imlay, 2006). The SODs possess the ability to interact (stabilise) and efficiently detoxify superoxide with a diffusion-limited rate by a proton-coupled electron transfer, with no requirement for external reductant supply (Sheng et al., 2014). They coordinate redox-active metals (Fe, Mn, Cu, Ni) in their active sites, which enable disproportionation of the two superoxide molecules, in a two-step 'ping-pong' reaction (Fielden et al., 1974), where the metal ion cycles between its oxidised and reduced state, with acquisition of one proton upon each superoxide molecule binding.



Equation 1.3 Superoxide dismutase reaction with superoxide anion.

1.4.1 Classification and properties of SODs

SODs are the front line defence systems for the detoxification of superoxide anion in aerobic organisms and in many anaerobes (Tally et al., 1977), across all domains of life (Sheng et al., 2014). They belong to an oxidoreductase class of enzymes (E.C. 1.15.1.1). Since the discovery of superoxide dismutase activities in the early 1970s (McCord & Fridovich, 1969; Keele et al., 1970; Yost & Fridovich, 1973), these important metalloenzymes were grouped based on the activating metal ion into three distinct families: proteins utilising either manganese (Mn) or iron (Fe) form the Mn/Fe SODs; proteins using Cu complexed with a structural Zn are known as Cu, Zn-SODs; and the third group is the Ni-SOD family of proteins employing Ni as cofactor (Hong-Duk et al., 1996).

Ni-, Cu-, and Mn/Fe-SODs are an example of functional convergence (Smith & Doolittle, 1992; Herbst et al., 2009), an independent evolution of ability to catalyse the same chemical reaction in non-homologous (not derived from the common ancestral protein) enzymes. Many organisms contain multiple forms of SODs, characterised by different expression profiles and cellular localisation. One of the best studied examples is the Gram-negative bacterium *Escherichia coli*, which contains three types of SODs: a constitutive Fe-SOD (SodB; Yost & Fridovich, 1973), a Mn-SOD (SodA; Keele et al., 1970), which is expressed in oxidative stress conditions, as well as a periplasmic Cu,Zn-SOD (SodC; Benov & Fridowich, 1994; Touati et al., 2000).

The Cu, Zn-SODs are generally homodimers (or dimers of dimers, but monomeric species are observed in the periplasm of some bacteria, such as *Salmonella Typhi*), where each monomer presents an immunoglobulin-like fold, known as a "Greek key" β -barrel (Figure 1.8 C).

The Cu and Zn ions are bound on the outside of the barrel by two loops, including a short helix. They localise to the eukaryotic cytosol (McCord & Fridovich, 1969), but also to the mitochondrial intermembrane space and nuclei, chloroplasts and peroxisomes, and the periplasm of some bacteria (Imlay & Imlay, 1996), and may also be secreted in the extracellular matrix in mammals and plants.

The Ni-SODs are homohexamers (or dimers of trimers) of four-helix bundles. Each four-helix bundle binds a Ni ion at the N-terminus, with a distinctive Ni-hook motif (Figure 1.8 D). They are the least characterised group of SODs, with representatives found in cytosol of *Streptomyces* and cyanobacteria (Barondeau et al., 2004), as well as a few green algae (Dupont et al., 2008).

The most common type of SOD, the Fe/Mn-SOD, is nearly ubiquitous being used by organisms belonging to all three kingdoms of life (Kirschvink et al., 2000), where it is found in the cytosolic fraction and in mitochondria, chloroplasts or peroxisomes (Sheng et al., 2014). Though unrelated to the two other families of SODs, all Mn- and Fe-dependent SODs are evolutionarily related to each other: they belong to a single protein superfamily (the Fe/Mn superoxide dismutase superfamily, SCOP accession 46609). Structurally, this family is highly homologous, sharing a substantial degree of similarity from primary to tertiary structure (Figure 1.8 A, B).

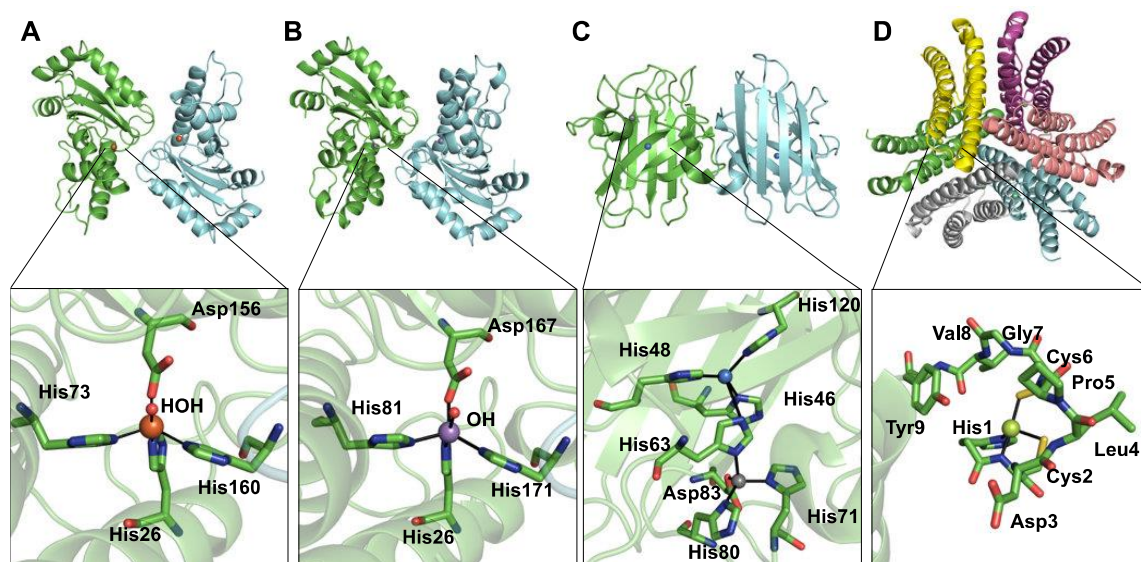


Figure 1.8 Structural models of the representatives of Fe/Mn-SOD, CuZn-SOD and Ni-SOD.

A comparison of the crystal structures (top panel) and the active sites (bottom panel) of (A) *E. coli* Fe-SOD (1ISB; (Lah et al., 1995)), (B) *E. coli* Mn-SOD (1VEV; Edwards et al., 1998)), (C) human Cu,Zn-SOD (1PU0; (DiDonato et al., 2003)), (D) *Streptomyces coelicolor* Ni-SOD (1T6U; (Barondeau et al., 2004)). Structural models coloured by polypeptide chain. The ligand residues represented as sticks, solvent ligand represented as red sphere. Coordinated metal ions represented as spheres, coloured orange (Fe), purple (Mn), blue (Cu), grey (Zn), and green (Ni). Figure produced with Pymol (Schrödinger, LLC).

1.4.2 Evolution of bacterial Fe-dependent and Mn-dependent specificity of SODs

The Fe/Mn-SODs can non-selectively bind both Fe and Mn cofactors, however, in most cases they present high specificity towards one of the metals, and the metal substitution usually results in loss of the catalytic activity (Ose & Fridovich, 1979; Kirby et al, 1980; Beyer & Fridovich, 1991). However, some members of the Mn/Fe-SOD family are catalytically active with either Mn or Fe, in the standard *in vitro* assay conditions. This group of SOD proteins is known as cambialistic enzymes, from Latin *cambium*, “exchange” or “change” (Meier et al., 1982; Gregory, 1985; Martin et al., 1986; Amano et al., 1990; Matsumoto et al., 1991; Yamano et al., 1999; Tabares et al., 2003; Lancaster et al., 2004; De Vendittis et al., 2012; Mandelli & Cairo, 2013). The truly cambialistic enzymes, i.e. exhibiting equal functionality with the two metal cofactors, are usually characterised as less active than the metal specific isoforms. The degree or the ability of an enzyme to exhibit cambialistic properties seem to differ among SODs. Some SODs are truly cambialistic, displaying approximately equal activity regardless of the bound cofactor (Gregory, 1985; Martin et al., 1986; Amano et al., 1990; Matsumoto et al., 1991), whereas others are only partially cambialistic, displaying far greater activity with one cofactor than with the other (Martin et al., 1986; Matsumoto et al., 1991; Sheng et al., 2014). To this date, only a few cambialistic enzymes have been isolated in both metal forms from their native organisms (Meier et al., 1982; Martin et al., 1986; Amano et al., 1990; Matsumoto et al., 1991). Even though the cambialistic variants of SODs present lower levels of catalytic activity they could provide a physiological advantage for organisms occupying specific habitats (i.e. limited availability of metals, anaerobic, extreme temperature, osmolarity conditions).

The early analyses of SOD protein sequences provided data suggesting that, metal-specificity of SODs can be predicted based on the primary structure of these enzymes. Numerous attempts have been made to identify and assign the sequential determinants of metal specificity within Mn/Fe-SOD superfamily (Parker & Blake, 1988; Kwasigroch et al., 2008; Sheng et al., 2014; Wintjens et al., 2004; Clements et al., 1999; Yamano & Maruyama, 1999; Wintjens et al., 2008). However, there are no comprehensive algorithms to accurately predict metal-specificity or cambialism based only on the amino acid sequence, and thus experimental determination or verification of bioinformatics predictions is necessary.

Cambialism was proposed to be a possible ancestral trait of SODs, based on the bioavailability of Fe and Mn predicted in the early low-oxygen atmosphere of the Earth (Kirschvink et al., 2000). The modern Fe/Mn SOD family members seem to have a range of metal specificities, with the Fe-specific SODs widely distributed between the species of all domains of life, and Mn-specific variants that were characterised mostly for Bacteria and Eukaryota (Kirschvink et al., 2000). Relatively high degree of similarity between Fe-SODs and Mn-SODs was suggested to reflect the common ancestry of the two groups (Wolfe-Simon et al., 2005; Fink & Scandalios, 2002; Miller, 2012). Often, multiple copies of enzymes with different metal-

specificities are expressed by a single cell, and can localise to different cellular compartments, e.g. chloroplasts and mitochondria of plants, indicating possible spatial determinants of intracellular metal availabilities, or possibly be due to a different origin of the enzymes (in this example an endosymbiotic origin of chloroplasts and mitochondria). On the other hand, SODs with different metal specificities can be also found in the same cellular compartment, which could suggest that they have evolved to adapt to variable metal availabilities in the environment or to the growth at the specific environmental conditions (e.g. aerobic and anaerobic; Hassan & Fridovich, 1977).

1.4.3 Structure of Fe/Mn SOD enzymes

Almost half of SOD crystal structures deposited in PDB database are for the proteins of Mn/Fe-SOD family (<http://www.ebi.ac.uk>; database 09-2017). The Mn-specific, Fe-specific, and cambialistic proteins belonging to Fe/Mn-SOD family share high level of similarity from a primary to a quaternary structure (Sheng et al., 2014). Coordination of both Fe and Mn in the mononuclear active site is conferred by the same ligands: three histidine residues, one aspartate and a solvent molecule; in distorted trigonal bipyramidal geometry. The characteristic two-domain fold (N-terminal α -helical domain and α/β -C-terminal domain, Figure 1.9), that these protein share encloses the active site at the hydrophobic interface between the two domains of each monomer. The active site is stabilised by a core of conserved hydrophobic amino acids, that potentially protect the active site from the radical-mediated damage or mis-metalation. The N-terminal domain mediates contact between the two subunits, leading to multimerisation (dimers or tetramers are characteristic assemblies in this family of proteins, Lah et al., 1995; Edwards et al., 1998; Ludwig et al., 1991).

The oligomeric assemblies also share a conserved dimer interface interactions, which is partially involved in formation of symmetry-related funnels, providing substrate access to the active site (Ludwig et al., 1991; Lah et al., 1995; Whittaker et al., 2006).

The superoxide anion is guided to the active site of these enzymes by the attraction with positively charged residues located on the surface of each monomer of these proteins, creating the mouth of the substrate access funnel. The superoxide reaches the active site through a narrow channel entrance to the metal-coordination sphere (the active site; Ludwig et al., 1991; Lah et al., 1995). In the example of *E. coli* Mn-SOD enzyme, the entries to the active sites are gated by some of the residues of the dimer interface: His30, Tyr34, His171, Trp169, Glu170', Arg181' (Ludwig et al., 1991; Lah et al., 1995). As proposed by Whittaker & Whittaker, 2008, His30 and Tyr34 form 'substrate gateway' which is thought to restrict access to the active site metal ion in *E. coli* MnSOD (PDB ID 1VEW; Edwards et al., 1998), conferring substrate selectivity and possibly facilitating proton transfer steps in the redox turnover mechanism.

The active site of Mn/Fe-SOD is involved in formation of a hydrogen bond network that extends from the metal bound solvent molecule, and engages interaction with the residues of the outer coordination sphere. Using the structures of a well-studied *E. coli* MnSOD and FeSOD

(PDB IDs: 1VEW, and 1ISB, respectively), as an example, the solvent ligand in the active site of these enzymes is directly connected by a hydrogen bond with Gln (structurally conserved residue Gln146 in *E. coli* MnSOD (PDB ID 1VEW; Edwards et al., 1998), and Gln69 in *E. coli* FeSOD (PDB ID 1ISB; Lah et al., 1995), from the outer sphere, which further connects the active site in interaction with Tyr34, Trp122, Asn72, as well as via another solvent molecule with His30 and Tyr174' from the other subunit of *E. coli* MnSOD. The interaction of the two active sites of *E. coli* MnSOD is also mediated by hydrogen bonding between ligand His171 and residue Glu171' (Whittaker & Whittaker, 1998). The hydrogen bond network interactions between metal cofactor and outer sphere amino acids has been suggested to support proton transfer in catalysis (Miller et al., 2003; Whittaker & Whittaker, 1997) and to be important in determining metal specificity (Grove et al., 2008).

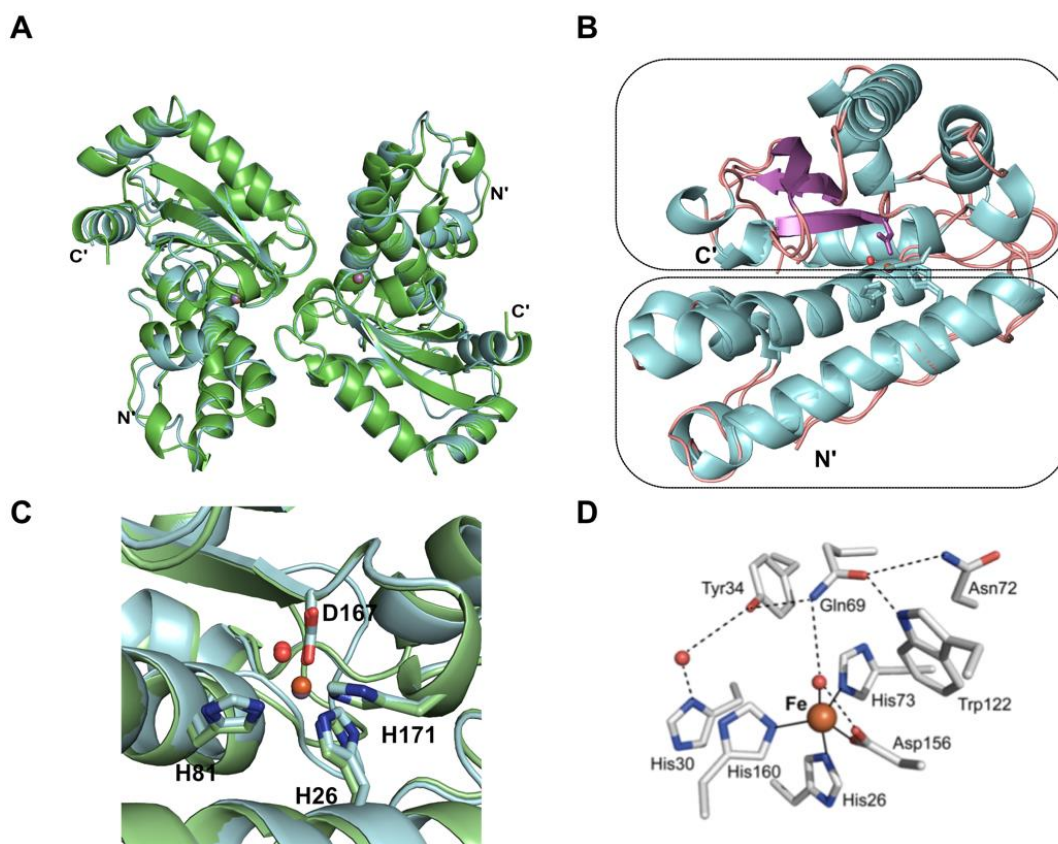


Figure 1.9 Manganese and iron superoxide dismutases of *E. coli*.

(A) A superimposed cartoon representation of dimers of MnSOD (green; PDB ID 1VEW; Edwards et al., 1998) and FeSOD (cyan, PDB ID 1ISB; Lah et al., 1995) of *Escherichia coli*, with Mn and Fe represented as purple and orange spheres, respectively. (B) A view of the monomer, coloured by secondary structure component (helix: cyan; sheet: purple; loop: salmon), depicting coordination of the metal ion in the active site, by residues from N-terminal domain and C-terminal domain, and solvent molecule represented as a red sphere. (C) Active site view of superimposed Mn-SOD (green) and Fe-SOD (cyan) *E. coli* structures, showing a trigonal bipyramidal coordination of Mn (purple sphere) by as labelled: His26, His81, His171 and Asp167 and Fe (orange sphere) coordinated by the equivalent residues: His26, His73, His160, Asp156 residues (depicted but not labelled). (D) Hydrogen bond (black dashed line) network surrounding the active site of *E. coli* FeSOD.

1.4.4 Proposed molecular mechanism of catalysis by MnSOD and FeSOD

The disproportionation of superoxide, that is catalysed by SODs, involves both oxidation and reduction of this substrate, concomitant with the cycling of the redox-active metal cofactors between the Mn^{2+}/Fe^{2+} and Mn^{3+}/Fe^{3+} oxidation states (Equation 1.3; “ping-pong” reaction; Fielden et al., 1974). The conserved solvent ligand, which is involved in proton transfer during dismutation in Fe/MnSODs, is proposed to be OH^- in the oxidised Mn^{3+}/Fe^{3+} (resting) state and H_2O in the reduced Mn^{2+}/Fe^{2+} state of the enzyme (Stallings et al., 1991).

In FeSOD from *E. coli* substrate is proposed to coordinate directly to Fe^{3+} , and form a six-coordinate intermediate (inner sphere binding was experimentally presented for a range of small anions, such as azide, fluoride and hydroxide; that alter coordination geometry to a distorted octahedral) in the first part of dismutation reaction. The reduction of metal ion to Fe^{2+} occurs upon superoxide anion binding to Fe^{3+} , in conjunction with uptake of proton by OH^- , and release of the oxygen (Stallings et al., 1991). The second part of the dismutation reaction and release of hydrogen peroxide product, was proposed not to occur via direct binding of superoxide anion to the reduced Fe^{2+} , but further away from the metal centre, in the alternate anion-binding site in the active site, possibly at the base of the funnel (outer sphere binding, Tyr34; the coordination of metal by 5-6-5 ligands mechanism, Lah et al., 1995). This outer sphere binding mechanism is postulated to prevent the occurrence of Fenton reaction of Fe^{2+} catalyst, and damage of the enzyme.

The irreversible inactivation of Fe(II)-SOD enzyme may occur via reaction of Fe^{2+} with the product of dismutation reaction, hydrogen peroxide (peroxidative reaction; type of Fenton reaction). The production of hydroxyl radical can further cause the loss of Fe, oxidation of the Trp residues (damaging protein core), and oxidation of Cys, and His residues. In the standard SOD assays, peroxide inhibition is treated as an indicator of Fe-specific activity, as the MnSODs does not seem to undergo the inhibition by peroxide (Sheng et al., 2014).

The MnSOD catalysis has been shown *in vitro* to be dependent on the concentration of available substrate, with an increased product inhibition at higher concentration of substrate. When a concentration of substrate exceeds a concentration of enzyme *in vitro*, the disproportionation occurs via two-stages: first-order (fast step; ‘outer sphere’), and a zero-order (slow step; ‘inner sphere’; formation of product-inhibited, Mn-peroxo complex). The ratio of the fast-to-slow reactions, namely “gating”, describes the level of product inhibition. The rate of catalysis by the human mitochondrial MnSOD is strongly limited in a high concentration of the superoxide (Hsu et al., 1996), while the yeast MnSODs are highly efficient in catalysis (Sheng et al., 2011).

The variable-temperature spectroscopy studies of MnSOD active site suggested temperature-dependent coordination geometry (analogous to the 5-6-5 mechanism; Lah et al., 1995). The mechanism of the ‘associative displacement’ has been proposed, by which the low-temperature structure (below physiological) favours binding of the anion (azide, fluoride) as a

sixth ligand in a (trapped) distorted octahedral geometry, however, physiological (or room) temperature promotes expansion of the coordinating ligands to trigonal bipyramidal geometry (Whittaker & Whittaker, 1996). In this mechanism, the inactive inhibitor-bound enzyme is six-coordinated, while the active form remains five-coordinated, with substrate binding causing the displacement of one of the manganese ligands. It was suggested that this flexibility of the coordination (reversible isomerisation) may have a physiological relevance for catalysis (Whittaker & Whittaker, 1996). Further studies shown that azide-adduct to active site of Mn³⁺SOD in physiological temperature can interact with either the Mn³⁺ or the outer sphere residue Tyr34 (Jackson et al., 2004). The role of interaction with outer sphere residue Tyr34 was suggested to play important role in the protonation during catalysis (Sheng et al., 2012).

1.4.5. Metal selectivity and metal specificity of Mn/Fe-SODs; electronic structure and 'redox tuning' model of metal specificity

The high level of conservation of the active site ligands in Mn/Fe-SOD family provides a stable frame for accommodation of redox-active metal cofactor. The interactions of the ligands with the residues from the outer sphere through the network of hydrogen bonds, are crucial for efficient catalysis by the Mn/Fe-SODs.

Binding of the redox-active metal cofactor in the active site was shown to be essential for conferring activity of SODs. The *E. coli* Mn-SOD metal binding selectivity was demonstrated to be dependent on the availability of metals in growth medium (Beyer and Fridovich, 1991). However, only binding of the cognate Mn was a condition for catalytic activity of the enzyme.

Mechanism of acquisition of metals by apo-SODs of *E. coli* was proposed to be based on an interdependence of metal uptake pathways and the structural features of the protein. A proposed model of post-translational metal uptake by the dimeric *E. coli* apo-MnSOD, was involving thermal activation leading to a conformational reorganisation ('gating'; transition between closed and opened conformation of domains, enclosing the active site), required for metal uptake (Whittaker & Whittaker, 2008), (M. M. Whittaker et al., 2011). Acquisition of the metal cofactor into protein structure *in vitro* was demonstrated to occur through subunit exchange (dimer dissociation), with the concomitant metal binding by the two subunits (J. W. Whittaker, 2003).

Electrochemistry of metal ions sets the limits of catalytic properties of the protein. However, a protein can utilise properties of ligands coordinating the metal, and the interactions within the second and even further sphere of residues, to modulate the cofactor's reduction potential and facilitate catalysis. The disproportionation of superoxide that is catalysed by SODs involves both oxidation and reduction of this substrate (Fielden et al., 1974). The standard reduction potentials of these two reactions are -0.180 V and +0.910 V, respectively (Sheng et al., 2014). In order to facilitate both these steps, and achieve the theoretical optimal turnover, the

enzymes should have a reduction potential near the average for the two reactions, e.g. ~ 0.360 V vs. normal hydrogen electrode (NHE). If the metal site had too low reduction potential, it would only be able to effectively reduce superoxide, and conversely, one with too high reduction potential could only extract the electrons from the substrate but would not be able to reduce the next molecule. The intrinsic E^0 of aqueous complexes (Table 1.1) of hexaaquo-Mn is over two-fold higher (1.510 V vs. NHE) than that of the hexaaquo-Fe (0.770 V vs. NHE), which implies that for the thermodynamically efficient (~ 0.360 V vs. NHE) catalysis, Mn-SOD needs to depress the potential of its metal to a much higher extent than Fe-specific SOD would need to accomplish for its Fe cofactor. The evaluated potentials of the *E. coli* Mn-specific SOD and Fe-specific SOD (Table 1.1) fit within the theoretical, appropriate intermediate range, ~ 0.3 V and 0.2 V, respectively (Miller, 2012); Figure 1.10).

Property/ ligand	Mn	Fe
Ionic radius of 3+ state, (pm)	78.5	78.5
Ionic radius of 2+ state, (pm)	97	92
E^0 of aqueous complex, (V vs NHE*)	1.510	0.770
Fe-SOD, (V vs NHE*)	>0.900	0.220
Mn-SOD, (V vs NHE*)	0.290	-0.240

Table 1.1 Ionic radii and midpoint potentials of 3+/2+ couples of Mn and Fe complexes (Sheng et al., 2014).

*NHE, normal hydrogen electrode.

The model presented by Miller (Miller, 2012; Figure 1.10) proposed that the catalytic inactivity due to swapping of metal cofactors (metal-substituted proteins) would have arisen from too low potential of Fe-reconstituted Mn-SOD and too high potential of Mn-reconstituted Fe-SOD. The determined potentials for these mis-metalated proteins fit in with the model, as they observed that they were at approximately -0.240 V and over 0.900 V, respectively (Vance & Miller, 1998; Yikilmaz et al., 2006; Miller, 2012). According to this model, the cambialistic enzymes would have evolved to be able to accommodate different interactions with the two metals, applying minimal changes to the overall structure of the protein (as they are very similar in the structure to metal specific variants). Their reduction potentials are predicted to fall in between the two of the metal-specific SODs. How the proteins sharing similar structural architecture can modulate redox potential is not clear.

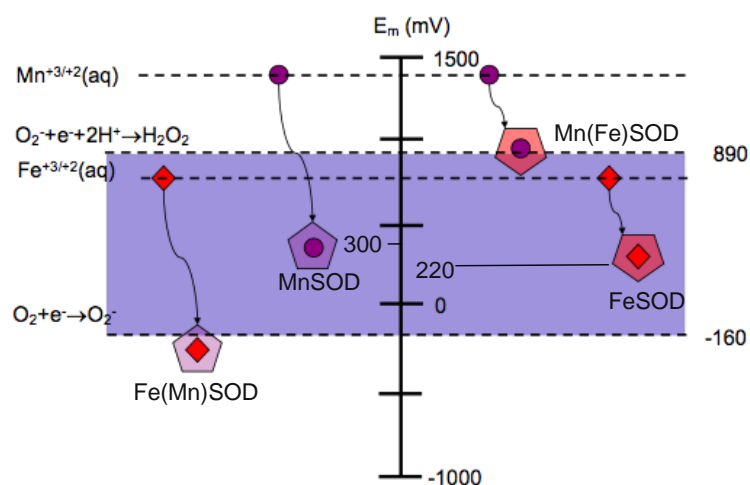


Figure 1.10 Model of redox potential tuning (Miller, 2012).

Reduction potentials of native (MnSOD, FeSOD) and metal-substituted (Fe-substituted MnSOD, Fe(Mn)SOD; and Mn-substituted FeSOD, Mn(Fe)SOD)). Mn represented as purple circle, and Fe represented as red rhombus.

1.4.6. Structure-based *in vitro* mutational analyses of Fe/Mn-SODs

Investigation of the importance of various structural elements of Mn/Fe-SODs by the means of mutagenesis studies *in vitro* provided information on the effects of the tested structural changes onto protein specific activity and catalysis. The conservation or similarity of certain residues in protein sequence and structure has been suggested to play a role in determining metal specificity, such as the Gln146 or Gly165 in Mn-specific enzymes vs. Ala146 and Thr165 in Fe-specific SOD (numbering based on *E. coli* Mn-SOD, 1VEW). The Gln146 is the only residue that directly interacts with a solvent molecule ligand, which implies its potential role in mediating proton-coupled electron transfer. In Mn/Fe-SODs, the pK_a of the water ligand is likely to be controlled by ligand residue Asp167 and Gln146 to which it respectively donates and accepts a hydrogen-bond. The role of Gln146 hydrogen-bonding water ligand had been presented as important determinant of Mn-specificity in *E. coli* and human SODs (Yikilmaz et al., 2007; Yikilmaz et al., 2002; Edwards et al., 2001a); (Schwartz et al., 2000); (Lévêque et al., 2000); (Miller, 2008); (Miller & Wang, 2017). The mutation of Gln146 to Leu, His, Ala, or Gly were demonstrated to cause a substantial decrease of catalytic activity of the *E. coli* MnSOD protein, relative to the wild-type enzyme (complete loss of activity was noted upon replacement of Gly with Glu). The structural change upon mutation of the Gln146 in *E. coli* MnSOD was demonstrated to alter the positioning of Tyr34 and Trp126 residues, and disrupts the hydrogen-bond network of the active site. Similar effect has been demonstrated in human MnSOD, where the mutation of Trp126 to Phe changed catalytic activity by modulating positions of the residues involved in hydrogen bond network (Greenleaf et al., 2004).

A His30-Tyr174 pair is involved in the hydrogen-bonding network, with His residue contributing to both, the dimer interface and the entrance of the active site channel in MnSOD of

E. coli, was also demonstrated to be important for catalytic activity. Upon mutation of His30 to Ala, the enzyme presented decrease in activity, relative to the wild-type. The Tyr174Phe mutation had a similar effect on the catalytic activity (decrease of Mn-specific activity and fractional increase of activity with Fe), however, it had more pronounced effect on the alteration of the local structure, and change to the hydrogen bond network (Edwardset al., 2001b).

The importance of the presence of Thr at position 165 for the Fe-specific activity of SODs was demonstrated experimentally. A mutation changing Gly165 to Thr in *E. coli* was shown not alter Mn-specific activity, but it significantly increased activity of protein loaded with Fe, relative to the MnSOD wild type (Osawa et al., 2010). The equivalent mutation in a cambialistic enzyme from *P. gingivalis* caused a similarly significant decrease in Mn-specific activity, accompanied by a 2-fold increase of Fe-specific activity of this protein (Yamakura et al., 2003). Based on the comparison of crystal structures of wild type and mutant variants of *PgSOD*, introduction of Thr in place of Gly165 influenced the position of the two Trp residues that surround the active site (Yamakura et al., 2003), and therefore, has been proposed to alter the hydrogen bonding network around the active site and in consequence metal-specific activity.

The mutagenesis studies confirmed that His165-Glu170' (Whittaker & Whittaker, 1998) and His30–Tyr174' (Edwards et al., 2001b; Hearn et al., 2004) bonds were essential for retaining the dimeric structure and metal-specific activity of SODs.

1.4.7. *S. aureus* SODs

The genomes of all strains of *Staphylococcus aureus* possesses two monocistronic superoxide dismutase genes, *sodA* and *sodM* (Poyart et al., 1995), (Clements et al., 1999; Valderas & Hart, 2001), which encode putative Fe/Mn-dependent SOD enzymes. The coagulase-negative staphylococci genomes lack *sodM* homologue (Valderas et al., 2002).

Transcription of both *sodA* and *sodM* was shown to initiate from the σ^A -type promoters, and increased levels of transcripts (significantly more *sodM*) were observed in a σ^B -deficient strain (Karavolos et al., 2003). Expression of *sodA* is constitutive, and confers the major source of catalytic activity, independent of the growth phase of staphylococci (Clements et al., 1999; Valderas & Hart, 2001; Karavolos et al., 2003). The transcription and activity of both SODs is induced by oxidative stress in the *S. aureus* growth environment; specifically, *sodA* was shown to be induced by internal stressors and *sodM* by exogenous. Both *sodA* and *sodM* are important to oxidative stress resistance in *S. aureus* (Clements et al., 1999; Valderas and Hart, 2001; Karavolos et al., 2003). As the *sodM* gene is only present in the *S. aureus* lineage and is absent from non-pathogenic staphylococci (Valderas et al., 2002), it could imply its crucial role in this significant mammalian pathogen.

Based on initial studies and sequence analysis, both *S. aureus* SODs were predicted to be Mn-dependent enzymes *in vivo* (Clements et al., 1999; Valderas & Hart, 2001), but the evidence presented in the literature is inconsistent. The relative resistance of SodM proteins to

hydrogen peroxide, an Fe-specific inhibitor, differed between studies, indicating potential Fe-binding by SodM (Valderas & Hart, 2001), (Clements et al., 1999). Metal depletion of *S. aureus* protein extracts, followed by reconstitution with Mn *in vitro*, led to detection of activity from SodA but not SodM, whereas neither activity could be restored with Fe reconstitution (Clements et al., 1999). Addition of Mn to the growth medium of *S. aureus* SH1000 cells led to an increase in SodA activity but a decrease in SodM activity (Karavolos et al., 2003). The addition of Mn to the growth medium of the SH1000 Δ sodM mutant led to an increase in total SOD activity (i.e. from SodA), whereas addition of Mn to the medium of the SH1000 Δ sodA mutant led to decreased total SOD activity (i.e. from SodM), (Karavolos et al., 2003).

The two superoxide dismutases of *S. aureus* were demonstrated to play a significant role in pathogenicity of this pathogenic bacteria. Both the *sodA* and *sodM* genes are transcriptionally regulated by the staphylococcal accessory regulator, SarA (Ballal & Manna, 2009b). Increased expression of SodA and SodM protein was detected in *S. aureus* cells after internalisation by human lung epithelial cells and human monocyte cell line, respectively (Figure 1.11), (Kristin Surmann, 2014; Mäder et al., 2016). Infection of mice with *S. aureus* strains devoid of *sodA* or *sodM* (or both) was shown to result in a decrease of bacteria recovered from lesions, relative to the wild type strain, in a skin model of infection or in a systemic mouse model (Karavolos et al., 2003; Kehl-Fie et al., 2011).

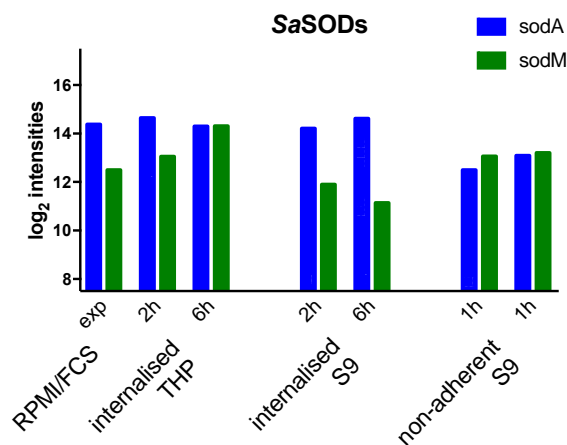


Figure 1.11 The quantile-normalized data of *sodA* and *sodM* expression profiles of *S. aureus* HG001.

The *sodA* (SAOUHSC_01695) and *sodM* (SAOUHSC_00093) expression data were extracted from a comprehensive analysis of the condition-dependent transcriptome profiles of *S. aureus* HG001 (Mäder et al., 2016). Cell culture infection experiments were performed with the human bronchial epithelial cell line S9 and the human monocyte cell line THP-1. Bacteria internalised by eukaryotic host cells were isolated from samples taken 2 hours and 6 hours (internalised THP, internalised S9) post infection. The following additional samples were taken: i) non-adherent bacteria at multiplicity of infection (MOI) of 25 or 50 retrieved from the supernatant of S9 cells after 1 hour of infection (non-adherent S9); ii) bacteria grown in RPMI medium with foetal calf serum (FCS) (RPMI/FCS), the pre-culture condition for the THP experiments. Data taken from (Mäder et al., 2016).

The importance of the SODs in *S. aureus* pathogenicity was emphasised by their apparent role in the nutritional immunity and neutrophil-mediated killing of the *S. aureus* (Kehl-Fie

et al., 2011). The mechanism of the growth inhibition of *S. aureus* in these conditions has been proposed to be caused by an action of host protein calprotectin, which chelates Mn and Zn at the site of infection (Corbin et al., 2008). Manganese starvation was shown to induce pronounced growth phenotype in *S. aureus* indicating an essential role of this micronutrient for a pathogen during infection (Corbin et al., 2008). Host-imposed Mn starvation mediated by CP was shown to reduce total staphylococcal SOD activity, both in culture and during infection, which renders *S. aureus* more sensitive to oxidative stress and the action of phagocytic immune cells (Kehl-Fie et al., 2011; Kehl-Fie et al., 2013; Damo et al., 2013). As the loss of both SodA and SodM in *S. aureus* resulted in the increased sensitivity of bacteria to Mn-sequestration by calprotectin it was proposed that SODs may contribute to the ability of *S. aureus* to resist metal starvation, potentially by being able to relay on the alternative metal cofactors when starved of manganese (Kehl-Fie et al., 2011).

1.5. Aims and objectives of the thesis

Research hypothesis

S. aureus SodM can function with Fe during Mn-starvation, to provide a mechanism for resisting the host imposed Mn-restriction during infection.

Research aims

The main goal of this study was to determine the metal requirements of the two *S. aureus* SODs belonging to Mn/Fe-SD family, and to characterise the role of these enzymes in the *S. aureus* ROS response. To achieve this goal, the following aims were set:

1. Production of recombinant proteins, followed by preparation of pure Fe- and Mn-loaded isoforms of the proteins, to quantitatively test their activities *in vitro*.
2. Determination of the crystal structures of all four form, and targeted mutagenesis to identify potential determinants of metal selectivity.
3. The *in vivo* characterisation of the role of SODs in bacterial culture of the wild type, $\Delta sodA$, $\Delta sodM$ and $\Delta sodA\Delta sodM$ strains under a range of stressed and control growth conditions.
4. Direct purification of SODs from *S. aureus* to determine metal usage in the native host and to subsequently determine the contribution of the SODs to the survival and infectivity of *S. aureus*.

Research objectives

To achieve the aims of this work, the following objectives were planned:

I. Preparation and initial characterisation of the SOD proteins *in vitro*.

1. Cloning of the *sodA* and *sodM* genes for heterologous expression and preparation of purified proteins from *E. coli*.
2. Determination of metal content of as-purified from *E. coli* using inductively-coupled plasma mass spectrometric elemental analysis.
3. Preparation of pure Fe- and Mn- loaded versions of proteins through *in vitro* unfolding/refolding protocols.

II. Structural and functional characterisation of metalated recombinant protein forms.

1. Determination of the activity of all four metalloprotein isoforms *in vitro*.
2. Determination of the crystal structure of all four forms by X-ray crystallography, followed by the structure-to-function analyses through site-directed mutagenesis, and determination of changes in metal specificity and activity of protein isoforms.

III. Determination of biophysical properties of recombinant proteins.

1. Investigation of the protein and/or metal specific features using combination of spectroscopic methods (CD, UV-vis, HF-EPR).

IV. Metal usage by the proteins purified directly from *S. aureus*.

1. Investigation of cofactor usage by the SODs in *S. aureus* using chromatographic separation of cell extracts and inductively-coupled plasma mass spectrometric elemental analysis.

2. Direct purification of proteins from *Staphylococcus aureus* using affinity-tagged proteins.

IV. Role SODs in an oxidative stress defence and their relationship with metal starvation.

1. Creation of strains and phenotyping.

2. Using neutrophil-derived protein calprotectin to study the manganese-starvation phenotypes in bacterial culture and determine the role and contribution of both proteins to infectivity of *S. aureus* in animal model of infection (*collaborative work*).

Chapter 2. Materials and methods

2.1. Bacterial strains and maintenance

Bacterial strains used in this study are listed in Table 2.1. Strains were stored at -80°C in a rich growth medium containing 25% (v/v) sterile glycerol, in 2 ml cryotubes. To recover bacteria for experimental manipulation, the frozen glycerol stock was used to inoculate an agar plate containing the appropriate antibiotics. The plate was incubated overnight at 37°C.

Strain	Genotype	Reference/ Source
<i>Escherichia coli</i>		
DH5 α	<i>fhuA2 lac(del)U169 phoA glnV44 Φ80' lacZ(del)M15 gyrA96 recA1 relA1 endA1 thi-1 hsdR17</i>	Lab stock
BL21(DE3)	<i>E. coli B dcm ompT hsdS(r_Bm_B) gal</i>	Novagen/Lab stock
AB1157	F ⁻ <i>thr-1 leuB6 proA2 his-4 thi-1 argE2 lacY1 galk2 rspL supE44 ara-14 xyl-15 mtl-1 tsx-33</i>	(Dewitt & Adelberg, 1962) ¹
PN134	<i>E. coli</i> AB1157 (<i>sodA</i> ::MudPR13)25 (<i>sodB</i> -Km) 1- Δ 2	(Imlay & Linn, 1987) ¹
AS391	<i>E. coli</i> AB1157 (<i>sodA</i> ::MudPR13)25 (<i>sodB</i> -Km) 1- Δ 2 (<i>sodC</i> ::Spec)	(Gort et al., 1999) ¹
BL21(DE3) Δ <i>sodA</i>	<i>E. coli</i> BL21(DE3) (<i>sodA</i> ::MudPR13)25	This work
BL21(DE3) Δ <i>sodB</i>	<i>E. coli</i> BL21(DE3) (<i>sodB</i> -Km) 1- Δ 2	This work
BL21(DE3) Δ <i>sodA</i> Δ <i>sodB</i>	<i>E. coli</i> BL21(DE3) (<i>sodA</i> ::MudPR13)25 (<i>sodB</i> -Km) 1- Δ 2	This work
<i>Staphylococcus aureus</i>		
SH1000	Wild type MSSA, 8325-4 rsbU ⁺	(Horsburgh et al., 2002a)
RN4220	Restriction negative 8325	(Kreiswirth et al., 1983)
Newman	Wild type MSSA	(Duthie & Lorenz, 1952)
SH1000 Δ <i>sodA</i>	SH1000 <i>sodA</i> ::Tn917	(Karavolos et al., 2003) ²
SH1000 Δ <i>sodM</i>	SH1000 <i>sodM</i> ::tet	(Karavolos et al., 2003) ²
SH1000 Δ <i>sodA</i> Δ <i>sodM</i>	SH1000 <i>sodA</i> ::Tn917 <i>sodM</i> ::tet	(Karavolos et al., 2003) ²
SH1000 Δ <i>mntA</i>	SH1000 <i>mntA</i> ::kan	(Horsburgh et al., 2002) ²
SH1000 Δ <i>mntR</i>	SH1000 <i>mntR</i> ::tet	(Horsburgh et al., 2002) ²
SH1000 Δ <i>sodA</i> Δ <i>mntA</i>	SH1000 <i>sodA</i> ::Tn917 <i>mntA</i> ::kan	This work
SH1000 Δ <i>sodA</i> Δ <i>mntR</i>	SH1000 <i>sodA</i> ::Tn917 <i>mntR</i> ::tet	This work
SH1000 Δ <i>mntA</i> Δ <i>sodM</i>	SH1000 <i>mntA</i> ::kan <i>sodM</i> ::tet	This work
Newman Δ <i>sodA</i>	Newman <i>sodA</i> ::tet	(Garcia et al., 2017) ³
Newman Δ <i>sodM</i>	Newman <i>sodM</i> ::erm	(Garcia et al., 2017) ³
Newman Δ <i>sodA</i> Δ <i>sodM</i>	Newman <i>sodA</i> ::tet <i>sodM</i> ::erm	(Kehl-Fie et al., 2011) ³

Table 2.1 Bacterial strains used through this study.

¹Prof J. A. Imlay, University of Illinois, USA; ²Prof S. Foster, University of Sheffield, UK; ³Dr T. E. Kehl-Fie, University of Illinois, USA

2.1.1. Growth media and supplementation of bacterial culture

Where indicated, media were sterilised by autoclaving at 120°C for 30 minutes at 1 atmosphere pressure. To filter sterilise large volumes of liquid, 150 ml Steritop (Millipore), vacuum-driven disposable filtration systems with a 0.22 µm pore size were used. To filter sterilise smaller volumes of liquids, plastic syringes and 0.2 µm Acrodisc® membrane filters (Pall) were applied. All supplements and media were made using Milli-Q grade water obtained with a Millipore Simplicity water purification system, with a rated resistivity $\geq 18 \text{ M}\Omega\cdot\text{cm}$ at room temperature (RT), unless otherwise stated.

2.1.1.1. *Escherichia coli*

The *E. coli* strains were propagated on solidified growth medium (containing 1.5 % w/v agar) and subsequently cultured in liquid broth. Lysogeny broth (LB; Bertani, 1951) and 2x YT rich media were used for standard cultures. For growth in defined, minimal medium conditions *E. coli* strains were cultured in M9 medium (Sambrook & Russel, 2001), containing 10 µM FeSO₄ heptahydrate.

When selective pressure was required, antibiotics were added at the following concentrations: 150 µg·ml⁻¹ carbenicillin (water solution), 50 µg·ml⁻¹ kanamycin (water solution), 10 µg·ml⁻¹ chloramphenicol (ethanol solution), or 100 µg·ml⁻¹ spectinomycin (water solution).

Each *E. coli* liquid culture was started by inoculation of 10 ml or 100 ml of fresh growth media with a single colony from an agar plate. The pre-culture was incubated overnight at 37°C, with 185 rpm orbital shaking. The bacterial pre-culture was subsequently used to inoculate a fresh batch of growth media (100 ml or 1000 ml) to an OD_{600nm} of 0.05. The sub-culture was also grown at 37°C, with 185 rpm orbital shaking.

Medium	Composition	Supplements
Lysogeny broth (LB)	10 g·L ⁻¹ tryptone	5 mM MnCl ₂
	5 g·L ⁻¹ yeast extract	0.2 mM ammonium ferric citrate
	10 g·L ⁻¹ NaCl	1 mM H ₂ O ₂
2x Yeast extract and Tryptone medium (2xYT)	16 g·L ⁻¹ tryptone	1 mM MnCl ₂
	10 g·L ⁻¹ yeast extract	
	5 g·L ⁻¹ NaCl	
M9 minimal medium (M9)	12.8 g·L ⁻¹ Na ₂ HPO ₄ x 7H ₂ O	0.01 mM ammonium iron (II) sulphate
	3 g·L ⁻¹ KH ₂ PO ₄	0.25 mM MnCl ₂
	0.5 g·L ⁻¹ NaCl	0.2 % (w/v) casamino acids
	1 g·L ⁻¹ NH ₄ Cl	1mM thiamine
	2 mM MgSO ₄	
	0.1 mM CaCl ₂	
	0.4 % (w/v) glucose	

Table 2.2 Composition of *E. coli* bacterial growth media and supplements used.

2.1.2.2. *Staphylococcus aureus*

The *S. aureus* strains were propagated on tryptic soy broth (TSB) agar (1.5 % w/v) plates and subsequently cultured in liquid TSB. For growth in nutrient-limiting conditions, *S. aureus* strains were cultured in modified Tris(hydroxymethyl)aminoethane (Tris) minimal (TM) medium (Sebulsky, 2000), where succinate was replaced with 0.25 % (w/v) glucose. For selective growth, antibiotics were added at the following concentrations: 50 µg·ml⁻¹ kanamycin (water solution), 5 µg·ml⁻¹ erythromycin (ethanol solution), 5 µg·ml⁻¹ tetracycline (ethanol solution), or 10 µg·ml⁻¹ chloramphenicol (ethanol solution).

Growth analyses of *S. aureus* SH1000 wild type and deletion mutant strains were performed under normal and induced superoxide stress conditions in TSB medium or modified TM medium. *S. aureus* SH1000 cultures were inoculated with a single colony and incubated overnight aerobically at 37°C with rotary shaking (185 rpm). Growth analysis was started with sub-culture of the overnight culture into 20 ml of fresh media (TSB or TM) containing appropriate antibiotic to an OD_{600nm} of 0.05, which was then split into two 50 ml Falcon tubes to give a control culture of 10 ml and corresponding stress-induced culture. The superoxide stress inducing agent, methyl viologen (MV; Sigma-Aldrich, UK), was added to the bacterial culture after 2 hours of initial growth to the final concentration of 1 mM. Hourly OD_{595nm} readings were taken using a plate reader (BioTek™ ELx800™).

Medium	Composition	Supplements
Tryptic soy broth (TSB)	17 g·L ⁻¹ tryptone 3 g·L ⁻¹ soytone 2.5 g·L ⁻¹ K ₂ HPO ₄ 5 g·L ⁻¹ NaCl 0.25 % (w/v) glucose	1 mM Methyl viologen Varying [MnCl ₂]
Tris minimal medium (TM)	5.8 g·L ⁻¹ NaCl 3.7 g·L ⁻¹ KCl 1.1 g·L ⁻¹ (NH ₄) ₂ SO ₄ 0.142 g·L ⁻¹ Na ₂ SO ₄ 0.272 g·L ⁻¹ KH ₂ PO ₄ 100 mM Tris pH 7.4 0.5 mM MgCl ₂ x 6H ₂ O 0.1 mM CaCl ₂ x 2H ₂ O 1 % (w/v) Casamino Acids 0.02 g·L ⁻¹ Tryptophan 0.022 g·L ⁻¹ Cysteine 0.05 mM Thiamine 0.01 mM Nicotinic Acid 0.5 mg·L ⁻¹ Pantothenic Acid 0.01 mg·L ⁻¹ Biotin 0.25 % (w/v) glucose	1 mM Methyl viologen Varying [MnCl ₂]
LK	10 g·L ⁻¹ tryptone 5 g·L ⁻¹ yeast extract 7 g·L ⁻¹ KCl	0.05% (w/v) sodium citrate

Table 2.3 Composition of *S. aureus* bacterial growth media.

2.2. DNA manipulations

2.2.1. Isolation of genomic and plasmid DNA

All the plasmids used and created throughout this work are listed in Table 2.4. Total DNA was isolated from overnight bacterial cultures. Cultures were centrifuged (10 minutes, 4000 g, 4°C) and harvested cells were washed with 10 mM Tris, pH 7.5, 10 mM EDTA buffer, followed by repeat centrifugation. Washed pellets were resuspended in 500 µl of buffer (100 mM NaCl, 10 mM Tris, pH 7.5). Glass beads (0.1 mm diameter, 0.1 g) were added to each cell suspension in a 2 ml screw cap tube. Cells were agitated in a cell disruptor (Biospec Mini-Bead Beater 16; 6 m/s, 2 x 40 seconds, with 1 minute on ice in between cycles) for lysis. Cell debris was removed by centrifugation (10 minutes, 21,100 g, 4°C). Soluble lysates were boiled for 10 minutes and

denatured material was removed by another round of centrifugation (10 minutes, 21,100 g, 4°C). Recovered supernatant was column-purified using a PCR clean-up kit (Sigma-Aldrich, UK) before being used as template in the relevant PCR reaction. Concentration of DNA was determined using a ThermoSci Nano-drop2000.

Plasmid	Description	Ab ^R	Reference/ source
pGEM-T	<i>E. coli</i> cloning vector	Ampicillin	Promega
pGEM-T- <i>sodA</i>		Ampicillin	Dr K. Waldron ¹
pGEM-T- <i>sodMqc</i>		Ampicillin	Dr K. Waldron ¹
pET29a(+)	<i>E. coli</i> expression vector	Kanamycin	Novagen/ Lab stock
pET29a- <i>sodA</i>		Kanamycin	This work
pET29a-FLAG- <i>sodA</i>		Kanamycin	This work
pET29a- <i>sodMqc1</i>		Kanamycin	This work
pET29a- <i>sodMqc2</i>		Kanamycin	This work
pET29a-StrepII- <i>sodM</i>		Kanamycin	This work
pET29a- <i>ecsodB</i>		Kanamycin	This work
pET29a- <i>ecsodBqc1</i>		Kanamycin	This work
pET151	<i>E. coli</i> expression vector	Ampicillin	(Rashid et al., 2015) ³
pET151- <i>sodA</i>		Ampicillin	This work
pET151- <i>sodM</i>		Ampicillin	This work
pS10t	pMK4-derivative <i>E. coli</i> / <i>S. aureus</i> shuttle vector with <i>S. aureus</i> S10 ribosomal gene promoter and T2 transcriptional terminator from <i>E. coli</i>	Ampicillin/ Chloramphenicol	(Morrissey et al., 2000) ²
pS10t-StrepII- <i>sodM</i>			This work
pS10t-Flag- <i>sodA</i>			This work
pS10t-StrepII- <i>sodA</i>			This work

Table 2.4 Plasmids used in this project.

¹ Dr K. J. Waldron, Institute for Cell and Molecular Bioscience, Newcastle University, United Kingdom; ² Dr J. Morrissey, Department of Genetics, University of Leicester, United Kingdom; ³ Dr T. D. H. Bugg, Department of Chemistry and School of Life Sciences, University of Warwick, United Kingdom

Plasmid DNA was prepared using a GenElute™ Plasmid Miniprep Kit (Sigma-Aldrich, UK). The standard manufacturer's protocol for preparing bacterial plasmids using a micro-centrifuge was followed. When preparing plasmids from *S. aureus*, an additional 100 µg·mL⁻¹ lysostaphin (Sigma-Aldrich, UK) was added to the resuspension buffer and this suspension was incubated at 37°C for 30 minutes to lyse the staphylococcal cell wall before treatment with the supplied lysis buffer. The final elution was performed with nuclease-free water instead of the supplied elution buffer.

2.2.2. Agarose gel electrophoresis, staining and visualisation

DNA samples were analysed using agarose gel electrophoresis. Samples were mixed with 6 x DNA loading buffer (Thermo-Fisher Scientific, UK) and resolved on a 1 % (w/v) agarose gel composed of TAE buffer (40 mM Tris, 20 mM acetic acid, and 1 mM EDTA, pH 8.0) and 0.01 % SYBR® Safe DNA Gel Stain (Thermo-Fisher Scientific, UK). A MassRuler™ DNA Ladder Mix (Thermo-Fisher Scientific, UK) was used to estimate DNA fragment size and concentration. The gel was run in TAE at 80-100 V until the gel front reached the required distance. Resolved DNA samples were then visualised using UV light in a ChemiDoc™ system (BioRad, UK).

2.2.3. Oligonucleotides

Oligonucleotide primers were designed in order to amplify genes of interest from the genomic DNA and clone them into the vectors. For standard cloning by restriction enzyme digestion and ligation, a restriction site (underlined) was incorporated in the forward and reverse primers. The sequences of all of the oligonucleotides used in this work are listed in Table 2.5, categorised by application: screening of constructs, amplification of genes for cloning, correction of sequence errors, mutagenesis and genotyping.

All of the oligonucleotides were synthesised by Sigma-Aldrich at 0.025 μ mol scale and purified by desalting. In capital letters are sequences incompatible with the amplifying template.

Name	Sequence	Application
T7_F	taatacgactcactatag	Screening of plasmids
T7_R	gctagttattgctcagcgg	Screening of plasmids
pGEM-T_R	caagctatgcatccaacg	Screening of plasmids
M13_F	gtaaacgacggccagt	Screening of plasmids
M13_R	caggaaacagctatgac	Screening of plasmids
sodA-amp_F	GGGCATatggctttgaattacc	Amplification of <i>sodA</i>
sodA-amp_R	GGGGATCCtattttgttcattatataattcg	Amplification of <i>sodA</i>
sodM-amp_F	GGGCATatggcattaaattacc	Amplification of <i>sodM</i>
sodM-amp_R	GGGGATCCtattattttgctgcttg	Amplification of <i>sodM</i>
sodA-amp_F2	ggggatccaggaggatgattttatggctttg	Amplification of <i>sodA</i> CDS
sodA-amp_R2	GGGATATCttttgttcattatataattc	Amplification of <i>sodA</i> CDS
sodM-amp_F2	ggggatccaggaggaatatacttatggcattaa	Amplification of <i>sodM</i> CDS
sodM-amp_R2	GGGATATCttttgctgctgtgataattc	Amplification of <i>sodM</i> CDS
bssodA-ampNdeI_F	gggcatatggcttacgaactcca	Amplification of <i>bssodA</i>
bssodA-ampSalI/BamHI_R	gtcgacggatcctattttgctcgcgtga	Amplification of <i>bssodA</i>
ecsodB-ampNcoI_F	gcgctccatggGCtattcgaattacc	Amplification of <i>ecsodB</i>
ecsodB-ampXhoI_R	gcgctcaggttatgcagcgg	Amplification of <i>ecsodB</i>
sodM-NdeIqc1_F	taaattaccaaatattaccataCgcGtatgatgcattggaaccatat	Removing internal NdeI
sodM-NdeIqc1_R	atatggtccaatgcatcataCgcGtatggtaaatttggaattta	Removing internal NdeI
sodM-A570qc2_F	ggaacattgtaactggAaaaaagtgtgaattataccaagcagc	Correcting A570 error
sodM-A570qc2_R	gctgcttggtataattcatcaactttttTccagttaacaatgttcc	Correcting A570 error
ecsodB-qc1_F	gccacgcggttccatgtcattcgaattacctg	Correction
ecsodB-qc1_R	caggaattcgaatgacatggaaccgctggc	Correction
SDM_SaSodA19_F	agaaccacatATTgacaaagaaac	F19I mutagenesis
SDM_SaSodA19_R	gtttctttgtcAATatgtggttct	F19I mutagenesis
SDM_SaSodA159/160_F	cacctatttaCTGTTCgacgtatgggaacacgcttattac	G159L, L160F mutagenesis
SDM_SaSodA159/160_R	gtaataagcgtgttcccatacgtcGAACAGtaaaataggtg	G159L, L160F mutagenesis
SDM_SaSodA159_F1	gggtaaacacacctattttaCTGtagacgtatgggaacacg	G159L mutagenesis
SDM_SaSodA159_R1	cggtgtcccatacgtctaaCAGtaaaataggtgttttacc	G159L mutagenesis
SDM_SaSodA159_F2	ggtaaacacacctattttaACTcagacgtatggG	G159T(XbaI) mutagenesis
SDM_SaSodA159_R2	CccatacgtctGaAGTtaaaataggtgttttacc	G159T(XbaI) mutagenesis
SDM_SaSodA164_F	ggtttagacgtatggGCCcagccttattacc	E164A (ApaI) mutagenesis
SDM_SaSodA164_R	ggtaataagcgtgGGCccatacgtctaaacc	E164A (ApaI) mutagenesis
SDM_SaSodM19_F	ggaaccatatTTCgatcaaagaacaatgg	I19F mutagenesis
SDM_SaSodM19_R	ccattgttctttgatcGAAataggttcc	I19F mutagenesis
SDM_SaSodM159/160_F	accaatcctaGGCCTGgatgtttgggagcatgcctac	L159G, F160L mutagenesis

Name	Sequence	Application
SDM_SaSodM159/160_R	gtaggcgatgctcccaaaccatcCAGGCCtaagattggt	L159G, F160L mutagenesis
SDM_SaSodM159_F1	caccaatcctaGGAttcgaattgtggagcatgcc	L159G mutagenesis
SDM_SaSodM159_R1	ggcatgctcccaaaccatcgaaTCCTaagattggtg	L159G mutagenesis
SDM_SaSodM159_F2	cccaaaccatcAaaAGTtaaTattggtgtttgc	L159T (Sspl) mutagenesis
SDM_SaSodM159_R2	gcaaaacaccaatAttaACTttTgatgtttggg	L159T (Sspl) mutagenesis
SDM_SaSodM164_F	ctatttgatgtttgggCCcatgcctactatctg	E164A (ApaI) mutagenesis
SDM_SaSodM164_R	cagatagtaggcatgGGcccaaaccatcaaatag	E164A (ApaI) mutagenesis
sodA_F	gcaaatcttgttgaaccagtcactgcttg	Genotyping
sodA_R	cggtctcatttaagagaccgaacaagtaac	Genotyping
sodM_F	catatgcatatgatgcattggaacc	Genotyping
sodM_R	gctgcttggtataattcatcaac	Genotyping
mntA_F	ggaggataaaacgttgttag	Genotyping
mntA_R	cgacaaactctaaccatgttatattgctcc	Genotyping
mntR_F	ctggattatcttcaatctttatgcagtg	Genotyping
mntR_R	ctgatataatatagacaatgtatgtgagg	Genotyping
rsbU_F	tcaaattattatatacccatc	Genotyping
rsbU_R	ccttgcttaagcatttgc	Genotyping

Table 2.5 Oligonucleotides used in this project.

2.2.4. Polymerase chain reaction (PCR)

All PCRs were performed using Taq DNA polymerase (NEB) or Phusion® High-Fidelity DNA Polymerase (NEB) in 10, 25 or 50 µl reaction volumes according to the manufacturers' protocols. Cycling conditions are listed in Table 2.6.

Step	Number of cycles	Taq DNA polymerase (NEB)	Phusion® High-Fidelity DNA Polymerase (NEB)
Initial denaturation	-	5 min, 95°C	30 sec, 98°C
Denaturation	35	30 sec, 95°C	15 sec, 98°C
Annealing		30 sec, 55-65°C	30 sec, 55-65°C
Extension		1 min / 1 kb, 68°C	30 sec - 1 min / 1 kb, 72°C
Final extension	-	5 min, 68°C	10 min, 72°C
Storage	-	12°C until stopped	12°C until stopped

Table 2.6 Polymerase chain reaction conditions.

2.2.5. Molecular cloning

PCR products were purified using either PCR clean-up kit (Sigma-Aldrich, UK) or GenElute™ Gel Extraction Kit (Sigma-Aldrich, UK). Plasmids were isolated and purified from bacterial cells using a GenElute™ Plasmid Miniprep Kit (Sigma-Aldrich, UK). Purified PCR products and plasmids (usually 1 µg) were digested using appropriate restriction enzymes (Table 2.5). All double digestions were performed sequentially using commercial restriction enzymes (NEB) in recommended buffers and recommended conditions (usually 1 hour or overnight incubation at 37°C with 5-10 U of restriction enzyme). When required, thermal inactivation of restriction enzyme was applied. A PCR clean-up kit was used to purify DNA fragments after digestion.

Purified restriction fragments were ligated into the accordingly digested and phosphatase treated (Antarctic Phosphatase, NEB) plasmids using T4 DNA Ligase (Thermo-Fisher Scientific, UK). The insert and vector DNAs were mixed in a thin-wall PCR tube to produce an insert:vector ratio of 3:1. The ligation reaction was incubated at room temperature or at 4°C overnight and stored at -20°C until required. Ligation products were used to transform chemically competent *E. coli* cells. Transformants were selected on agar plates containing appropriate antibiotics at 37°C overnight. Initially colony PCR was performed on selected transformants, with primers specific to regions of the plasmid upstream and downstream from the cloning site. Patch-plated colonies were used to start overnight broth cultures with the appropriate antibiotics at 37°C. Plasmids were isolated and purified from bacterial cells using a GenElute™ Plasmid Miniprep Kit (Sigma-Aldrich, UK) and digested using the same set of restriction enzymes that were used for cloning in order to verify the presence of an insert. The sequence of the insert and its integration into the vector was verified by Sanger sequencing (GATC Biotech, Germany).

2.2.5.1. Cloning of *S. aureus* *sodA* and *sodM* genes for heterologous expression

Initial work predating this project conducted by Dr K. Waldron involved amplification of both *sodA* (SAOUHSC_01653) and *sodM* (SAOUHSC_00093) genes from *S. aureus* SH1000 genomic DNA by polymerase chain reaction (PCR) using Phusion DNA polymerase (Thermo-Fisher Scientific, UK). In order to amplify genes of interest, the primer pairs *sodA*-amp_F and *sodA*-amp_R or *sodM*-amp_F and *sodM*-amp_R were used, respectively (Table 2.5). The PCR product was A-tailed by incubation with *Taq* polymerase (NEB) with dATP at 72°C for 30 min, purified by agarose gel electrophoresis using GenElute™ Gel Extraction Kit (Sigma-Aldrich, UK), and ligated into the pGEM-T vector (Promega). After transformation of *E. coli* DH5α and selection on carbenicillin, resulting clones were screened for the presence of insert by *NcoI/Spel* restriction digest. An internal *NdeI* restriction site in the *sodM* gene was subsequently removed using QuikChange site-directed mutagenesis (Stratagene) using the primer pair *sodM*-*NdeI*qc1_F and *sodM*-*NdeI*qc1_R, with resulting clones screened by *NdeI* restriction digest. The genetic insert in

the resulting pGEM-T-sodA and pGEM-T-sodMqc plasmids was verified by DNA sequencing (GATC Biotech, Germany).

At the start of this project the *sodA* and *sodMqc* genes were sub-cloned from the previously prepared pGEM-T plasmids (pGEM-T-*sodA* and pGEM-T-*sodMqc*) into the pET29a *E. coli* expression vector. Each plasmid was double digested (*NdeI/BamHI*), the inserts (each ~600bp) purified by agarose gel electrophoresis followed by gel extraction, and ligated into *NdeI/BamHI*-digested, phosphatase-treated pET29a vector (Novagen). After transformation and selection on kanamycin, resulting clones were screened by PCR using the primer pair T7_F and T7_R with *Taq* DNA polymerase. The plasmid from one successful clone containing each insert, designated pET29a-*sodA* and pET29a-*sodMqc* respectively, was verified by DNA sequencing. A detected error, a deletion of A570 in the pET29a-*sodMqc* sequence, was fixed using QuikChange site-directed mutagenesis with the primer pair sodM-A570qc2_F and sodM-A570qc2_R (Table 2.5). A resulting clone pET29a-*sodMqc2* was subsequently verified by Sanger DNA sequencing (GATC Biotech, Germany).

2.2.5.2. Site directed mutagenesis of *sodA* and *sodM* genes

The constructs of pET29a-*sodA* F19I (single mutant F19I); G159L, L160F (double mutant); F19I, G159L, L160F (triple mutant); G159L (single mutant G159L); G159T (single mutant G159T); E164A (single mutant 164A), and of pET29a-*sodMqc* I19F (single mutant I19F); L159G, F160L (double mutant); I19F, L159G, F160L (triple mutant); L159G (single mutant L159G); L159T (single mutant L159T); and E164A (single mutant E164A) were prepared using a site directed mutagenesis approach. Mutagenesis was performed using 5-50 ng of pET29a-*sodA* and pET29a-*sodMqc2* plasmid DNA templates, 250 ng of appropriate primer pairs listed in Table 2.5 with Phusion® High-Fidelity DNA Polymerase, according to the QuikChange site-directed mutagenesis kit (Stratagene). Applied conditions are listed in Table 2.7.

10 U of *DpnI* restriction enzyme was added to each reaction and incubated at 37°C for 1 hour to digest the parental, supercoiled dsDNA. *DpnI*-treated DNA was then used to transform chemically-competent *E. coli* DH5α cells. Resulting transformants, selected on kanamycin, were initially screened by PCR using the primer pair T7_F and T7_R with *Taq* DNA polymerase. Where possible a diagnostic restriction digest was performed to confirm the introduction of specific mutation (restriction sites indicated within oligonucleotide sequences listed in Table 2.5), and in all cases the final sequence was verified by Sanger sequencing (GATC BioTech, Germany).

Controls for SDM reactions were set up with no polymerase added. Non-modified DNA (parental strand) gets digested by *DpnI*, and thus DH5α transformation with a control reaction resulted in no colonies grown on plates.

Step	Number of cycles	Temperature	Time
Initial denaturation	1	95°C	1 min
Denaturation		95°C	1 min
Annealing	16-18	60°C	1 min
Extension		72°C	7 min
Final extension	1	72°C	10 min
DpnI digest	-	37°C	60 min

Table 2.7 QuikChange reaction conditions.

2.2.5.3. Cloning of *Bacillus subtilis* *sodA* for heterologous expression in *E. coli* BL21(DE3)

The *B. subtilis* *sodA* (NP_390381; herein *bssodA*) gene was amplified by PCR from *Bacillus subtilis* 168 genomic DNA using Phusion DNA polymerase and the primer pair *bssodA*-ampNdeI_F and *bssodA*-ampSallBamHI_R (listed in Table 2.5) incorporating 5' *NdeI* and 3' *BamHI* restriction sites. The resulting PCR product was cloned into the *Escherichia coli* expression vector, pET29a, through *NdeI/BamHI* restriction cloning, to yield pET29a-*bssodA* expression vector.

2.2.5.4 Cloning of *Escherichia coli* *sodB* and expression in *E. coli* BL21(DE3) wild type and Δ *sodA* strains

The *E. coli* *sodB* gene (herein *ecsodB*) was amplified from *Escherichia coli* K12 genomic DNA using Phusion DNA polymerase with the primer pair *ecsodB*-ampNcoI_F and *ecsodB*-ampXhoI_R, introducing 5' *NcoI* and 3' *XhoI* restriction sites (Table 2.5). The genetic insert was cloned into *NcoI/XhoI* (NEB) digested pET29a *E. coli* expression vector. QuikChange site-directed mutagenesis with the *sodB*-qc1_F and *sodB*-qc1_R primer pair was used to correct for a mutation that introduced a Gly2 residue (G5, C6 bases) and revert to the wild type sequence, as confirmed by Sanger sequencing.

2.2.6. Gene synthesis

The FLAG epitope (DYKDDDDK) and StrepII epitope (WSHPQFEK) tagged versions of the *sodA* and *sodM* genes were prepared synthetically in pIDTSmart Amp plasmids (Integrated DNA Technologies, Germany). Codon optimisation of a protein and epitope-coding sequence was applied to improve efficiency of heterologous expression in *E. coli*. The *sodA* gene was tagged N-terminally with a FLAG octapeptide, whereas *sodM* had a StrepII-tag incorporated at the C-terminus.

A lyophilised 4 µg sample of purified, double-stranded DNA of a circularized plasmid was resuspended in 80 µL of 10 mM Tris, 0.1 mM EDTA buffer, pH 8.0. An aliquot (1 µL) of resuspended DNA was used to transform chemically competent *E. coli* DH5α cells. Transformants were selected on ampicillin-supplemented LB agar media.

Plasmid DNA was isolated from positive transformants with GenElute™ Plasmid Miniprep Kit. Tagged genes were sub-cloned from pDTSmart plasmids into pET29a *E. coli* expression vector using *NdeI/EcoRI* restriction digest followed by ligation of the resulting inserts into pET29a with T4 DNA Ligase to form pET29a-FLAG-*sodA* and pET29a-StrepII-*sodM* constructs. The sequences were verified by Sanger sequencing.

2.2.7. Preparation of pS10t-StrepII/FLAG constructs for constitutive SOD expression in *S. aureus* SH1000

The epitope-tagged genes were introduced into the *E. coli*-*S. aureus* shuttle vector pS10t (Morrissey et al., 2000), an *S. aureus* expression vector containing a strong, constitutive promoter and a transcriptional terminator. Firstly, the synthesised N-terminal FLAG tag and C-terminal-StrepII tag SOD constructs (section 2.2.6) were inserted into pS10t plasmid sequence using *BamHI/PstI* restriction sites. Subsequently, wild type copies of *sodA* and *sodM*, including Shine-Dalgarno sequences, were amplified from SH1000 genomic DNA using primers *sodA*-amp_F2/R2, *sodM*-amp_F2/R2; and ligated with pS10t plasmids downstream of the FLAG tag and upstream of StrepII tag, to form pS10t-FLAG-*sodA* and pS10t-StrepII-*sodM* constructs. Ligation products were used to transform chemically competent *E. coli* DH5α cells. *E. coli* transformants were selected on agar plates containing 150 µg·ml⁻¹ carbenicillin (*E. coli* selection marker). Screening of the clones was performed using the primer pairs M13_F and M13_R with *Taq* DNA polymerase. Plasmid DNA from positive clones, confirmed by DNA sequencing, was isolated using the GenElute™ Plasmid Miniprep Kit and used to transform electrocompetent *S. aureus* RN4220 cells. Subsequently plasmid DNA was extracted from *S. aureus* RN4220 cells to transform the wild type *S. aureus* strains by electroporation. *S. aureus* transformants were selected on agar plates containing 10 µg·ml⁻¹ chloramphenicol (*S. aureus* selection marker).

Phage transduction (section 2.5.2) was used to introduce pS10t-FLAG-*sodA* and pS10t-StrepII-*sodM* constructs into the SH1000 mutant backgrounds. Phage lysate stocks were prepared using the wild type strain transformed with the pS10t-FLAG-*sodA* and pS10t-StrepII-*sodM* constructs. Transduction and selection was performed as described in section 2.5.2, using chloramphenicol selection for pS10 plasmid.

2.3. Preparation of competent cells

2.3.1. Chemically competent *E. coli*

An overnight culture of *E. coli* cells was used to inoculate 100 ml of fresh growth media containing appropriate antibiotics. Cultures were grown at 37°C until OD_{600nm} reached 0.5. Cell suspension was chilled for 15 minutes on ice and subsequently spun down at 4000 g for 10 minutes. Supernatant was discarded, and harvested cells were resuspended in 30 ml of ice-cold buffer I (100 mM RbCl₂, 50 mM MnCl₂·4 H₂O, 30 mM potassium acetate, 10 mM CaCl₂·2 H₂O, 15 % (v/v) glycerol, pH 5.8) and incubated on ice for 2 hours. Following incubation, suspension was centrifuged at 4000 g for 10 minutes and pellet was resuspended in 8 ml of ice-cold buffer II (10 mM MOPS, 10 mM RbCl₂, 75 mM CaCl₂·2 H₂O, 15 % (v/v) glycerol, pH 6.8) and incubated on ice for 15 minutes. Aliquots (50 µl) of cells were flash frozen in liquid nitrogen and stored at -80°C until required.

2.3.2. Electrocompetent *S. aureus*

An overnight culture of *S. aureus* cells was used to start a culture in fresh TSB and incubated with 185 rpm orbital shaking at 37°C up to OD_{600nm} of 0.4. Cells were harvested by centrifugation at 4000 g for 10 minutes. The pellet was resuspended in one volume ((v/v) of bacterial culture) of ice-cold filter-sterilised 0.5 M sucrose and centrifuged at 4000 g for 10 minutes. Supernatant was discarded and cells resuspended in a 50 % volume ((v/v) of bacterial culture) of ice-cold 0.5 M sucrose. The cell suspension was incubated on ice for 15-30 minutes and after that centrifuged at 4000 g for 10 minutes. Pellets were resuspended in 10 % volume ((v/v) of bacterial culture) of ice-cold 0.5 M sucrose. Aliquots (50 µl) of cells in 1.5 ml Eppendorf tubes were flash frozen in liquid nitrogen and stored at -80°C until required.

2.4. Transformations of bacterial cells with plasmid DNA

2.4.1. *Escherichia coli*

Chemically competent *E. coli* cells were thawed on ice, 1-5 µl of the DNA (plasmid or ligation mixture, respectively) was added, and then incubated on ice for 20 minutes. After incubation, the mixture was promptly transferred to a 42°C thermoblock for 45 seconds heat shock followed by an additional incubation on ice for 2 minutes. The cell recovery process was initiated by addition of 450 µl of a room temperature rich growth medium (LB) to 50 µl of transformed bacterial cells, followed by incubation for 1 hour at 37°C with 185 rpm orbital shaking. Cells were finally plated out onto the LB agar plates containing the appropriate antibiotics and incubated overnight at 37°C.

2.4.2. *Staphylococcus aureus*

DNA intended to transform competent *S. aureus* cells was firstly dialysed for 30 minutes by aspirating 30 µl onto a 0.025 µm 13 mm nitrocellulose filter (Millipore) placed on the surface of a MilliQ water-filled Petri dish. Following dialysis, DNA was mixed with an aliquot of competent *S. aureus* cells and incubated for 30 minutes at room temperature. This solution was aspirated into an electroporation cuvette and then pulsed briefly in a Bio-Rad gene pulser II (Bio-Rad, UK) at 2.5 kV, 200 Ω and 25 µF. Immediately after the pulse, 900 µl of room temperature TSB medium containing 500 mM sucrose was added and the solution transferred to a 15 ml universal tube and incubated with shaking at 37°C for three hours. An aliquot (100 µl) of the transformation was then spread onto several replicate solid media plates with the appropriate antibiotics. Restriction-deficient *S. aureus* RN4220 was used when transforming with plasmid DNA harvested from *E. coli*. A control reaction was also performed using competent cells but no external DNA.

2.5. Phage transductions

2.5.1. Preparation of *E. coli* BL21(DE3) SOD deletion mutant strains using P1 phage transduction

P1 phage was kindly provided by Dr David Bulmer (Newcastle University, UK). The *E. coli* PN134 (*sodA::cam sodB::kan*), (Imlay & Linn, 1987) and AS391 (*sodA::cam sodB::kan sodC::spec*) strains, (Gort et al., 1999) were acquired from Dr James A. Imlay (University of Illinois, USA).

Fresh phage lysate was prepared in BL21(DE3) strain. An overnight culture of BL21(DE3) cells was used to inoculate 10 ml of fresh LB supplemented with 10 mM MgSO₄ and 10 mM CaCl₂ and cultured at 37°C with 185 rpm agitation. When an OD_{600nm} = 0.3 was reached, the culture was infected with 100 µl of P1 stock lysate. Following addition of phage, the culture was incubated statically at 42°C for 1 hour, and subsequently at 37°C with 185 rpm orbital shaking, until cell lysis occurred. Chloroform was added (1 ml per 10 ml of culture) and mixed by vortex to mechanically disrupt the remaining cells. Cell debris was removed by centrifugation at 4200 g for 10 minutes and pellet was discarded. Collected supernatant was filtered using plastic syringe with 0.2 µm Acrodisc® membrane filter and stored at 4°C.

In order to transduce *sod* mutations from AB1157 strain into BL21(DE3) background, phage lysates were prepared by infection by P1 of the donor strains: PN134 (*sodA::cam sodB::kan*) and AS391 (*sodA::cam sodB::kan sodC::spec*).

BL21(DE3) recipient strain was cultured overnight in 10 ml of LB at 37°C with 185 rpm shaking. The culture was supplemented with 5 mM CaCl₂, required for phage infectivity, and incubated at 37°C with 185 rpm agitation for 20 minutes. Aliquots (1ml) of cells were inoculated with 100 µl of the following P1 stock lysates: AB1157 (*sodA::cam sodB::kan*) and AB1157 (*sodA::cam sodB::kan sodC::spec*) and incubated statically at 37°C for 10 minutes. LB (500 µl)

containing 10 mM sodium citrate was added to infected cells followed by 1 hour incubation at 37°C with 185 rpm orbital shaking, to allow expression of the antibiotic resistance markers. Cells were harvested by centrifugation for 5 minutes at 4000 g and pellets were resuspended in 300 µl of LB containing 10 mM sodium citrate. The cell suspension (100 µl) was plated onto 10 mM sodium citrate-supplemented solid media containing appropriate antibiotic to select for allelic transfer of *sodA::cam*, *sodB::kan* and *sodC::spec* into BL21(DE3). After overnight incubation at 37°C, colonies of transductants were patch-plated onto fresh 10 mM sodium citrate-supplemented, selective solid media to remove remaining phage contamination. Transductants were screened with in-gel SOD assay (see section 2.9.1) to confirm loss of activity.

2.5.2. Preparation of *S. aureus* SH1000 deletion mutant strains using ϕ 11 transduction

The mutant donor strains (*S. aureus* SH1000 *mntA::kan*, SH1000 *mntR::tet*) were cultured in 10 ml of LB broth supplemented with 10 mM CaCl₂ with 185 rpm shaking at 37°C until an OD_{600 nm} of 0.2 was reached. The culture was further diluted into fresh 25 ml of LB containing 10 mM CaCl₂. Phage lysate production was initiated by addition of 1 ml of phage ϕ 11 lysate, followed by incubation with shaking at 37°C until complete lysis occurred. After centrifugation for 10 minutes at 4000 g, the supernatant was filter-sterilised using 0.2 µm Acrodisc® membrane filter and stored at 4°C.

The recipient *S. aureus* strains, SH1000 *sodA::Tn917*, SH1000 *sodM::tet*, were cultured overnight with 185 rpm agitation at 37°C. The cells were harvested by centrifugation at 4000 g for 10 minutes and re-suspended in 1 ml LK supplemented with 10 mM CaCl₂. The donor phage lysate (0.5 ml) was added to the cells and incubated statically at 37°C for 25 minutes, followed by 15 minutes at 37°C with 185 rpm orbital shaking. Ice-cold 1 M sodium citrate (1 ml); (Ca chelator to prevent further cell lysis during transduction) was added to each reaction and the tubes were centrifuged for 10 minutes at 4000 g. The pellets were re-suspended in 1 ml ice-cold 1 M sodium citrate and incubated on ice for 2 hours. The aliquots (0.3 ml) of each reaction were plated onto several LK agar plates containing 0.05 % (v/v) sodium citrate and selective antibiotics. Plates were incubated at 37°C for 24-72 hours. Resulting colonies were patch-plated onto a fresh LB selective agar plate containing 0.05 % (v/v) sodium citrate. Genotypes of mutants SH1000 (*sodA::Tn917*, *mntA::kan*), SH1000 (*sodM::tet*, *mntA::kan*), SH1000 (*sodA::Tn917*, *mntR::tet*) were confirmed with PCR (primers listed in Table 2.5).

2.6. Complementation of *Ec*SODs' mutant strains with *Sa*SODs

Constructs for complementation of *E. coli* BL21(DE3) Δ *sodA* Δ *sodB* strain with *S. aureus* SODs were prepared in plasmids pET151 (IPTG-inducible expression vector) and pS10t (*E. coli*-*S. aureus* shuttle vector, with strong, constitutive promoter S10).

The *sodA* and *sodM* genes were sub-cloned from pET29a*sodA* and pET29a*sodM*qc2 vectors, by *NdeI*, *SacI* restriction cloning into pET151 plasmid. The pET151*sodA*, pET151*sodM* constructs were verified by sequencing (GATC Biotech, Germany) with T7 primers (Table 5.2). Validated vectors were introduced into the *E. coli* SOD-deficient strain by heat-shock transformation (section 2.4.1) and transformants were selected on LB-agar plates containing 1 % (w/v) glucose and 10 $\mu\text{g}\cdot\text{ml}^{-1}$ chloramphenicol, 50 $\mu\text{g}\cdot\text{ml}^{-1}$ kanamycin, 100 $\mu\text{g}\cdot\text{ml}^{-1}$ ampicillin.

The preparation of DH5 α pS10t transformants was described in section 2.2.7. Plasmid DNA extracted from positive clones was used to transform *E. coli* BL21(DE3) $\Delta\text{sodA}\Delta\text{sodB}$ strain (section 2.4.1). Transformed bacteria were selected on LB-agar plates containing 1 % (w/v) glucose and 10 $\mu\text{g}\cdot\text{ml}^{-1}$ cam, 50 $\mu\text{g}\cdot\text{ml}^{-1}$ kan, 100 $\mu\text{g}\cdot\text{ml}^{-1}$ amp.

The complementation of the SOD-deficient growth phenotype of *E. coli* was evaluated by comparison of the growth of wild type BL21(DE3), BL21(DE3) $\Delta\text{sodA}\Delta\text{sodB}$ mutant, and the mutant strain transformed with pET151*sodA*, pET151*sodM*, pS10Flag*sodA*, pS10StrepII*sodM* constructs. The growth curve was started by inoculating a 10 ml LB (1% (w/v) glucose) containing appropriate antibiotics and culturing all strains overnight at 37°C with 185 rpm shaking. Pre-cultures were subsequently diluted into fresh medium to an OD_{600nm} of 0.05 and grown for 8 hours, with OD_{595nm} measurement taken hourly, using microtiter plate reader (BioTek™ ELx800™).

2.7. Purification of proteins

2.7.1. Small-scale protein expression testing

In order to determine the optimal conditions for protein over-expression, small-scale expression trials were performed. Typically, 10 ml of LB containing an appropriate antibiotic was inoculated with a single colony of *E. coli* transformed with the expression plasmid, and cultured overnight at 37°C with 185 rpm orbital shaking. The stationary phase culture was diluted into 50 ml of fresh LB containing an appropriate antibiotic and incubated for approximately 2.5 hours until the OD_{600nm} had reached the value of 0.5 – 0.8. Protein expression was induced by the addition of isopropyl β -D-1-thiogalactopyranoside (IPTG). Several growth parameters were optimised, including duration (1 - 18 h) of growth and IPTG concentration (0.05 - 1.0 mM).

Routinely, 5 ml samples of the cultures were collected every few hours (typically at 0, 2, 4, 6, 20 h), harvested by centrifugation and sonicated using a MSE Soniprep150, and the lysate centrifuged for 10 minutes at 21,100 *g*. Expression level of a soluble protein was assessed comparing samples of cleared lysate (soluble supernatant) and cell suspension collected after sonication (total extract) by SDS-PAGE electrophoresis.

2.7.2. Large scale over-expression of recombinant proteins in *E. coli*

BL21(DE3) and BL21(DE3) sod-deficient strains

The pET29a-*sodA*, pET29a-*sodMqc2* and pET29a-*bssodA* constructs were transformed into *E. coli* BL21(DE3) or BL21(DE3) Δ *sodA* Δ *sodB* chemically competent cells and selected on LB agar plates containing 50 μ g·ml⁻¹ kanamycin. The pET29a-*ecsodB* plasmid was transformed into *E. coli* BL21(DE3) Δ *sodA* mutant strain and selected on LB agar plates containing 50 μ g·ml⁻¹ kanamycin and 10 μ g·ml⁻¹ chloramphenicol.

For overproduction of the proteins, transformants of *E. coli* cells were inoculated into selective media (LB or M9; Table 2.2) and cultured overnight at 37°C with 185 rpm orbital shaking. The overnight pre-culture was then used to inoculate 1 L of fresh media containing appropriate antibiotics to an OD_{600nm} 0.05. Protein expression was induced at OD_{600nm} ~0.5 by addition of 1 mM IPTG followed by incubation for the determined for all expression strains optimum of 4 h at 37°C with 185 rpm orbital shaking. Cells were harvested by centrifugation (4000 g, 30 min, 4°C), washed in 20 mM Tris pH 7.5, 10mM EDTA and frozen at -20°C.

Addition of MnCl₂, H₂O₂ and ammonium ferric citrate or (NH₄)₂Fe(SO₄)₂·6H₂O to growth media (LB or M9) was used in some experiments during over-expression of recombinant proteins in *E. coli* to manipulate metal content of yielded proteins. The MnCl₂ was added at the point of induction with 1 mM IPTG in varying concentrations of 0.25 mM, 0.5 mM or 5 mM, separately or in combination with 1 mM H₂O₂, while for testing with iron the ammonium ferric citrate or ammonium ferric sulphate (0.2 mM) were also added to the *E. coli* cultures at the point of induction with IPTG. Cultures were incubated for 4 h at 37°C with 185 rpm orbital shaking. Cells were harvested by centrifugation (4000 g, 30 min, 4°C), washed in 20 mM Tris pH 7.5, 10 mM EDTA and frozen at -20°C.

2.7.3. Protein extraction from *Escherichia coli* cells

Frozen cell pellets of bacteria expressing the recombinant proteins were thawed on ice and resuspended in 10 volumes (v/v) of 20 mM Tris buffer, pH 7.5, supplemented with cComplete EDTA-free protease inhibitors (Roche). Resuspended cells were lysed by sonication on ice (cycling: 5 min of alternate 5 seconds sonication, 5 seconds rest, using MSE Soniprep150). Resulting lysates were clarified by centrifugation (43549.6 g, 30 min, 4°C). The soluble cell extract was filtered using a 0.45 μ m syringe filter before commencing liquid chromatography.

2.7.4. Gradient anion exchange chromatography of soluble cell lysate (AEC)

Liquid chromatography purification of proteins was performed using the ÄKTA fast performance liquid chromatography (FPLC) system (GE Healthcare). The cleared cell lysate was loaded onto a 5 ml HiTrap Q HP anion exchange column (GE Healthcare), previously equilibrated with 2 column volumes (CV) of 20 mM Tris buffer, pH 7.5 (binding buffer), with the flow through of the

column collected. Unbound proteins were washed off the column with 5 CV of binding buffer, and the wash fraction was also collected. Protein elution was performed with a 9 CV linear (0-1 M) NaCl gradient at 5 ml/min, collecting 2 ml fractions. Eluted fractions were analysed by SDS-PAGE (see section 2.8.1), and the fractions containing the recombinant proteins were further purified or frozen at -20°C.

An additional AEC step was applied for the purification of *EcSodB* from the contaminating proteins that remained present after the initial AEC. Fractions containing the recombinant protein were pooled and further purified on a 5 ml HiTrap Q HP column in 20 mM MES pH 6.5 buffer with a linear 0-1 M NaCl gradient elution. Eluted fractions were treated as above.

2.7.5. Size-exclusion chromatography

All size-exclusion chromatography (SEC) columns were stored and maintained according to manufacturer's instructions (GE Healthcare). The columns were calibrated using low MW and high MW calibration kits (GE Healthcare): blue dextran (2000 kDa), thyroglobulin (669kDa), ferritin (440 kDa), aldolase (158 kDa), conalbumin (75 kDa), ovalbumin (44 kDa), carbonic anhydrase (29 kDa), ribonuclease A (13.7 kDa) and aprotinin (6.5 kDa). Analytical SEC was used to determine an apparent molecular weight of a protein and its oligomeric state, whereas preparative SEC was used to further resolve initially purified protein species.

2.7.5.1. Preparative size-exclusion chromatography

Peak AEC fractions containing recombinant SaSodA, SaSodM and BsSodA proteins were further purified through preparative SEC on a Superdex 200 16/600 PG column (GE Healthcare) in 20 mM Tris, pH 7.5, 150 mM NaCl buffer. An aliquot (1 ml) of AEC-eluted protein sample was loaded onto the column, previously equilibrated with 1.5 CV of the same buffer, and resolved at 1 ml·min⁻¹ flow rate, either at room temperature or at 4°C, collecting 2 ml fractions. The *EcSodB* SEC was performed as above, except using the buffer 20mM MES, 150 mM NaCl, pH 6.5.

Eluted fractions were analysed for protein by SDS-PAGE and for SOD activity by non-denaturing polyacrylamide gel electrophoresis (Native-PAGE; section 2.8.2) in-gel SOD assay (2.9.1). Protein concentration was assessed by Bradford assay (section 2.13), using bovine serum albumin (BSA) as standard. Purified recombinant proteins were frozen and stored at -20°C.

2.7.5.2. Analytical size-exclusion chromatography

Analytical SEC was performed using Superdex 200 increase 10/300 GL column (GE Healthcare). Depending on the analysed samples, SEC was performed either in 20 mM Tris, pH 7.5, 150 mM NaCl buffer for samples after metal-exchange or in 20 mM Tris, pH 7.5, 150 mM NaCl, 5 mM EDTA buffer for apo-proteins. An aliquot (0.5 ml) of a protein sample was loaded onto the

column, previously equilibrated with 1.5 CV of the appropriate buffer, and resolved at 0.75 ml·min⁻¹ flow rate, either at room temperature or at 4°C, collecting 0.5 ml fractions. Eluted fractions were analysed for protein by SDS-PAGE and for SOD activity by Native-PAGE in-gel assay. Protein concentration was assessed by Bradford assay, using BSA as standard. Purified samples were subjected to metal analysis before any further experiments (see section 2.11).

2.7.6. Size-exclusion chromatography - multi-angle light scattering (SEC-MALS)

The absolute molar mass of protein in solution was determined using size-exclusion chromatography combined with multi-angle light scattering analysis (SEC-MALS). Protein samples (100 µl; 1 mg·ml⁻¹) were loaded onto a Superdex 200 increase 10/300 GL column, in either 20 mM Tris pH 7.5, 150 mM NaCl for holo-enzymes, or in 20 mM Tris pH 7.5, 150 mM NaCl, 5 mM EDTA buffer for apo-proteins, and resolved at 0.5 ml·min⁻¹ using an ÄKTA FPLC system. Samples eluting from the column passed through a DAWN HELEOS II light scattering detector (Wyatt Technology), coupled to an Optilab T-rEX refractive index detector (Wyatt Technology). Data were collected and weight averaged molecular mass was calculated based on refractive index and light scattering measurements using Astra 6 software (Wyatt Technology).

2.7.7. Protein extraction from *Staphylococcus aureus* cells

S. aureus total protein cell extracts were prepared using freeze-grinding under liquid nitrogen. Cells were harvested from 500 ml-1000 ml large-scale, 6-hour cultures by centrifugation at 4000 g for 20 minutes at 4°C. Harvested cells were washed twice in 20 mM Tris pH 7.5, 10 mM EDTA, and for the third, final wash 20 mM Tris pH 7.5 buffer was used to remove EDTA. Collected pellets were resuspended in 20 mM Tris pH 7.5 and mechanically lysed using pestle and mortar under liquid nitrogen. Thawed, ground material was centrifuged (4000 g, 20 minutes, 4°C) to remove cell debris, and the resulting supernatant was subjected to ultracentrifugation at 48,384 g, 30 min, 4°C. If required, buffer exchange was applied by centrifugal ultrafiltration (Amicon Ultra15, 10 kDa MWCO, Millipore).

Whole cell lysates of *S. aureus* small-scale cultures were prepared using a Biospec Mini-Bead Beater 16, following a previously described protocol (Valderas & Hart, 2001), which was also used, with modification, for isolation of total DNA (section 2.2.1).

2.7.8. Affinity chromatography

The StrepTrapTM HP (GE Healthcare) and ANTI-FLAGTM M2 agarose (Sigma-Aldrich, UK) systems were used to detect and purify tagged SaSOD proteins using affinity chromatography. The target proteins with affinity tags, N'-FLAG-SaSodA, SaSodM-StrepII-C', were constitutively

expressed in *S. aureus* SH1000 $\Delta sodA$ and SH1000 $\Delta sodM$ background strains, respectively. Cell extracts were prepared using freeze-grinding under liquid nitrogen (as described in section 2.7.7), using 20 mM Tris pH 8.0, 150 mM NaCl, 1 mM EDTA as a lysis buffer. Thawed, ground material was centrifuged (4000 g, 20 minutes, 4°C) to remove cell debris, and the resulting supernatant was filtered through a 0.45 μm membrane filter. Chromatographic separation steps were performed at room temperature using a manual peristaltic pump or gravitationally using PolyPrep columns (BioRad, UK).

StrepII-tagged proteins were specifically and reversibly bound to StrepTactin Sepharose (ligand, engineered streptavidin). The soluble protein extract was applied to the StrepTrap column (GE Healthcare), previously washed with 3 CV of water and equilibrated with 3 CV of 20 mM Tris pH 8.0, 150 mM NaCl, 1 mM EDTA buffer, and then the unbound material was washed out of the column with this same buffer. A specific StrepII-tag competitor, 2.5 mM desthiobiotin (PanReac AppliChem) in 20 mM Tris pH 8.0, 150 mM NaCl, 1 mM EDTA buffer, was used for elution using 1 ml fractionation. The collected fractions were analysed for purity by SDS-PAGE, and for metal content by ICP-MS (see section 2.11).

Purification of FLAG-tagged proteins was performed using the agarose resin-conjugated anti-FLAG-tag monoclonal antibody, clone M2 (Sigma-Aldrich, UK). Cell extracts were prepared using the freeze-grinding method (see section 2.7.7) under liquid nitrogen, followed by ultracentrifugation and filtration (0.45 μm membrane filter). Resin was packed into PolyPrep column (Bio-Rad, UK) and prepared by passing 3 CV of 100 mM glycine, pH 3.5 through the column to remove any contaminants blocking the binding sites. Following column equilibration with 10 CV of 20 mM Tris, 150 mM NaCl, pH 7.5 buffer, the protein sample was loaded onto the column under gravity flow. Multiple passes over the column were performed to improve the binding efficiency. Unbound material was washed out of the column with 20 mM Tris, 150 mM NaCl, pH 7.5 buffer. The bound FLAG-tagged protein was eluted from the column with 150 $\text{ng}\cdot\mu\text{l}^{-1}$ FLAG peptide. Tag cleavage was not required prior to further use of the protein. Collected fractions were analysed for purity by SDS-PAGE (see section 2.8.1) and metal content by ICP-MS (see section 2.11).

2.8. Polyacrylamide gel electrophoresis (PAGE), staining and visualisation

2.8.1. Sodium dodecyl sulphate-polyacrylamide gel electrophoresis (SDS-PAGE)

The expression and purity of proteins were assessed using sodium dodecyl sulphate-polyacrylamide gel electrophoresis (SDS-PAGE). All Tris-glycine SDS-polyacrylamide gels were prepared using the Mini-PROTEAN Handcast system (Bio-Rad) with 1 mm spacers. The gels consisted of a top layer of 5 % stacking gel (5 % (w/v) acrylamide:bis-acrylamide (Bio-Rad, UK), 125 mM Tris pH 6.8, 0.1 % (v/v) SDS, 0.1 % (v/v) ammonium persulfate (APS) and 0.04 % (v/v)

N,N,N',N'-tetramethylene diamine (TEMED, Melford) and a bottom layer of 12 % (w/v) or 15 % (w/v) resolving gel (12 - 15 % (w/v) acrylamide/bis-acrylamide, 375 mM Tris pH 8.8, 0.1 % (w/v) SDS, 0.1 % (w/v) APS and 0.04 % (v/v) TEMED).

Protein extracts were prepared in Laemmli sample buffer (50 mM Tris pH 6.8, 2% (w/v) SDS, 10% (v/v) Glycerol, 0.1% (w/v) Bromphenol Blue and 100 mM DTT) by incubation at 95°C for 10 minutes. Gels were run at a constant voltage (180 V) using the Mini-PROTEAN Tetra cell system and PowerPac Basic power supply (Bio-Rad) in a Tris-Glycine running buffer (25 mM Tris pH 8.3, 250 mM glycine, 0.1 % (w/v) SDS). PageRuler protein ladder (Thermo-Fisher Scientific, UK) or SigmaMarker™ low range protein ladder (Sigma-Aldrich, UK) were used as the molecular weight markers. Resolved proteins were stained in-gel with Coomassie blue G-250-based gel stain, InstantBlue™ (Expedeon, UK) for 1 hour. Images of the gels were acquired using Bio-Rad ChemiDoc system with white light conversion screen.

2.8.2. Non-denaturing- polyacrylamide gel electrophoresis (Native-PAGE)

In order to verify native protein oligomeric state, charge and activity, proteins were resolved by PAGE in a non-denaturing, native conditions. 10 % (w/v) or 12 % (w/v) Tris-glycine native-polyacrylamide gels were prepared following previously described protocol (2.8.1), in the absence of SDS detergent. To eliminate a change in pH between two layers of a native gel, 5 % (w/v) stacking gel consisted of 125 mM Tris pH 8.8, 5 % (w/v) acrylamide:bis-acrylamide, 0.1 % (w/v) APS and 0.04 % (v/v) TEMED. Protein samples were prepared in a non-reducing, non-denaturing sample buffer (50 mM Tris pH 8.8, 10 % (v/v) Glycerol, 0.1 % (w/v) Bromphenol Blue), to maintain the secondary structure and native charge density. Gels were run at a constant voltage (180 V) using Mini-PROTEAN Tetra cell system and PowerPac Basic power supply (Bio-Rad) in a Tris-Glycine native running buffer (25 mM Tris pH 8.3, 250 mM glycine). Resolved proteins were stained in-gel with InstantBlue™ for 1 hour and visualised using Bio-Rad ChemiDoc system with white light conversion screen. Protein activity was verified using SOD-specific negative staining described in detail in section 2.9.1.

2.9. SOD activity assays

Superoxide dismutase activity was assessed using qualitative and quantitative methods. Both in-gel and spectrophotometric assays are based on the inhibition of reduction of yellow nitroblue tetrazolium (NBT) to dark blue precipitate (formazan) by photochemically-generated superoxide in the presence of superoxide dismutase.

2.9.1. In-gel assay

SOD activity was assessed qualitatively in-gel by the NBT (Sigma-Aldrich, UK) negative staining of purified protein samples or crude cell extracts, resolved on non-denaturing 10 % (w/v) or 12 %

(w/v) polyacrylamide gels (Beauchamp & Fridovich, 1971). Resolved proteins were stained in-gel with NBT-riboflavin stain consisting of 0.5 mM NBT, 28 mM TEMED, 28 μ M riboflavin in 100 mM sodium phosphate pH 7.0 buffer. Staining was performed by incubation of the gel, soaked in 20 ml of NBT-riboflavin stain, on a rotary shaker at room temperature in the dark. Assay visualisation was initiated by exposing the gel to bright white light. Under light exposure (2-5 minutes), the riboflavin underwent TEMED-catalysed reduction, leading to production of superoxide. NBT in-gel was reduced by superoxide to a dark-blue formazan precipitate. The presence of SOD activity, that scavenges superoxide and, in consequence prevents the formation of formazan, was observed as an achromatic zone on a dark blue background. The assay results were captured by scanning the stained and developed gels using Bio-Rad ChemiDoc system with a white light conversion screen and then inverting display to enhance the view of activity zones.

2.9.2. Peroxide inhibition assay

Inactivation of Fe-SODs by hydrogen peroxide was used as one of the indicative tools to determine the enzyme's metal content in-gel. Protein samples were resolved in native conditions with Native-PAGE on two gel replicas. Following Native-PAGE and prior to NBT-riboflavin SOD activity staining processes, one gel was soaked in 20 mM H_2O_2 solution for 30 min with shaking at room temperature and the control gel was incubated in water, in the same conditions. After incubation gels were rinsed with distilled water, and the remaining process of SOD activity staining was followed as described in section 2.9.1.

2.9.3. Liquid assay

The enzymatic activity of SOD proteins was determined quantitatively using a commercial SOD Assay Kit-WST (Sigma-Aldrich, UK). The assay utilizes water-soluble tetrazolium salt, WST-1 that produces a water-soluble formazan dye upon reduction with a superoxide anion generated in the system by xanthine oxidase (XO) activity.

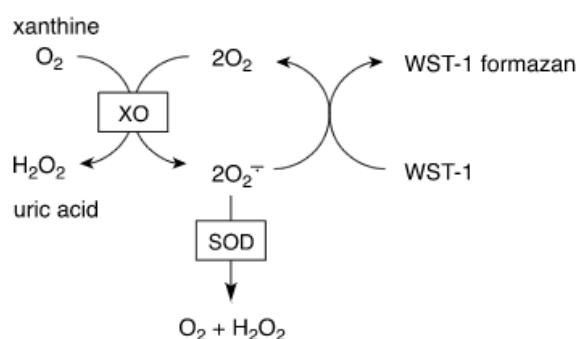


Figure 2.1 SOD assay Kit-WST reaction.

The rate of the reduction of WST-1 is inhibited by SOD, therefore the IC_{50} (50% inhibition of WST-1 reduction) activity of SOD was determined with a colorimetric method by monitoring 450

nm absorbance of WST-1 formazan product in relation to known concentrations ($\text{U}\cdot\text{ml}^{-1}$) of SOD standards. The assay was set up following the manufacturer's instructions, in a flat-bottom microplate. Results were acquired using a plate reader spectrophotometer (BioTek™ ELx800™). The sigmoidal fit of the inhibition curve (see Figure 2.2) was generated with the Origin software (OriginLab, Northampton, MA) using a standard 4-parameter logistic model (see Equation 2.1), where x_0 = center, p = power, A_1 = initial Y value, A_2 = final Y value; The y value at x_0 is half way between the two limiting values A_1 and A_2 (IC_{50}).

$$y = A_2 + \frac{A_1 - A_2}{1 + \left(\frac{x}{x_0}\right)^p}$$

Equation 2.1 A standard 4-parameter logistic model used for the sigmoidal fit of the inhibition curve.

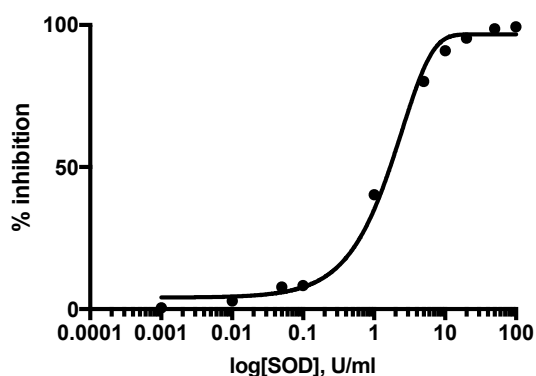


Figure 2.2 A representative inhibition curve (standard 4-parameter logistic model used for the sigmoidal fit).

Specific activity was expressed in terms of enzyme units per mg protein ($\text{U}\cdot\text{mg}^{-1}$). Protein concentration was determined by Bradford assay and corrected by amino acid analysis (see section 2.13). The amount of protein used for the assay was optimised to fit within a linear range closest to 50 % inhibition of WST-1 reduction, based on a standard curve. The standard curve of known U ml^{-1} concentration was prepared using commercially available recombinant superoxide dismutase from bovine erythrocytes and *E. coli* Mn-SOD.

2.10. Western blotting

Protein samples were resolved by SDS-PAGE and transferred to a nitrocellulose membrane in wet transfer (Bio-Rad Mini Trans-Blot Cell, 30 V overnight in a cold-room) or semi-dry transfer (Bio-Rad Trans-Blot Turbo 25 V, 30 min) system according to manufacturer's protocols. Wet transfer was performed in the Towbin buffer (25 mM Tris, 192 mM glycine, pH 8.3, 20 % (v/v) methanol), whereas semi-dry protocol was carried out in the Bjerrum-Schafer-Nielsen buffer (48 mM Tris, 39 mM glycine, pH 9.2, 20 % (v/v) methanol). Efficiency of the transfer of proteins from gel to membrane was assessed by reversible Ponceau S (Sigma-Aldrich, UK) staining of a membrane. Membrane after transfer was incubated in filtered 5 % (w/v) milk, 50 mM Tris, pH 7.6,

150 mM NaCl, 0.1 % (v/v) Tween-20 buffer (TBST) for 1 hour at room temperature to block non-specific binding of antibodies to membrane followed by 1-hour or overnight incubation with primary antibody solution in 5 % (w/v) milk-TBST at 4°C. After incubation with primary antibodies, membrane was rinsed 3x10 min with TBST buffer to remove unbound antibodies. Subsequently membrane was incubated with secondary horseradish peroxidase (HRP) conjugated antibodies in 5 % (w/v) milk-TBST for 1 hour at 4°C. The membrane was finally washed 3x10 min with TBST buffer and 1x10 min in TBS buffer. Detection of chemiluminescent signal was carried out using Clarity™ Western ECL Blotting Substrate (Bio-Rad) according to manufacturer's instructions and visualised using Bio-Rad ChemiDoc XRS+ system.

2.11. Inductively coupled plasma mass-spectrometry (ICP-MS)

Inductively coupled plasma mass spectrometry (ICP-MS) technique was used to identify and quantify the concentrations of metals in protein and cell samples (Ammann, 2007). Samples, prepared by dissolving in nitric acid (Suprapur, Merck), containing known concentration of matrix-matched internal metal standards (20 µg·L⁻¹ of ⁵⁹Co and ¹⁹⁵Pt or ¹⁰⁹Ag and ¹⁹⁵Pt) were loaded with an auto-sampler (Cetac 900) onto the instrument (Thermo x-series) operating in collision cell mode (CCT), using 3.0 ml·min⁻¹ flow of 8% (v/v) H₂ in He as the collision gas. Following sample ionisation within an argon plasma (99.99% purity), ions with specific mass/charge ratios were quantified by comparing the number of ions colliding with the detector during analysis of the unknown samples to those detected during analysis of elemental standards of the target ions (⁵⁵Mn, ⁵⁶Fe, ⁵⁹Co, ⁶⁵Cu, ⁶⁶Zn).

The samples were analysed, each in triplicate using the peak-jump method (100 sweeps, 20-30 ms dwell time on 3-5 channels per isotope, separated by 0.02 atomic mass units) and compared to elemental standards using a standard curve.

2.11.1. *Elemental analysis of purified, recombinant and native proteins*

Purified recombinant protein samples analysed by ICP-MS were diluted 50 or 5-fold in 2.5% (v/v) Suprapur HNO₃ containing 20 µg·L⁻¹ Co and Pt, whereas purified tagged proteins were diluted 10-fold in 2.5% (v/v) Suprapur HNO₃ containing 20 µg·L⁻¹ Ag and Pt as internal standards. Standard curves of the target transition metals (⁵⁵Mn, ⁵⁶Fe, ⁵⁹Co, ⁶⁵Cu, ⁶⁶Zn) were prepared using metal standard solutions (VWR) at concentrations of 0, 1, 5, 10, 50 and 100 µg·L⁻¹.

Stoichiometry of metal to protein was determined by comparing quantified analytes with the protein concentration (see section 2.13).

2.11.2. *S. aureus* SH1000 whole cell metal content analysis

Crude lysates of *S. aureus* cells were subjected to ICP-MS analysis to determine whole cell metal content. *S. aureus* SH1000 wild-type and deletion mutant strains ($\Delta sodA$, $\Delta sodM$, $\Delta sodA\Delta sodM$, $\Delta mntA$, $\Delta sodA\Delta mntA$, $\Delta sodM\Delta mntA$) were cultured in rich TSB medium or modified TM medium, as described in section 2.1.1. Cultures (50 ml) were grown in technical triplicate for 6 hours at 37°C with 185 rpm orbital shaking. All cultures were matched for the lowest OD_{600nm} and cells were harvested by centrifugation at 4000 g for 10 minutes at 4°C. Three sequential buffer washes with: 1) 20 mM Tris pH 8.0, 10 mM EDTA followed by 2) and 3) 20 mM Tris pH 7.5, 150 mM NaCl were performed to remove any growth media, or external metal contamination, before cell lysis. Collected pellets were digested for 24-72 hours, directly in high concentration (65%, 0.35 ml) nitric acid before dilution prior to ICP-MS analysis.

Acid-digested cell samples were clarified by centrifugation (13000 g, 10 min) and set up for ICP-MS analysis as described in section 2.11.2. Samples of supernatant collected after buffer washes were analysed alongside cell extracts to verify efficiency of removing extracellular metal contamination. Analyses were carried out using the same instrument setup as described in section 2.11.

2.12. *In vitro* refolding

In order to remove any natively bound metal ions protein solution was subjected to unfolding through dialysis in the presence of chaotropic agents and metal chelators, followed by refolding through the removal of denaturing agents.

2.12.1. *Preparation of metal-free dialysis tubing*

Metal free tubing used for dialysis (14 kDa MWCO, Sigma-Aldrich, UK) was prepared by processing pre-cut tubing through a series of solutions as follows: 10 minutes boiling in 2% (w/v) NaHCO₃, 1 mM EDTA, rinsing with MilliQ water, 10 minutes boiling in 1 mM EDTA solution. Dialysis tubing was cooled to room temperature, rinsed in water, and stored in sterile MilliQ water at 4°C.

2.12.2. *Optimisation of unfolding and refolding protocols*

Multiple unfolding protocols were tested in a process of optimisation of metal exchange. For Mn reconstitution, both proteins were denatured in 8 M urea and 1 mM EDTA for 1 hour at room temperature and renatured by dialysis against 20mM Tris pH 7.5, 1mM EDTA for 2 hours, followed by metal reconstitution in 20mM Tris pH 7.5, 100mM NaCl, 1 mM MnCl₂ at 4°C for 16 hours and removal of excess metal by dialysis against 20mM Tris pH 7.5, 100mM NaCl for 3 hours. Only the SodA protein was found to have incorporated Mn, but not to completely replace

its native Fe content after the size-exclusion step. Increasing the concentration of EDTA to 10 mM in unfolding buffer (Tu et al., 2012) was found to improve the content of Mn in SodA.

Several attempts were made to generate the Fe-free form of SodM including unfolding by dialysis against 6 M guanidine and 1 mM EDTA, 6 M guanidine and 25 mM EDTA, 6 M guanidine and 1 mM deferoxamine mesylate (DFM; iron chelator,) or incubation with 6 M guanidine and sodium citrate, 25mM Tris, 200mM NaCl pH 7.5 at room temperature for 24 hours ('A periplasmic iron-binding protein contributes toward inward copper supply', 2007). The first Fe-free preparations of SodM were produced by unfolding against 20 mM 8-hydroxyquinoline, 2.5 M guanidine hydrochloride, 5 mM Tris, and 0.1 mM EDTA at pH 3.8 and at 4°C for 12 hours (Kirby et al., 1980).

2.12.3. Preparation of apo-proteins

The protein sample was mixed in a 1:10 (v/v) ratio with denaturing buffer (Kirby et al., 1980), consisting of: 2.5 M Guanidine hydrochloride (Gdn-HCl), 20 mM 8-hydroxyquinoline (8-HQ), 5 mM EDTA, 20 mM Tris at pH 3.8. The mixture was enclosed into metal-free dialysis tubing and dialysed against 4 L of denaturing buffer for 8 hours at 4°C. To remove 8-HQ, protein was dialysed against 4 L of 2.5 M Gdn-HCl, 5 mM EDTA, 20 mM Tris buffer overnight. Denaturing agent, Gdn-HCl, was dialysed away against 20 mM Tris, 100 mM NaCl, 5 mM EDTA buffer, exchanged twice over a 24-hour period. Any precipitate was removed by centrifugation of the content of dialysis tubing at 21100 g for 10 minutes at 4°C. The supernatant was concentrated to a final volume of 0.5 ml, by centrifugal ultrafiltration in a 10 kDA MWCO Amicon Ultra-15 concentrator in 10-minute intervals at 4000 g. The concentrate was resolved by gel-filtration on analytical S200 10/300 column to verify oligomeric state of the proteins and tested for metal content by ICP-MS (see section 2.11.1).

2.12.4. Metal cofactor exchange

Substitution of an iron cofactor of recombinant protein purified from *E. coli* was achieved by *in vitro* unfolding and refolding in excess manganese. The SaSodA was unfolded overnight in metal depletion buffer (Tu et al., 2012; 8 M urea, 10 mM EDTA) to extract the bound iron, followed by 2-hour dialysis against 8 M urea, 1 mM MnCl₂, 5 mM Tris and 6-hour refolding by dialysis against 20 mM Tris pH 7.5, 100 mM NaCl buffer containing 1 mM MnCl₂. Excess of non-incorporated metal was removed by two steps of dialysis against 20 mM Tris, 100 mM NaCl pH 7.5 buffer over the course of 20 hours. SaSodM was prepared and unfolded by dialysis against 4 L of denaturing buffer consisting of 2.5 M Gdn-HCl, 20 mM 8-HQ, 5 mM EDTA, 20 mM Tris at pH 3.8, for 8 hours at 4°C. Subsequently to unfolding of the protein, chelators were removed by dialysis against 4 L of 2.5 M Gdn-HCl, 5 mM EDTA, 20 mM Tris buffer over-night. The introduction of the substituting cofactor was performed by dialysis against excess manganese for 2 hours (4 L buffer: 2.5 M Gdn-HCl, 10 mM MnCl₂, 20 mM Tris, 100 mM NaCl). Guanidine hydrochloride was removed by 3-

hour dialysis in 10 mM MnCl_2 , 20 mM Tris, 100 mM NaCl buffer. Excess of non-incorporated external metal was removed through two steps of dialysis against 20 mM Tris, 100 mM NaCl pH 7.5 buffer over the course of 20 hours. The content of the dialysis tubing was centrifuged at 21100 g for 10 minutes at 4°C. The supernatant was concentrated to a final volume of 0.5 ml, by centrifugal ultrafiltration in a 10 kDa MWCO Amicon Ultra-15 concentrator in 10-minute intervals at 4000 g . Concentrate was resolved by gel-filtration on analytical S200 10/300 column to remove any residual free metal and verify oligomeric state of the proteins and tested for metal content by ICP-MS (see section 2.11.1).

2.13. Determination of protein concentration

Protein concentration was routinely determined by use of the Bradford assay (Coomassie Plus protein assay; Thermo-Fisher Scientific, UK) or Pierce BCA protein assay (Thermo-Fisher Scientific, UK), in a microplate format according to manufacturer's instructions. Absorbance readings were taken at 595 nm and 562 nm respectively for the two different assays using a plate reader spectrophotometer (BioTek™ ELx800™), and protein concentration determined by comparison to a standard curve prepared from known concentrations of bovine serum albumin (BSA).

The concentrations of proteins were also determined by monitoring absorbance of aromatic residues at 280 nm ($A_{280\text{nm}}$), in a quartz cuvette with a UV-Vis Spectrometer, Lambda 35, (Perkin Elmer), using theoretical extinction coefficients $\epsilon_{A_{280\text{nm}}}$: SodA $\epsilon=48930 \text{ M}^{-1}\cdot\text{cm}^{-1}$, MW=22711.3 Da, SodM $\epsilon=51910 \text{ M}^{-1}\cdot\text{cm}^{-1}$, MW=23040.9 Da, values estimated with ProtParam, ExPasy.

To correlate outcomes of the different assays the 2.5 μM sample of purified SaSodA and 2.64 μM sample of purified SaSodM were analysed by Alta Biosciences Ltd, to determine their amino acid composition and verify the total protein concentration. The output of analysis (Table 2.8) represented the amino acid composition of the acid extract of the protein samples, with exception of cysteic acid, hydroxyproline, cystine and tryptophan, which were not-determined due to the limitations of the analysis type.

Residue name	Residue mass	SaSodA			SaSodM		
		µg/ml	No in sequence	µM	µg/ml	No in sequence	µM
Aspartic acid	115.10	5.21	26	1.74	5.89	29	1.76
Threonine	101.10	2.22	11	2.00	2.82	14	1.99
Serine	87.08	1.42	8	2.04	1.48	6	2.83
Glutamic acid	129.10	4.64	26	1.38	4.23	21	1.56
Proline	97.12	1.38	9	1.58	1.45	9	1.66
Glycine	57.05	1.17	12	1.71	1.46	11	2.33
Alanine	71.08	1.91	16	1.68	1.78	14	1.79
Valine	99.13	2.42	14	1.74	1.93	11	1.77
Methionine	131.20	0.127	2	0.48	0.86	6	1.10
Isoleucine	113.20	1.67	8	1.84	1.66	8	1.83
Leucine	113.20	3.88	18	1.90	3.98	18	1.95
Tyrosine	163.20	2.05	7	1.79	2.79	9	1.90
Phenylalanine	147.20	2.28	8	1.94	2.63	9	1.99
Histidine	137.10	6.02	8	5.49	5.88	8	5.36
Lysine	128.20	3.32	15	1.73	3.4	15	1.77
Arginine	156.20	1.18	4	1.89	1.4	4	2.24

Table 2.8 Amino acid analysis output.

2.14. Protein mass spectrometry

Identification of SodA was performed by MALDI-TOF peptide mass fingerprinting (PMF) by Dr Kevin Waldron (ICAMB, Newcastle University, UK) prior to my PhD project. Extracts of *S. aureus* cells were separated by anion exchange and size-exclusion chromatography. Collected fractions were resolved by SDS-PAGE and visualised using SyproRuby. Densitometry analysis of bands intensity was correlated with metal analysis of the corresponding fractions. Principal component analysis (PCA) was used to find correlation between the concentration of identified Mn pool and the abundance of individual proteins. Potential candidate proteins were resolved on 12 % SDS-PAGE and visualised using Coomassie G250 (Invitrogen, UK). Bands of interest were excised from the gel and purified. Trypsin digests of purified gel bands were analysed using a Voyager-DE (ABI) matrix- assisted laser desorption ionization time-of-flight (MALDI- TOF) mass spectrometer. Peptide mass fingerprints were analysed using the Mascot search tool (matrixscience.com), (Tottey et al., 2008).

Whole-protein mass analysis of the purified, recombinant SaSODs was performed by Dr Emma Tarrant (ICAMB, Newcastle University, UK) and Dr J. Gray (Pinnacle, Newcastle University, UK). The molecular weight (MW) of recombinant proteins was determined with a whole-protein mass protocol using an Applied Biosystems Voyager-DE STR matrix assisted laser desorption ionisation time-of-flight (MALDI-TOF) mass spectrometer (MS) system.

2.15. X-ray crystallography

2.15.1. *Initial screens and optimisation*

Protein samples of over 95 % homogeneity were concentrated to 10 – 20 mg·ml⁻¹ using centrifugal ultrafiltration (Amicon Ultra-15 10 kDa MWCO, Millipore and Vivaspin 500 10 kDa MWCO, Sartorius, UK). Initial crystallisation trials were performed using commercially available matrix screens: PACT, JCSG⁺ and Structure (Molecular Dimensions, UK) in 96-well MRC crystallisation plates (Molecular Dimensions), using the sitting-drop of vapour-diffusion method at 20°C. A Mosquito (TTP LabTech, UK) robot was used for setting up two sitting drops (100 nl + 100 nl and 200 nl + 100 nl of protein and crystallisation liquor, respectively) per condition, equilibrated against 80 µl of reservoir solution. Crystal plates were incubated at 20°C and periodically examined for formation of crystals using 16x optical zoom light microscope (Leica).

The initial conditions producing crystals were optimised for salt, polyethylene glycol (PEG) precipitant concentration and pH, using the hanging drop of vapour diffusion method at 20°C, in 24-well Linbro plates (Molecular Dimensions, UK). Drops were set manually at 1 µl + 1 µl and 2 µl + 1 µl of protein and crystallisation liquor, respectively per condition, equilibrated against 500 µl of reservoir solution. Crystals were harvested by Dr Arnaud Baslé (Newcastle University, UK) in a 20 % PEG-400 cryoprotectant and flash-frozen in liquid nitrogen.

2.15.2. *Data collection*

X-ray diffraction data were collected by Dr Arnaud Baslé (Newcastle University, UK) at the Diamond Light Source (DLS) synchrotron (Didcot, UK) on 5 trips: mx7864-57, mx7864-62, mx7864-67, mx9948-1, mx9948-22. The presence of the metal cofactors was evaluated by the fluorescence scans taken at the K edge of Fe, Mn and/ or Zn excitation wavelength allowing detection of peaks of metals coordinated in proteins, upon diffraction data collection. Anomalous difference maps were calculated using data sets collected above (high-energy remote) and/or below (low-energy remote) the Fe or Mn K-edge (peak) to confirm the presence or absence of the anomalous signal (Figure 2.3).

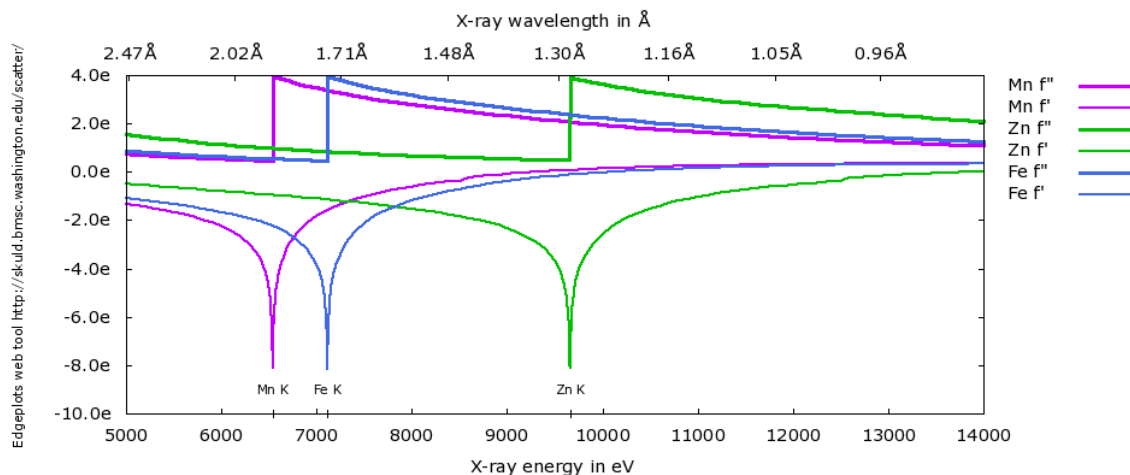


Figure 2.3 Anomalous Scattering Factors of Mn, Fe and Zn as a function of energy generated with http://skuld.bmsc.washington.edu/scatter/AS_form.html

The metal K-edge energies (keV) and corresponding wavelength (Å) of Fe (7.1120 keV, 1.7433 Å); Mn (6.5390 keV, 1.8961 Å) and Zn (9.6586 keV, 1.2837 Å).

2.15.3. Structure determination, refinement and validation

Structures of *S. aureus* SODs were determined by molecular replacement using Collaborative Computational Project (CCP4) software suit (Winn et al., 2011).

Data were processed and integrated using iMOSFLM (Battye et al., 2011) or XDS (Kabsch, 2010) and scaled with AIMLESS (Evans & Murshudov, 2013). Models were built using molecular replacement with MOLREP (Lebedev et al., 2008) or Phaser (Airlie J McCoy, 2007) and 1IDS (Cooper et al., 1995), 2RCV (Liu et al., 2007) as the search models. Anomalous difference Fourier maps were calculated with Fast Fourier Transform (FFT) using additional data sets collected above the metals' K-edge, (high-energy remote) and below the metals' K-peak, (low-energy remote). Final models were produced by the cycles of refinement (REFMAC5 (Murshudov et al., 2011)) and model-building using COOT (Emsley et al., 2010), Phenix (Adams et al., 2010) and PdbRedo (Joosten et al., 2012). MOLPROBITY (Chen et al., 2010) and Phenix were used to validate outcomes of modelling. Additional analysis of the structures was performed with PDBePISA (Proteins, Interfaces, Structures and Assemblies), (Krissinel & Henrick, 2007), PDBsum (Pictorial database of 3D structures in the Protein Data Bank), (Laskowski & Chistyakov, 2005) and CheckMyMetal (CMM), (Zheng et al., 2014). All graphic representation of structural models were created using PyMOL Molecular Graphics System (Schrödinger, LLC).

2.16. Tryptophan fluorescence measurements

Protein fluorescence measurements were performed using a Cary Eclipse Fluorescence Spectrophotometer (Varian Inc., Agilent Technologies). Samples of proteins at 10 μM

concentration in either 20 mM Tris, 150 mM NaCl buffer pH 7.5, 8 M urea or 6 M guanidine were analysed at room temperature, using 10 mm path length quartz cuvettes (Hellma). Excitation and emission band-pass slits were set to 5 nm width. Intrinsic tryptophan residues were excited at 285 nm. The emission spectra were recorded between 300 nm and 450 nm.

2.17. Circular dichroism spectroscopy

Circular dichroism (CD) data were collected using a JASCO J-810 spectropolarimeter with a PTC-4235 Peltier temperature controller. Spectra measurements were performed at a protein concentration of 2 μ M (300 μ l aliquot) in 10 mM sodium phosphate buffer, pH 7.0 at 20°C. The exchange of Tris and NaCl containing protein buffers for sodium phosphate buffer was performed to eliminate high absorbance in the far-UV region by these compounds, using Micro Bio-Spin P-6 columns (Bio-Rad), according to manufacturer's instructions. Wavelength scans were recorded within a far-UV range (185-260 nm), in 1 mm path length quartz cuvette (Hellma), at a scan rate of 100 nm \cdot min $^{-1}$, with a response time of 2 s, a data pitch of 0.2 nm and a bandwidth of 2 nm. For each sample 5 accumulated scans were averaged, corrected for buffer reference and then converted into mean residue ellipticity (MRE, θ). Deconvolution was performed using the CDSSTR program with a reference data set 4 (250-190 nm) on the DichroWeb (Whitmore & Wallace, 2004) server (<http://dichroweb.cryst.bbk.ac.uk>).

The thermal denaturation curves were measured by monitoring the absorbance change at 222 nm, between 20°C and 90°C, with 1°C per minute ramping rate in 1 mm path length cuvette. Raw data were converted to mean residue ellipticity (MRE₂₂₂, θ_{222}). Melting temperature (T_m) value was calculated from the maximum of the first derivative.

Mean residue ellipticity was calculated using following equation (Equation 2.2), where θ_{obs} is the observed ellipticity signal (deg), MRW is a Mean Residue Weight (Da; Molecular mass of a peptide chain/ (number of amino acids – 1), l is path length (cm) and c is concentration (mgml $^{-1}$).

$$\theta_{\lambda} = \frac{MRW \cdot \theta_{obs}}{10 \cdot l \cdot c}$$

Equation 2.2 Mean residue ellipticity.

The mid-points of the thermal denaturation curves, (T_m) were calculated by taking derivatives of the spectra, within Jasco J-810 software.

2.18. UV-Vis spectroscopy

Optical spectra of as-purified, reduced (by sodium dithionite) and oxidised (by potassium permanganate) protein samples were acquired using a Perkin-Elmer λ 35 spectrophotometer in a range of 200 - 800 nm, at room temperature. Measurements were conducted using 10 mm path length quartz cuvette (Hellma). Native datasets were collected for samples of proteins in 10 mM

sodium phosphate buffer, pH 7.0. Protein reduction was monitored spectrophotometrically upon equimolar titration of sodium dithionite into 0.15-0.3 mM native protein sample. Reduced proteins were subjected to buffer exchange for 10 mM sodium phosphate, pH 7.0 using centrifugal ultrafiltration (VivaSpin 500, 10 kDa MWCO, Sartorius) to remove sodium dithionite. Subsequently the samples were oxidized by incubation with 0.75 molar equivalents of potassium permanganate pH 7.5 (Sheng et al., 2012). Spectra of oxidized proteins were acquired upon permanganate addition and after 10, 20, 30, 45 and 60 min incubation. In order to determine the reducing effect of sodium ascorbate, fully oxidized samples were mixed with one molar equivalent of sodium ascorbate and optical spectra were recorded.

2.19. High-field high frequency Electron Paramagnetic Resonance (HF-EPR)

2.19.1. *Sample preparation*

Purified proteins samples for EPR were prepared in 20mM Tris pH 7.5, 150mM NaCl buffer. In order to remove free manganese contamination, an additional chelation step was performed by addition of EDTA to a final concentration of 10 mM and incubation at room temperature for 30 minutes. EDTA was removed by buffer exchange with centrifugal ultrafiltration (10 kDa MWCO) prior to the final concentration step. Concentrated samples were prepared with VivaSpin 500 (10 kDa MWCO) concentrators.

To reduce the oxidation state of manganese in the protein solution, samples were treated with a strong reducing agent, sodium dithionite. A 1 M stock of dithionite in 20 mM Tris pH 7.5 buffer was prepared and added to the protein solutions. Reduction was monitored by UV-Vis spectroscopy (section 2.18). To prepare fully reduced (MnII) samples, Mn-SodA was treated with 10-molar equivalents of dithionite and Mn-SodM with 2-molar equivalents of dithionite. Reduced protein samples were flash-frozen in liquid nitrogen and stored at -80°C.

2.19.2. *Hydrogen/Deuterium exchange*

Hydrogen/deuterium exchange was performed in preparation for ELDOR EPR experiments. Aliquots of proteins were diluted 10-fold in 20 mM Tris, 150 mM NaCl buffer prepared in deuterium oxide 99.9 atom % D (Sigma-Aldrich, UK), pH 7.5 adjusted with deuterium chloride 35 wt. % in D₂O, 99 atom % D (Sigma-Aldrich, UK). Following 30-minutes incubation at room temperature, protein samples were concentrated down to 50 µl total volume using VivaSpin 500 (10 kDa MWCO) and buffer exchange was carried out, keeping a 5:1 ratio of fresh deuterated buffer to the concentrate. Resulting deuterated proteins were subjected to dithionite treatment (stock prepared in deuterium oxide) following a general sample preparation protocol (see section 2.19.1). Protein samples were flash-frozen in liquid nitrogen and stored at -80°C.

2.19.3. **Experimental procedures**

Data collection, processing and analysis was performed by Dr Sun Un (Department of Biochemistry, Biophysics and Structural Biology, Institute for Integrative Biology of the Cell (I2BC), Université Paris-Saclay, CEA, Saclay, France).

The 94 GHz EPR (The field-sweep echo; FSECHO) and ELDOR-NMR spectra were obtained at 6 K (liquid helium) using a Bruker Elexsys II 680 EPR spectrometer, equipped with an Oxford Instruments CF935 flow cryostat. The EPR spectra were obtained by measuring the amplitude of a standard two-pulse Hahn echo ($t_p(\pi)=24$ ns and interpulse time of 400 ns) as a function of the magnetic-field. The ELDOR-NMR spectra were obtained by measuring the integrated two-pulse echo intensity detected at ν_{obs} as a function ν_{ex} .

	Cavity Tuning Frequency¹	t_{ex} (μs)²	π_{ex} (ns)³	π_{obs} (ns)⁴
¹⁴ N SQ, D _{zz}	ν_{obs}	20	1600	240
¹⁴ N SQ, D _{xx}	ν_{obs}	6	160	200
¹⁴ N DQ, D _{zz}	ν_{obs}	2	200	200
¹ H SQ, D _{zz}	$\nu_{\text{obs}}+\nu_{\text{NMR}}$	2	210	200
¹ H SQ, D _{xx}	$\nu_{\text{obs}}+\frac{1}{2}\nu_{\text{NMR}}$	2	200	200
¹ H DQ, D _{zz}	$\nu_{\text{obs}}+\nu_{\text{NMR}}$	2	70	200
Broad	$\nu_{\text{obs}}+\nu_{\text{1H,NMR}}$	2	-	200

Table 2.9 EPR experiments' acquisition parameters.

Acquisition parameters: ¹The cavity was over-coupled to the same extent for all samples; ²Length of excitation pulse; ³ π -pulse time measured at the $\nu_{\text{obs}}+\nu_{\text{NMR}}$ for SQ and $\nu_{\text{Detect}}+2\nu_{\text{NMR}}$ for DQ spectra; ⁴ π -pulse time at observation frequency (ν_{obs}).

2.20. Bioinformatics and phylogenetics

2.20.1. **Database searches and identification of SOD homologues**

Homologues of superoxide dismutase (SOD) were identified using Blast (Altschul et al., 1990) and HMM profile searches (Eddy, 2001). Amino acid sequences of *S. aureus* SODs were downloaded from online GenBank (NCBI) databases and used as queries in BlastP and tBlastN searches performed using an online NCBI Blast server (Altschul et al., 1990). HMM profiles for HMMER profile searches (Eddy, 2001) were, downloaded from Pfam-A database. HMM profile searches were performed with an online HMMER server (Eddy, 2001).

2.20.2. **Multiple sequence alignments and phylogenetic analyses**

MAFFT v7.271 (Kato & Standley, 2013) in the --auto mode, was used to generate multiple sequence alignments (MSA) of SODs. MSAs were trimmed with the trimAL 1.2rev59 (Capella-Gutiérrez et al., 2009) using manual mode with gap threshold (-gt) set to 0.4. PhyloBayes-MPI v1.7 (Lartillot et al., 2009) was used to generate bayesian phylogenies. All the PhyloBayes

analyses were performed in two chains run in parallel (each on 6 CPUs) until convergence. The convergence was determined using the bpcomp and tracecomp programs of the PhyloBayes package according to the manual (Lartillot et al., 2009).

Seaview (Gouy et al., 2010), Jalview (Waterhouse et al., 2009), and ALINE (Bond & Schüttelkopf, 2009) were used for formatting and analysis of the multiple sequence alignments.

Chapter 3. SaSodA is Mn-specific, whereas SaSodM is cambialistic

3.1. Introduction

Superoxide dismutase (SOD) proteins are involved in the oxidative stress response systems of most of the known organisms across all domains of life (Fink & Scandalios, 2002; Wolfe-Simon et al., 2005; Miller, 2012). They are classified based on their metal cofactor into a Mn/Fe-dependent family, a Cu,Zn-dependent family and a Ni-dependent family of enzymes. SODs are characterised by a high degree of conservation within the specific families, but not between families.

The studies conducted on these proteins from various organisms revealed that manganese and iron superoxide dismutase usually possess very high metal specificity for catalytic activity, or more rarely presents cambialistic properties, that is the capacity to function with either Fe or Mn. However, all characterised members of Mn/Fe family are highly homologous in sequence and share highly similar structural organisation, including the coordination of metal in the active site. Often multiple copies of SOD enzymes with different metal specificity are expressed by a single cell, and both can localise to the same cellular components; for example *E. coli* possesses two Fe/Mn-dependent superoxide dismutases; a constitutively expressed Fe-SOD, and a Mn-SOD whose expression is induced by high aeration and ROS. These are highly metal-specific enzymes, which could suggest that they may have evolved to confer cell adaptability to changes in metal content or specific growth conditions. The high level of similarity between the two types of enzymes as well as their ability to bind both cofactors makes them prone to mismetalation. *E. coli* Mn-SOD metal binding selectivity was demonstrated to be metal availability-dependent (Beyer et al., 1991), however only binding of the cognate metal (Mn) confers catalytic activity of the enzyme (Whittaker, 2003).

Most predictions and annotation of metal specificity is often based on the analysis of the amino acid sequence, which is highly conserved in this family of proteins. The short sequence of the protein (~200 amino acids) with the high level of identity makes it inherently difficult to accurately assign metal-determining residues. Multiple attempts have been made to assign these signatures, however, it has proven inconsistent (Parker & Blake, 1988; Clements et al., 1999; Yamano & Maruyama, 1999; Wintjens et al., 2004; Wintjens et al., 2007; Sheng et al., 2014).

The two superoxide dismutases of *S. aureus* have been classified as Mn-dependent enzymes. This initial classification was firstly based on sequence analysis and similarity to Mn-SOD enzymes. Further, the activity arising from Mn-reconstitution of metal-depleted wild type lysates (Clements et al., 1999), and Mn-dependent growth studies of isogenic mutants (Karavolos et al., 2003) indicated the Mn-dependence of the SaSODs. However, the relative, though inconsistent, sensitivity to hydrogen peroxide, which is regarded as a specific Fe-SOD inhibitor

(Valderas & Hart, 2001; Clements et al., 1999), hinted the possibility that SodM may utilise Fe as a cofactor.

For a comprehensive characterisation of SaSODs and to clarify their metal-specific activity, the following chapter will present work addressing their evolutionary relations, and the biochemical and initial biophysical analyses of recombinant proteins, including identification, quantification and correlation of the metal content with catalytic activity.

3.2. Results and discussion

The phylogenetic data presented in this chapter indicates the possible origin of the two paralogues of the superoxide dismutase, encoded by *sodA* and the *sodM* in *S. aureus* genome.

The *in vitro* characterisation of the two superoxide dismutases from *S. aureus*, SodA and SodM, gives new insight into the metal-specific activities and the physical properties differentiating these proteins. Addressing the difficulty in bioinformatically predicting metal usage by SOD enzymes, this work aimed to investigate metal specificities of SodA and SodM using recombinantly produced proteins. Collected data demonstrated that SaSODs could bind, and be catalytically active, with both permitted Fe and Mn cofactors *in vitro*. However, SodA was found to present strong Mn preference reflected by its enzymatic activity, whereas SodM demonstrated cambialistic properties, and the higher degree of chemical stability.

Sections of the work presented in this chapter have been published as part of my second-author manuscript, in collaboration with the group of Dr Kehl-Fie:

Garcia, Y.M., Barwinska-Sendra, A., Tarrant, E., Skaar, E.P., Waldron, K.J. & Kehl-Fie, T.E. (2017) A Superoxide Dismutase Capable of Functioning with Iron or Manganese Promotes the Resistance of *Staphylococcus aureus* to Calprotectin and Nutritional Immunity. *PLoS Pathogens*. 13 (1), e1006125.

3.2.1. Staphylococcus aureus possesses two SOD proteins detected as three bands of activity

The superoxide dismutase protein SodA is highly conserved and spread across all domains of life. The presence of multiple copies of SodA is observed amongst many bacteria, including Firmicutes. Taxonomic distribution analysis, using profile hidden Markov Models (HMMER) across the Firmicutes tree derived from the NCBI taxonomy database, indicates the highest number of 3 copies present in 14 representative proteomes, such as those of *Clostridium saccharolyticum*, *Bacillus anthracis*, *Bacillus cereus* or *Bacillus thuringiensis*. Two copies of SodA

are found in 120 out of 711 proteomes analysed (UniProt-ref Prot, database version 2017_07), and amongst these, only in one species from the staphylococci, namely *Staphylococcus aureus*.

SOD activity was assessed in-gel by the nitroblue tetrazolium (NBT-riboflavin) negative staining of soluble lysates of various *S. aureus* wild type strains (SH1000, Newman, USA300, ATCC12600, and PM64) resolved on non-denaturing 15% polyacrylamide gels (Beauchamp and Fridovich, 1971). The assay is based on the inhibition of reduction of yellow NBT to dark blue formazan by photochemically-generated superoxide in the presence of superoxide dismutase. Presence of SOD activity is observed as an achromatic zone on a dark blue background. The assay results can be visualised by scanning the stained and developed gels and inverting display to enhance the view of activity zones.

The two superoxide dismutases of *S. aureus*, denoted SodA and SodM, combine to form three SOD activity zones *in vivo*, that can be observed by resolving *S. aureus* cell extracts by non-denaturing PAGE (Native-PAGE) and using in-gel staining assay (Figure 3.1). The three bands represent activities of SodA and SodM homodimers, and a SodA/SodM heterodimer, which is a mixture of both proteins that migrate on the gel between two homodimers (Valderas and Hart, 2001).

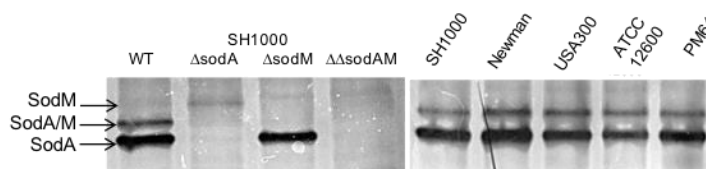


Figure 3.1 In-gel assay of SOD activity of *Staphylococcus aureus* cell extracts.

Detection of SOD activity in *Staphylococcus aureus* strains on a non-denaturing polyacrylamide gel stained for SOD activity. Lanes: 1, *S. aureus* wild type; 2, *S. aureus* *sodA::erm*; 3, *S. aureus* *sodM::tet*; 4, *S. aureus* *sodAsodM*; 5-9 selection of wild type strains of *S. aureus*. Lanes contain 15 μ g of total proteins in crude extracts of aerobic cultures.

3.2.2. Bioinformatics and phylogenetic analyses of the origin of SaSODs

Bayesian phylogenetic analyses of Fe/Mn-SOD homologues identified four major, strongly supported groups, separated by long branches (posterior probabilities of 1), (Figure 3.2 A). The overall tree topology resembled that of the previously published phylogenies (Kirschvink et al., 2000). Sequences of the plastid SODs (e.g. three SODs from *Arabidopsis thaliana*) grouped together with cyanobacterial SODs (e.g. *Nostoc punctiforme*) in group 2, consistent with the endosymbiotic theory of origin of this eukaryotic organelle. Mitochondrial SODs, including that from *Homo sapiens*, grouped together with sequences from chlamydiae in group 4. Most of the archaeal sequences were in group 3 although some were also found in group 1. Sequences of the two *E. coli* SODs were found in group 1 (Mn-SodA) and group 2 (Fe-SodB), respectively.

In the published phylogenetic research, metal-specificities of SODs available at the time were mapped onto a phylogenetic tree, and it was observed that SODs that utilise the same metal grouped together (Kirschvink et al., 2000). To further test this, herein, the available metal-specificities of SODs (Figure 3.2 A), including some characterised more recently, were mapped onto the generated phylogenetic tree. Similar to the previous observations (Kirschvink et al., 2000), Fe-specific SODs were found mostly in groups 2 and 3. Group 4 consisted exclusively of the Mn-SODs; whereas group 1, distinct from the published research (Kirschvink et al., 2000), contained Mn-specific SODs with a single (more recently characterised) Fe-specific SOD from *Bacillus anthracis* (Tu et al., 2012). The cambialistic SODs were broadly distributed across the tree, and were present in groups 1, 2, and 3; but not in group 4 (Figure 3.2 A).

Based on the observed distribution of the Fe-, Mn-SODs, and Fe/Mn-SODs, three alternative hypotheses can be formulated. The first hypothesis is that the last common ancestor of each major group (1, 2, 3 and 4) was cambialistic followed by sub-functionalization into Fe-, or Mn-specific modern SODs, respectively, after descent from that ancestor. In that case, many cambialistic enzymes could present an ancestral phenotype. In an alternative hypothesis, the ancestor of each major group was Fe- or Mn-specific followed by adaptations to evolve cambialism in some SODs. The third hypothesis is that metal specificity of SODs is flexible and can be changed upon the selective pressures of the environment, such as relative bioavailability of Fe and Mn.

In the published research, based on the comprehensive analyses of geological and phylogenetic data (Kirschvink et al., 2000), it was hypothesized that in the early reductive atmosphere of the Earth, a high abundance of soluble Mn and Fe could have favoured a cambialistic ancestral-SOD (Kirschvink et al., 2000). The increase in the oxygenation of the Earth's atmosphere and oceans led to the decreased bioavailability of both metals (Kirschvink et al., 2000). Lowered concentrations of the soluble metal ions may have provided a selective pressure for the sub-functionalization of SODs towards Mn- or Fe-specificity, possibly depending on metal availability within the specific habitat. At the same time, it is likely that presence of higher concentrations of the oxygen in the atmosphere increased the importance of the oxygen-stress response pathways including SOD. Although such comprehensive studies (Kirschvink et al., 2000) can provide evidence supporting the hypothesis of the ancestral cambialistic SOD, interpretation of phylogenetic analyses as well as geological data (especially dating) can have a high level of uncertainty. The complex topology of the SOD protein tree often does not follow predicted species trees. For example, whereas the Mn/Fe-SOD from the *Bacillus anthracis* (Tu et al., 2012) grouped together with *Staphylococci* (group 1), the *B. anthracis* Fe-SOD (Tu et al., 2012) was placed on one of the unresolved (polytomic) branches in group 1, while the third *B. anthracis* SOD (of uncharacterised metal-specificity) grouped together with sequences from archaea such as *Candidatus bathyarchaeota*, and bacteria including *Clostridium botulinum* in group 3. The observed tree topology may be a result of the short length of SOD protein sequences (on average approximately 200 amino acids) that provides a small sample size for the phylogenetic inference algorithms. The possibility of a complex evolutionary history of SODs

including multiple gene loss and gene gain (e.g. by gene duplication or by lateral gene transfer) events, as well as convergent evolution, cannot be excluded and will be further investigated following on from this work.

Staphylococcus aureus provides an example of an organism with more than one SOD. Most of the experimental data presented so far pointed at the Mn-specificity of both SaSODs (Clements et al., 1999; Valderas & Hart, 2001; Karavolos et al., 2003), however a possible cambialistic character of the SaSodM was hypothesized based on the relative sensitivity to hydrogen peroxide (Clements et al., 1999; Karavolos et al., 2003) and the relative contribution to resisting host-imposed manganese starvation mediated by calprotectin (Kehl-Fie et al., 2011).

To better understand the origin of the SaSODs, the broad sampling of SODs from all major phylogenetic groups of staphylococci (Lamers et al., 2012) including four *S. aureus* isolates (Figure 3.2 A, B) were analysed. All *Staphylococcus* sequences used in the analyses grouped together within group 1 alongside sequences from some eukaryotes (e.g. *Perkinus marinus*, *Chlamydomonas* sp., *Encephalitozoon* sp.), some archaea (e.g. *Nitrosopumilus* sp.), as well as many bacteria, including *E.coli* SodA. Despite the overall poor resolution within group 1, all *Staphylococcus* sequences grouped together with very strong support (posterior probability of 1). The single SOD from *Macrococcus caseoliticus*, the closest relative of staphylococci used in the analyses, formed a highly supported (posterior probability of 0.99) outgroup to the staphylococci, which is consistent with vertical inheritance of all the analysed SODs within the *Macrococcus/Staphylococcus* group. SaSodAs and SaSodMs (Figure 3.2B) formed two separate and strongly supported groups (posterior probabilities of 1), indicating that the last common ancestor of all analysed *S. aureus* species encoded two SODs in its genome. SaSodAs and SaSodMs grouped together with other *staphylococcal* SOD sequences on a weakly supported (posterior probability of 0.54) polytomic (unresolved relationship between three or more relatives) branch. The observed polytomy is likely to be due to a high sequence identity (83.12%) between the *Staphylococcus* SODs resulting in a low level of sequence variation that can be used to resolve the relationships.

Although the relationship between the SaSodM and the SaSodA was unresolved, thorough analyses of the 9310 (reference assemblies) *Staphylococcal* genomes using BlastP, tBlastN (Altschul et al., 1990), and HMMER profile searches (Eddy, 2001) did not identify any *Staphylococcus* species other than *S. aureus* that encoded more than one SOD gene. All 8167 analysed *S. aureus* genomes encoded a single SaSodM and a single SaSodA homologue. The presence of the two SODs in *S. aureus* but not in other staphylococci or *Macrococcus*, together with the grouping of the two SaSods within the *Staphylococcus* clade, suggests that the presence of SaSodM and the SaSodA in the *S. aureus* genomes resulted from a gene duplication of a single SOD gene in the last common ancestor of the analysed *S. aureus* strains (paralogy). The SaSodA sequences group on a relatively short branch and share higher identity (87.79%) with SODs from other *Staphylococcus* species indicating that the SaSodA is the more conserved paralogue. Conversely, SaSodM sequences group on a longer branch and share lower level of

sequence identity (74.46%) with SODs from other *Staphylococcus* species, suggesting that the SaSodM is the more divergent paralogue.

Following the gene duplication event, either one of the copies can be lost, both copies can continue performing the same function as their ancestor, two copies can specialise in performing a subset of the functions of the ancestral gene (sub-functionalisation), or one of the copies can evolve new functionality (neo-functionalisation) while the second copy retains functions of the ancestral gene. Based on the phylogenetics and the sequence analyses it can be hypothesized that the more divergent SaSodM has undergone a neo-functionalization while SaSodA performs the ancestral SOD functions.

To further test the hypothesized neo-functionalization of SaSodM, the protein sequences of SODs from staphylococci were aligned (Figure 3.3; arbitrary numbering of amino acid positions based on *B. subtilis* SOD sequence in multiple sequence alignment, MSA) with the SODs from the representatives of the major phylogenetic groups identified by phylogenetic analyses (Figure 3.2A). It was previously hypothesized that the metal-specificity of SODs can be predicted based on the presence or absence of specific amino acid residues (Wintjens et al., 2008). To test the reliability of these predictions, the proposed metal-specificity determinants (according to (Wintjens et al., 2008)) were mapped onto the alignment (Figure 3.3). Many of the proposed residues provided a relatively good prediction of metal-specificities, although in each case, at least one exception was found. For example, Met105 (position 105 in MSA) provided a good prediction of Mn-specificity with an exception of *S. cerevisiae* SOD. No obvious patterns enabling prediction of cambialism were observed. The observed variation within the proposed determination sites suggest that prediction of metal-specificity based on the presence or absence of these sequence features will not be sufficient. Consistent with that, the published characterisation of an iron-specific SOD from *B. anthracis* (Tu et al., 2012) provides an example of a sequence of the FeSOD protein that contains all but two predicted determinants of Mn-specificity (Met105, Val189 of *B. anthracis* SOD; arbitrary numbering, based on the MSA), but no putative determinants of Fe-specificity. Despite the inability to accurately predict metal specificity, analyses of the proposed determinants can help to guide formulation of initial hypotheses about metal specificity, that can be later tested using experimental approaches. In the sequences of SaSodA, all previous predicted determinants of Mn-specificity with the exception of Ser239 were present. In SaSodM, all proposed Mn-specific conserved residues except Ser239, and Val189 were found. Val189 was also substituted in *B. anthracis* Fe-SOD, suggesting that SaSodM may also use iron. However, Ile189 found in SaSodM is also present in the Mn-specific *C. elegans* SOD, further signifying the importance of experimental verification of metal-specificity of Fe/MnSODs.

Altogether, this phylogenetic and sequence analyses provided evidence in support of the hypothesis of this thesis that the more divergent SaSodM has undergone neo-functionalization, potentially to enable it to utilise Fe during the Mn-starvation imposed by the immune system of the infected host. Whereas the more conserved SaSodA retained the ancestral Mn-specificity, which can function in non-restricted, environmental concentrations of manganese.

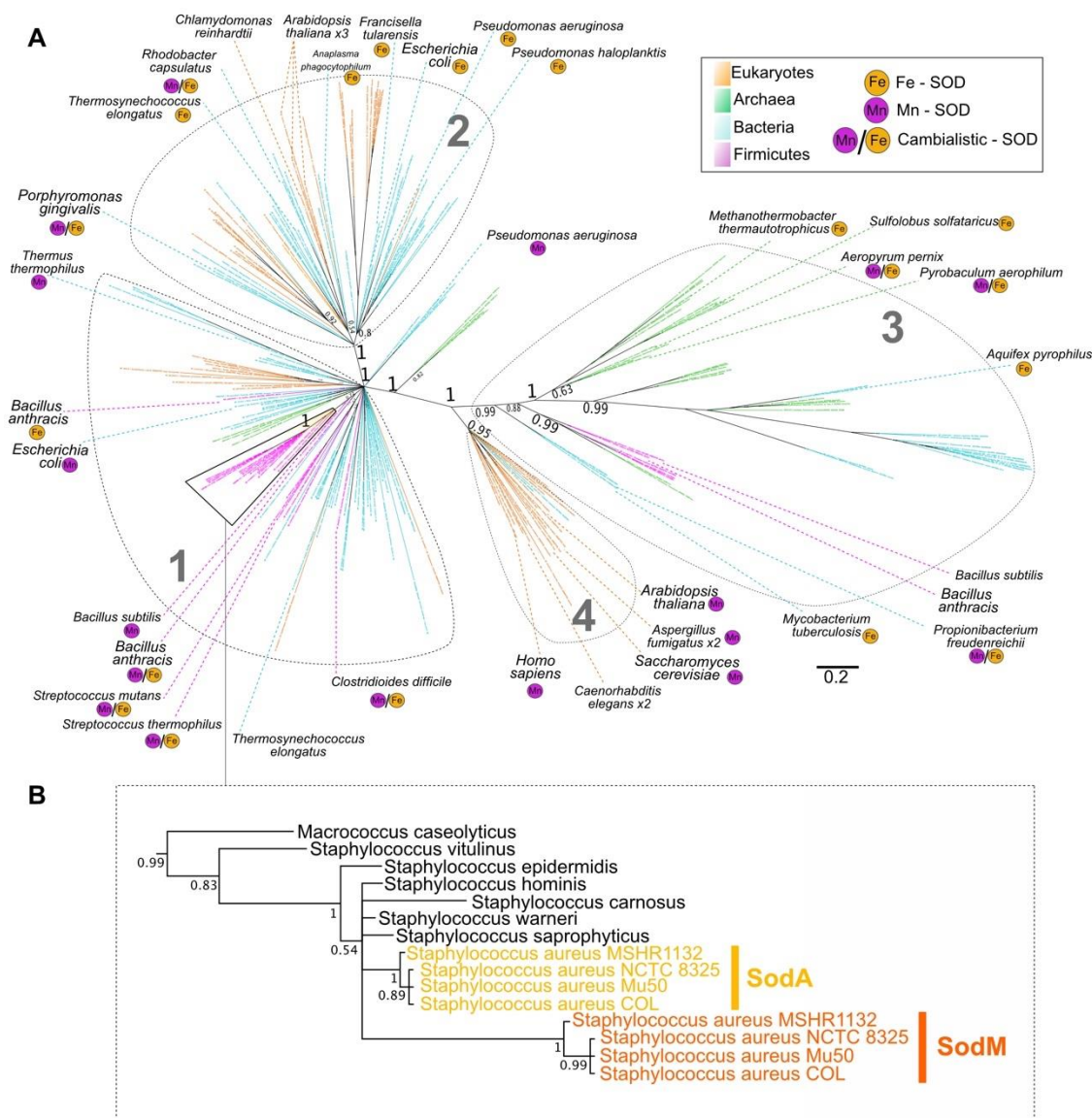


Figure 3.2 Bayesian phylogenetic tree of Mn/Fe-SOD homologues.

(A) Phylogeny generated based on an alignment of 217 Fe/Mn SOD homologues from the NCBI database including sequences from bacteria (cyan), eukaryotes (orange), and archaea (green). Firmicutes are indicated in magenta. Four major groups (1, 2, 3 and 4) were separated by long branches. (B) Magnification of the region indicated with black triangle in A that included all analysed SOD sequences from staphylococci. *S. aureus* SodAs (yellow) and SodMs (orange) are indicated. Metal-specificity of enzymes, based on the available research literature, was annotated next to the species name, with Mn-specificity marked as purple circle, and Fe-specificity marked as an orange circle.

Support values (posterior probabilities) are displayed only for the key branches. The tree was generated using PhyloBayes (Lartillot et al., 2009) under the CAT60 model based on trimmed alignment of 206 amino acid positions. Scale bar represents number of substitutions per site.

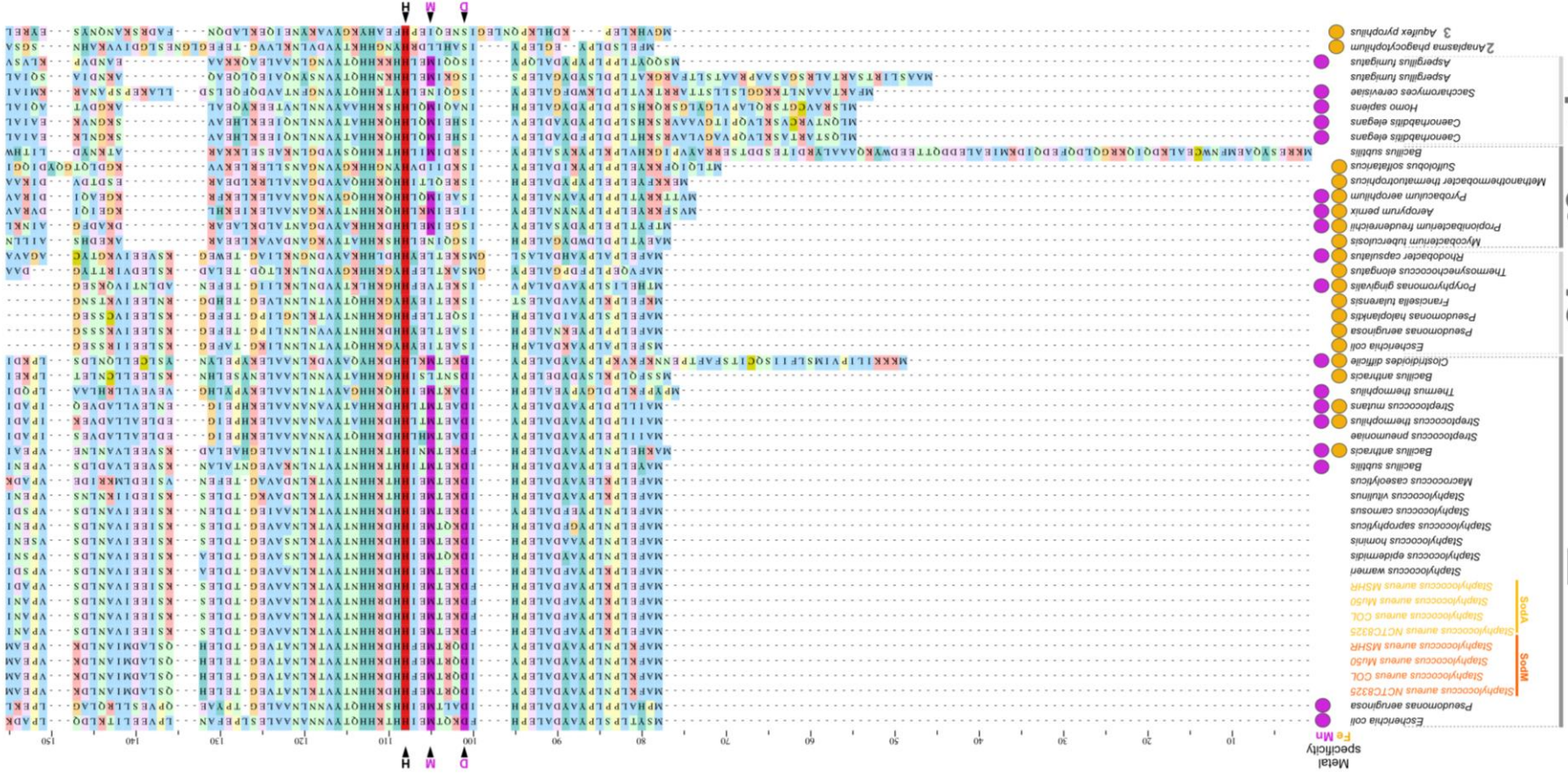


Figure 3.3 Multiple sequence alignment of representative Mn/Fe-SODs (continued on the following page).

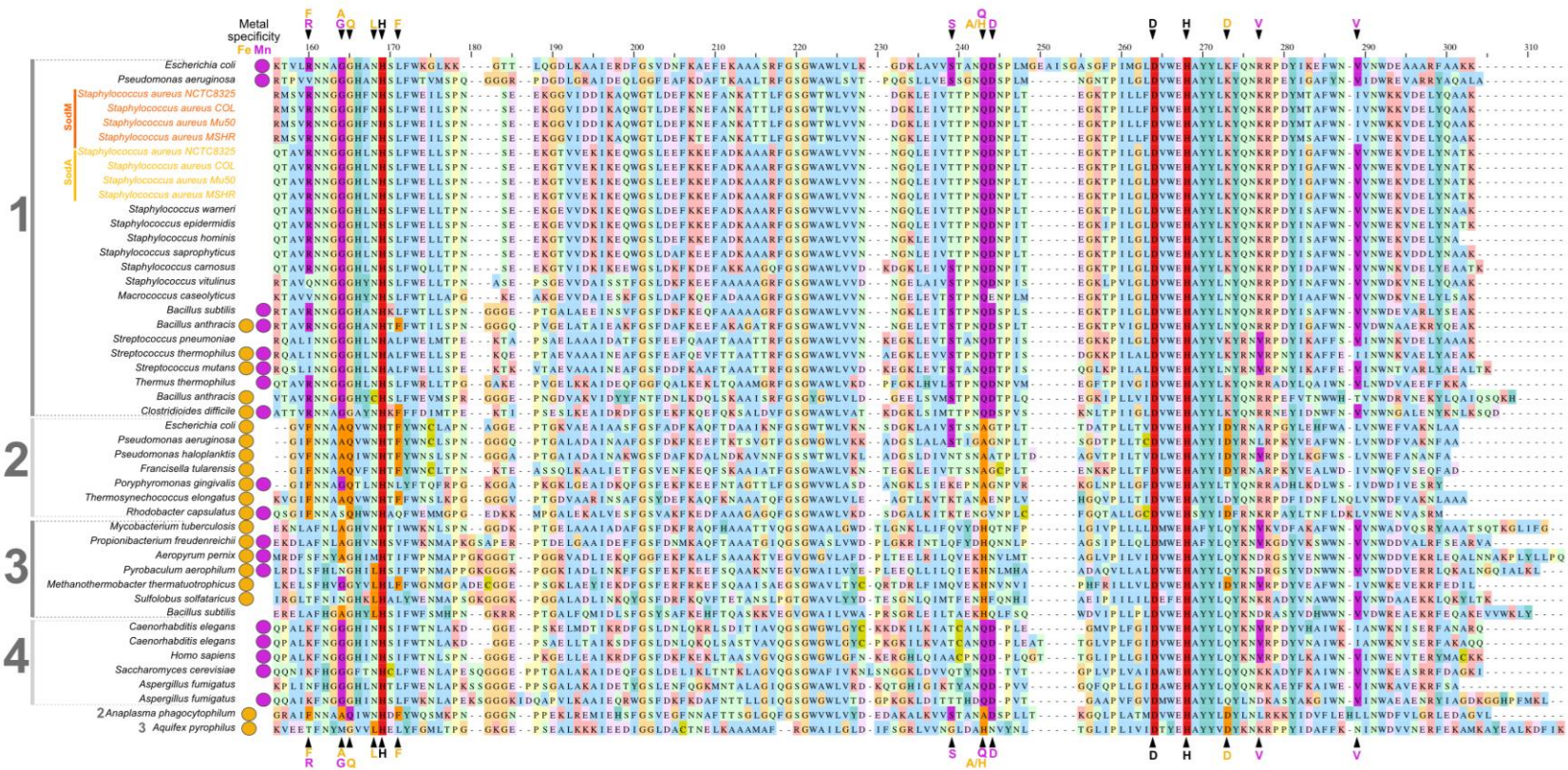


Figure 3.3 continued. Multiple sequence alignment of representative Mn/Fe-SODs

The alignment of 47 Fe/Mn SOD homologues from *Staphylococcus* genus, and organisms sampled from across the major phylogenetic groups (1, 2, 3, and 4) identified in the phylogenetic analyses (Figure 3.2). The experimentally verified metal-specificities of SODs were indicated (Fe in yellow, Mn in magenta). The conserved residues involved in binding of metal were indicated in red. The residues predicted to be as determinants of metal-specificity according to (Wintjens et al., 2008) were indicated in orange (Fe), or magenta (Mn).

The alignment was generated using MAFFT, '--auto' algorithm (Katoch & Standley, 2013). The order of sequences in the alignment was automatically sorted using MAFFT '--reorder'. Jalview (Waterhouse et al., 2009) was used to display and colour the alignment.

3.2.3. Purification of recombinant proteins SaSodA and SaSodM

The *sodA* (SAOUHSC_01653) and *sodM* (SAOUHSC_00093) genes were each cloned into the pET29a expression vector (sections 2.2.5.1) and heterologously expressed in *E. coli* BL21 (DE3) cells (sections 2.7.1-2.7.2). As outlined in section 2.7, SaSOD proteins were initially purified by anion exchange chromatography (AEC), eluted using a linear (0-1 M) NaCl gradient, in 20 mM Tris pH 7.5 buffer. SaSodA and SaSodM recombinant proteins eluted respectively at 230 mM and 250 mM NaCl concentration (Figure 3.4 A, B).

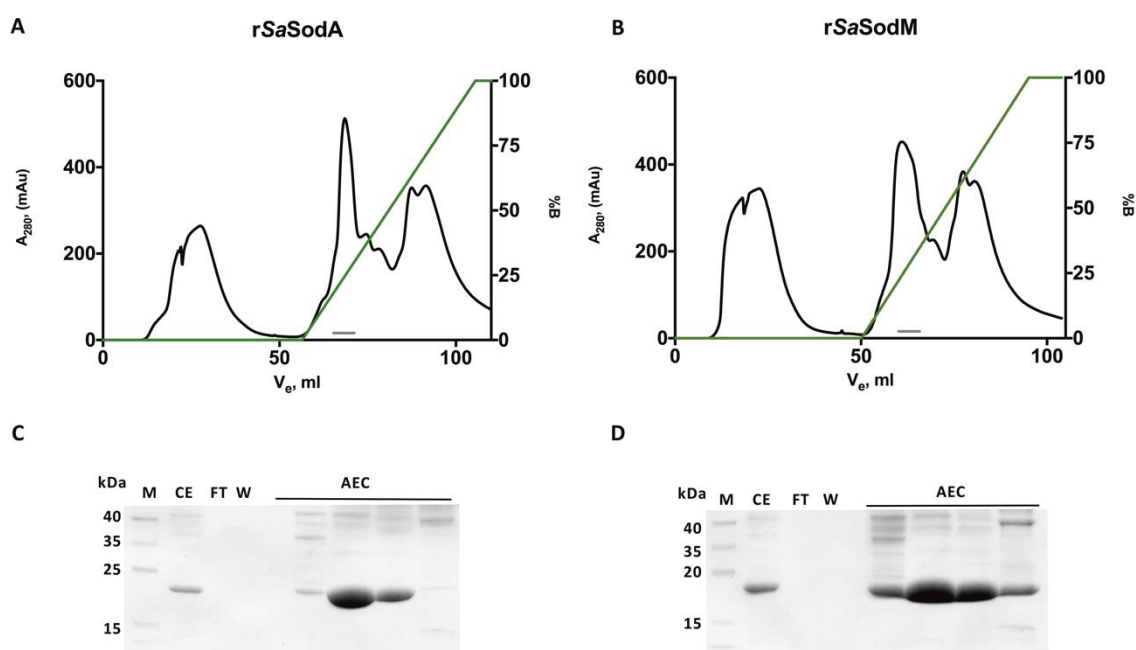


Figure 3.4 Protein purification: anion exchange chromatography.

Representative AEC chromatograms of (A) SaSodA and (B) SaSodM purification showing a linear NaCl gradient elution (%B, green line) of proteins (A₂₈₀, black line). AEC purification was performed at room temperature using 5 ml HiTrap Q HP anion exchange column on ÄKTA Basic or Start (GE Healthcare) system. Binding buffer consisted of 20 mM Tris pH 7.5 and the elution buffer contained 1 M NaCl in 20 mM Tris pH 7.5. Column equilibration was performed according to manufacturer instructions. Flow through of the column was collected upon loading of the crude extract. Unbound protein was washed off the column with 5 column volumes (CV) of binding buffer. Linear salt gradient elution was performed over 9 CV, with 2 ml fractionation. SOD elution peaks, marked with a grey line along V_e axes, were identified by SDS-PAGE (C, D); 1 μ l of cell extract loaded (CE); flow through of the column (FT), unbound wash (W); and gradient elution (AEC) were resolved on 15 % (w/v) gel, stained for protein using Instant Blue (Expedeon) Coomassie stain and visualised with Image Lab™ software on BioRad ChemiDoc XRS+ system.

Further purification was conducted with preparative size-exclusion chromatography (SEC), (see section 2.7.5) using Superdex 200 16/600 column (V_{total} 120 ml, V_{void} 46.12 ml) in 20 mM Tris, pH 7.5, 150 mM NaCl buffer. The elution profiles of SEC (Figure 3.5 A, B), based on calibration with known molecular weight (MW) standards, suggested that SaSodA and SaSodM proteins had

apparent molecular masses 46218.2 Da and 45035.5 Da, respectively (theoretical masses of a monomer: SodA 22711.3 Da, SodM 23040.9 Da; according to ProtParam, ExPASy). The SEC eluate was analysed with SDS-PAGE (section 2.8.1) and both proteins were found to be >95 % homogenous (Figure 3.5 C, D). SEC purification was performed at different temperature conditions, and the observed elution profiles under the given conditions were as follow: at 4°C (n=3), SodA eluted at an average 83.4 ml (± 0.5 ml SD), and SodM eluted at an average 84.0 ml (± 0.5 ml SD); at room temperature (n=15), SodA eluted at an average 82.4 ml (± 0.5 ml SD) and SodM eluted at an average 83.1 ml (± 0.5 ml SD).

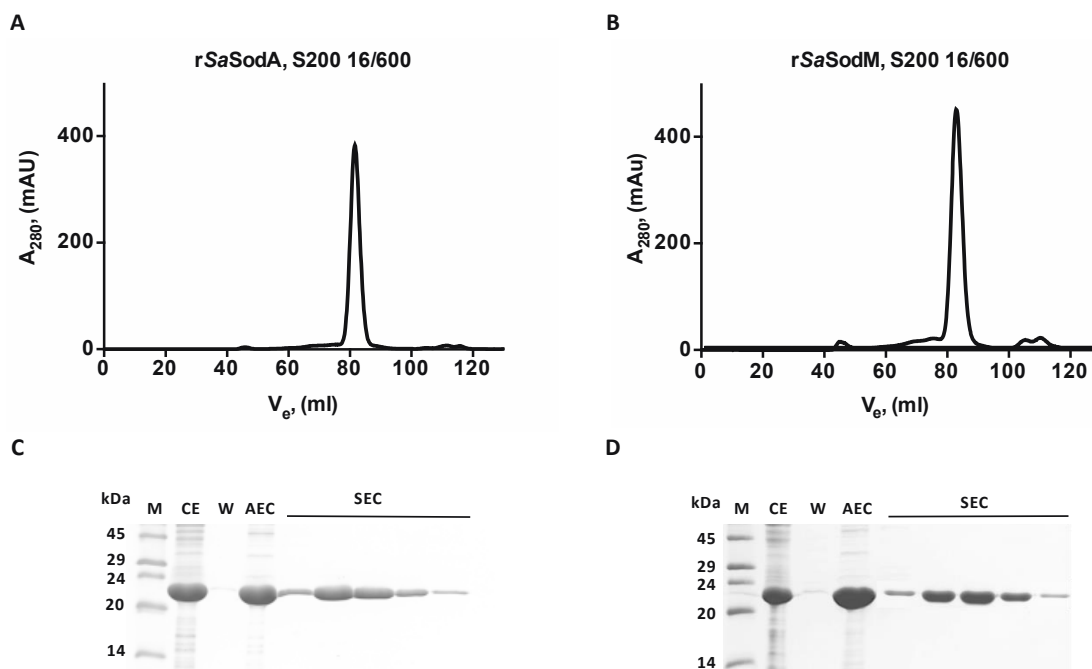


Figure 3.5 Protein purification: size exclusion chromatography (SEC).

Representative chromatograms (A, B) of SEC purification of SaSodA and SaSodM respectively, in 20 mM Tris, 150 mM NaCl pH 7.5. SEC purification was performed using Superdex S200 16/600 preparative column on ÄKTA Prime purification system at room temperature or on ÄKTA Pure system at 4°C. On any occasion, up to 1 ml of the AEC purified protein fraction was loaded onto the column and resolved with 2 ml fractionation over 1.5 CV. The main elution peak (A, B) corresponds to the high purity recombinant protein, as confirmed by SDS-PAGE (C, D), performed on 15 % gel with 5 μ l loading of cell extract (CE), unbound wash (W), AEC peak of SOD eluate from Q HP column, and size-exclusion peak eluate (SEC), stained for protein using Instant Blue (Expedeon) Coomassie and visualised with Image Lab™ software on BioRad ChemiDoc XRS+ system.

3.2.4. Quantification of purified recombinant SODs

As described in Materials and methods, section 2.13, the concentration of purified proteins was routinely determined by the use of the Bradford assay (Coomassie Plus protein assay; Thermo-Fisher Scientific) or Pierce BCA protein assay (Thermo-Fisher Scientific), by comparison to a standard curve of known concentrations of bovine serum albumin (BSA); or by monitoring absorbance of aromatic residues at 280 nm (A_{280nm}) by UV-visible spectroscopy, using theoretical

extinction coefficients ϵ_{A280nm} : SodA $\epsilon=48930 \text{ M}^{-1}\cdot\text{cm}^{-1}$, MW=22711.3 Da, SodM $\epsilon=51910 \text{ M}^{-1}\cdot\text{cm}^{-1}$, MW=23040.9 Da, values estimated with ProtParam, ExPasy.

Due to discrepancies between the outcomes of different assays, both recombinant SodA and SodM samples were analysed by Alta Biosciences Ltd to quantitatively determine their amino acid composition and verify the total protein concentration. The average of all determined amino acids was correlated with protein concentration as assessed by the routinely used assays; A_{280nm} , Bradford assay and BCA. This allowed generation of correction factors for these assays based on the amino acid analysis (AAA) (Table 3.1). Based on these calculations, the corrected extinction coefficients were determined to be: SodA $\epsilon=62681 \text{ M}^{-1}\cdot\text{cm}^{-1}$, SodM $\epsilon=64949 \text{ M}^{-1}\cdot\text{cm}^{-1}$.

Protein	Correction factor	
	Bradford Assay	BCA
SaSodA	0.45	0.52
SaSodM	0.52	0.59

Table 3.1 A correction factors calculated for standard protein assays based on amino acid analysis outcome.

Both Bradford and BCA assays overestimate the concentration of SaSodA and SaSodM proteins, and can be accordingly adjusted by multiplying their output by a listed correction factor determined based on amino acid content analysis.

3.2.5. Recombinant SODs acquire Fe in the heterologous host

Purified recombinant SaSOD proteins were subjected to elemental analysis by ICP-MS to determine their metal content (section 2.12.1) and metal-to-protein stoichiometry. Elemental analysis of SaSodA and SaSodM purified from *E. coli* host cells (Figure 3.6) showed that predominantly iron was found to co-migrate with both proteins. Multiple preparations of SaSodA were isolated, containing an average of 0.8 ± 0.1 iron equivalents per monomer of protein, and 0.2 equivalent contamination with Zn. Total metal detected was always stoichiometrically equal to the protein yield, implying complete occupancy (Table 3.2).

Higher iron occupancy was noted in multiple preparations of SaSodM, containing on average 0.9 ± 0.1 iron equivalents per monomer of protein. Numerous preparations of both SodA and SodM were found to contain low levels of Zn, and occasionally trace Mn contamination. Optimisation of the medium composition (using iron-supplemented minimal medium, M9) and expression conditions was crucial to prepare pure Fe forms of the SODs, for reliable assessment of metal-specific activity (sections 2.7.1, 2.7.2, 2.11.1). For any further downstream applications, only the proteins containing above 0.9 molar equivalents of iron and no detectable Mn were used.

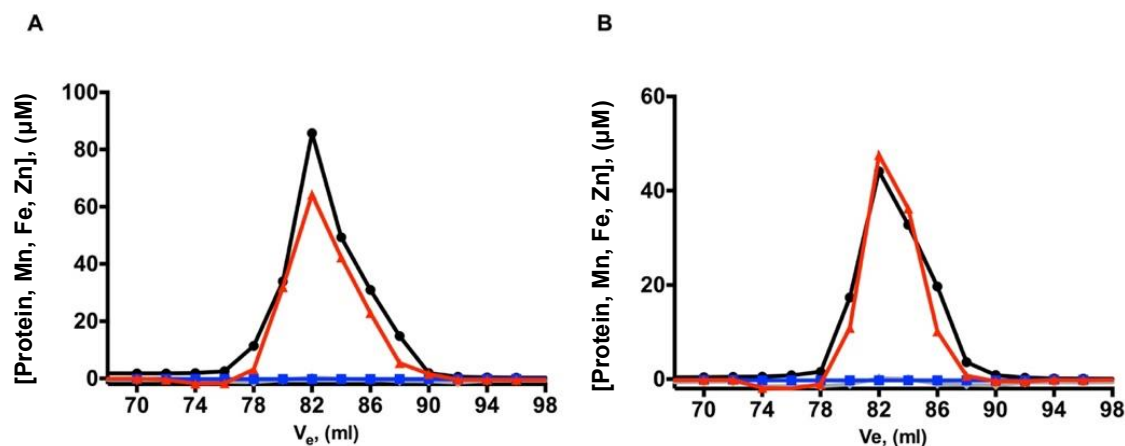


Figure 3.6 Elemental analysis of purified SaSOD proteins.

A representative chromatogram of an elemental analysis of SaSOD protein fractions resolved by preparative size-exclusion chromatography. All standards and samples were prepared in a solution of 2.5% HNO₃ (Suprapur, Merck) containing 20 µg·L⁻¹ Co and Pt as internal standards. Concentration of Fe (red triangles), Mn (blue squares), and Zn (grey diamonds) in analysed samples was determined from a standard curve. Protein concentration in analysed fractions was determined with Bradford assay, corrected by amino acid analysis, depicted as black circles.

Metal content (% ± SD)			
Protein	Mn	Fe	Zn
SaSodA	2.1 ± 01.4	92.6 ± 5.4	6.0 ± 3.8
SaSodM	1.7 ± 1.3	94.8 ± 7.1	5.6 ± 3.9

Table 3.2 Average metal content of preparations of as-purified recombinant SODs.

Metal content represented as a percent of total metal content of the protein. Mean ± standard deviation values of n=10 runs.

3.2.6. Purified SODs are free of contaminating native *E. coli* SODs

Aliquots of 2 µg of each purified protein, in 20 mM Tris, pH 7.5, 150 mM NaCl, and 20 µg total protein (as determined by Bradford assay) of soluble extracts of BL21 (DE3)-pET29a (empty vector), BL21 (DE3)-pET29a-sodA, BL21 (DE3)-pET29a-sodM/qc were analysed for enzyme activity using the in-gel NBT-riboflavin SOD activity assay (Figure 3.7). No trace of contamination with host's native SODs was found in the preparations of recombinant proteins after protein purification protocol.

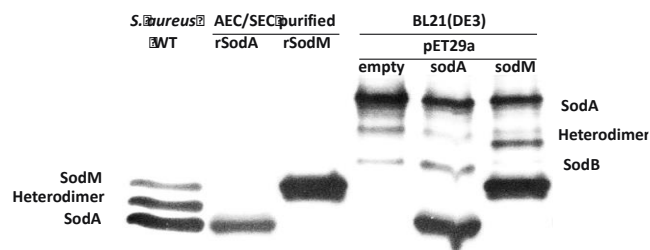


Figure 3.7 In-gel SOD activity assay shows absence of contamination of purified SaSODs by EcSODs.

In-gel SOD activity assay of cell lysates of *E. coli* BL21 (DE3) containing pET29a plasmid, BL21 (DE3) transformed with pET29a-sodA and BL21 (DE3) transformed with pET29a-sodMqc constructs, in comparison to purified SaSodA and SaSodM recombinant proteins and a sample of *S. aureus* wild type cell lysate. SOD activity was assessed in-gel by the nitroblue tetrazolium (NBT-riboflavin) negative staining of purified protein samples resolved on non-denaturing 15 % polyacrylamide gels (Beauchamp and Fridovich, 1971). The assay output represents SOD activity as an achromatic zone on a dark blue background. The assay results were visualised using Image Lab™ software on BioRad ChemiDoc XRS+ system and inverting the display to enhance the view of activity zones.

3.2.7. Evaluation of the secondary structure and thermal stability of SOD proteins by CD spectroscopy

To assess the secondary structure of the recombinant proteins, samples of SodA and SodM were subjected to circular dichroism (CD) spectroscopy analysis (see section 2.17). Spectra (Figure 3.8) were recorded in the far-UV region, where signal arises from the peptide bond when it is located in a regular, folded environment. Alpha helix, beta-sheet, and random coil structures each give rise to a characteristic shape and magnitude of CD spectrum. Alpha-helix gives negative bands at 222 nm and 208 nm, beta-sheet gives a negative band at 218 nm, and both have a positive band at around 190 nm.

The approximate fraction of each secondary structure type present in the studied proteins (Figure 3.8) was calculated using the SVD algorithm of the CDSSTR analysis programme within the Dichroweb server (Whitmore & Wallace, 2004; Sreerama & Woody, 2000). Predominantly helical composition of the two proteins was reflected by the CD data, with SodA containing 52 % helix, 13 % strand, 12 % turn, and 23 % unordered residues, and SodM secondary structure composition of 56 % helix, 12 % strand, 12 % turn and 20 % unordered residues. The determined composition of secondary structure of SaSODs was similar to the content extracted from PDBSum (Laskowski & Chistyakov, 2005) for the examples of published crystal structures of SODs from Mn/Fe superfamily, as illustrated by *B. subtilis* 2RCV composed of 53 % helix, 12 % strand and 35 % of other elements, or *E. coli* 11SB with 51 % helix, 11 % strand and 38 % other elements composition.

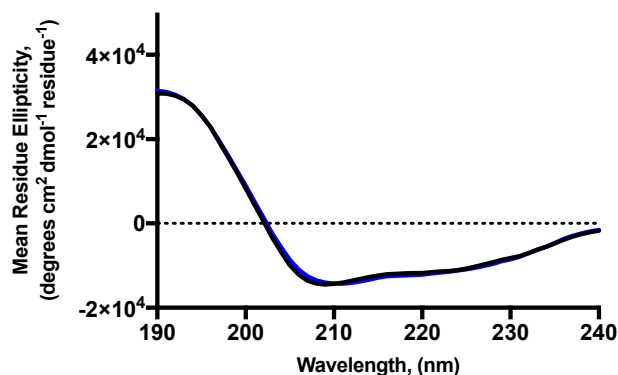


Figure 3.8 CD spectra of SaSodA and SaSodM.

A representative far-UV circular dichroism spectra of SodA (black) and SodM (blue) in 10 mM sodium phosphate buffer, pH 7.0. All measurements were performed at 20 °C, within 260-185 nm range. Collected scans resulted from averaging of the 5 accumulated measurements corrected for buffer blank. Mean residue ellipticity values of collected data, were generated with the CDSSTR method, using reference data set: 4 optimised for 240 – 190 nm, with a normalised root mean squared deviation (NRMSD) of 0.010.

CD measurements in the far-UV range allowed quantitative estimation of secondary structure, reflecting an average of the entire population of protein in solution. The loss of CD signal by an increase in temperature was subsequently used to assess the stability of the folded proteins. As both SodA and SodM were indicated to possess predominantly helical composition, the thermal denaturation was performed by following the change in ellipticity at a fixed wavelength of 222 nm (α -helix band) as a function of temperature, increasing from 20 to 90°C (Figure 3.9).

The inspection of changes in the 222 nm band of the SodA CD spectrum indicated that the thermal denaturation was not a simple, two state process; the melt curve presented two inflection points (i.e., $T_{m1}=45.2^{\circ}\text{C}$ and $T_{m2}=69^{\circ}\text{C}$), indicative of two temperature-induced transitions. The SodM dimer was found to be more thermally stable than SodA in solution, with unfolding occurring in a single transition at T_m of 72.7°C.

For both proteins, thermal unfolding was irreversible (or only partially reversible) as confirmed by the comparison of the CD spectrum taken at 20°C, at 90°C upon loss of protein secondary structure (5% helical content retained), and again after the return to the start temperature of 20°C (approximately 20% helical content recovered, data not shown).

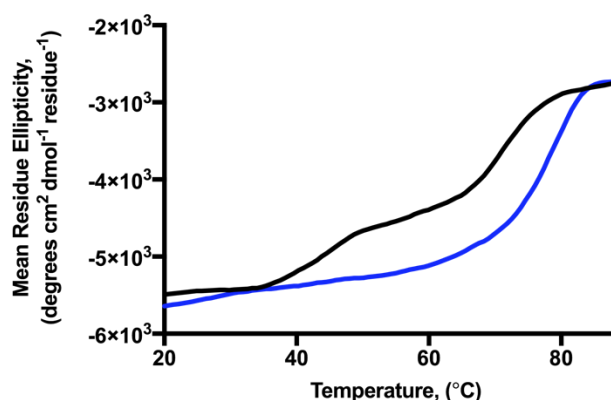


Figure 3.9 SaSODs' thermal denaturation monitored by CD spectroscopy.

The variable temperature measurements were performed at 222 nm wavelength over a temperature range from 20°C to 90°C, with 1°C/min temperature ramping. A T_m of analysed proteins was calculated from the first derivative. SodA thermal denaturation curve (black) represents two-step process with T_m of 45.2°C and 69°C, SodM thermal melt curve depicted in blue with T_m of 72.7°C.

3.2.7.1. SaSodM presents higher stability than SaSodA when subjected to chemical denaturation

To analyse the structural changes of *S. aureus* SODs upon unfolding, fluorescence of tryptophan residues (Teale & Weber, 1957; Ghisaidoobe, 2014) was measured. Tryptophan (Trp) is one of the probes of intrinsic protein fluorescence, as its indole ring is sensitive to the polarity of the local environment, which changes when a protein undergoes structural or environmental changes. In the native, folded state, aromatic residues are located within the hydrophobic core of the protein, and fluorescence of Trp emission is observed at ~330 nm, whereas in a partially folded or unfolded state, they become exposed to solvent, which is reflected in a shift in wavelength of the emitted fluorescence towards ~355 nm (e.g. glucagon, or aqueous solution of tryptophan), (Teale & Weber, 1957; Vivian & Callis, 2001).

There are 7 tryptophan residues per subunit of SaSOD proteins' structures (residues mapped onto crystal structures, which will be introduced in Chapter 4, section 4.2.2), at positions 85, 106, 128, 130, 163, 183 and 188 (Figure 3.10 A). Residues W128, W163, W85, and W130 contribute to the formation of a hydrophobic core, surrounding the metal coordination centre, and potentially may influence the reactivity of metals in SOD proteins. Residue W163 facilitates interactions at the dimer interface, and 80 % of its solvent-accessible surface is buried upon formation of the dimer (Figure 3.10 B).

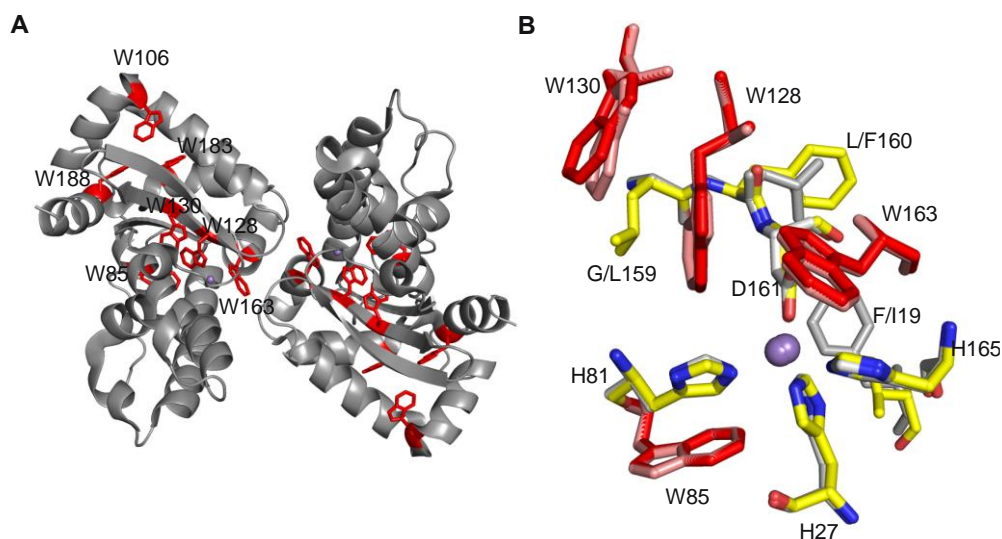


Figure 3.10 Tryptophan residues contributing to the fluorescence emission spectra of SaSODs.

(A) All Trp residues are represented as red sticks, and mapped onto Mn-SodA dimer structure. (B) Tryptophan residues involved in the hydrophobic core around the active site of the superimposed Mn-SodA (white carbons; salmon Trp) and Mn-SodM (yellow carbons; red Trp).

Tryptophan fluorescence of SodA and SodM protein was measured at room temperature using an excitation wavelength of 280 nm. The emission spectra of the native proteins in 20 mM Tris, 150 mM NaCl buffer pH 7.5 (Figure 3.11, black trace), recorded between 300 nm and 450 nm, contained a single emission peak with emission maxima at 331 nm and 334 nm for SodA and SodM, respectively.

As the tryptophan fluorescence emission maximum (λ_{max}) changes with the degree of solvent exposure of the residues, proteins were exposed to chemical unfolding by 8 M urea or 6 M guanidine hydrochloride. Protein denaturation by chaotropic agents, such as urea and guanidine, is proposed to occur via direct interaction of the chaotrope with protein through displacement of water molecules surrounding the protein and hydrogen bonding of amide groups of the peptide bond (“push-pull” mechanism”; (Robinson & Jencks, 1963; Das & Mukhopadhyay, 2009; de Oliveira & Silva, 2015)) and/or indirectly by altering water structure, leading to solvation of hydrophobic side chains (Watlauer et al., 1964).

The red-shift (from ~330 nm to 355 nm) in Trp fluorescence of both proteins treated with 6 M guanidine (Figure 3.11, blue trace) suggest that the fluorophores had become more solvent-accessible, implying both proteins unfolded in the presence of guanidine hydrochloride. When the two proteins were treated with 8 M urea, only SodA was denatured, reflected by the shift of the emission maximum to 355 nm (Figure 3.11, red trace). SodM in 8 M urea presented the peak of fluorescence at 335 nm, matching the one recorded for the native protein, implying the protein remained folded and suggesting higher stability of SodM against urea denaturation. This observation is consistent with a higher melting temperature determined for SodM than SodA, by means of CD spectroscopy (Figure 3.9). Changes of the intrinsic fluorescence properties of SaSODs report on the difference in chemical stability of proteins.

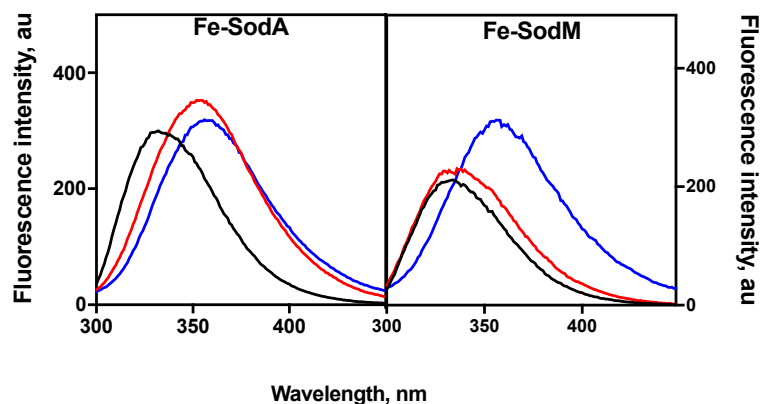


Figure 3.11 Tryptophan fluorescence spectroscopy of as-purified (Fe-loaded) forms of SaSODs.

Fluorescence emission measurements were performed using samples of proteins (10 μ M) in either 20 mM Tris, 150 mM NaCl buffer pH 7.5 (black trace), 8 M urea (red trace) or 6 M guanidine-HCl (blue trace). Fluorescence emission analysis was performed at room temperature, and spectra were recorded between 300 nm and 450 nm upon excitation at 280 nm, at 30 nm/min scan rate and 0.5 nm data interval.

3.2.8. Metal content of the SaSODs can be manipulated by metal supplementation of bacterial host culture

Most organisms require Fe to facilitate metabolic functions, and thus they also accumulate levels of iron sufficient to catalyse a variety of biochemical processes. Based on the Irving-Williams series (Mn < Fe < Co < Ni < Cu > Zn; Irving & Williams, 1953), iron is predicted to bind preferentially to cellular ligands over manganese (flexibility of proteins can influence steric selection between metals, and the relative affinities of metals for proteins depend greatly on ligand field stabilization energies of the metals). This creates the universal orders of preference, which for divalent metals is the Irving-Williams series. It has been proposed that the metalation of cytosolic proteins is often determined by the environment in which the protein is expressed (Cotruvo & Stubbe, 2012), in this case the *E. coli* cytosol. A greater intracellular concentration of Fe than Mn in *E. coli* under standard growth conditions has been described (Outten & O'Halloran, 2001) and it is thought to be the reason for which many recombinant, cytosolic metalloenzymes expressed in *E. coli* are found to predominantly acquire iron under normal conditions (Whittaker & Whittaker, 1999; Lamarre et al., 2001).

Unlike *E. coli*, Gram positive bacteria such as *B. subtilis* (Helmann, 2014) and *B. anthracis* (Tu et al., 2012) or *S. aureus* (chapter 6, section 6.2.2) are reliant on manganese for growth and maintain pools of both total and labile iron and manganese. *Treponema pallidum* or *Borrelia burgdorferi* have evolved without a cellular requirement for iron (Posey et al., 1999; Aguirre et al., 2014), and normally accumulate high levels of manganese compared to other organisms such as *E. coli* or *S. cerevisiae*.

Selectivity of metal binding by enzymes, including SODs, can be critical for conferring enzymatic activity. Metal content of recombinant SodA and SodM, expressed in *E. coli* in LB under standard growth conditions (sections 3.2.5), highlighted a requirement for optimisation of growth and expression conditions to prepare pure Fe and Mn forms of the SODs, for reliable assessment of metal-specific activity.

To investigate the influence of external metal supplementation of the bacterial culture media on the metalation status of the SaSOD proteins produced in *E. coli*, varying concentrations of Mn and Fe were added to the rich (LB) and minimal (M9) growth media for overexpression of SodA and SodM in BL21 (DE3) cells. Protein expression was carried out in standard, optimised conditions as described in section 2.7.2, with metal supplementation upon induction with IPTG.

Metal analysis of LB medium, prepared according to the standard laboratory protocol, revealed that it contained an average of $0.36 \pm 0.08 \mu\text{M}$ Mn, $6.52 \pm 0.44 \mu\text{M}$ Fe and $15.76 \pm 1.02 \mu\text{M}$ Zn (results of technical triplicate). Approximately 10-fold lower total metal content was detected in M9 minimal medium, which contained $0.09 \pm 0.02 \mu\text{M}$ Mn, $0.80 \pm 0.24 \mu\text{M}$ Fe and $1.21 \pm 0.06 \mu\text{M}$ Zn.

Negligible effect on the metal content of recombinant SaSODs (Figure 3.12 B) was observed under supplementation of LB growth medium with $200 \mu\text{M}$ Fe. The determined metal content showed only 1-2 % increase in Fe content of SodA and SodM in comparison to preparations from non-supplemented medium. Overexpression of proteins in M9 minimal medium supplemented with an equivalent amount of Fe (Figure 3.12 C) yielded almost exclusively Fe-loaded versions of SodA and SodM, that contained less than 1 % Mn in total.

Supplementation of rich growth medium (Figure 3.12 B) with increasing concentration of Mn yielded proteins with Mn content that increased in a dose-dependent manner. Nearly 5 and 6-fold gain of Mn content at the expense of Fe was noted for SodM and SodA respectively, when overexpressed in the presence of $250 \mu\text{M}$ Mn. Addition of 5 mM Mn to the growth medium resulted in SodA and SodM preparations containing mostly Mn, at 98 % and 81 % of total metal, respectively.

Mn supplementation in minimal growth medium (Figure 3.12 C) at 1 mM concentration resulted in protein preparations containing 78 % and 50 % manganese in SodA and SodM, respectively. A general trend of lower levels of Mn and higher levels of Fe bound to the protein was observed for SodM compared to SodA, at a given Mn and Fe supplementation in rich or minimal growth conditions (Figure 3.12), which may suggest different ability to acquire metal *in vivo*.

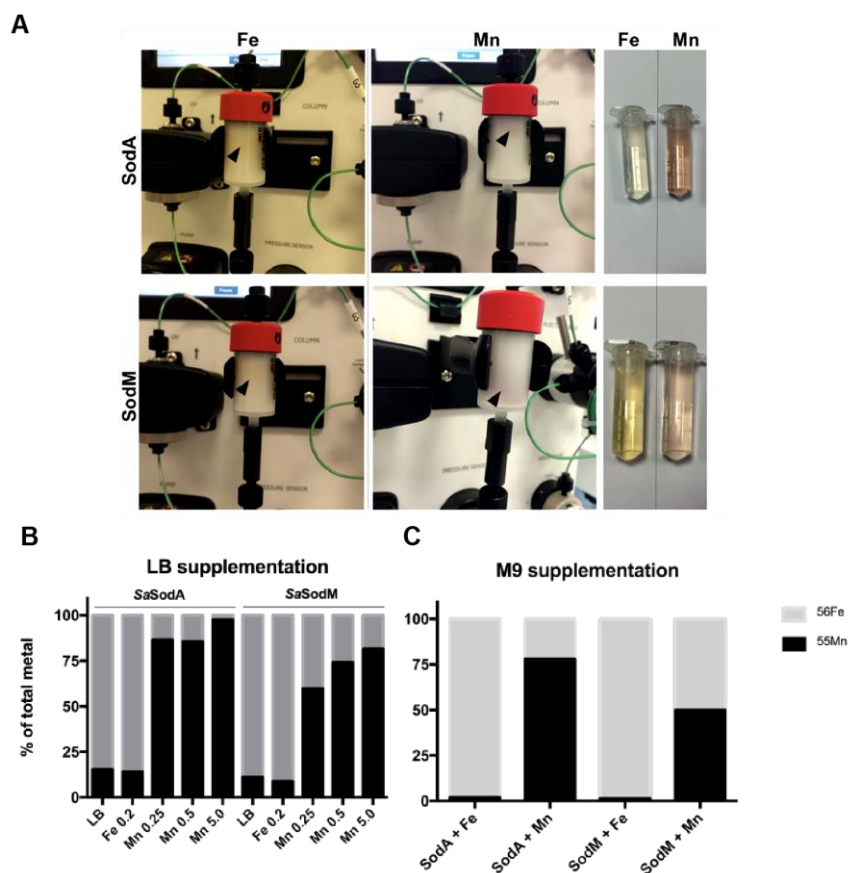


Figure 3.12 Manipulation of the metal content of recombinant SaSOD proteins expressed in LB and M9.

The AEC purification set up (A) used for initial purification of SaSODs, depicting a 5 ml QHP column connected to ÄKTA Start purifier, in a process of elution of proteins overexpressed in LB supplemented with Fe or Mn, as indicated. The arrowheads pinpoint fraction of coloured protein coming off the column. Collected yellow and pink samples corresponding to SaSOD fractions are a visible indication of a metal cofactor bound to the protein.

An elemental analysis of recombinant SaSOD proteins, overexpressed in LB (B) under standard conditions with either 200 μ M Fe or 250 μ M, 500 μ M or 5 mM Mn supplementation of growth medium upon induction of protein expression. Metal content represented as a percent of total metal content of the protein, with Mn depicted as black bars and Fe depicted as grey bars. The effects of external metal supplementation on the metal content of recombinant proteins were also assessed in M9 minimal medium (C), with addition of 200 μ M Fe or 1 mM Mn.

Cultivating *E. coli* in medium supplemented with ferrous or manganese salts resulted in substitution of Mn or Fe in the active site of the protein, reflecting relatively indiscriminate uptake of either Mn or Fe by the recombinant protein, presumably by altering intracellular metal bioavailability.

The conditions of oxidative stress (addition of peroxide) in the *E. coli* culture were shown to cause an increase of Mn content (relative to Fe content) in the proteins expressed and purified from such culture. This Fe to Mn switch was proposed to occur as a consequence of the iron uptake repression and the induction of manganese uptake under oxidative stress conditions (Anjem et al., 2009). Addition of hydrogen peroxide to final concentration of 1 mM in liquid culture, in LB supplemented with Mn salts (Figure 3.13) resulted in a negligible increase in the level of Mn (on the account of Fe) bound to purified protein, in the case of both SodA and SodM.

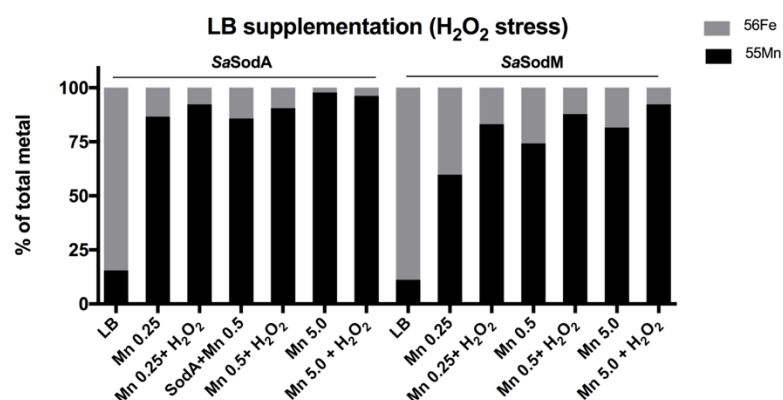


Figure 3.13 Peroxide treatment of bacterial cultures increases Mn content of SaSODs overexpressed in LB.

ICP-MS analysis of recombinant SaSOD proteins overexpressed in LB under standard conditions with 250 μ M, 500 μ M or 5 mM Mn supplementation, as well as with peroxide treatment upon 1 mM hydrogen peroxide addition to growth medium at the point of induction of protein expression by IPTG. Metal content is represented as a percent of total metal content of the protein, with Mn depicted as black bars and Fe as grey bars.

3.2.9. *In vitro* metal exchange yields Mn-loaded SODs

The detected difference in the proteins' stability against the two tested chaotropic denaturants (section 3.2.7.1) was useful in achieving the preparation of fully Mn-loaded versions of the two proteins. As supplementation of growth medium with high concentrations of metal (section 3.2.8) failed to yield both proteins containing exclusively Mn (Figure 3.12), SaSodA and SaSodM proteins were refolded *in vitro* to fully exchange their iron cofactor for manganese. Multiple unfolding protocols were tested in the process of optimisation of metal exchange (see section 2.12.2).

Optimisation lead to successful production of Fe-free, Mn-loaded versions of SodA and SodM (Table 3.3). As outlined in section 2.12.4 SaSodA was unfolded in 8 M urea in the presence of 10 mM EDTA to extract the bound iron, followed by refolding through dialysis against 20 mM Tris pH 7.5, 100 mM NaCl buffer containing 1 mM MnCl₂. Conversely SaSodM was unfolded in 2.5 M guanidine hydrochloride in the presence of 5 mM EDTA and 20 mM 8-hydroxyquinoline to extract the bound iron, followed by refolding through dialysis against 20 mM Tris pH 7.5, 100 mM NaCl buffer containing 10 mM MnCl₂. Equivalent results were obtained for SaSodA protein with both described methods, allowing unification of unfold-refold protocols for subsequent experiments using exclusively guanidine based method. Finally, each protein was resolved on a Superdex 200 Increase 10/300 analytical SEC column (V_{total} 24 ml, V_{void} 8.33 ml; see section 2.7.5.2) in 20 mM Tris pH 7.5, 150 mM NaCl, 0.5 mM EDTA buffer, eluting as stable dimers, and the eluate fractions were analysed for protein content by Bradford assay (see section 2.13). Metal content determination was performed with ICP-MS and samples were analysed for manganese, iron and zinc (Figure 3.14). In each case, exclusively manganese (> 98% total metal

content), and not iron (< 1% total metal content) or zinc, was found to co-migrate with the protein (Table 3.3).

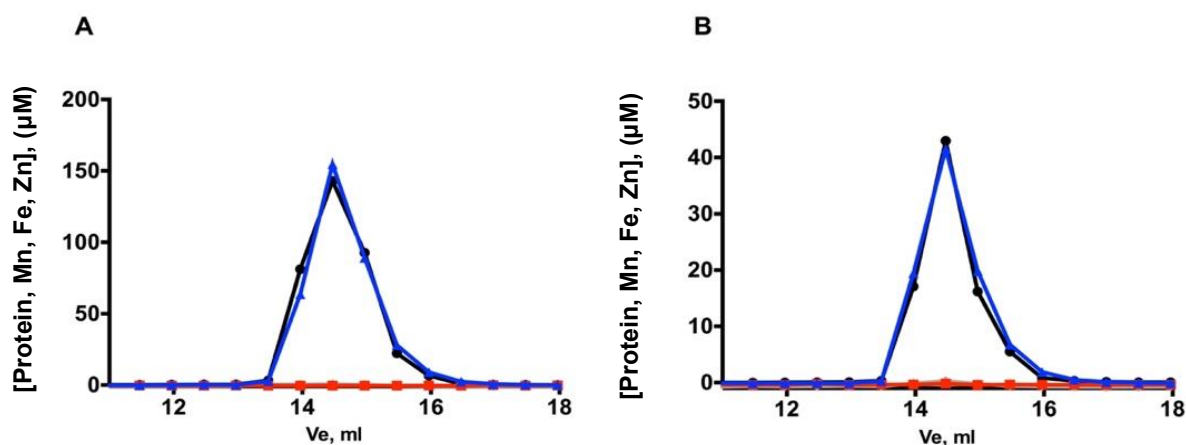


Figure 3.14 ICP-MS elemental analysis of metalated proteins.

Elemental analysis of SodA (A) and SodM (B) protein fractions after an analytical size exclusion chromatography step post unfolding and refolding in Mn. All standards and samples were prepared in a solution of 2.5% HNO₃ (Suprapur, Merck) containing 20 μg·l⁻¹ Co and Pt as internal standards. Isotopes Fe (red squares), Mn (blue triangles), Zn (grey diamonds), Co and Pt were monitored in triplicate, and metal concentrations determined from the standard curve. Protein concentration determined with Bradford assay corrected by amino acid analysis depicted as black circles.

Metal content (% ± SD)			
Protein	Mn	Fe	Zn
Mn-SaSodA	98.6 ± 1.0	0.7 ± 0.6	0.8 ± 0.5
Mn-SaSodM	98.1 ± 1.0	0.3 ± 0.2	1.6 ± 0.9

Table 3.3 An average metal content of Mn-refolded SaSOD proteins.

Metal content represented as a percent of total metal content of the protein. Mean values of n=10 runs ± standard deviation.

3.2.10. CD spectroscopy and Tryptophan fluorescence assays demonstrate Mn-SODs have similar properties as Fe-SODs

The elution profiles of refolded proteins on size exclusion chromatography suggested a correct folding of polypeptides into dimeric structures in solution, with no apparent aggregation (data not shown). To compare Mn forms with Fe-loaded SODs, the secondary structure and unfolding properties of Mn-loaded isoforms were subjected to CD spectroscopy. Analysis of collected far-UV spectrum scans (Figure 3.15) confirmed that the secondary structure content of refolded proteins did not vary significantly from the one determined for overexpressed and purified from *E. coli*, Fe-loaded equivalents (see Figure 3.8, Table 3.4). As in the case of Fe-SODs, the spectra presented a double minimum at 208 nm and 222 nm, implying that chemical unfolding and

refolding of the proteins and exchange of metal cofactor did not alter their predominantly helical composition.

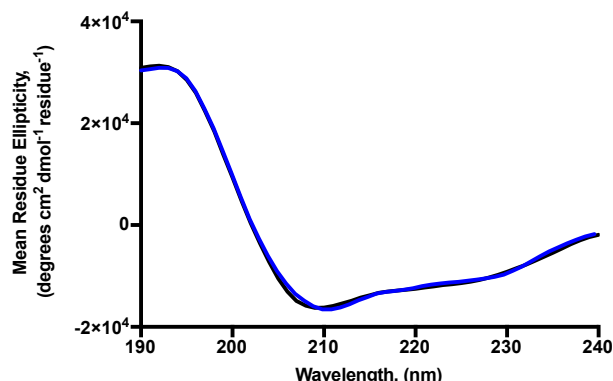


Figure 3.15 CD spectroscopy of Mn-loaded SaSODs.

The representative far-UV circular dichroism spectra of Mn-SodA (black) and Mn-SodM (blue) in 10 mM sodium phosphate buffer, pH 7.0. All measurements were performed at 20°C within 260–185 nm range. Collected scans resulted from averaging of the 5 accumulated measurements corrected for buffer blank. Data presented as mean residue ellipticity (MRE) over the range of wavelengths 240–190 nm were processed within Dichroweb server with the CDSSTR method using reference data set: 4 optimised for 240–190 nm, with a normalised root mean squared deviation (NRMSD) of 0.010.

Protein	Secondary structure, %		
	Helix	β -sheet	Other
Fe-SodA	52	13	35
Mn-SodA	52	12	36
Fe-SodM	56	12	32
Mn-SodM	59	14	27

Table 3.4 Comparison of the overall secondary structure contents of SaSODs quantified from far-UV CD spectra.

Comparison of the secondary structure contents of metalated isoforms of SODs as calculated from the far-UV CD spectra using Dichroweb (outputs were generated with the CDSSTR method using reference data set: 4 optimised for 240–190 nm).

A monitoring of temperature-dependent unfolding by CD (temperature range 20°C to 90°C) was used as a comparative measure of stability between metalated isoforms of SodA and SodM recombinant proteins. Mn-loaded SodA exhibited biphasic thermal unfolding behaviour (Figure 3.16), with T_{m1} of 53.8°C and T_{m2} =65.2°C, similar to its Fe-containing counterpart (Figure 3.9) unfolding at T_{m1} =45.2°C and T_{m2} =69°C. The native CD spectra were not fully recovered after heating of the samples to 90°C and cooling back to 20°C, with an approximately 20% of helical content being recovered. These results imply that the temperature-induced unfolding of these two proteins was irreversible (or partially reversible), however no visible aggregation was observed and the residual enzyme activity of the protein was not assessed. Denaturation of both metalated

forms of SodA involved transitions occurring approximately 20°C apart, implying stepwise conformational changes upon heating.

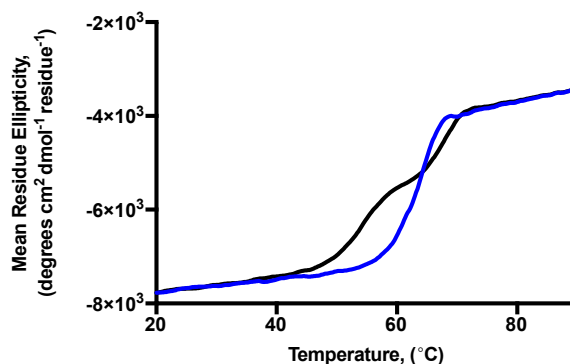


Figure 3.16 Mn-loaded SaSODs' thermal denaturation monitored by CD spectroscopy.

The variable temperature measurements were performed on Jasco J-810 spectropolarimeter equipped with Peltier temperature controller. Spectra were taken at 222 nm wavelength over a temperature range from 20°C to 90°C, with 4 sec response, standard sensitivity, 0.2°C data pitch, 1°C/min temperature ramping, 2 nm spectral bandwidth in 0.1 cm optical path length cuvette. SodA thermal denaturation curve (black) with T_m of 53.8°C and 65.2°C, SodM thermal melt curve depicted in blue with T_m of 62.6°C. The T_m of analysed proteins was calculated from the first derivative.

CD signals and observed temperature-induced transitions reflect an average of the entire molecular population of protein in solution. The exact cause of the occurring transitions is not clear, but it can be speculated that the first unfolding event represents the dissociation of the dimer and the following transition occurring at higher temperature corresponds to the denaturation of the folded domains of a monomer containing the active site. However, the assessment of the oligomeric state of the proteins at the point corresponding with the first thermal transition was not performed to allow the speculation on the structural intermediate between native and unfolded state. Possible occurrence of the intermediate state along the denaturation process was evaluated by performing sequential scans in variable temperature mode. Scans were taken at 5°C increments. Gradual decrease in helical content of each protein sample was observed with increasing temperature, but no obvious plateau indicating intermediate structure was observed. Between 50°C and 55°C total helical content of Mn-SodA decreased from 51% to 36% and further to 18% at 65°C. Mn-SodM retained 50% of total helical content at 55°C, which dropped down to 30% at 60°C-65°C.

An approximately 10°C difference between the midpoints of unfolding was observed between the two metalated isoforms of SodM (Figure 3.9, Figure 3.16). Fe-SodM dimer was found to be more thermally stable than Mn-SodM in solution with an unfolding occurring in single transition at T_m of 72.7°C as oppose to 62.6°C calculated for Mn-loaded protein.

The observed trend of relatively lower thermal stability of Mn-loaded, with respect to Fe-loaded forms of SODs could imply a possible role of metal cofactor in thermostability of the *S. aureus* protein, as has been described for *E. coli* metal-specific SODs (Hunter et al., 2002). Mn-binding (increased Mn to Fe content) has been shown to decrease the enthalpy of the heat inactivation process of recombinant cambialistic SODs of *Streptococcus mutans* (De Vendittis et al., 2010), and *Propionibacterium shermanii* (Meier et al., 1997). Conversely, due to stronger Fe-ligand bonds than Mn-ligand bonds, tighter binding of Fe-cofactor could influence the overall stability of Fe-SaSOD isoforms. Increased stability of SodM in comparison to SodA could potentially result from greater numbers of electrostatic interactions (i.e., hydrogen bonds and salt bridges) contributing to higher resistance to disruption of structure as heat increases the kinetic energy within the protein.

The metal cofactor did not seem to alter chemical stability of SaSODs, evaluated upon urea or guanidine hydrochloride mediated denaturation. As observed in the case of purified, recombinant SodM (Figure 3.11), chemical unfolding did not occur upon treatment of the Mn-loaded form of the protein with 8 M urea, monitored by tryptophan fluorescence (Figure 3.17 and Table 3.5). Both Fe and Mn-SodA presented a red-shift of tryptophan fluorescence in 8 M urea and 6 M guanidine, arising from the exposure of hydrophobic residues to solvent environment, during protein unfolding.

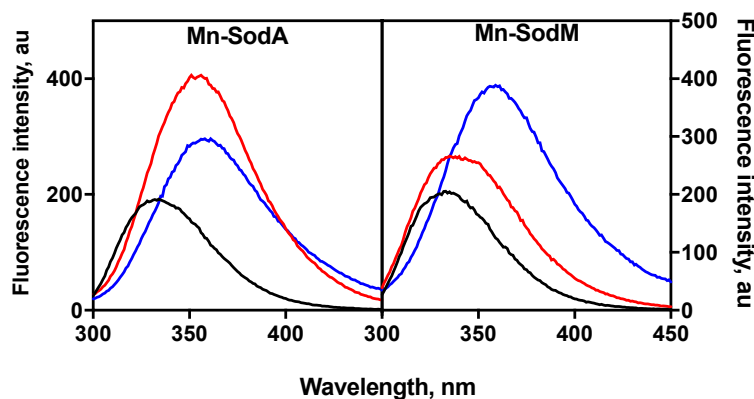


Figure 3.17 Tryptophan fluorescence spectroscopy of refolded (Mn-loaded) forms of SaSODs.

Fluorescence emission measurements were performed using Cary Eclipse Fluorescence Spectrophotometer (Varian Inc., Agilent Technologies). Samples of proteins at 10 μ M concentration in either 20 mM Tris, 150 mM NaCl buffer pH 7.5 (black trace), 8 M urea (red trace) or 6 M guanidine (blue trace) were analysed at room temperature. Collected fluorescence emission spectra were recorded between 300 nm and 450 nm upon excitation at 280 nm, at 30 nm/min scan rate.

Protein	Fluorescence emission wavelength, [nm]		
	Tris/ NaCl buffer	8M Urea	6M Gdm
Fe-SaSodA	331	355	355
Fe-SaSodM	334	335	355
Mn-SaSodA	332	351	358
Mn-SaSodM	332	335	359

Table 3.5 Overview of the chemical stability of SaSODs evaluated by Trp fluorescence.

Fluorescence emission spectra were collected between 300 nm and 450 nm under 280 nm excitation using Cary Eclipse Fluorescence Spectrophotometer (Varian Inc., Agilent Technologies). Summarised are the maximum intensity peaks of fluorescence emission, recorder for samples in 20 mM Tris, 150 mM NaCl buffer pH 7.5, 8 M urea or 6 M guanidine. Red shift of fluorescence emission (~330 nm to ~350 nm) is reporting of solvent exposure of tryptophan residues occurring during protein unfolding.

3.2.11. All four forms of SaSODs are catalytically active

Both SaSodA and SaSodM recombinant proteins purified from *E. coli* were tested for catalytic activity with either Mn or Fe bound as their metal cofactor. Homogenous preparations were used to ensure accurate interpretation of metal dependent activity. In-gel NBT-riboflavin SOD activity assay performed using equal amount of proteins (Figure 3.18) suggested a quantitative difference. To measure the specific activity of different metalated forms of proteins, a commercially available WST-1 SOD Assay Kit from Sigma-Aldrich was used. Assessment of the specific enzymatic activity with a spectrophotometric assay showed that SaSodA possessed substantially (~400-fold) higher activity when utilizing manganese ($1594 \pm 81 \text{ U}\cdot\text{mg}^{-1}$) as a cofactor in respect to Fe-loaded ($4 \pm 1 \text{ U}\cdot\text{mg}^{-1}$) isozyme. However, in the case of SaSodM, catalytic analysis revealed that both metalated forms of the protein had lower activity than Mn-SodA. Both Mn-loaded and Fe-loaded SodM had comparable levels of activity (210 and $215 \pm 21 \text{ U}\cdot\text{mg}^{-1}$), demonstrating cambialistic properties of this enzyme.

Equal activity observed for both metalated forms of SodM imply possibility of a metal switch under varying growth condition, conferring protein activity and resistance to oxidative stress.









	Fe		Mn	
	SaSodA	SaSodM	SaSodA	SaSodM
SDS-PAGE				
In-gel SOD assay				
SOD activity (U mg⁻¹_{protein})	4.28	209.53	1593.93	214.63
SD	0.69	21.34	80.88	21.34
mole equivalents				
Fe	1.01	1.00	0.01	0.01
Mn	0.00	0.01	1.04	1.04

Figure 3.18 SOD activity assay.

Relative activity of metalated isoforms of recombinant SaSODs (aliquots of 2 µg of protein in 20 mM Tris, pH 7.5, 150 mM NaCl buffer) was assessed in-gel by the nitroblue tetrazolium (NBT-riboflavin) negative staining of protein samples resolved on non-denaturing 15 % (w/v) polyacrylamide gel (Beauchamp and Fridovich, 1971). The assay output represents SOD activity as an achromatic zone on a dark blue background. The assay results were visualised using Image Lab™ software on BioRad ChemiDoc XRS+ system and inverting the display to enhance the view of activity zones.

The specific enzymatic activity was determined using a commercial assay kit (SOD Assay Kit-WST-1, Sigma Aldrich). Protein concentration was determined by absorbance at A₂₈₀. The assay results showing the percentage of superoxide dismutase-mediated inhibition of the rate of reduction of tetrazolium salt by xanthine oxidase-generated, were collected using 96-well plate reader, by monitoring absorbance at 450 nm. Protein samples were analysed against a standard curve of known concentrations of SOD from bovine erythrocytes as well as recombinant *E. coli* SodA. The sigmoidal fit of the standard curve was generated using OriginLab software, which was also used to interpolate value of U·ml⁻¹ in analysed SOD samples. Based on the determined protein concentration, the final number of SOD units per milligram of protein was calculated. Data presented as an average of 10 assays in U·mg⁻¹ ± SD.

Molar equivalents of metal content per subunit of protein were determined based on the elemental analysis of proteins by ICP-MS and protein concentration measured by A₂₈₀ absorbance.

3.2.12. Direct metal competition and EDTA effect on the metalation of SaSODs

Stability of binding of the metal cofactor was addressed by exposing previously purified protein samples to a relatively high concentration of metal chelator, EDTA (10 mM), for half an hour at room temperature and then resolving by SEC in 20 mM Tris pH 7.5, 150 mM NaCl and 1 mM EDTA buffer. Metal analysis performed on SEC eluate (data not shown) did not show any significant change in the metal content of proteins that underwent EDTA treatment with respect to non-treated equivalents (Table 3.2, Table 3.3).

Potential inter-metal competition and/or displacement of bound cofactor with other permitted metals was tested/challenged by incubation of samples of metal-loaded proteins (from

Figure 3.12) with two mole-equivalents of competitor metal (Fe or Mn) at 37°C. A visible colour change from transparent to light-orange was noted (Figure 3.19) following incubation for 1 hour at 37°C in the case of Mn-SOD preparations with a two-fold excess of FeSO₄. After 10 min of centrifugation at 21100 g, a brown precipitate was observed in the discoloured samples. No change of colour or precipitate was visible in the preparations of Fe-SODs exposed to MnCl₂ two-fold excess.

Following the incubation, soluble supernatants were resolved by size exclusion chromatography in 20 mM Tris pH 7.5, 150 mM NaCl and 1 mM EDTA buffer, and metal content was verified by ICP-MS (Figure 3.19). No change to their native metal content was observed for the samples of Fe-SODs incubated with Mn, implying no direct metal exchange upon heating up of the proteins to 37°C. When the preparations of Mn-SODs were subjected to competition with 2-fold excess of FeSO₄, an increase in Fe content was noted in the case of both SodA (from 1.3 % to 5.2 %) and SodM (from 6.5 % to 9.3 %) at the expense of the Zn contaminant, but with a negligible change of Mn content.

As described in sections 3.2.3, 3.2.7.1, 3.2.9 denaturing conditions are required to remove the metal from SodA and SodM, implying the existence of relatively high kinetic barriers for changes in the metalation state of the folded protein. As indicated by different behaviour of the two proteins under thermal (Figure 3.9, Figure 3.16) and chemical unfolding (Figure 3.11, Figure 3.17), these barriers are probably related to the stability of the protein structure. Metal binding to *E. coli* Mn-SOD was shown to be kinetically controlled, dependent on thermal excitation of the apo-Mn-SOD protein (Ose & Fridovich, 1979; Beyer et al., 1991; Mizuno et al., 2004). A direct titration of competitor metal into metalated and folded SaSODs at 37°C did not yield metal-exchanged isoforms of proteins. Observed subtle changes in metalation state could have originated from a metal-EDTA chelate to protein-surface complexes, co-eluting in SEC.

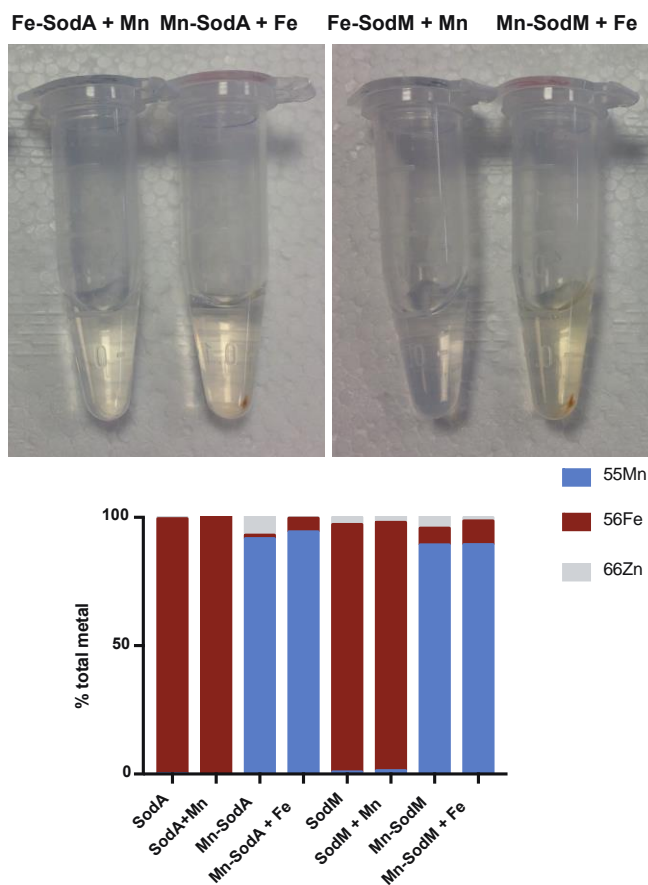


Figure 3.19 Fractional metal content of SaSOD proteins incubated with another permitted metal cofactor.

Purified preparations of proteins overexpressed in a presence of external metal supply, at the average concentration of 50 μM were mixed with 2 molar-equivalents of the opposite metal cofactor solution (FeSO_4 or MnCl_2), mixed by vortex, and incubated at 37°C for 1 hour. Samples were centrifuged and resolved by an analytical size-exclusion chromatography in 20 mM Tris, 150 mM NaCl pH 7.5, 1 mM EDTA buffer. Collected fractions were analysed for metal content using ICP-MS. Isotopes Fe (red bar), Mn (blue bar), Zn (grey bar), Ag and Pt were monitored in triplicate, and metal concentrations determined from the standard curve. Metal content is represented as a percent of total determined metal. Bar plot represents a single replicate experiment.

3.2.13. *In vitro* substitution with non-physiological metal cofactors yields inactive proteins

To study binding of alternative metals to SaSODs, SodA and SodM proteins at approximately 2.5 μM concentration were subjected to *in vitro* unfolding in guanidine hydrochloride in presence of metal chelators as described in a previous section 2.12. Refolding was carried out with addition of 1 mM manganese or non-physiological metal (Co, Cu, Zn) to dialysis buffer. Following several rounds of dialysis against 20 mM Tris pH 7.5, 150 mM NaCl, the post-dialysis sample was centrifuged to remove any potential precipitate (none was visible) and concentrated down to 0.5 ml final volume. The concentrate was resolved by SEC on Superdex 200 increase 10 300 GL in 20 mM Tris pH 7.5, 150 mM NaCl, 1 mM EDTA buffer and the collected fractions were analysed for metal content using ICP-MS.

In comparison to Mn-refolding used as a control, SodA (Figure 3.20 A) was found to bind on average 1.1 equivalents of Co, Cu or Zn, whereas SodM (Figure 3.20 B) bound approximately 0.9 molar equivalents of metal per subunit of enzyme.

Binding of Co, Zn, Ni, Fe or Cu has been reported for *E. coli* Mn-superoxide dismutase (Ose & Fridovich, 1976), (Ose & Fridovich, 1979), Mn-superoxide dismutase from *Bacillus stearothermophilus* (Brock & Harris, 1977) or Fe-superoxide dismutase from *Pseudomonas ovalis* (Yamakura & Suzuki, 1980). In all examples mentioned above, metal-reconstituted enzymes presented no catalytic activity, when loaded with non-native metal cofactor. Similarly to previously reported examples, SaSODs did not retain their enzymatic activity after loading with metals other than Mn or Fe (Figure 3.20 C-E). Native and reconstituted enzymes exhibited identical elution profiles on SEC and mobility upon polyacrylamide gel electrophoresis.

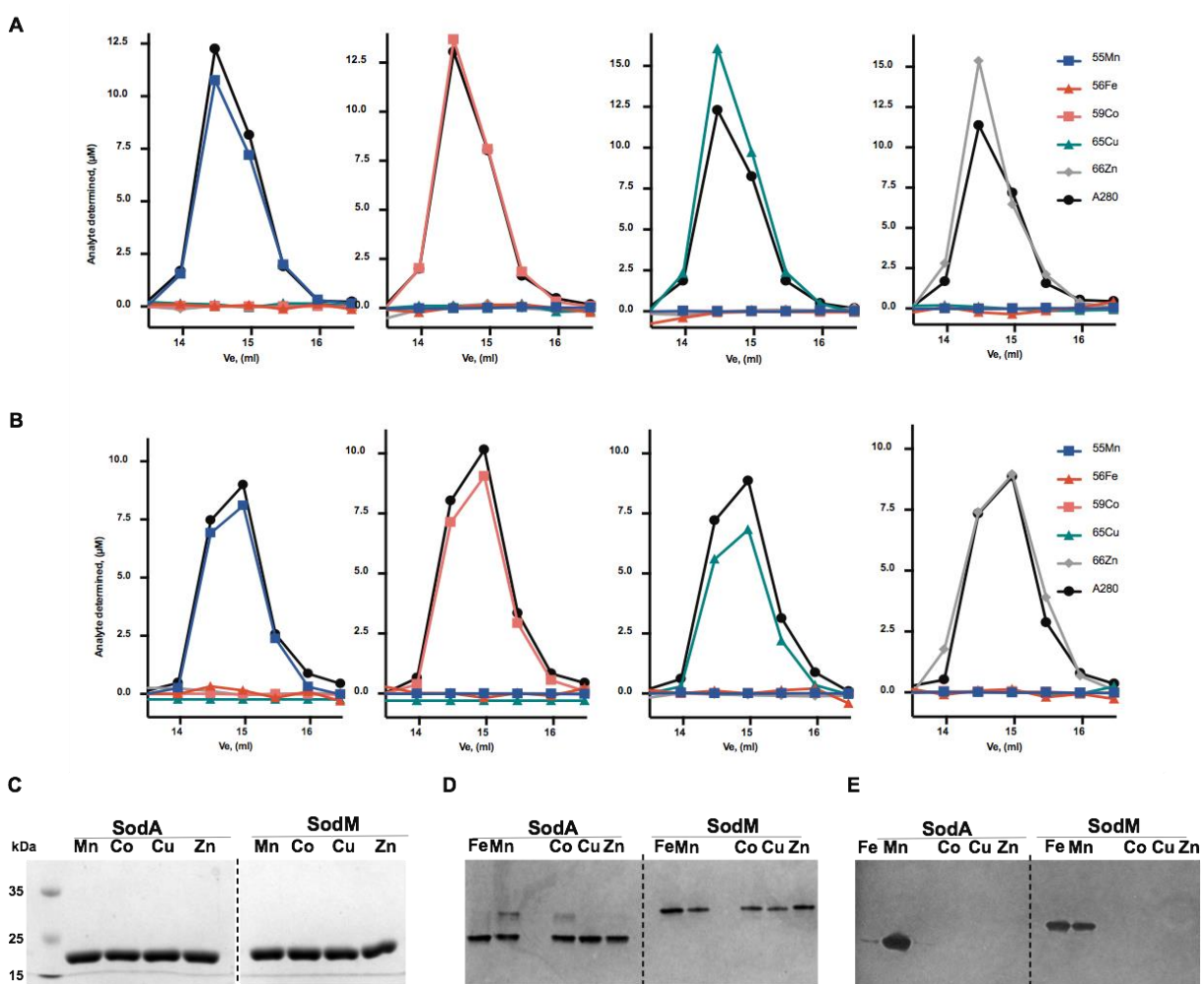


Figure 3.20 ICP-MS analysis of proteins after forced mis-metalation through *in vitro* refolding.

Elemental analysis of protein fractions after an analytical size exclusion chromatography step. All standards and samples were prepared in a solution of 2.5% (v/v) HNO₃ containing 20 µg·L⁻¹ Ag and Pt as internal standards. Isotopes Fe (red squares), Mn (blue triangles), Co (salmon squares), Cu (teal triangles), Zn (grey diamonds), Ag and Pt were monitored in triplicate, and metal concentrations determined from the standard curve. Protein concentration determined with A280 is depicted as black circles.

Protein fractions were analysed by electrophoresis, for purity using SDS-PAGE (C); and mobility (D), and catalytic activity (E) by Native-PAGE.

3.2.14. *In vitro* interaction of SodA and SodM (heterodimer formation)

The interaction of subunits of SodA and SodM leads to formation of a heterodimer, which produces a third superoxide dismutase activity band visible through the in-gel NBT-riboflavin SOD assay of *S. aureus* cell extract (Figure 3.1), (Valderas & Hart, 2001; Valderas et al., 2002). Formation of a hybrid enzyme *in vitro* has been described in *E. coli*, where monomer of Mn-SOD was found to interact with a monomer of Fe-SOD to form a heterodimer (Clare et al., 1984). In *E. coli* as well as in *S. aureus*, it is not known whether the formation of a hybrid SOD protein has physiological relevance or is merely the result of subunit exchange between two related proteins.

The molecular masses of both metalated forms of each SaSOD protein in solution were determined using size-exclusion chromatography combined with multi-angle light scattering (SEC-MALS). Sample analysis and data collection were performed by Dr Owen Davies (ICAMB, Newcastle University). SEC-MALS is a direct measurement of the light scattering of the molecules in solution, and provides an accurate way of determining mass and, therefore, oligomeric state of the proteins. Both metalated forms of the two proteins behaved as stable dimers (i.e. elutes as monodisperse peaks). Differences in the retention properties of the two SaSODs by size exclusion chromatography (section 3.2.3) indicated small variance between their apparent molecular masses of 46.22 kDa for SodA and 45.04 Da for SodM, when compared to elution profiles of proteins of known masses. The combination of SEC retention with the light scattering and refractive index analyses allowed for determination of an absolute molar mass of studied proteins, as following: Fe-SodA 43.63 kDa ($\pm 0.136\%$), Mn-SodA 41.90 ($\pm 0.107\%$), Fe-SodM 45.24 ($\pm 0.175\%$) and Mn-SodM 44.96 ($\pm 0.129\%$), (Figure 3.21). Even though the elution profile of SodM, relative to SodA, indicated its apparent mass to be smaller, when corrected for light scattering and refractive indexes, the absolute determined mass of SodM was in fact bigger than SodA, consistent with their theoretical masses (theoretical masses according to ProtParam: 23.04 kDa and 22.71 kDa, respectively).

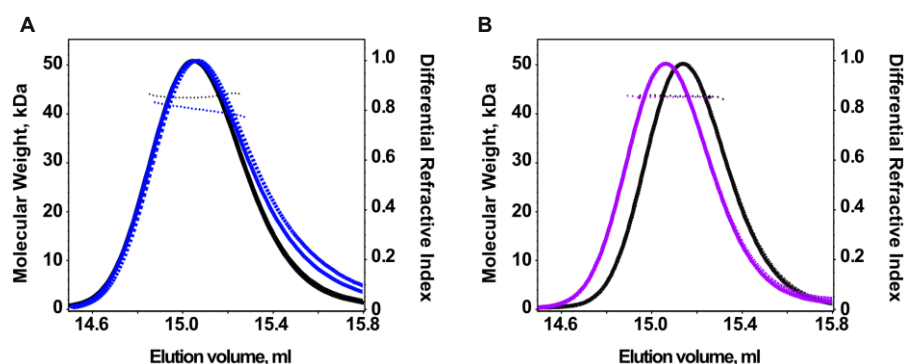


Figure 3.21 Analysis of the oligomeric state of SaSODs in solution by SEC-MALS.

The absolute molar mass of protein in solution was determined using size-exclusion chromatography combined with multi-angle light scattering analysis (SEC-MALS) of SodA (A) and SodM (B). Protein samples (100 μl ; 1 $\text{mg}\cdot\text{ml}^{-1}$) were resolved on size exclusion column, in 20 mM Tris pH 7.5, 150 mM NaCl, at $0.5\text{ ml}\cdot\text{min}^{-1}$ rate, using an ÄKTA FPLC system. Samples eluting from the column passed through light scattering detector, coupled to a refractive index detector. A weight average molecular mass was calculated from collected data, based on refractive index and light scattering measurements using Astra 6 software (Wyatt Technology): Fe-SodA 43.63 kDa ($\pm 0.136\%$), Mn-SodA 41.90 ($\pm 0.107\%$), Fe-SodM 45.24 ($\pm 0.175\%$) and Mn-SodM 44.96 ($\pm 0.129\%$).

The *S. aureus* SodA and SodM form a heterodimer *in vivo*, which is a SodA/SodM hybrid of subunits. To evaluate heterodimer formation *in vitro*, co-unfolding/co-refolding of SodA and SodM in the presence of Mn, was performed following protocols established for preparation of Mn-loaded proteins. Following dialysis, the proteins mixture was resolved by size exclusion chromatography, and collected fractions were subjected to metal analysis. The dimeric species eluting from size-exclusion chromatography were loaded with Mn (Figure 3.22 A) and consisted of a mixture of SodA and SodM homodimers, and the SodA/SodM heterodimer, as was confirmed by PAGE (Figure 3.22 B), and all exhibited catalytic activity (in-gel NBT-riboflavin SOD assay). This indicated that SodA and SodM can exchange subunits and form an active hybrid form of SodA/SodM, through co-refolding in the presence of Mn cofactor.

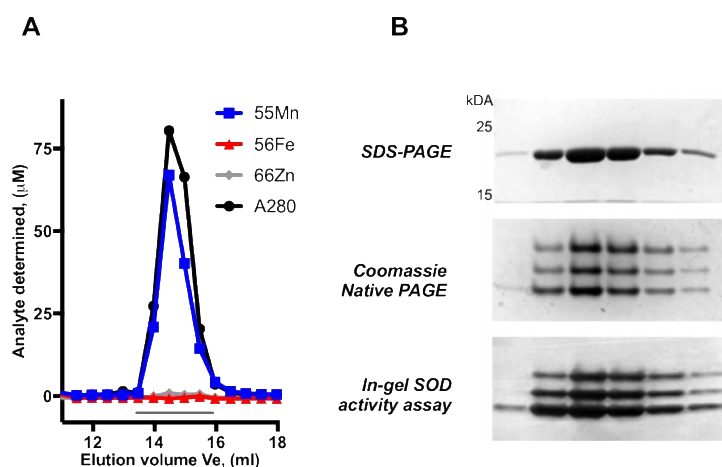


Figure 3.22 *In vitro* SodA/SodM heterodimer formation by refolding in presence of Mn.

Metal analysis of the mixture of SodA and SodM refolded in a presence of Mn, after resolving on size exclusion column (A), confirmed co-migration of Mn (blue squares) with protein in fractions of eluate (black circles). Gel electrophoresis (B), performed across fractions indicated with grey line (A), confirmed purity of the eluate (SDS-PAGE) and activity and formation of SodA/SodM hybrid (Native-PAGE, in-gel assay).

To test the possible influence of an identity of metal cofactor of recombinant proteins on the capacity of these enzymes to form a hybrid of SodA/SodM, the pairs of Mn/Mn; Fe/Fe; Mn/Fe-loaded proteins were assessed. The combinations of different metalated versions of SaSodA and SaSodM proteins were prepared in 1:1 ratio and incubated at room temperature or at 37°C for a period of 24 hours (Figure 3.23). Subsequently, single protein controls and protein mixture samples were resolved by 15% (w/v) native PAGE, in duplicate, with one gel stained with Coomassie to verify the protein content and the other gel used to perform qualitative NBT-riboflavin SOD activity assay. The obtained results suggested the formation of SodA/SodM heterodimer *in vitro* to be a temperature-dependent process as the occurrence of the middle band was noted for samples incubated at 37°C, with no indication of heterodimer being formed after 24 hours at room temperature.

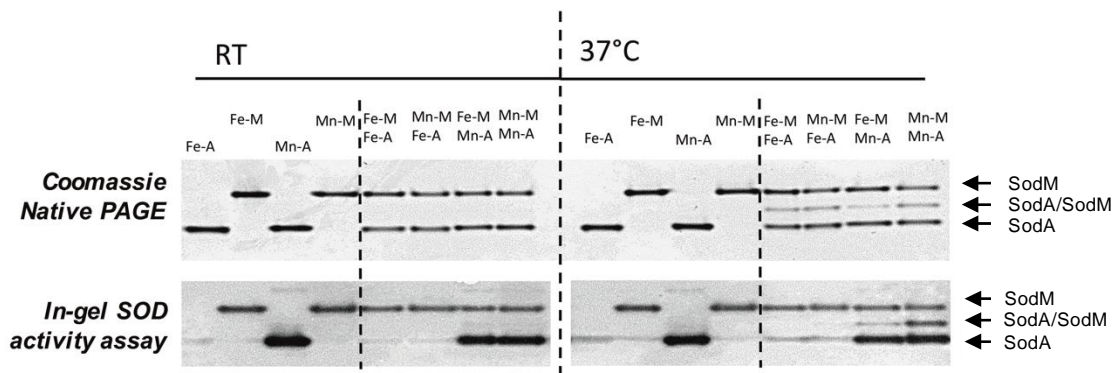


Figure 3.23 *In vitro* SodA/SodM heterodimer formation in varying temperature conditions.

First column of lanes (dashed line borders) in each temperature condition, represents single protein controls. In the second column lanes contain mixtures of SodA and SodM metalated forms in combinations: Fe + Fe, Fe + Mn and Mn + Mn. Samples were resolved by 15 % Native-PAGE and stained either with Coomassie or NBT-riboflavin mix for SOD activity detection, after 24 hours of incubation at either room temperature (RT) or at 37°C. Formation of heterodimer is observed as the appearance of a third and of activity, migrating in between SodA and SodM.

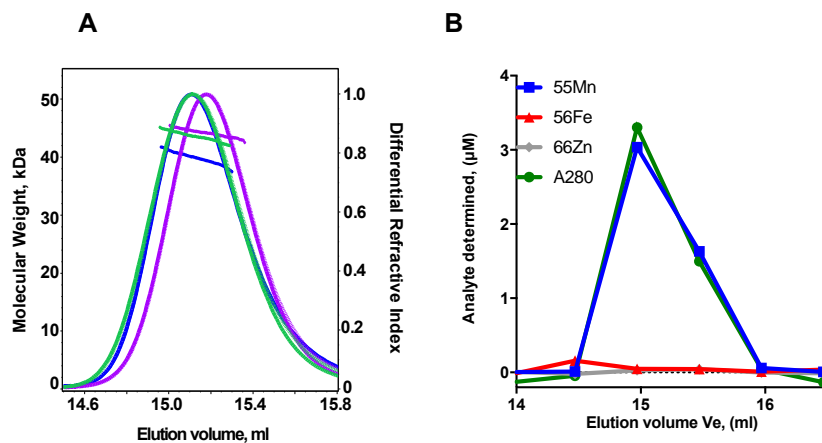


Figure 3.24 SEC-MALS analysis of Mn-loaded heterodimer.

Oligomeric state of heterodimer mixture (green trace), relative to Mn-SodA (blue trace) and Mn-SodM (purple trace) was assessed by SEC-MALS (A). Metal content of SEC-purified heterodimer was determined by ICP-MS (B). Only Mn (blue squares) and no other metal contamination (Fe, red triangles; Zn, grey diamonds), was found to co-migrate with the protein trace (green circles) collected after SEC-MALS run.

A complex of Mn-SodA/Mn-SodM subunits formed a stable heterodimer. An equimolar mixture of Mn-loaded SODs was incubated for 24 hours at 37°C, and subsequently resolved on size exclusion column in 20 mM Tris, pH 7.5, 150 mM NaCl, 5 mM EDTA buffer. Following a chromatography step, SEC-MALS analysis (Figure 3.24) was performed on concentrated eluate peak fractions. It is important to note that the actual sample contained a population of homodimers of SodA and SodM as well as the SodA/SodM heterodimer.

A SodA/SodM hybrid (green trace, Figure 3.24) presented slightly altered retention properties by size exclusion column, eluting earlier than any of the homodimers, but closer to SodA (blue trace) homodimer. Mass calculation determined absolute mass of heterodimer to be 44.29 kDa ($\pm 0.131\%$, green trace), which lays between masses of Mn-SodA (41.90 kDa $\pm 0.107\%$, blue trace) and Mn-SodM (44.80 kDa $\pm 0.154\%$, purple trace), but closer to Mn-SodM. Altered elution profile and molecular mass indicated formation of the hybrid of SodA and SodM subunits. A fraction of 2.8 % of total determined mass was found to elute further in the profile, with a molecular mass of 21.82 kDa ($\pm 0.154\%$), suggesting a monomeric species (single subunits) was also present in equilibrium with the dimers.

The presence of the metal associated with a protein, eluted from the size exclusion column after the SEC-MALS analysis, was confirmed by ICP-MS (Figure 3.24 B). Mn (blue squares) was found to co-migrate with an eluate protein trace (green circles), suggesting that any subunit exchange occurring between SodA and SodM at 37°C did not influence the binding of metal in the active sites of proteins.

3.3. Conclusions

The two genes encoding superoxide dismutase SodA and SodM proteins of *S. aureus* were cloned and expressed in a heterologous host. Purification of proteins from *E. coli* cultured in standard growth conditions indicated the acquisition of primarily Fe cofactor by both recombinant proteins. Manipulation of the metal content in bacterial culture, in both standard and minimal growth conditions, suggested that the metalation of the recombinant proteins could be altered by changing availability of the external source of metal. Culture conditions were optimised to yield Fe loaded proteins, containing negligible level of Mn. An efficient way to prepare metalated isoforms of recombinant SODs was achieved by means of optimised *in vitro* unfolding in the presence of metal chelators, followed by refolding through dialysis in buffer containing Mn. Metal-pure forms of SaSODs were prepared with Fe, Mn, Co, Cu and Zn cofactors, suggesting no absolute metal binding selectivity of the two proteins. The physiological relevance of cofactors was confirmed by assessment of enzymatic activity, which was demonstrated for the two metals, Fe and Mn.

The two proteins presented distinct metal-specific catalytic properties. SodA was found to resemble a typical Mn-specific enzyme; SodM however displayed cambialistic properties, manifested by equal activity with Fe and Mn cofactors. Both proteins formed stable dimers in solution as confirmed by SEC-MALS analysis. Recombinant proteins were found capable of inter-protein subunit exchange, leading to formation of SodA/SodM heterodimer, upon either chemical

or thermal induction of conformational change. The two proteins were found to be very similar in their secondary structure composition. However, biophysical analysis by CD spectroscopy and tryptophan fluorescence revealed that SodM presented higher thermal and chemical stability, relative to SodA.

The requirement for conformational rearrangements in protein structure (induced by temperature or chaotropes), for removal and exchange of a metal cofactor of SaSODs, or for subunit exchange and formation of the heterodimer, and quantitative incorporation of metal into proteins eluting off size-exclusion column, suggested the role of kinetic trapping as a determinant of stability of the active, i.e. metalated SaSODs.

The evolution of a Mn-specific enzyme into cambialistic isoform most probably occurred after a duplication of the common ancestor of both the SodA, and the SodM in staphylococcal lineage, and the subsequent divergence. The SaSodA sequence shares a high level of similarity with SOD sequences from other species of *Staphylococcus* genus, whereas SodM is highly conserved amongst *S. aureus* strains (99% identity at protein level), but is absent from the genomes of other staphylococci. This could indicate a potential specialisation of the SodM and its contribution to the increased adaptability of pathogenic *S. aureus* bacteria.

Chapter 4. Identification of residues determining cambialism of SaSodM

4.1. Introduction

There are 333 structures of superoxide dismutases deposited in the public database Protein Data Bank in Europe (PDBe, database accessed 09/2017); <https://www.ebi.ac.uk>. The majority of the published structures have been solved for eukaryotic (215 structures from 33 species) and bacterial (107 structures from 36 species) SODs, with only 10 structures of underrepresented archaeal enzymes and one structure of SOD from a megavirus. Out of all 333 structures representing the three distinct families of Cu,Zn-dependent, Mn/Fe-dependent, and Ni-dependent SODs, 131 are models of superoxide dismutases belonging to the Mn/Fe-superfamily. Mn/Fe-dependent SODs are ubiquitous enzymes conferring enzymatic activity against superoxide stress in prokaryotes, archaea, blue-green algae, protists, chloroplasts, and mitochondria.

The superfamily of Mn/Fe-SOD proteins comprises the highly metal-specific enzymes, Fe-specific or Mn-specific, and a small number of characterised cambialistic enzymes, which are active with both cofactors. All these proteins share a high degree of structural homology. A monomer comprises two conserved domains, an α -N-terminal domain and an α/β -C-terminal domain, connected by a loop (Chapter 1, section 1.4.3). Often the helices of the N-terminal domain of the Fe-specific enzymes are found to be longer than the equivalents in Mn-specific enzymes. The Mn/Fe-SODs form biological dimers or tetramers. Two very well studied members of the Mn/Fe-SODs, *E. coli* Fe-SOD and Mn-SOD, share a conserved protein fold and a dimer interface that involves active site residues, as well as the funnel by which substrate gains access to the catalytic metal ion, which is coordinated by three histidine residues and one aspartate. The Fe or Mn ion is also coordinated by a fifth ligand, the solvent molecule that engages in hydrogen bonds with outer sphere residues (a glutamine mediates the contact between the solvent and other amino acids). The metal coordination site of the Mn-SOD and the Fe-SOD does not provide structural clues that could explain the distinct metal-specific activities of these two enzymes. Moreover, both active sites can bind either metal ion with similar coordination geometries, but only one metal confers the protein's catalytic activity (Lah et al., 1995; Edwards et al., 1998).

As shown in the previous Chapter 3, the *S. aureus* SODs (SaSODs) can each bind both Fe and Mn cofactors. Preparation of recombinant proteins allowed for the characterisation of their metal requirements and catalytic activities. SodA was characterised as a typical Mn-specific enzyme, showing only negligible activity when loaded with Fe, and therefore reflecting characteristics of well characterised Mn-SOD of *E. coli*. SodM, however, displayed an equally high degree of activity regardless of Mn or Fe-bound cofactor, but with a lower overall efficiency than Mn-SodA. Differences in stability between the two recombinant *S. aureus* SOD proteins were also described, with SodM displaying higher resistance to unfolding.

The ability to confer activity with both metals requires that the protein controls the chemistry of the metal cofactors, by accommodating changes that are necessary to provide redox potential that is appropriate for catalysis. To investigate the distinct properties of the two SaSODs, the following work will address the structural determinants that potentially distinguish the cambialistic active site of SodM, and the Mn-specific site of SodA, with an aim to translate the findings from this system onto the wider Mn/Fe-dependent SOD protein family.

4.2. Results and discussion

4.2.1. Crystallisation and determination of the structure of SaSODs

Both Fe-loaded and Mn-loaded forms of the two *S. aureus* SOD enzymes were first subjected to crystallisation trials and optimisation. Diffraction experiments were performed at the Diamond Light Source (Didcot, UK) synchrotron and data were collected and processed by Dr Arnaud Baslé (Newcastle University, UK). The structural solution was performed either by, or under the supervision of Dr Arnaud Baslé. The deposited structures of Mn-SodA and Mn-SodM were assigned PDB codes 5N56 and 5N57, respectively. At the time of submission of this thesis, the remaining crystal structures have not yet been published, however they have been deposited and were assigned a PDB identifiers: 6EX3 (Fe-SodA), 6EX4 (Fe-SodM), and 6EX5 (Mn-SodM triple mutant).

4.2.1.1. Data collection and structure solution

The two SaSOD enzymes, which share 75 % protein sequence identity (Figure 3.3) and originated from a duplication and a divergence event (Figure 3.2), possess distinct metal-dependent activities (Figure 3.17). To identify structural factors that could potentially determine these critical differences, SodA and SodM were crystallised for structure determination. Purified proteins of over 95% purity, as confirmed by SDS-PAGE (data not shown); containing exclusively target metal ion, as measured by ICP-MS; were concentrated to 10-15 mg·ml⁻¹, and initial sitting-drop vapour-diffusion crystallisation trials were set up against commercially available systematic grid (PACT; Molecular Dimensions, UK) and sparse matrix (JCSG+, Structure; Molecular Dimensions, UK) screens in 96-well MRC crystallisation plates at 20°C, as described in section 2.15. From all positive hits of the initial screening (Appendix, Table 8.1), selected conditions were further manually optimised around the original composition of the crystallisation liquor (section 2.15.1) for salt, precipitant concentration and pH, using the hanging drop of vapour diffusion method at 20°C, in 24-well Linbro plates (Molecular Dimensions, UK). Crystal trays were examined for formation of crystals using 16x optical zoom light microscope (Leica). The crystals of visually good quality were harvested by Dr Arnaud Baslé (Newcastle University, UK) using CryoLoops (Hampton Research, UK), cryo-protected in reservoir solution supplemented with 20

% (w/v) PEG400, and flash-frozen in liquid nitrogen for storage and transfer to the Diamond Light Source.

Diffraction patterns were collected for the crystals of four metalated forms of the SaSOD proteins, produced in conditions listed in Table 4.1, by Dr Arnaud Baslé (Newcastle University, UK) at the Diamond Light Source on four experiments (BAG numbers: mx7864-57, mx7864-62, mx7864-67, mx9948-1).

Protein	Condition
Fe-SaSodA	0.2 M MgCl ₂ , 30 % PEG 4000, 0.1 M Tris pH8.5
Mn-SaSodA	0.2 M MgCl ₂ , 30 % PEG 4000, 0.1 M Tris pH8.5
Fe-SaSodM	25 % PEG 1500, 0.1 M PCTP pH 7.0
Mn-SaSodM	0.05 M KSCN, 30 % PEG 2000 MME

Table 4.1 Protein crystallisation final conditions.

Protein	Model	Reference	Sequence Identity (%)
Fe-SaSodA	2RCV (1.6 Å, Mn-Sod, <i>B. subtilis</i>)	Liu <i>et al.</i> , 2007	71.8
Mn-SaSodA	Fe-SodA	This study	100
Fe-SaSodM	2RCV (1.6 Å, Mn-Sod, <i>B. subtilis</i>)	Liu <i>et al.</i> , 2007	62.4
Mn-SaSodM	Fe-SodM	This study	100

Table 4.2 Phase problem search models.

The test images (Figure 4.1) were indexed with iMosflm (Battye *et al.*, 2011) to determine the unit cell parameters and space group of the crystals, and select the best strategy for collecting a complete dataset. The datasets were processed (indexed and integrated) using XDS (Kabsch, 2010). Reflections were scaled to average all symmetry equivalent reflections, and merged using Aimless (symmetry check, space group determination, twinning check) in CCP4 suite (Collaborative Computational Project, 1994; Evans, 2006; Evans, 2011, Evans and Murshudov, 2013). A summary of the data collection statistics is given in Table 4.3.

Upon data collection, metal content analysis was performed *in crystallo* to confirm the identity of the bound metal cofactor (Figure 4.1 C). Fluorescence scans were taken at the K edge of the Fe, Mn and/or Zn excitation wavelength allowed detection of peaks of metals coordinated in proteins. The representative fluorescence edge scans shown on Figure 4.1 C were collected for Fe-loaded SodM, and confirmed qualitatively the presence of the Fe cofactor and absence of Mn or Zn bound to the SodM protein in the crystal, indicating homogeneity of metal loading of crystallised protein, in accordance with ICP-MS analysis of protein samples (Table 3.2, Table 3.3).

The quality of the data and high resolution limits were assessed by a combination of indicators, such as reliability factor (R_{merge}), signal-to-noise ratio of all recorded reflections (I/σ), completeness and correlation coefficient ($CC_{1/2}$), (Evans & Murshudov, 2013; Diederichs & Karplus, 2013; Karplus & Diederichs, 2012).

Matthews coefficient calculations (Matthews, 1968) performed in CCP4i to determine unit cell contents (probability of multimeric state), suggested for Fe-SodA at the given resolution limit, either three or four molecules were present per asymmetric unit, with a solvent content of 50 % or 34 %, respectively. The Mn-SodA, Fe-SodM, and Mn-SodM were indicated to possess two molecules per asymmetric unit with solvent content of 43-58 %.

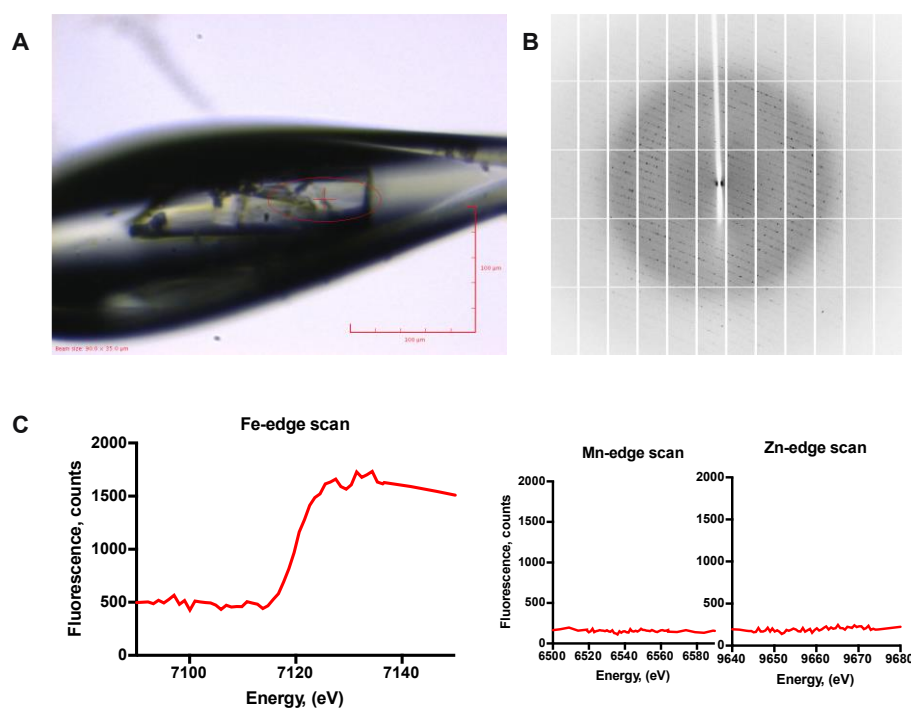


Figure 4.1 Fe-SodM X-ray data collection.

An example of a crystal in a crystal loop, (A), and diffraction data (B) collected at the Diamond Light Source as part of mx7864-57 experiment on I03 beamline, for an Fe-SodM crystal at 2.2 Å resolution, with 90 x 35 μM beam (A; represented by red ellipse) at 0.97 Å wavelength. A native dataset comprising 1000 images was collected over 322° of crystal rotation with 0.2° oscillation and 0.1 s exposure per image. Fluorescence edge scans (C) assessing metal presence in the studied protein crystal. The peak (C, red line) corresponds to the K-edge excitation wavelength of iron. No peaks were observed for either Mn or Zn, that were often observed as a contaminant in protein preparations as purified from *E. coli*.

Determination of structural models was performed by molecular replacement using MolRep (Lebedev et al., 2008). Amino acid sequences of SaSodA (ABD30729.1) and SaSodM (ABD29276.1) were used to perform sequence similarity check in PDBe, to identify adequate search models for molecular replacement (Table 4.2). The 1.6 Å structure of a dimeric BsSodA from *B. subtilis* (Liu et al., 2007), sharing 62 % identity, was used as a search model to solve the phase problem for Fe-SaSodM. The molecular replacement calculations for Fe-SaSodA were more complex. The phases were obtained using the dimer of a 2 Å structure of tetrameric Fe-SOD from *M. tuberculosis* (38.8 % identity; Cooper et al., 1995) and the 1.6 Å structure of a dimeric Mn-SodA from *B. subtilis* (72 % identity; Liu et al., 2007). The initial molecular replacement solutions presented poor statistics. To improve the quality of signal, data were scaled in P1 space group, to remove any symmetry constraint on the unit cell parameters and molecular replacement was performed with Phaser. Multiple cycles of automated model building

with ARP/wARP and Buccaneer software allowed determination of the search model, presenting acceptable R factors, which was subsequently used as a source of experimental phase information to build models of Fe-SaSodA in P2₁ space group. Initial structure models were improved by iterative cycle of refinement in Refmac5 (Murshudov *et al.*, 1997) in tandem with manual model rebuilding in COOT. Models of Fe-SaSODs were subsequently used to solve the structures of the Mn-loaded isoforms.

Data collection	SaSodA (Fe)	SaSodA (Mn)	SaSodM (Fe)	SaSodM (Mn)
Beamline	I24	I04	I03	I02
Date	02/02/14	24/04/14	07/12/13	23/02/14
Wavelength (Å)	0.96862	1.88138	0.97957	1.28162
Resolution (Å)	47.01-2.20 (2.27 – 2.20)	43.30 – 2.07 (2.12 – 2.07)	46.47 – 2.40 (2.49-2.40)	46.55 – 2.30 (2.38 – 2.30)
Space group	P2 ₁	P2 ₁	P6 ₁	P6 ₁
Unit-cell parameters				
a, b, c (Å)	47.6, 66.4, 108.3	51.3, 68.4, 56.7	141.9, 141.9, 46.2	142.2, 142.2, 46.4
α, β, γ (°)	90.0, 98.7, 90.0	90.0, 99.5, 90.0	90.0, 90.0, 120.0	90.0, 90.0, 120.0
Unit-cell volume (Å³)	337976	196115	805531	813284
Solvent content (%)	34	43	58	58
Total reflections	118068 (9551)	77487 (1527)	69671 (7378)	78873 (7817)
Unique reflections	33834 (2914)	21845 (936)	21099 (2214)	24136 (2339)
CC_{1/2}	0.998 (0.733)	0.995 (0.971)	0.993 (0.664)	0.968 (0.760)
Completeness (%)	99.3 (98.5)	91.6 (51.7)	99.8 (99.9)	99.8 (100.0)
Redundancy	3.5 (3.3)	3.5 (1.6)	3.3 (3.3)	3.3 (3.3)
R_{merge} (%)	7.6 (72.3)	6.3 (23.5)	9.8 (56.0)	9.2 (38.5)
I/σ(I)	9.1 (1.6)	9.0 (1.5)	7.6 (1.9)	7.0 (1.5)

Table 4.3 Summary of data collection statistics of the wild type Fe and Mn-loaded SaSODs.

Summary of parameters of the datasets collected for the Fe and Mn-loaded SodA and SodM protein crystals. Values in parenthesis are for the highest resolution shell.

Generated models were validated in COOT, Phenix (Polygon), PdbRedo (Joosten *et al.*, 2012), and MOLPROBITY (Chen *et al.*, 2010) webserver. Output from PdbRedo presented better statistics for Mn-SaSodA and Mn-SaSodM, and were used for the further refinement and analysis. Final pdb models were validated with COOT (Emsley and Cowtan, 2004), MOLPROBITY (Chen *et al.*, 2010) and wwPDB validation service to check geometry, Ramachandran outliers and clashes. The final data refinement statistics are summarised in Table 4.4.

Data refinement	SaSodA (Fe)	SaSodA (Mn)	SaSodM (Fe)	SaSodM (Mn)
Rwork (%)	21.21	14.97	17.30	19.22
Rfree# (%)	27.18	23.89	23.27	23.74
No. of non-H atoms				
No. of protein, atoms	6245	3202	3244	3242
No. of solvent atoms	146	140	167	121
No. of metal atoms	4	2	2	2
R.m.s. deviation from ideal values				
Bond angle (°)	1.5	1.6	1.4	1.7
Bond length (Å)	0.014	0.014	0.011	0.017
Average B factor (Å ²)				
Protein	50.85	39.30	42.72	43.89
Solvent	44.82	38.56	40.58	35.22
Metal	41.03	27.29	31.04	30.06
Ramachandran plot*, residues in				
Most favoured regions (%)	95.24	97.19	95.41	96.43

Table 4.4 Summary of refinement statistics of the determined crystal structures of wild type SaSODs.

#5% of the randomly selected reflections excluded from refinement. *Calculated using MOLPROBITY.

Following structure solution, anomalous difference maps were calculated. Phases obtained by molecular replacement, after a few cycles of refinement with Refmac5 (Murshudov et al., 1997), were combined with anomalous data using CAD of the CCP4 software suite. FFT (Ten Eyck, 1985; Read and Schierbeek, 1988) was then used to calculate the anomalous difference map. Anomalous difference maps were calculated with data collected at the wavelength above the K-edge of either Mn (1.896 Å) or Fe (1.743 Å), which revealed anomalous difference peaks greater than 3.8 σ in Fe-SodA, 5 σ in Fe and Mn-SodM and 15 σ in Mn-SodM, corresponding to the location of the catalytic metal ion (Figure 4.2).

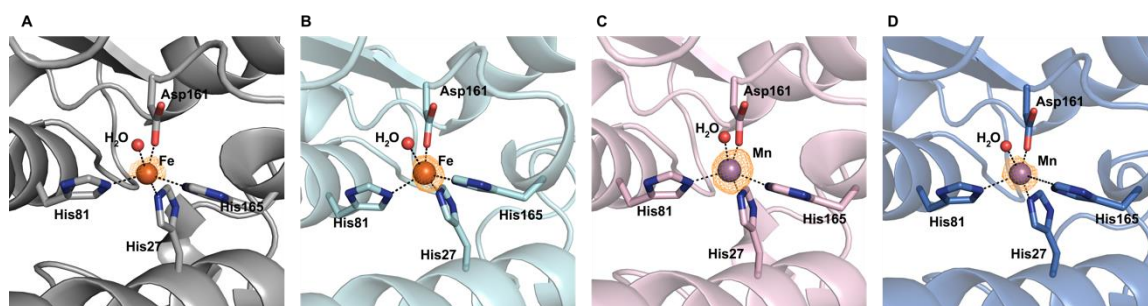


Figure 4.2 Anomalous difference maps of native proteins.

Graphic representation of metal coordination in the active sites of the homodimers of (A) Fe-SodA, (B) Fe-SodM, (C) Mn-SodA and (D) Mn-SodM. Anomalous difference maps, represented as an orange mesh, were contoured at 3.0 σ on the metal ion in the active site of Fe-SodA, at 5.0 σ on metal ion in both Mn-SodM and Fe-SodM and 15.0 σ on the Mn ion in the active site of Mn-SodA respectively. Metal ions depicted as spheres, with Fe coloured orange and Mn in purple. Metal-coordinating ligand residues are shown in the stick representation with grey (Fe-SodA), pink (Mn-SodA), aquamarine (Fe-SodM) and blue (Mn-SodM) carbon atoms, oxygens in red, nitrogens in blue and a water molecule represented as a red sphere.

4.2.2. Crystal structures of Fe and Mn containing SaSodA and SaSodM are nearly identical

4.2.2.1. Structure analysis

The crystal structures of Fe-SodA and Mn-SodA have been determined (Table 4.2, Table 4.3) at 2.20 Å and 2.07 Å resolution and refined to a crystallographic R factor of 21.21 % and 14.97 % (Table 4.4), respectively. Both isoforms of SodA crystallised in a primitive monoclinic system, in space group $P2_1$. Four chains were found in the asymmetric unit of Fe-SodA, forming a set of two dimers. The structural model of the Mn-loaded SodA consisted of two molecules in the asymmetric unit. The SodM protein isoforms crystallised in a primitive hexagonal space group $P6_1$. Structures of Fe and Mn-SodM were determined at the resolution of 2.40 Å and 2.30 Å, respectively. The crystal packing (Figure 4.3) shows close-packed and compact organisation of the SodA protein in crystal (Figure 4.3 C). SodM, however, presented looser arrangements of protein molecules in the crystal, with hexagonal-shaped channels (Figure 4.3 D), and higher solvent content than SodA (Table 4.3).

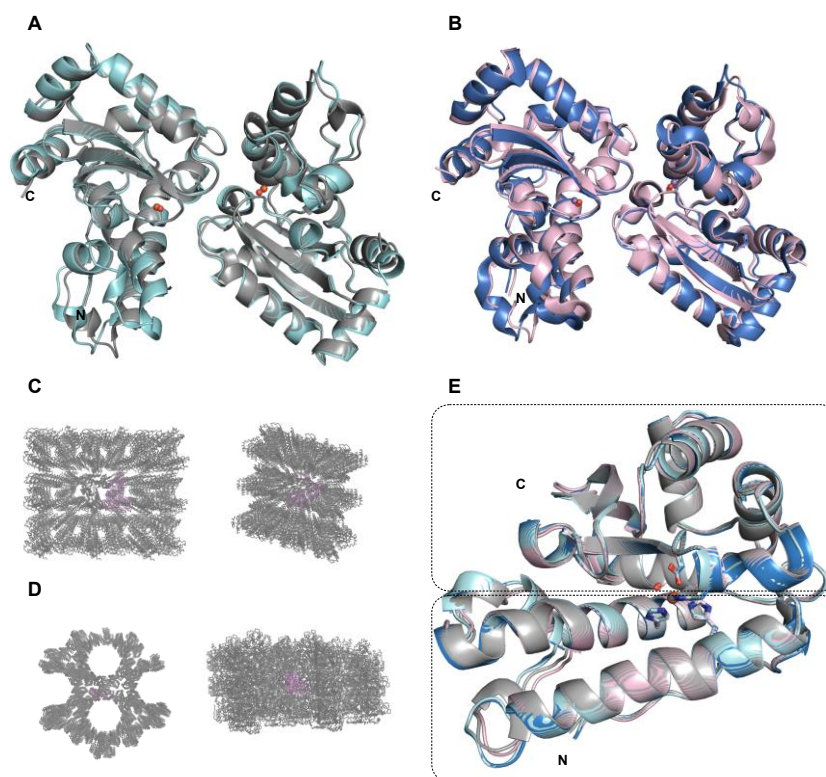


Figure 4.3 Crystal structures of SaSodA and SaSodM.

Ribbon representation of the superimposed crystal structure models of (A) the Fe-SodA (light grey), Fe-SodM (cyan), and (B) Mn-SodA (light pink) and Mn-SodM (blue) homodimers. Metal cofactor and solvent molecule represented as spheres (orange Fe, purple Mn, red water). Models of crystal packing of proteins in $P2_1$ (C, SodA) and $P6_1$ (D, SodM) space group. The molecules in the asymmetric unit (origin of symmetry-mates) are coloured in pink. The conserved two-domain fold (E) with α -helical N-terminal motif and α/β -C-terminal domain of SaSODs is shown.

Both metalated isoforms of SodA and SodM were present in the crystal as homodimers, with monomers presenting the characteristic fold conserved amongst superoxide dismutases (Figure 4.3 E) with a helical N-terminal domain and an α/β -C-terminal domain, connected by a loop. Dimers of SodA and SodM were superimposable in protein backbone with an average root mean square deviation (RMSD) of 0.602 Å. Given the average resolution of determined structures at an average 2.24 Å, this implies that they are almost identical. Most of the differences between structures were found in loops connecting helical elements within N-terminal domains (Figure 4.4 B). These regions of the most pronounced differences in protein backbone correspond with the highest B-factors of the protein backbone (Figure 4.4 C).

The Fe-SodA structure was not modelled to completion, with only one chain out of four found in the asymmetric unit that had enough data to model residues 2-199. Unmodelled residues 59-68 in chains A, C and D suggest a high degree of lability in the loop linking two helices of the N-terminal domain of the protein. All models were built without the N-terminal methionine (Appendix Table 8.2).

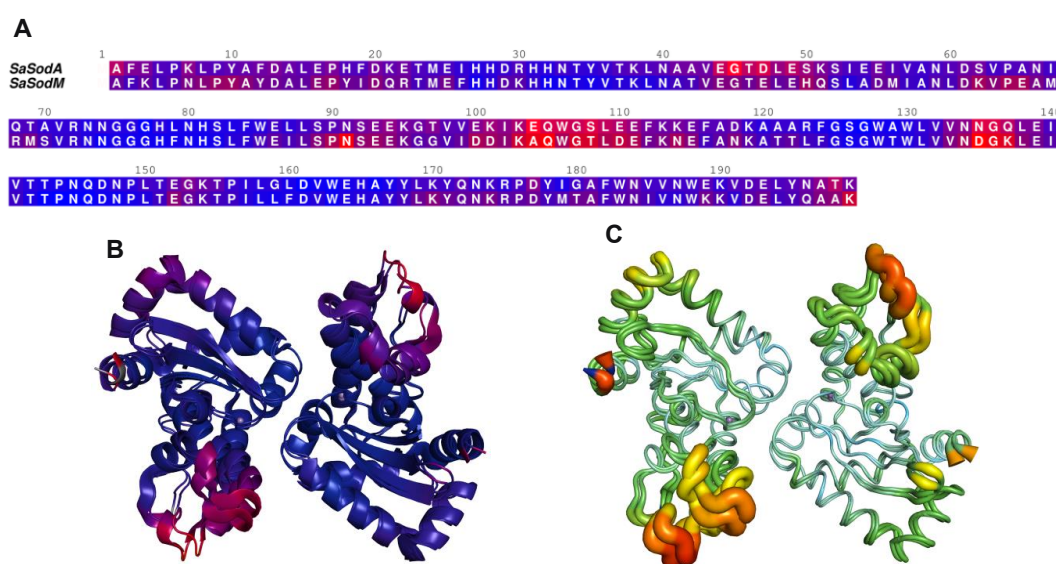


Figure 4.4 The Root-Mean-Square-deviation (RMSD) within the backbone of SaSodA and SaSodM.

Sequence alignment (A) of SaSodA (5N56) and SaSodM (5N57) coloured by RMSD using ALINE (Bond & Schüttelekopf, 2009). Ribbon representation (B) of superimposed Mn-SaSodA (5N56) and Mn-SaSodM (5N57) structures, coloured by RMSD of protein backbone, with blue (most similar) to red (most divergent) colour gradient. B-factor putty representation (C) of superimposed SaSodA (5N56) and SaSodM (5N57), coloured with blue to red gradient of colours and a narrow to wide tube size, indicating regions of lower to higher B-factors, respectively.

Biological assemblies of SodA and SodM structures were assessed in the the PDBePisa tool (Krissinel & Henrick, 2007); (Appendix Table 8.2). Both structural models were described as symmetry-related homodimers, with approximately 10 % of buried surface conferring the dimer interface. Dimeric assemblies were stabilised by a set of 12 hydrogen bonds, involving residues

S126, E164, H165, H31, Y168, and salt bridges formed between conserved residues H165 and E164 (Appendix: Figure 8.1, Table 8.2). An additional pair of residues (R30 and N173) was involved in formation of a hydrogen bond at the dimer interface of SodA. The role of H165–E164 (Whittaker & Whittaker, 1998) and H31–Y168 (Edwards et al., 2001b; Hearn et al., 2004) bonds has previously been described as essential for retaining the dimeric structure and metal-specific activity of SODs. A qualitative electrostatic representation of charge-smoothed potential generated with Pymol (Figure 4.5) indicated a relative negative net-charge of SodA and SodM, potentially playing protective role against negatively charged radicals or inhibitors.

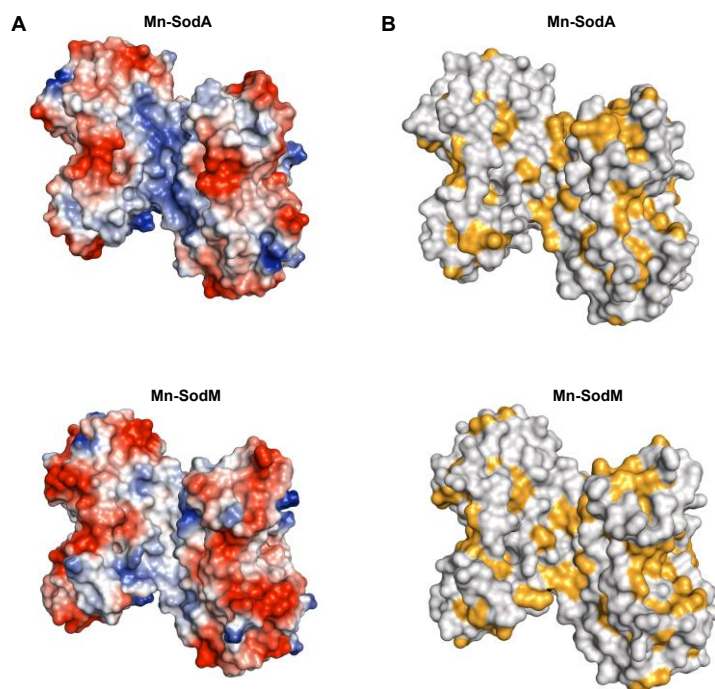


Figure 4.5 A qualitative protein electrostatic potential mapped on molecular surface.

(A) A qualitative electrostatic representation of charge-smoothed potential generated with Pymol (Schrödinger, LLC). The molecules were rendered as a surface that was coloured according to the electrostatic potential. The red colour (negative potential) arises from an excess of negative charges near the surface and the blue colour (positive potential) occurs when the surface is positively charged. The white regions correspond to neutral potentials. (B) Yellow patches of hydrophobic amino acids (Ala, Ile, Leu, Met, Phe, Val, Pro, Gly) in surface representation.

The positively charged zone at the bottom of each monomer of the two proteins creates the mouth of the substrate access funnel (Figure 4.6 A). This localised positive charge (Figure 4.6 B), attracting negatively charged substrate, is attributable principally to a hydrogen-bonded network of amino acid side-chains near the active site. The superoxide reaches the active site through a funnel leading to a narrow channel entrance to the active site. Two symmetry-related substrate-access channels leading from bulk solvent towards the metal sites are buried between the N-terminal and C-terminal domains of the monomers. The entries to the active sites are gated (Figure 4.6 C in stick representation) by some of the residues of the dimer interface: H31, Y35, H165, W163, E164B, R175B. As proposed by (Whittaker & Whittaker, 2008) H31 and Y35 form

half of the substrate and metal binding gateway and which is thought to restrict access to the active site metal ion in *E. coli* SodA, conferring substrate selectivity and possibly facilitating proton transfer steps in the redox turnover mechanism.

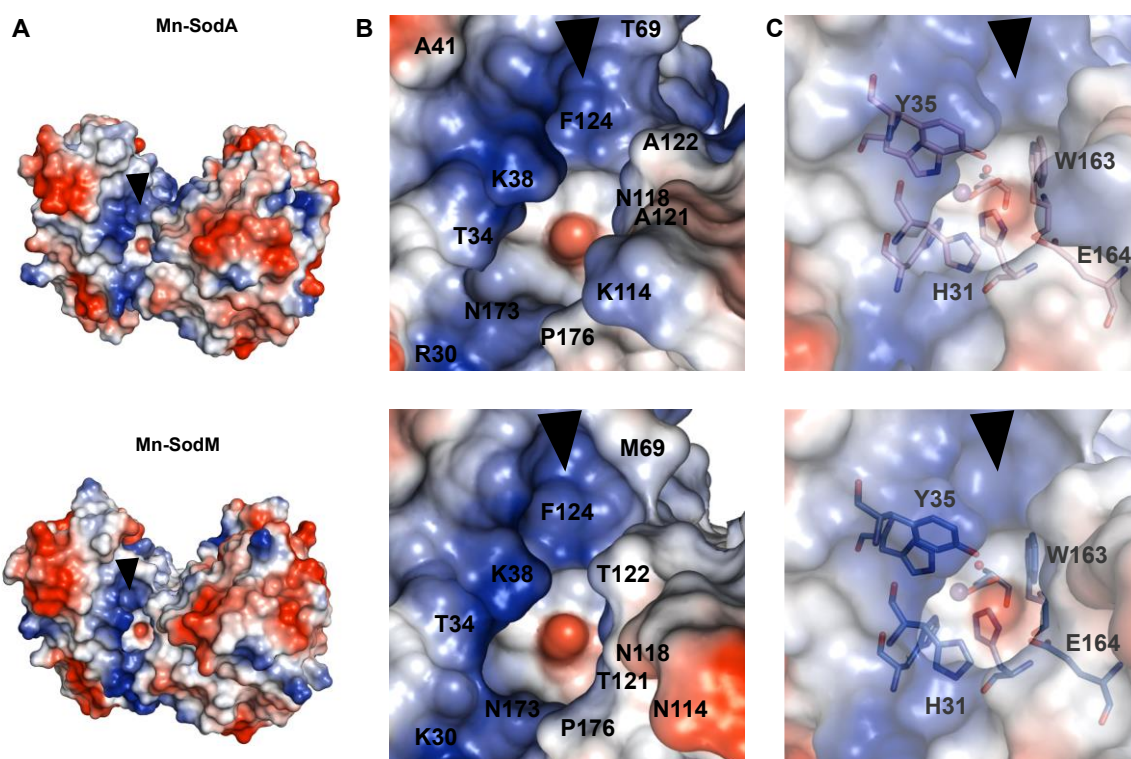


Figure 4.6 Electrostatic potential at the surface of substrate access funnel.

Top panels represent SodA, and bottom panels represent SodM, respectively. (A) A bottom view of the Mn-SodA and Mn-SodM dimers, represented as a surface, coloured according to the electrostatic potential (blue, positive and red, negative). The black arrowheads indicate the entrance to the substrate access funnel from bulk solvent. (B) A zoomed-in view on the substrate access funnel of Mn-SodA (top) and Mn-SodM (bottom). A black arrowhead placed in an equivalent position to panel (A). (C) The innermost residues of substrate access channel: H31, Y35, W163, H165, E164B, gating the entrance to the metal binding site, shown as sticks in transparent surface model. Mn-ligands of Mn-SodA (pink) and Mn-SodM (blue) are represented as sticks, with Mn ions and water molecules depicted as purple and red spheres, respectively.

In the SaSODs, the metal ion is ligated by amino acid side chains (histidines, aspartate) arising from both the N- and C-terminal regions of each monomer. Both Fe and Mn are coordinated in a distorted trigonal bipyramidal geometry by H65, D161, H165 in the equatorial plane and by H27 and a solvent molecule in the axial plane (Figure 4.2, Figure 4.7, Appendix Table 8.3). The metal binding site is surrounded by a cluster of aromatic residues that serves as a central hydrophobic core for the molecular architecture, shielding the metal coordination centre from exposure to bulk solvent. Such an electron-rich hydrophobic environment may contribute to

controlling the catalytic reactivity of the metal centre (Figure 4.7) by maintaining the appropriate redox potential of the metal ion during two-step disproportionation reactions.

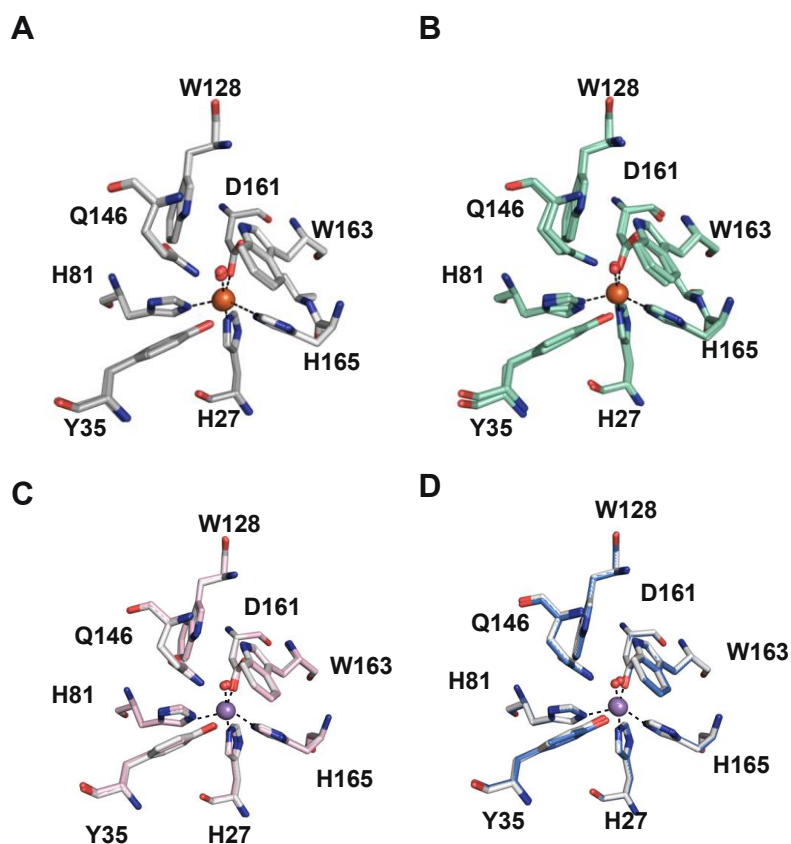


Figure 4.7 Active sites of SaSodA and SaSodM.

A stick representation of the metal coordination site, showing residues within approximately 5 Å radius from the metal ion, in crystal structure models of Fe-SodA (A), Mn-SodA (B), Fe-SodM (C) and Mn-SodM (D). Metal cofactors and a coordinating water molecule are represented as spheres (orange: Fe; purple: Mn; water: red). Coordinating bonds represented by black dashed line. Represented are superimposed chains of each of the dimers.

Analysis of the solved crystal structures of SaSODs did not reveal any major differences that could explain distinct stability or catalytic properties of these proteins. In light of a high conservation of the metal coordination between Mn/Fe-SODs, including the two SaSODs, it could be presumed that metal-specific activity of these proteins may only be conferred by very subtle differences in protein structure, beyond the resolution of determined crystal structures. Comparison of SodA, which is highly metal-specific, and cambialistic SodM (section 3.2.11) indicated a small alteration (unlikely to be statistically significant at the resolution of determined crystal structures) in the bond length of H165 and D161 to the metal, appearing shorter in SodM

(2.2 Å, 2.0 Å) than SodA (2.3 Å, 2.1 Å). The reverse characteristic was observed for the bond between H81–metal ion, which was shorter in SodA (2.1 Å) than SodM (2.2 Å), (Appendix Table 8.3). To evaluate differences in the geometry of the coordination sphere (primary sphere; ligand sphere), structures of *E. coli* Mn-SodA (1VEW), Fe-SodB (1ISB) and cambialistic *Porphyromonas gingivalis* Fe-SodB (1UER) were superimposed onto the metalated isoforms of SaSODs (Figure 4.8). A general pattern was observed for Fe–ligand bonds being shorter than Mn–ligand bonds in SaSODs. Similar correlation was observed for the bonds of H81, H165 and D161 to the metal ion, in comparison of SaSODs with the highly Mn-specific *E. coli* SodA (Figure 4.8 A; green carbons) and Fe-specific *E. coli* SodB (Figure 4.8 B; teal carbons), but not cambialistic *P. gingivalis* Fe-SodB (Figure 4.8C; orange carbons), implying the role of other, potentially distant from the active site (second-sphere) interactions contributing to its cambialistic properties.

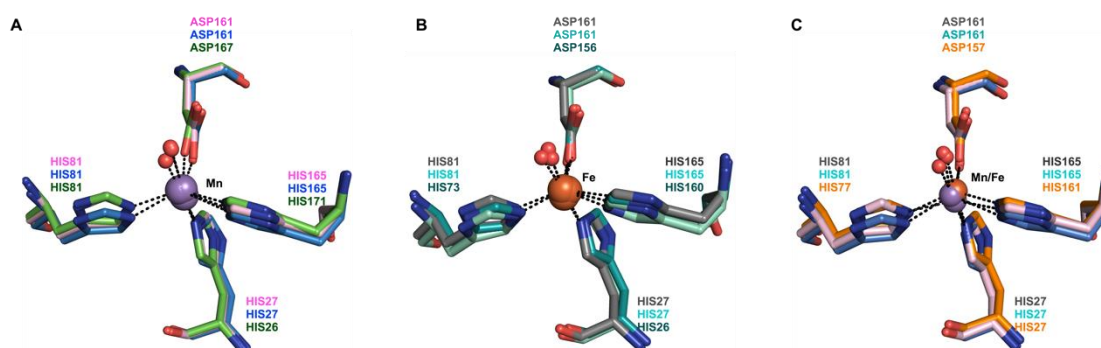


Figure 4.8 Superimposed metal site geometry.

Superimposed stick representation of the active site residues of: (A) *E. coli* Mn-SodA (1VEW; green carbons), *S. aureus* Mn-SodA (5N56; pink carbons), and *S. aureus* Mn-SodM (5N57; blue carbons); (B) Fe-SodB (1ISB; teal carbons) and *S. aureus* Fe-SodA (grey carbons), *S. aureus* Fe-SodM (aquamarine carbons); and (C) cambialistic *P. gingivalis* Fe-Sod (1UER; orange carbons) with *S. aureus* Mn-SodA (5N56; pink carbons), and Mn-SodM (5N57; blue carbons). Metal ion represented as sphere coloured by element: purple Mn, orange Fe, and solvent molecule depicted as red sphere.

4.2.3. Identification of candidate residues potentially determining the distinct properties of SaSodA and SaSodM

The importance of residues situated up to 10 Å from the coordinated metal has been previously described as important for metal specific catalysis, proposed to be due to their participation in a hydrogen bond network important in the proton-coupled electron transfer mechanism (Yamakura et al., 2003); (Osawa et al., 2010; Yikilmaz et al., 2007; Yikilmaz et al., 2002; Edwards et al., 2001a; Schwartz et al., 2000; Lévêque et al., 2000; Miller, 2008; Miller & Wang, 2017). To assess the possible contribution of residues from this secondary sphere to distinct activity of *S. aureus* SodA and SodM proteins, all 50 of the non-identical residues (according to point accepted

mutation, PAM250, scoring matrix (Pearson, 2013) used in ClustalΩ) in the aligned protein sequences were mapped onto the superimposed structures (Figure 4.9 A, B; coloured in red, green and dark blue). Expanding further beyond the conserved ligand sphere, all the residues facilitating contacts at the dimer interface were conserved, similarly to the structures of other Fe/Mn-SODs. Most of the residues differentiating SodA and SodM localised to the protein surface or in the regions of the labile loops linking secondary structure elements within the two domains. Within 10 Å radius from the metal ion, six residues were identified as non-conserved (positions 19, 26, 30, 79, 159, 160). Out of these six candidates, three residues (SaSodA: F19, G159, L160; SaSodM: I19, L159, F160, marked with red arrowheads in the alignment Figure 4.9 A), due to their spatial orientation in relation to the active site, were subjected to site directed mutagenesis to swap the residues between two proteins (Figure 4.9 C), aiming at swapping their specific activity.

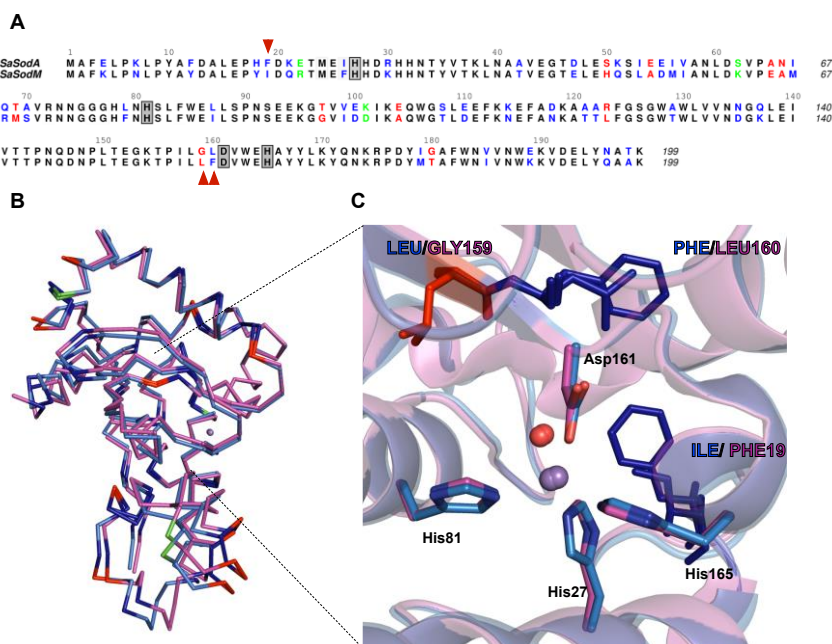


Figure 4.9 Identification of residues potentially determining the distinct properties of SaSodA and SaSodM.

(A) Sequence alignment generated using ClustalΩ. Colouring was applied according to consensus symbols assigned by ClustalΩ on basis of point accepted mutation (PAM250) scoring matrix (Pearson, 2013). Fully conserved residues (75 %) coloured in black, dark blue indicates conservative amino acid changes (37 residues; conservation between residues of strongly similar properties; scoring > 0.5 in the Gonnet PAM 250 matrix), whereas green depicts semi-conservative changes (3 residues; conservation between residues of weakly similar properties; scoring ≤ 0.5 but >0.0 in the Gonnet PAM 250 matrix), and non-conservative mutations (fully non-conserved; ; scoring =0.0 in the Gonnet PAM 250 matrix) are indicated in red (10 residues). Residues presented in grey boxes are the ligands for metal cofactor that are conserved across the Mn/Fe-SOD superfamily. (B) All sequence differences (red, green, dark blue) were depicted on superimposed ribbon-representations of SaSodA (pink) and SaSodM (blue) structures. (C) The three different residues (red arrowheads; SaSodA: F19, G159, L160; SaSodM: I19, L159, F160) identified that are spatially close to the active site of both enzymes were targeted for site directed mutagenesis.

4.2.4. *BsSodA* is a manganese dependent protein and exhibits similar enzymatic activity profile as *SaSodA*

Having identified three residues spatially close to the metal ion that differ between *SodA* and *SodM*, we first used a potential ‘natural experiment’, aiming to test the hypothesis that these three residues influence the metal specificity of enzyme activity (Figure 4.10 A).

BsSodA shares 72 % identity with *SodA* and 63 % identity with *SodM* proteins of *S. aureus*. Looking at the positions of the three residues that were selected for mutagenesis in staphylococcal SODs, *BsSodA* resembles *SodM* sequence at position 19 and *SodA* at positions 159, 160 (Figure 4.10). The crystal structure of *BsSodA* (P. Liu et al., 2007) shows a conserved geometry of the active site of the enzyme, and especially the orientation of the residues at positions 19, 159 and 169 in comparison to *SaSODs* (Figure 4.10 B).

The *sodA* gene of *B. subtilis* 168 strain was cloned into the pET29a vector (section 2.2.5.3), and protein expression was performed in the BL21 (DE3) *E. coli* host under optimised expression conditions in M9 minimal medium (section 2.7.2). Protein purification was conducted by a combination of anion exchange and size exclusion chromatography (section 2.7). Purified protein was found to contain primarily a Fe metal cofactor, which was exchanged for Mn by means of *in vitro* refolding (section 2.12.4). Elemental analysis confirmed that prepared isoforms of the protein were metal-pure (Figure 4.11 A).

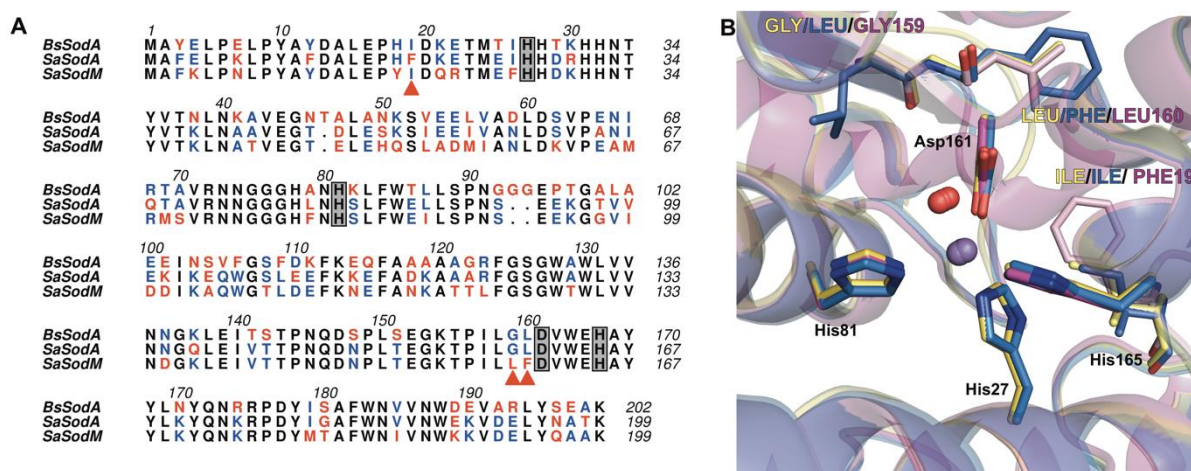


Figure 4.10 *Bacillus subtilis* *SodA*.

(A) The Clustal alignment of *BsSodA* and *SaSODs*, with conserved residues coloured in black, similar residues marked in blue and non-conserved coloured red. Red arrowheads indicate positions of three identified residues, targeted for mutagenesis in *SaSODs*. Grey boxes indicate ligands coordinating metal ion in the active site. (B) The superimposed active sites of *BsSodA* (yellow carbons), *SaSodA* (pink carbons) and *SaSodM* (blue carbons), with ligand residues represented as sticks, Mn and water molecule shown as purple and red sphere, respectively.

The superimposition of the backbones of *BsSodA* and *SaSODs* reveals a higher level of similarity between the structures of the *BsSodA* and *SaSodA* proteins, than between *BsSodA* and *SaSodM*. Determination of enzymatic activity of recombinant *SodA* from *B. subtilis* (Figure 4.11 B, Table 4.5) also places it closer to the catalytic properties of *SodA* (section 3.2.11). This is consistent with the Firmicutes *SodA* being the ancestral enzyme as shown by phylogenetics (Chapter 3, section 3.2.2).

The sequence and structural alignments between *BsSodA* and *SaSODs*, and the catalytic activities of the three proteins, allowed us to hypothesise an important role of residues G159 and L160 in conferring high activity with Mn and low activity with Fe for the staphylococcal *SODs*.

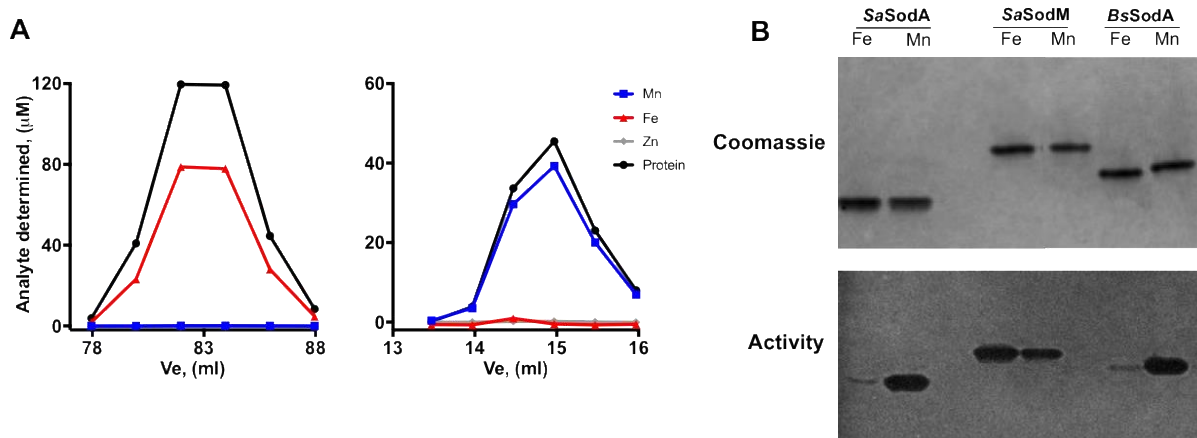


Figure 4.11 Metal analysis and enzymatic activity of recombinant *BsSodA*.

(A) A representative metal analysis of as-purified *BsSodA* (left chromatogram), showing Fe (red triangles) loading of analysed protein (black circles), and Mn-loading (blue squares) of protein post *in vitro* refolding in the presence of manganese (right chromatogram), quantified ICP-MS. Protein concentration determined by Bradford assay, based on a standard curve. (B) 12% Native-PAGE of an equal amount (0.3 μ g) of purified protein, stained with Coomassie (upper) and NBT-riboflavin stain for *SOD* activity (lower). Gels were scanned using BioRad ChemiDoc XRS+ system.

	Fe-BsSodA			Mn-BsSodA		
	Mn	Fe	Zn	Mn	Fe	Zn
Metal content (% ± SD)	0.2 ± 0.0	92.2 ± 0.5	0.7 ± 0.5	99.5 ± 0.3	0.1 ± 0.0	0.4 ± 0.3
Molar equivalent (average ± SD)	0.001 ± 0.000	0.656 ± 0.013	0.004 ± 0.003	0.909 ± 0.065	0.001 ± 0.000	0.003 ± 0.002
Activity (U mg ⁻¹)		20			2200	

Table 4.5 Metal content and specific activity of *BsSodA*.

A summary of elemental analysis of metalated isoforms of *BsSodA* and specific activity of enzymes. Activity was quantified per mg of protein, as determined by Bradford assay, based on the percentage of inhibition of WST-1 reduction, compared to known concentrations of SOD standard (using WST SOD assay, Sigma, UK). A percentage of inhibition was determined by monitoring A450nm after a 30-minute long incubation of assay mixture at 37°C in a microtiter plate.

4.2.5. Mutated versions of *SaSodA* and *SaSodM* purify from a heterologous host exclusively with an iron cofactor, which can be exchanged *in vitro* for manganese

A comparative analysis of the crystal structures obtained for all metalated forms of *SaSodA* and *SaSodM* proteins resulted in identification of three residues different between the two proteins (Figure 4.9), which were hypothesised as potentially important for determining metal specificity. The mutated versions of *sodA* ([F19I]; [G159L, L160F]; [F19I, G159L, L160F], [G159L]) and *sodM* ([I19F]; [L159G, F160L]; [I19F, L159G, F160L], [L159G]) genes were prepared using a site-directed mutagenesis approach (section 2.2.5.2). Each of the eight mutants was heterologously expressed in *E. coli* BL21 (DE3) cells in M9 minimal medium supplemented with 30 µM Fe (section 2.7.2). Initial protein purification was performed as previously described by anion exchange (AEX) chromatography with a linear (0-1 M) NaCl gradient in 20 mM Tris pH7.5 buffer. Anion exchange fractions were subsequently resolved by preparative size exclusion chromatography (SEC) using Superdex 200 16/600 column (GE Healthcare) in 20 mM Tris, pH 7.5, 150 mM NaCl buffer. All isoforms of *SodA* and *SodM* behaved as stable and homogenous dimers in size exclusion elution profiles, based on calibration with known MW standards. Eluant fractions were analysed for homogeneity by SDS-PAGE, protein content by A₂₈₀, and for metal content using ICP-MS. Similarly to the wild type proteins (Chapter 3, Figure 3.6), each of the mutants purified from *E. coli* containing predominantly iron, and not manganese or zinc (Figure 4.12 A, C).

To prepare exclusively Mn-loaded isoforms of these proteins, all mutant versions of *SodA* and *SodM* proteins were treated *in vitro* to exchange their cofactor for manganese (section 2.12). *SodA* and *SodM* isoforms were unfolded using the optimised protocol (section 2.12.4), in 2.5 M guanidinium HCl in the presence of 1 mM EDTA and 20 mM 8-hydroxyquinoline to extract the bound iron, followed by refolding through dialysis against 20 mM Tris pH 7.5, 100 mM NaCl buffer containing 1 mM MnCl₂. Further, each refolded protein was resolved on a Superdex 200 Increase 10/300 analytical SEC column in 20 mM Tris pH 7.5, 150 mM NaCl buffer. Elemental analysis by ICP-MS confirmed quantitatively that only manganese, and not iron or zinc, was found to co-

migrate with the refolded proteins (Figure 4.12 B, D). Relatively low recovery yield was noted for SodM I19F and SodA G159L, L160F isoforms after *in vitro* refolding.

The swapping of the residues 19, 159, 160 between the sequences of the two proteins did not alter their native capacity to bind Fe in the heterologous host, and Fe was successfully exchanged for Mn using *in vitro* refolding, as was demonstrated for the wild type enzymes (Chapter 3, sections 3.2.9, 3.2.13).

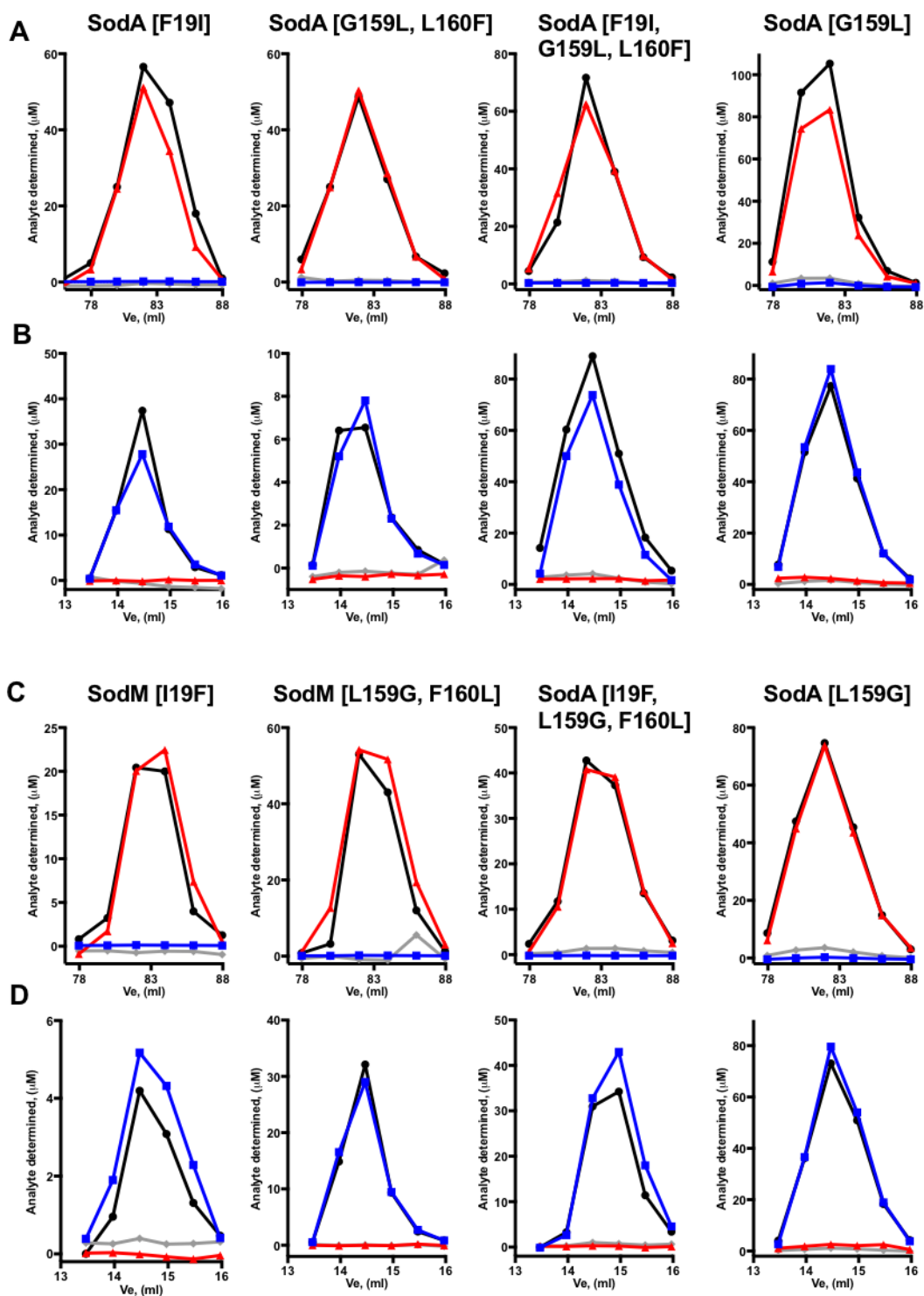


Figure 4.12 Purification and elemental analysis of mutated recombinant proteins SaSodA and SaSodM expressed in *E. coli* and subjected to *in vitro* metal cofactor exchange.

The mutated isoforms of SaSodA and SaSodM proteins were overexpressed in BL21(DE3) cells and purified from the heterologous host using a combination of anion exchange and size exclusion chromatography. Purified proteins were refolded *in vitro* to exchange the Fe cofactor for Mn and make metal-pure isoforms of mutant proteins. The concentration of Fe (red squares), Mn (blue triangles), and Zn (grey diamonds) in mutant protein fractions after an analytical size exclusion chromatography step was determined from the standard curve. Protein concentration determined with Bradford assay depicted as black circles.

4.2.6. Mutations introduced to the secondary sphere of SaSODs alter their relative activity

Amongst the three residues that were mutagenized in the sequence of the SaSODs, a couple of the residues occupying positions 19 and 160 share hydrophobic properties. The F19 is paired with L160 in SodA, whereas I19 is paired with F160 in SodM, and swapping these pairs with respect to each other between two proteins should not introduce major chemical changes into the protein environment. A third residue of the mutagenized triad shows more substantial difference in sidechain chemical properties, with G159 in SodA being replaced with L159 in SodM. The residues G159 and L160 were anticipated to play an important role in conferring substantial Mn-specific activity, based on the conservation amongst Mn-specific enzymes (Wintjens et al., 2008); (Sheng et al., 2014), including *BsSodA* biochemically characterised in this study as a Mn-specific enzyme (Liu et al., 2007); (Chapter 4, section 4.2.4).

The relative activities of all the studied proteins were assessed qualitatively by comparing enzymatic activity arising from aliquots of Fe-SodA, Fe-SodM, Mn-SodA and Mn-SodM, with both wild type and mutated versions of proteins analysed by the in-gel SOD activity assay (section 2.9.1). The specific enzymatic activities of recombinant SaSOD protein isoforms were determined quantitatively using a commercial WST SOD assay kit (Sigma Aldrich, UK, section 2.9.3).

4.2.6.1. SaSodA mutants do not yield a cambialistic SodM-like protein, though the G159L; L160F mutation significantly improves catalytic activity with Fe

The metalated isoforms of wild type SodA displayed distinct relative activities (section 3.2.11, Figure 4.13), with negligible activity observed for the Fe-loaded form and substantial activity displayed by the Mn-loaded isoform. This characteristic was not significantly altered by introduced point mutations, except for the [G159L; L160F] mutant, when analysed by the semi-quantitative in-gel activity assay. The double mutant presented qualitatively similar levels of activity (implying cambialism) between both metalated forms, however, they did not match the level of truly cambialistic SodM wild type enzyme.

A quantitative analysis of the enzymatic activity of the metalated SodA isoforms (Table 4.6) was performed with a spectrophotometric assay (section 2.9.3).

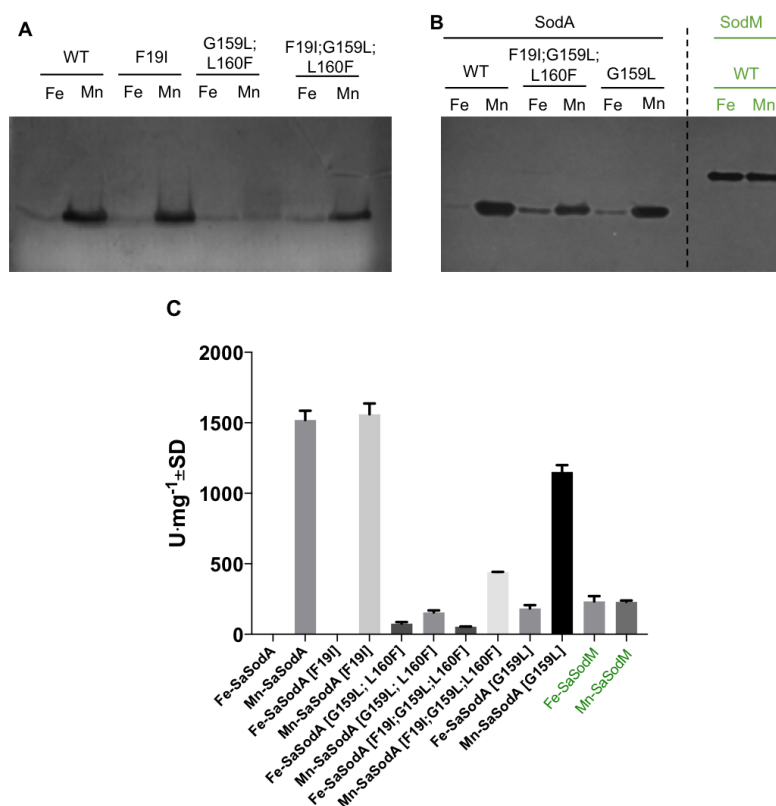


Figure 4.13 SOD activity in-gel assays across all recombinant SaSodA versions, showing semi-quantitative differences between the activities of the proteins.

An equal amount of proteins (0.3 μ g in 20 mM Tris, pH 7.5, 150 mM NaCl) was resolved by 12 % (w/v) Native-PAGE and subsequently stained for superoxide dismutase activity using in-gel NBT-riboflavin based staining protocol (section 2.9.1). Post incubation with the dye, gels were exposed to bright white light, and activity bands were recorded using BioRad ChemiDoc XRS+ system. Comparative assay of the wild type and mutants of SodA (A) and relative activity of SodA isoforms correlated with the activity of SodM wild type protein. Column representation (C) of the activity quantified using liquid assay detailed in Table 4.6.

No significant change of activity was observed upon introduction of hydrophobic isoleucine in a place of another hydrophobic residue, phenylalanine, at position 19. Mutation of the conserved glycine at position 159 to leucine substantially increased the Fe-specific activity of the SodA isoform (50-fold increase) and only moderately altered (1.3-fold decrease) its Mn-specific activity relative to the wild type. Approximately 20-fold increase in the activity of Fe-loaded SodA with respect to the wild type enzyme was noted for the [G159L; L160F] isoform of SodA, where two bulky hydrophobic residues replaced glycine and leucine, possibly restricting structural flexibility in the surrounding protein environment (Yamakura et al., 2003). The increase in Fe-specific activity and almost 10-fold decrease in Mn-specific activity of that mutant relative to the wild type SodA brought its catalytic properties closer to those of cambialistic SodM. A combination of mutations introduced into the SodA sequence at the three positions: [F19I; G159L; L160F] caused a gradual increase (2.8-fold) of Mn-specific activity and a gradual decrease of its Fe-specific activity, relative to the double mutant isoform. Changes introduced into the SodA sequence decreased the enzyme's strong Mn preference, and increased the level of catalytic activity with Fe. The greatest inversion of metal specificity towards cambialism was

observed when substitutions were made at positions 159 and 160, indicating their combined importance in determining the metal specificity of catalysis in SodA.

Sample number	SOD isoform	U mg ⁻¹ ± SD
1	Fe-SaSodA	3.5 ± 0.1
2	Mn-SaSodA	1820.6 ± 65.2
3	Fe-SaSodA [F19I]	4.2 ± 0.4
4	Mn-SaSodA [F19I]	1560.4 ± 77.2
5	Fe-SaSodA [G159L; L160F]	75.6 ± 10.7
6	Mn-SaSodA [G159L; L160F]	155.3 ± 13.4
7	Fe-SaSodA [F19I; G159L; L160F]	54.1 ± 1.6
8	Mn-SaSodA [F19I; G159L; L160F]	526.4 ± 1.6
9	Fe-SaSodA [G159L]	183.5 ± 23.5
10	Mn-SaSodA [G159L]	942.8 ± 48.2
11	Fe-SaSodM	233.1 ± 37.9
12	Mn-SaSodM	230.0 ± 9.4

Table 4.6 A specific SOD activity assay of SodA isozymes.

SOD activity was assessed using a spectrophotometric WST SOD assay kit (Sigma, UK). Summary of the activity, expressed in units per mg protein (U mg⁻¹), shows the average of at least 3 replicates of the specific activity assay for all studied versions of proteins +/- SD. Protein concentrations were determined by A₂₈₀. The amount of protein used for the assay was optimised to fit within a range closest to 50 % inhibition of WST reduction, based on a standard curve. The standard curve of known U ml⁻¹ concentration was prepared using commercially available recombinant superoxide dismutase from bovine erythrocytes and *E. coli* Mn-SOD. The assay mix was prepared in a 96-well microplate format, using kit-supplied buffer at pH 7.0. The absorbance at 450 nm was measured using plate reader spectrophotometer, following 30 min incubation at 37°C.

4.2.6.2. Mutations within SaSodM sequence result in a non-cambialistic, highly Mn-specific protein, analogous to SaSodA

The two metalated forms of wild type SodM displayed comparable activities, with the ratio of Fe-specific activity to Mn-specific activity (Chapter 3, Figure 4.14, Table 4.7).

To test whether the cambialistic properties of SodM can be altered towards metal-specific activity, the three targeted residues (Figure 4.9) were swapped for amino acids occurring in its Mn-specific homologue, SodA. The effect of point mutations were assessed by performing SOD activity assays (Figure 4.14, Table 4.7). The introduced mutations had an equivalent, but opposite, effect on the metal-specific activity of SodM as had been observed with mutations in SodA (section 4.2.6.1).

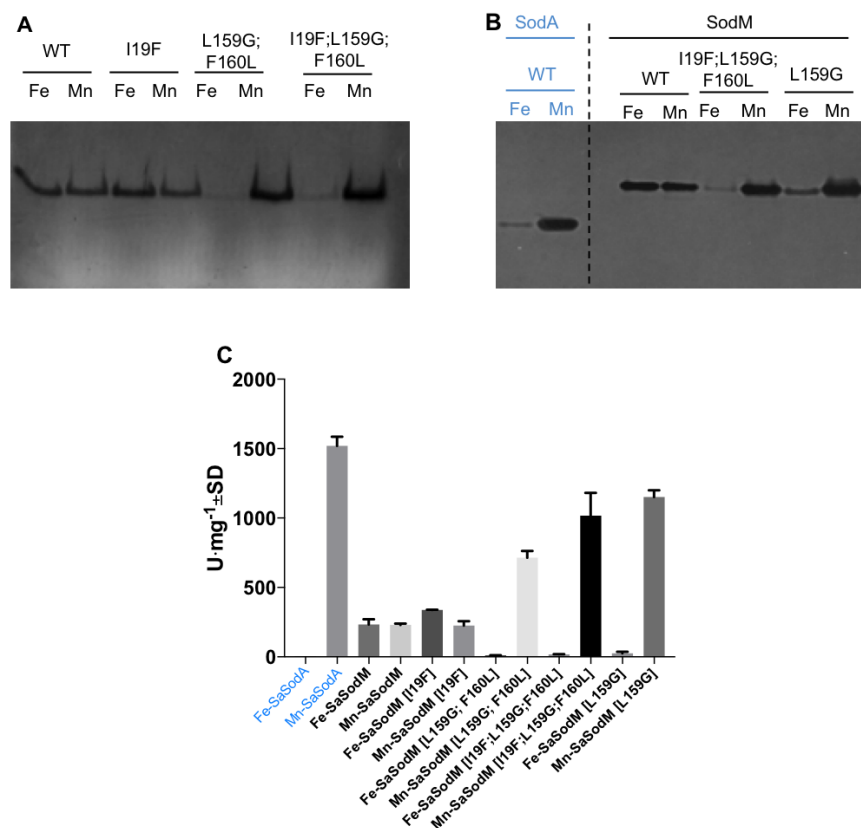


Figure 4.14 SOD activity in-gel assays of recombinant SaSodM versions.

An equal amount of proteins (0.3 μg in 20 mM Tris, pH 7.5, 150 mM NaCl) was resolved by 12 % (w/v) Native-PAGE and subsequently stained for superoxide dismutase activity using in-gel NBT-riboflavin based staining protocol (section 2.9.1). Post incubation with the dye, gels were exposed to bright white light, and activity bands were recorded using BioRad ChemiDoc XRS+ system. Comparative assay of the wild type and mutants of SodM (A) and relative activity of SodM isoforms correlated with the activity of SodA wild type protein. Column representation (C) of the activity quantified using liquid assay detailed in Table 4.7.

Mutations of [L159G; F160L] and [I19F; L159G; F160L] introduced into the SaSodM sequence inverted the cambialistic properties of the protein, resulting in a SodA-like Mn-specific version of SodM, increasing its Mn-specific activity 3 and 4-fold, respectively, relative to the wild type (Table 4.7). Interestingly, a single mutation of leucine to glycine at position 159 had an equally strong effect, bringing the ratio of the Fe-specific to the Mn-specific activity of the mutant to 0.023, relative to 0.003 of SodA. The equal ratio of Fe-supported activity to Mn-supported activity (Fe:Mn=1.0) for the wild type SodM was brought down to 0.019 by the introduction of the triple (19, 159, 160) mutation, causing a change of catalytic properties of the protein towards Mn-specificity. Unexpectedly, the highest activity with Fe was observed for the I19F isoform of the SodM protein, which presented a 1.5-fold increase in Fe-specific activity in relation to wild type SodM, and over 95-fold increase relative to Fe-SodA.

Sample number	SOD isoform	U mg ⁻¹ ± SD
1	Fe-SaSodA	3.5 ± 0.1
2	Mn-SaSodA	1820.6 ± 65.2
3	Fe-SaSodM	253.1 ± 37.9
4	Mn-SaSodM	250.0 ± 9.4
5	Fe-SaSodM[I19F]	338.1 ± 1.2
6	Mn-SaSodM[I19F]	224.9 ± 32.4
7	Fe-SaSodM[L159G; F160L]	11.2 ± 1.3
8	Mn-SaSodM[L159G; F160L]	714.2 ± 48.6
9	Fe-SaSodM[I19F; L159G; F160L]	38.9 ± 1.2
10	Mn-SaSodM[I19F; L159G; F160L]	789.8 ± 15.8
11	Fe-SaSodM[L159G]	26.1 ± 10.9
12	Mn-SaSodM[L159G]	808.3 ± 21.8

Table 4.7 A specific SOD activity assay of SodM isozymes.

SOD activity was measured using spectrophotometric WST-based assay kit (Sigma). The amount of protein used for the assay was optimised to fit within a range closest to 50 % inhibition of WST reduction, based on a standard curve. The standard curve of known U ml⁻¹ concentration was prepared using commercially available recombinant superoxide dismutase from bovine erythrocytes and *E. coli* Mn-SOD. The assay mix was prepared in a 96-well microplate format, using kit-supplied buffer at pH 7.0. The absorbance at 450 nm was measured using plate reader spectrophotometer, following 30 min incubation at 37°C. Summary of the relative activity expressed in units per mg protein (U mg⁻¹) shows the average of at least 3 replicates of the assay +/- SD. Protein concentration was determined by A₂₈₀.

4.2.7. Crystal structure of [I19F; L159G; F160L] SaSodM triple mutant demonstrates only subtle structural changes in protein backbone

The observed effects of point mutations on metal specific activity of SaSODs suggest that the substitution of the residues at positions 19, 159 and 160, result in the apparent switch between cambialistic and metal specific properties of these enzymes. To address the effects of these amino acid substitution on the overall and active site structure of SodM, the crystal structure of the Mn-loaded form of SodM carrying the triple mutation was determined and analysed.

Diffraction quality crystals were produced using the sitting drop vapour diffusion technique in 100 mM potassium thiocyanate, 30% (w/v) PEG 2000 MME (original condition G9 of JCSG+ matrix screen; Molecular Dimension, UK). Crystals were harvested and cryo-protected in reservoir solution supplemented with 20 % (w/v) PEG400 by Dr Arnaud Baslé (Newcastle University, UK), who also performed data collection and initial structure solution. Diffraction data collection was performed at the Diamond Light Source (mx9948-22 experiment). The structure was solved by molecular replacement with MolRep (Lebedev et al., 2008), using the native SaSodM structural model determined in this study, as search model.

Generated models were validated in COOT, Phenix (Polygon) and PdbRedo (Joosten et al., 2012) webserver. Final pdb models were validated with COOT (Emsley and Cowtan, 2004), MOLPROBITY (Chen *et al.*, 2010) and wwPDB validation service to check geometry, Ramachandran outliers and clashes. The data collection statistics and final data refinement statistics are summarised in Table 4.8.

The Mn-SaSodM [I19F; L159G; F160L] structure was determined at 1.8 Å resolution (Figure 4.15 A), with two molecules in the asymmetric unit (48.01 % solvent), in primitive orthorhombic space group $P2_1$ (Table 4.8). As with the previous structures, the mutant structure presented the conserved two-domain fold of the polypeptide chain, with residues 2-89 forming the helical N-terminal domain, and residues 94-194 of C-terminal α/β domain. Two polypeptide chains formed a symmetrical dimer, with 10 % interface surface between interacting chains. Dimer stability was conferred by 12 hydrogen bonds and 2 salt bridges between conserved residues (Appendix, Table 8.2). Manganese ions were found to be coordinated in trigonal bipyramidal geometry by H65, D161, H165 in the equatorial plane, and H27 with solvent molecule in the axial plane. The active site of the mutant was superimposable to 0.097 Å with SodA and 0.130 Å with SodM, by least squares (LSQ) fit. Proteins were superimposable within the core with 0.521 Å RMSD by secondary structure matching. Structure analysis revealed that the three substituted residues adopted spatial positions in the mutant analogous to these in wild type SodA (Figure 4.15 B, C). The structural data confirmed that the mutations yielded similar active site structures to the wild type enzymes, maintained the conserved dimer interface, and did not cause any major changes to the overall structure. This suggests that amongst an overall number of 50 non-conserved mutations differentiating the two *S. aureus* SODs, potentially just these three mutations, located away from the catalytic centre, are sufficient to alter metal cofactor specificity.

Data statistics	
Beamline	I04
Date	24/11/2014
Wavelength (Å)	0.97949
Resolution (Å)	43.17 – 1.80 (1.84 – 1.80)
Space group	P2 ₁ 2 ₁ 2 ₁
Unit-cell parameters	
a, b, c (Å)	58.2, 58.2, 128.64
α, β, γ (°)	90.0, 90.0, 90.0
Unit-cell volume (Å ³)	436224
Solvent content (%)	48
Total reflections	299146 (17872)
Unique reflections	41450 (2460)
CC _{1/2}	0.993 (0.827)
Completeness (%)	100.0 (100.0)
Redundancy	7.2 (7.3)
R _{merge} (%)	15.0 (67.4)
I/σ(I)	6.7 (1.6)
Refinement statistics	
Rwork (%)	14.72
Rfree [#] (%)	21.38
No. of non-H atoms	
No. of protein, atoms	3241
No. of solvent atoms	321
No. of metal atoms	2
R.m.s. deviation from ideal values	
Bond angle (°)	1.6
Bond length (Å)	0.016
Average B factor (Å ²)	
Protein	23.02
Solvent	29.89
Metal	13.11
Ramachandran plot*, residues in Most favoured regions (%)	97.39

Table 4.8 Data collection and refinement statistics of Mn-SodM triple mutant.

The diffracting crystals were obtained in 100 mM potassium thiocyanate, 30% (w/v) PEG 2000 MME, for the Mn-loaded triple mutant isoform of SodM. Samples were cryo-protected using the reservoir solution complemented with 20% (w/v) PEG 400. Diffraction experiments were performed by Dr Arnaud Basle, (Newcastle University, UK) at the Diamond Light Source synchrotron during mx9948-22 experiment. Values in parenthesis quoted for the highest resolution shell. # 5% of the randomly selected reflections excluded from refinement. * Calculated using MOLPROBITY.

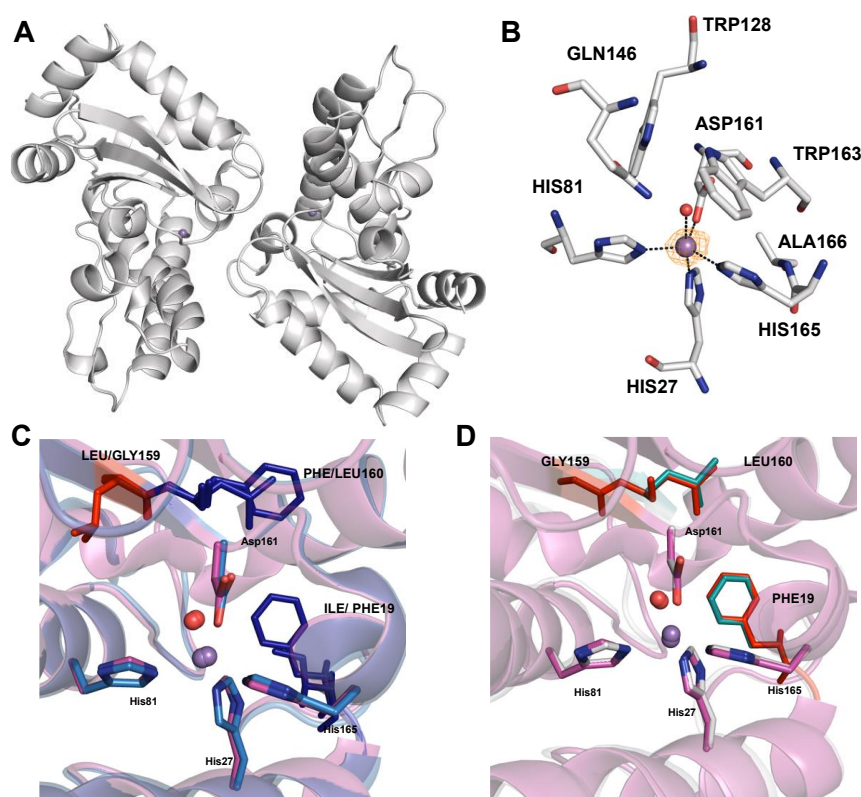


Figure 4.15 Crystal structure of Mn-SodM triple mutant.

Cartoon representation (A) of two chains present in the asymmetric unit of Mn-SodM triple mutant crystal, forming biological dimer. Mn ion (purple sphere) coordination sphere (B), with ligand residues in stick format, solvent molecule represented as red sphere, and the anomalous difference map, contoured at 5 σ level, represented as orange mesh. Superimposed by secondary structure matching of the Mn-SodA (pink carbons) and the triple mutant (white carbons), (C), and Mn-SodM (blue carbons) and mutant (D).

Coordinating residue/molecule	Atom ID	Distance to metal atom, (Å)				
		FeSodA	MnSodA	FeSodM	MnSodM	MnSodM (mutant)
Chain A						
His27	NE2	2.23	2.36	2.25	2.36	2.16
His81	NE2	2.06	2.13	2.17	2.33	2.14
His165	NE2	2.31	2.41	2.14	2.30	2.23
Asp161	OD2	2.06	2.12	2.02	1.97	2.03
HOH	O	2.12	2.22	2.29	2.21	2.22
Ligand – metal – ligand angle, (°)						
His27-M-His81		92.1	95.1	92.7	91.1	96.8
His27-M-Asp161		82.9	80.2	92	87.4	84.3
His27-M-His165		90.5	89.6	91.5	89.3	92.9
His27-M-HOH		170.1	167.6	172.8	174.3	169.2
His81-M-Asp161		111	116.5	119.6	120	111.9
His81-M-His165		136.2	131.1	122.6	124.7	129.6
His81-M-HOH		93.5	95.5	91.8	84.2	89.7
His165-M-HOH		91.2	89.3	90.8	96.1	89.5
Asp161-M-His165		112.7	112.3	117.4	115.2	118.3
Asp161-M-HOH		87.4	88.9	80.9	92.1	85.3

Table 4.9 Bond distances and bond angles of the metal coordination sphere in single chain A.

Distances (Å) and angles (°) measured using Pymol (Schrödinger, LLC).

The importance of Gly159 to metal-specific activity was previously proposed based on mutagenesis studies of the metal-specific enzymes from *E. coli* (Osawa et al., 2010) and the cambialistic enzyme from *Porphyromonas gingivalis* (Yamakura et al., 2003). This position is usually occupied by a Thr residue in Fe-specific SODs (Thr154 in *E. coli* FeSOD) but is usually a glycine in MnSODs (Gly165 in *E. coli* MnSOD) and cambialistic SODs (Gly155 in *P. gingivalis*). A mutation of Gly165 to Thr in *E. coli* did not alter Mn-specific activity, but increased activity of protein loaded with Fe by 10-fold relative to the MnSOD wild type (Osawa et al., 2010). The equivalent mutation in *P. gingivalis* caused a 10-fold decrease in Mn-specific activity and a 2-fold increase of Fe-specific activity of the cambialistic enzyme (Yamakura et al., 2003). Modulation of catalytic activity in *P. gingivalis* G156T mutant was proposed to be conferred by changes to the conserved hydrogen bond network that extends from the active site to the outer sphere and supports proton transfer during catalysis (Yamakura et al., 2003).

Based on the comparison of crystal structures of the wild type and mutant variants of the *P. gingivalis* SOD enzyme, the introduction of threonine influenced the position of the two tryptophan residues (W123, W125) that surround the active site (Yamakura et al., 2003), (Figure 4.16 A). This has been proposed to alter the hydrogen bonding network around the active site (involving residues Q70, N73, and W123; Figure 4.16A), and in consequence metal-specific activity, by altering the cofactor's redox tuning. Comparison of the superimposed residues involved in H-bond interactions within 10 Å radius of the metal cofactor in the two wild type enzymes of *S. aureus* (Figure 4.16 B) and the SodM mutant (Figure 4.16 B) indicated a difference in the relative orientation of W128 and W130. Swapping of the residues [I19; L159; F160] in cambialistic SaSodM for its Mn-specific SaSodA equivalents [F19; G159; L160], which altered the enzyme's activity, similar to *P. gingivalis* SOD variants, caused an alteration in the positioning of the residues Trp128 and Trp130 (Figure 4.16 C). However, there was no significant changes observed in the hydrogen bond network observed within the 10 Å radius from the coordinated metal ion. The subtle differences observed within the protein backbone between the two *S. aureus* SODs, could, however, potentially influence the (length) strength of H-bonds in the network, and influence catalysis.

Analogously to the mutagenesis performed on the *E. coli* (Osawa et al., 2010), and the *P. gingivalis* SODs (Yamakura et al., 2003), the G159T mutation was also introduced into SaSODs' sequences to assess the potential increase in Fe-specific activity. Due to the time constraints, a comprehensive analysis of the these protein isoforms was not completed. The initial result obtained for SodA [G159T] and SodM [L159T] showed that both proteins purified from the heterologous host as dimeric, Fe-loaded forms with approximately 5 % Mn and 14 % Zn contamination. The cofactor exchange was performed for Mn by standardised protocol (section 2.12.4) and yielded Mn-loaded proteins. Introduction of threonine at position 159 seemed to increase Fe-specific activity of both the SodA [G159T] and the SodM [L159T], as was indicated by initial activity in-gel assay (Figure 4.17). Replication of these preliminary experiments is required to confirm that observed increase of Fe-specific activity, consistent with previously

observed for the *Ec*SOD and the *Pg*SOD mutants, was not due to contamination of the sample with Mn.

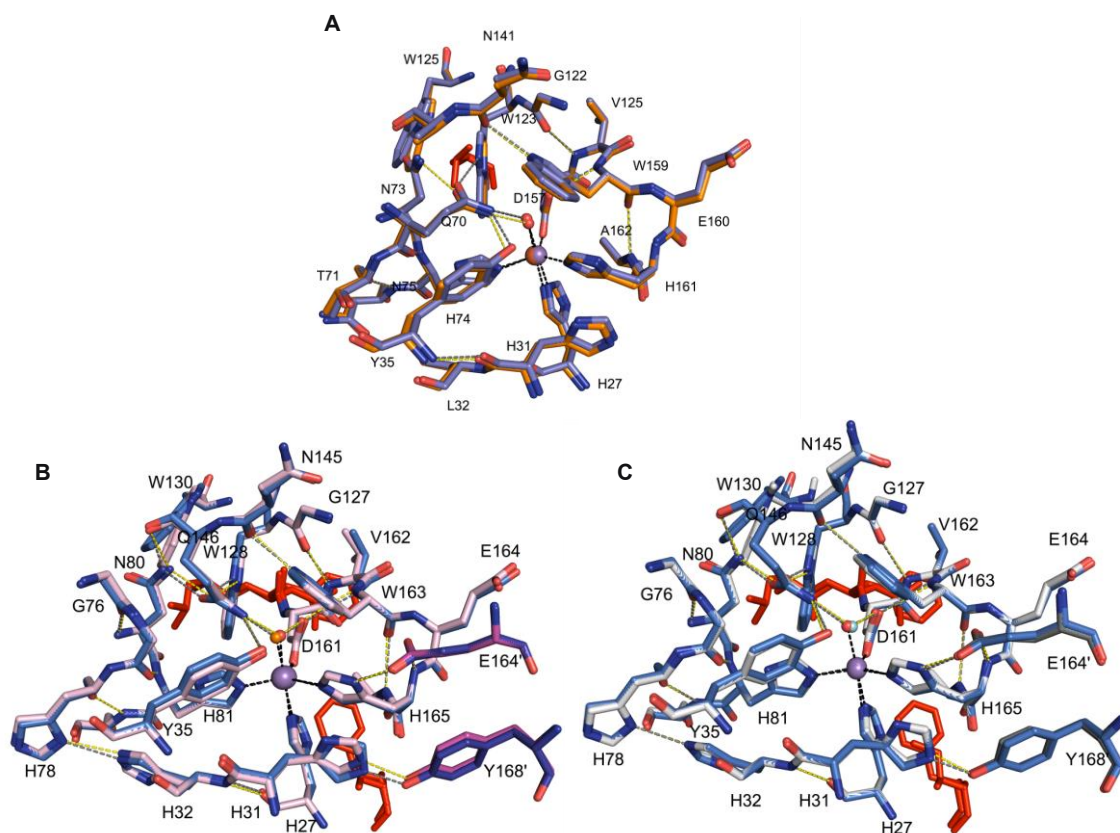


Figure 4.16 Comparison of the active site coordination and estimated hydrogen bond network within ~10 Å radius of metal ion.

Superimposed stick models of selected residues within ~10 Å radius from coordinated metal ion (Mn as purple sphere, Fe as orange sphere) in Mn-SodA (pink), Mn-SodM (blue), Mn-SodM triple mutant (white), cambialistic *Porphyromonas gingivalis* SodB wild type (1UER, orange) and SodBT155 mutant (1UES, purple). Hydrogen bonds coloured in: yellow (SodA, SodM mutant, *Pg*SOD wild type) and in grey (SodM and the mutant PgT155). Hydrogen bonds assigned using measurement tool in Pymol. Mutated residues coloured in red. (A) Comparison of bond network in *Pg*SOD wild type and mutant. (B) Comparison of Mn-loaded SodA and SodM wild type enzymes of *S. aureus* and (C) comparison of Mn-SodM and SodM mutant [I19F; L159G; F160L].

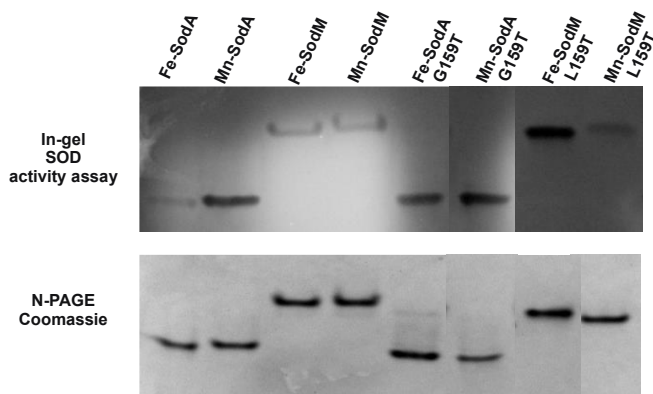


Figure 4.17 Activity assay of the SodA [G159T] and the SodM [L159T] mutants.

Aliquots (0.3 µg of each protein in 20 mM Tris, pH 7.5, 150 mM NaCl) were resolved by 12 % Native-PAGE and stained for SOD activity using in-gel NBT-riboflavin based assay, or for protein using Coomassie stain. Gels were visualised using BioRad ChemiDoc XRS+ system.

4.3. Conclusions

The two superoxide dismutases of *S. aureus*, SodA and SodM were crystallised in both Fe and Mn-loaded isoforms. The proteins crystallised in primitive monoclinic and hexagonal space groups, respectively. Determination of structural models was performed by molecular replacement. Conducted structural studies revealed that both SodA and SodM proteins adopted identical folds and active site geometry (section 4.2.1), aligning within protein backbone with RMSD of 0.684 Å. Subtle differences were detected in the estimated net-charge of the two proteins, with Mn-SodA presenting more positively charged residues at the surface creating the substrate access funnel then Mn-SodM, which could potentially contribute to the higher activity of this form of protein by the increased attraction of the negatively charged substrate ion.

Close investigation of the solved structures enabled identification of residues for targeted mutagenesis, which were hypothesised to be potential structural determinants of the different biochemical properties (section 4.2.3). Isoforms of both SodA and SodM proteins were prepared in the two metalated forms, and their activities were assessed and compared to the wild type enzymes.

A single residue at position 159 was identified as critical to inverse cambialistic properties of SodM protein towards Mn-specificity (sections 4.2.5 - 4.2.6). Conversely, mutations introduced into SodA structure decreased activity of Mn-loaded protein and increased its Fe-specific activity. Swapping of two residues (159 and 160) did create a cambialistic version of the SodA enzyme. However, the swapping of residues between the two proteins did not invert their activity completely, indicating importance of additional (as yet unidentified) residues in conferring the specific activity of the two SaSODs.

Chapter 5. Biophysical characterisation of the cambialistic and non-cambialistic SaSODs

5.1. Introduction

The superoxide dismutase enzymes catalyse the conversion of two superoxide molecules into oxygen and hydrogen peroxide. In principle, the disproportionation of superoxide anion by the SOD enzyme is based on the sequential steps of a reduction of metal cofactor in the active site, concomitant with an oxidation of one superoxide molecule to oxygen; followed by an oxidation of the metal cofactor associated with a reduction of another superoxide molecule to hydrogen peroxide (Stallings et al., 1991). Both steps are dependent on the capacity of the protein to accommodate the appropriate redox active metal cofactor (Chapter 1; sections 1.4.4, 1.4.5).

Transition metals, such as Fe and Mn, can cycle (i.e. transition) between two oxidation states (e.g. M^{3+}/M^{2+}) during redox catalysis. As the cofactors differ in the intrinsic reduction potentials (1.51 V and 0.77 V for the $Mn^{3+/2+}$, and $Fe^{3+/2+}$ pairs, respectively), the SOD proteins evolved to differentially control the electrochemistry of their metal cofactors to facilitate optimal turnover (~ 0.3 V; Figure 1.10); (Sheng et al., 2014). This requirement implies structural differences between the MnSODs and FeSOD that could account for the distinct depression in the Mn and Fe reduction potentials (Miller and Sorokin, 1997), (Vance and Miller, 1998). According to this 'redox tuning' model, the cambialistic Fe/Mn-SOD proteins, such as SaSodM, should impose an intermediate redox tuning to accommodate either of the two metal ions for catalysis. A substitution of the metal cofactor in enzymes that evolved to perform the metal-specific function is proposed to result in a metal redox potential that does not sit within the range required to perform both steps of the superoxide dismutation (Vance and Miller, 1998), (Yikilmaz et al., 2006), (Miller, 2012).

The structural determinants enabling this redox tuning capacity of the metal-specific and the cambialistic enzymes are unclear. Determined crystal structures of the SaSODs are superimposable with 0.684 ± 0.084 Å RMSD. A comparison of the structural data of both enzymes in the two metalated forms shows conservation of the metal-ligating residues in the active site, the outer sphere, and the hydrogen-bonding network surrounding the metal atom. The differences in stability detected for the wild type SaSODs suggest that, despite the highly similar crystal structures, these proteins display some physical variations that could also be contributing to their distinct activities. The results from mutagenesis performed on the two *S. aureus* proteins identified a number of residues that enable switching of the Mn-specific and the cambialistic properties of SaSODs (positions 159, 160), that are located within 10 Å radius from the metal cofactor, and not directly interacting with the active site. The limits of crystal structure resolution

did not allow for identification of physical changes within the structure that could explain the influence of mutations on the modulation of the electrochemistry of the metal sites.

Electron paramagnetic resonance (EPR) spectroscopy of the Mn(II) centres appears to be a sensitive probe of their electronic structure although its interpretation can be complex. The zero-field interaction, which is a magnetic property of paramagnetic species that have more than one unpaired electron such as Mn(II), has been shown to respond to local electrostatic interactions and was postulated to act as a semi-quantitative measure of the changes in redox potentials that correlated with SOD-like catalytic activity (Sjödin et al., 2008; Gätjens et al., 2007; Tabares et al., 2007).

I would like to acknowledge Dr Sun Un, CEA Saclay, France, for accommodating me in his lab and providing us with the state of the art equipment to perform EPR measurements and expert knowledge for analysis of the collected spectra. The results of this collaborative work are published in a manuscript:

Barwinska-Sendra, A., Baslé, A., Waldron, K.J. and Un, S., 2018. A charge polarization model for the metal-specific activity of superoxide dismutases. Physical Chemistry Chemical Physics.

5.2. Results and discussion

The aim of work presented in this chapter was to further examine the potential influence of the subtle physical differences detected between the two wild types of *S. aureus* SODs on their specific catalytic properties.

Apo-proteins were prepared and their properties were determined with SEC-MALS and spectrofluorimetry to evaluate stability related to the metal binding.

Previous mutagenesis that was performed on both SodA and SodM to swap the three residues identified that differ in their primary sequences that lie spatially close to the active site yielded proteins with altered catalytic properties. Here, the biophysical properties of these isoforms were assessed by means of tryptophan fluorescence measurement and circular dichroism spectroscopy, to determine possible changes to the stability of created mutants.

High magnetic field (HF)-EPR spectroscopy was used to study the electronic and structural interactions within the Mn(II) centres of the two SaSODs, relative to the catalytically inactive Mn-substituted Fe-SOD of *E. coli*, to further investigate possible determinants of the metal specificity of these proteins.

5.2.1. SaSodM reversibly changes oligomeric state from dimeric holo-enzyme to monomeric apo-enzyme, when stripped of metal cofactor

Metal binding in the active site of SODs is essential for the formation of a functional enzyme. The identity of the metal is crucial in the case of the metal-specific SOD enzymes, which due to a relatively low selectivity of binding can acquire other metals from their environment, but attain activity only with one metal ion. However, Mn/Fe-cambialistic enzymes can bind and function with both metals.

To assess the properties of SaSOD apo-proteins *in vitro*, unfolding and refolding in the presence of strong metal chelators was used in an effort to prepare metal-free isoforms of the wild type protein (Materials and methods, section 2.12.3). As for preparation of Mn-loaded forms of enzymes, the preparations of Fe-SodA and Fe-SodM produced by heterologous expression and purified with anion-exchange and size-exclusion chromatography were unfolded by dialysis against 6 M guanidine hydrochloride, 8-hydroxyquinoline and EDTA (pH 3.8) buffer at 4°C for 12 hours. Further, the chaotropic agent and 8-hydroxyquinoline were subsequently removed from dialysis buffers (20 mM Tris, 100 mM NaCl pH 7.5), but 5 mM EDTA was retained throughout all steps of dialysis to prevent metalation of proteins by contaminating metal ions. After dialysis, recovered proteins were subjected to size-exclusion chromatography in 20 mM Tris, 150 mM NaCl, 5 mM EDTA, pH7.5, and subsequent elemental analysis by ICP-MS (Figure 5.1 A, B).

Apo-SodA eluted from the size-exclusion column as a dimer (Figure 5.1 A, black trace), similar to all previously observed metalated forms of SaSODs (Chapter 4, section 4.2.5) and the apo-(Mn)SOD of *E. coli* (Whittaker et al., 2011). Changes to the oligomeric state were observed

for non-metalated SodM (Figure 5.1 A, green trace). Predominantly monomeric species were observed in the elution profile from size exclusion chromatography, with approximately 0-30 % of the protein eluting as a dimer (taking into account prep-to-prep variations). It should be noted that production of apo-SodM was often difficult, giving a lower yield of recovered protein in comparison to apo-SodA, most likely due to precipitation of apo-SodM in dialysis.

Elemental analysis conducted on the recovered apo-proteins (Figure 5.1 B) confirmed loss of metal content in these preparations. Catalytic activity of the apo-proteins was assessed by a comparative SOD *in-gel* assay (Figure 5.1 C). Equal amounts of the apo-proteins, as well as the Fe-loaded and the Mn-loaded SodA and SodM as controls, were resolved by 12 % (w/v) Native-PAGE and subjected to activity analysis by staining with the NBT-riboflavin assay mix. No bands of activity were observed for the samples of apo-SaSODs in comparison to the metalated, functional forms of the proteins. Binding a metal cofactor also significantly alters the net charge of SaSOD proteins (on top of small difference in mass) demonstrated by the observation that metalated isoforms of SodA and SodM exhibit distinct electrophoretic mobility (Figure 5.1 C). Removal of the metal ion charge contribution changes the migration of apo-proteins (indicated with black arrow on Figure 5.1 C) in Native-PAGE in relation to metalated isoforms. The difference in migration of apo-SaSODs is much smaller and reflects the net charge of the two proteins.

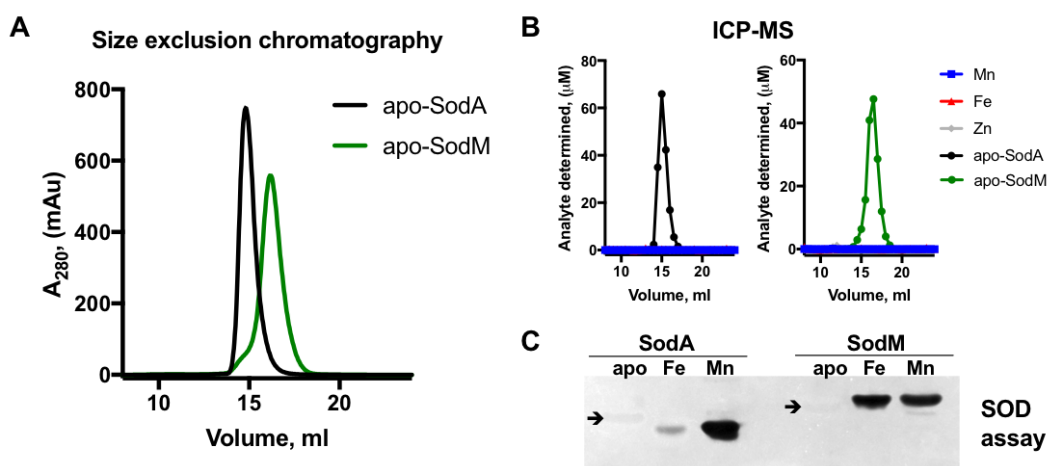


Figure 5.1 Production and initial characterisation of apo-SaSODs.

(A) A representative size-exclusion chromatography of the preparations of apo-SodA (black trace) and apo-SodM (green trace), following *in vitro* unfolding and refolding protocol. Proteins were resolved in 10 mM Tris, 150 mM NaCl, 5 mM EDTA, pH 7.5 buffer at 4°C. The main elution peaks were observed at 14.93 ml and 16.33 ml for apo-SodA and apo-SodM, corresponding with dimer and monomer, respectively, based on standard elution profiles. (B) Elemental analysis of SEC eluant presented lack of metal content in analysed samples (apo-SodA, black trace; apo-SodM, green trace), as verified against matrix of known concentrations of standards. (C) Loss of catalytic activity was observed for apo-SaSODs in comparison with metalated forms of SodA and SodM. A NBT-riboflavin staining for SOD activity was performed on the equal amount of samples resolved by 12 % (w/v) Native-PAGE at room temperature. Black arrow indicates position of apo-protein on the native gel, as confirmed by Coomassie staining of an equivalent gel (not shown).

The molecular masses of apo-SaSOD proteins in solution were determined using SEC-MALS (Figure 5.2 A, C). Sample analysis and data collection were performed by Dr Owen Davies (ICAMB, Newcastle University). SEC-MALS analysis allows for an accurate determination of a molecular mass and stable oligomeric state of the protein in solution. Size-exclusion chromatography indicated differences in oligomerisation of the two apo-SaSODs (Figure 5.1 A). A combination of SEC retention with the light scattering and refractive index analysis allowed determination of the absolute molar masses of apo-SodA (Figure 5.2 A, black trace) as a dimer of 41.60 kDa ($\pm 0.132\%$) and apo-SodM as predominantly a monomer (Figure 5.2 C) of 22.75 kDa ($\pm 0.181\%$). A small fraction of dimeric species was also identified for apo-SodM by SEC-MALS. Even multiple size-exclusion separation steps of a monomeric species did not separate the two fractions (data not shown), indicating that the two forms can interconvert, leading to monomer-dimer equilibrium under size-exclusion conditions.

Manganese reconstitution of apo-SaSODs was performed by the incubation of approximately 10 μM concentration of each protein with 2 mole-equivalents of MnCl_2 at 37°C for 24 hours. Following incubation, the mixtures were desalted by size-exclusion chromatography in 20 mM Tris, 150 mM NaCl and 5 mM EDTA, pH 7.5 at 4°C . The collected peak fractions were subjected to SEC-MALS and subsequent ICP-MS analyses (Figure 5.2). The dimeric state of Mn-reconstituted apo-SodA (Figure 5.2 A, grey trace) was preserved after incubation with Mn. The determined mass of this isoform (41.90 kDa $\pm 0.107\%$) was consistent with as-isolated Fe-SodA (43.63 kDa $\pm 0.136\%$) and refolded Mn-SodA (43.90 kDa $\pm 0.097\%$), (Chapter 3, section 3.2.14, Figure 3.21). A quantitative metal analysis performed on Mn-reconstituted apo-SodA (Figure 5.2 B, grey trace) did not detect Mn (blue squares) corresponding with the protein trace, implying lack of incorporation of metal cofactor into protein structure.

Under the same incubation conditions, a formation of dimeric Mn-reconstituted apo-SodM was observed (Figure 5.2 C, teal trace). Approximately 15 % of the monomeric species did not convert into dimer. A molecular mass of the Mn-reconstituted apo-SodM was determined to be 44.96 kDa ($\pm 0.129\%$), which was consistent with previously determined masses for Fe-SodM (45.24 $\pm 0.175\%$) and refolded Mn-SodM (45.13 $\pm 0.100\%$), (Chapter 3, section 3.2.14, Figure 3.21).

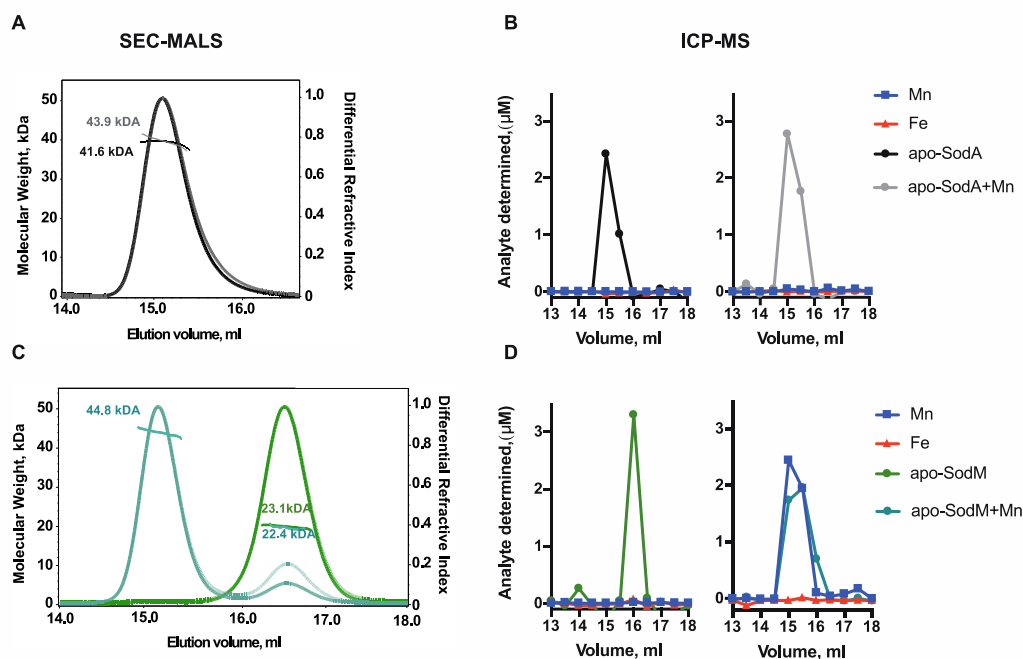


Figure 5.2 SEC-MALS analysis of apo-SaSODs and apo-(Mn)SaSODs.

Approximately 100 µg of apo-SodA (A, black trace) and apo-SodM (C, green trace) were resolved on size exclusion column, in 20 mM Tris pH 7.5, 150 mM NaCl. Samples eluting from the column passed through a light scattering detector, coupled to a refractive index detector. Aliquots of apo-SaSODs were incubated for 24 h at 37°C with 2 molar-equivalents of Mn and desalted by gel filtration chromatography. Following desalting, 100 µg of Mn-reconstituted apo-SodA (A, grey trace) and Mn-reconstituted apo-SodM (C, teal trace) were each resolved by size exclusion, coupled with light scattering detector and a refractive index detector. A weighted average molecular mass was calculated from the collected data, based on refractive index and light scattering measurements using Astra 6 software (Wyatt Technology). A 1 ml fractions of apo-SodA (B, black trace), Mn-reconstituted apo-SodA (B, grey trace), apo-SodM (D, grey trace) and Mn-reconstituted apo-SodM (D, teal trace), collected post SEC-MALS were subjected to elemental analysis to determine their metal content (Mn, blue square; Fe, red triangle).

A phenomenon of quenching of the intrinsic protein fluorescence by metal ions has been used in fluorimetric metal uptake assay to determine mechanism and kinetics of metal binding by *E. coli* apo-MnSOD (M. M. Whittaker et al., 2006). Metal binding by the protein causes a decrease (quenching) of the intrinsic fluorescence of aromatic residues due to energy transfer between the excited tryptophan residues and the metal centre via a Förster mechanism. Comparison of Mn-loaded and Fe-loaded proteins with the apo-enzymes (Figure 5.3 A, B) indicated efficient quenching of the tryptophan fluorescence in comparison to samples with absent metal cofactors. Upon metal binding, there was 10 % (Mn-SodA), 25 % (Fe-SodA), 50 % (Mn-SodM) and 65 % (Fe-SodM) decrease in the measured fluorescence intensity in comparison to the respective apo-SaSOD. A clear difference was observed in both intensity and emission wavelength of the fluorescence between apo-SodM (Figure 5.3 B, blue trace) and apo-SodA (Figure 5.3 A, blue trace). This effect may potentially have arisen from the conformational variation between the two proteins, with a monomeric apo-SodM possibly having more solvent exposed aromatic residues than dimeric apo-SodA.

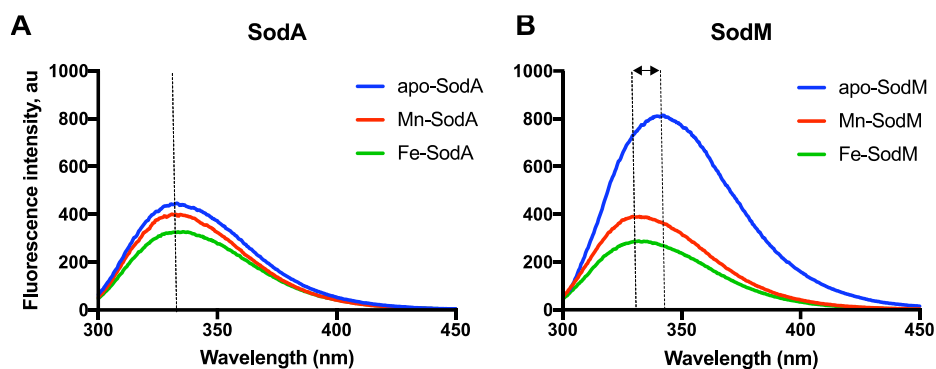


Figure 5.3 Tryptophan fluorescence emission changes upon metal binding to apo-SaSodA.

(A) Approximately 3 μM protein in 20 mM Tris, 100 mM NaCl, pH 7.5 at room temperature was incubated with 10 molar-equivalents of MnCl_2 and tryptophan fluorescence was measured upon excitation at 280 nm, before addition of Mn, at the point of Mn titration and after 1h, 2h, 24h incubation. Fluorescence was recorded for a region around the wavelength of maximum fluorescence of tryptophan, at ~ 330 nm. (B, C) Comparison of tryptophan fluorescence emission intensity of apo (blue trace) and stoichiometrically metalated isoforms (Mn, red; Fe, green) of wild type SaSODs. Approximately 10 μM samples of proteins in 20 mM Tris, 150 mM NaCl pH 7.5 were excited at 280 nm and fluorescence measurements were taken at room temperature, recording emission between 300 nm and 450 nm.

The post-translational mechanism of acquisition of metals by the dimeric *E. coli* apo-MnSOD, involving thermal activation and a conformational transition required for metal binding, was proposed by Whittaker & Whittaker, 2008. The crystal structure of apo-MnSOD (PDB 3OT7; Whittaker et al., 2011) suggested that coordination of the metal centre is not organised around the metal ion upon the acquisition of cofactor, but may comprise a stable structure within the native folded protein, as a non-metalated active centre showed the same positioning of its ligands arranged in a distorted, trigonal bipyramidal geometry as in the metalated Mn-SOD protein (1VEW; Edwards et al., 1998). Incorporation of the metal cofactor into the protein structure *in vitro* was demonstrated to occur through subunit exchange, coordinated with metal binding by the two subunits of the dimeric protein. Subunit exchange between holo-enzyme and apo-enzyme was shown to be a concentration-dependent process, implying the importance of protein dissociation to metal binding (Whittaker et al., 2011).

The difficulty experienced in extracting the metal cofactor from the metalated SaSODs, together with the thermally triggered metal uptake *in vitro* demonstrated for other SOD homologues, could imply kinetic-trapping of the metal cofactor as the basis for the apparent metalation-dependent stability of the proteins. Analysis of determined crystal structures (Chapter 4, section 4.2.2) suggests that access to the metal binding site is kinetically gated, restricting access to the active site only to the small anionic substrate. The positively charged substrate access funnel's mouth attracts superoxide anion and constitutes an electrostatic barrier to binding the cationic metal in the 'closed' form of the protein. The properties of apo-SodA suggest that it presumably represents the 'closed' form of the enzyme, with higher barriers for metal uptake, according to Whittakers' model (Whittaker & Whittaker, 2008). Dissociation of subunits of apo-SodM, and recovery of the protein in the monomeric state, suggest there may be fewer constraints for reorganisation of the domains within a polypeptide chain (i.e. interconversion to an

'open' form), potentially enabling less demanding metal uptake *in vitro*. Quantitative incorporation of metal in apo-SodM (and re-association of subunits into a dimer), but not in apo-SodA, after 24 hours of incubation with 2 molar-equivalents of Mn could imply different metal acquisition pathways by the two proteins in these conditions.

Crystallisation trials were initiated for the apo-SodM, but yielded crystals only in a single condition, which unfortunately contained 0.005 M cobalt chloride, 0.005 M cadmium chloride, 0.005 M magnesium chloride, 0.005 M nickel chloride; 0.1 M HEPES; pH 7.5; 12% PEG 3350 (JCSG+, G5); (192 conditions tested; not optimised; not solved; metal binding indicated by electron density but not verified by fluorescence scans), which subsequently was found to contain a bound metal ion (data not shown). This could suggest a stabilising role of metal binding for the formation of the structure of holoenzyme of SodM in crystal.

5.2.2. Tryptophan fluorescence spectroscopy indicate changes in chemical stability of SodM upon introduction of point mutations

Given that the biophysical differences between the two wild type proteins were observed (Chapter 3, sections 3.2.7.1; 3.2.10), to evaluate an influence of the mutations introduced into SodA and SodM sequence, on the overall stability of resulting mutants, protein samples were subjected to the tryptophan fluorescence analysis.

Comparison of the tryptophan fluorescence emission for all SOD isoforms is presented in Table 5.1. SaSodA protein isoforms exposed to either urea or guanidine hydrochloride were all susceptible to denaturation, just like the wild type, presenting a characteristic red shift of tryptophan fluorescence maximum from 330 nm to ~350 nm. This implies that the mutagenesis did not alter the chemical stability of SodA isoforms, relative to wild type enzyme.

Variations in the behaviour of SaSodM mutant proteins were observed under exposure of the proteins to equivalent conditions. All mutant forms were equally susceptible to guanidine denaturation, similar to the wild type enzyme. Comparison of the wild type SaSodM with the mutated isoforms indicated that the introduction of mutations at the single position [19], or at the two positions [159 and 160] did not alter the resistance of proteins to urea-mediated denaturation. The single mutant [L159G] and the triple mutant [I19F, L159G, F160L], however, exhibited a more denaturation-tolerant characteristic, manifested by a shift of Trp fluorescence emission towards 350 nm under urea denaturation (Figure 5.4, Table 5.1). This observation could imply that site-specific mutagenesis of the SodM protein had an effect on the resistance to urea denaturation, similar to one observed for all SodA proteins.

The hydrophobic environment around the active site potentially may influence the reactivity of metals in proteins by maintaining the appropriate redox potential of the metal ion during two-step superoxide dismutation reaction. Cumulatively, mutations introduced into the SodM sequence at positions [19, 159 and 160] which inverted enzyme's cambialistic properties

into Mn-specificity, influenced the chemical stability of the protein in a similar manner, yielding a SodA-like version of SodM, as indicated by the change in Trp fluorescence.

Protein	Fluorescence emission maximumwavelength, [nm]		
	Tris/ NaCl buffer	8M Urea	6M Gdm
Fe-SaSodA	331	<u>355</u>	<u>355</u>
Fe-SaSodA [F19I]	335	<u>351</u>	<u>358</u>
Fe-SaSodA [G159L]	334	<u>355</u>	<u>356</u>
Fe-SaSodA [G159L; L160F]	332	<u>355</u>	<u>356</u>
Fe-SaSodA [F19I; G159L; L160F]	332	<u>354</u>	<u>357</u>
Mn-SaSodA	332	<u>351</u>	<u>358</u>
Mn-SaSodA [F19I]	332	<u>354</u>	<u>361</u>
Mn-SaSodA [G159L]	331	<u>355</u>	<u>357</u>
Mn-SaSodA [G159L; L160F]	330	<u>356</u>	<u>358</u>
Mn-SaSodA [F19I; G159L; L160F]	333	<u>355</u>	<u>355</u>
Fe-SaSodM	334	335	<u>355</u>
Fe-SaSodM [I19F]	333	335	<u>352</u>
Fe-SaSodM [L159G]	332	<u>347</u>	<u>356</u>
Fe-SaSodM [L159G; F160L]	333	336	<u>356</u>
Fe-SaSodM [I19F; L159G; F160L]	333	<u>342</u>	<u>356</u>
Mn-SaSodM	332	335	<u>359</u>
Mn-SaSodM [I19F]	333	335	<u>358</u>
Mn-SaSodM [L159G]	332	<u>349</u>	<u>357</u>
Mn-SaSodM [L159G; F160L]	334	338	<u>358</u>
Mn-SaSodM [I19F; L159G; F160L]	333	<u>349</u>	<u>357</u>

Table 5.1 Summary of the maxima of the tryptophan fluorescence emission spectra of all studied native and mutated versions of SaSodA and SaSodM.

Fluorescence emission spectra obtained for samples of all protein forms at 10-12 μ M concentration in 20 mM Tris buffer pH 7.0, 150 mM NaCl, 8 M urea and 6 M guanidine at room temperature. The emission spectra were recorded between 300 nm and 450 nm, upon excitation at 280 nm. A shift in the emission maximum of tryptophan residues, from ~330 nm to ~350 nm, is indicative of a transition from a folded to an unfolded state in given environment. (Teale & Weber, 1957).

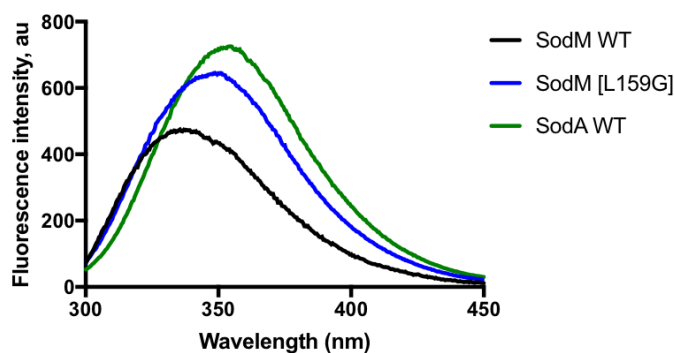


Figure 5.4 Tryptophan fluorescence emission spectroscopy of Mn-loaded SaSodA, SaSodM and SodM L159G proteins in 8 M urea.

Fluorescence emission spectra obtained for samples of SodM wild type (WT, black trace), SodM L159G (L159G, blue trace) and SodA wild type (SodA, green trace), at 12 μ M concentration in 8 M urea. A shift in the emission maximum of tryptophan residues from 330 nm to 350 nm is observed for SodA treated with urea. Wild type SodM does not unfold in urea and presents maximum of fluorescence emission at \sim 330 nm. A mutation of L159G residue, that inverts catalytic properties into Mn-specificity, alters chemical stability of protein, as indicated by a shift of Trp fluorescence, with a maximum at \sim 350 nm.

5.2.3. Circular dichroism spectroscopy demonstrates that mutant isoforms of SaSODs have similar properties to the wild type proteins

The effects of the mutations introduced into the sequences of both SodA and SodM on their overall secondary structure compositions were assessed with far-UV CD spectroscopy. Comparison of the contents determined from the wild type crystal structures and estimated by the means of CD spectroscopy indicates that all isoforms of the proteins had very similar, predominantly α -helical composition, as summarised in Table 5.2 and Figure 5.5 A, C.

Multiple thermal unfolding transitions were observed for the Fe-loaded mutants of SodA, similar to the wild type protein, which presented two inflection points (i.e., T_{m1} =45.2°C and T_{m2} =69°C. A small change, approximately 5°C decrease, in the melting temperature of the second transition was observed between SodA wild type, the single G159L mutant; and the triple mutant (Figure 5.5 B). Fe-SodM isoforms were found to be consistently more resistant to thermal denaturation than Fe-SodA in solution, with an unfolding occurring in single transition at T_m around 79°C (Figure 5.5 D).

Protein	Data source	Secondary structure, %		
		Helix	β -sheet	Other
SaSodA	X-ray	54.8	11.8	33.3
	Far-UV CD	52	13	35
Mn-SaSodA	X-ray	52.6	11.6	35.9
	Far-UV CD	52	12	36
SaSodM	X-ray	57.1	11.6	31.3
	Far-UV CD	56	12	32
Mn-SaSodM	X-ray	56.1	11.6	32.3
	Far-UV CD	59	14	27
Mn-SaSodM [I19F;L159G;F160L]	X-ray	56.1	11.6	32.3
	Far-UV CD	53	15	32

Table 5.2 Comparison of the secondary structure contents of SaSODs.

The secondary structure contents determined from available structures using PDB-SUM (X-ray structures) and calculated from the far-UV CD spectra using Dichroweb (Far-UV CD).

Relatively higher stability was observed for Fe-loaded wild type forms of SaSODs, in respect to the equivalent Mn-loaded proteins (Chapter 3, sections 3.2.7). This observation was consistent with similar behaviour described for the metal-specific *E. coli* SODs (Hunter et al., 2002), the cambialistic *S. mutans* SOD (De Vendittis et al., 2010), and the cambialistic *P. shermanii* enzyme (Meier et al., 1997). It has been proposed that protein stability (estimated by an apparent melting temperature) is linked with metal selectivity and Mn-specificity (Miller & Wang, 2017). The [Q146E]_{Ec} mutant of MnSOD from *E. coli* was isolated as an apo-protein (unable to acquire substantial amount of any metal inside the cells, even when supplemented in abundance), but presented a 30°C higher melting temperature than the wild type apo-MnSOD (which is easily reconstituted with Mn). This example suggested that the conservation of Q146 in Mn-specific SOD of *E. coli* favours the protein's high affinity specific metal binding, required for its efficient catalysis at the cost of protein stability.

Both SaSODs have conserved Q146 position in their structures, however, different residues could potentially be involved in linking the metal specificity and stability of these two proteins, as indicated by the subtle fluctuations in T_m of SodA mutants Figure 5.5 B).

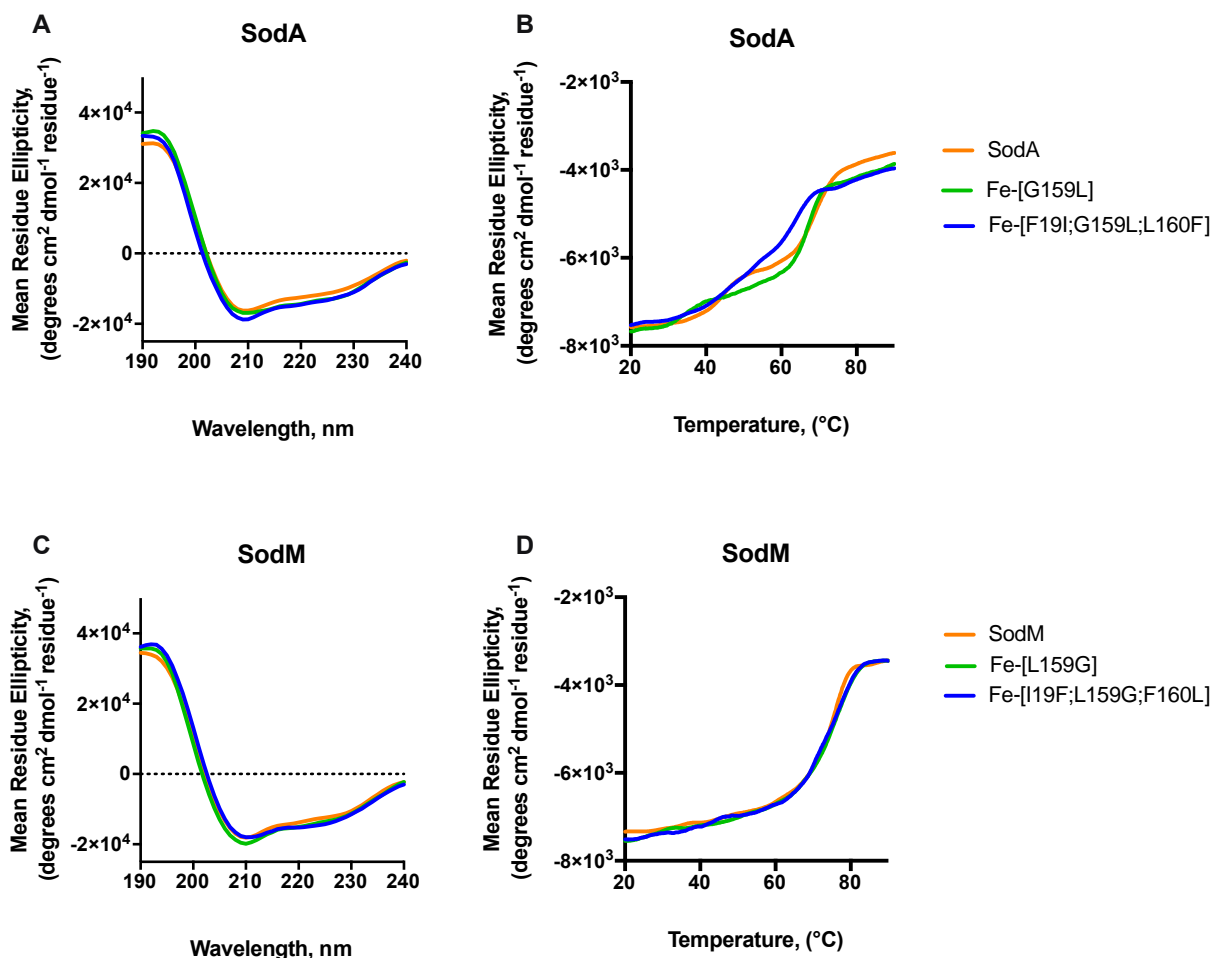


Figure 5.5 The circular dichroism spectroscopy of Fe-loaded, native and mutated SaSodA and SaSodM proteins.

The far-UV circular dichroism spectra of Fe-SODs (WT, orange; 159 single mutant, green; triple mutant, blue) at the concentration of approximately 1 μM in 10 mM sodium phosphate buffer, pH 7.0, processed using CDSSTR analysis programme with a reference set 4 optimised for 190-240 nm within Dichroweb server. Data presented as mean residue ellipticity over the range of wavelengths 190-240 nm. (B) A CD spectrum measured at 222 nm wavelength as a function of a temperature gradient from 20°C to 90°C, presenting unfolding of helical component of the proteins at approximately 8 μM concentration in 10 mM sodium phosphate buffer, pH 7.0 (WT, orange; residue 159 single mutant, green; triple mutant, blue).

5.2.4. UV-vis spectroscopy reveals strong propensity of SodA to autooxidation

A mechanism of superoxide dismutation by Mn/Fe-SODs involves the cyclical reduction and oxidation of the metal cofactor ($\text{M}^{3+} \leftrightarrow \text{M}^{2+}$; Chapter 1, section 1.4.4, 1.4.5). To evaluate differences in the effect of the metal sites of the two SaSODs on their oxidation state at rest, visible absorption spectra of the two metalated versions of both proteins were measured and compared (Figure 5.6).

The UV/visible absorption spectrum of as-isolated (i.e. Fe-containing) SodM protein (Figure 5.6 A) was characterised by a broad maximum around 350 nm and a long absorption tail extending up to 600 nm. The strong absorption in the visible region ($\epsilon_{350\text{nm}}=1508 \text{ M}^{-1}\cdot\text{cm}^{-1}$) occurs due to ligand-to-metal charge transfer in the Fe(III)-coordinated active site. Similar properties were observed for Fe-SOD or the Fe-loaded [E170A]_{Ec} mutant of MnSOD from *E. coli* (Slykhouse

& Fee, 1976), (Whittaker & Whittaker, 1998). The native form of *S. aureus* SodA, which was purified from the heterologous host containing Fe, did not exhibit such a pronounced spectral feature around 350 nm. The weaker SodA absorption in a visible region may reflect a difference in the ratio of species containing the reduced state (Fe(II)) of the protein-bound metal.

The UV-vis spectra of Mn-SaSODs exhibited features that can be associated with the presence of a Mn(III) centre, with maximum absorption around 480 nm and a second, smaller peak at around 600 nm (Figure 5.6 B; Whittaker et al., 1991). Similarly to the observation for Fe-loaded proteins, Mn-SaSODs presented different levels of absorption in these regions. Mn-SodA exhibited a stronger absorption peak at 480 nm ($\epsilon_{480\text{nm}}=495 \text{ M}^{-1}\cdot\text{cm}^{-1}$) than Mn-SodM ($\epsilon_{480\text{nm}}=261 \text{ M}^{-1}\cdot\text{cm}^{-1}$). The higher Mn(III)-SodA extinction coefficient, calculated based on protein concentration, potentially indicated higher oxidation levels of the bound Mn in this protein, in comparison to a partial reduction of the Mn(III) signal in SodM.

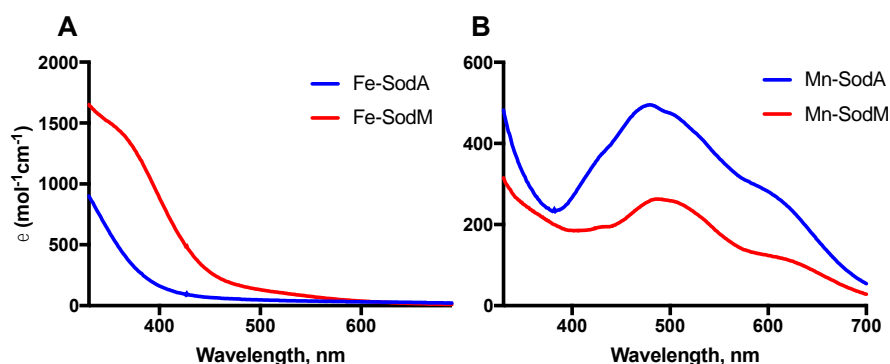


Figure 5.6 Optical absorption spectra of metalated isoforms of wild type SaSODs.

UV-vis spectra of (A) Fe-SaSODs and (B) Mn-SaSODs samples at approximately 300 μM concentration in 10 mM phosphate buffer pH 7.0. Spectra were recorded at room temperature in the visible region for SodA (blue trace) and SodM (red trace) using different metalated versions of wild type proteins.

The reduction of Mn(III)-SaSODs to Mn(II) by dithionite titration led to a loss of the visible spectrum. However, Mn-SodA was found to be more resistant to treatment with dithionite, requiring a 10 times higher dose of the reducing agent than SodM to eliminate the spectral feature produced by the Mn(III) centre. These observations imply that the population of the recombinant Mn-SodA in solution was dominated by the Mn(III)-bound form, whereas cambialistic Mn-loaded SodM seems on average more reduced i.e. potentially has a different (higher) redox potential than Mn-SodA. This would potentially correlate with the differences in activities of the Mn-loaded forms of these proteins (Chapter 3, section 3.2.11).

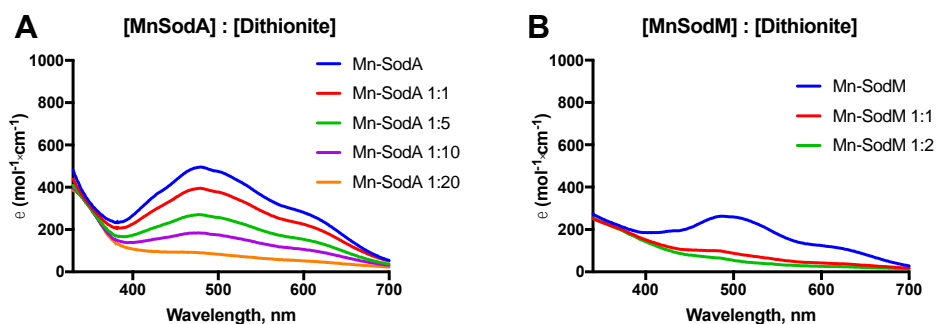


Figure 5.7 Optical absorption spectra of metalated isoforms of wild type SaSODs upon reduction with dithionite.

The change in the visible absorption spectrum of $\sim 300 \mu\text{M}$ Mn-SodA (A) and Mn-SodM (B) in 10 mM Na-phosphate buffer pH7.0 upon stoichiometric titration of protein with increasing concentration of dithionite.

SodA presented features typical to the Mn-specific enzymes, and its behaviour indicated strong propensity for auto-oxidation (at high concentration, the protein solution was pink coloured) relative to Mn-loaded SodM (which was a clear solution regardless of concentration). The cambialistic properties of SodM were reflected by the loss of $\sim 50\%$ of signal arising from Mn(III), which is characteristic for Mn-specific proteins like SodA, and gain of the signal reflecting Fe-specific activity, characteristic for the metal-tolerant SOD type. As was previously shown, the mutation of Gly165 to Thr in *E. coli* Mn-SOD which yielded a metal-tolerant enzyme (increase of activity with Fe, while still keeping high Mn-activity), showed the loss of some of the Mn(III)-spectral feature in UV-vis, and possibly some gain of the Fe(III)-specific feature, in comparison to the native Mn-SOD (Osawa et al., 2010). The equivalent mutation in the cambialistic *P. gingivalis* enzyme, which yielded an Fe-specific SOD, presented nearly complete loss of the Mn-spectral feature, and substantial gain of the Fe-specific one (Yamakura et al., 2003).

5.2.5. Mn-specific SodA and cambialistic SodM of *S. aureus* can be distinguished by the Zero Field Interaction of Mn in magnetic field (94 GHz)

The crystal structures obtained for the SaSOD proteins shared a high level of structural similarity, and did not provide sufficient structural detail to explain the distinct catalytic properties of these proteins. EPR spectroscopy is particularly sensitive to subtle changes in the environment of paramagnetic species, such as Mn. To investigate differences in the metal sites of the SaSODs, EPR spectroscopy analysis was conducted on reduced Mn-loaded forms of the SodA and the SodM proteins, in comparison to an inactive Mn-substituted Fe-SOD from *E. coli*, to seek detailed and quantitative information about the electronic structure of the Mn(II)-containing active sites. Collection and processing of the EPR spectra were performed by Dr Sun Un, CEA, Saclay, France, using purified protein samples that were prepared in Newcastle.

As indicated by the visible absorption analysis (Figure 5.6, Figure 5.7), purified Mn-loaded SaSOD proteins exhibited characteristics of the mixed oxidation states of Mn, with a strong contribution of oxidised species to UV-vis spectra. Therefore for EPR measurements, aliquots of SOD proteins at approximately 2 mM concentration were treated with the strong reductant, dithionite (Figure 5.7), to prepare homogenous, reduced Mn(II)-SOD samples.

The spectra of Mn(II) [$3d^5$, $S=5/2$, $L=5/2$] were recorded at the liquid helium temperature of 5 K, by applying high-magnetic field (3 T) and high microwave frequency (94 GHz) EPR (HF-EPR). The HF-EPR allows for a robust characterisation of the magnetic parameters of the metal-ligand interaction in the active site, such as zero-field interaction (which arises from magnetic spin-spin and spin-orbit interactions; determines shape and width of a spectrum), which distinguishes SOD enzymes, and hyperfine interactions (which describe in detail the distances and orientation of Mn and interacting nuclei, such as protons and nitrogen atoms; in relation to the magnetic field and the zero-field interaction), (Figure 5.8).

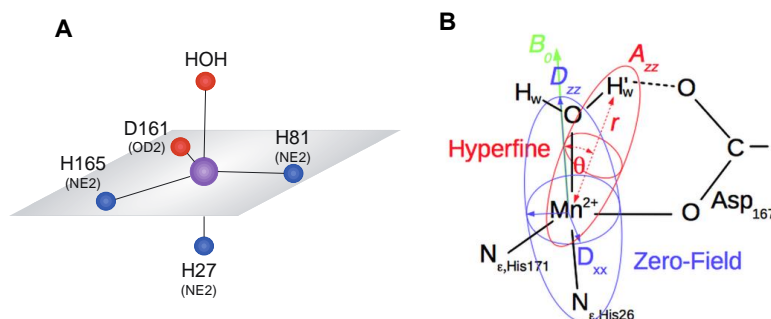


Figure 5.8 The models of the Mn-SodA active site structure.

(A) Simplified model representation of a distorted trigonal bipyramidal geometry of Mn-SodA active site. (B) The geometry of the hyperfine interaction (in red) between the Mn(II) and a water ligand proton with the magnetic-field (B_0 , green) applied along Mn-N_{ε,His26} bond and, in blue, the orientation of the zero-field interaction axes (D_{xx} , yy , zz) with respect to the Mn(II) ligands. Figure B was taken from Barwinska-Sendra et al., 2018; fig 2.

Interactions within the Mn coordination sphere were first assessed by 94 GHz field-swept echo spectrum scans, performed for both wild type and the mutants of SaSOD enzymes, as well as comparative spectra that were obtained with the two wild type SaSODs and Mn-substituted FeSOD from *E. coli*. All studied proteins presented distinctive spectra (Figure 5.9; Figure 5.11), implying different electronic structures of the metal centres. The zero-field interactions that differentiated the analysed proteins were described by the magnetic parameters ($|D|+E$), which were derived from the specific field positions relative to the applied microwave frequency (Un et al., 2004), (Figure 5.10 inset; Figure 5.11). Although no significant differences were observed in the determined crystal structures of SaSODs, the observed electronic differences could be reflecting the subtle physical differences in metal coordination sphere, beyond the resolution of the crystal structures; or they may be caused by electronic interactions in the outer sphere.

The correlation between zero-field interaction and Mn-specific activity was described based on the comparative analysis of multiple proteins of characterised activity and their

magnetic spin parameters (Un et al., 2004; Tabares et al., 2010). The enzymes that presented a high level of Mn-specific activity also presented broader HF-EPR spectra and high zero-field interaction, described by the value of $[|D|+E]$. Conversely, enzymes that were inactive with Mn, such as Mn-substituted Fe-specific SODs, were found at the opposite site of scale, presenting lowest $[|D|+E]$ factor, with the cambialistic enzymes exhibiting intermediate values of zero-field interaction, reflective of their activity. The zero-field interaction parameters of the wild type SaSOD proteins were consistent with this trend. The D and E parameters derived from the collected spectra of Mn-SodA, $D=-10.60$ and $E=0.63$ GHz, were similar to *E. coli* MnSOD; for Mn-SodM, -10.66 and 0.43 GHz, they were comparable to the *R. capsulatus* camSOD. As a point of reference, the inactive Mn(Fe)SOD was characterised by $D=-10.46$ and $E=0.33$ GHz.

The EPR spectra recorded for the mutants of SodA [159] and [19, 159, 160]; and SodM [159], showed that the introduced mutations, which altered their catalytic activities, had an analogous effect on the parameters describing their zero-field interaction. The only outlier from this trend was the triple mutant of SodM [19, 159, 160], which presented high Mn-dependent activity but its $[|D|+E]$ parameters resembled those of inactive enzymes. The mutations introduced into the SaSODs' sequence changed the properties of the wild type enzymes by swapping their characteristics. This inversion of catalytic properties, however, was not complete, i.e. the mutants did not gain the exact catalytic properties of the opposite (homologue) wild type. This biochemical property is also reflected by the zero-field interactions of the protein isoforms. The linear correlation of the two properties was observed for most of analysed SaSODs, but the outlier mutant of SodM [19, 159, 160] remains to be further characterised to address the observed discrepancy.

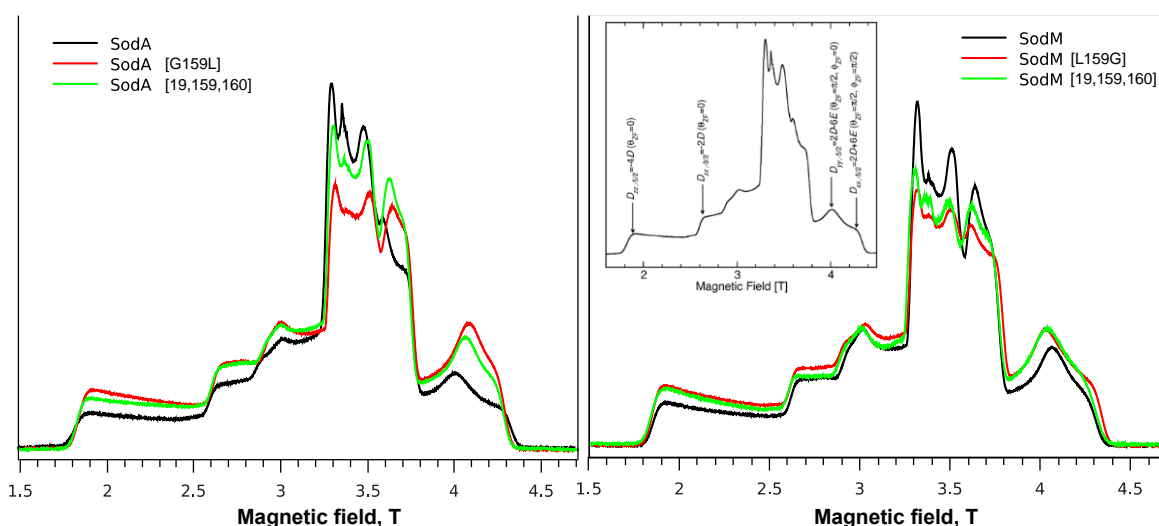


Figure 5.9 A 5K 94 GHz Mn(II) field-swept echo EPR spectra of SaSOD proteins.

HF-EPR spectra of Mn-SaSODs wild types (coloured in black), single [159] mutants (coloured in red) and triple [19, 159, 160] mutants (coloured in green). Inset shows representative spectrum with indicated (arrows) positions of the magnetic field, that were used to calculate $|D|$ and E parameters of the zero-field interaction (Un et al., 2004).

Protein	D	E	D +E	Activity, (U/mg)
Mn-sub.FeSOD	-10.46	0.33	10.79	-
SodM [19, 159, 160]	-10.46	0.50	10.96	789
SodM	-10.64	0.43	11.08	251
SodA [G159L]	-10.71	0.39	11.11	526
SodM [L159G]	-10.54	0.63	11.18	808
SodA [19, 159, 160]	-10.80	0.44	11.24	942
SodA	-10.67	0.66	11.34	1836

Table 5.3 The Mn(II) zero-field parameters and specific SOD activity of SaSODs.

Magnetic parameters listed were determined by HF-EPR and SOD activity was measured using commercial spectrophotometric assay based on WST-1. For the SaSODs, the |D|+E values were correlated with SOD activity and are presented on Figure 5.11.

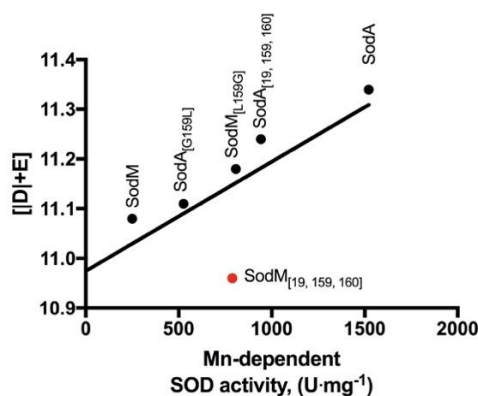


Figure 5.10 Correlation of Mn-dependent activity of SaSODs and their magnetic zero-field interaction.

The relationship between zero-field interaction parameters determined by HF-EPR and SOD activity determined by standard spectrophotometric assay. Linear regression excluding SodM triple mutant outlier with goodness of fit expressed as $R^2=0.9764$.

The correlation of the Mn-specific activity of SaSODs and the zero-field interaction shows that the zero-field respond to electrostatic interactions within catalytic centre, and thus could reflect changes in the redox potential of these metalloproteins. Therefore, zero-field interaction was postulated to serve as a semi-quantitative measure of this parameter.

The complexity of HF-EPR spectra of SaSODs reflects the complexity of interactions involved in determination of their distinct properties. The role of a hydrogen bond between the metal-bound water ligand and the sidechain of residue Q146 has been postulated to be the critical factor related to metal-specific activity for *E. coli* SODs (Yikilmaz et al., 2002; Emine Yikilmaz et al., 2007; Miller & Wang, 2017; Grove et al., 2008; Miller, 2008). The shorter distance between the solvent ligand and Q146 in *E. coli* MnSOD than in FeSOD (the structurally equivalent position is Q69) imply a stronger hydrogen-bond with the water ligand, leading to a greater depression of the $Mn^{3+/2+}$ redox potential in MnSOD (1VEW) than FeSOD (1ISB), and thus conferring different redox tuning for the two metal specific enzymes. The distance between the water and Q146 in *S. aureus* Mn-SodM crystal structure was 3.0 Å and the equivalent distance for Mn-SodA measured 2.9 Å, which corresponds with the observations for *E. coli* MnSOD, supporting the potential importance of this hydrogen-bonding interaction of Mn(II) with the outer sphere via solvent ligand to conferring specific redox potential of SaSODs.

The importance of the strength and polarity of the bonds mediated with the active site by the solvent ligand, without perturbation of the active site's physical and electronic structure, seem important for conferring the different properties of various types of SODs, given the high level of conservation of the coordination and the outer sphere structure amongst Mn/Fe-SODs. This has been demonstrated particularly well using synthetic Mn(II) complexes, which while keeping the stable structure were able to meet the thermodynamic requirements for SOD-like activity, and thus mimicked various types of specific and cambialistic activity with good accuracy (Tabares et al., 2010). The Mn or Fe complexes of 4'-(*R*)-substituted bis-terpy (bis-terpyridine), and Mn-complexes of (N,N-bis(2-ethyl-5-methylimidazol-4-ylmethyl)aminopropane)(*p*-(*R*)-benzoate), were substituted at a position distant from the metal ion, with the *R*-group differing in electron-donating/accepting capacity, measurable by the Hammett constant (Hansch et al., 1991; Gätjens et al., 2007; Tabares et al., 2007; Sjödin et al., 2008). A linear relationship was observed between the increase of electron-donating capacity of the *R* groups (Hammett constant, σ) in the outer sphere, influencing the charge of the interacting ligand nitrogen atom and the net charge of the whole metal complex; and further the zero-field interaction $[|D|+E]$ of the complex, which in turn was following the changes in redox potential of the metal centre. This correlation between the charge of the ligating atom and the zero-field interaction indicates potential importance of the electrostatic interactions between the outer and inner sphere for determination of redox potential, and thus the activity of SODs, without alteration of the physical structure of the metal site.

5.2.6. ENDOR and ELDOR-NMR provide an insight into positions of protons involved in SOD catalysis

Mn(II) electron nuclear double resonance (ENDOR) and electron double resonance detected NMR (ELDOR-NMR) are spectroscopic methods allowing detailed inspection of the local structure of the metal centres, in principle providing precise distance measurements down to 0.05Å. The ENDOR and ELDOR-NMR were used to determine the distances between Mn(II) and surrounding (coupled) nuclei, i.e. to map the positions of the ligands' protons and nitrogen atoms in the metal binding site, by recording the change in EPR signal in response to excitation of the spin of nuclei.

The ENDOR and ELDOR-NMR spectra were recorded for Mn-loaded SaSODs, in comparison to an inactive Mn-substituted FeSOD from *E. coli*, at positions of the magnetic field indicated on the 94 GHz EPR spectra of these proteins (Figure 5.11).

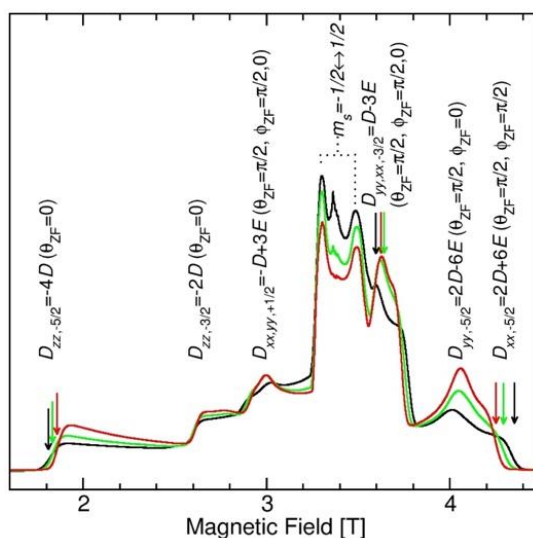


Figure 5.11 A 5 K 94 GHz Mn(II) field-swept echo HF-EPR spectra of Mn(II) SaSODs and Mn-substituted FeSOD of *E. coli*.

Represented are spectra of Mn-SodA (black), Mn-SodM (green) and Mn-substituted FeSOD (red). The indicated zero-field positions are relative to applied microwave frequency. Arrows indicate the magnetic-field positions where the ENDOR and ELDOR-NMR spectra were taken (their colours corresponding to the proteins). Figure taken from Barwinska-Sendra et al., 2017, manuscript submitted.

Overall, the ^1H ELDOR-NMR (Figure 5.12 A, B) and ENDOR (Figure 5.13) spectra of the three proteins presented very similar shape and intensity. The two resonances that were best resolved and were detected by ^1H ELDOR-NMR (Figure 5.12 B) at 8 MHz and 16 MHz, and at -6.3 MHz and -9.2 MHz in ENDOR spectra (Figure 5.13), arose from the two protons of the metal bound water. Both features were present in the spectra recorded for all three proteins, implying that the water molecule occupied a similar position in the active SaSODs as well as the inactive enzyme, Mn-loaded FeSOD.

The Mn-substituted FeSOD ^1H ELDOR-NMR single quantum (SQ) transition spectrum (4-8 MHz region, Figure 5.12 B; lower amplitude than SaSODs), and ^1H double quantum (DQ) transition spectrum (shift of low frequency edge, Figure 5.12 B), as well as the ENDOR spectra (-3 MHz; Figure 5.13, orange region), indicated the presence of at least one pair of protons that distinguished this inactive enzyme from the two catalytically active SaSODs.

Inspection of the ^{14}N ELDOR-NMR spectra (Figure 5.12 A, C) suggested some degree of similarity between the SaSODs and the Mn-substituted FeSOD in a DQ transition signal with a pair of resonances detected at 12 and 20 MHz, however, the intensity of the peak in the spectra from the SaSODs' differed from that of the *E. coli* Mn-substituted FeSOD. This could imply that the nitrogen atoms of the ligands occupy similar positions in the SaSODs but potentially different positions in the *E. coli* protein. The apparent differences in the amplitude of this feature in the spectra of Mn-substituted FeSOD, relative to SaSODs, unfortunately could not be addressed in a structural context due to low resolution of the spectra.

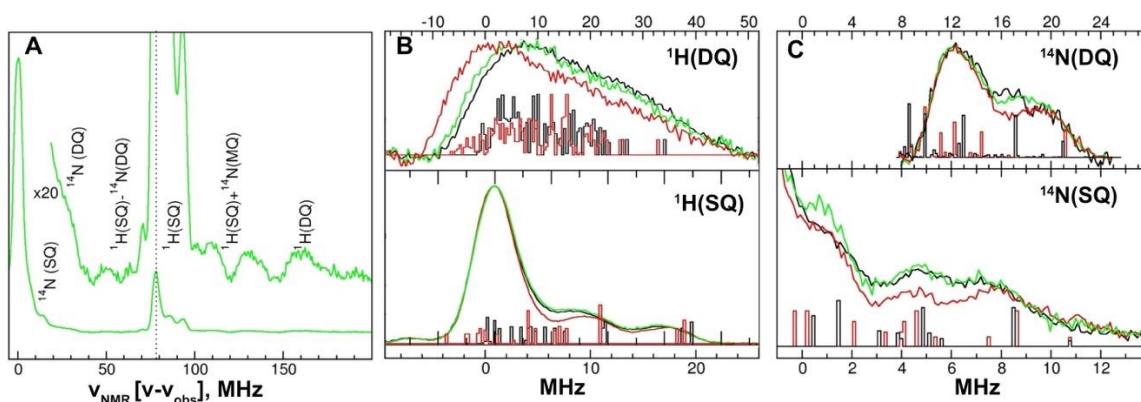


Figure 5.12 The 5K 94 GHz ELDOR-NMR spectra of Mn(II)-SaSODs and Mn-substituted Fe-SOD.

A full Mn(II) ELDOR-NMR spectrum of Mn-SodM obtained at the $D_{zz,-5/2}$ magnetic-field position of the EPR spectrum. The inset (x20) shows the ^1H ELDOR-NMR spectrum taken at the $D_{xx,-5/2}$ field position. Dotted black line indicates proton NMR resonance frequency. (B) ^1H ELDOR-NMR spectra and (C) ^{14}N ELDOR-NMR of Mn-SodA (black), Mn-SodM (green) and Mn-substituted FeSOD (red), taken at $D_{zz,-5/2}$; top represents double quantum (DQ) transition and bottom represents single quantum (SQ) transition resonance. The hyperfine histograms calculated based on the Density Functional Theory (see 5.2.7) for the models describing Mn-substituted FeSOD (GO, black) and SaSODs (CD(NH), red) models are superimposed.

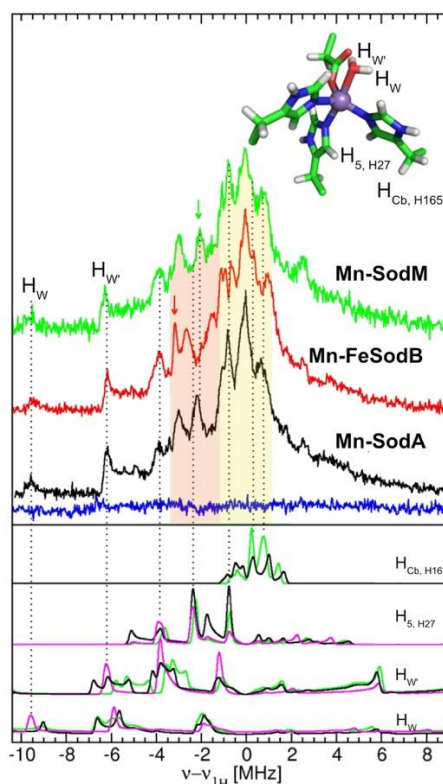


Figure 5.13 The 5 K, 94 GHz Davies ^1H ENDOR spectra of Mn-SodA, Mn-substituted FeSOD and Mn-SodM.

Spectra of Mn-SodA (black), Mn-SodM (green) and Mn-substituted FeSOD (red) were taken at the $D_{yy,-3/2}$ magnetic field positions (see Figure 5.11) after applying the initial pulse of 200 ns, followed by a 16 μs radio-frequency pulse and standard spin-echo detection. Hydrogen atoms are labelled, based on the crystal structures of SaSODs. The bottom panel shows corresponding spectra calculated based on DFT models describing Mn-substituted FeSOD (green), and SaSODs (magenta), and manually fitted DFT data (black). Dashed lines represent correlating signals, red arrow indicates distant feature of Mn-FeSOD, and green arrow points at the feature differentiating all three proteins' spectra.

5.2.7. Density Functional Theory (DFT) modelling together with hyperfine measurements and crystal structures provides an overview of the electronic structure of the SOD Mn(II) centre

Density functional theory (DFT) modelling was paired with the structural information available from the known crystal structures of the Mn/Fe-superoxide dismutases, including the structures of the SaSODs, in order to calculate the ligand sphere geometry models to account for the data acquired from ENDOR and ELDOR-NMR measurements. The three models were derived from computational building (denoted CD(NH), CD(OH), and GO) which each consisted of a Mn(II) centre, with D161 modelled by a propanoate or acetate ligand, and the histidine residues modelled by 4-methylimidazoles (Figure 5.14 B, C, D). The hyperfine tensors derived from DFT calculations agreed with the spectroscopic data (histograms superimposed onto ELDOR-NMR spectra Figure 5.12, and the linear fitting presented on the bottom panel of Figure 5.13).

The first two models, CD(NH) (Figure 5.14 C), and CD(OH) (Figure 5.14 D), which originated from the crystallographic data set and were geometry-optimised fitted equally well the available structural and electronic information for the two *S. aureus* SODs. The inactive Mn-substituted Fe-dependent *Ec*SOD was assigned a different model according to DFT calculations, representing a global energy-minimum structure (GO). The GO model accommodated an altered orientation of the imidazole moiety of the His171 (H165 in *S. aureus*) sidechain, in relation to this ligand in a native MnSOD protein (1VEW) and in the two Mn-SaSODs (Figure 5.14 B, C, D). This conformational change reflected the differences observed in the proton spectra between the SaSODs and the Mn-substituted FeSOD (Figure 5.12 B, Figure 5.13).

In both *E. coli* SODs and the SaSODs, the ligand histidine 165 (His171 in *E. coli*) interacts via two hydrogen bonds with the residue Glu164' (Glu170' in *E. coli*) from the second monomer. Destabilisation of the interaction between H171 and E170' in Mn-substituted FeSOD is postulated to cause a shift in charge polarisation between the two residues that could lead to altered catalytic activity. The spectroscopic data and results of DFT calculations together suggested that the H165 ligand of SaSODs may share its proton with E164' from the second subunit, and thus the negative charge is located between the two residues, contributing negative charge to H165 and stabilising metal coordination.

Due to the alteration of the conformation of His171 in an inactive *E. coli* SOD (Figure 5.14 B), the position of this proton was distinct from that in the SaSODs, as suggested by ¹H ELDOR-NMR and ENDOR spectra. This disruption of the Glu170'-His171-Mn(II) interaction, which left the coordinating histidine partially positively charged, was therefore postulated to be a possible source of the lack of catalytic activity with a Mn cofactor in the Fe-dependent enzyme.

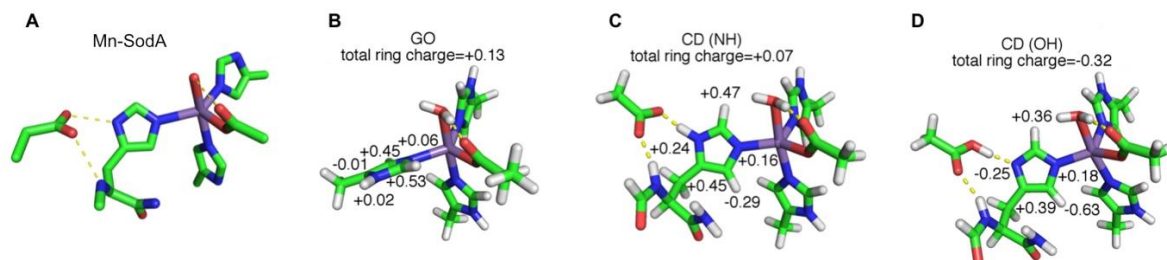


Figure 5.14 Comparison of the structure of the Mn(II) active site in Mn(Mn)SOD and the DFT GO, N- and O-protonated CD model structures.

Stick representation of a model of Mn(II) coordination site. Carbon atoms are coloured in green, nitrogen atoms are represented in blue, and oxygen atoms in red. Manganese is also depicted in stick representation, and coloured in purple. Hydrogen atoms shown in white. Predicted hydrogen bonds are marked as yellow dashed lines. The numbers indicate the Mulliken charges (partial atomic charges from calculations carried out by the methods of computational chemistry) of each atom of the His165 ring with the protons charges included.

These findings are supported by the correlated differences in the Mn(II) zero-field interactions of the three SOD-types and their catalytic activity. The importance of charge localisation, and its subsequent effect on enzyme reactivity, of the conformation of the Mn-H-E' triad was interpreted based on the previously determined relationship between the electron-donating/withdrawing capacity of the acid group (*R*) hydrogen-bonded to the ligand and the resulting SOD-like activity of the synthetic Mn(II) complexes (see section 5.2.5). In this light, E164 of SaSODs was predicted to be a greater electron donor to the ligand histidine, contributing to a greater zero-field interaction of SaSODs, than in the inactive Mn(Fe)SOD (as represented by $[[D]+E]$, Table 5.3), and giving rise a lower reduction potential of the metal site.

Residues from the metal's outer sphere, via their interaction with the primary coordination sphere ligands, were shown to modulate the properties of the active site and thus the enzyme's catalytic properties. Importantly, the dimer interface interactions are conserved between these two enzymes (Chapter 4, Figure 4.9; Appendix, Figure 8.1), and indeed amongst Fe/Mn-SODs in general. The role of this glutamate bridge (Whittaker & Whittaker, 1998) has been previously described as essential for the dimerisation of *E. coli* MnSOD and important for conferring Mn-specific activity. Other interacting residues from the dimer interface, such as His31-Tyr168', have also been described as important in stabilising the dimeric structure, influencing Mn-specific activity and catalytic mechanisms (specifically the pH dependence of catalysis by Mn-SOD) in *E. coli* and humans (Hearn et al., 2004; Edwards et al., 2001a). Based on the spectroscopic data (¹H-ENDOR) collected for SaSODs, no difference was observed in the bond lengths, and thus in the electron donating properties, of the Gln146-water-Mn(II) triad that could determine the distinct properties of these enzymes. The predicted increased electron donating capacity of Glu164' to His165, and consequently the higher zero-field interaction and lower redox potential, was suggested to confer activity with Mn on SaSODs, as opposed to Mn-substituted, inactive FeSOD of *E. coli* which lacks this interaction.

Previous examples of catalytic active sites containing catalytically important triads (metal-water-Asp/Glu or metal-His-Asp/Glu) showed how the outer sphere residues can influence the orientation and polarization of bonds with the ligands of inner shell sidechains and can modulate catalytic activity (Smulevich et al., 1988; El Yazal et al., 2000; Dudev et al., 2003; Dudev & Lim, 2013; Frison & Ohanessian, 2009). The complexity of the spectroscopic data did not allow us to exclusively confirm or disprove any of the proposed interactions as definite determinants of metal specificity of SaSODs, but such studies are ongoing.

5.3. Conclusions

A potential importance of subunit dissociation for the acquisition of metal by the apo-SaSOD proteins was indicated from *in vitro* studies. Differences in the oligomeric states of the recombinant apo-proteins were confirmed by SEC-MALS analysis, to complement the observations of biophysical differences in the structural stability of these enzymes (. Non-metalated SodA retained its dimeric quaternary structure, whereas apo-SodM dissociates into monomeric species. The temperature-dependent capacity of quantitative acquisition of Mn by apo-SodM and its re-association into the dimeric form was also observed, however this phenomenon was not reproduced for apo-SodA. Attempts at Mn-loading of apo-SodA under the equivalent conditions led to a lack of incorporation of the metal into apo-SodA. This physical difference between the two proteins forms a good basis for further studies of potentially different pathways for metal acquisition by the two apo-proteins.

The visible absorption spectra collected indirectly revealed potential differences in the redox potential of the two wild type SaSODs that correlated with their catalytic activity. SodA presented spectral features typical of a Mn-specific enzyme, and exhibited a strong propensity for autooxidation. A higher titre of reductant (dithionite) was require to fully reduce the Mn(III), relative to Mn-loaded SodM. Indeed the SodM visible absorption spectra reflected the loss of ~50% of signal arising from Mn(III) at resting condition, characteristic for Mn-specific proteins like SodA, and a concomitant gain of signal characteristic for metal-tolerant type.

The HF-EPR studies of Mn(II)-SaSODs provided insight into the different electronic structures of the two wild type proteins, that were described by the zero-field interaction component, which correlated with the wild type protein activity, and was consistent with previous observations for multiple SOD proteins. The exact structural determinants of this distinct structure remain to be identified, and these detailed analyses of the EPR spectra are continuing.

A comparative analysis of active vs. inactive enzymes allowed for evaluation of the contribution of specific interactions within the active centre including the outer sphere environment to catalytic activity. A combination of the magnetic spin parameters and hyperfine interactions in the Mn(II) centres indicated general conservation of the positions of the protons of the water ligand in both active *S. aureus* enzymes and in the inactive Mn-substituted Fe-SOD of

E. coli, indicating the importance of outer sphere interactions to the different activity of these enzymes.

The EPR, ENDOR and ELDOR-NMR measurements and subsequent DFT calculations indicated that interactions at the axis between the two active sites within the SOD dimer, specifically between a liganding histidine and a nearby glutamate, play a critical role in facilitating proton coupled electron transfer via distribution of charge between the ligand histidine and the glutamate spanning the dimer interface. This interaction was observed to differ between the active and inactive enzyme forms.

Chapter 6. Role of cambialism of SodM *in vivo*

6.1. Introduction

In the process of establishing infection, pathogens such as *S. aureus* must employ mechanisms to overcome the host immune system's defensive strategies. Staphylococci can escape innate immune defence and cause infection in invaded tissues, inducing a robust inflammatory response that attracts professional phagocytes such as macrophages and neutrophils. The host immune cells utilise a strategy called 'nutritional immunity', by which they restrict the pathogen's access to essential metal ions (Fe, Mn, Zn), (Weinberg, 1978; Pishchany et al., 2010; Corbin et al., 2008) that are essential for the growth and proliferation of bacteria in the host environment. Neutrophils restrict the growth of *S. aureus* by creating an environment devoid of available iron, manganese, and zinc. The host also restricts the amount of available iron in the serum through the iron-binding activity of lactoferrin and transferrin, whereas manganese and zinc are sequestered by the activity of a heterodimeric complex of two EF-hand proteins, called calprotectin (CP), (Gagnon et al., 2015).

Calprotectin possesses a high affinity binding site for Mn(II) (Kehl-Fie et al., 2011) that enables Mn sequestration, leading to inhibition of growth of *S. aureus* in culture in the presence of CP. An increase in the expression of the *S. aureus* Mn uptake systems (Kehl-Fie et al., 2013) has been observed in response to calprotectin treatment, indicating the importance of metal uptake systems in conferring the growth and infection of pathogenic bacteria by overcoming nutritional immunity.

Amongst the other host immune responses to bacterial infection is the generation of reactive oxygen species such as superoxide anion through the oxidative burst. Bacterial pathogens detoxify these effector molecules by the action of oxidative stress response enzymes, such as superoxide dismutase and catalase (Mandell, 1975; Horsburgh et al., 2002). The sequestration of manganese by calprotectin increases the sensitivity of *S. aureus* to superoxide stress during infection. Increased accumulation of superoxide has been observed in *S. aureus* in consequence of Mn depletion by CP, with concomitant reduction of superoxide dismutase activity in cells (Kehl-Fie et al., 2011).

The two superoxide dismutases of *S. aureus* have been demonstrated to play a significant role in the pathogenicity of this mammalian pathogen. Increased expression of SodA and SodM protein were detected in *S. aureus* cells after internalisation by human lung epithelial cells and human monocyte cell lines (Kristin Surmann, 2014; Mäder et al., 2016). Infection of mice with *S. aureus* strains lacking either *sodA* or *sodM* (or both) resulted in lower bacterial load isolated from lesions relative to the wild type strain in a mouse subcutaneous model of infection (Karavolos et al., 2003).

The *sodM* gene is only present in the *S. aureus* lineage and is absent from the genomes of other staphylococci (Valderas et al., 2002), (Chapter 3, section 3.2.2), which implies that it may play a crucial role in this significant mammalian pathogen. The *in vitro* characterisation of metal-specific activity of both SodA and SodM showed that SodA is a canonical Mn-dependent enzyme, whereas SodM presents cambialistic properties. Both proteins presented conserved protein fold and cofactor coordination. The two recombinant proteins were shown to present distinct biophysical properties such as thermal and chemical stability, metal binding-dependent oligomerisation, and electrochemical structure, all of which may play a physiological role in *S. aureus*. The role of both proteins in their native host, with an emphasis on the cambialistic enzyme, will be addressed in this chapter.

I would like to acknowledge the contribution of Dr Kevin Waldron and Dr Emma Tarrant, ICAMB, Newcastle University, UK, who performed metalloproteomics experiments, and whose work is presented in this chapter. All experiments with the use of calprotectin or involving animal models were conducted in collaboration with Yuritz Garcia and Dr Thomas Kehl-Fie from University of Illinois Urbana-Champaign, USA.

6.2. Results and discussion

The primary aim of work described in this chapter was to determine the metal usage of the *S. aureus* SODs *in vivo*. The role of SodA and SodM in *S. aureus* physiology in response to externally generated oxidative stress was investigated. The putative Mn-dependence of both proteins' activity was evaluated in bacterial culture, and in an animal model of infection in collaboration with the Kehl-Fie lab (University of Illinois Urbana-Champaign, USA), both in the context of mutants lacking their Mn-uptake systems and in response to the immune effector calprotectin. Pulldown purification assays were used to determine the metalation state of SodM in *S. aureus*. Pathogenicity studies in a mouse model of infection were applied to verify the role of the cambialistic property of SodM in the infectivity of *S. aureus* during the innate immune response.

Sections of the work presented in this chapter have been published as part of the following manuscript, in collaboration with the group of Dr Kehl-Fie:

Garcia, Y.M., Barwinska-Sendra, A., Tarrant, E., Skaar, E.P., Waldron, K.J. & Kehl-Fie, T.E. (2017) A Superoxide Dismutase Capable of Functioning with Iron or Manganese Promotes the Resistance of *Staphylococcus aureus* to Calprotectin and Nutritional Immunity. *PLoS Pathogens*. 13 (1), e1006125.

Determination of the metal content *in vivo* and calprotectin-related studies are part of the following manuscript, in preparation for submission to Nature Chemical Biology in 2018:

Barwinska-Sendra, A., Garcia, Y.M., Baslé, A., Tarrant, E., Sendra, K., Un, S., Kehl-Fie, T.E. & Waldron, K.J. & (2018) An evolutionary path to altered cofactor specificity in a metalloenzyme.

6.2.1. Superoxide induces growth phenotypes in SH1000 strains deficient in SOD activity or in Mn uptake

The two superoxide dismutases of *Staphylococcus aureus*, each belonging to the Mn/Fe-dependent superfamily of SODs, SodA and SodM are essential for endogenous superoxide stress resistance. SodA is conserved in all staphylococci and accounts for most SOD activity through all growth stages in standard culture conditions, whereas SodM is unique to *S. aureus* and becomes a major source of activity during the late exponential and stationary phases of growth under superoxide stress (Valderas and Hart, 2001).

Growth curves (Figure 6.1) of wild type and mutants defective in SOD activity or Mn uptake, in two distinct *S. aureus* strains (SH1000 and Newman; wild type, SOD mutant strains: $\Delta sodA$, $\Delta sodM$, $\Delta sodA\Delta sodM$, and a putative manganese transporter, $\Delta mntA$), were performed aerobically under standard conditions, and also under oxidative stress conditions induced by the superoxide-generating compound methyl viologen (MV) to assess the effects of oxidative stress on growth *in vitro*. Genotypes of all parental strains (wild type, $\Delta sodA$, $\Delta sodM$, $\Delta sodA\Delta sodM$, $\Delta mntA$) as well as the mutants created for this study ($\Delta sodA\Delta mntA$, $\Delta sodM\Delta mntA$) using the phage $\phi 11$ transduction protocol (section 2.5.2, Baker *et al.*, 2010) were confirmed by PCR performed on genomic DNA with the appropriate primer pairs listed in Table 2.4. The transductants were initially screened for antibiotic resistance, and the genotypes of all the strains were subsequently confirmed by DNA gel electrophoresis and sequencing.

Growth analysis of both SH1000 and Newman wild type and SOD mutant strains ($\Delta sodA$, $\Delta sodM$, $\Delta\Delta sodA\Delta sodM$) in TSB rich medium, was conducted in control conditions (Figure 6.1 A, C) and under oxidative stress-inducing conditions with 1 mM MV addition in an early exponential phase (Figure 6.1 B, D). Comparison of growth curves showed that the strains lacking the primary SOD activity of SodA ($\Delta sodA$, $\Delta\Delta sodA\Delta sodM$) exhibited a growth defect phenotype when challenged with this stress generating agent in the early exponential growth phase (2 h). The SH1000 $\Delta mntA$ strain, which has a compromised high affinity Mn uptake system, also grew at a reduced rate and to a lower final yield than the wild type in normal growth conditions and presented increased sensitivity to intracellular superoxide radicals (Figure 6.1 A, B). This effect was observed potentially due to limited availability of Mn to SodA and other Mn-dependent proteins.

Analogous growth analysis was also performed for SH1000 strains in the modified Tris minimal medium (TM, section 2.1.1, Sebulsky *et al.*, 2000), (Figure 6.1 E, F). Experiments conducted in minimal conditions showed a reduced growth yield in comparison to culture in TSB, but overall led to the same observation that, regardless of medium complexity, strains lacking *sodA* or the *mntA* Mn-importer exhibited a reduced growth rate compared to wild type in normal growth conditions (Figure 6.1 E) and present a higher sensitivity to superoxide stress (Figure 6.1 F).

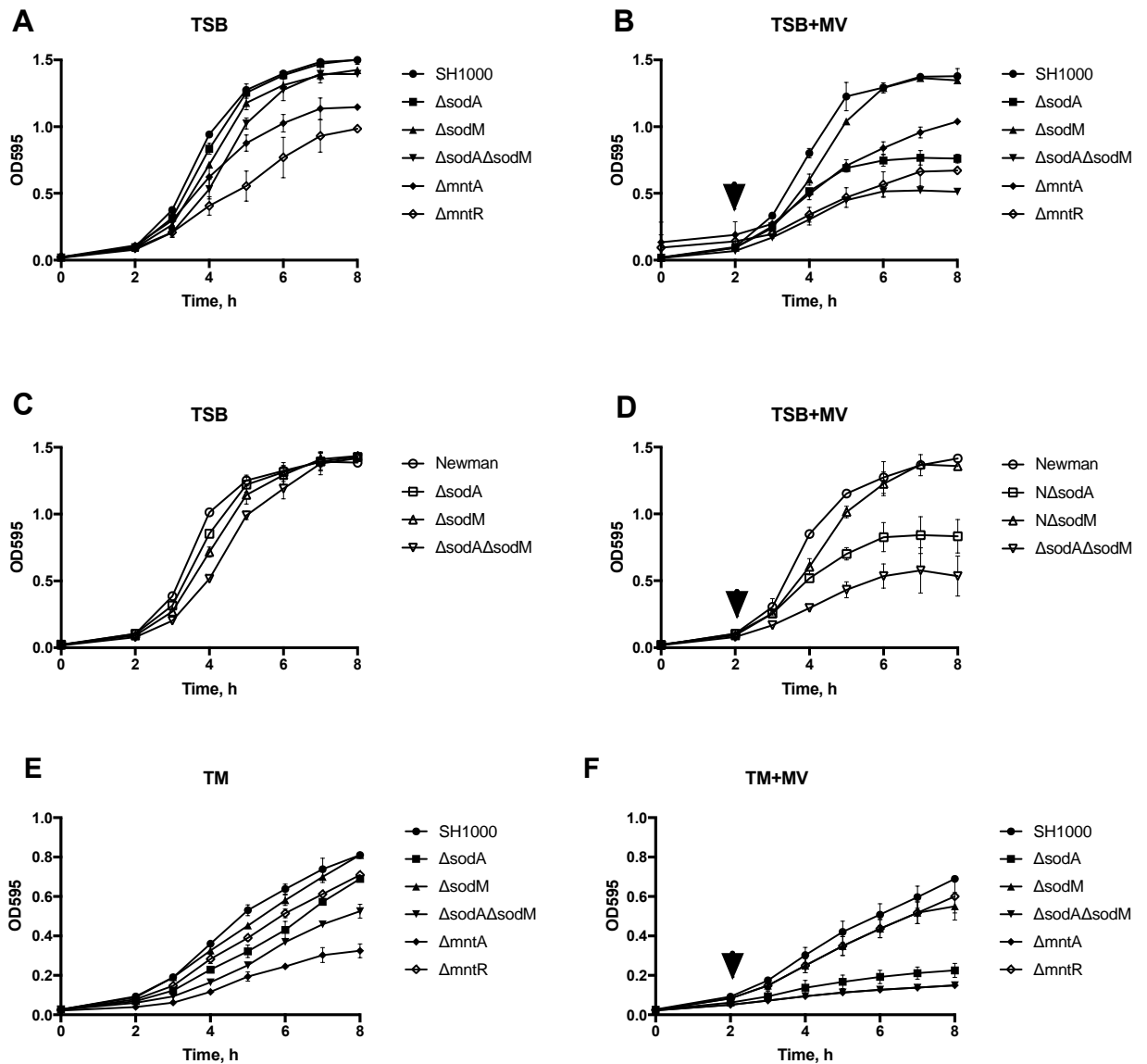


Figure 6.1 Growth analysis of *S. aureus* SH1000 and Newman wild type and mutant strains in rich growth medium TSB and minimal medium TM.

S. aureus SH1000 (A, B, E, F) and Newman (C, D) cultures were inoculated into 10 ml TSB with a single colony and incubated aerobically overnight at 37°C with 180 rpm orbital shaking. Growth analysis was started with a subculture of the overnight culture into 20 ml of fresh media (TSB or TM) with appropriate antibiotic to an OD_{600nm} of 0.05, which was then split into two 50 ml Falcon tubes to give a control culture of 10 ml and corresponding culture for methyl viologen (MV) treatment. The superoxide stress inducing agent, methyl viologen (Sigma Aldrich), was added to the bacterial culture after 2 h of initial growth to a final concentration of 1 mM (point of addition depicted with black arrow on graphs). Hourly OD_{595nm} readings were taken using a microplate reader.

6.2.2. Manganese-dependence of SH1000 Δ sodA Δ mntA and SH1000 Δ sodM Δ mntA growth.

Based on initial experimental studies and on bioinformatics sequence analysis, the *S. aureus* SODs were originally predicted to be Mn-dependent enzymes *in vivo* (Clements et al., 1999; Valderas and Hart, 2001), but conflicting data has been reported in the literature. Both SodA and SodM activities were shown to be relatively resistant to inhibition by H₂O₂ in one study (Valderas and Hart, 2001), which is generally inhibitory to FeSODs but not MnSODs, whereas SodM was seen to be inhibited by H₂O₂ in another study (Clements et al., 1999). Metal depletion of *S. aureus* protein extracts, followed by reconstitution with Mn *in vitro*, was shown to lead to detection of activity from SodA but not SodM, whereas neither activity could be restored with *in vitro* Fe reconstitution (Clements et al., 1999). Addition of Mn to the growth medium of *S. aureus* SH1000 cells led to an increase in SodA activity but a decrease in SodM activity, apparently due to post-transcriptional effects, as no change of expression of *soda* or *sodM* was observed in these conditions (Karavolos et al., 2003). The addition of Mn to the growth medium of the SH1000 Δ sodM mutant has previously been shown to cause an increase in total SOD activity (i.e. from SodA), whereas addition of Mn to the medium of the SH1000 Δ sodA mutant led to decreased total SOD activity (i.e. from SodM), (Karavolos et al., 2003).

The *in vitro* analysis of recombinant SodA and SodM proteins (Chapter 3, section 3.2.11; Chapter 4, section 4.2.6) showed that the two proteins present distinct metal-specific activities. SodA was characterised by a strong Mn-dependency, whereas SodM exhibited equal activities when loaded with either Mn or Fe, *in vitro*.

In *S. aureus*, Mn homeostasis is controlled primarily by MntR, which regulates an ABC-type permease, the MntABC Mn uptake system. The action of MntABC directly affects the expression of the PerR regulon (the Mn-dependent repressor of the genes encoding antioxidant proteins as well as of the metalloregulators Fur and PerR itself; Horsburgh *et al.*, 2001a). Mn uptake systems are important for the defence against superoxide stress in *S. aureus* (Kehl-Fie *et al.*, 2013; Horsburgh *et al.*, 2002).

S. aureus expresses two metal uptake systems that promote Mn acquisition *in vitro*, the MntABC transporter (cation-transporting ATP Binding Cassette type permease) and the Nramp1 (natural resistance-associated macrophage protein) homologue, MntH. In *S. aureus*, MntA and MntB are the ATP binding protein and permease, respectively, of the ABC transporter, while MntC is a surface-associated solute binding protein. Both MntABC and MntH Mn transport systems have been shown to contribute to resisting CP-dependent metal limitation and the development of invasive staphylococcal infection (Kehl-Fie *et al.*, 2013).

The SH1000 strain of *S. aureus* used in some of the presented experiments has previously been shown to possess a mutation in the *mntH* gene, creating a premature stop codon in the S286 codon in the sequence of manganese transport protein MntH (SAOUHSC_01053), (O'Neill, 2010). The presence of this mutation in our laboratory SH1000 strain was confirmed by

PCR and Sanger sequencing (data not shown). The functionality of the mutated protein was not assessed; however, it was presumed that the truncation would lead to reduction or complete loss of the ability of the protein to transport Mn (non-measurable levels of *mntH* expression were previously reported for SH1000 strain; Horsburgh et al., 2002).

Growth analysis in TM minimal medium (Figure 6.1 E) revealed that SH1000 Δ *sodA*, SH1000 Δ *sodA* Δ *sodM* and SH1000 Δ *mntA* all grew at a reduced rate when compared to the wild type under Mn-limited growth conditions. Similarly to these strains, SH1000 Δ *sodA* Δ *mntA* and SH1000 Δ *sodM* Δ *mntA* also grew to a lower final growth yield (Figure 6.2 A, B) in comparison to the wild type in minimal growth medium.

The observed phenotypes for SH1000 Δ *sodA* Δ *mntA* and SH1000 Δ *sodM* Δ *mntA* presumably resulted primarily from diminished uptake of manganese, because they were rescued by the supplementation of excess MnCl_2 to the bacterial culture (Figure 6.3 A). After 5 hours of growth (Figure 6.2 A) of SH1000 Δ *sodM* Δ *mntA* (open triangle) in comparison to the single mutant strains SH1000 Δ *sodA* (closed square), SH1000 Δ *sodM* (closed triangle) and SH1000 Δ *mntA* (closed diamond), it was noted that the knockout of *sodM* in the Δ *mntA* background caused an additive phenotype defect (Figure 6.2 B). Lack of this effect (lower statistical significance) in SH1000 Δ *sodA* Δ *mntA* may imply that *sodM* and *mntA* can at least partially function in independent pathways. At the later stage of growth (Figure 6.3 A, C), a similar pattern of growth defects of the SH1000 Δ *mntA*, SH1000 Δ *sodA* Δ *mntA* and SH1000 Δ *sodM* Δ *mntA* strains was observed with increasing concentration of external Mn source.

In a minimal medium, superoxide stress induces almost identical phenotypes for the SH1000 Δ *sodA*, SH1000 Δ *sodA* Δ *sodM* and SH1000 Δ *mntA* mutants that can be attributed to the absence of SodA or to the compromised Mn uptake system that supplies Mn to SodA in these strains (Figure 6.1 F). In equivalent experimental conditions of superoxide stress challenge, but with additional supplementation of cultures with increasing concentrations of Mn up to 10 μM (Figure 6.3 B, D), it was observed that SH1000 Δ *sodA*, SH1000 Δ *sodA* Δ *sodM* and SH1000 Δ *sodA* Δ *mntA* mutants were struggling to grow. In comparison to those strains, sensitivity to superoxide stress when induced at early growth stages of growth was decreased for the SH1000 Δ *mntA*, SH1000 Δ *sodM* Δ *mntA* strains in the presence of high Mn concentrations, which may suggest possible involvement of alternative Mn delivery systems contributing to oxidative stress resistance.

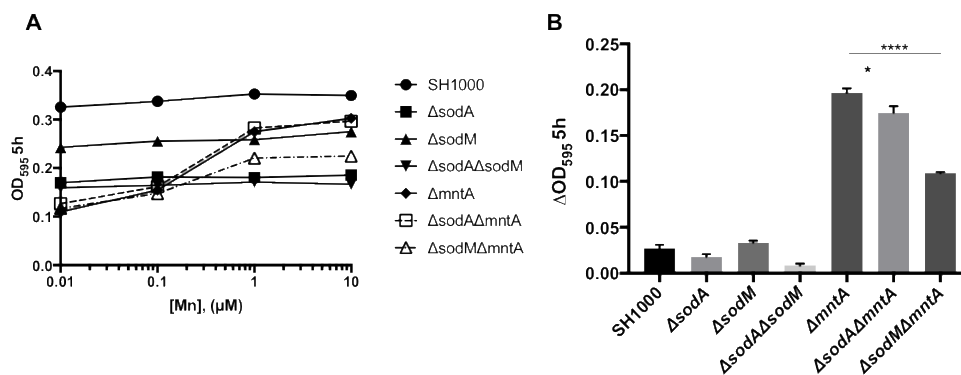


Figure 6.2 A 5-hour growth rate change in TM upon Mn supplementation.

Growth rate (A; relative to initial OD_{595nm}) of *S. aureus* SH1000 strains (wild type, ΔsodA, ΔsodM, ΔsodAΔsodM, ΔmntA, ΔsodAΔmntA, ΔsodMΔmntA) cultured for 5 hours in minimal medium (TM) with varying concentration of added MnCl₂. (B) Effect of 10 μM supplementation of TM medium on the growth rate of cultured SH1000 strains, after 5-hour culture, relative to non-supplemented cultures. The change of optical density (OD_{595nm}) was measured using microplate reader. *, p=0.0104; ****, p<0.0001 relative to ΔmntA via two-way ANOVA with Tukey's multiple comparison test. Error bars indicate SD (n = 3).

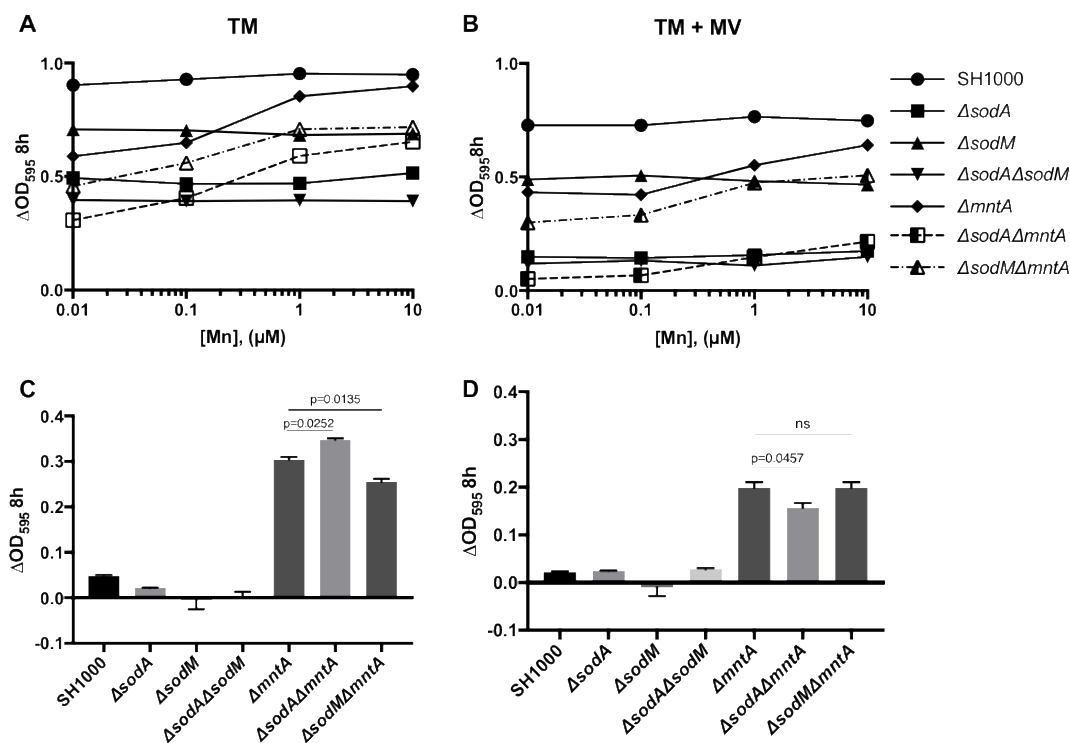


Figure 6.3 Manganese dependent growth of SH1000 wild type, SOD mutant strains (ΔsodA, ΔsodM, ΔsodAΔsodM), a putative manganese transporter (ΔmntA, ΔsodAΔmntA, ΔsodMΔmntA) deletion strains.

Growth rate of *S. aureus* SH1000 wild type, SOD mutant strains (ΔsodA, ΔsodM, ΔsodAΔsodM), and a putative manganese transporter (ΔmntA, ΔsodAΔmntA, ΔsodMΔmntA) deletion strains in TM, (A, B) with varying concentration of added MnCl₂ and (B), upon exposure to the superoxide stress inducer, MV. The change of optical density (OD_{595nm}) across differing concentration of MnCl₂ was measure using microplate reader after 8 hours of total growth in culture. (C, D) Effect of 10 μM supplementation of TM on the growth rate of cultures SH1000 strains, after 8-hour culture (± MV), relative to non-supplemented cultures. Statistical analysis relative to ΔmntA via two-way ANOVA with Tukey's multiple comparison test. Error bars indicate SD (n = 3).

Mn availability has been shown to differentially regulate the expression of the *S. aureus* SODs. SodM expression was found to be increased in *S. aureus* during growth under Mn-deplete conditions (Garcia et al., 2017). The high level of SodA transcription observed under standard conditions, however, was not affected by Mn-limitation. Calprotectin, the innate immune effector,

possesses a high affinity binding site for Mn(II), determined *in vitro* to be $K_d=1.3$ nM (Kehl-Fie et al., 2011)), which enables Mn chelation and leads to Mn-depletion conditions when CP is added to *S. aureus* growth medium. In experiments conducted by Yuritz Garcia (University of Illinois Urbana-Champaign, USA) in collaboration, we were able to show that sequestration of Mn by calprotectin inhibits growth of *S. aureus* in bacterial culture. By comparing the effects of metal sequestration by calprotectin in standard growth conditions on the wild type Newman strain and the SOD mutant strains, a gradual inhibition of growth rate was observed in a dose-dependent manner (Figure 6.4 A). Upon introduction of the superoxide-generating agent MV, a significant decrease of the final bacterial yield after 8-hour culture was observed in the growth of Newman $\Delta sodA$ and $\Delta sodA\Delta sodM$ mutants in manganese-replete conditions. A combination of oxidative stress and Mn-depletion (> 240 $\mu\text{g/ml}$ CP) led to a notable inhibition of the growth of Newman $\Delta sodM$ and $\Delta sodA\Delta sodM$, implying a role of SodM in conferring resistance to oxidative stress of *S. aureus* *in vitro* under Mn-deplete conditions (Kehl-Fie et al., 2011), (Garcia et al., 2017)

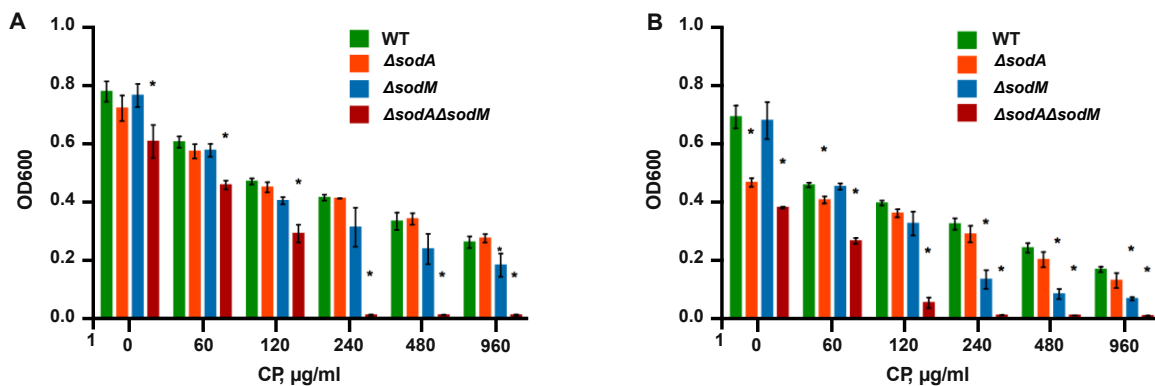


Figure 6.4 Effects of calprotectin (CP) on the growth of *S. aureus* Newman wild type and SOD mutant strains in response to oxidative stress.

Wild type, $\Delta sodA$, $\Delta sodM$ and $\Delta sodA\Delta sodM$ *S. aureus* Newman strains were grown in the presence of increasing concentrations of CP, in the (A) absence and (B) presence of 0.1 mM methyl viologen. Growth was assessed after 8 hours by measuring optical density (OD₆₀₀). * = $p < 0.05$ relative to wild type at the same concentration of CP via two-way ANOVA with Dunnett's post-test. Error bars indicate SEM (n = 3 or more). Data collected and processed by Yuritz Garcia (University of Illinois Urbana-Champaign, USA).

6.2.3. Estimation of the whole-cell metal content and specific SOD activity of *S. aureus* strains in post exponential phase.

The overall change in the abundance of manganese in cellular extracts of *S. aureus* SH1000 wild type, $\Delta mntA$ and SOD mutant strains ($\Delta sodA$, $\Delta sodM$, $\Delta sodA\Delta sodM$, $\Delta sodA\Delta mntA$, $\Delta sodM\Delta mntA$) was assessed by elemental analysis of whole-cell lysates (Figure 6.5 A, C). All strains were cultured in both minimal and rich medium (Figure 6.5 B, D respectively), for 5 hours in aerobic conditions. Harvested cells were washed thoroughly with 20 mM Tris pH 7.5 buffer, containing metal chelator (10 mM EDTA, in excess to metals potentially present in medium), to remove any metals introduced with medium and associated with the cell surface, before the lysis was performed. Chelation of metals was important to prevent any metals present in the extracellular fraction from mixing with the cytoplasmic fraction upon lysis. Two additional washes with a 20 mM Tris, 150 mM NaCl pH 7.5 buffer were performed to eliminate EDTA-chelated complexes. A total metal content of washes was verified by ICP-MS to be less than 0.1 μM (for determined Mn, Fe, Cu, Zn). Total metal content analysis of the acid-digested cells showed a significant decrease in manganese abundance in the $\Delta sodA$ mutant in comparison to the wild type strain (Figure 6.5 A). Significant decrease was also observed between a single mutant of $\Delta sodA$ and the double $\Delta sodA\Delta mntA$ delete, but the difference between $\Delta mntA$ and $\Delta sodA\Delta mntA$ was not statistically significant. Taken together these observations imply that Mn content of the total proteome of *S. aureus* SH1000 strains in post-exponential growth phase, under these experimental conditions was affected by deletion of one of the components of Mn-uptake system and that the significant portion of cellular Mn is associated with SOD proteins.

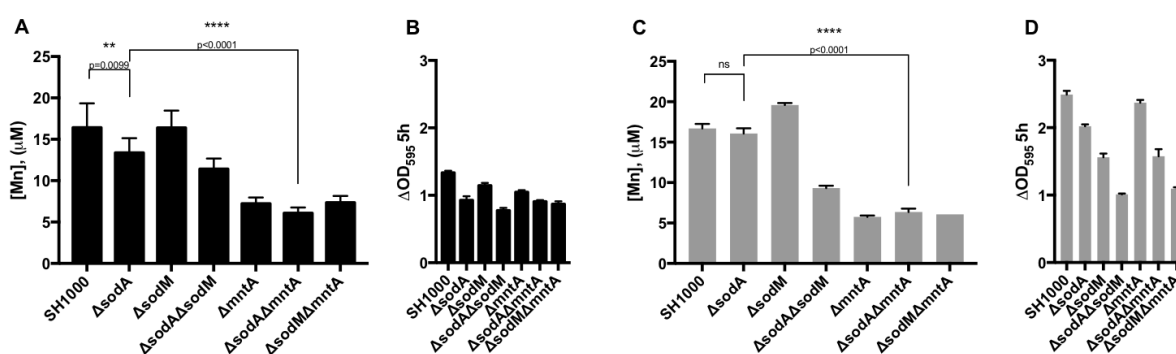


Figure 6.5 Whole cell metal content of SH1000 wild type, SOD mutant strains ($\Delta sodA$, $\Delta sodM$, $\Delta sodA\Delta sodM$), and a putative manganese transporter ($\Delta mntA$, $\Delta sodA\Delta mntA$, $\Delta sodM\Delta mntA$) deletion strains.

(A, C) Whole-cell elemental analysis of *S. aureus* wild type and Δsod , $\Delta mntA$ mutant strains after 5-hour culture (B) in TM minimal medium supplemented with 0.1 μM Mn or (D) in TSB medium. After 5 h culture with 185 rpm orbital shaking at 37 °C, cells were harvested by centrifugation at 4000 g and washed with 20 mM Tris, 10 mM EDTA pH 8.0, followed by two washes with 20 mM Tris pH 7.5, 150 mM NaCl. Collected cell pellets were finally digested in 65 % HNO_3 for 48 hours. Debris free acid digest of the cells was further diluted 10-fold in 2.5 % v/v HNO_3 containing 20 ppb Co, Pt internal standards and analysed using ICP-MS against matrix-matched metal standards. Data represents an average and SEM of triplicated experiments. Output of statistical analysis Two-way ANOVA with Tukey's multiple comparisons test between relevant strains.

The SOD activity (Figure 6.6) of SH1000 cell extracts was assessed with a spectrophotometric WST SOD assay (section 2.9.3) using aliquots of the extracts that were subjected to metal analysis (Figure 6.5). Deletion of *sodA* abolished nearly 90% of total SOD activity of SH1000 strain in the post exponential phase of growth in TM (Figure 6.56). Conversely, the Δ *sodM* strain presented only 10% less SOD activity per milligram of total protein than the wild type strain at this stage of growth. In a minimal growth medium, Δ *sodM* Δ *mntA* presented 50% of the total activity determined in a wild type strain and Δ *sodA* Δ *mntA* activity was determined at around 10% level of the total SOD activity.

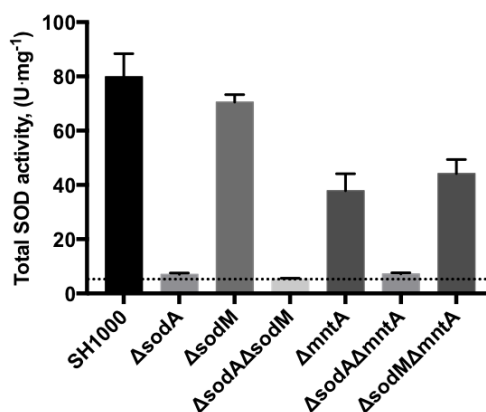


Figure 6.6 A total SOD activity of SH1000 wild type, SOD mutant strains (Δ *sodA*, Δ *sodM*, Δ *sodA* Δ *sodM*), and a putative manganese transporter (Δ *mntA*, Δ *sodA* Δ *mntA*, Δ *sodM* Δ *mntA*) deletion strains.

The SOD activity was measured in total protein extracts of SH1000 wild type, Δ *sod* and Δ *mntA* mutants, using a standard WST spectrophotometric SOD assay kit. Assay was performed in a microtiter plate format at 37°C for 20 minutes and the endpoint absorbance at 450 nm was measured using a plate reader. Data represent mean and SD of three experiments.

In the analysed culture conditions, the predominant SOD activity determined in total cell extracts was attributed to SodA (Figure 6.6). Deletion of the *mntA* component of the high affinity Mn-transporter reduced the detectable level of Mn to 44% of that determined in the wild type strain (Figure 6.5), and SOD activity measured in the extract of the Δ *mntA* strain was at 50 % of the level of the wild type (Figure 6.6). This implies that the remaining functional components of the MntABC transport system, or alternative transporters, worked efficiently enough under these conditions to provide metals to Mn-requiring cytosolic enzymes, including the SODs. As shown previously (Kehl-Fie et al., 2013), MntABC and MntH systems both promote *S. aureus* Newman resistance to Mn starvation and contribute to the retention of superoxide dismutase activity upon Mn-starvation conditions.

Experiments performed by Yuritz Garcia (University of Illinois Urbana-Champaign, USA, published in Garcia et al., 2017 on the wild type Newman strain showed that when *S. aureus* is grown under Mn-replete conditions, the majority of the detectable SOD activity comes from SodA

(Figure 6.7). Calprotectin treatment in culture leads to Mn-starvation of the cells, and leads to inhibition of the superoxide dismutase activity overall, especially from SodA. The fractional contribution of the two isozymes to overall SOD activity changes, with SodM becoming the major source of activity.

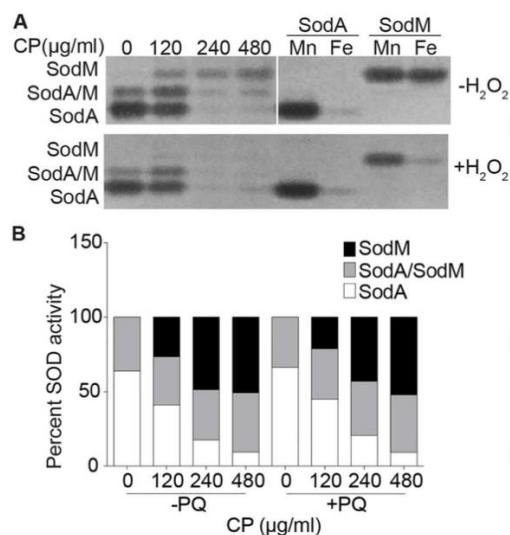


Figure 6.7 Fractional contribution of SaSODs to total activity during Mn starvation (Garcia et al., 2017).

Wild type *S. aureus* Newman was grown in increasing concentrations of CP in the (A, B) absence and (B) presence of 0.1 mM methyl viologen (PQ). (A) The activities of the SODs and (B) the fractional contribution of SodA and SodM to total SOD activity in cell lysates was determined. Cell extracts (5.17 µg) were resolved by 10% (w/v) Native-PAGE and stained for SOD activity. The bottom gel was treated with 20 mM hydrogen peroxide prior to staining for SOD activity. Purified recombinant metalated isoforms of SodA and SodM (0.3 µg), were included as controls. The experiment was repeated 3 times and representative gels are shown.

The ability for the proposed Mn-dependent enzyme SodM to function in a Mn-limited environment is hereby postulated to arise from its ability to also use Fe as a cofactor in *S. aureus* cells, as has been shown *in vitro* (Chapter 3, section 3.2.11). Treatment of the enzymes with hydrogen peroxide (Figure 6.7), a specific inhibitor of Fe-SODs, indicated that the activity of SodM under Mn-deplete conditions is inhibited by H₂O₂, suggesting the possibility of Fe binding by SodM *in vivo* (Figure 6.67 A, bottom panel).

6.2.4. SodM contributes to *S. aureus* pathogenicity under Mn-limitation during infection in the presence of calprotectin

SodM was shown to influence *S. aureus* resistance to oxidative stress *in vitro* (Figure 6.4) in Mn-depleted growth conditions (Garcia et al., 2017). To investigate the contribution of SodA and SodM to establishing bacterial infection in varying Mn availability conditions, the respective mutant strains of *S. aureus* Newman were tested in an established mouse model of systemic

6.2.5. What is the metal content of the *S. aureus* SODs in vivo?

The intracellular distribution of metal ions within *S. aureus* cells was first tested using a published metalloproteomic approach (Tottey et al., 2008). Whole-cell soluble extracts of wild type and relevant mutant strains, prepared under anaerobic conditions, were resolved by two-dimensional liquid chromatography (2D-LC). Initial experiments were performed by Dr Kevin Waldron before this PhD project started. This metalloproteomics approach was further used by Dr Emma Tarrant to perform initial evaluation of the metal cofactor associated with the two SODs in *S. aureus* SH1000.

Extraction and chromatography were performed under non-denaturing conditions to maintain native metal-protein associations. The extracts were prepared using a freeze-grinding method of lysis, under liquid nitrogen. Cleared, soluble lysates were obtained by high-speed ultracentrifugation. Initial separation was performed by anion exchange chromatography, with a step-wise NaCl gradient. The collected salt cuts were subsequently resolved by size exclusion by high performance liquid chromatography (HPLC). Each resulting 2D-LC fraction was analysed by inductively coupled plasma mass spectrometry (ICP-MS) for metal content (Tottey et al., 2008).

The resulting profile of manganese distribution (Figure 6.9 A) demonstrated the presence of two abundant soluble Mn pools, one of high molecular weight (MW), labelled Mn^{HMW}, and one of low MW, labelled Mn^{LMW}, in a wild type SH1000 cell extract.

The Mn^{HMW} was eluted from the anion exchange column by 300-400 mM NaCl. After resolution of this fraction on a size exclusion column (Figure 6.9 B), SDS-PAGE combined with densitometry analysis (Figure 6.9 C, bottom) identified the distribution of a single protein species as matching that of the manganese distribution. This protein was excised from the gel and subjected to peptide mass fingerprinting, which identified SodA in the gel band (Tottey et al., 2008). An in-gel SOD activity assay (Figure 6.9 C, top) performed on the same fractions of SEC eluate indicated the presence of all three SOD activity bands in these fractions derived from wild type SH1000. Analogous 2D-LC profile analysis performed on $\Delta sodA\Delta sodM$ double deletion strain (Figure 6.9 D) showed that the loss of SodA and SodM proteins abolished this high molecular weight Mn pool completely.

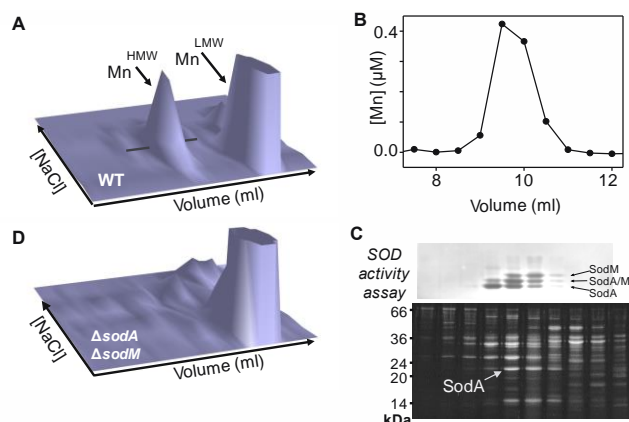


Figure 6.9 A 2D-LC profiles of soluble *S. aureus* extracts with two identified manganese pools (Dr Kevin Waldron).

(A) A 3D elution profile and elemental analysis of *S. aureus* SH1000 wild type and (D) $\Delta sodA \Delta sodM$ double mutant cell extracts. Bacteria were cultured in TSB and harvested cells were lysed anaerobically using freeze-grinding under liquid nitrogen. Lysates were cleared by ultracentrifugation and resolved by first dimension of chromatography, anion exchange (Q HP column), using NaCl 0-1M gradient in 20 mM Tris pH 8.0. Collected salt cuts were further resolved by a second dimension of chromatography, by size-exclusion on a Tosoh SW3000 column, in 10 mM Tris, pH 7.5, 50 mM NaCl. (B) Collected size-exclusion eluate of *S. aureus* SH1000 wild type was analysed for Mn content with ICP-MS, using matrix-matched standards. (C, bottom) SDS-PAGE of fractions containing Mn^{HMW} stained with SyproRuby. Correlation between the concentration of manganese in Mn^{HMW} and the abundance of individual proteins quantified by densitometry following SDS-PAGE of fractions containing Mn^{HMW}. The best corresponding band, identified by principal component analysis (PCA), was excised for MALDI-MS mass fingerprinting and designated SodA, is marked. (C, top) SOD activity assay of the fractions containing Mn^{HMW} showing presence of both SodA and SodM in samples recovered from SH1000 wild type extract.

Following on from the initial identification of the HMW Mn pool detected in wild type *S. aureus* cell extracts as being associated with SodA and SodM, Dr Emma Tarrant (Waldron Lab, ICAMB, Newcastle University) conducted a series of separations aiming to identify the metal occupancy of SOD isozymes *in vivo*, in isogenic mutant strains (Figure 6.10 A). A mixed population of Mn and Fe was detected in fractions corresponding with SodA and SodM elution peak in the wild type SH1000. Peroxide treatment of the gels (Figure 6.10 B, C, D bottom) inhibited activity of the highest of the three activity bands, corresponding to the SodM homodimer, indicating Fe-loading of SodM. Comparison of the wild type and $\Delta sodA$ mutant of SH1000 showed the loss of the Mn peak in the latter extracts.

Analysis of the mutants was hindered by multiple technical difficulties of these complex analyses. Even though a clear loss of the Mn peak was observed upon deletion of *sodA*, getting a clear analysis of Fe content proved inconsistent due to the very low Fe abundance, higher Fe background, and inherent difficulties in measuring Fe using ICP-MS (due to ArO mass of 56). The abundance of the SodM protein in the analysed culture conditions was also quite low. Ultimately, these analyses were operating close to the ICP-MS instrument's detection levels, resulting in noisy readings. Nonetheless, a mixed population of metals was detectable in the case of the SH1000 $\Delta sodM$ mutant, potentially implying varied metalation of SodA in the analysed sample.

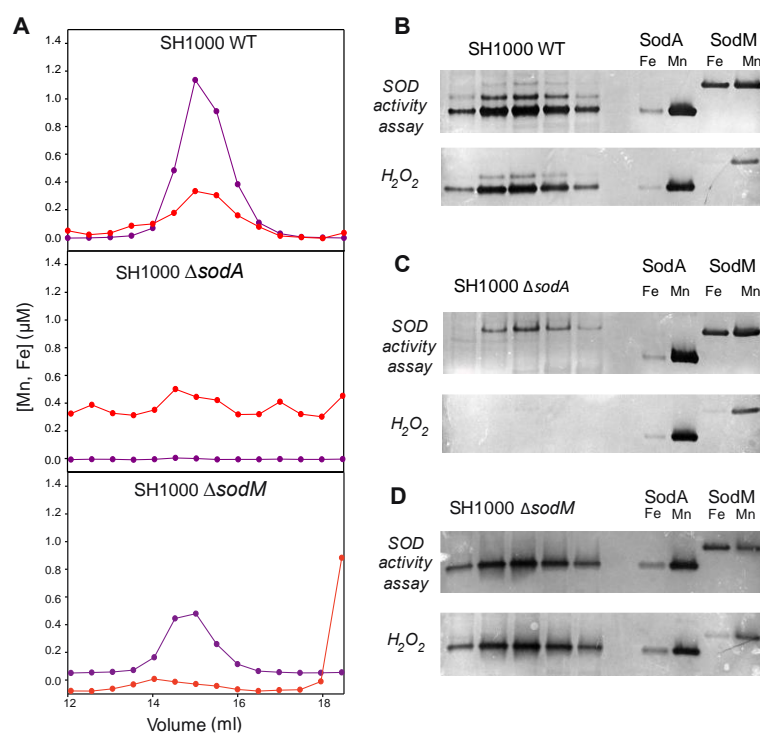


Figure 6.10 A 2D-LC Mn and Fe profiles of SH1000 strains (Dr Emma Tarrant).

(A) ICP-MS analysis of cell extracts resolved by two dimensions of chromatography: anion exchange and size exclusion, of the wild type, $\Delta sodA$, and $\Delta sodM$ strains. Mn trace represented as purple circles and Fe trace shown as red circles. (B, C, D) A control (top gel) and a peroxide-treated (bottom gel) *in-gel* SOD activity assay performed by resolving S200 eluate by 12% (w/v) Native-PAGE and staining for enzymatic activity. Metalated isoforms of recombinant SodA and SodM included as control of metalation state.

6.2.6. Complementation with tagged isoform of cambialistic SodM rescues the phenotype of *E. coli* strain lacking SODs

To directly address metalation of *S. aureus* SODs *in vivo*, affinity tags were introduced into the protein sequences to allow for an affinity chromatography pull down followed by elemental analysis of a single-protein species (Chapter 2, section 2.11). Initially, the C-terminal StrepII tag was added to *sodM* and N-terminal Flag-tagged *sodA* constructs were prepared for overexpression in BL21 cells and to verify whether addition of either tag at either end of the protein constructtag altered protein solubility and/or activity.

The tagged isoforms of the genes were sub-cloned from the commercially synthesised pUC-IDT plasmids (Integrated DNA Technologies) (section 2.2.6) into pET29a expression vectors. The pET29a constructs were transformed into BL21 (DE3) *E. coli* cells and protein expression was carried out in the standard conditions, optimised for heterologous expression (Chapter 2, section 2.7.2). Following a 4-hour overexpression in M9 supplemented with 200 μ M Fe, harvested cells were lysed by sonication and purified using anion exchange and size exclusion chromatography. No change in protein solubility was observed, and the final yield of purified tagged proteins was comparable to the wild type proteins. Metal analysis performed on the tagged versions of SodA and SodM proteins demonstrated stoichiometric loading with Fe

(data not shown), as expected. Enzymatic activity of the Fe-loaded tagged SODs was assayed using the in-gel and spectrophotometric WST SOD assays, which confirmed that addition of affinity tags to the termini of SodA and SodM did not alter their catalytic activity (Figure 6.11). Size exclusion elution profiles were the same between native and tagged versions of proteins (data not shown). However, the electrophoretic migration on native gel was slightly altered in comparison with the non-tagged proteins.

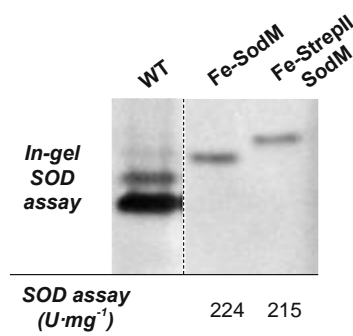


Figure 6.11 A representative SOD activity assay of recombinant and the StreptII-tagged isoform of Fe-SodM.

An aliquot of 20 μg of the cell extract of SH1000 wild type cells was resolved on a 10% (w/v) Native-PAGE alongside a 0.3 μg of recombinant wild type and StreptII-tagged SodM protein. Gel was stained for SOD activity using NBT-riboflavin assay mix.

The ability of the tagged constructs to complement the growth phenotype of a SOD-deficient *E. coli* strain was tested by introduction of tagged and non-tagged versions of SaSODs into the $\Delta\text{sodA}\Delta\text{sodB}$ deletion strain of BL21(DE3) (Figure 6.12). The expression strains of BL21(DE3) *sodA::cam sodB::kan* was prepared by P1 phage transduction (Chapter 2, section 2.5.1). The phage stock was kindly provided by Dr David Bulmer (Newcastle University, UK). The donor strains of *E. coli* AB1157: PN134 (*sodA::cam sodB::kan*; Imlay & Linn, 1987) and AS391 (*sodA::cam sodB::kan sodC::spec*; Gort et al., 1999) were acquired from Dr James A. Imlay (University of Illinois, USA).

The BL21(DE3) $\Delta\text{sodA}\Delta\text{sodB}$ cells were transformed with either ampicillin-resistant pET151*sodA* and pET151*sodM* (Chapter 2, section 2.2.5) *E. coli* expression constructs (Figure 6.12 A) or constructs made in the *E. coli*-*S. aureus* shuttle vector pS10, containing the affinity-tagged coding sequences of *sodA* and *sodM* (Chapter 2, section 2.2.7; Figure 6.12 B). Growth analysis was performed by sub-culturing of an overnight culture into fresh medium, containing appropriate antibiotics, to an OD_{600nm} of 0.05. A standard BL21(DE3) expression strain was cultured alongside BL21(DE3) $\Delta\text{sodA}\Delta\text{sodB}$ and the double mutant carrying plasmids with native or tagged staphylococcal *sodA* and *sodM*. The OD_{595nm} was measured hourly using 96-well microtiter plate reader.

Introduction of pET151*sodA* and pET151*sodM* constructs into BL21(DE3) $\Delta\text{sodA}\Delta\text{sodB}$ (Figure 6.12 A), followed by induction of expression by addition of 0.1 mM IPTG at OD_{600nm} of

approximately 0.5, improved the growth defect of the SOD-deficient *E. coli* strain. The growth rate of that complemented strains did not reach the growth of the wild type, but a noticeably shorter lag phase was observed in comparison to the double mutant during the early exponential phase of growth.

Constitutive expression (Figure 6.12 B) of tagged *sodA* or *sodM* in the *E. coli* SOD-deficient strain led to complementation of the growth phenotype of the BL21(DE3) $\Delta sodA\Delta sodB$ mutant. The BL21(DE3) $\Delta sodA\Delta sodB$ delete strain carrying the pS10*sodM* construct seemed to grow nearly as well as the wild type strain of BL21(DE3), in comparison to weakly complementing pS10*sodA*. The difference in the level of complementation may have been caused by sub-optimal composition of the growth medium (too low levels of Mn) or potentially due to a non-functional construct of pS10*sodA* (toxicity of N-terminal FLAG tag), although the data from recombinant protein would argue against the latter.

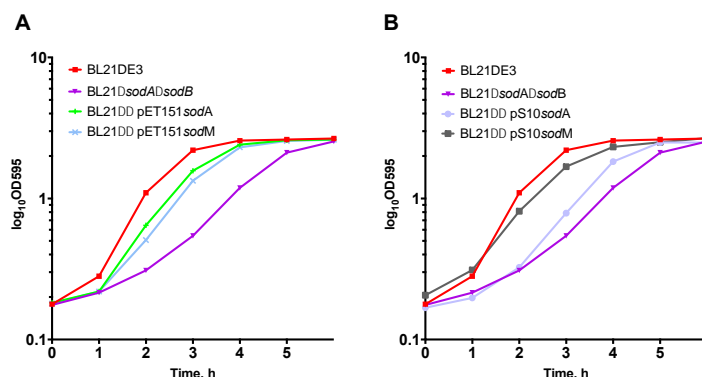


Figure 6.12 Complementation of *E. coli* *sod* mutant phenotype in rich medium liquid culture.

A representative growth curve of *E. coli* BL21 (DE3) wild type and BL21(DE3) $\Delta sodA\Delta sodB$ mutant, as well as complementation strains containing (A) pET151*sodA* and pET151*sodM* or (B) pS10*sodA*, pS10*sodM* plasmids. Cultures were started from an overnight pre-culture, in LB supplemented with 1 % glucose and appropriate antibiotics: 50 $\mu\text{g}\cdot\text{ml}^{-1}$ kanamycin, 10 $\mu\text{g}\cdot\text{ml}^{-1}$ chloramphenicol, for selection of mutant strain; 100 $\mu\text{g}\cdot\text{ml}^{-1}$ ampicillin for selection of plasmids. To induce protein expression from pET151 constructs, 0.1 mM IPTG was added at the point of $\text{OD}^{595} \sim 0.5$. Hourly time points were measured using 96-well microtiter plate reader.

6.2.7. Manipulation of protein metal content by external supply

The *E. coli*-*S. aureus* shuttle vector pS10 (Morrissey et al., 2000) was used to express the tagged versions of *sodA* and *sodM* *in trans* in *S. aureus* SH1000 or Newman (Chapter 2, section 2.2.7). The pS10^{amp^R, cam^R} vector contains the constitutive S10 promoter and the T2 transcriptional terminator, flanking a region containing a limited multiple cloning site (MCS). The coding sequence of the *sodA* and *sodM* genes from *S. aureus* SH1000, including the Shine-Dalgarno sequence and N-terminal Flag or C-terminal StrepII tag sequence, were ligated into pS10 using *Bam*HI and *Pst*I restriction sites. The generated pS10-*sodA* and pS10-*sodM* constructs,

introduced into BL21(DE3) $\Delta sodA\Delta sodB$ background, conferred a complementation of SOD-deficient growth phenotype of the mutant strain (Figure 6.12 B).

To evaluate the expression of tagged SODs, pS10 constructs were introduced into *S. aureus* SH1000 background by electroporation. Selected transformants were cultured in 20 ml of TSB medium overnight, sub-cultured in fresh medium and grown for a further 6 hours. Cell lysates were prepared by bead beating and normalised for total protein content by Bradford assay. The soluble lysates were examined for the presence of Flag-SodA and StrepII-SodM by immunoblotting with mouse anti-Flag and mouse anti-StrepII antibodies, respectively (Figure 6.13).

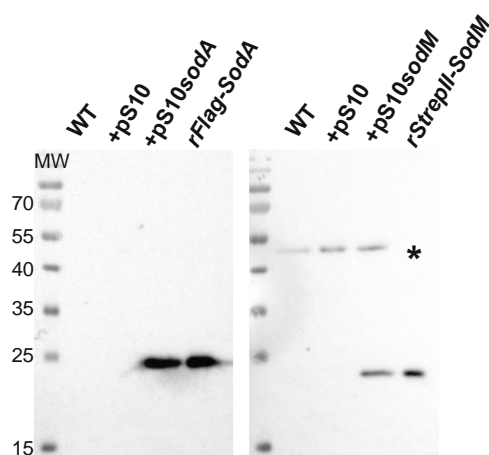


Figure 6.13 Immunoblotting of extracts of SH1000 cells.

Whole-cell lysates of *S. aureus* SH1000 wild type, strain transformed with empty pS10 plasmid and with pS10sodA, pS10sodM constructs. Soluble proteins were normalised for concentration by Bradford assay and resolved by 12% (w/v) SDS-PAGE. Separated lysates were transferred onto a nitrocellulose membrane using wet transfer (Bio-Rad Mini Trans-Blot Cell, 30 V overnight at 4°C), in the Towbin buffer (25 mM Tris, 192 mM glycine, pH 8.3, 20 % (v/v) methanol). Western blotting analysis was performed with mouse monoclonal antibodies against the affinity tags, and the anti-mouse immunoglobulin, HRP-conjugate (Promega) used as a secondary antibody. Detection of chemiluminescent signal was carried out using Clarity™ Western ECL Blotting Substrate (Bio-Rad) according to manufacturer's instructions and visualised using Bio-Rad ChemiDoc XRS+ system. The non-specific band, detected ~40-55 kDa (black asterisk) presumably arisen from binding of the antibodies to protein A.

The expression of both N-Flag-SodA and C-StrepII-SodM was detected in soluble lysates of SH1000 cells after 6-hour culture. No signal was detected in the cells of the wild type strain (WT) or those transformed with an empty pS10 plasmid (+pS10). Recombinant, purified protein containing the tag was used as a positive control. The higher-molecular-weight band (~40-55 kDa; marked with an asterisk) is presumably due to non-specific binding of the antibodies to contaminating staphylococcal protein A. Equivalent lysate samples were resolved by Native-PAGE and stained for SOD activity to assess functional production of the tagged proteins (Figure 6.14). C-terminally tagged sodM expressed in SH1000 $\Delta sodM$ showed production of functional StrepII-tagged SodM enzyme, complementing the lack of the native protein, and engaging in

formation of the heterodimer with SaSodA. However, introduction of the pS10-Flag-tagged *sodA* construct did not seem to produce a functional copy of Flag-SodA protein. Non-specific activity bands were observed in an in-gel Sod assay. Due to time constraints of this project, subsequent protein characterisation was performed only for Strep-tagged SodM.

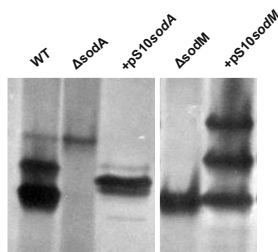


Figure 6.14 Activity assay of complemented SH1000 SOD mutants.

An aliquot of 20 μ g of the cell extract of SH1000 wild type, SH1000 Δ *sodA*, SH1000 Δ *sodM* cells; and the cell extracts of isogenic mutant strains complemented with pS10*sodA* and pS10*sodM* plasmid constructs; were resolved on a 10% Native-PAGE and stained for SOD activity using NBT-riboflavin assay mix.

As previously demonstrated (Figure 6.1, Figure 6.3, Figure 6.4, Figure 6.7), the enzymatic activity of SodM in *S. aureus* cells increases during growth under manganese-deficient conditions, induced in culture by the presence of the human immune effector calprotectin. To address the role of the cambialistic SodM in *S. aureus* physiology, the metal loading of tagged SodM was determined using pull-down assays in comparison to the non-cambialistic SodM L159G mutant (Chapter 4, section 4.2.6).

Overnight cultures of Newman Δ *sodM* pS10-StrepII*sodM*, Newman Δ *sodM* pS10-StrepII*sodML159G*, SH1000 Δ *sodM* pS10-StrepII*sodM* and SH1000 Δ *sodM* pS10-StrepII*sodML159G* were used to inoculate 100 ml of TM media, non-supplemented (TM), or supplemented with 100 μ M MnCl₂ (TM+Mn) or with 30 μ M FeSO₄ (TM+Fe) to an OD₆₀₀ of 0.05. Change of OD_{595nm} (Figure 6.15) was measured after 8-hour culture at 37°C with 185 rpm orbital shaking, and the cells were harvested for protein analysis.

Cells were lysed, and extracts were affinity-purified by StrepII pulldown affinity purification (Chapter 2, section 2.7.8). Collected eluate fractions were analysed for protein content by A280 (Nanodrop) and SDS-PAGE. All fractions containing the SodM protein were combined and resolved by size exclusion (Figure 6.16) on S200 10/300 increase column in 20 mM Tris, 150 mM NaCl and 1 mM EDTA buffer, pH 8.0.

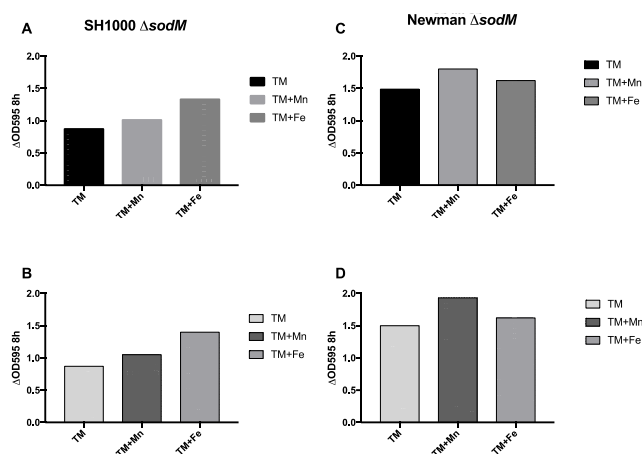


Figure 6.15 Change of growth of *S. aureus* *sodM* mutant strains complemented *in trans* with StrapII-tagged *sodM* and *sodM* L159G mutant.

The *S. aureus* SH1000 or Newman Δ *sodM* strains, carrying a plasmid for constitutive expression of a Strep-tagged version of either (A, C) wild type or (B, D) the L159G isoform of SodM, were cultured in Tris minimal (TM) medium in the absence or presence of excess manganese (100 μ M, TM+Mn) or excess iron (30 μ M, TM+Fe). Growth change was monitored after 8 hours of culture using microtiter plate reader.

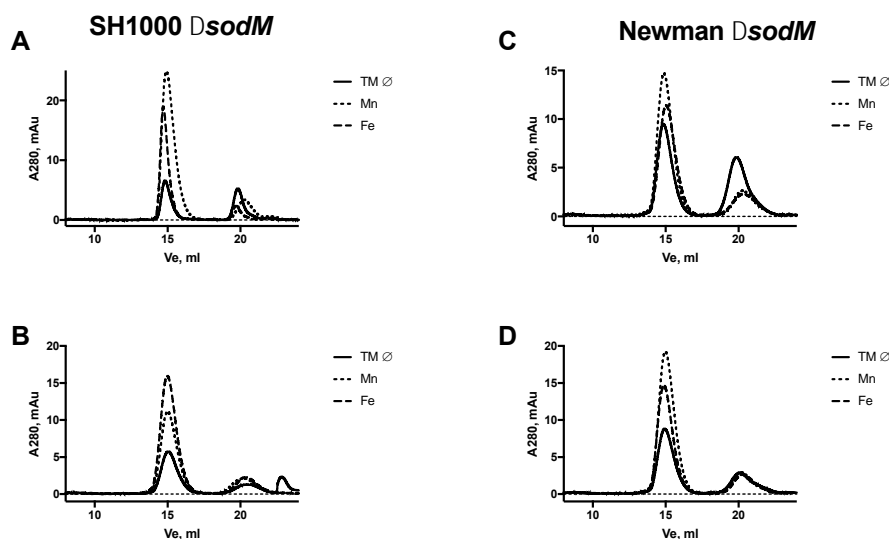


Figure 6.16 The representative chromatograms of size exclusion step following the StrepTrap purification.

A StrepTrap eluate was loaded onto S200 10 300 increase column and resolved at 4 °C in 20 mM Tris, 150 mM NaCl and 1 mM EDTA pH 8.0 buffer with 0.5 ml fractionation starting at 0.45 CV. Represented chromatograms are overlaid A280nm traces of preparation from basal minimal medium (TMØ, solid line), Mn-supplemented culture (Mn, dotted line) and Fe-supplemented medium (Fe, dashed line).

Peak fractions were subjected to elemental analysis using ICP-MS (Figure 6.17), which showed that the metal acquired by SodM in *S. aureus* was influenced by the availability of metal in bacterial culture (Table 6.1). Culturing of *S. aureus* in basal, non-supplemented TM minimal medium yielded low amounts of pulled down protein from both SH1000 Δ *sodM* and Newman Δ *sodM* cultures.

The wild type SodM purified from non-supplemented TM culture of both SH1000 and Newman cells contained a mixture of the two cofactors: manganese (22 % and 21 %) and iron (36 % and 47 %), and significant amounts of zinc (42 % and 32 %), (Table 6.1). Supplementation of the bacterial culture with 100 μ M manganese significantly (SH1000 $p=0.0328$; Newman

p<0.0001, with Tukey's test) increased the total yield of protein and resulted in an enzyme that contained predominantly manganese (88 % and 70 %, p<0.0001 with Tukey's test), at the expense of iron (10 % and 20) and zinc (3 % and 11 %) levels. Addition of 30 μ M Fe iron to the culture of wild type SodM increased the total amount of iron (76 % and 69 %, p<0.0001 with Tukey's test) incorporated into protein. The total yield of protein recovered from Fe-supplemented cultures was not statistically different from that determined for the basal minimal.

The general results obtained from cells expressing the SodM L159G (Figure 6.17 B, D) isoform were similar to those determined for the wild type protein. A statistically significant increase of the recovered protein was again noted in Mn supplemented culture when compared to the preparations from TM. In the case of both analysed strains of *S. aureus* containing constitutively expressed mutant protein, an increased yield of recovered protein was noted for preparations from iron supplemented cultures (SH1000 p=0.0393 and Newman p<0.001, with Sidak's test), nearly matching the highest recovered yield from Mn-supplemented cultures of the wild type expressing strains.

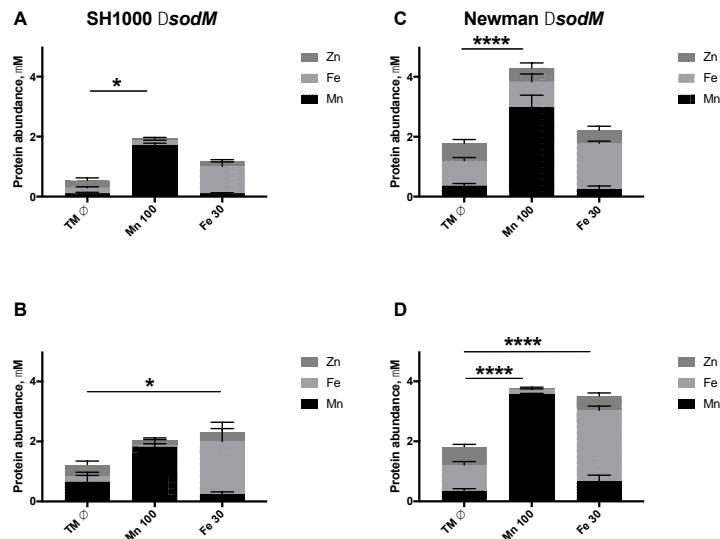


Figure 6.17 Metal analysis of StrepTrap and size exclusion purified proteins from *S. aureus* cells exposed to external metal supply in culture.

The *S. aureus* SH1000 or Newman $\Delta sodM$ strains, carrying a plasmid for constitutive expression of a Strep-tagged version of either (A, C) wild type or (B, D) the L159G isoform of SodM, were cultured in Tris minimal medium (TM) in the absence or presence of excess manganese (100 μ M, Mn100) or iron (30 μ M, Fe30) for 8 hours. Cell pellets were resuspended in 500 μ l of 20 mM Tris, 150 mM NaCl and 1 mM EDTA pH 8.0 buffer, containing protease inhibitors and transferred to 2 ml screw-cup tubes, compatible with cell disruptor. Approximately 0.2 g of glass beads was added to each tube and lysis was performed in 2 cycles of 40 second bead beating, with 1 min incubation on ice to cool down. Cell lysates were cleared by centrifugation multiple rounds at 21.1 k x rpm for 10 minutes at 4°C. Recovered, cleared lysate (~ 400 μ l) was loaded on 1 ml StrepTrap column (GE Healthcare) prepared as per manufacturer instructions and equilibrated in 20 mM Tris, 150 mM NaCl and 1 mM EDTA pH 8.0 buffer. Flow-through from the column was collected and unbound protein was washed off the column with 5 CV of 20 mM Tris, 150 mM NaCl and 1 mM EDTA pH 8.0 buffer. Elution was performed using 20 mM Tris, 150 mM NaCl and 1 mM EDTA pH 8.0, 2.5 mM desthiobiotin buffer with 0.5 ml fractionation over 3 CV. Column was subsequently recovered according to manufacturer instructions. Extracted proteins were analysed for metal content by ICP-MS. Metal content is presented as a fraction relative to the abundance of recovered protein. Data represent a mean of (n=2) SH1000 strain experiments and (n=4) of Newman experiments, error bars represent standard deviation. 2wayANOVA, *, p=0.0328; ****, p<0.0001 with Tukey's test.

A	Mn, %			Fe, %			Zn, %			Protein μ M
	Mean	SD	N	Mean	SD	N	Mean	SD	N	
TM	21.9	0.4	2	35.8	1.2	2	42.3	0.8	2	0.6
Mn 100	87.8	1.6	2	9.7	1.6	2	2.6	0.0	2	2.6
Fe 30	9.4	0.2	2	75.9	0.5	2	14.6	0.4	2	1.7
B										
TM	34.4	0.1	2	21.1	2.7	2	44.5	2.5	2	1.1
Mn 100	87.6	4.9	2	3.9	1.8	2	8.5	3.1	2	2.1
Fe 30	16.8	0.2	2	72.7	0.3	2	10.5	0.5	2	2.7
C										
TM	20.9	3.7	4	46.7	5.7	4	32.4	7.1	4	1.8
Mn 100	69.5	9.3	4	19.7	6.0	4	10.8	3.9	4	4.3
Fe 30	11.8	4.2	4	68.7	3.2	4	19.5	6.2	4	2.2
D										
TM	19.0	3.8	4	47.4	6.2	4	33.5	4.1	4	1.8
Mn 100	94.4	0.9	4	4.3	0.6	4	1.3	0.8	4	3.8
Fe 30	18.9	5.9	4	67.3	4.0	4	13.8	2.8	4	3.5

Table 6.1 Fractional metal content of a purified preparation of Strep-tagged SodM and SodM L159G, purified from *S. aureus* $\Delta sodM$ culture.

Elemental analysis of wild type (A, C) or the L159G isoform (B, D) of SodM as purified from *S. aureus* SH1000 (A, B) or Newman Δ sodM (C, D) strains, cultured in TM, with Mn or Fe supplementation, by StrepTrap pulldown followed by size exclusion. Metal content is presented as a fraction of total metal determined for recovered protein. Data represent mean of (n=2) SH1000 strain experiments and (n=4) of Newman experiments, error bars represent standard deviation. Total yield of protein (Protein, μ M) recovered from a given preparation after final purification step.

The effects of the addition of either hydrogen peroxide (800 μ M, 0.0024 % v/v) or methyl viologen (100 μ M) to the bacterial culture to induce oxidative stress were also tested on the Newman Δ sodM strain expressing wild type SodM (Figure 6.18). 20 ml cultures of Newman Δ sodM carrying pS10-StrepII sodM were set up in TM from an overnight pre-culture to an OD_{595nm} of 0.05. A control triplet of cultures consisted of non-supplemented TM, TM with 100 μ M addition of Mn, and TM supplemented with 30 μ M Fe. Oxidative stress conditions were created by addition of methyl viologen or hydrogen peroxide to the culture sets at a concentration equivalent to those of the controls in the early exponential phase (2 hours) at the concentration of 100 μ M and 800 μ M, respectively (Figure 6.18 A).

A significant increase in Mn (3 % up to 23 %) and decrease of Fe (51 % down to 26 %) content of wild type SodM was observed in non-supplemented TM culture of Newman Δ sodM upon exposure to methyl viologen stress (Figure 6.18 B).

A similar and pronounced effect of MV on the Fe content of the protein (69 % to 53 %) was noted even with external supplementation of the culture with 30 μ M Fe. A decrease of Fe was accompanied by a simultaneous, moderate increase of Mn content (8 % to 18 %). Peroxide treatment of the minimal medium or metal supplemented culture did not seem to significantly influence the metal content of purified proteins, relative to the controls. Addition of 100 μ M Mn to the culture effectively abolished the effects induced by oxidative stress observed in cells not supplemented with Mn.

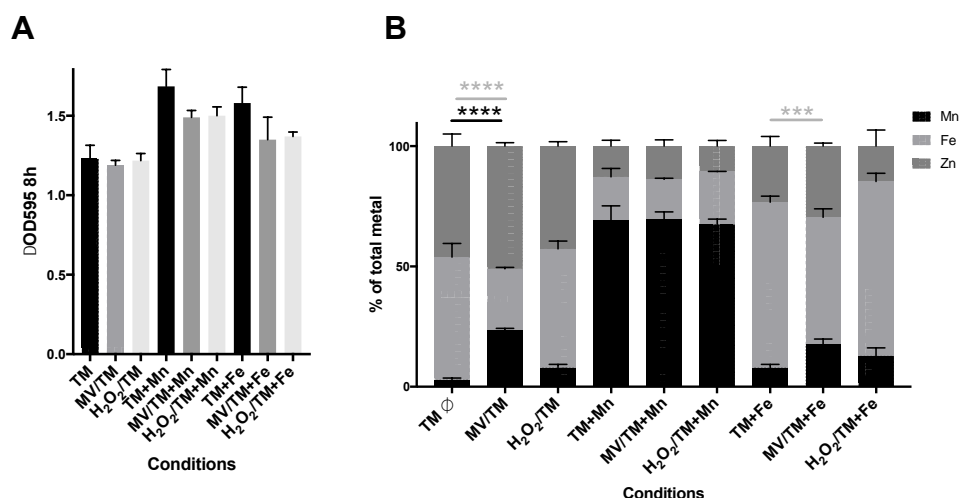


Figure 6.18 Change of growth of *S. aureus* Newman Δ sodM expressing wild type SodM, grown under oxidative stress and metal content of subsequent protein preparations.

(A) Overnight cultures were used to inoculate 20 ml of fresh TM, TM supplemented with 100 μ M Mn or 30 μ M Fe with *S. aureus* Newman Δ sodM pS10sodM and cultured for 8 hours, with either an aliquot of TM (black bar), hydrogen peroxide (800 μ M, 0.0024 %; grey bar) or methyl viologen (100 μ M; white bar) added after 2 hours into the growth of cultures. (B) Fractional content of Mn (black bar), Fe (light grey bar) and Zn (dark grey bar) determined in protein preparations recovered from cells cultured in control and induced oxidative stress conditions. Statistically significant changes in Mn and Fe in relation to a control culture in given conditions marked as asterisk, coloured respectively to the metal representation (2way ANOVA with Tukey's test: ***, $p=0.0007$; ****, $p<0.0001$). Data represent mean and standard deviation of two independent experiments.

6.2.8. Manipulation of protein metal content by external supply with non-native metal cofactor

The metal content of cambialistic SodM in *S. aureus* was influenced by the availability of metal in its growth environment (Figure 6.17; Table 6.1). The binding selectivity of metal ions was tested *in vitro* (Chapter 3, section 3.2.13), and showed that SodA and SodM can bind Zn, Co or Cu through unfolding and refolding, each yielding inactive protein.

The ability of SodM to bind non-physiological ions was tested by supplementation of TM culture of SH1000 Δ sodM carrying plasmid pS10StrepII-sodM with varying, non-toxic concentrations (50 μ M, 500 μ M) of ZnCl₂, CoCl₂, or CuSO₄. Proteins extracted from cells after 8-hour culture were StrepII-tag purified and further resolved by size exclusion chromatography. Collected fractions were analysed for metal content using ICP-MS (Figure 6.19 A, B) and catalytic activity (Figure 6.19 C) of the proteins was assessed by in-gel SOD assay.

A general increase of the recovered protein yield was observed for the cultures supplemented with ZnCl₂, in a dose-dependent manner (Figure 6.19 A). Relative to the preparation from a basal TM medium, higher incorporation of Zn was observed for these proteins at the expense of Fe and Mn (Figure 6.19 B). As a consequence of increased contribution of Zn to total metal composition of SodM, a decrease in total activity of the enzyme was observed

(Figure 6.19 C), indicating that mis-metalation with zinc yielded inactive SodM, consistent with *in vitro* results.

Cobalt has been shown to form stable complexes *in vitro* in the active site of MnSOD of *E. coli* (Ose & Fridovich, 1979). *In vitro* reconstitution of SodA and SodM of *S. aureus* led to formation of stable complexes with both proteins (Chapter 3, section 3.2.13, figure 3.20). Supplementation of 50 μM CoCl_2 in TM culture of SH1000 ΔsodM cells complemented *in-trans* with wild type SodM had a stimulating effect on growth and on protein recovery, in comparison to TM culture (Figure 6.19 A). Regardless of the applied dose, the most significant incorporation of Co into the protein was determined (Figure 6.19 B), amongst all used metals. Similar to Zn-loaded SodM, the Co-metallated isoform presented lower level of activity relative to wild type protein (Figure 6.19 C), implying lack of catalytic functionality of this form of the enzyme. Finally, 50 μM Cu seemed to have improved the growth rate and the protein yield purified from Cu supplemented culture (Figure 6.19 A). Contrary to Zn or Co, no copper was detected in the protein purified from Cu-containing cultures (Figure 6.19 B). It seems that exposure of SH1000 ΔsodM to Cu influenced the relative content of the native metals associated with SodM, without being directly incorporated. Increasing the concentration of Cu resulted in a change of Zn to Fe ratio of protein preparations. An increase in total content of Mn (25%) and Zn (61%), together with a 45% decrease of Fe content was observed in SodM recovered from the culture with addition of 500 μM Cu, in comparison to non-supplemented culture, probably due to displacement of other proteins' metal cofactors by copper, and altering availability of Mn, Fe or Zn to SODs.

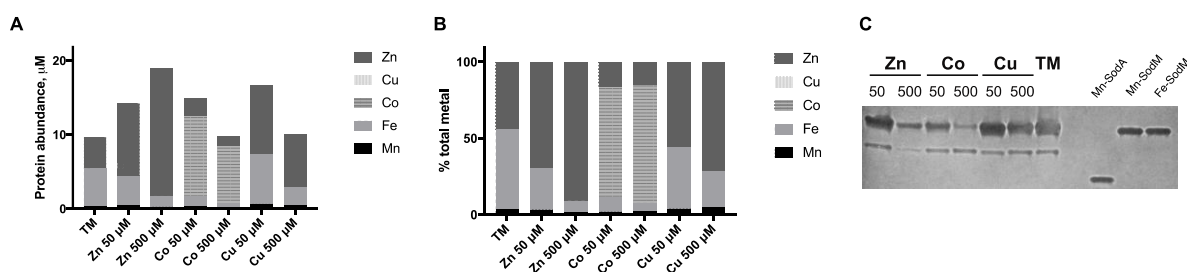


Figure 6.19 Elemental and catalytic analysis of proteins subjected to mis-metalation in *S. aureus* culture.

(A) A relative abundance of metal in total protein (A280nm) from preparations of StrepTrap and size exclusion chromatography purified SodM. Proteins were recovered from 20 ml TM cultures which were supplemented with 50 μM and 500 μM concentrations of Zn, Co or Cu and cultured aerobically for 8 hours at 37°C with 185 rpm shaking. (B) Fractional contribution (%) of detected metals was assessed relative to a total metal content determined in given preparation. (C) SOD activity assay was performed by resolving equal amount (2.5 μg) of proteins by 10% (w/v) Native-PAGE and staining for activity using NBT-riboflavin based stain. The aliquots of 0.3 μg of recombinant Mn-SodA, Fe-SodM and Mn-SodM were loaded as controls. Experiment was conducted once.

6.2.9. *S. aureus* Δ sodM strain expressing a non-cambialistic isoform of SodM is more sensitive than WT to Mn starvation.

The role of the cambialistic SodM in survival of *S. aureus* under manganese starvation was demonstrated both in bacterial culture and in a mouse model of infection (Figure 6.8; Garcia et al., 2017). The ability to switch from using Mn to using Fe, depending on relative bioavailability in the environment, was demonstrated by a direct measurement of the metal content of SodM purified from *S. aureus* cells. The loss of the cambialistic properties by SodM was demonstrated to have an influence on the acquisition of metal by the mutant protein, using the pulldown purification of the SodM mutant expressed in *S. aureus*.

To further verify the role of cambialism *in vivo*, the effect of manganese starvation was tested in cultures of *S. aureus* Newman Δ sodM containing (integrated into *sodM* native locus) a mutated, non-cambialistic isoform of SodM [L159G] (Figure 6.20). The bacterial culture of *S. aureus* was carried out in the medium supplemented with increasing concentrations of calprotectin, and under conditions of oxidative stress caused by addition of methyl viologen. The growth of the *S. aureus* wild type strain was compared to the isogenic Δ sodM mutant strain, as well as the Δ sodM strain complemented with [L159G] *sodM*, this time re-introduced into the native *sodM* locus to ensure normal, wild type regulation of gene expression. As previously shown, the *S. aureus* Δ sodM mutant strain presented a substantial growth defect under Mn-starvation, and increased sensitivity to oxidative stress (Figure 6.1, Figure 6.4) in comparison to the wild type. Integration of the [L159G] *sodM* variant into *S. aureus* Δ sodM genome led to only partial complementation of the Mn-starvation growth phenotype. The reduced growth of the strain producing a Mn-specific SodM relative to WT in the presence of calprotectin was observed at the high doses of this Mn-chelator (>120 $\mu\text{g}\cdot\text{ml}^{-1}$), i.e. under the more extreme Mn starvation conditions. This could potentially reflect a limited capacity of this protein to functionally use Fe under these conditions in *S. aureus*, and thus partially compensating Mn-starvation phenotype of *S. aureus* Δ sodM mutant. It has been shown *in vitro* that the recombinant isoform of this [L159G] SodM protein showed approximately 10-times lower level of activity with Fe than the wild type SodM, and not as low as determined for recombinant SodA (Chapter 4, section 4.2.6);

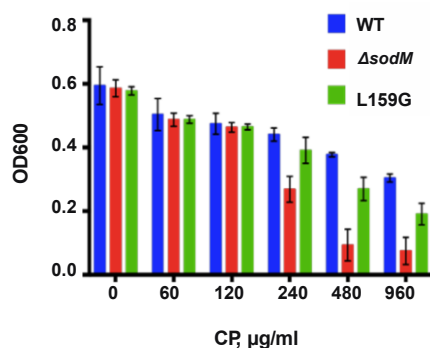


Figure 6.20 Non-cambialistic SodM presents reduced growth rate upon Mn-starvation and oxidative stress.

Wild type *S. aureus*, Δ sodM and sodM L159G mutant *S. aureus* Newman strains were grown in the presence of increasing concentrations of CP, in the presence of 0.1 mM methyl viologen. Growth was assessed after 8 hours by measuring optical density (OD₆₀₀). Data collected by Yuritzi Garcia, University

6.3. Conclusions

The role of SodA and SodM in *S. aureus* physiology was addressed in a series of growth analyses in minimal medium (TM). The phenotypes arising in response to externally generated oxidative stress were characterised in bacterial culture treated with methyl viologen at the early exponential phase of growth. Strains lacking sodA or the mntA Mn-importer exhibited a reduced growth rate and higher sensitivity to superoxide stress, compared to the wild type. The Mn-dependence of SodA and MntA proteins was evaluated in bacterial culture, with the growth defects being rescued by increasing concentration of Mn-supplemented into growth medium. SodM was found to play a major role in conferring resistance to oxidative stress of *S. aureus in vitro* under Mn restricted growth conditions, induced in culture by addition of the immune effector calprotectin, mediating metal depleted conditions in bacterial culture.

Integration of microbiology and biochemistry approaches enabled the determination of the fractional contribution of both SodA and SodM to the overall SOD activity, in conditions of varying metal availability, both in bacterial culture and an animal model of infection. SodA was shown to act as a canonical Mn-dependent enzyme, accounting for most of the total SOD activity and playing the key role in infectivity of *S. aureus* in metal-replete conditions (i.e. in the absence of calprotectin), whereas cambialistic SodM was more important for providing activity under conditions of Mn-starvation during bacterial growth in culture and at the infection site.

The mixed Mn and Fe metal usage and cambialistic properties of SodM were determined *in vivo* in bacterial culture of *S. aureus*. The metalloproteomics showed that both SodA and SodM are present in the major high molecular weight Mn pool in *S. aureus* but Fe concentration in this same pool could not be accurately assessed. This was further confirmed using a more direct method, through purification of Strep-tagged SodM from cells of the *S. aureus* Δ sodM

background. Strep-tagged SodM was shown to be able to switch to using a different metal cofactor depending on the relative abundance of Mn and Fe supplemented in bacterial culture. The relative lack of selectivity (binding of non-native Zn, and Co, but not Cu) and specificity of metal binding (activity conferred by Mn, and Fe, but not any other metals) by a cambialistic SodM in *S. aureus* was shown by exposing cells to non-toxic doses of non-physiological metals.

The residues previously identified to play a role in cambialism, identified using structure-function analysis with site-directed mutagenesis of the recombinant proteins, were verified *in vivo* in *S. aureus* culture. The *S. aureus* Δ sodM cells expressing a mutated SodM showed reduced growth rate relative to WT in the presence of calprotectin. This suggested that abolishing the cambialistic properties of SodM in the [L159G] SodM mutant had limited the ability of *S. aureus* to resist oxidative stress under Mn starvation. An increase of Mn content of SodM was observed in *S. aureus* expressing the mutated variant of SodM in relation to the wild type protein in Mn-supplemented culture, which could imply that the introduced mutation may have altered the ability of enzyme to acquire metals *in vivo*.

Pathogenicity studies allowed for determination of SodM activity as the major contributor to the infectivity of *S. aureus* in Mn-deplete conditions, imposed on bacteria during innate immune response by the action of calprotectin. The presence of additional superoxide dismutase enzyme able to use both Mn and Fe cofactors was shown to be an evolutionary adaptation of this pathogen, to contribute to the increased virulence of *S. aureus*.

Chapter 7. General discussion

Metal ions play roles as essential protein cofactors, estimated to be required by between one-third and a half of all enzymes. Zinc and magnesium are the most commonly utilised metal cofactors (16 and 9% of all enzymes, respectively), and iron and manganese are the next most common cofactors estimated to be exploited by 8 and 6% of enzymes (Andreini et al., 2008; Waldron et al., 2009). The *d*-block or 'transition' metals, such as manganese and iron, are especially found at the active sites of a great number of proteins catalysing reduction-oxidation reactions. Despite their essential role across all domains of life, metals can also cause toxic effects including oxidative damage to cellular components due to formation of deleterious reactive oxygen species.

Interactions between pathogenic bacteria and their host provide a good example of this Janus-faced nature of metals. On the one hand many bacterial proteins, including those involved in the infection process, require essential metals, giving an opportunity to the host to restrict pathogen growth through nutrient restriction; essential metal ions are sequestered by components of the immune system (termed nutritional immunity), making it difficult for the pathogen to acquire them. On the other hand, some immune cells such as macrophages can use increased concentrations of metals such as copper to kill bacteria (White et al., 2009; Shittisak et al., 2007). These processes impose two types of selective pressure on bacterial pathogens: they must overcome metal starvation within the host during some stages of infection, but must also be able to resist the toxicity caused by metal excess during other stages of infection.

Staphylococcus aureus is an important pathogen, which due to its increasing antibiotic resistance, virulence and ability to spread in the community, poses a serious threat to human health (WHO, CDC). The successful evasion of host's immune system by *S. aureus* leading to invasive infection has been markedly associated with the ability of this pathogen to overcome nutrient starvation (Hammer & Skaar, 2011; Corbin et al., 2008). Host phagocytic immune cells produce large quantities of a high-affinity Mn-binding protein (calprotectin), which efficiently chelate metal ions (Mn, Zn) at the site of *S. aureus* infection. Metal sequestration by the calprotectin was demonstrated to inhibit the growth of *S. aureus* (Corbin et al., 2008) and lead to inactivation of Mn-dependent superoxide dismutase (Kehl-Fie et al., 2011).

The genome of *S. aureus* possesses two genes that encode superoxide dismutases (SODs), metalloenzymes catalysing the conversion of superoxide into molecular oxygen and hydrogen peroxide. *S. aureus* SODs play a key role in defence against endogenous (i.e. as a by-product of *S. aureus* aerobic metabolism) and exogenous (e.g. caused by the immune system's 'oxidative burst') oxidative stress. The presence of two copies of the SODs in *S. aureus* genome, both of which were previously suggested to utilise manganese as their essential redox-active metal cofactor, was hypothesised to be a possible adaptation to infecting humans (Valderas et al., 2002).

In this thesis, a range of complementary experimental approaches including bioinformatics, metalloproteomics, protein crystallography and spectroscopy was used to provide a comprehensive characterisation of SaSODs, to detect functional differences between the SaSODs, and to investigate their role in *S. aureus* pathogenicity.

Bioinformatics analyses identified that the two SOD homologues are encoded in all available genomes of *S. aureus* whereas only a single SOD homologue was found in the genomes of other Staphylococci. Phylogenetic analyses and sequence comparisons suggested that the second *S. aureus* SOD, encoded by the *sodM* gene, was most likely acquired through a species-specific gene duplication of the pre-existing *sodA* gene, that occurred in the genome of the ancestor of all sequenced *S. aureus* strains. Based on the level of the sequence identity and length of branches in the phylogenetic trees, SodM appears to be the more divergent homologue suggesting that it was relieved from selective pressure at the point of duplication and had subsequently undergone sub- or neo-functionalisation. The *S. aureus* SodA is highly similar to the single SOD present in other *Staphylococcus* sp. genomes, suggesting that it has conserved properties and performs conserved SOD functions.

Two homologues of the Fe/Mn-dependent SODs can be also found in other bacteria, including the *Escherichia coli* and *Bacillus anthracis*. In *E. coli*, *sodA* encodes a SOD enzyme that utilises exclusively manganese in its catalytic centre, displaying negligible activity with an iron cofactor *in vitro*, and functions under conditions of oxidative stress (Hassan & Fridovich, 1977a). The product of the *E. coli* *sodB* gene, conversely, is an iron-specific enzyme, displaying negligible activity with a manganese cofactor *in vitro*, and is expressed constitutively (Hassan & Fridovich, 1977b; Baez & Shiloach, 2017). *B. anthracis* also possesses two SOD enzymes which exhibit differing metal specificities.

Published *in silico* analyses and initial experimental work classified both *S. aureus* SODs as probable manganese-dependent enzymes (Valderas & Hart, 2001); (Clements et al., 1999). Furthermore, Mn-depletion of *S. aureus* cells by culture in the presence of the immune effector protein complex calprotectin, indicated an increase in the expression of *S. aureus* Mn uptake systems (Kehl-Fie et al., 2013), reduction of the superoxide dismutase activity, as well as increased sensitivity of *S. aureus* to superoxide stress during infection (Kehl-Fie et al., 2011); indicating a Mn-starvation phenotype of the bacteria due to the nutritional immunity of the host, caused by calprotectin. However, experiments using the Fe-specific SOD inhibitor, hydrogen peroxide, suggested possible use of iron in the catalytic centre of one of the *S. aureus* SODs (Clements et al., 1999) which could be potentially explained by the neo-functionalization of the SodM to function with iron.

Here, functional diversity of both SodA and SodM enzymes, and their significance for the virulence of *S. aureus* was investigated in infection studies and *in vitro* culture experiments. In the *S. aureus*-infected mice as well as the *in vitro* growth assays of the *sodA* and the *sodM* mutant strains, SodA played the main role in Mn-abundant conditions whereas SodM appeared to be important under Mn-depletion. These results gave further support for the conserved role of SodA

in the general oxidative stress response, and the specialised role of SodM, potentially functioning in stress conditions such as host-imposed manganese-starvation.

The observed significant differences in oxidative stress tolerance of the *S. aureus* SOD deletion strains in Mn-rich and Mn-depleted conditions suggested that the two homologues could utilise different metals in their catalytic centres. In order to further study the role of different metals in the two *S. aureus* SOD homologues, we characterised their catalytic activities in the presence of different metals. In the enzyme activity assays using recombinant proteins, SodA was active only with Mn, making it a canonical Mn-dependent SOD enzyme, whereas SodM was active with both Mn and Fe, and thus presented cambialistic properties (capacity to use different metal cofactors). The Mn-specific activity of the recombinant SodM was seven times lower than that of the recombinant SodA loaded with Mn. Consistent with that, SodA accounted for most of the SOD activity in lysates of *S. aureus* grown under oxidative stress conditions in Mn replete conditions, whereas SodM activity was enriched in Mn-restricted conditions. The mixed Mn and Fe metal usage, and cofactor switching by SodM in *S. aureus*, were further demonstrated using a direct measurement of the metal content of protein purified from the *S. aureus* cells cultured in defined metal conditions.

All these data give support for the hypothesis that the activity of SodM with an Fe cofactor helps the pathogen to survive host-imposed oxidative stress and concomitant manganese starvation. However, the molecular bases determining the metal specificity of the superoxide dismutases remain elusive. In order to investigate the potential metal specificity-determinants, we have solved crystal structures of both *S. aureus* SODs, each with both Fe and Mn in their catalytic centres. Crystal structures of the Fe-loaded and Mn-loaded isoforms of both proteins shared a high level of structural similarity, including no observed differences in the residues involved in binding the metal cofactors, and no significant differences in the geometry of metal coordination (within the limits of resolution of the solved structures). This indicated that the observed differences in metal specificity between the two SOD homologues are likely due to very subtle structural variation in metal coordination, alteration to the relative strength of the hydrogen bond network surrounding the catalytic metal ion, or charge distribution between residues involved in the catalysis.

Based on detailed analyses of the primary and the tertiary structures of the *S. aureus* SODs, we identified residues in the outer coordination sphere (non-metal coordinating amino acid residues that are nonetheless in close spatial proximity), which could be potentially involved in determination of the observed differences in SaSODs metal specificities. These non-conserved residues (positions 19, 159, 160) were identified mainly based on their spatial orientation in relation to the active site, and were selected for mutagenesis experiments. Swapping of one pair of residues, [G159, L160]_{SodA} and [L159, F160]_{SodM}, between the sequence of the two SaSODs, had a pronounced effect on their metal specificity, turning SodA [G159L, L160F] into a cambialistic enzyme and SodM [L159G, F160L] into a Mn-specific enzyme. The cambialistic properties of SodM were changed towards Mn-specificity to the same extent when the protein was mutated at a single position, residue 159; the SodM L159G, the double mutant L159G,

F160L, or the triple mutant I19F, L159G, F160L all demonstrated similar preference for Mn, indicating the importance of residue 159 in conferring metal-specificity in SodM. Although mutagenesis of selected residues significantly altered the metal-specific properties of SaSODs, it did not inverse their native activities completely. This indicates importance of additional (than identified) residues in conferring the specific activity of the two SaSODs.

The *S. aureus* Δ sodM strain expressing the [L159G] SodM was more susceptible to Mn starvation and oxidative stress than the wild type. Determined activity of the [L159G] SodM was predominantly Mn-dependent, however, the enzyme also presented a very low-level activity with Fe. The very limited ability of the [L159G] SodM to function with Fe-cofactor in *S. aureus* Δ sodM cells led to decreased capacity of the enzyme to support the growth of bacteria in the conditions that inhibit Mn-specific SOD. This is consistent with an important role of the cambialistic activity of SodM (conditional metal cofactor switch) for the ability of *S. aureus* to resist oxidative stress and nutritional immunity; when the cambialistic property of SodM is inhibited by a mutation, the cells are less able to survive the stress conditions.

The crystal structure was also solved for the non-cambialistic SodM triple mutant isoform, which confirmed that the introduced mutations did not significantly alter the structure of the active site, the predicted hydrogen bonding network around the active site, or the overall protein structure which resembled those of the wild type enzymes. The conserved active site of the enzymes stabilises the redox-active metal coordination, and provides an optimal structure for efficient electron and proton transfer between the metal ion and the superoxide anion during catalysis.

The changes in activity of the two SaSODs achieved by mutagenesis together with the conservation of the high level of structural similarity between wild type and mutant proteins imply that the structural changes responsible for altering metal specificity must be structurally very subtle (electronic, i.e. modulating the redox potential). To support activity with either of these two metal cofactors, which vary in their intrinsic redox potentials, a cambialistic enzyme must provide a relatively flexible electronic scaffold. As there are no significant differences between the determined crystal structures of the cambialistic and the Mn-specific enzymes of *S. aureus* it can be hypothesized that the required flexibility could be conferred by subtle structural differences. We have demonstrated herein that some of these differences are facilitated by the amino acid residues identified in the mutagenesis studies. In order to further investigate determinants of the protein redox properties, the recombinant *S. aureus* SODs were analysed using electron paramagnetic resonance (EPR), electron nuclear double resonance (ENDOR), and electron double resonance detected NMR (ELDOR-NMR) spectroscopy. The electronic structures were assessed by contrasting SodA and SodM, both loaded with a functional Mn cofactor; and the *E. coli* SodB enzyme, which had its native Fe cofactor swapped for Mn, and therefore was inactive. The HF-EPR spectroscopy of these Mn(II) paramagnetic centres provided insight into electronic interactions, coupling and structural dynamics of the active SaSOD proteins. The spectroscopic measurements revealed differences in the EPR spectra (zero field interaction component) of SaSodA and SaSodM, indicating distinct electronic structures between the two homologues. Due

to the complexity of the collected data and computational limitations, most of the distinctive spectral determinants of the two proteins could not be directly ascribed to specific structural components.

However, spectroscopic measurements identified a key interaction between the metal centre, one of its direct ligands, and a residue from the second subunit, across the dimer interface [Mn-H165(ligand)-E164'(second monomer)], as being potentially important in conferring the metal specificity of the catalytic activities of the SodA and the SodM, as well as the lack of activity of the Mn-substituted form of the Fe-specific SOD from *E. coli*. The E164'-H165 pair of residues form a double bridge of hydrogen bonds across the dimer interface, interconnecting the two subunits of the SaSODs. E164 was previously shown to be important for the stability of the dimer and also for metal-specific activity of the SODs in *E. coli* (Whittaker & Whittaker, 1998). It was hypothesised that this interaction may play a role in proton-coupled electron transfer in the SOD catalysis.

The investigation of the complex electron-nuclear hyperfine interactions (distances) between Mn and the surrounding protons, as well as between Mn and nitrogen atoms of the metal's ligands was carried out using ENDOR and ELDOR-NMR. To aid interpretation of the hyperfine measurements, computational/statistical modelling was used to integrate available structural information with the spectroscopic measurements and to determine the positions of critical protons and charges of the redox metal centre and its environment. These calculations confirmed similar positions of the critical water-ligand protons in both the active Mn-loaded SaSODs and the inactive Mn-substituted Fe-SOD from *E. coli*, coupled to electron transfer in superoxide dismutation. It also indicated sharing of the proton and distribution of the charge between both E164' and H165 only in the active SaSODs, which was broken in inactive enzyme due to a change in the relative position of these sidechains, indicating a key role of this interaction for the catalytic activity of SODs.

The measured electron and proton spectra of SaSODs, and inactive *E. coli* SOD; together with the solved crystal structures, and the measurements based on isostructural $[M(4'-R\text{-terpyridine})_2]^{2+}$ (M=Mn or Fe) complexes (Gätjens et al., 2007; Sjöin et al., 2008; Tabares et al., 2010), provided sufficient preliminary data to postulate the correlation between the measured zero field interaction, specific activity, and the protein's redox potential. The predicted correlation could arise from the increased electron donating capacity of E164' to the metal ligand, H165, in SaSODs, which is not observed in the Mn-substituted, inactive FeSOD of *E. coli*. The proposed model is consistent with the examples of metal sites containing triads Metal-water-Asp/Glu or Metal-His-Asp/Glu, in which the outer sphere residues were shown to influence the orientation and polarization of bonds with the metal ligands and in consequence modulate catalytic activity of enzymes (Smulevich et al., 1988; Jamal El Yazal et al., 2000; Frison & Ohanessian, 2009).

The exact mechanisms that could provide the proposed redox-tuning in SaSODs remain unresolved, but changes in the interactions between the metal and the protein, including hydrogen bond interactions with the metal-bound water, seem to be important contributors. Charge distribution between residues on the axis between the two metal centres cycling between

oxidation states during dismutation reaction, is hypothesised to be important in catalysis of SaSODs.

Due to the time constraints of this work, the identification of the exact source of the electronic differences between the two proteins remains to be determined in future. The complexity of spectra acquired by HF-EPR suggested that more work and/or instrumental/computational power should be invested to accurately interpret the detected features. Assessment of the mutants of the two SaSODs, both prepared in this work, or identified in the course of spectroscopic analyses as potentially important for proton coupled electron transfer, could be included in the further HF-EPR studies, to aid correlation of the specific changes in the enzymes with the modulation of catalytic activities. Further investigation of the spectroscopic properties will be carried out in collaboration with EPR expert, Dr Sun Un, CEA Saclay, France.

Furthermore, the direct measurement of the redox potential of versions of these proteins is necessary to provide a quantitative characterisation of the redox biochemistry of these two proteins, and provide insight into the exact molecular mechanism of cambialism vs metal specificity of SaSODs. This work is planned in collaboration with Dr Alison Parkin, University of York, an expert in protein film Fourier transform alternating current cyclic voltammetry (PF-FTacV).

Further biochemical characterisation of the two proteins could address the metal preference and also the kinetics of the metal binding in metal competition experiments. Measuring affinity of the metals in SODs with high precision is difficult due to necessity of chemical unfolding to extract the native cofactor and the requirement for working in anaerobic conditions due to the oxidation of Fe(II). This difficulty could be potentially addressed by measuring the protein-bound metal content in proteins folded in presence of different metal ratios (Fe:Mn).

Further studies of the SodA/SodM heterodimer could provide insight into metal-specificity of this hybrid form of protein. Comparison of the catalytic properties of the heterodimer and the two homodimers could address potential differences in activities of these forms. Finally, any properties of the homodimer determined *in vitro* would aid determination of the potential physiological role and relevance of this hydride protein in *S. aureus*.

Overall, this thesis provided insights into elusive mechanisms determining different metal specificity of two highly identical SOD proteins from bacterial pathogen *Staphylococcus aureus*. It also provided a strong experimental evidence and phylogenetic background supporting cambialism of the *S. aureus* SodM, which evolved capacity of mixed-metal usage to confer defence against the nutritional immunity of the infected host.

Appendix

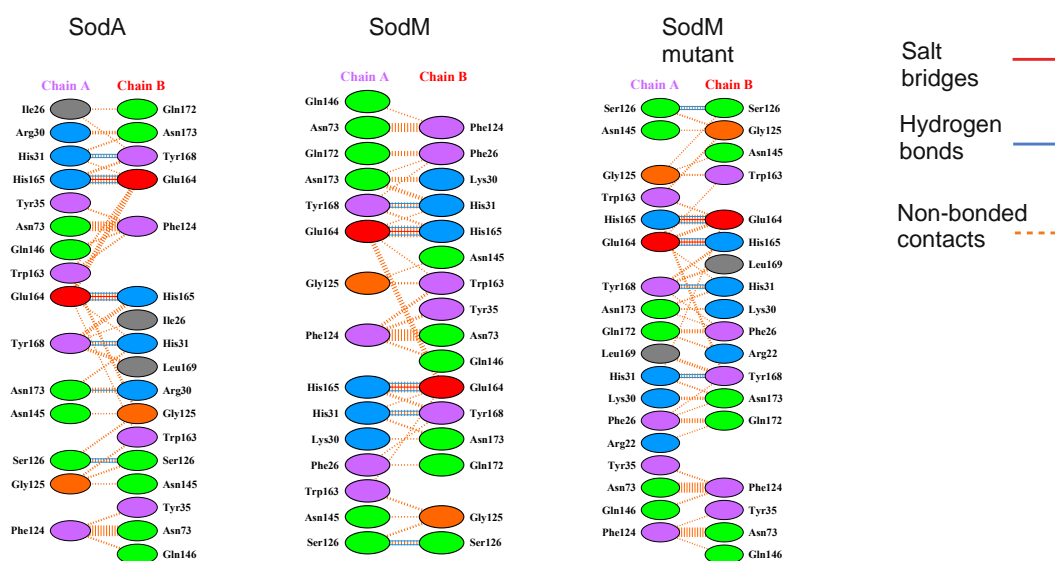
Protein	Condition	Screen
SaSodA	0.2 M calcium acetate hydrate, 18 % PEG 8000, 0.1 M Na cacodylate pH 6.5	MD, Structure
	0.2 M magnesium chloride, 30 % PEG 4000, 0.1 M Tris pH 8.5	MD, Structure
	0.2 M lithium sulphate, 30 % PEG 4000, 0.1 M Tris pH 8.5	MD, Structure
	0.2 M ammonium sulphate, 30 % PEG 8000	MD, Structure
	0.2 M ammonium phosphate monobasic, 50 % MPD, 0.1 M Tris pH 8.5	MD, Structure
SaSodM	25 % PEG 1500, 0.1M PCTP pH 6.0	MD, PACT
	25 % PEG 1500, 0.1M PCTP pH 7.0	MD, PACT
	25 % PEG 1500, 0.1M PCTP pH 8.0	MD, PACT
	0.2 M magnesium chloride, 20 % PEG 6000, 0.1 M HEPES pH 7.0	MD, PACT
	0.01 M zinc chloride, 20 % PEG 6000, 0.1 M HEPES pH 7.0	MD, PACT
	0.2 M sodium chloride, 20 % PEG 6000, 0.1 M Tris, pH 8.0	MD, PACT
	0.2 M magnesium chloride, 20 % PEG 6000, 0.1 M Tris pH 8.0	MD, PACT
	0.2 M lithium chloride, 20 % PEG 6000, 0.1 M Tris pH 8.0	MD, PACT
	0.002 M zinc chloride, 20 % PEG 6000, 0.1 M Tris pH 8.0	MD, PACT
	0.2 M sodium acetate, 25 % PEG 3350, 0.1 M Bis Tris propane, pH 7.5	MD, PACT
	0.2 M sodium fluoride, 25 % PEG 3350, 0.1 M Bis Tris propane, pH 7.5	MD, PACT
	0.1 M potassium thiocyanate, 30 % PEG 2000 MME	MD, JCSG+
	0.15 M potassium bromide, 30 % PEG 2000 MME	MD, JCSG+
	20 % PEG 6000, 0.1 M Bicine pH 9.0	MD, JCSG+
	10 % PEG 20000, 2 % Dioxane, 0.1 M Bicine pH 9.0	MD, JCSG+

Table 8.1 Summary of initial screening conditions resulting in positive hits of SodA and SodM crystals.

All listed experiments were performed at 20°C, using Mosquito robot (TTP LabTech, UK). The initial screening was carried out at 10 mg/ml protein concentration with commercially available matrix crystallisation screens Structure, PACT and JCSG+ (Molecular Dimensions, UK) using sitting drop vapour-diffusion technique (100 nl:100 nl and 200 nl:100 nl mixture of protein-crystallisation reservoir) and equilibrated against 80 µl reservoir in 96-well MRC crystallisation plates.

Protein name, resolution (Å)	Chain ID	B-factor, (Å ²)	Range of modelled residues/ atoms/molecules	PISA Surface, (Å ²)	PISA Interface			PDBSum Interface		
					Average Interface Area, Interacting chains (Å ²)	N _{HB}	N _{SB}	Average Interface Area, Interacting chains (Å ²)	N _{HB}	N _{SB}
FeSodA (6EX3), 2.20	A	52.129	2-60; 63-198	9287.3	884.9	12	2	881.3	11	2
	B	46.938	2-198 (mediating crystal contact)	9467	C x A: 893.1	12	2	889.5	11	
	C	53.179	2-62; 68-198	9224.6	D x B: 876.8	12	2	873.0	11	
	D	51.137	2-58; 69-198	9105.1						
	Fe	41.025	4							
	HOH	44.815	146							
MnSodA (5N56), 2.07	A	41.726	2-199	9600.8	880.8	12	2	879	11	2
	B	36.869	2-199	9562.6						
	Mn	27.286	2							
	HOH	38.556	140							
FeSodM (6EX4), 2.40	A	41.34	2-199	9632.6	941.7	12	2	942.5	10	2
	B	44.096	2-199	9822.8						
	Fe	40.583	2							
	HOH	31.035	167							
MnSodM (5N57), 2.30	A	44.85	2-199	9742	939.7	12	2	941.5	10	2
	B	42.929	2-199	9765						
	Mn	35.215	2							
	HOH	30.055	121							
MnSodM (6EX5), 1.80 (mutant)	A	21.813	2-199	9582.2	927.0	12	2	927	10	2
	B	24.231	2-199	9630.1						
	Mn	29.885	2							
	HOH	13.113	312							

Table 8.2 Dimer interface and surface description.



Residue colours: Positive (H,K,R); negative (D,E); S,T,N,Q = neutral; A,V,L,I,M = aliphatic; F,Y,W = aromatic; P,G = Pro&Gly; C = cysteine.

Figure 8.1 All the potential bonded and non-bonded contacts identified at the dimer interface of SaSODs.

The number of blue H-bond lines between any two residues indicates the number of potential hydrogen bonds between them. For non-bonded contacts, the width of the dashed orange line is proportional to the number of predicted atomic contacts.

Distance to metal atom, (Å)						
Coordinating residue/molecule	Atom ID	FeSodA	MnSodA	FeSodM	MnSodM	MnSodM (mutant)
Chain A						
His27	NE2	2.23	2.36	2.25	2.36	2.16
His81	NE2	2.06	2.13	2.17	2.33	2.14
His165	NE2	2.31	2.41	2.14	2.30	2.23
Asp161	OD2	2.06	2.12	2.02	1.97	2.03
HOH	O	2.12	2.22	2.29	2.21	2.22
Chain B						
His27	NE2	2.16	2.38	2.02	2.35	2.24
His81	NE2	2.06	2.17	2.22	2.33	2.23
His165	NE2	2.29	2.20	2.09	2.34	2.25
Asp161	OD2	2.06	2.06	1.92	1.91	2.00
HOH	O	2.04	2.22	2.26	2.14	2.19
Chain C						
His27	NE2	2.18				
His81	NE2	2.14				
His165	NE2	2.20				
Asp161	OD2	2.05				
HOH	O	2.19				
Chain D						
His27	NE2	2.11				
His81	NE2	2.04				
His165	NE2	2.30				
Asp161	OD2	2.06				
HOH	O	2.04				

Table 8.3 Bond distances between active site metal and coordinating ligands.

References

- Acton, D. S., Plat-Sinnige, M. T., van Wamel, W., de Groot, N., & van Belkum, A. (2009). Intestinal carriage of *Staphylococcus aureus*: how does its frequency compare with that of nasal carriage and what is its clinical impact? *European Journal of Clinical Microbiology & Infectious Diseases*, 28(2), 115.
- Adams, P.D., Afonine, P.V., Bunkóczy, G., Chen, V.B., Davis, I.W., Echols, N., Headd, J.J., Hung, L.-W., Kapral, G.J., Grosse-Kunstleve, R.W., McCoy, A.J., Moriarty, N.W., Oeffner, R., Read, R.J., Richardson, D.C., Richardson, J.S., Terwilliger, T.C. & Zwart, P.H. (2010) PHENIX: a comprehensive Python-based system for macromolecular structure solution. *Acta Crystallographica Section D: Biological Crystallography*. 66 (Pt 2), 213–221.
- Adl, S.M., Simpson, A.G.B., Lane, C.E., Lukeš, J., Bass, D., Bowser, S.S., Brown, M.W., Burki, F., Dunthorn, M., Hampl, V., Heiss, A., Hoppenrath, M., Lara, E., le Gall, L., Lynn, D.H., McManus, H., Mitchell, E.A.D., Mozley-Stanridge, S.E., Parfrey, L.W., et al. (2012) The Revised Classification of Eukaryotes. *Journal of Eukaryotic Microbiology*. 59 (5), 429–514.
- Aguirre, J.D., Clark, H.M., McIlvin, M., Vazquez, C., Palmere, S.L., Grab, D., Seshu, J., Hart, P.J., Saito, M. & Culotta, V.C. (2014) A Manganese-Rich Environment Supports Superoxide Dismutase Activity in a Lyme Disease Pathogen, *Borrelia burgdorferi*. *Journal of Biological Chemistry*.
- Altschul, S.F., Gish, W., Miller, W., Myers, E.W. & Lipman, D.J. (1990) Basic local alignment search tool. *Journal of Molecular Biology*. 215 (3), 403–410.
- Amano A., Shizukuishi S., Tamagawa H., Iwakura K., Tsunasawa S., Tsunemitsu A. (1990) Characterization of superoxide dismutases purified from either anaerobically maintained or aerated *Bacteroides gingivalis*, *Journal of Bacteriology*. 172, 1457-63.
- Amar B T Ghisaidoobe, S.J.C. (2014) Intrinsic Tryptophan Fluorescence in the Detection and Analysis of Proteins: A Focus on Förster Resonance Energy Transfer Techniques - *ijms-15-22518.pdf*. *International Journal of Molecular Sciences*. 15 (12), 22518.
- Ammann, A.A. (2007) Inductively coupled plasma mass spectrometry (ICP MS): a versatile tool. *Journal of Mass Spectrometry*. 42 (4), 419–427.
- Ando, M., Manabe, Y.C., Converse, P.J., Miyazaki, E., Harrison, R., Murphy, J.R. & Bishai, W.R. (2003) Characterization of the role of the divalent metal ion-dependent transcriptional repressor MntR in the virulence of *Staphylococcus aureus*. *Infection and Immunity*. 71 (5), 2584–2590.
- Andreini, C., Bertini, I., Cavallaro, G., Holliday, G.L. & Thornton, J.M. (2008) Metal ions in biological catalysis: from enzyme databases to general principles. *Journal of Biological Inorganic Chemistry*. 13 (8), 1205–1218.

- Anjem, A., Varghese, S. & Imlay, J.A. (2009) Manganese import is a key element of the OxyR response to hydrogen peroxide in *Escherichia coli*. *Molecular Microbiology*. 72 (4), 844–858.
- Archer, G.L. (1998) *Staphylococcus aureus*: A Well-Armed Pathogen. *Clinical Infectious Diseases*. 26 (5), 1179–1181.
- Azarian, T., Daum, R.S., Petty, L.A., Steinbeck, J.L., Yin, Z., Nolan, D., Boyle-Vavra, S., Hanage, W.P., Salemi, M. & David, M.Z. (2016) Intrahost Evolution of Methicillin-Resistant *Staphylococcus aureus* USA300 Among Individuals with Reoccurring Skin and Soft-Tissue Infections. *Journal of Infectious Diseases*. 214 (6), 895–905.
- Baba, T., Takeuchi, F., Kuroda, M., Yuzawa, H., Aoki, K.-I., Oguchi, A., Nagai, Y., Iwama, N., Asano, K., Naimi, T., Kuroda, H., Cui, L., Yamamoto, K. & Hiramatsu, K. (2002) Genome and virulence determinants of high virulence community-acquired MRSA. *The Lancet*. 359 (9320), 1819–1827.
- Baez, A. & Shiloach, J. (2017) Increasing dissolved-oxygen disrupts iron homeostasis in production cultures of *Escherichia coli*. *Antonie van Leeuwenhoek*. 110 (1), 115–124.
- Baker-Austin, C., Wright, M.S., Stepanauskas, R. & McArthur, J.V. (2006) Co-selection of antibiotic and metal resistance. *Trends in Microbiology*. 14 (4), 176–182.
- Baker, J., Sitthisak, S., Sengupta, M., Johnson, M., Jayaswal, R.K. & Morrissey, J.A. (2010) Copper stress induces a global stress response in *Staphylococcus aureus* and represses *sae* and *agr* expression and biofilm formation. *Applied and Environmental Microbiology*. 76 (1), 150–160.
- Ballal, A. & Manna, A.C. (2009a) Control of Thioredoxin Reductase Gene (*trxB*) Transcription by *SarA* in *Staphylococcus aureus*. *Journal of Bacteriology*. 192 (1), 336–345.
- Ballal, A. & Manna, A.C. (2009b) Regulation of superoxide dismutase (*sod*) genes by *SarA* in *Staphylococcus aureus*. *Journal of Bacteriology*. 191 (10), 3301–3310.
- Barondeau, D. P., Kassmann, C. J., Bruns, C. K., Tainer, J. A., & Getzoff, E. D. (2004). Nickel superoxide dismutase structure and mechanism. *Biochemistry*, 43(25), 8038-8047.
- Battye, T.G.G., Kontogiannis, L., Johnson, O., Powell, H.R. & Leslie, A.G.W. (2011) iMOSFLM: a new graphical interface for diffraction-image processing with MOSFLM. *Acta Crystallographica Section D: Biological Crystallography*. 67 (Pt 4), 271–281.
- Beasley, F.C. & Heinrichs, D.E. (2010) Siderophore-mediated iron acquisition in the staphylococci. *Journal of inorganic biochemistry*. 1;104(3):282-8.
- Beasley, F.C., Marolda, C.L., Cheung, J., Buac, S. & Heinrichs, D.E. (2011) *Staphylococcus aureus* transporters Hts, Sir, and Sst capture iron liberated from human transferrin by Staphyloferrin A, Staphyloferrin B, and catecholamine stress hormones, respectively, and contribute to virulence. *Infection and Immunity*. 79 (6), 2345–2355.

- Beauchamp, C. & Fridovich, I. (1971) Superoxide dismutase: improved assays and an assay applicable to acrylamide gels. *Analytical biochemistry*. 44 (1), 276–287.
- Begier, E., Seiden, D.J., Patton, M., Zito, E., Severs, J., Cooper, D., Eiden, J., Gruber, W.C., Jansen, K.U., Anderson, A.S. & Gurtman, A. (2017) SA4Ag, a 4-antigen *Staphylococcus aureus* vaccine, rapidly induces high levels of bacteria-killing antibodies. *Vaccine*. 35 (8), 1132–1139.
- Benito, D., Lozano, C., Rezusta, A. & Ferrer, I. (2014) Characterization of tetracycline and methicillin resistant *Staphylococcus aureus* strains in a Spanish hospital: Is livestock-contact a risk factor in infections caused by MRSA CC398?. *International Journal of Medical Microbiology*, 304(8), 1226-1232.
- Benov, L. T., & Fridovich, I. (1994). *Escherichia coli* expresses a copper-and zinc-containing superoxide dismutase. *Journal of Biological Chemistry*, 269(41), 25310-25314.
- Bergey, D. H. & Breed, R. S. *Bergey's Manual of Determinative Bacteriology* 464–466 (Williams & Wilkins Co., 1957)
- Berntzen, H.B., Ölmez, Ü., Fagerhol, M.K. and Munthe, E. (1991). The leukocyte protein L1 in plasma and synovial fluid from patients with rheumatoid arthritis and osteoarthritis. *Scandinavian Journal of Rheumatology*, 20(2), pp.74-82.
- Bertani, G. (1951) Studies on lysogenesis. I. The mode of phage liberation by lysogenic *Escherichia coli*. *Journal of Bacteriology*. 62 (3), 293–300.
- Berube, B.J. & Wardenburg, J. B. (2013) *Staphylococcus aureus* α -toxin: nearly a century of intrigue. *Toxins*. 5 (6), 1140–1166.
- Beyer, W. F., & Fridovich, I. (1991). *In vivo* competition between iron and manganese for occupancy of the active site region of the manganese-superoxide dismutase of *Escherichia coli*. *Journal of Biological Chemistry*, 266(1), 303-308.
- Bhalla, A., Aron, D.C. & Donskey, C.J. (2007) *Staphylococcus aureus* intestinal colonization is associated with increased frequency of *S. aureus* on skin of hospitalized patients. *BMC Infectious Diseases*. 7(1):105.
- Bischoff, M. & Berger-Bachi, B. (2001) Teicoplanin stress-selected mutations increasing ζ B activity in *Staphylococcus aureus*. *Antimicrobial Agents and Chemotherapy*, 45(6), 1714-1720.
- Bischoff, M., Dunman, P., Kormanec, J., Macapagal, D., Murphy, E., Mounts, W., Berger-Bachi, B. & Projan, S. (2004) Microarray-Based Analysis of the *Staphylococcus aureus* B Regulon. *Journal of Bacteriology*. 186 (13), 4085–4099.
- Bond, C.S. & Schüttelkopf, A.W. (2009) ALINE: a WYSIWYG protein-sequence alignment editor for publication-quality alignments. *Acta Crystallographica Section D: Biological Crystallography*. 65 (5), 510–512.

- Botella, H., Peyron, P., Levillain, F., Poincloux, R., Poquet, Y., Brandli, I., et al. (2011). Mycobacterial P1-type ATPases mediate resistance to zinc poisoning in human macrophages. *Cell Host & Microbe*, 10, 248–259.
- Bourgeois-Nicolaos, N., Lucet, J.-C., Daubié, C., Benchaba, F., Rajguru, M., Ruimy, R., Andremont, A. & Armand-Lefèvre, L. (2010) Maternal vaginal colonisation by *Staphylococcus aureus* and newborn acquisition at delivery. *Paediatric and Perinatal Epidemiology*. 24 (5), 488–491.
- Brock, C.J. & Harris, J.I. (1977) Superoxide dismutase from *Bacillus stearothermophilus*: reversible removal of manganese and its replacement by other metals. *Journal of Molecular Biology*. 5 (5), 1537–1539.
- Bronner, S., Monteil, H. & Prévost, G. (2004) Regulation of virulence determinants in *Staphylococcus aureus*: complexity and applications. *FEMS Microbiology Reviews*, 28 (2): 183–200.
- Brosnahan, A.J. & Schlievert, P.M. (2011) Gram-positive bacterial superantigen outside-in signaling causes toxic shock syndrome. *The FEBS Journal*. 278 (23), 4649–4667.
- Brown, A.F., Leech, J.M., Rogers, T.R. & McLoughlin, R.M. (2014) *Staphylococcus aureus* Colonization: Modulation of Host Immune Response and Impact on Human Vaccine Design. *Frontiers in immunology*. 4, 507.
- Burlak, C., Hammer, C.H., Robinson, M.-A., Whitney, A.R., McGavin, M.J., Kreiswirth, B.N. & DeLeo, F.R. (2007) Global analysis of community-associated methicillin-resistant *Staphylococcus aureus* exoproteins reveals molecules produced *in vitro* and during infection. *Cellular Microbiology*. 9 (5), 1172–1190.
- Butaye, P., Argudín, M.A. & Smith, T.C. (2016) Livestock-Associated MRSA and Its Current Evolution. *Current Clinical Microbiology Reports*. 3 (1), 19–31.
- Canonne-Hergaux, F. (2002) Expression and subcellular localization of NRAMP1 in human neutrophil granules. *Blood*. 100 (1), 268–275.
- Capella-Gutiérrez, S., Silla-Martínez, J.M. & Gabaldón, T. (2009) trimAl: a tool for automated alignment trimming in large-scale phylogenetic analyses. *Bioinformatics (Oxford, England)*. 25 (15), 1972–1973.
- Carleton, H.A., Diep, B.A., Charlebois, E.D., Sensabaugh, G.F. & Perdreau Remington, F. (2004) Community-Adapted Methicillin-Resistant *Staphylococcus aureus* (MRSA): Population Dynamics of an Expanding Community Reservoir of MRSA. *Journal of Infectious Diseases*. 190 (10), 1730–1738.
- Casey, A.L., Adams, D., Karpanen, T.J., Lambert, P.A., Cookson, B.D., Nightingale, P., Miruszenko, L., Shillam, R., Christian, P. & Elliott, T.S.J. (2010) Role of copper in reducing hospital environment contamination. *The Journal of Hospital Infection*. 74 (1), 72–77.

- Cassat, J.E. & Skaar, E.P. (2011) Metal ion acquisition in *Staphylococcus aureus*: overcoming nutritional immunity. *Seminars in Immunopathology*. 34 (2), 215–235.
- Cavaco, L. M., Hasman, H., & Aarestrup, F. M. (2011). Zinc resistance of *Staphylococcus aureus* of animal origin is strongly associated with methicillin resistance. *Veterinary Microbiology*. 150(3–4), 344–348.
- Cavaco, L. M., Hasman, H., Stegger, M., Andersen, P. S., Skov, R., Fluit, A. C. (2010). Cloning and occurrence of *czrC*, a gene conferring cadmium and zinc resistance in methicillin-resistant *Staphylococcus aureus* CC398 isolates. *Antimicrobial Agents and Chemotherapy*, 54(9), 3605–3608.
- Cellier, M.F., Courville, P. & Campion, C. (2007) Nramp1 phagocyte intracellular metal withdrawal defense. *Microbes and Infection*. 9(14), 1662-1670.
- Centers for Disease Control and Prevention (CDC). (2015) Antibiotic resistance threats in the United States, Atlanta: CDC; 2013. (<https://www.cdc.gov/drugresistance/threat-report-2013/pdf/ar-threats-2013-508.pdf>, accessed 18 August 2017).
- Chaibenjawong, P. & Foster, S.J. (2011). *Archives of Microbiology*. 193(2), 125-135.
- Chan, P.F. & Foster, S.J. (1998) The role of environmental factors in the regulation of virulence-determinant expression in *Staphylococcus aureus* 8325-4. *Microbiology*. 144 (9), 2469–2479.
- Chan, P.F., Foster, S.J., Ingham, E. & Clements, M.O. (1998) The *Staphylococcus aureus* alternative sigma factor sigmaB controls the environmental stress response but not starvation survival or pathogenicity in a mouse abscess model. *Journal of Bacteriology*. 180 (23), 6082–6089.
- Chang, S., Sievert, D.M., Hageman, J.C., Boulton, M.L., Tenover, F.C., Downes, F.P., Shah, S., Rudrik, J.T., Pupp, G.R., Brown, W.J., Cardo, D. & Fridkin, S.K. (2003) Infection with Vancomycin-Resistant *Staphylococcus aureus* Containing the *vanA* Resistance Gene. *New England Journal of Medicine*. 348 (14), 1342–1347.
- Chang, W., Small, D.A., Toghrol, F. & Bentley, W.E. (2006) Global Transcriptome Analysis of *Staphylococcus aureus* Response to Hydrogen Peroxide. *Journal of Bacteriology*. 188 (4), 1648–1659.
- Chen, P.R., Nishida, S., Poor, C.B., Cheng, A., Bae, T., Kuechenmeister, L., Dunman, P.M., Missiakas, D. & He, C. (2009) A new oxidative sensing and regulation pathway mediated by the MgrA homologue SarZ in *Staphylococcus aureus*. *Molecular Microbiology*. 71 (1), 198–211.
- Chen, V.B., Arendal, W.B.I., Headd, J.J., Keedy, D.A., Immormino, R.M., Kapral, G.J., Murray, L.W., Richardson, J.S. & Richardson, D.C. (2010) MolProbity: all-atom structure validation for macromolecular crystallography. *Acta Crystallographica Section D: Biological Crystallography*. 66 (1), 12.

- Cheng, A.G., Kim, H.K., Burts, M.L., Krausz, T., Schneewind, O. & Missiakas, D.M. (2009) Genetic requirements for *Staphylococcus aureus* abscess formation and persistence in host tissues. *The FASEB Journal*. 23 (10), 3393–3404.
- Cheung, A.L., Bayer, A.S., Zhang, G., Gresham, H. & Xiong, Y.Q. (2004) Regulation of virulence determinants *in vitro* and *in vivo* in *Staphylococcus aureus*. *FEMS Immunology & Medical Microbiology*, 40 (1): 1–9.
- Cheung, A.L., Nishina, K. A, Trottonda, M.P. & Tamber, S. (2008) The SarA protein family of *Staphylococcus aureus*. *The International Journal of Biochemistry & Cell Biology*, 40 (3): 355–61.
- Cheung, G.Y.C., Joo, H.-S., Chatterjee, S.S. & Otto, M. (2014) Phenol-soluble modulins-critical determinants of staphylococcal virulence. *FEMS Microbiology Reviews*. 38 (4), 698–719.
- Christine C. Winterbourn and Anthony J. Kettle. *Antioxidants & Redox Signaling*. 2013, 18(6): 642-660.
- Chu, V.H., Crosslin, D.R., Friedman, J.Y. & Reed, S.D. (2005) *Staphylococcus aureus* bacteremia in patients with prosthetic devices: costs and outcomes. *The American Journal of Medicine*, 118(12), 1416-e19.
- Clare, D.A., Blum, J. & Fridovich, I. (1984) A hybrid superoxide dismutase containing both functional iron and manganese. *Journal of Biological Chemistry*. 259 (9), 5932–5936.
- Clements, M.O., Watson, S.P. & Foster, S.J. (1999) Characterization of the major superoxide dismutase of *Staphylococcus aureus* and its role in starvation survival, stress resistance, and pathogenicity. *Journal of Bacteriology*. 181 (13), 3898–3903.
- Clohessy, P.A. & Golden, B.E. (1995) Calprotectin-mediated zinc chelation as a biostatic mechanism in host defence. *Scandinavian Journal of Immunology*. 42 (5), 551–556.
- Cooper, J.B., McIntyre, K., Badasso, M.O., Wood, S.P., Zhang, Y., Garbe, T.R. & Young, D. (1995) X-ray Structure Analysis of the Iron-dependent Superoxide Dismutase from *Mycobacterium tuberculosis* at 2.0 Ångstroms Resolution Reveals Novel Dimer–Dimer Interactions. *Journal of Molecular Biology*. 246 (4), 531–544.
- Corbin, B.D., Seeley, E.H., Raab, A., Feldmann, J., Miller, M.R., Torres, V.J., Anderson, K.L., Dattilo, B.M., Dunman, P.M., Gerads, R., Caprioli, R.M., Nacken, W., Chazin, W.J. & Skaar, E.P. (2008) Metal chelation and inhibition of bacterial growth in tissue abscesses. *Science*. 319 (5865), 962–965.
- Cosgrove, K., Coutts, G., Jonsson, I.M., Tarkowski, A., Kokai-Kun, J.F., Mond, J.J. & Foster, S.J. (2007) Catalase (KatA) and Alkyl Hydroperoxide Reductase (AhpC) Have Compensatory Roles in Peroxide Stress Resistance and Are Required for Survival, Persistence, and Nasal Colonization in *Staphylococcus aureus*. *Journal of Bacteriology*. 189 (3), 1025–1035.

- Cotruvo, J.A., Jr & Stubbe, J. (2012) Metalation and mismetalation of iron and manganese proteins in vitro and in vivo: the class I ribonucleotide reductases as a case study. *Metallomics*. 4 (10), 1020.
- Cue, D., Lei, M.G. & Lee, C.Y. (2012) Genetic regulation of the intercellular adhesion locus in staphylococci. *Frontiers in Cellular and Infection Microbiology*. (2), 38.
- Damo, S.M., Kehl-Fie, T.E., Sugitani, N., Holt, M.E., Rathi, S., Murphy, W.J., Zhang, Y., Betz, C., Hench, L., Fritz, G., Skaar, E.P. & Chazin, W.J. (2013) Molecular basis for manganese sequestration by calprotectin and roles in the innate immune response to invading bacterial pathogens. *Proceedings of the National Academy of Sciences*, 110(10), 3841-3846.
- Das, A. & Mukhopadhyay, C. (2009) Urea-mediated protein denaturation: a consensus view. *The Journal of Physical Chemistry*. 113 (38), 12816–12824.
- Davies, M.J. (2005) The oxidative environment and protein damage. *Biochimica et Biophysica Acta (BBA) - Proteins and Proteomics*. 1703 (2), 93–109.
- de Haas, C.J.C., Veldkamp, K.E., Peschel, A., Weerkamp, F., Van Wamel, W.J.B., Heezius, E.C.J.M., Poppelier, M.J.J.G., Van Kessel, K.P.M. & van Strijp, J.A.G. (2004) Chemotaxis Inhibitory Protein of *Staphylococcus aureus*, a Bacterial Antiinflammatory Agent. *The Journal of experimental medicine*. 199 (5), 687–695.
- de Oliveira, G.A.P. & Silva, J.L. (2015) A hypothesis to reconcile the physical and chemical unfolding of proteins. *Proceedings of the National Academy of Sciences*. 112 (21), E2775–84.
- De Vendittis, A., Amato, M., Mickiewicz, A., Parlato, G., De Angelis, A., Castellano, I., Rullo, R., Riccitiello, F., Rengo, S., Masullo, M. & De Vendittis, E. (2010) Regulation of the properties of superoxide dismutase from the dental pathogenic microorganism *Streptococcus mutans* by iron- and manganese-bound co-factor. *Molecular bioSystems*. 6 (10), 1973–1982.
- De Vendittis, A., Marco, S., Di Maro, A., Chambery, A., Albino, A., Masullo, M., Michniewicz, A., Parlato, G., De Angelis, A., De Vendittis, E. & Rullo, R. (2012) Properties of a putative cambialistic superoxide dismutase from the aerotolerant bacterium *Streptococcus thermophilus* Strain LMG 18311. *Protein & Peptide Letters*. 19 (3), 333–344.
- Dewitt, S.K. & Adelberg, E.A. (1962) The Occurrence of a genetic transposition in a strain of *Escherichia Coli*. *Genetics*. 47 (5), 577–585.
- Diederichs, K. & Karplus, P.A. (2013) Better models by discarding data? *Acta Crystallographica Section D: Biological Crystallography*. 69 (7), 1215–1222.
- Diekema, D.J., Pfaller, M.A., Schmitz, F.J., Smayevsky, J., Bell, J., Jones, R.N., Beach, M. SENTRY Participants Group (2001) Survey of Infections Due to Staphylococcus Species: Frequency of Occurrence and Antimicrobial Susceptibility of Isolates Collected in the United States, Canada, Latin America, Europe, and the Western Pacific Region for the SENTRY Antimicrobial Surveillance Program, 1997–1999. *Clinical Infectious Diseases*. 32 (2), S114–S132.

- Dinges, M.M., Orwin, P.M. & Schlievert, P.M. (2000) Exotoxins of *Staphylococcus aureus*. *Clinical Microbiology Reviews*. 13 (1), 16–34.
- Dudev, T. & Lim, C. (2013) Competition among metal ions for protein binding sites: determinants of metal ion selectivity in proteins. *Chemical reviews*, 114(1), 538-556.
- Dudev, T., Lin, Y.-L., Dudev, M. & Lim, C. (2003) First-second shell interactions in metal binding sites in proteins: a PDB survey and DFT/CDM calculations. *Journal of the American Chemical Society*. 125 (10), 3168–3180.
- DuMont, A.L. & Torres, V.J. (2014) Cell targeting by the *Staphylococcus aureus* pore-forming toxins: it's not just about lipids. *Trends in Microbiology*. 22 (1), 21–27.
- Dupont, C. L., Neupane, K., Shearer, J., & Palenik, B. (2008). Diversity, function and evolution of genes coding for putative Ni-containing superoxide dismutases. *Environmental microbiology*. 10(7), 1831-1843.
- Duthie, E. and Lorenz, L.L., 1952. Staphylococcal coagulase: mode of action and antigenicity. *Microbiology*, 6(1-2). 95-107.
- Eddy, R.S. (2001) HMMER: Profile hidden Markov models for biological sequence analysis. Available from: <http://hmmer.wustl.edu/>. (Accessed 19 September 2017).
- Edwards, R.A., Baker, H.M., Whittaker, M.M., Whittaker, J.W., Jameson, G.B. & Baker, E.N. (1998) Crystal structure of *Escherichia coli* manganese superoxide dismutase at 2.1-Å resolution. *JBIC Journal of Biological Inorganic Chemistry*. 3 (2), 161–171.
- Edwards, R.A., Whittaker, M.M., Whittaker, J.W., Baker, E.N. & Jameson, G.B. (2001a) Outer sphere mutations perturb metal reactivity in manganese superoxide dismutase. *Biochemistry*. 40 (1), 15–27.
- Edwards, R.A., Whittaker, M.M., Whittaker, J.W., Baker, E.N. & Jameson, G.B. (2001b) Removing a hydrogen bond in the dimer interface of *Escherichia coli* manganese superoxide dismutase alters structure and reactivity. *Biochemistry*. 40 (15), 4622–4632.
- EFSA (European Food Safety Authority) and ECDC (European Centre for Disease Prevention and Control), 2017. The European Union summary report on antimicrobial resistance in zoonotic and indicator bacteria from humans, animals and food in 2015. *EFSA Journal*. 15(2):4694,212
- Eiff, Von, C., Becker, K., Machka, K., Stammer, H. & Peters, G. (2001) Nasal carriage as a source of *Staphylococcus aureus* bacteremia. *New England Journal of Medicine*. 344 (1), 11–16.
- Elbir, H., Robert, C., Nguyen, T.T., Gimenez, G., Sanousi, El, S.M., Flock, J.-I., Raoult, D. & Drancourt, M. (2013) *Staphylococcus aureus* subsp. *anaerobius* strain ST1464 genome sequence. *Standards in Genomic Sciences*. 9 (1), 1–11.
- Emine Yikilmaz, Jason Porta, Laurie E Grove, Ardeschir Vahedi-Faridi, Yuriy Bronshteyn, Thomas C Brunold, Gloria E O Borgstahl, A. & Anne-Frances Miller (2007) How can a single

second sphere amino acid substitution cause reduction midpoint potential changes of hundreds of millivolts? *Journal of the American Chemical Society*. 129 (32), 9927–9940.

Emsley, P., Lohkamp, B., Scott, W.G. & Cowtan, K. (2010) Features and development of Coot. *Acta Crystallographica Section D: Biological Crystallography*. 66 (4), 486–501.

European Centre for Disease Prevention and Control (ECDC). (2015). Antimicrobial resistance surveillance in Europe 2015. Annual Report of the European Antimicrobial Resistance Surveillance Network (EARS-Net).

(<https://ecdc.europa.eu/sites/portal/files/media/en/publications/Publications/antimicrobial-resistance-europe-2015.pdf>, accessed 18 August 2017).

Evans, P.R. & Murshudov, G.N. (2013) How good are my data and what is the resolution? *Acta Crystallographica Section D: Biological Crystallography*. 69 (Pt 7), 1204–1214.

Fang, F.C. (2004) Antimicrobial reactive oxygen and nitrogen species: concepts and controversies. *Nature reviews. Microbiology*, 2(10), 820.

Feil, E.J., Cooper, J.E., Grundmann, H., Robinson, D.A., Enright, M.C., Berendt, T., Peacock, S.J., Smith, J.M., Murphy, M., Spratt, B.G., Moore, C.E. & Day, N.P.J. (2003) How clonal is *Staphylococcus aureus*? *Journal of Bacteriology*. 185 (11), 3307–3316.

Feng, Y., Chen, C.J., Su, L.H., Hu, S. & Yu, J. (2008) Evolution and pathogenesis of *Staphylococcus aureus*: lessons learned from genotyping and comparative genomics. *FEMS Microbiology Reviews*. 32(1), 23-37.

Fernandes, S., Geueke, B., Delgado, O., Coleman, J. & Hatti-Kaul, R. (2002) β -Galactosidase from a cold-adapted bacterium: purification, characterization and application for lactose hydrolysis. *Applied Microbiology and Biotechnology*. 58 (3), 313–321.

Fielden, E.M., Roberts, P.B., Bray, R.C., Lowe, D.J., Mautner, G.N., Rotilio, G. & Calabrese, L. (1974) Mechanism of action of superoxide dismutase from pulse radiolysis and electron paramagnetic resonance. Evidence that only half the active sites function in catalysis. *The Biochemical Journal*. 139 (1), 49–60.

Fink, R.C. & Scandalios, J.G. (2002) Molecular evolution and structure-function relationships of the superoxide dismutase gene families in angiosperms and their relationship to other eukaryotic and prokaryotic superoxide dismutases. *Archives of Biochemistry and Biophysics*. 399 (1), 19–36.

Fitzgerald, J. R., Sturdevant, D. E., Mackie, S. M., Gill, S. R. and Musser, J. M. (2001). Evolutionary genomics of *Staphylococcus aureus*: insights into the origin of methicillin-resistant strains and the toxic shock syndrome epidemic. *Proceedings of the National Academy of Sciences*. 98(15), 8821-8826.

Flint, D.H., Tuminello, J.F. & Emptage, M.H. (1993) The inactivation of Fe-S cluster containing hydro-lyases by superoxide. *The Journal of Biological Chemistry*. 268 (30), 22369–22376.

- Foster, T.J. (2017) Antibiotic resistance in *Staphylococcus aureus*. Current status and future prospects. FEMS Microbiology Reviews. 41 (3), 430–449.
- Foster, T.J. & Höök, M. (1998) Surface protein adhesins of *Staphylococcus aureus*. Trends in Microbiology. 6 (12), 484–488.
- Friedman, D.B., Stauff, D.L., Pishchany, G., Whitwell, C.W., Torres, V.J. & Skaar, E.P. (2006) *Staphylococcus aureus* redirects central metabolism to increase iron availability. PLoS Pathogens. 2 (8), e87.
- Frison, G. & Ohanessian, G. (2009) Metal-histidine-glutamate as a regulator of enzymatic cycles: a case study of carbonic anhydrase. Physical Chemistry Chemical Physics. 11(2), 374-383.
- Fuchs, S., Zühlke, D., Pané-Farré, J., Kusch, H., Wolf, C., Reiß, S., Binh, L.T.N., Albrecht, D., Riedel, K., Hecker, M. & Engelmann, S. (2013) Aureolib - a proteome signature library: towards an understanding of *Staphylococcus aureus* pathophysiology. PLOS ONE. 8 (8), e70669.
- Gagnon, D.M., Brophy, M.B., Bowman, S.E.J., Stich, T.A., Drennan, C.L., Britt, R.D. & Nolan, E.M. (2015) Manganese binding properties of human calprotectin under conditions of high and low calcium: X-ray crystallographic and advanced electron paramagnetic resonance spectroscopic analysis. Journal of the American Chemical Society. 137 (8), 3004–3016.
- Gao, R. & Stock, A.M. (2009) Biological insights from structures of two-component proteins. Annual Review of Microbiology. 63, 133-154.
- Garcia, Y.M., Barwinska-Sendra, A., Tarrant, E., Skaar, E.P., Waldron, K.J. & Kehl-Fie, T.E. (2017) A Superoxide dismutase capable of functioning with iron or manganese promotes the resistance of *Staphylococcus aureus* to calprotectin and nutritional immunity. PLoS Pathogens. 13 (1), e1006125.
- Gardete, S. & Tomasz, A. (2014) Mechanisms of vancomycin resistance in *Staphylococcus aureus*. The Journal of Clinical Investigation. 124(7), 2836.
- Garrity, G. M., Bell, J. A., & Lilburn, T. (2015). Epsilonproteobacteria class. nov In: Bergey's Manual® of Systematics of Archaea and Bacteria.
- Gätjens, J., Sjödin, M., Pecoraro, V.L. & Un, S. (2007) The Relationship between the Manganese(II) zero-field interaction and Mn(II)/Mn(III) redox potential of Mn(4'-X-terpy) complexes. Journal of the American Chemical Society. 129 (45), 13825–13827.
- Gaupp, R., Ledala, N., & Somerville, G. A. (2012). Staphylococcal response to oxidative stress. Frontiers in Cellular and Infection Microbiology. (2), 33
- Gordon, R.J. & Lowy, F.D. (2008) Pathogenesis of methicillin-resistant *Staphylococcus aureus* infection. Clinical Infectious Diseases. 46, S350-S359.
- Gort, A.S., Ferber, D.M., & Imlay, J.A. (1999) The regulation and role of the periplasmic copper, zinc superoxide dismutase of *Escherichia coli*. Molecular Microbiology. 32(1), 179-191.

- Gouy, M., Guindon, S. & Gascuel, O. (2010) SeaView version 4: A multiplatform graphical user interface for sequence alignment and phylogenetic tree building. *Molecular Biology and Evolution*. 27 (2), 221–224.
- Graveland, H., Duim, B., van Duijkeren, E., Heederik, D. & Wagenaar, J.A. (2011) Livestock-associated methicillin-resistant *Staphylococcus aureus* in animals and humans. *International Journal of Medical Microbiology*. 301 (8), 630–634.
- Greenleaf, W.B., Perry, J.J.P., Hearn, A.S., Cabelli, D.E., Lepock, J.R., Stroupe, M.E., Tainer, J.A., Nick, H.S. & Silverman, D.N. (2004) Role of hydrogen bonding in the active site of human manganese superoxide dismutase. *Biochemistry*. 43 (22), 7038–7045.
- Gregory E.M. (1985) Characterization of the O₂-induced manganese-containing superoxide dismutase from *Bacteroides fragilis*. *Archives of Biochemistry and Biophysics*. 238, 83-9.
- Gribenko, A., Mosyak, L., Ghosh, S., Parris, K., Svenson, K., Moran, J., Chu, L., Li, S., Liu, T., Woods, V.L., Jr., Jansen, K.U., Green, B.A., Anderson, A.S. & Matsuka, Y.V. (2013) Three-dimensional structure and biophysical characterization of *Staphylococcus aureus* cell surface antigen–manganese transporter MntC. *Journal of Molecular Biology*. 425 (18), 3429–3445.
- Grossoehme, N., Kehl-Fie, T.E., Ma, Z., Adams, K.W., Cowart, D.M., Scott, R.A., Skaar, E.P. & Giedroc, D.P. (2011) Control of copper resistance and inorganic sulfur metabolism by paralogous regulators in *Staphylococcus aureus*. *Journal of Biological Chemistry*. 286 (15), 13522–13531.
- Grove, L.E., Xie, J., Yikilmaz, E., Karapetyan, A., Miller, A.-F. & Brunold, T.C. (2008) Spectroscopic and computational insights into second-sphere amino-acid tuning of substrate analogue/active-site interactions in iron(III) superoxide dismutase. *Inorganic Chemistry*. 47 (10), 3993–4004.
- Hammer, N.D. & Skaar, E.P. (2011) Molecular mechanisms of *Staphylococcus aureus* iron acquisition. *Annual Review of Microbiology*. (65), 129–147.
- Handke, L.D., Hawkins, J.C., Miller, A.A., Jansen, K.U. & Anderson, A.S. (2013) Regulation of *Staphylococcus aureus* MntC expression and its role in response to oxidative stress. *PLOS ONE*. 8 (10), e77874.
- Hansch, C., Leo, A. & Taft, R.W. (1991) A survey of Hammett substituent constants and resonance and field parameters. *Chemical Reviews*. 91(2), 165-195.
- Harris, L.G., Foster, S.J. and Richards, R.G., 2002. An introduction to *Staphylococcus aureus*, and techniques for identifying and quantifying *S. aureus* adhesins in relation to adhesion to biomaterials: review. *European Cell and Materials*, 4(3), 39 – 60.
- Hartman, B.J. & Tomasz, A. (1984) Low-affinity penicillin-binding protein associated with beta-lactam resistance in *Staphylococcus aureus*. *Journal of Bacteriology*. 158 (2), 513–516.
- Haslinger-Löffler, B., Kahl, B.C., Grundmeier, M., Strangfeld, K., Wagner, B., Fischer, U., Cheung, A.L., Peters, G., Schulze-Osthoff, K. & Sinha, B. (2005) Multiple virulence factors are

required for *Staphylococcus aureus*-induced apoptosis in endothelial cells. *Cellular Microbiology*. 7 (8), 1087–1097.

Hassan, H. M., & Fridovich, I. (1977a). Regulation of the synthesis of superoxide dismutase in *Escherichia coli*. Induction by methyl viologen. *Journal of Biological Chemistry*. 252(21), 7667-7672.

Hassan, H. M., & Fridovich, I. (1977b). Enzymatic defenses against the toxicity of oxygen and of streptonigrin in *Escherichia coli*. *Journal of Bacteriology*. 129(3), 1574-1583.

Hearn, A.S., Fan, L., Lepock, J.R. & Luba, J.P. (2004) Amino acid substitution at the dimeric interface of human manganese superoxide dismutase. *Journal of Biological Chemistry*. 279(7), 5861-5866.

Hecker, M., Engelmann, S. & Cordwell, S.J. (2003) Proteomics of *Staphylococcus aureus*—current state and future challenges. *Journal of Chromatography B*. 787(1), 179-195.

Hecker, M., Reder, A., Fuchs, S. & Pagels, M. (2009) Physiological proteomics and stress/starvation responses in *Bacillus subtilis* and *Staphylococcus aureus*. *Research in Microbiology*. 160(4), 245-258.

Helmann, J.D. (2014) Specificity of metal sensing: iron and manganese homeostasis in *Bacillus subtilis*. *Journal of Biological Chemistry*. 289 (41), 28112–28120.

Henriques, I., Tacão, M., Leite, L., Fidalgo, C., Araújo, S., Oliveira, C. & Alves, A. (2016) Co-selection of antibiotic and metal(loid) resistance in gram-negative epiphytic bacteria from contaminated salt marshes. *Marine Pollution Bulletin*. 109 (1), 427–434.

Herbert, S., Bera, A., Nerz, C., Kraus, D., Peschel, A., Goerke, C., Götz, F. (2007). Molecular basis of resistance to muramidase and cationic antimicrobial peptide activity of lysozyme in staphylococci. *PLoS pathogens*. 3(7), e102.

Herbst, R.W., Guce, A., Bryngelson, P.A., Higgins, K.A., Ryan, K.C., Cabelli, D.E., Garman, S.C. & Maroney, M.J. (2009) Role of conserved tyrosine residues in NiSOD catalysis: a case of convergent evolution. *Biochemistry*. 48 (15), 3354–3369.

Hiramatsu, K., Hanaki, H., Ino, T., Yabuta, K., Oguri, T. & Tenover, F.C. (1997) Methicillin-resistant *Staphylococcus aureus* clinical strain with reduced vancomycin susceptibility. *The Journal of Antimicrobial Chemotherapy*. 40 (1), 135–136.

Holden, M. T., & Lindsay, J. A. (2008). Whole genomes: sequence, microarray and systems biology. *Staphylococcus: molecular genetics*. Caister Academic Press, Norfolk, UK, 1-28.

Holden, M.T.G., Hsu, L.Y., Kurt, K., Weinert, L.A., Mather, A.E., Harris, S.R., Strommenger, B., Layer, F., Witte, W., de Lencastre, H., Skov, R., Westh, H., Zemlickova, H., Coombs, G., Kearns, A.M., Hill, R.L.R., Edgeworth, J., Gould, I., Gant, V., et al. (2013) A genomic portrait of the emergence, evolution, and global spread of a methicillin-resistant *Staphylococcus aureus* pandemic. *Genome Research*. 23 (4), 653–664.

- Hong-Duk, Y., Eun-Ja, K., Jung-Hye, R., HAH, Y. C., & Sa-Ouk, K. (1996). A novel nickel-containing superoxide dismutase from *Streptomyces* spp. *Biochemical Journal*. 318(3), 889-896.
- Horsburgh, M.J., Aish, J.L., White, I.J., Shaw, L., Lithgow, J.K. & Foster, S.J. (2002) sigmaB modulates virulence determinant expression and stress resistance: characterization of a functional rsbU strain derived from *Staphylococcus aureus* 8325-4. *Journal of Bacteriology*. 184 (19), 5457–5467.
- Horsburgh, M.J., Clements, M.O., Crossley, H., Ingham, E. & Foster, S.J. (2001) PerR controls oxidative stress resistance and iron storage proteins and is required for virulence in *Staphylococcus aureus*. *Infection and Immunity*. 69 (6), 3744–3754.
- Horsburgh, M.J., Ingham, E. & Foster, S.J. (2001) In *Staphylococcus aureus*, Fur is an interactive regulator with PerR, contributes to virulence, and is necessary for oxidative stress resistance through positive regulation of catalase and iron homeostasis. *Journal of Bacteriology*. 183 (2), 468–475.
- Horsburgh, M.J., Wharton, S.J., Cox, A.G., Ingham, E., Peacock, S. & Foster, S.J. (2002) MntR modulates expression of the PerR regulon and superoxide resistance in *Staphylococcus aureus* through control of manganese uptake. *Molecular Microbiology*. 44 (5), 1269–1286.
- Horsburgh, M.J., Wharton, S.J., Karavolos, M. & Foster, S.J. (2002) Manganese: elemental defence for a life with oxygen. *Trends in microbiology*. 10(11), 496-501.
- Howard, B. J., & Kloss, W. E. (1987). *Staphylococci in clinical and pathogenic microbiology*. Edited by Howard BJ, Tilton RC. The CV Mosby Comp. St. Louis, 238.
- Hsu, J.-L., Hsieh, Y., Tu, C., O'Connor, D., Nick, H.S. & Silverman, D.N. (1996) Catalytic properties of human manganese superoxide dismutase. *Journal of Biological Chemistry*. 271 (30), 17687–17691.
- Hung, H.C. & Chang, G.G. (2001) Differentiation of the slow-binding mechanism for magnesium ion activation and zinc ion inhibition of human placental alkaline phosphatase. *Protein Science*. 10 (1), 34–45.
- Hunter, T., Bannister, J.V. & Hunter, G.J. (2002) Thermostability of manganese- and iron-superoxide dismutases from *Escherichia coli* is determined by the characteristic position of a glutamine residue. *The FEBS Journal*. 269 (21), 5137–5148.
- Hurd, A.F., Garcia-Lara, J., Rauter, Y., Cartron, M., Mohamed, R. and Foster, S.J., 2012. The iron-regulated surface proteins IsdA, IsdB, and IsdH are not required for heme iron utilization in *Staphylococcus aureus*. *FEMS Microbiology Letters*. 329(1),93-100.
- Huseby, M., Shi, K., Brown, C.K., Digre, J., Mengistu, F., Seo, K.S., Bohach, G.A., Schlievert, P.M., Ohlendorf, D.H. & Earhart, C.A. (2007) Structure and biological activities of beta toxin from *Staphylococcus aureus*. *Journal of Bacteriology*. 189 (23), 8719–8726.

- Huttenhower, C., Gevers, D., Knight, R., Abubucker, S., Badger, J.H., Chinwalla, A.T., Creasy, H.H., Earl, A.M., FitzGerald, M.G., Fulton, R.S. and Giglio, M.G., 2012. Structure, function and diversity of the healthy human microbiome. *Nature*, 486(7402), 207-214.
- Imlay, J.A. (2006) Iron-sulphur clusters and the problem with oxygen. *Molecular Microbiology*. 59 (4), 1073–1082.
- Imlay, J.A. (2008) Cellular defenses against superoxide and hydrogen peroxide. *Annual Review of Biochemistry*. (77), 755–776.
- Imlay, J.A. & Linn, S. (1987) Mutagenesis and stress responses induced in *Escherichia coli* by hydrogen peroxide. *Journal of Bacteriology*. 169 (7), 2967–2976.
- Imlay, K. R., & Imlay, J. A. (1996). Cloning and analysis of *sodC*, encoding the copper-zinc superoxide dismutase of *Escherichia coli*. *Journal of Bacteriology*. 178(9), 2564-2571.
- Inkinen, J., Mäkinen, R., Keinänen-Toivola, M.M., Nordström, K. & Ahonen, M. (2016) Copper as an antibacterial material in different facilities. *Letters in Applied Microbiology*. 64 (1), 19–26.
- Irving, H. & Williams, R. (1953) 637. The stability of transition-metal complexes. *Journal of the Chemical Society*. 3192-3210.
- Ito, T., Okuma, K., Ma, X.X., Yuzawa, H. & Hiramatsu, K. (2003) Insights on antibiotic resistance of *Staphylococcus aureus* from its whole genome: genomic island SCC. *Drug Resistance Updates*. 6(1), 41-52.
- Jackson, T.A., Karapetian, A., Miller, A.-F. & Brunold, T.C. (2004) Spectroscopic and computational studies of the azide-adduct of manganese superoxide dismutase: definitive assignment of the ligand responsible for the low-temperature thermochromism. *Journal of the American Chemical Society*. 126 (39), 12477–12491.
- Jamal El Yazal, Rachel R Roe, A. & Pang, Y.-P. (2000) Zinc's affect on proton transfer between imidazole and acetate predicted by ab initio calculations. *The Journal of Physical Chemistry B*. 104(28), 6662-6667.
- Jang, S. & Imlay, J.A. (2007) Micromolar intracellular hydrogen peroxide disrupts metabolism by damaging iron-sulfur enzymes. *Journal of Biological Chemistry*. 282 (2), 929–937.
- Jenkinson, H.F. & Jakubovics, N.S. (2001) Out of the iron age: new insights into the critical role of manganese homeostasis in bacteria. *Microbiology*. 147 (7), 1709–1718.
- Jensen, S.O. & Lyon, B.R. (2009) Genetics of antimicrobial resistance in *Staphylococcus aureus*. *Future Microbiology*. 4 (5), 565–582.
- John P Lisher, D.P.G. (2013) Manganese acquisition and homeostasis at the host-pathogen interface. *Frontiers in Cellular and Infection Microbiology*. (3), 91
- Joint scientific report of ECDC, EFSA and EMEA on meticillin resistant *Staphylococcus aureus* (MRSA) in livestock, companion animals and foods. (2009). 301, 1-10.

- Johnson, D.A. and Nelson, P.G., 1995. Factors determining the ligand field stabilization energies of the hexaaqua 2+ complexes of the first transition series and the Irving-Williams order. *Inorganic Chemistry*. 34(22), 5666-5671.
- Joosten, R.P., Joosten, K., Murshudov, G.N. & Perrakis, A. (2012) PDB_REDO: constructive validation, more than just looking for errors. *Acta Crystallographica Section D: Biological Crystallography*. 68 (4), 484–496.
- Kabsch, W. (2010) XDS. *Acta Crystallographica Section D: Biological Crystallography*. 66 (2), 125–132.
- Karavolos, M.H., Horsburgh, M.J., Ingham, E. & Foster, S.J. (2003) Role and regulation of the superoxide dismutases of *Staphylococcus aureus*. *Microbiology*. 149 (10), 2749–2758.
- Karplus, P.A. & Diederichs, K. (2012) Linking crystallographic model and data quality. *Science*. 336 (6084), 1030–1033.
- Kato, T., Kouzaki, H., Matsumoto, K., Hosoi, J., & Shimizu, T. (2017). The effect of calprotectin on TSLP and IL-25 production from airway epithelial cells. *Allergy International*. 66(2), 281-289.
- Katoh, K. & Standley, D.M. (2013) MAFFT multiple sequence alignment software version 7: improvements in performance and usability. *Molecular Biology and Evolution*. 30 (4), 772–780.
- Keele, B. B., McCord, J. M., & Fridovich, I. (1970). Superoxide dismutase from *Escherichia coli* B a new manganese-containing enzyme. *Journal of Biological Chemistry*. 245(22), 6176-6181.
- Kehl-Fie, T.E. & Skaar, E.P. (2010) Nutritional immunity beyond iron: a role for manganese and zinc. *Current Opinion in Chemical Biology*. 14 (2), 218–224.
- Kehl-Fie, T.E., Chitayat, S., Hood, M.I., Damo, S., Restrepo, N., Garcia, C., Munro, K.A., Chazin, W.J. & Skaar, E.P. (2011) Nutrient metal sequestration by calprotectin inhibits bacterial superoxide defense, enhancing neutrophil killing of *Staphylococcus aureus*. *Cell Host and Microbe*. 10 (2), 158–164.
- Kehl-Fie, T.E., Zhang, Y., Moore, J.L., Farrand, A.J., Hood, M.I., Rathi, S., Chazin, W.J., Caprioli, R.M. & Skaar, E.P. (2013) MntABC and MntH contribute to systemic *Staphylococcus aureus* infection by competing with calprotectin for nutrient manganese. *Infection and Immunity*. 81 (9), 3395–3405.
- Keyer, K. & Imlay, J.A. (1996) Superoxide accelerates DNA damage by elevating free-iron levels. *Proceedings of the National Academy of Sciences*. 93 (24), 13635–13640.
- Keyer, K., Keyer, K., Gort, A.S., Gort, A.S., Imlay, J.A. & Imlay, J.A. (1995) Superoxide and the production of oxidative DNA damage. *Journal of Bacteriology*. 177 (23), 6782–6790.

- Kim, H.K., DeDent, A., Cheng, A.G., McAdow, M., Bagnoli, F., Missiakas, D.M. & Schneewind, O. (2010) IsdA and IsdB antibodies protect mice against *Staphylococcus aureus* abscess formation and lethal challenge. *Vaccine*. 28 (38), 6382–6392.
- Kirby, T., Blum, J., Kahane, I. & Fridovich, I. (1980) Distinguishing between Mn-containing and Fe-containing superoxide dismutases in crude extracts of cells. *Archives of Biochemistry and Biophysics*. 201 (2), 551–555.
- Kirschvink, J.L., Gaidos, E.J., Bertani, L.E., Beukes, N.J., Gutzmer, J., Maepa, L.N. & Steinberger, R.E. (2000) Paleoproterozoic snowball Earth: Extreme climatic and geochemical global change and its biological consequences. *Proceedings of the National Academy of Sciences*. 97 (4), 1400–1405.
- Kloos, W.E. (1980) Natural populations of the genus *Staphylococcus*. *Annual Reviews in Microbiology*, 34(1), 559-592.
- Knight, G.M., Budd, E.L., Whitney, L., Thornley, A., Al-Ghusein, H., Planche, T. & Lindsay, J.A. (2012) Shift in dominant hospital-associated methicillin-resistant *Staphylococcus aureus* (HA-MRSA) clones over time. *Journal of Antimicrobial Chemotherapy*. 67 (10), 2514–2522.
- Kohler, T., Weidenmaier, C., & Peschel, A. (2009). Wall teichoic acid protects *Staphylococcus aureus* against antimicrobial fatty acids from human skin. *Journal of bacteriology*, 191(13), 4482-4484.
- Kreiswirth, B.N., Löfdahl, S., Betley, M.J. & O'Reilly, M. (1983) The toxic shock syndrome exotoxin structural gene is not detectably transmitted by a prophage. *Nature*. 305(5936), 709-712.
- Krismer, B., Weidenmaier, C., Zipperer, A., & Peschel, A. (2017). The commensal lifestyle of *Staphylococcus aureus* and its interactions with the nasal microbiota. *Nature Reviews Microbiology*. 15(11), 675.
- Krissinel, E. & Henrick, K. (2007) Inference of macromolecular assemblies from crystalline state. *Journal of Molecular Biology*. 372(3), 774-797.
- Kuklin, N.A., Clark, D.J., Secore, S., Cook, J., Cope, L.D., McNeely, T., Noble, L., Brown, M.J., Zorman, J.K., Wang, X.M., Pancari, G., Fan, H., Isett, K., Burgess, B., Bryan, J., Brownlow, M., George, H., Mainz, M., Liddell, M.E., et al. (2006) A novel *Staphylococcus aureus* vaccine: iron surface determinant B induces rapid antibody responses in rhesus macaques and specific increased survival in a murine *S. aureus* sepsis model. *Infection and Immunity*. 74 (4), 2215–2223.
- Kullik, I. & Giachino, P. (1997) The alternative sigma factor σ_B in *Staphylococcus aureus*: regulation of the sigB operon in response to growth phase and heat shock. *Archives of Microbiology*. 167 (2-3), 151–159.

- Kuroda, M., Hayashi, H. & Ohta, T. (1999) Chromosome-determined zinc-responsible operon *czr* in *Staphylococcus aureus* strain 912. *Microbiology and Immunology*. 43 (2), 115–125.
- Kuroda, M., Ohta, T., Uchiyama, I., Baba, T., Yuzawa, H., Kobayashi, I., Cui, L., Oguchi, A., Aoki, K., Nagai, Y., Lian, J., Ito, T., Kanamori, M., Matsumaru, H., Maruyama, A., Murakami, H., Hosoyama, A., Mizutani-Ui, Y., Takahashi, N.K., et al. (2001) Whole genome sequencing of methicillin-resistant *Staphylococcus aureus*. *Lancet*. 357 (9264), 1225–1240.
- Kwasigroch J.M., Wintjens R., Gillis D., Rooman M. (2008) SODA: An Mn/Fe superoxide dismutase prediction and design server. *BMC Bioinformatics*. 9, 257.
- La Fuente, De, R., Suarez, G. & Schleifer, K.H. (1985) *Staphylococcus aureus* subsp. *anaerobius* subsp. nov., the causal agent of abscess disease of sheep. *International Journal of Systematic Bacteriology*. 35 (1), 99–102.
- Ladhani, S., Joannou, C.L., Lochrie, D.P., Evans, R.W. & Poston, S.M. (1999) Clinical, microbial, and biochemical aspects of the exfoliative toxins causing staphylococcal scalded-skin syndrome. *Clinical Microbiology Reviews*. 12 (2), 224–242.
- Lah, M.S., Dixon, M.M., Patridge, K.A., Stallings, W.C., Fee, J.A. & Ludwig, M.L. (1995) Structure-function in *Escherichia coli* iron superoxide dismutase: comparisons with the manganese enzyme from *Thermus thermophilus*. *Biochemistry*. 34 (5), 1646–1660.
- Lamarre, C., LeMay, J.D., Deslauriers, N. & Bourbonnais, Y. (2001) *Candida albicans* expresses an unusual cytoplasmic manganese-containing superoxide dismutase (SOD3 gene product) upon the entry and during the stationary phase. *Journal of Biological Chemistry*. 276 (47), 43784–43791.
- Lamers, R.P., Muthukrishnan, G., Castoe, T.A., Tafur, S., Cole, A.M. & Parkinson, C.L. (2012) Phylogenetic relationships among *Staphylococcus* species and refinement of cluster groups based on multilocus data. *BMC Evolutionary Biology*. 12 (1), 71.
- Lancaster, V. L., LoBrutto, R., Selvaraj, F. M., & Blankenship, R. E. (2004). A cambialistic superoxide dismutase in the thermophilic photosynthetic bacterium *Chloroflexus aurantiacus*. *Journal of Bacteriology*. 186(11), 3408-3414.
- Lartillot, N., Lepage, T. & Blanquart, S. (2009) PhyloBayes 3: a Bayesian software package for phylogenetic reconstruction and molecular dating. *Bioinformatics*. 25 (17), 2286–2288.
- Laskowski, R.A. & Chistyakov, V.V. (2005) PDBsum more: new summaries and analyses of the known 3D structures of proteins and nucleic acids. *Nucleic Acids Research*. 33, D266-D268.
- Le, K. Y., & Otto, M. (2015). Quorum-sensing regulation in staphylococci—an overview. *Frontiers in microbiology*. 6, 1174.
- Lebedev, A.A., Vagin, A.A. & Murshudov, G.N. (2008) Model preparation in MOLREP and examples of model improvement using X-ray data. *Acta Crystallographica Section D: Biological Crystallography*. 64 (1), 33–39.

- Lee, J.-W. & Helmann, J.D. (2006) The PerR transcription factor senses H₂O₂ by metal-catalysed histidine oxidation. *Nature*. 440 (7082), 363–367.
- Lentino, J.R. (2003) Prosthetic joint infections: bane of orthopedists, challenge for infectious disease specialists. *Clinical Infectious Diseases*. 36 (9), 1157–1161.
- Lévêque, V.J., Stroupe, M.E., Lepock, J.R., Cabelli, D.E., Tainer, J.A., Nick, H.S. & Silverman, D.N. (2000) Multiple replacements of glutamine 143 in human manganese superoxide dismutase: effects on structure, stability, and catalysis. *Biochemistry*. 39 (24), 7131–7137.
- Li, L.-G., Xia, Y., & Zhang, T. (2017). Co-occurrence of antibiotic and metal resistance genes revealed in complete genome collection. *The ISME Journal*. 11, 651–662.
- Li, Y. X., Xiong, X., Chun-ye, L., Feng-song, Z., Wei, L., & Wei, H. (2010). Cadmium in animal production and its potential hazard on Beijing and Fuxin farmlands. *Journal of Hazardous Materials*. 177(1), 475–480.
- Lindsay, J.A. (2010) Genomic variation and evolution of *Staphylococcus aureus*. *International Journal of Medical Microbiology*. 300(2), 98-103.
- Lindsay, J.A. & Foster, S.J. (2001) zur: a Zn²⁺-responsive regulatory element of *Staphylococcus aureus*. *Microbiology*. 147 (5), 1259–1266.
- Lindsay, J.A. & Holden, M. (2006) Understanding the rise of the superbug: investigation of the evolution and genomic variation of *Staphylococcus aureus*. *Functional & Integrative Genomics*. 6(3), 186-201.
- Lindsay, J.A. & Holden, M.T.G. (2004) *Staphylococcus aureus*: superbug, super genome? *Trends in Microbiology*. 12 (8), 378–385.
- Liu, C., Bayer, A., Cosgrove, S.E., Daum, R.S., Fridkin, S.K., Gorwitz, R.J., Kaplan, S.L., Karchmer, A.W., Levine, D.P., Murray, B.E., Rybak, M.J., Talan, D.A. & Chambers, H.F. (2011) Clinical practice guidelines by the infectious diseases society of america for the treatment of methicillin-resistant *Staphylococcus aureus* infections in adults and children. *Clinical Infectious Diseases*. 52 (3), e18–e55.
- Liu, G.Y., Essex, A., Buchanan, J.T., Datta, V., Hoffman, H.M., Bastian, J.F., Fierer, J. & Nizet, V. (2005) *Staphylococcus aureus* golden pigment impairs neutrophil killing and promotes virulence through its antioxidant activity. *The Journal of Experimental Medicine*. 202 (2), 209–215.
- Liu, P., Ewis, H.E., Huang, Y.J., Lu, C.D., Tai, P.C. & Weber, I.T. (2007) Structure of *Bacillus subtilis* superoxide dismutase. *Acta Crystallographica Section F Structural Biology and Crystallization Communications*. 63 (12), 1003–1007.
- Lowy, F.D. (1998) *Staphylococcus aureus* Infections. *New England Journal of Medicine*. 339 (8), 520–532.

- Ludwig, M.L., Metzger, A.L., Pattridge, K.A. & Stallings, W.C. (1991) Manganese superoxide dismutase from *Thermus thermophilus*. A structural model refined at 1.8 Å resolution. *Journal of Molecular Biology*. 219 (2), 335–358.
- Lushchak, V.I. (2001) Oxidative stress and mechanisms of protection against it in bacteria. *Biochemistry*. 66 (5), 476–489.
- Macomber, L. & Imlay, J.A. (2009) The iron-sulfur clusters of dehydratases are primary intracellular targets of copper toxicity. *Proceedings of the National Academy of Sciences*. 106 (20), 8344–8349.
- Mäder, U., Nicolas, P., Depke, M., Pané-Farré, J., Debarbouille, M., van der Kooi-Pol, M.M., Guérin, C., Dérozier, S., Hiron, A., Jarmer, H., Leduc, A., Michalik, S., Reilman, E., Schaffer, M., Schmidt, F., Bessières, P., Noirot, P., Hecker, M., Msadek, T. (2016) *Staphylococcus aureus* transcriptome architecture: from laboratory to infection-mimicking conditions. *PLOS Genetics*. 12 (4), e1005962.
- Majerczyk, C.D., Dunman, P.M., Luong, T.T., Lee, C.Y., Sadykov, M.R., Somerville, G.A., Bodi, K. & Sonenshein, A.L. (2010) Direct targets of CodY in *Staphylococcus aureus*. *Journal of Bacteriology*. 192 (11), 2861–2877.
- Makris, G. (2004) The hyaluronate lyase of *Staphylococcus aureus* - a virulence factor? *Microbiology*. 150 (6), 2005–2013.
- Malachowa, N. & DeLeo, F.R. (2010) Mobile genetic elements of *Staphylococcus aureus*. *Cellular and Molecular Life Sciences*. 67 (18), 3057–3071.
- Malachowa, N., Whitney, A.R., Kobayashi, S.D., Sturdevant, D.E., Kennedy, A.D., Braughton, K.R., Shabb, D.W., Diep, B.A., Chambers, H.F., Otto, M. & DeLeo, F.R. (2011) Global changes in *Staphylococcus aureus* gene expression in human blood. *PLOS ONE*. 6 (4), e18617.
- Maltezou, H.C. & Giamarellou, H. (2006) Community-acquired methicillin-resistant *Staphylococcus aureus* infections. *International Journal of Antimicrobial Agents*. 27(2), 87-96.
- Mandell, G.L. (1975) Catalase, superoxide dismutase, and virulence of *Staphylococcus aureus*. *In vitro* and *in vivo* studies with emphasis on staphylococcal-leukocyte interaction. *Journal of Clinical Investigation*. 55 (3), 561–566.
- Mandelli, F. & Cairo, J.F. (2013) The characterization of a thermostable and cambialistic superoxide dismutase from *Thermus filiformis*. *Letters in Applied Microbiology*. 57(1), 40-46.
- Mariotti, P., Malito, E., Biancucci, M., Surdo, Lo, P., Mishra, R.P.N., Nardi-Dei, V., Savino, S., Nissum, M., Spraggon, G., Grandi, G., Bagnoli, F. & Bottomley, M.J. (2013) Structural and functional characterization of the *Staphylococcus aureus* virulence factor and vaccine candidate FhuD2. *The Biochemical Journal*. 449 (3), 683–693.
- Marshall, C. & McBryde, E. (2014) The role of *Staphylococcus aureus* carriage in the pathogenesis of bloodstream infection. *BMC Research Notes*. 7 (1), 428.

- Martin M.E., Byers B.R., Olson M.O., Salin M.L., Arceneaux J.E., Tolbert C. (1986) A *Streptococcus mutans* superoxide dismutase that is active with either manganese or iron as a cofactor. *Journal of Biological Chemistry*. 261 (20), 9361-7.
- Martins-Costa, M.T.C., Anglada, J.M., Francisco, J.S. & Ruiz-Lopez, M.F. (2012) Reactivity of atmospherically relevant small radicals at the air-water interface. *Angewandte Chemie International Edition*. 51 (22), 5413–5417.
- Mashruwala, A.A. & Boyd, J.M. (2017) The *Staphylococcus aureus* SrrAB regulatory system modulates hydrogen peroxide resistance factors, which imparts protection to aconitase during aerobic growth. *PLOS ONE*. 12 (1), e0170283.
- Masse, E. & Gottesman, S. (2002) A small RNA regulates the expression of genes involved in iron metabolism in *Escherichia coli*. *Proceedings of the National Academy of Sciences*. 99 (7), 4620–4625.
- Matsumoto T., Terauchi K., Isobe T., Matsuoka K., Yamakura F. (1991) Iron- and manganese-containing superoxide dismutases from *Methylobionas*: identity of the protein moiety and amino acid sequence. *Biochemistry*. 30, 3210-6.
- Mazmanian, S.K., Skaar, E.P., Gaspar, A.H., Humayun, M., Gornicki, P., Jelenska, J., Joachmiak, A., Missiakas, D.M. & Schneewind, O. (2003) Passage of heme-iron across the envelope of *Staphylococcus aureus*. *Science*. 299 (5608), 906–909.
- McCord, J. M., & Fridovich, I. (1969). Superoxide dismutase an enzymic function for erythrocyte hemocuprein. *Journal of Biological Chemistry*, 244(22), 6049-6055.
- McCoy, A.J., Grosse-Kunstleve, R.W., Adams, P.D., Winn, M.D., Storoni, L.C. & Read, R.J. (2007) Phaser crystallographic software. *Journal of Applied Crystallography*. 40 (4), 658–674.
- McGuinness, W., Kobayashi, S. & DeLeo, F. (2016) Evasion of neutrophil killing by *Staphylococcus aureus*. *Pathogens*. 5 (1), 32.
- Meier B., Barra D., Bossa F., Calabrese L., Rotilio G. (1982) Synthesis of either Fe- or Mn-superoxide dismutase with an apparently identical protein moiety by an anaerobic bacterium dependent on the metal supplied. *Journal of Biological Chemistry*. 257 (23), 13977-80.
- Meier, B., Parak, F., Desideri, A. & Rotilio, G. (1997) Comparative stability studies on the iron and manganese forms of the cambialistic superoxide dismutase from *Propionibacterium shermanii*. *FEBS Letters*. 414 (1), 122–124.
- Merchant, A.T. & Spatafora, G.A. (2014) A role for the DtxR family of metalloregulators in gram-positive pathogenesis. *Molecular Oral Microbiology*. 29 (1), 1–10.
- Merlino, A., Russo Krauss, I., Castellano, I., Ruocco, M.R., Capasso, A., De Vendittis, E., Rossi, B. & Sica, F. (2014) Structural and denaturation studies of two mutants of a cold adapted superoxide dismutase point to the importance of electrostatic interactions in protein stability. *Biochimica et Biophysica Acta (BBA)-Proteins and Proteomics*. 1844 (3), 632–640.

- Merriman, J.A., Klingelhutz, A.J., Diekema, D.J., Leung, D.Y.M. & Schlievert, P.M. (2015) Novel *Staphylococcus aureus* secreted protein alters keratinocyte proliferation and elicits a proinflammatory response *in vitro* and *in vivo*. *Biochemistry*. 54 (31), 4855–4862.
- Miller, A.-F. (2008) Redox tuning over almost 1 V in a structurally conserved active site: lessons from Fe-containing superoxide dismutase. *Accounts of Chemical Research*. 41 (4), 501–510.
- Miller, A.-F. (2012) Superoxide dismutases: ancient enzymes and new insights. *FEBS Letters*. 586 (5), 585–595.
- Miller, A.-F. & Wang, T. (2017) A single outer-sphere mutation stabilizes apo-mn superoxide dismutase by 35 °C and disfavors mn binding. *Biochemistry*. 56 (29), 3787–3799.
- Miller, A.-F., Padmakumar, K., Sorkin, D.L., Karapetian, A. & Vance, C.K. (2003) Proton-coupled electron transfer in Fe-superoxide dismutase and Mn-superoxide dismutase. *Journal of Inorganic Biochemistry*. 93 (1-2), 71–83.
- Miller, L.G. & Diep, B.A. (2008) Colonization, Fomites, and Virulence: Rethinking the pathogenesis of community-associated methicillin-resistant *Staphylococcus aureus* infection. *Clinical Infectious Diseases*. 46 (5), 752–760.
- Mishra, R.P.N., Mariotti, P., Fiaschi, L., Nosari, S., Maccari, S., Liberatori, S., Fontana, M.R., Pezzicoli, A., De Falco, M.G., Falugi, F., Altindis, E., Serruto, D., Grandi, G. & Bagnoli, F. (2012) *Staphylococcus aureus* FhuD2 is involved in the early phase of staphylococcal dissemination and generates protective immunity in mice. *Journal of Infectious Diseases*. 206 (7), 1041–1049.
- Mizuno, K., Whittaker, M.M., Bächinger, H.P. & Whittaker, J.W. (2004) Calorimetric studies on the tight binding metal interactions of *Escherichia coli* manganese superoxide dismutase. *Journal of Biological Chemistry*. 279 (26), 27339–27344.
- Monk, I.R., Shah, I.M., Xu, M., Tan, M.-W. & Foster, T.J. (2012) Transforming the untransformable: application of direct transformation to manipulate genetically *Staphylococcus aureus* and *Staphylococcus epidermidis*. *mBio*. 3 (2), e00277-11
- Morrissey, J.A., Cockayne, A., Brummell, K. & Williams, P. (2004) The staphylococcal ferritins are differentially regulated in response to iron and manganese and via PerR and Fur. *Infection and Immunity*. 72 (2), 972–979.
- Morrissey, J.A., Cockayne, A., Hill, P.J. & Williams, P. (2000) Molecular cloning and analysis of a putative siderophore ABC transporter from *Staphylococcus aureus*. *Infection and Immunity*. 68 (11), 6281–6288.
- Murshudov, G.N., Skubák, P., Lebedev, A.A., Pannu, N.S., Steiner, R.A., Nicholls, R.A., Winn, M.D., Long, F. & Vagin, A.A. (2011) REFMAC5 for the refinement of macromolecular crystal structures. *Acta Crystallographica Section D: Biological Crystallography*. 67 (4), 355–367.
- Nakashige, T.G., Zhang, B., Krebs, C. & Nolan, E.M. (2015) Human calprotectin is an iron-sequestering host-defense protein. *Nature Chemical Biology*. 11 (10), 765–771.

- Nakashige, T.G., Zygiel, E.M., Drennan, C.L. & Nolan, E.M. (2017) Nickel sequestration by the host-defense protein human calprotectin. *Journal of the American Chemical Society*. 139 (26), 8828–8836.
- Nathan, C. & Shiloh, M.U. (2000) Reactive oxygen and nitrogen intermediates in the relationship between mammalian hosts and microbial pathogens. *Proceedings of the National Academy of Sciences of the United States of America*. 97 (16), 8841–8848.
- Nemeth, E. (2002) Hepcidin, a putative mediator of anemia of inflammation, is a type II acute-phase protein. *Blood*. 101 (7), 2461–2463.
- Nemeth, E. (2004) Hepcidin regulates cellular iron efflux by binding to ferroportin and inducing its internalization. *Science*. 306 (5704), 2090–2093.
- Notredame, C., Higgins, D.G. & Heringa, J. (2000) T-Coffee: A novel method for fast and accurate multiple sequence alignment. *Journal of Molecular Biology*. 302 (1), 205–217.
- O'Neill, A.J. (2010) *Staphylococcus aureus* SH1000 and 8325-4: comparative genome sequences of key laboratory strains in staphylococcal research. *Letters in Applied Microbiology*. 51(3), 358-361.
- O'Riordan, K. & Lee, J.C. (2004) *Staphylococcus aureus* capsular polysaccharides. *Clinical Microbiology Reviews*. 17(1), 218-234.
- Ogston, A. (1881) Report upon micro-organisms in surgical diseases. *British Medical Journal*. 1 (1054), 369.b2–375.
- Okuma, K., Iwakawa, K., Turnidge, J.D., Grubb, W.B., Bell, J.M., O'Brien, F.G., Coombs, G.W., Pearman, J.W., Tenover, F.C., Kapi, M., Tiensasitorn, C., Ito, T. & Hiramatsu, K. (2002) Dissemination of new methicillin-resistant *Staphylococcus aureus* clones in the community. *Journal of Clinical Microbiology*. 40 (11), 4289–4294.
- Osawa, M., Yamakura, F., Mihara, M., Okubo, Y., Yamada, K. & Hiraoka, B.Y. (2010) Conversion of the metal-specific activity of *Escherichia coli* Mn-SOD by site-directed mutagenesis of Gly165Thr. *Biochimica et Biophysica Acta*. 1804 (9), 1775–1779.
- Ose, D. E., & Fridovich, I. (1979). Manganese-containing superoxide dismutase from *Escherichia coli*: reversible resolution and metal replacements. *Archives of Biochemistry and Biophysics*. 194(2), 360-364.
- Ose, D.E. & Fridovich, I. (1976) Superoxide dismutase. Reversible removal of manganese and its substitution by cobalt, nickel or zinc. *Journal of Biological Chemistry*. 251 (4), 1217–1218.
- Ose, D.E. & Fridovich, I. (1979) Manganese-containing superoxide dismutase from *Escherichia coli*: reversible resolution and metal replacements. *Archives of Biochemistry and Biophysics*. 194(2), 360-364.

- Otto, M. (2010) Basis of virulence in community-associated methicillin-resistant *Staphylococcus aureus*. Annual review of microbiology. 64:143–162.
- Otto, M. (2013) Community-associated MRSA: what makes them special? International Journal of Medical Microbiology, 303(6), 324-330.
- Outten, C.E. & O'Halloran, T.V. (2001) Femtomolar sensitivity of metalloregulatory proteins controlling zinc homeostasis. Science. 292 (5526), 2488–2492.
- Pagels, M., Fuchs, S., Pané-Farré, J., Kohler, C., Menschner, L., Hecker, M., McNamarra, P.J., Bauer, M.C., Wachenfeldt, von, C., Liebeke, M., Lalk, M., Sander, G., Eiff, Von, C., Proctor, R.A. & Engelmann, S. (2010) Redox sensing by a Rex-family repressor is involved in the regulation of anaerobic gene expression in *Staphylococcus aureus*. Molecular Microbiology. 76 (5), 1142–1161.
- Pal, C., Bengtsson-Palme, J., Kristiansson, E., & Larsson, D. G. J. (2015). Co-occurrence of resistance genes to antibiotics, biocides and metals reveals novel insights into their co-selection potential. BMC Genomics. 16(1), 964.
- Pal, C., Bengtsson-Palme, J., Kristiansson, E., & Larsson, D. G. J. (2016). The Structure and diversity of human, animal and environmental resistomes. Microbiome. 4(1), 54.
- Pané-Farré, J., Jonas, B., Förstner, K. & Engelmann, S. (2006) The σ B regulon in *Staphylococcus aureus* and its regulation. International Journal of Medical Microbiology. 296(4), 237-258.
- Parker M.W., Blake C.C. (1988) Iron- and manganese-containing superoxide dismutases can be distinguished by analysis of their primary structures. FEBS Letters. 229(2), 377-82.
- Peacock, S.J., de Silva, I. & Lowy, F.D. (2001) What determines nasal carriage of *Staphylococcus aureus*? Trends in Microbiology. 9 (12), 605–610.
- Peacock, S.J., Justice, A., Griffiths, D., de Silva, G.D.I., Kantzanou, M.N., Crook, D., Sleeman, K. & Day, N.P.J. (2003) Determinants of acquisition and carriage of *Staphylococcus aureus* in infancy. Journal of Clinical Microbiology. 41(12), 5718-5725.
- Peake, S.L., Peter, J.V., Chan, L., Wise, R.P., Butcher, A.R. & Grove, D.I. (2006) First report of septicemia caused by an obligately anaerobic *Staphylococcus aureus* infection in a human. Journal of Clinical Microbiology. 44 (6), 2311–2313.
- Pearson, W.R. (2013) Selecting the Right Similarity-Scoring Matrix. Current Protocols in Bioinformatics. 3-5.
- Pennella, M.A., Arunkumar, A.I. & Giedroc, D.P. (2006) Individual metal ligands play distinct functional roles in the zinc sensor *Staphylococcus aureus* CzrA. Journal of Molecular Biology. 356(5), 1124-1136.

- Perera, V. R., Newton, G. L., & Pogliano, K. (2015). Bacillithiol: a key protective thiol in *Staphylococcus aureus*. *Expert Review of Anti-Infective Therapy*, 13(9), 1089–1107.
- Pishchany, G., McCoy, A.L., Torres, V.J., Krause, J.C., Crowe, J.E., Fabry, M.E. & Skaar, E.P. (2010) Specificity for human hemoglobin enhances *Staphylococcus aureus* infection. *Cell Host and Microbe*. 8 (6), 544–550.
- Pletinckx, L.J., Verheghe, M., Crombé, F. & Dewulf, J. (2013) Evidence of possible methicillin-resistant *Staphylococcus aureus* ST398 spread between pigs and other animals and people residing on the same farm. *Preventive Veterinary Medicine*. 109(3), 293-303.
- Posada, A.C., Kolar, S.L., Dusi, R.G., Francois, P., Roberts, A.A., Hamilton, C.J., Liu, G.Y. & Cheung, A. (2014) Importance of bacillithiol in the oxidative stress response of *Staphylococcus aureus*. *Infection and Immunity*. 82(1), 316–332.
- Posey, J.E., Hardham, J.M., Norris, S.J. and Gherardini, F.C., 1999. Characterization of a manganese-dependent regulatory protein, TroR, from *Treponema pallidum*. *Proceedings of the National Academy of Sciences*. 96(19),10887-10892.
- Poyart, C., Berche, P. & Trieu-Cuot, P. (1995) Characterization of superoxide dismutase genes from gram-positive bacteria by polymerase chain reaction using degenerate primers. *FEMS Microbiology Letters*. 131(1), 41-45.
- Prajsnar, T.K., Hamilton, R., Garcia-Lara, J., McVicker, G., Williams, A., Boots, M., Foster, S.J. & Renshaw, S.A. (2012) A privileged intraphagocyte niche is responsible for disseminated infection of *Staphylococcus aureus* in a zebrafish model. *Cellular Microbiology*. 14(10), 1600-1619.
- Price, C.W., Fawcett, P., C er monie, H., Su, N., Murphy, C.K. & Youngman, P. (2001) Genome-wide analysis of the general stress response in *Bacillus subtilis*. *Molecular Microbiology*. 41 (4), 757–774.
- Purves, J., Thomas, J., Riboldi, G.P., Zapotoczna, M., Tarrant, E., Andrew, P.W., Londo o, A., Planet, P.J., Geoghegan, J.A., Waldron, K.J. and Morrissey, J.A., 2018. A horizontally gene transferred copper resistance locus confers hyper-resistance to antibacterial copper toxicity and enables survival of community acquired methicillin resistant *Staphylococcus aureus* USA300 in macrophages. *Environmental Microbiology*. 20(4), 1576-1589
- Pynnonen, M., Stephenson, R. E., Schwartz, K., Hernandez, M., & Boles, B. R. (2011). Hemoglobin promotes *Staphylococcus aureus* nasal colonization. *PLoS pathogens*. 7(7), e1002104
- Quiles-Melero, I., Garc a-Perea, A. & de Pablos, M. (2012) Resistance to linezolid in a methicillin-susceptible *Staphylococcus aureus* clinical isolate without previous exposure to oxazolidinones. *International Journal of Medical Microbiology*. 302(3), 145-147.

- Rachid, S., Ohlsen, K., Wallner, U. & Hacker, J. (2000) Alternative transcription factor ζ b is involved in regulation of biofilm expression in a *Staphylococcus aureus* mucosal isolate. *Journal of Bacteriology*. 182(23), 6824-6826.
- Rashid, G.M.M., Taylor, C.R., Liu, Y., Zhang, X., Rea, D., Fülöp, V. & Bugg, T.D.H. (2015) Identification of manganese superoxide dismutase from *Sphingobacterium* sp. T2 as a novel bacterial enzyme for lignin oxidation. *ACS Chemical Biology*. 10 (10), 2286–2294.
- Ray, M.D., Boundy, S. & Archer, G.L. (2016) Transfer of the methicillin resistance genomic island among staphylococci by conjugation. *Molecular Microbiology*. 100 (4), 675–685.
- Richardson, A.R., Dunman, P.M. & Fang, F.C. (2006) The nitrosative stress response of *Staphylococcus aureus* is required for resistance to innate immunity. *Molecular Microbiology*. 61 (4), 927–939.
- Rinke, C., Schwientek, P., Sczyrba, A., Ivanova, N.N., Anderson, I.J., Cheng, J.-F., Darling, A., Malfatti, S., Swan, B.K., Gies, E.A., Dodsworth, J.A., Hedlund, B.P., Tsiamis, G., Sievert, S.M., Liu, W.-T., Eisen, J.A., Hallam, S.J., Kyrpides, N.C., Stepanauskas, R., et al. (2013) Insights into the phylogeny and coding potential of microbial dark matter. *Nature*. 499 (7459), 431–437.
- Robinson, D.N.J. & Pohl, D.E. (2013) Zinc sensors in bacteria. *Encyclopedia of Metalloproteins*. 2499–2506.
- Robinson, D.R. & Jencks, W.P. (1963) Effect of denaturing agents of the urea-guanidinium class on the solubility of acetyltetraglycine ethyl ester and related compounds. *Journal of Biological Chemistry*. 238(4), 1558-1560.
- Ryu, S.Y., Jeong, K.S., Kang, B.N., Park, S.J., Yoon, W.K., Kim, S.H. & Kim, T.H. (2000) Modulation of transferrin synthesis, transferrin receptor expression, iNOS expression and NO production in mouse macrophages by cytokines, either alone or in combination. *Anticancer Research*. 20 (5A), 3331–3338.
- Sambrook, J. & Russell, D.W. (2001) *Molecular cloning: a laboratory manual* 3rd edition. Coldspring-Harbour Laboratory Press, UK.
- Sanz, R., Marín, I., Ruiz-Santa-Quiteria, J.A., Orden, J.A., Cid, D., Diez, R.M., Silhadi, K.S., Amils, R. & la Fuente, de, R. (2000) Catalase deficiency in *Staphylococcus aureus* subsp. *anaerobius* is associated with natural loss-of-function mutations within the structural gene. *Microbiology*. 146(2), 465–475.
- Scharn, C.R., Tenover, F.C. & Goering, R.V. (2013) Transduction of staphylococcal cassette chromosome mec elements between strains of *Staphylococcus aureus*. *Antimicrobial Agents and Chemotherapy*. 57 (11), 5233–5238.
- Schauber, J., & Gallo, R. L. (2008). Antimicrobial peptides and the skin immune defense system. *Journal of Allergy and Clinical Immunology*. 122(2), 261-266.

- Schleifer, K.-H. & Bell, J.A. (2015) *Staphylococcus*. 9(17). Chichester, UK: John Wiley & Sons, Ltd.
- Schwartz, A.L., Yikilmaz, E., Vance, C.K. & Vathyam, S. (2000) Mutational and spectroscopic studies of the significance of the active site glutamine to metal ion specificity in superoxide dismutase. *Journal of Inorganic Biochemistry*. 80(3), 247-256.
- Scientific Opinion of the Panel on Biological Hazards on a request from the European Commission on Assessment of the Public Health significance of meticillin resistant *Staphylococcus aureus* (MRSA) in animals and foods. *The EFSA Journal* (2009) 993, 1-73
- Sebulsky, M.T., Hohnstein, D., Hunter, M.D. & Heinrichs, D.E. (2000) Identification and characterization of a membrane permease involved in iron-hydroxamate transport in *Staphylococcus aureus*. *Journal of Bacteriology*. 182 (16), 4394.
- Seidl, K., Müller, S., Francois, P., Kriebitzsch, C., Schrenzel, J., Engelmann, S., Bischoff, M. & Berger-Bächi, B. (2009) Effect of a glucose impulse on the CcpA regulon in *Staphylococcus aureus*. *BMC Microbiology*. 9(1), 95.
- Senn, M.M., Giachino, P., Homerova, D., Steinhuber, A., Strassner, J., Kormanec, J., Flückiger, U., Berger-Bächi, B. & Bischoff, M. (2005) Molecular analysis and organization of the sigmaB operon in *Staphylococcus aureus*. *Journal of Bacteriology*. 187 (23), 8006–8019.
- Sheng, Y., Abreu, I.A., Cabelli, D.E., Maroney, M.J., Miller, A.-F., Teixeira, M. & Valentine, J.S. (2014) Superoxide dismutases and superoxide reductases. *Chemical Reviews*. 114 (7), 3854–3918.
- Sheng, Y., Butler Gralla, E., Schumacher, M., Cascio, D., Cabelli, D.E. & Valentine, J.S. (2012) Six-coordinate manganese (3+) in catalysis by yeast manganese superoxide dismutase. *Proceedings of the National Academy of Sciences*. 109 (36), 14314–14319.
- Sheng, Y., Stich, T.A., Barnese, K., Gralla, E.B., Cascio, D., Britt, R.D., Cabelli, D.E. & Valentine, J.S. (2011) Comparison of two yeast MnSODs: mitochondrial *Saccharomyces cerevisiae* versus cytosolic *Candida albicans*. *Journal of the American Chemical Society*. 133(51), 20878-20889.
- Sievert, D.M., Rudrik, J.T., Patel, J.B., McDonald, L.C., Wilkins, M.J. & Hageman, J.C. (2008) Vancomycin-resistant *Staphylococcus aureus* in the United States, 2002-2006. *Clinical Infectious Diseases*. 46 (5), 668–674.
- Singh, V.K., Xiong, A., Usgaard, T.R., Chakrabarti, S., Deora, R., Misra, T.K. & Jayaswal, R.K. (1999) ZntR is an autoregulatory protein and negatively regulates the chromosomal zinc resistance operon znt of *Staphylococcus aureus*. *Molecular Microbiology*. 33 (1), 200–207.
- Sitthisak, S., Knutsson, L., Webb, J.W. & Jayaswal, R.K. (2007) Molecular characterization of the copper transport system in *Staphylococcus aureus*. *Microbiology*. 153 (12), 4274–4283.

- Sjödin, M., Gättjens, J., Tabares, L.C., Thuéry, P., Pecoraro, V.L. & Un, S. (2008) Tuning the redox properties of manganese(II) and its implications to the electrochemistry of manganese and iron superoxide dismutases. *Inorganic Chemistry*. 47 (7), 2897–2908.
- Skaar, E.P. & Schneewind, O. (2004) Iron-regulated surface determinants (Isd) of *Staphylococcus aureus*: stealing iron from heme. *Microbes and Infection*, 6(4), 390-397.
- Slykhouse, T.O. & Fee, J.A. (1976) Physical and chemical studies on bacterial superoxide dismutases. Purification and some anion binding properties of the iron-containing protein of *Escherichia coli* B. *Journal of Biological Chemistry*. 251(18), 5472-5477.
- Smith, M.W. & Doolittle, R.F. (1992) A comparison of evolutionary rates of the two major kinds of superoxide dismutase. *Journal of Molecular Evolution*. 34 (2), 175–184.
- Smulevich, G., Mauro, J.M., Fishel, L.A. & English, A.M. (1988) Heme pocket interactions in cytochrome c peroxidase studied by site-directed mutagenesis and resonance Raman spectroscopy. *Biochemistry*, 27(15), 5477-5485.
- Soe-Lin, S., Sheftel, A.D., Wasyluk, B. & Ponka, P. (2008) Nramp1 equips macrophages for efficient iron recycling. *Experimental Hematology*, 36(8), 929-937.
- Speziali, C.D., Dale, S.E., Henderson, J.A., Vinés, E.D. & Heinrichs, D.E. (2006) Requirement of *Staphylococcus aureus* ATP-binding cassette-ATPase FhuC for iron-restricted growth and evidence that it functions with more than one iron transporter. *Journal of Bacteriology*. 188 (6), 2048–2055.
- Sreerama, N. & Woody, R.W. (2000) Estimation of protein secondary structure from circular dichroism spectra: comparison of CONTIN, SELCON, and CDSSTR methods with an expanded reference set. *Analytical Biochemistry*. 287 (2), 252–260.
- Stallings, W.C., Metzger, A.L., Patridge, K.A., Fee, J.A. & Ludwig, M.L. (1991) Structure-function relationships in iron and manganese superoxide dismutases. *Free Radical Research Communications*. 12-13 Pt 1259–268.
- Stapels, D.A.C., Ramyar, K.X., Bischoff, M., Köckritz-Blickwede, von, M., Milder, F.J., Ruyken, M., Eisenbeis, J., McWhorter, W.J., Herrmann, M., Van Kessel, K.P.M., Geisbrecht, B.V. & Rooijackers, S.H.M. (2014) *Staphylococcus aureus* secretes a unique class of neutrophil serine protease inhibitors. *Proceedings of the National Academy of Sciences*. 111 (36), 13187–13192.
- Stefani, S., Chung, D. R., Lindsay, J. A., Friedrich, A. W., Kearns, A. M., Westh, H., & MacKenzie, F. M. (2012). Meticillin-resistant *Staphylococcus aureus* (MRSA): global epidemiology and harmonisation of typing methods. *International Journal Of Antimicrobial Agents*. 39(4), 273-282.
- Sun, G. & Budde, R.J. (1999) Substitution studies of the second divalent metal cation requirement of protein tyrosine kinase CSK. *Biochemistry*. 38 (17), 5659–5665.

- Surmann, K., Michalik, S., Hildebrandt, P., Gierok, P., Depke, M., Brinkmann, L., Bernhardt, J., Salazar, M.G., Sun, Z., Shteynberg, D., Kusebauch, U., Moritz, R.L., Wollscheid, B., Lalk, M., Völker, U. & Schmidt, F. (2014) Comparative proteome analysis reveals conserved and specific adaptation patterns of *Staphylococcus aureus* after internalization by different types of human non-professional phagocytic host cells. *Frontiers in Microbiology*. 5, 392.
- Suttisansanee, U., Lau, K., Lagishetty, S., Rao, K.N., Swaminathan, S., Sauder, J.M., Burley, S.K. & Honek, J.F. (2011) Structural variation in bacterial glyoxalase I enzymes. *Journal of Biological Chemistry*. 286 (44), 38367–38374.
- Tabares, L. C., Bittel, C., Carrillo, N., Bortolotti, A., & Cortez, N. (2003). The single superoxide dismutase of *Rhodobacter capsulatus* is a cambialistic, manganese-containing enzyme. *Journal of Bacteriology*, 185(10), 3223-3227.
- Tabares, L.C., Cortez, N. & Un, S. (2007) Role of tyrosine-34 in the anion binding equilibria in manganese(II) superoxide dismutases. *Biochemistry*. 46 (32), 9320–9327.
- Tabares, L.C., Gätjens, J. & Un, S. (2010) Understanding the influence of the protein environment on the Mn(II) centers in superoxide dismutases using High-Field Electron Paramagnetic Resonance. *Biochimica et Biophysica Acta*. 1804 (2), 308–317.
- Tachikawa, H. (2014) Electron detachment dynamics of O₂ – (H₂O): direct *ab initio* molecular dynamics (AIMD) approach. *RSC Advances*. 4 (1), 516–522.
- Tally, F.P., Goldin, B.R., Jacobus, N.V. & Gorbach, S.L. (1977) Superoxide dismutase in anaerobic bacteria of clinical significance. *Infection and Immunity*. 16 (1), 20–25.
- Teale, F.W. & Weber, G. (1957) Ultraviolet fluorescence of the aromatic amino acids. *The Biochemical Journal*. 65 (3), 476–482.
- Thakker, M., Park, J.S., Carey, V. & Lee, J.C. (1998) *Staphylococcus aureus* serotype 5 capsular polysaccharide is antiphagocytic and enhances bacterial virulence in a murine bacteremia model. *Infection and Immunity*. 66 (11), 5183–5189.
- Totter, S., Waldron, K.J., Firbank, S.J., Reale, B., Bessant, C., Sato, K., Cheek, T.R., Gray, J., Banfield, M.J., Dennison, C. & Robinson, N.J. (2008) Protein-folding location can regulate manganese-binding versus copper- or zinc-binding. *Nature*. 455 (7216), 1138–1142.
- Touati, D. (2000). Iron and oxidative stress in bacteria. *Archives of Biochemistry and Biophysics*. 373(1), 1-6.
- Tu, W.Y., Pohl, S., Gray, J., Robinson, N.J., Harwood, C.R. & Waldron, K.J. (2012) Cellular iron distribution in *Bacillus anthracis*. *Journal of Bacteriology*. 194 (5), 932–940.
- Tuscherr, L., Heitmann, V., Hussain, M., Viemann, D., Roth, J., Eiff, Von, C., Peters, G., Becker, K. & Löffler, B. (2010) *Staphylococcus aureus* small-colony variants are adapted phenotypes for intracellular persistence. *Journal of Infectious Diseases*. 202 (7), 1031–1040.

- Tzagolo, H. & Novick, R. (1977) Geometry of cell division in *Staphylococcus aureus*. *Journal of Bacteriology*. 129, 343–350
- Ulrich, M., Bastian, M., Cramton, S.E., Ziegler, K., Pragman, A.A., Bragonzi, A., Memmi, G., Wolz, C., Schlievert, P.M., Cheung, A. & Döring, G. (2007) The staphylococcal respiratory response regulator SrrAB induces *ica* gene transcription and polysaccharide intercellular adhesin expression, protecting *Staphylococcus aureus* from neutrophil killing under anaerobic growth conditions. *Molecular Microbiology*. 65 (5), 1276–1287.
- Un, S., Tabares, L.C., Cortez, N. & Hiraoka, B.Y. (2004) Manganese (II) zero-field interaction in cambialistic and manganese superoxide dismutases and its relationship to the structure of the metal binding site. *Journal of the American Chemical Society*, 126(9), 2720-2726.
- Valderas, M.W. & Hart, M.E. (2001) Identification and characterization of a second superoxide dismutase gene (*sodM*) from *Staphylococcus aureus*. *Journal of Bacteriology*. 183 (11), 3399–3407.
- Valderas, M.W., Gatson, J.W., Wreyford, N. & Hart, M.E. (2002) The superoxide dismutase gene *sodM* is unique to *Staphylococcus aureus*: absence of *sodM* in coagulase-negative staphylococci. *Journal of Bacteriology*. 184 (9), 2465–2472.
- Valente, A.M., Jain, R., Scheurer, M., Fowler, V.G., Corey, G.R., Bengur, A.R., Sanders, S. & Li, J.S. (2005) Frequency of infective endocarditis among infants and children with *Staphylococcus aureus* bacteremia. *Pediatrics*. 115 (1), e15–e19.
- van Cleef, B.A.G.L., Graveland, H., Haenen, A.P.J., van de Giessen, A.W., Heederik, D., Wagenaar, J.A. & Kluytmans, J.A.J.W. (2011) Persistence of livestock-associated methicillin-resistant *Staphylococcus aureus* in field workers after short-term occupational exposure to pigs and veal calves. *Journal of Clinical Microbiology*. 49 (3), 1030–1033.
- van Cleef, B.A.G.L., Monnet, D.L., Voss, A., Krziwanek, K., Allerberger, F., Struelens, M., Zemlickova, H., Skov, R.L., Vuopio-Varkila, J., Cuny, C., Friedrich, A.W., Spiliopoulou, I., Pászti, J., Hardardottir, H., Rossney, A., Pan, A., Pantosti, A., Borg, M., Grundmann, H., et al. (2011) Livestock-associated methicillin-resistant *Staphylococcus aureus* in humans in Europe. *Emerging Infectious Diseases*. 17 (3), 502–505.
- van Rijen, M.M.L., Bosch, T., Verkade, E.J.M., Schouls, L., Kluytmans, J.A.J.W. & CAM Study Group (2014) Livestock-associated MRSA carriage in patients without direct contact with livestock. *PLOS ONE*. 9 (6), e100294.
- Vance, C. K., & Miller, A. F. (1998). A simple proposal that can explain the inactivity of metal-substituted superoxide dismutases. *Journal of the American Chemical Society*, 120(3), 461-467.
- Vivian, J.T. & Callis, P.R. (2001) Mechanisms of tryptophan fluorescence shifts in proteins. *Biophysical Journal*. 80 (5), 2093–2109.

- Voyich, J.M., Braughton, K.R., Sturdevant, D.E., Whitney, A.R., Saïd-Salim, B., Porcella, S.F., Long, R.D., Dorward, D.W., Gardner, D.J., Kreiswirth, B.N., Musser, J.M. & DeLeo, F.R. (2005) Insights into mechanisms used by *Staphylococcus aureus* to avoid destruction by human neutrophils. *Journal of Immunology*. 175 (6), 3907–3919.
- Vyoral, D. & Petrák, J. (2005) Hcpidin: a direct link between iron metabolism and immunity. *The International Journal of biochemistry and Cell Biology*. 37(9), 1768-1773.
- Wakeman, C.A. & Skaar, E.P. (2012) Metalloregulation of Gram-positive pathogen physiology. *Current Opinion in Microbiology*. 15 (2), 169–174.
- Waldron, D.E. & Lindsay, J.A. (2006) Sau1: a novel lineage-specific type I restriction-modification system that blocks horizontal gene transfer into *Staphylococcus aureus* and between *S. aureus* isolates of different lineages. *Journal of Bacteriology*. 188 (15), 5578–5585.
- Waldron, K.J. & Robinson, N.J. (2009) How do bacterial cells ensure that metalloproteins get the correct metal? *Nature*. 7 (1), 25–35.
- Waldron, K.J., Rutherford, J.C., Ford, D. & Robinson, N.J. (2009) Metalloproteins and metal sensing. *Nature*. 460 (7257), 823–830.
- Waldron, K.J., Tottey, S. & Yanagisawa, S. (2007) A periplasmic iron-binding protein contributes toward inward copper supply. *Journal of Biological Chemistry*, 282(6), 3837-3846.
- Wang R., Braughton K. R., Kretschmer D., Bach T. H., Queck S. Y., Li M., Kennedy A. D., Dorward D. W., Klebanoff S. J., Peschel A., DeLeo F. R., Otto M. (2007) Identification of novel cytolytic peptides as key virulence determinants for community-associated MRSA. *Nat. Med.* 13, 1510–1514
- Wassenberg, M.W.M., Bootsma, M.C.J., Troelstra, A., Kluytmans, J.A.J.W. & Bonten, M.J.M. (2011) Transmissibility of livestock-associated methicillin-resistant *Staphylococcus aureus* (ST398) in Dutch hospitals. *Clinical Microbiology and Infection*. 17 (2), 316–319.
- Waterhouse, A.M., Procter, J.B., Martin, D.M.A., Clamp, M. & Barton, G.J. (2009) Jalview Version 2-a multiple sequence alignment editor and analysis workbench. *Bioinformatics*. 25 (9), 1189–1191.
- Watlafer, D.B., Malik, S.K. & Stoller, L. (1964) Nonpolar group participation in the denaturation of proteins by urea and guanidinium salts. Model compound studies. *Journal of the American Chemical Society*, 86(3), 508-514.
- Weber, H., Engelmann, S., Becher, D. & Hecker, M. (2004) Oxidative stress triggers thiol oxidation in the glyceraldehyde-3-phosphate dehydrogenase of *Staphylococcus aureus*. *Molecular Microbiology*. 52 (1), 133–140.
- Weems, J.J. (2001) The many faces of *Staphylococcus aureus* infection. Recognizing and managing its life-threatening manifestations. *Postgraduate Medicine*. 110 (4), 24–36.
- Weinberg, E.D. (1978) Iron and infection. *Microbiological reviews*. 42 (1), 45–66.

- Wendlandt, S., Schwarz, S. & Silley, P. (2013) Methicillin-resistant *Staphylococcus aureus*: A food-borne pathogen? Annual Review of Food Science and Technology. 4 (1), 117–139.
- Wertheim, H., Vos, M.C., Ott, A., van Belkum, A. & Voss, A. (2004) Risk and outcome of nosocomial *Staphylococcus aureus* bacteraemia in nasal carriers versus non-carriers. Lancet, 364(9435), 703-705.
- Wertheim, H.F.L., Melles, D.C., Vos, M.C., van Leeuwen, W., van Belkum, A., Verbrugh, H.A. & Nouwen, J.L. (2005) The role of nasal carriage in *Staphylococcus aureus* infections. The Lancet Infectious Diseases. 5 (12), 751–762.
- Wessling-Resnick, M. (2015) Nramp1 and other transporters involved in metal withholding during infection. Journal of Biological Chemistry, 290(31), 18984-18990.
- White, C., Lee, J., Kambe, T., Fritsche, K. & Petris, M.J. (2009) A role for the ATP7A copper-transporting ATPase in macrophage bactericidal activity. Journal of Biological Chemistry. 284 (49), 33949–33956.
- Whitmore, L. & Wallace, B.A. (2004) DICHROWEB, an online server for protein secondary structure analyses from circular dichroism spectroscopic data. Nucleic acids research. 32, W668–W673.
- Whittaker, J. W., & Whittaker, M. M. (1991). Active site spectral studies on manganese superoxide dismutase. Journal of the American Chemical Society, 113(15), 5528-5540.
- Whittaker, J.W. (2003) The irony of manganese superoxide dismutase. Biochemical Society Transactions. 31 (6), 1318–1321.
- Whittaker, M. M., Lerch, T. F., Kirillova, O., Chapman, M. S., & Whittaker, J. W. (2011). Subunit dissociation and metal binding by *Escherichia coli* apo-manganese superoxide dismutase. Archives of Biochemistry and Biophysics, 505(2), 213-225.
- Whittaker, M.M. & Whittaker, J.W. (1996) Low-temperature thermochromism marks a change in coordination for the metal ion in manganese superoxide dismutase. Biochemistry, 35(21), 6762-6770.
- Whittaker, M.M. & Whittaker, J.W. (1997) Mutagenesis of a proton linkage pathway in *Escherichia coli* manganese superoxide dismutase. Biochemistry. 36 (29), 8923–8931.
- Whittaker, M.M. & Whittaker, J.W. (1998) A glutamate bridge is essential for dimer stability and metal selectivity in manganese superoxide dismutase. The Journal of Biological Chemistry. 273 (35), 22188–22193.
- Whittaker, M.M. & Whittaker, J.W. (1999) Thermally triggered metal binding by recombinant *Thermus thermophilus* manganese superoxide dismutase, expressed as the apo-enzyme. The Journal of Biological Chemistry. 274 (49), 34751–34757.

- Whittaker, M.M. & Whittaker, J.W. (2008) Conformationally gated metal uptake by apomanganese superoxide dismutase. *Biochemistry*, 47(44), 11625-11636.
- Whittaker, M.M., Mizuno, K., Bächinger, H.P. & Whittaker, J.W. (2006) Kinetic analysis of the metal binding mechanism of *Escherichia coli* manganese superoxide dismutase. *Biophysical Journal*. 90 (2), 598–607.
- Wielders, C., Vriens, M.R. & Brisse, S. (2001) Evidence for in-vivo transfer of *mecA* DNA between strains of *Staphylococcus aureus*. *The Lancet*, 357(9269), 1674-1675.
- Williams, T.A., Szöllösi, G.J., Spang, A., Foster, P.G., Heaps, S.E., Boussau, B., Ettema, T.J.G. & Embley, T.M. (2017) Integrative modeling of gene and genome evolution roots the archaeal tree of life. *Proceedings of the National Academy of Sciences*. 114 (23), E4602–E4611.
- Winn, M.D., Ballard, C.C., Cowtan, K.D., Dodson, E.J., Emsley, P., Evans, P.R., Keegan, R.M., Krissinel, E.B., Leslie, A.G.W., McCoy, A., McNicholas, S.J., Murshudov, G.N., Pannu, N.S., Potterton, E.A., Powell, H.R., Read, R.J., Vagin, A. & Wilson, K.S. (2011) Overview of the CCP4 suite and current developments. *Acta Crystallographica Section D: Biological Crystallography*. 67 (4), 235–242.
- Winterbourn, C.C. & Kettle, A.J. (2013) Redox reactions and microbial killing in the neutrophil phagosome. *Antioxidants & Redox Signaling*. 18 (6), 642–660.
- Wintjens, R., Gilis, D. & Rooman, M. (2008) Mn/Fe superoxide dismutase interaction fingerprints and prediction of oligomerization and metal cofactor from sequence. *Proteins: Structure, Function, and Bioinformatics*, 70(4), 1564-1577.
- Wintjens, R., Noël, C., May, A.C.W., Gerbod, D., Dufernez, F., Capron, M., Viscogliosi, E. & Rooman, M. (2004) Specificity and Phenetic Relationships of Iron- and Manganese-containing Superoxide Dismutases on the Basis of Structure and Sequence Comparisons. *The Journal of Biological Chemistry*. 279 (10), 9248–9254.
- Witte, W. (2009) Community-acquired methicillin-resistant *Staphylococcus aureus*: what do we need to know? *Clinical Microbiology and Infection*. 1517–25.
- Witte, W., Strommenger, B., Stanek, C., & Cuny, C. (2007). Methicillin-resistant *Staphylococcus aureus* ST398 in humans and animals, Central Europe. *Emerging Infectious Diseases*, 13(2), 255.
- Wolf, C., Hochgräfe, F., Kusch, H., Albrecht, D., Hecker, M. & Engelmann, S. (2008) Proteomic analysis of antioxidant strategies of *Staphylococcus aureus*: diverse responses to different oxidants. *Proteomics*. 8 (15), 3139–3153.
- Wolfe-Simon, F., Grzebyk, D., Schofield, O. & Falkowski, P.G. (2005) The role and evolution of superoxide dismutases in algae. *Journal of Phycology*. 41 (3), 453–465.
- Wulf, M. & Voss, A. (2008) MRSA in livestock animals—an epidemic waiting to happen? *Clinical Microbiology and Infection*. 14 (6), 519–521.

- Xiong, A., Singh, V.K., Cabrera, G. & Jayaswal, R.K. (2000) Molecular characterization of the ferric-uptake regulator, Fur, from *Staphylococcus aureus*. *Microbiology*, 146: 659–68.
- Xu, S. X., & McCormick, J. K. (2012). Staphylococcal superantigens in colonization and disease. *Frontiers in Cellular and Infection Microbiology*. 2, 52.
- Yamakura, F. & Suzuki, K. (1980) Cadmium, Chromium, and Manganese replacement for iron in iron-superoxide dismutase from *Pseudomonas ovalis*. *The Journal of Biochemistry*. 88(1), 191-196.
- Yamakura, F., Sugio, S., Hiraoka, B.Y., Ohmori, D. & Yokota, T. (2003) Pronounced conversion of the metal-specific activity of superoxide dismutase from *Porphyromonas gingivalis* by the mutation of a single amino acid (Gly155Thr) located apart from the active site. *Biochemistry*. 42 (36), 10790–10799.
- Yamano, S. & Maruyama, T. (1999) An azide-insensitive superoxide dismutase from a hyperthermophilic archaeon, *Sulfolobus solfataricus*. *Journal of Biochemistry*. 125 (1), 186–193.
- Yamano, S., Sako, Y., Nomura, N., & Maruyama, T. (1999). A cambialistic SOD in a strictly aerobic hyperthermophilic archaeon, *Aeropyrum pernix*. *The Journal of Biochemistry*, 126(1), 218-225.
- Yikilmaz, E., Rodgers, D. W., & Miller, A. F. (2006). The crucial importance of chemistry in the structure– function link: manipulating hydrogen bonding in iron-containing superoxide dismutase. *Biochemistry*, 45(4), 1151-1161.
- Yikilmaz, E., Xie, J., Brunold, T.C. & Miller, A.-F. (2002) Hydrogen-bond-mediated tuning of the redox potential of the non-heme Fe site of superoxide dismutase. *Journal of the American Chemical Society*. 124 (14), 3482–3483.
- Yocum, C.F. & Pecoraro, V.L. (1999) Recent advances in the understanding of the biological chemistry of manganese. *Current Opinion in Chemical Biology*. 3 (2), 182–187.
- Yost, F. J., & Fridovich, I. (1973). An iron-containing superoxide dismutase from *Escherichia coli*. *Journal of Biological Chemistry*, 248(14), 4905-4908.
- Yui, S., Nakatani, Y. & Mikami, M. (2003) Calprotectin (S100A8/S100A9), an inflammatory protein complex from neutrophils with a broad apoptosis-inducing activity. *Biological & Pharmaceutical Bulletin*. 26 (6), 753–760.
- Zheng, H., Chordia, M.D., Cooper, D.R. & Chruszcz, M. (2014) Validation of metal-binding sites in macromolecular structures with the CheckMyMetal web server. *Nature protocols*. 9(1), 156.
- Zhu, Y., Nandakumar, R., Sadykov, M.R., Madayiputhiya, N., Luong, T.T., Gaupp, R., Lee, C.Y. & Somerville, G.A. (2011) RpiR homologues may link *Staphylococcus aureus* RNAIII synthesis and pentose phosphate pathway regulation. *Journal of Bacteriology*. 193 (22), 6187–6196.

References

- Acton, D. S., Plat-Sinnige, M. T., van Wamel, W., de Groot, N., & van Belkum, A. (2009). Intestinal carriage of *Staphylococcus aureus*: how does its frequency compare with that of nasal carriage and what is its clinical impact? *European Journal of Clinical Microbiology & Infectious Diseases*, 28(2), 115.
- Adams, P.D., Afonine, P.V., Bunkóczi, G., Chen, V.B., Davis, I.W., Echols, N., Headd, J.J., Hung, L.-W., Kapral, G.J., Grosse-Kunstleve, R.W., McCoy, A.J., Moriarty, N.W., Oeffner, R., Read, R.J., Richardson, D.C., Richardson, J.S., Terwilliger, T.C. & Zwart, P.H. (2010) PHENIX: a comprehensive Python-based system for macromolecular structure solution. *Acta Crystallographica Section D: Biological Crystallography*. 66 (Pt 2), 213–221.
- Adl, S.M., Simpson, A.G.B., Lane, C.E., Lukeš, J., Bass, D., Bowser, S.S., Brown, M.W., Burki, F., Dunthorn, M., Hampl, V., Heiss, A., Hoppenrath, M., Lara, E., le Gall, L., Lynn, D.H., McManus, H., Mitchell, E.A.D., Mozley-Stanridge, S.E., Parfrey, L.W., et al. (2012) The Revised Classification of Eukaryotes. *Journal of Eukaryotic Microbiology*. 59 (5), 429–514.
- Aguirre, J.D., Clark, H.M., McIlvin, M., Vazquez, C., Palmere, S.L., Grab, D., Seshu, J., Hart, P.J., Saito, M. & Culotta, V.C. (2013) A Manganese-Rich Environment Supports Superoxide Dismutase Activity in a Lyme Disease Pathogen, *Borrelia burgdorferi*. *Journal of Biological Chemistry*. 288(12), 8468-8478.
- Altschul, S.F., Gish, W., Miller, W., Myers, E.W. & Lipman, D.J. (1990) Basic local alignment search tool. *Journal of Molecular Biology*. 215 (3), 403–410.
- Amano A., Shizukuishi S., Tamagawa H., Iwakura K., Tsunasawa S., Tsunemitsu A. (1990) Characterization of superoxide dismutases purified from either anaerobically maintained or aerated *Bacteroides gingivalis*, *Journal of Bacteriology*. 172, 1457-63.
- Amar B T Ghisaidoobe, S.J.C. (2014) Intrinsic Tryptophan Fluorescence in the Detection and Analysis of Proteins: A Focus on Förster Resonance Energy Transfer Techniques - *ijms-15-22518.pdf*. *International Journal of Molecular Sciences*. 15 (12), 22518.
- Ammann, A.A. (2007) Inductively coupled plasma mass spectrometry (ICP MS): a versatile tool. *Journal of Mass Spectrometry*. 42 (4), 419–427.
- Ando, M., Manabe, Y.C., Converse, P.J., Miyazaki, E., Harrison, R., Murphy, J.R. & Bishai, W.R. (2003) Characterization of the role of the divalent metal ion-dependent transcriptional repressor MntR in the virulence of *Staphylococcus aureus*. *Infection and Immunity*. 71 (5), 2584–2590.
- Andreini, C., Bertini, I., Cavallaro, G., Holliday, G.L. & Thornton, J.M. (2008) Metal ions in biological catalysis: from enzyme databases to general principles. *Journal of Biological Inorganic Chemistry*. 13 (8), 1205–1218.

- Anjem, A., Varghese, S. & Imlay, J.A. (2009) Manganese import is a key element of the OxyR response to hydrogen peroxide in *Escherichia coli*. *Molecular Microbiology*. 72 (4), 844–858.
- Archer, G.L. (1998) *Staphylococcus aureus*: A Well-Armed Pathogen. *Clinical Infectious Diseases*. 26 (5), 1179–1181.
- Azarian, T., Daum, R.S., Petty, L.A., Steinbeck, J.L., Yin, Z., Nolan, D., Boyle-Vavra, S., Hanage, W.P., Salemi, M. & David, M.Z. (2016) Intrahost Evolution of Methicillin-Resistant *Staphylococcus aureus* USA300 Among Individuals with Reoccurring Skin and Soft-Tissue Infections. *Journal of Infectious Diseases*. 214 (6), 895–905.
- Baba, T., Takeuchi, F., Kuroda, M., Yuzawa, H., Aoki, K.-I., Oguchi, A., Nagai, Y., Iwama, N., Asano, K., Naimi, T., Kuroda, H., Cui, L., Yamamoto, K. & Hiramatsu, K. (2002) Genome and virulence determinants of high virulence community-acquired MRSA. *The Lancet*. 359 (9320), 1819–1827.
- Baez, A. & Shiloach, J. (2017) Increasing dissolved-oxygen disrupts iron homeostasis in production cultures of *Escherichia coli*. *Antonie van Leeuwenhoek*. 110 (1), 115–124.
- Baker-Austin, C., Wright, M.S., Stepanauskas, R. & McArthur, J.V. (2006) Co-selection of antibiotic and metal resistance. *Trends in Microbiology*. 14 (4), 176–182.
- Baker, J., Sitthisak, S., Sengupta, M., Johnson, M., Jayaswal, R.K. & Morrissey, J.A. (2010) Copper stress induces a global stress response in *Staphylococcus aureus* and represses *sae* and *agr* expression and biofilm formation. *Applied and Environmental Microbiology*. 76 (1), 150–160.
- Ballal, A. & Manna, A.C. (2009a) Control of Thioredoxin Reductase Gene (*trxB*) Transcription by SarA in *Staphylococcus aureus*. *Journal of Bacteriology*. 192 (1), 336–345.
- Ballal, A. & Manna, A.C. (2009b) Regulation of superoxide dismutase (*sod*) genes by SarA in *Staphylococcus aureus*. *Journal of Bacteriology*. 191 (10), 3301–3310.
- Barondeau, D. P., Kassmann, C. J., Bruns, C. K., Tainer, J. A., & Getzoff, E. D. (2004). Nickel superoxide dismutase structure and mechanism. *Biochemistry*, 43(25), 8038-8047.
- Battye, T.G.G., Kontogiannis, L., Johnson, O., Powell, H.R. & Leslie, A.G.W. (2011) iMOSFLM: a new graphical interface for diffraction-image processing with MOSFLM. *Acta Crystallographica Section D: Biological Crystallography*. 67 (Pt 4), 271–281.
- Beasley, F.C. & Heinrichs, D.E. (2010) Siderophore-mediated iron acquisition in the staphylococci. *Journal of inorganic biochemistry*. 1;104(3):282-8.
- Beasley, F.C., Marolda, C.L., Cheung, J., Buac, S. & Heinrichs, D.E. (2011) *Staphylococcus aureus* transporters Hts, Sir, and Sst capture iron liberated from human transferrin by Staphyloferrin A, Staphyloferrin B, and catecholamine stress hormones, respectively, and contribute to virulence. *Infection and Immunity*. 79 (6), 2345–2355.
- Beauchamp, C. & Fridovich, I. (1971) Superoxide dismutase: improved assays and an assay applicable to acrylamide gels. *Analytical biochemistry*. 44 (1), 276–287.

- Begier, E., Seiden, D.J., Patton, M., Zito, E., Severs, J., Cooper, D., Eiden, J., Gruber, W.C., Jansen, K.U., Anderson, A.S. & Gurtman, A. (2017) SA4Ag, a 4-antigen *Staphylococcus aureus* vaccine, rapidly induces high levels of bacteria-killing antibodies. *Vaccine*. 35 (8), 1132–1139.
- Benito, D., Lozano, C., Rezusta, A. & Ferrer, I. (2014) Characterization of tetracycline and methicillin resistant *Staphylococcus aureus* strains in a Spanish hospital: Is livestock-contact a risk factor in infections caused by MRSA CC398?. *International Journal of Medical Microbiology*, 304(8), 1226-1232.
- Benov, L. T., & Fridovich, I. (1994). *Escherichia coli* expresses a copper-and zinc-containing superoxide dismutase. *Journal of Biological Chemistry*, 269(41), 25310-25314.
- Bergey, D. H. & Breed, R. S. *Bergey's Manual of Determinative Bacteriology* 464–466 (Williams & Wilkins Co., 1957)
- Berntzen, H.B., Ölmez, Ü., Fagerhol, M.K. and Munthe, E. (1991). The leukocyte protein L1 in plasma and synovial fluid from patients with rheumatoid arthritis and osteoarthritis. *Scandinavian Journal of Rheumatology*, 20(2), pp.74-82.
- Bertani, G. (1951) Studies on lysogenesis. I. The mode of phage liberation by lysogenic *Escherichia coli*. *Journal of Bacteriology*. 62 (3), 293–300.
- Berube, B.J. & Wardenburg, J. B. (2013) *Staphylococcus aureus* α -toxin: nearly a century of intrigue. *Toxins*. 5 (6), 1140–1166.
- Beyer, W. F., & Fridovich, I. (1991). *In vivo* competition between iron and manganese for occupancy of the active site region of the manganese-superoxide dismutase of *Escherichia coli*. *Journal of Biological Chemistry*, 266(1), 303-308.
- Bhalla, A., Aron, D.C. & Donskey, C.J. (2007) *Staphylococcus aureus* intestinal colonization is associated with increased frequency of *S. aureus* on skin of hospitalized patients. *BMC Infectious Diseases*. 7(1):105.
- Bischoff, M. & Berger-Bachi, B. (2001) Teicoplanin stress-selected mutations increasing ζ B activity in *Staphylococcus aureus*. *Antimicrobial Agents and Chemotherapy*, 45(6), 1714-1720.
- Bischoff, M., Dunman, P., Kormanec, J., Macapagal, D., Murphy, E., Mounts, W., Berger-Bachi, B. & Projan, S. (2004) Microarray-Based Analysis of the *Staphylococcus aureus* B Regulon. *Journal of Bacteriology*. 186 (13), 4085–4099.
- Bond, C.S. & Schüttelkopf, A.W. (2009) ALINE: a WYSIWYG protein-sequence alignment editor for publication-quality alignments. *Acta Crystallographica Section D: Biological Crystallography*. 65 (5), 510–512.
- Botella, H., Peyron, P., Levillain, F., Poincloux, R., Poquet, Y., Brandli, I., et al. (2011). Mycobacterial P1-type ATPases mediate resistance to zinc poisoning in human macrophages. *Cell Host & Microbe*, 10, 248–259.

- Bourgeois-Nicolaos, N., Lucet, J.-C., Daubié, C., Benchaba, F., Rajguru, M., Ruimy, R., Andremont, A. & Armand-Lefèvre, L. (2010) Maternal vaginal colonisation by *Staphylococcus aureus* and newborn acquisition at delivery. *Paediatric and Perinatal Epidemiology*. 24 (5), 488–491.
- Brock, C.J. & Harris, J.I. (1977) Superoxide dismutase from *Bacillus stearothermophilus*: reversible removal of manganese and its replacement by other metals. *Journal of Molecular Biology*. 5 (5), 1537–1539.
- Bronner, S., Monteil, H. & Prévost, G. (2004) Regulation of virulence determinants in *Staphylococcus aureus*: complexity and applications. *FEMS Microbiology Reviews*, 28 (2): 183–200.
- Brosnahan, A.J. & Schlievert, P.M. (2011) Gram-positive bacterial superantigen outside-in signaling causes toxic shock syndrome. *The FEBS Journal*. 278 (23), 4649–4667.
- Brown, A.F., Leech, J.M., Rogers, T.R. & McLoughlin, R.M. (2014) *Staphylococcus aureus* Colonization: Modulation of Host Immune Response and Impact on Human Vaccine Design. *Frontiers in immunology*. 4, 507.
- Burlak, C., Hammer, C.H., Robinson, M.-A., Whitney, A.R., McGavin, M.J., Kreiswirth, B.N. & DeLeo, F.R. (2007) Global analysis of community-associated methicillin-resistant *Staphylococcus aureus* exoproteins reveals molecules produced *in vitro* and during infection. *Cellular Microbiology*. 9 (5), 1172–1190.
- Butaye, P., Argudín, M.A. & Smith, T.C. (2016) Livestock-Associated MRSA and Its Current Evolution. *Current Clinical Microbiology Reports*. 3 (1), 19–31.
- Canonne-Hergaux, F. (2002) Expression and subcellular localization of NRAMP1 in human neutrophil granules. *Blood*. 100 (1), 268–275.
- Capella-Gutiérrez, S., Silla-Martínez, J.M. & Gabaldón, T. (2009) trimAl: a tool for automated alignment trimming in large-scale phylogenetic analyses. *Bioinformatics (Oxford, England)*. 25 (15), 1972–1973.
- Carleton, H.A., Diep, B.A., Charlebois, E.D., Sensabaugh, G.F. & Perdreau Remington, F. (2004) Community-Adapted Methicillin-Resistant *Staphylococcus aureus* (MRSA): Population Dynamics of an Expanding Community Reservoir of MRSA. *Journal of Infectious Diseases*. 190 (10), 1730–1738.
- Casey, A.L., Adams, D., Karpanen, T.J., Lambert, P.A., Cookson, B.D., Nightingale, P., Miruszenko, L., Shillam, R., Christian, P. & Elliott, T.S.J. (2010) Role of copper in reducing hospital environment contamination. *The Journal of Hospital Infection*. 74 (1), 72–77.
- Cassat, J.E. & Skaar, E.P. (2011) Metal ion acquisition in *Staphylococcus aureus*: overcoming nutritional immunity. *Seminars in Immunopathology*. 34 (2), 215–235.

- Cavaco, L. M., Hasman, H., & Aarestrup, F. M. (2011). Zinc resistance of *Staphylococcus aureus* of animal origin is strongly associated with methicillin resistance. *Veterinary Microbiology*. 150(3–4), 344–348.
- Cavaco, L. M., Hasman, H., Stegger, M., Andersen, P. S., Skov, R., Fluit, A. C. (2010). Cloning and occurrence of *czrC*, a gene conferring cadmium and zinc resistance in methicillin-resistant *Staphylococcus aureus* CC398 isolates. *Antimicrobial Agents and Chemotherapy*, 54(9), 3605–3608.
- Cellier, M.F., Courville, P. & Campion, C. (2007) Nramp1 phagocyte intracellular metal withdrawal defense. *Microbes and Infection*. 9(14), 1662-1670.
- Centers for Disease Control and Prevention (CDC). (2015) Antibiotic resistance threats in the United States, Atlanta: CDC; 2013. (<https://www.cdc.gov/drugresistance/threat-report-2013/pdf/ar-threats-2013-508.pdf>, accessed 18 August 2017).
- Chaibenjawong, P. & Foster, S.J. (2011). Desiccation tolerance in *Staphylococcus aureus*. *Archives of Microbiology*. 193(2), 125-135.
- Chan, P.F. & Foster, S.J. (1998) The role of environmental factors in the regulation of virulence-determinant expression in *Staphylococcus aureus* 8325-4. *Microbiology*. 144 (9), 2469–2479.
- Chan, P.F., Foster, S.J., Ingham, E. & Clements, M.O. (1998) The *Staphylococcus aureus* alternative sigma factor sigmaB controls the environmental stress response but not starvation survival or pathogenicity in a mouse abscess model. *Journal of Bacteriology*. 180 (23), 6082–6089.
- Chang, S., Sievert, D.M., Hageman, J.C., Boulton, M.L., Tenover, F.C., Downes, F.P., Shah, S., Rudrik, J.T., Pupp, G.R., Brown, W.J., Cardo, D. & Fridkin, S.K. (2003) Infection with Vancomycin-Resistant *Staphylococcus aureus* Containing the *vanA* Resistance Gene. *New England Journal of Medicine*. 348 (14), 1342–1347.
- Chang, W., Small, D.A., Toghrol, F. & Bentley, W.E. (2006) Global Transcriptome Analysis of *Staphylococcus aureus* Response to Hydrogen Peroxide. *Journal of Bacteriology*. 188 (4), 1648–1659.
- Chen, P.R., Nishida, S., Poor, C.B., Cheng, A., Bae, T., Kuechenmeister, L., Dunman, P.M., Missiakas, D. & He, C. (2009) A new oxidative sensing and regulation pathway mediated by the MgrA homologue SarZ in *Staphylococcus aureus*. *Molecular Microbiology*. 71 (1), 198–211.
- Chen, V.B., Arendal, W.B.I., Headd, J.J., Keedy, D.A., Immormino, R.M., Kapral, G.J., Murray, L.W., Richardson, J.S. & Richardson, D.C. (2010) MolProbity: all-atom structure validation for macromolecular crystallography. *Acta Crystallographica Section D: Biological Crystallography*. 66 (1), 12.
- Cheng, A.G., Kim, H.K., Burts, M.L., Krausz, T., Schneewind, O. & Missiakas, D.M. (2009) Genetic requirements for *Staphylococcus aureus* abscess formation and persistence in host tissues. *The FASEB Journal*. 23 (10), 3393–3404.

- Cheung, A.L., Bayer, A.S., Zhang, G., Gresham, H. & Xiong, Y.Q. (2004) Regulation of virulence determinants *in vitro* and *in vivo* in *Staphylococcus aureus*. *FEMS Immunology & Medical Microbiology*, 40 (1): 1–9.
- Cheung, A.L., Nishina, K. A, Trottonda, M.P. & Tamber, S. (2008) The SarA protein family of *Staphylococcus aureus*. *The International Journal of Biochemistry & Cell Biology*, 40 (3): 355–61.
- Cheung, G.Y.C., Joo, H.-S., Chatterjee, S.S. & Otto, M. (2014) Phenol-soluble modulins-critical determinants of staphylococcal virulence. *FEMS Microbiology Reviews*. 38 (4), 698–719.
- Christine C. Winterbourn and Anthony J. Kettle. *Antioxidants & Redox Signaling*. 2013, 18(6): 642-660.
- Chu, V.H., Crosslin, D.R., Friedman, J.Y. & Reed, S.D. (2005) *Staphylococcus aureus* bacteremia in patients with prosthetic devices: costs and outcomes. *The American Journal of Medicine*, 118(12), 1416-e19.
- Clare, D.A., Blum, J. & Fridovich, I. (1984) A hybrid superoxide dismutase containing both functional iron and manganese. *Journal of Biological Chemistry*. 259 (9), 5932–5936.
- Clements, M. O., & Foster, S. J. (1999). Stress resistance in *Staphylococcus aureus*. *Trends in microbiology*, 7(11), 458-462.
- Clements, M.O., Watson, S.P. & Foster, S.J. (1999) Characterization of the major superoxide dismutase of *Staphylococcus aureus* and its role in starvation survival, stress resistance, and pathogenicity. *Journal of Bacteriology*. 181 (13), 3898–3903.
- Clohessy, P.A. & Golden, B.E. (1995) Calprotectin-mediated zinc chelation as a biostatic mechanism in host defence. *Scandinavian Journal of Immunology*. 42 (5), 551–556.
- Cooper, J.B., McIntyre, K., Badasso, M.O., Wood, S.P., Zhang, Y., Garbe, T.R. & Young, D. (1995) X-ray Structure Analysis of the Iron-dependent Superoxide Dismutase from *Mycobacterium tuberculosis* at 2.0 Ångstroms Resolution Reveals Novel Dimer–Dimer Interactions. *Journal of Molecular Biology*. 246 (4), 531–544.
- Corbin, B.D., Seeley, E.H., Raab, A., Feldmann, J., Miller, M.R., Torres, V.J., Anderson, K.L., Dattilo, B.M., Dunman, P.M., Gerads, R., Caprioli, R.M., Nacken, W., Chazin, W.J. & Skaar, E.P. (2008) Metal chelation and inhibition of bacterial growth in tissue abscesses. *Science*. 319 (5865), 962–965.
- Cosgrove, K., Coutts, G., Jonsson, I.M., Tarkowski, A., Kokai-Kun, J.F., Mond, J.J. & Foster, S.J. (2007) Catalase (KatA) and Alkyl Hydroperoxide Reductase (AhpC) Have Compensatory Roles in Peroxide Stress Resistance and Are Required for Survival, Persistence, and Nasal Colonization in *Staphylococcus aureus*. *Journal of Bacteriology*. 189 (3), 1025–1035.
- Cotruvo, J.A., Jr & Stubbe, J. (2012) Metalation and mismetalation of iron and manganese proteins *in vitro* and *in vivo*: the class I ribonucleotide reductases as a case study. *Metallomics*. 4 (10), 1020.

- Cue, D., Lei, M.G. & Lee, C.Y. (2012) Genetic regulation of the intercellular adhesion locus in staphylococci. *Frontiers in Cellular and Infection Microbiology*. (2), 38.
- Damo, S.M., Kehl-Fie, T.E., Sugitani, N., Holt, M.E., Rathi, S., Murphy, W.J., Zhang, Y., Betz, C., Hench, L., Fritz, G., Skaar, E.P. & Chazin, W.J. (2013) Molecular basis for manganese sequestration by calprotectin and roles in the innate immune response to invading bacterial pathogens. *Proceedings of the National Academy of Sciences*, 110(10), 3841-3846.
- Das, A. & Mukhopadhyay, C. (2009) Urea-mediated protein denaturation: a consensus view. *The Journal of Physical Chemistry*. 113 (38), 12816–12824.
- Davies, M.J. (2005) The oxidative environment and protein damage. *Biochimica et Biophysica Acta (BBA) - Proteins and Proteomics*. 1703 (2), 93–109.
- de Haas, C.J.C., Veldkamp, K.E., Peschel, A., Weerkamp, F., Van Wamel, W.J.B., Heezius, E.C.J.M., Poppelier, M.J.J.G., Van Kessel, K.P.M. & van Strijp, J.A.G. (2004) Chemotaxis Inhibitory Protein of *Staphylococcus aureus*, a Bacterial Antiinflammatory Agent. *The Journal of experimental medicine*. 199 (5), 687–695.
- de Oliveira, G.A.P. & Silva, J.L. (2015) A hypothesis to reconcile the physical and chemical unfolding of proteins. *Proceedings of the National Academy of Sciences*. 112 (21), E2775–84.
- De Vendittis, A., Amato, M., Mickiewicz, A., Parlato, G., De Angelis, A., Castellano, I., Rullo, R., Riccitiello, F., Rengo, S., Masullo, M. & De Vendittis, E. (2010) Regulation of the properties of superoxide dismutase from the dental pathogenic microorganism *Streptococcus mutans* by iron- and manganese-bound co-factor. *Molecular bioSystems*. 6 (10), 1973–1982.
- De Vendittis, A., Marco, S., Di Maro, A., Chambery, A., Albino, A., Masullo, M., Michniewicz, A., Parlato, G., De Angelis, A., De Vendittis, E. & Rullo, R. (2012) Properties of a putative cambialistic superoxide dismutase from the aerotolerant bacterium *Streptococcus thermophilus* Strain LMG 18311. *Protein & Peptide Letters*. 19 (3), 333–344.
- Dewitt, S.K. & Adelberg, E.A. (1962) The Occurrence of a genetic transposition in a strain of *Escherichia Coli*. *Genetics*. 47 (5), 577–585.
- Diederichs, K. & Karplus, P.A. (2013) Better models by discarding data? *Acta Crystallographica Section D: Biological Crystallography*. 69 (7), 1215–1222.
- Diekema, D.J., Pfaller, M.A., Schmitz, F.J., Smayevsky, J., Bell, J., Jones, R.N., Beach, M. SENTRY Participants Group (2001) Survey of Infections Due to Staphylococcus Species: Frequency of Occurrence and Antimicrobial Susceptibility of Isolates Collected in the United States, Canada, Latin America, Europe, and the Western Pacific Region for the SENTRY Antimicrobial Surveillance Program, 1997–1999. *Clinical Infectious Diseases*. 32 (2), S114–S132.
- Dinges, M.M., Orwin, P.M. & Schlievert, P.M. (2000) Exotoxins of *Staphylococcus aureus*. *Clinical Microbiology Reviews*. 13 (1), 16–34.

- Dudev, T. & Lim, C. (2013) Competition among metal ions for protein binding sites: determinants of metal ion selectivity in proteins. *Chemical reviews*, 114(1), 538-556.
- Dudev, T., Lin, Y.-L., Dudev, M. & Lim, C. (2003) First-second shell interactions in metal binding sites in proteins: a PDB survey and DFT/CDM calculations. *Journal of the American Chemical Society*. 125 (10), 3168–3180.
- DuMont, A.L. & Torres, V.J. (2014) Cell targeting by the *Staphylococcus aureus* pore-forming toxins: it's not just about lipids. *Trends in Microbiology*. 22 (1), 21–27.
- Dupont, C. L., Neupane, K., Shearer, J., & Palenik, B. (2008). Diversity, function and evolution of genes coding for putative Ni-containing superoxide dismutases. *Environmental microbiology*. 10(7), 1831-1843.
- Duthie, E. and Lorenz, L.L., 1952. Staphylococcal coagulase: mode of action and antigenicity. *Microbiology*, 6(1-2). 95-107.
- Eddy, R.S. (2001) HMMER: Profile hidden Markov models for biological sequence analysis. Available from: <http://hmmer.wustl.edu/>. (Accessed 19 September 2017).
- Edwards, R.A., Baker, H.M., Whittaker, M.M., Whittaker, J.W., Jameson, G.B. & Baker, E.N. (1998) Crystal structure of *Escherichia coli* manganese superoxide dismutase at 2.1-Å resolution. *JBIC Journal of Biological Inorganic Chemistry*. 3 (2), 161–171.
- Edwards, R.A., Whittaker, M.M., Whittaker, J.W., Baker, E.N. & Jameson, G.B. (2001a) Outer sphere mutations perturb metal reactivity in manganese superoxide dismutase. *Biochemistry*. 40 (1), 15–27.
- Edwards, R.A., Whittaker, M.M., Whittaker, J.W., Baker, E.N. & Jameson, G.B. (2001b) Removing a hydrogen bond in the dimer interface of *Escherichia coli* manganese superoxide dismutase alters structure and reactivity. *Biochemistry*. 40 (15), 4622–4632.
- EFSA (European Food Safety Authority) and ECDC (European Centre for Disease Prevention and Control), 2017. The European Union summary report on antimicrobial resistance in zoonotic and indicator bacteria from humans, animals and food in 2015. *EFSA Journal*. 15(2):4694,212
- Eiff, Von, C., Becker, K., Machka, K., Stammer, H. & Peters, G. (2001) Nasal carriage as a source of *Staphylococcus aureus* bacteremia. *New England Journal of Medicine*. 344 (1), 11–16.
- Elbir, H., Robert, C., Nguyen, T.T., Gimenez, G., Sanousi, El, S.M., Flock, J.-I., Raoult, D. & Drancourt, M. (2013) *Staphylococcus aureus* subsp. *anaerobius* strain ST1464 genome sequence. *Standards in Genomic Sciences*. 9 (1), 1–11.
- Emine Yikilmaz, Jason Porta, Laurie E Grove, Ardeschir Vahedi-Faridi, Yuriy Bronshteyn, Thomas C Brunold, Gloria E O Borgstahl, A. & Anne-Frances Miller (2007) How can a single second sphere amino acid substitution cause reduction midpoint potential changes of hundreds of millivolts? *Journal of the American Chemical Society*. 129 (32), 9927–9940.

- Emsley, P., Lohkamp, B., Scott, W.G. & Cowtan, K. (2010) Features and development of Coot. *Acta Crystallographica Section D: Biological Crystallography*. 66 (4), 486–501.
- European Centre for Disease Prevention and Control (ECDC). (2015). Antimicrobial resistance surveillance in Europe 2015. Annual Report of the European Antimicrobial Resistance Surveillance Network (EARS-Net). (<https://ecdc.europa.eu/sites/portal/files/media/en/publications/Publications/antimicrobial-resistance-europe-2015.pdf>, accessed 18 August 2017).
- Evans, P.R. & Murshudov, G.N. (2013) How good are my data and what is the resolution? *Acta Crystallographica Section D: Biological Crystallography*. 69 (Pt 7), 1204–1214.
- Fang, F.C. (2004) Antimicrobial reactive oxygen and nitrogen species: concepts and controversies. *Nature reviews. Microbiology*, 2(10), 820.
- Feil, E.J., Cooper, J.E., Grundmann, H., Robinson, D.A., Enright, M.C., Berendt, T., Peacock, S.J., Smith, J.M., Murphy, M., Spratt, B.G., Moore, C.E. & Day, N.P.J. (2003) How clonal is *Staphylococcus aureus*? *Journal of Bacteriology*. 185 (11), 3307–3316.
- Feng, Y., Chen, C.J., Su, L.H., Hu, S. & Yu, J. (2008) Evolution and pathogenesis of *Staphylococcus aureus*: lessons learned from genotyping and comparative genomics. *FEMS Microbiology Reviews*. 32(1), 23-37.
- Fernandes, S., Geueke, B., Delgado, O., Coleman, J. & Hatti-Kaul, R. (2002) β -Galactosidase from a cold-adapted bacterium: purification, characterization and application for lactose hydrolysis. *Applied Microbiology and Biotechnology*. 58 (3), 313–321.
- Fielden, E.M., Roberts, P.B., Bray, R.C., Lowe, D.J., Mautner, G.N., Rotilio, G. & Calabrese, L. (1974) Mechanism of action of superoxide dismutase from pulse radiolysis and electron paramagnetic resonance. Evidence that only half the active sites function in catalysis. *The Biochemical Journal*. 139 (1), 49–60.
- Fink, R.C. & Scandalios, J.G. (2002) Molecular evolution and structure-function relationships of the superoxide dismutase gene families in angiosperms and their relationship to other eukaryotic and prokaryotic superoxide dismutases. *Archives of Biochemistry and Biophysics*. 399 (1), 19–36.
- Fitzgerald, J. R., Sturdevant, D. E., Mackie, S. M., Gill, S. R. and Musser, J. M. (2001). Evolutionary genomics of *Staphylococcus aureus*: insights into the origin of methicillin-resistant strains and the toxic shock syndrome epidemic. *Proceedings of the National Academy of Sciences*. 98(15), 8821-8826.
- Flint, D.H., Tuminello, J.F. & Emptage, M.H. (1993) The inactivation of Fe-S cluster containing hydro-lyases by superoxide. *The Journal of Biological Chemistry*. 268 (30), 22369–22376.
- Foster, T.J. (2017) Antibiotic resistance in *Staphylococcus aureus*. Current status and future prospects. *FEMS Microbiology Reviews*. 41 (3), 430–449.

- Foster, T.J. & Höök, M. (1998) Surface protein adhesins of *Staphylococcus aureus*. Trends in Microbiology. 6 (12), 484–488.
- Friedman, D.B., Stauff, D.L., Pishchany, G., Whitwell, C.W., Torres, V.J. & Skaar, E.P. (2006) *Staphylococcus aureus* redirects central metabolism to increase iron availability. PLoS Pathogens. 2 (8), e87.
- Frison, G. & Ohanessian, G. (2009) Metal-histidine-glutamate as a regulator of enzymatic cycles: a case study of carbonic anhydrase. Physical Chemistry Chemical Physics. 11(2), 374-383.
- Fuchs, S., Zühlke, D., Pané-Farré, J., Kusch, H., Wolf, C., Reiß, S., Binh, L.T.N., Albrecht, D., Riedel, K., Hecker, M. & Engelmann, S. (2013) Aureolib - a proteome signature library: towards an understanding of *Staphylococcus aureus* pathophysiology. PLOS ONE. 8 (8), e70669.
- Gagnon, D.M., Brophy, M.B., Bowman, S.E.J., Stich, T.A., Drennan, C.L., Britt, R.D. & Nolan, E.M. (2015) Manganese binding properties of human calprotectin under conditions of high and low calcium: X-ray crystallographic and advanced electron paramagnetic resonance spectroscopic analysis. Journal of the American Chemical Society. 137 (8), 3004–3016.
- Gao, R. & Stock, A.M. (2009) Biological insights from structures of two-component proteins. Annual Review of Microbiology. 63, 133-154.
- Garcia, Y.M., Barwinska-Sendra, A., Tarrant, E., Skaar, E.P., Waldron, K.J. & Kehl-Fie, T.E. (2017) A Superoxide dismutase capable of functioning with iron or manganese promotes the resistance of *Staphylococcus aureus* to calprotectin and nutritional immunity. PLoS Pathogens. 13 (1), e1006125.
- Gardete, S. & Tomasz, A. (2014) Mechanisms of vancomycin resistance in *Staphylococcus aureus*. The Journal of Clinical Investigation. 124(7), 2836.
- Garrity, G. M., Bell, J. A., & Lilburn, T. (2015). Epsilonproteobacteria class. nov In: Bergey's Manual® of Systematics of Archaea and Bacteria.
- Gätjens, J., Sjödin, M., Pecoraro, V.L. & Un, S. (2007) The Relationship between the Manganese(II) zero-field interaction and Mn(II)/Mn(III) redox potential of Mn(4'-X-terpy) complexes. Journal of the American Chemical Society. 129 (45), 13825–13827.
- Gaupp, R., Ledala, N., & Somerville, G. A. (2012). Staphylococcal response to oxidative stress. Frontiers in Cellular and Infection Microbiology. (2), 33
- Gordon, R.J. & Lowy, F.D. (2008) Pathogenesis of methicillin-resistant *Staphylococcus aureus* infection. Clinical Infectious Diseases. 46, S350-S359.
- Gort, A.S., Ferber, D.M., & Imlay, J.A. (1999) The regulation and role of the periplasmic copper, zinc superoxide dismutase of *Escherichia coli*. Molecular Microbiology. 32(1), 179-191.
- Gouy, M., Guindon, S. & Gascuel, O. (2010) SeaView version 4: A multiplatform graphical user interface for sequence alignment and phylogenetic tree building. Molecular Biology and Evolution. 27 (2), 221–224.

- Graveland, H., Duim, B., van Duijkeren, E., Heederik, D. & Wagenaar, J.A. (2011) Livestock-associated methicillin-resistant *Staphylococcus aureus* in animals and humans. *International Journal of Medical Microbiology*. 301 (8), 630–634.
- Greenleaf, W.B., Perry, J.J.P., Hearn, A.S., Cabelli, D.E., Lepock, J.R., Stroupe, M.E., Tainer, J.A., Nick, H.S. & Silverman, D.N. (2004) Role of hydrogen bonding in the active site of human manganese superoxide dismutase. *Biochemistry*. 43 (22), 7038–7045.
- Gregory E.M. (1985) Characterization of the O₂-induced manganese-containing superoxide dismutase from *Bacteroides fragilis*. *Archives of Biochemistry and Biophysics*. 238, 83-9.
- Gribenko, A., Mosyak, L., Ghosh, S., Parris, K., Svenson, K., Moran, J., Chu, L., Li, S., Liu, T., Woods, V.L., Jr., Jansen, K.U., Green, B.A., Anderson, A.S. & Matsuka, Y.V. (2013) Three-dimensional structure and biophysical characterization of *Staphylococcus aureus* cell surface antigen–manganese transporter MntC. *Journal of Molecular Biology*. 425 (18), 3429–3445.
- Grossoehme, N., Kehl-Fie, T.E., Ma, Z., Adams, K.W., Cowart, D.M., Scott, R.A., Skaar, E.P. & Giedroc, D.P. (2011) Control of copper resistance and inorganic sulfur metabolism by paralogous regulators in *Staphylococcus aureus*. *Journal of Biological Chemistry*. 286 (15), 13522–13531.
- Grove, L.E., Xie, J., Yikilmaz, E., Karapetyan, A., Miller, A.-F. & Brunold, T.C. (2008) Spectroscopic and computational insights into second-sphere amino-acid tuning of substrate analogue/active-site interactions in iron(III) superoxide dismutase. *Inorganic Chemistry*. 47 (10), 3993–4004.
- Hammer, N.D. & Skaar, E.P. (2011) Molecular mechanisms of *Staphylococcus aureus* iron acquisition. *Annual Review of Microbiology*. (65), 129–147.
- Handke, L.D., Hawkins, J.C., Miller, A.A., Jansen, K.U. & Anderson, A.S. (2013) Regulation of *Staphylococcus aureus* MntC expression and its role in response to oxidative stress. *PLOS ONE*. 8 (10), e77874.
- Hansch, C., Leo, A. & Taft, R.W. (1991) A survey of Hammett substituent constants and resonance and field parameters. *Chemical Reviews*. 91(2), 165-195.
- Harris, L.G., Foster, S.J. and Richards, R.G., 2002. An introduction to *Staphylococcus aureus*, and techniques for identifying and quantifying *S. aureus* adhesins in relation to adhesion to biomaterials: review. *European Cell and Materials*, 4(3), 39 – 60.
- Hartman, B.J. & Tomasz, A. (1984) Low-affinity penicillin-binding protein associated with beta-lactam resistance in *Staphylococcus aureus*. *Journal of Bacteriology*. 158 (2), 513–516.
- Haslinger-Löffler, B., Kahl, B.C., Grundmeier, M., Strangfeld, K., Wagner, B., Fischer, U., Cheung, A.L., Peters, G., Schulze-Osthoff, K. & Sinha, B. (2005) Multiple virulence factors are required for *Staphylococcus aureus*-induced apoptosis in endothelial cells. *Cellular Microbiology*. 7 (8), 1087–1097.

- Hassan, H. M., & Fridovich, I. (1977a). Regulation of the synthesis of superoxide dismutase in *Escherichia coli*. Induction by methyl viologen. *Journal of Biological Chemistry*. 252(21), 7667-7672.
- Hassan, H. M., & Fridovich, I. (1977b). Enzymatic defenses against the toxicity of oxygen and of streptonigrin in *Escherichia coli*. *Journal of Bacteriology*. 129(3), 1574-1583.
- Hearn, A.S., Fan, L., Lepock, J.R. & Luba, J.P. (2004) Amino acid substitution at the dimeric interface of human manganese superoxide dismutase. *Journal of Biological Chemistry*. 279(7), 5861-5866.
- Hecker, M., Engelmann, S. & Cordwell, S.J. (2003) Proteomics of *Staphylococcus aureus*—current state and future challenges. *Journal of Chromatography B*. 787(1), 179-195.
- Hecker, M., Reder, A., Fuchs, S. & Pagels, M. (2009) Physiological proteomics and stress/starvation responses in *Bacillus subtilis* and *Staphylococcus aureus*. *Research in Microbiology*. 160(4), 245-258.
- Helmann, J.D. (2014) Specificity of metal sensing: iron and manganese homeostasis in *Bacillus subtilis*. *Journal of Biological Chemistry*. 289 (41), 28112–28120.
- Henriques, I., Tacão, M., Leite, L., Fidalgo, C., Araújo, S., Oliveira, C. & Alves, A. (2016) Co-selection of antibiotic and metal(loid) resistance in gram-negative epiphytic bacteria from contaminated salt marshes. *Marine Pollution Bulletin*. 109 (1), 427–434.
- Herbert, S., Bera, A., Nerz, C., Kraus, D., Peschel, A., Goerke, C., Götz, F. (2007). Molecular basis of resistance to muramidase and cationic antimicrobial peptide activity of lysozyme in staphylococci. *PLoS pathogens*. 3(7), e102.
- Herbst, R.W., Guce, A., Bryngelson, P.A., Higgins, K.A., Ryan, K.C., Cabelli, D.E., Garman, S.C. & Maroney, M.J. (2009) Role of conserved tyrosine residues in NiSOD catalysis: a case of convergent evolution. *Biochemistry*. 48 (15), 3354–3369.
- Hiramatsu, K., Hanaki, H., Ino, T., Yabuta, K., Oguri, T. & Tenover, F.C. (1997) Methicillin-resistant *Staphylococcus aureus* clinical strain with reduced vancomycin susceptibility. *The Journal of Antimicrobial Chemotherapy*. 40 (1), 135–136.
- Holden, M. T., & Lindsay, J. A. (2008). Whole genomes: sequence, microarray and systems biology. *Staphylococcus: molecular genetics*. Caister Academic Press, Norfolk, UK, 1-28.
- Holden, M.T.G., Hsu, L.Y., Kurt, K., Weinert, L.A., Mather, A.E., Harris, S.R., Strommenger, B., Layer, F., Witte, W., de Lencastre, H., Skov, R., Westh, H., Zemlickova, H., Coombs, G., Kearns, A.M., Hill, R.L.R., Edgeworth, J., Gould, I., Gant, V., et al. (2013) A genomic portrait of the emergence, evolution, and global spread of a methicillin-resistant *Staphylococcus aureus* pandemic. *Genome Research*. 23 (4), 653–664.
- Hong-Duk, Y., Eun-Ja, K., Jung-Hye, R., HAH, Y. C., & Sa-Ouk, K. (1996). A novel nickel-containing superoxide dismutase from *Streptomyces* spp. *Biochemical Journal*. 318(3), 889-896.

- Horsburgh, M.J., Aish, J.L., White, I.J., Shaw, L., Lithgow, J.K. & Foster, S.J. (2002) sigmaB modulates virulence determinant expression and stress resistance: characterization of a functional rsbU strain derived from *Staphylococcus aureus* 8325-4. *Journal of Bacteriology*. 184 (19), 5457–5467.
- Horsburgh, M.J., Clements, M.O., Crossley, H., Ingham, E. & Foster, S.J. (2001) PerR controls oxidative stress resistance and iron storage proteins and is required for virulence in *Staphylococcus aureus*. *Infection and Immunity*. 69 (6), 3744–3754.
- Horsburgh, M.J., Ingham, E. & Foster, S.J. (2001) In *Staphylococcus aureus*, Fur is an interactive regulator with PerR, contributes to virulence, and is necessary for oxidative stress resistance through positive regulation of catalase and iron homeostasis. *Journal of Bacteriology*. 183 (2), 468–475.
- Horsburgh, M.J., Wharton, S.J., Cox, A.G., Ingham, E., Peacock, S. & Foster, S.J. (2002) MntR modulates expression of the PerR regulon and superoxide resistance in *Staphylococcus aureus* through control of manganese uptake. *Molecular Microbiology*. 44 (5), 1269–1286.
- Horsburgh, M.J., Wharton, S.J., Karavolos, M. & Foster, S.J. (2002) Manganese: elemental defence for a life with oxygen. *Trends in microbiology*. 10(11), 496-501.
- Howard, B. J., & Kloss, W. E. (1987). *Staphylococci in clinical and pathogenic microbiology*. Edited by Howard BJ, Tilton RC. The CV Mosby Comp. St. Louis, 238.
- Hsu, J.-L., Hsieh, Y., Tu, C., O'Connor, D., Nick, H.S. & Silverman, D.N. (1996) Catalytic properties of human manganese superoxide dismutase. *Journal of Biological Chemistry*. 271 (30), 17687–17691.
- Hung, H.C. & Chang, G.G. (2001) Differentiation of the slow-binding mechanism for magnesium ion activation and zinc ion inhibition of human placental alkaline phosphatase. *Protein Science*. 10 (1), 34–45.
- Hunter, T., Bannister, J.V. & Hunter, G.J. (2002) Thermostability of manganese- and iron-superoxide dismutases from *Escherichia coli* is determined by the characteristic position of a glutamine residue. *The FEBS Journal*. 269 (21), 5137–5148.
- Hurd, A.F., Garcia-Lara, J., Rauter, Y., Cartron, M., Mohamed, R. and Foster, S.J., 2012. The iron-regulated surface proteins IsdA, IsdB, and IsdH are not required for heme iron utilization in *Staphylococcus aureus*. *FEMS Microbiology Letters*. 329(1),93-100.
- Huseby, M., Shi, K., Brown, C.K., Digre, J., Mengistu, F., Seo, K.S., Bohach, G.A., Schlievert, P.M., Ohlendorf, D.H. & Earhart, C.A. (2007) Structure and biological activities of beta toxin from *Staphylococcus aureus*. *Journal of Bacteriology*. 189 (23), 8719–8726.
- Huttenhower, C., Gevers, D., Knight, R., Abubucker, S., Badger, J.H., Chinwalla, A.T., Creasy, H.H., Earl, A.M., FitzGerald, M.G., Fulton, R.S. and Giglio, M.G., 2012. Structure, function and diversity of the healthy human microbiome. *Nature*, 486(7402), 207-214.

- Imlay, J.A. (2006) Iron-sulphur clusters and the problem with oxygen. *Molecular Microbiology*. 59 (4), 1073–1082.
- Imlay, J.A. (2008) Cellular defenses against superoxide and hydrogen peroxide. *Annual Review of Biochemistry*. (77), 755–776.
- Imlay, J.A. & Linn, S. (1987) Mutagenesis and stress responses induced in *Escherichia coli* by hydrogen peroxide. *Journal of Bacteriology*. 169 (7), 2967–2976.
- Imlay, K. R., & Imlay, J. A. (1996). Cloning and analysis of *sodC*, encoding the copper-zinc superoxide dismutase of *Escherichia coli*. *Journal of Bacteriology*. 178(9), 2564-2571.
- Inkinen, J., Mäkinen, R., Keinänen-Toivola, M.M., Nordström, K. & Ahonen, M. (2016) Copper as an antibacterial material in different facilities. *Letters in Applied Microbiology*. 64 (1), 19–26.
- Irving, H. & Williams, R. (1953) 637. The stability of transition-metal complexes. *Journal of the Chemical Society*. 3192-3210.
- Ito, T., Okuma, K., Ma, X.X., Yuzawa, H. & Hiramatsu, K. (2003) Insights on antibiotic resistance of *Staphylococcus aureus* from its whole genome: genomic island SCC. *Drug Resistance Updates*. 6(1), 41-52.
- Jackson, T.A., Karapetian, A., Miller, A.-F. & Brunold, T.C. (2004) Spectroscopic and computational studies of the azide-adduct of manganese superoxide dismutase: definitive assignment of the ligand responsible for the low-temperature thermochromism. *Journal of the American Chemical Society*. 126 (39), 12477–12491.
- Jamal El Yazal, Rachel R Roe, A. & Pang, Y.-P. (2000) Zinc's affect on proton transfer between imidazole and acetate predicted by ab initio calculations. *The Journal of Physical Chemistry B*. 104(28), 6662-6667.
- Jang, S. & Imlay, J.A. (2007) Micromolar intracellular hydrogen peroxide disrupts metabolism by damaging iron-sulfur enzymes. *Journal of Biological Chemistry*. 282 (2), 929–937.
- Jenkinson, H.F. & Jakubovics, N.S. (2001) Out of the iron age: new insights into the critical role of manganese homeostasis in bacteria. *Microbiology*. 147 (7), 1709–1718.
- Jensen, S.O. & Lyon, B.R. (2009) Genetics of antimicrobial resistance in *Staphylococcus aureus*. *Future Microbiology*. 4 (5), 565–582.
- John P Lisher, D.P.G. (2013) Manganese acquisition and homeostasis at the host-pathogen interface. *Frontiers in Cellular and Infection Microbiology*. (3), 91
- Joint scientific report of ECDC, EFSA and EMEA on meticillin resistant *Staphylococcus aureus* (MRSA) in livestock, companion animals and foods. (2009). 301, 1-10.
- Johnson, D.A. and Nelson, P.G., 1995. Factors determining the ligand field stabilization energies of the hexaaqua 2+ complexes of the first transition series and the Irving-Williams order. *Inorganic Chemistry*. 34(22), 5666-5671.

- Joosten, R.P., Joosten, K., Murshudov, G.N. & Perrakis, A. (2012) PDB_REDO: constructive validation, more than just looking for errors. *Acta Crystallographica Section D: Biological Crystallography*. 68 (4), 484–496.
- Kabsch, W. (2010) XDS. *Acta Crystallographica Section D: Biological Crystallography*. 66 (2), 125–132.
- Karavolos, M.H., Horsburgh, M.J., Ingham, E. & Foster, S.J. (2003) Role and regulation of the superoxide dismutases of *Staphylococcus aureus*. *Microbiology*. 149 (10), 2749–2758.
- Karplus, P.A. & Diederichs, K. (2012) Linking crystallographic model and data quality. *Science*. 336 (6084), 1030–1033.
- Kato, T., Kouzaki, H., Matsumoto, K., Hosoi, J., & Shimizu, T. (2017). The effect of calprotectin on TSLP and IL-25 production from airway epithelial cells. *Allergology International*. 66(2), 281-289.
- Katoh, K. & Standley, D.M. (2013) MAFFT multiple sequence alignment software version 7: improvements in performance and usability. *Molecular Biology and Evolution*. 30 (4), 772–780.
- Keele, B. B., McCord, J. M., & Fridovich, I. (1970). Superoxide dismutase from *Escherichia coli* B a new manganese-containing enzyme. *Journal of Biological Chemistry*. 245(22), 6176-6181.
- Kehl-Fie, T.E. & Skaar, E.P. (2010) Nutritional immunity beyond iron: a role for manganese and zinc. *Current Opinion in Chemical Biology*. 14 (2), 218–224.
- Kehl-Fie, T.E., Chitayat, S., Hood, M.I., Damo, S., Restrepo, N., Garcia, C., Munro, K.A., Chazin, W.J. & Skaar, E.P. (2011) Nutrient metal sequestration by calprotectin inhibits bacterial superoxide defense, enhancing neutrophil killing of *Staphylococcus aureus*. *Cell Host and Microbe*. 10 (2), 158–164.
- Kehl-Fie, T.E., Zhang, Y., Moore, J.L., Farrand, A.J., Hood, M.I., Rathi, S., Chazin, W.J., Caprioli, R.M. & Skaar, E.P. (2013) MntABC and MntH contribute to systemic *Staphylococcus aureus* infection by competing with calprotectin for nutrient manganese. *Infection and Immunity*. 81 (9), 3395–3405.
- Keyer, K. & Imlay, J.A. (1996) Superoxide accelerates DNA damage by elevating free-iron levels. *Proceedings of the National Academy of Sciences*. 93 (24), 13635–13640.
- Keyer, K., Keyer, K., Gort, A.S., Gort, A.S., Imlay, J.A. & Imlay, J.A. (1995) Superoxide and the production of oxidative DNA damage. *Journal of Bacteriology*. 177 (23), 6782–6790.
- Kim, H.K., DeDent, A., Cheng, A.G., McAdow, M., Bagnoli, F., Missiakas, D.M. & Schneewind, O. (2010) IsdA and IsdB antibodies protect mice against *Staphylococcus aureus* abscess formation and lethal challenge. *Vaccine*. 28 (38), 6382–6392.
- Kirby, T., Blum, J., Kahane, I. & Fridovich, I. (1980) Distinguishing between Mn-containing and Fe-containing superoxide dismutases in crude extracts of cells. *Archives of Biochemistry and Biophysics*. 201 (2), 551–555.

- Kirschvink, J.L., Gaidos, E.J., Bertani, L.E., Beukes, N.J., Gutzmer, J., Maepa, L.N. & Steinberger, R.E. (2000) Paleoproterozoic snowball Earth: Extreme climatic and geochemical global change and its biological consequences. *Proceedings of the National Academy of Sciences*. 97 (4), 1400–1405.
- Kloos, W.E. (1980) Natural populations of the genus *Staphylococcus*. *Annual Reviews in Microbiology*, 34(1), 559-592.
- Knight, G.M., Budd, E.L., Whitney, L., Thornley, A., Al-Ghusein, H., Planche, T. & Lindsay, J.A. (2012) Shift in dominant hospital-associated methicillin-resistant *Staphylococcus aureus* (HA-MRSA) clones over time. *Journal of Antimicrobial Chemotherapy*. 67 (10), 2514–2522.
- Kohler, T., Weidenmaier, C., & Peschel, A. (2009). Wall teichoic acid protects *Staphylococcus aureus* against antimicrobial fatty acids from human skin. *Journal of bacteriology*, 191(13), 4482-4484.
- Kreiswirth, B.N., Löfdahl, S., Betley, M.J. & O'Reilly, M. (1983) The toxic shock syndrome exotoxin structural gene is not detectably transmitted by a prophage. *Nature*. 305(5936), 709-712.
- Krismer, B., Weidenmaier, C., Zipperer, A., & Peschel, A. (2017). The commensal lifestyle of *Staphylococcus aureus* and its interactions with the nasal microbiota. *Nature Reviews Microbiology*. 15(11), 675.
- Krissinel, E. & Henrick, K. (2007) Inference of macromolecular assemblies from crystalline state. *Journal of Molecular Biology*. 372(3), 774-797.
- Kuklin, N.A., Clark, D.J., Secore, S., Cook, J., Cope, L.D., McNeely, T., Noble, L., Brown, M.J., Zorman, J.K., Wang, X.M., Pancari, G., Fan, H., Isett, K., Burgess, B., Bryan, J., Brownlow, M., George, H., Meinz, M., Liddell, M.E., et al. (2006) A novel *Staphylococcus aureus* vaccine: iron surface determinant B induces rapid antibody responses in rhesus macaques and specific increased survival in a murine *S. aureus* sepsis model. *Infection and Immunity*. 74 (4), 2215–2223.
- Kullik, I. & Giachino, P. (1997) The alternative sigma factor σ_B in *Staphylococcus aureus*: regulation of the sigB operon in response to growth phase and heat shock. *Archives of Microbiology*. 167 (2-3), 151–159.
- Kuroda, M., Hayashi, H. & Ohta, T. (1999) Chromosome-determined zinc-responsible operon *czr* in *Staphylococcus aureus* strain 912. *Microbiology and Immunology*. 43 (2), 115–125.
- Kuroda, M., Ohta, T., Uchiyama, I., Baba, T., Yuzawa, H., Kobayashi, I., Cui, L., Oguchi, A., Aoki, K., Nagai, Y., Lian, J., Ito, T., Kanamori, M., Matsumaru, H., Maruyama, A., Murakami, H., Hosoyama, A., Mizutani-Ui, Y., Takahashi, N.K., et al. (2001) Whole genome sequencing of methicillin-resistant *Staphylococcus aureus*. *Lancet*. 357 (9264), 1225–1240.
- Kwasigroch J.M., Wintjens R., Gilis D., Rooman M. (2008) SODa: An Mn/Fe superoxide dismutase prediction and design server. *BMC Bioinformatics*. 9, 257.

- La Fuente, De, R., Suarez, G. & Schleifer, K.H. (1985) *Staphylococcus aureus* subsp. *anaerobius* subsp. nov., the causal agent of abscess disease of sheep. *International Journal of Systematic Bacteriology*. 35 (1), 99–102.
- Ladhani, S., Joannou, C.L., Lochrie, D.P., Evans, R.W. & Poston, S.M. (1999) Clinical, microbial, and biochemical aspects of the exfoliative toxins causing staphylococcal scalded-skin syndrome. *Clinical Microbiology Reviews*. 12 (2), 224–242.
- Lah, M.S., Dixon, M.M., Patridge, K.A., Stallings, W.C., Fee, J.A. & Ludwig, M.L. (1995) Structure-function in *Escherichia coli* iron superoxide dismutase: comparisons with the manganese enzyme from *Thermus thermophilus*. *Biochemistry*. 34 (5), 1646–1660.
- Lamarre, C., LeMay, J.D., Deslauriers, N. & Bourbonnais, Y. (2001) *Candida albicans* expresses an unusual cytoplasmic manganese-containing superoxide dismutase (SOD3 gene product) upon the entry and during the stationary phase. *Journal of Biological Chemistry*. 276 (47), 43784–43791.
- Lamers, R.P., Muthukrishnan, G., Castoe, T.A., Tafur, S., Cole, A.M. & Parkinson, C.L. (2012) Phylogenetic relationships among *Staphylococcus* species and refinement of cluster groups based on multilocus data. *BMC Evolutionary Biology*. 12 (1), 71.
- Lancaster, V. L., LoBrutto, R., Selvaraj, F. M., & Blankenship, R. E. (2004). A cambialistic superoxide dismutase in the thermophilic photosynthetic bacterium *Chloroflexus aurantiacus*. *Journal of Bacteriology*. 186(11), 3408-3414.
- Lartillot, N., Lepage, T. & Blanquart, S. (2009) PhyloBayes 3: a Bayesian software package for phylogenetic reconstruction and molecular dating. *Bioinformatics*. 25 (17), 2286–2288.
- Laskowski, R.A. & Chistyakov, V.V. (2005) PDBsum more: new summaries and analyses of the known 3D structures of proteins and nucleic acids. *Nucleic Acids Research*. 33, D266-D268.
- Le, K. Y., & Otto, M. (2015). Quorum-sensing regulation in staphylococci—an overview. *Frontiers in microbiology*. 6, 1174.
- Lebedev, A.A., Vagin, A.A. & Murshudov, G.N. (2008) Model preparation in MOLREP and examples of model improvement using X-ray data. *Acta Crystallographica Section D: Biological Crystallography*. 64 (1), 33–39.
- Lee, J.-W. & Helmann, J.D. (2006) The PerR transcription factor senses H₂O₂ by metal-catalysed histidine oxidation. *Nature*. 440 (7082), 363–367.
- Lentino, J.R. (2003) Prosthetic joint infections: bane of orthopedists, challenge for infectious disease specialists. *Clinical Infectious Diseases*. 36 (9), 1157–1161.
- Lévêque, V.J., Stroupe, M.E., Lepock, J.R., Cabelli, D.E., Tainer, J.A., Nick, H.S. & Silverman, D.N. (2000) Multiple replacements of glutamine 143 in human manganese superoxide dismutase: effects on structure, stability, and catalysis. *Biochemistry*. 39 (24), 7131–7137.
- Li, L.-G., Xia, Y., & Zhang, T. (2017). Co-occurrence of antibiotic and metal resistance genes revealed in complete genome collection. *The ISME Journal*. 11, 651–662.

- Li, Y. X., Xiong, X., Chun-ye, L., Feng-song, Z., Wei, L., & Wei, H. (2010). Cadmium in animal production and its potential hazard on Beijing and Fuxin farmlands. *Journal of Hazardous Materials*. 177(1), 475–480.
- Lindsay, J.A. (2010) Genomic variation and evolution of *Staphylococcus aureus*. *International Journal of Medical Microbiology*. 300(2), 98-103.
- Lindsay, J.A. & Foster, S.J. (2001) Zur: a Zn²⁺-responsive regulatory element of *Staphylococcus aureus*. *Microbiology*. 147 (5), 1259–1266.
- Lindsay, J.A. & Holden, M. (2006) Understanding the rise of the superbug: investigation of the evolution and genomic variation of *Staphylococcus aureus*. *Functional & Integrative Genomics*. 6(3), 186-201.
- Lindsay, J.A. & Holden, M.T.G. (2004) *Staphylococcus aureus*: superbug, super genome? *Trends in Microbiology*. 12 (8), 378–385.
- Liu, C., Bayer, A., Cosgrove, S.E., Daum, R.S., Fridkin, S.K., Gorwitz, R.J., Kaplan, S.L., Karchmer, A.W., Levine, D.P., Murray, B.E., Rybak, M.J., Talan, D.A. & Chambers, H.F. (2011) Clinical practice guidelines by the infectious diseases society of america for the treatment of methicillin-resistant *Staphylococcus aureus* infections in adults and children. *Clinical Infectious Diseases*. 52 (3), e18–e55.
- Liu, G.Y., Essex, A., Buchanan, J.T., Datta, V., Hoffman, H.M., Bastian, J.F., Fierer, J. & Nizet, V. (2005) *Staphylococcus aureus* golden pigment impairs neutrophil killing and promotes virulence through its antioxidant activity. *The Journal of Experimental Medicine*. 202 (2), 209–215.
- Liu, P., Ewis, H.E., Huang, Y.J., Lu, C.D., Tai, P.C. & Weber, I.T. (2007) Structure of *Bacillus subtilis* superoxide dismutase. *Acta Crystallographica Section F Structural Biology and Crystallization Communications*. 63 (12), 1003–1007.
- Lowy, F.D. (1998) *Staphylococcus aureus* Infections. *New England Journal of Medicine*. 339 (8), 520–532.
- Ludwig, M.L., Metzger, A.L., Patridge, K.A. & Stallings, W.C. (1991) Manganese superoxide dismutase from *Thermus thermophilus*. A structural model refined at 1.8 Å resolution. *Journal of Molecular Biology*. 219 (2), 335–358.
- Lushchak, V.I. (2001) Oxidative stress and mechanisms of protection against it in bacteria. *Biochemistry*. 66 (5), 476–489.
- Macomber, L. & Imlay, J.A. (2009) The iron-sulfur clusters of dehydratases are primary intracellular targets of copper toxicity. *Proceedings of the National Academy of Sciences*. 106 (20), 8344–8349.
- Mäder, U., Nicolas, P., Depke, M., Pané-Farré, J., Debarbouille, M., van der Kooi-Pol, M.M., Guérin, C., Dérozier, S., Hiron, A., Jarmer, H., Leduc, A., Michalik, S., Reilman, E., Schaffer, M., Schmidt, F., Bessières, P., Noirot, P., Hecker, M., Msadek, T. (2016) *Staphylococcus aureus*

- transcriptome architecture: from laboratory to infection-mimicking conditions. *PLOS Genetics*. 12 (4), e1005962.
- Majerczyk, C.D., Dunman, P.M., Luong, T.T., Lee, C.Y., Sadykov, M.R., Somerville, G.A., Bodi, K. & Sonenshein, A.L. (2010) Direct targets of CodY in *Staphylococcus aureus*. *Journal of Bacteriology*. 192 (11), 2861–2877.
- Makris, G. (2004) The hyaluronate lyase of *Staphylococcus aureus* - a virulence factor? *Microbiology*. 150 (6), 2005–2013.
- Malachowa, N. & DeLeo, F.R. (2010) Mobile genetic elements of *Staphylococcus aureus*. *Cellular and Molecular Life Sciences*. 67 (18), 3057–3071.
- Malachowa, N., Whitney, A.R., Kobayashi, S.D., Sturdevant, D.E., Kennedy, A.D., Braughton, K.R., Shabb, D.W., Diep, B.A., Chambers, H.F., Otto, M. & DeLeo, F.R. (2011) Global changes in *Staphylococcus aureus* gene expression in human blood. *PLOS ONE*. 6 (4), e18617.
- Maltezou, H.C. & Giamarellou, H. (2006) Community-acquired methicillin-resistant *Staphylococcus aureus* infections. *International Journal of Antimicrobial Agents*. 27(2), 87-96.
- Mandell, G.L. (1975) Catalase, superoxide dismutase, and virulence of *Staphylococcus aureus*. *In vitro* and *in vivo* studies with emphasis on staphylococcal-leukocyte interaction. *Journal of Clinical Investigation*. 55 (3), 561–566.
- Mandelli, F. & Cairo, J.F. (2013) The characterization of a thermostable and cambialistic superoxide dismutase from *Thermus filiformis*. *Letters in Applied Microbiology*. 57(1), 40-46.
- Mariotti, P., Malito, E., Biancucci, M., Surdo, Lo, P., Mishra, R.P.N., Nardi-Dei, V., Savino, S., Nissum, M., Spraggon, G., Grandi, G., Bagnoli, F. & Bottomley, M.J. (2013) Structural and functional characterization of the *Staphylococcus aureus* virulence factor and vaccine candidate FhuD2. *The Biochemical Journal*. 449 (3), 683–693.
- Marshall, C. & McBryde, E. (2014) The role of *Staphylococcus aureus* carriage in the pathogenesis of bloodstream infection. *BMC Research Notes*. 7 (1), 428.
- Martin M.E., Byers B.R., Olson M.O., Salin M.L., Arceneaux J.E., Tolbert C. (1986) A *Streptococcus mutans* superoxide dismutase that is active with either manganese or iron as a cofactor. *Journal of Biological Chemistry*. 261 (20), 9361-7.
- Martins-Costa, M.T.C., Anglada, J.M., Francisco, J.S. & Ruiz-Lopez, M.F. (2012) Reactivity of atmospherically relevant small radicals at the air-water interface. *Angewandte Chemie International Edition*. 51 (22), 5413–5417.
- Mashruwala, A.A. & Boyd, J.M. (2017) The *Staphylococcus aureus* SrrAB regulatory system modulates hydrogen peroxide resistance factors, which imparts protection to aconitase during aerobic growth. *PLOS ONE*. 12 (1), e0170283.

- Masse, E. & Gottesman, S. (2002) A small RNA regulates the expression of genes involved in iron metabolism in *Escherichia coli*. *Proceedings of the National Academy of Sciences*. 99 (7), 4620–4625.
- Matsumoto T., Terauchi K., Isobe T., Matsuoka K., Yamakura F. (1991) Iron- and manganese-containing superoxide dismutases from *Methylobionas*: identity of the protein moiety and amino acid sequence. *Biochemistry*. 30, 3210-6.
- Mazmanian, S.K., Skaar, E.P., Gaspar, A.H., Humayun, M., Gornicki, P., Jelenska, J., Joachmiak, A., Missiakas, D.M. & Schneewind, O. (2003) Passage of heme-iron across the envelope of *Staphylococcus aureus*. *Science*. 299 (5608), 906–909.
- McCord, J. M., & Fridovich, I. (1969). Superoxide dismutase an enzymic function for erythrocyte (hemocuprein). *Journal of Biological Chemistry*, 244(22), 6049-6055.
- McCoy, A.J., Grosse-Kunstleve, R.W., Adams, P.D., Winn, M.D., Storoni, L.C. & Read, R.J. (2007) Phaser crystallographic software. *Journal of Applied Crystallography*. 40 (4), 658–674.
- McGuinness, W., Kobayashi, S. & DeLeo, F. (2016) Evasion of neutrophil killing by *Staphylococcus aureus*. *Pathogens*. 5 (1), 32.
- Meier B., Barra D., Bossa F., Calabrese L., Rotilio G. (1982) Synthesis of either Fe- or Mn-superoxide dismutase with an apparently identical protein moiety by an anaerobic bacterium dependent on the metal supplied. *Journal of Biological Chemistry*. 257 (23), 13977-80.
- Meier, B., Parak, F., Desideri, A. & Rotilio, G. (1997) Comparative stability studies on the iron and manganese forms of the cambialistic superoxide dismutase from *Propionibacterium shermanii*. *FEBS Letters*. 414 (1), 122–124.
- Merchant, A.T. & Spatafora, G.A. (2014) A role for the DtxR family of metalloregulators in gram-positive pathogenesis. *Molecular Oral Microbiology*. 29 (1), 1–10.
- Merlino, A., Russo Krauss, I., Castellano, I., Ruocco, M.R., Capasso, A., De Vendittis, E., Rossi, B. & Sica, F. (2014) Structural and denaturation studies of two mutants of a cold adapted superoxide dismutase point to the importance of electrostatic interactions in protein stability. *Biochimica et Biophysica Acta (BBA)-Proteins and Proteomics*. 1844 (3), 632–640.
- Merriman, J.A., Klingelutz, A.J., Diekema, D.J., Leung, D.Y.M. & Schlievert, P.M. (2015) Novel *Staphylococcus aureus* secreted protein alters keratinocyte proliferation and elicits a proinflammatory response *in vitro* and *in vivo*. *Biochemistry*. 54 (31), 4855–4862.
- Miller, A.-F. (2008) Redox tuning over almost 1 V in a structurally conserved active site: lessons from Fe-containing superoxide dismutase. *Accounts of Chemical Research*. 41 (4), 501–510.
- Miller, A.-F. (2012) Superoxide dismutases: ancient enzymes and new insights. *FEBS Letters*. 586 (5), 585–595.
- Miller, A.-F. & Wang, T. (2017) A single outer-sphere mutation stabilizes apo-mn superoxide dismutase by 35 °C and disfavors mn binding. *Biochemistry*. 56 (29), 3787–3799.

- Miller, A.-F., Padmakumar, K., Sorkin, D.L., Karapetian, A. & Vance, C.K. (2003) Proton-coupled electron transfer in Fe-superoxide dismutase and Mn-superoxide dismutase. *Journal of Inorganic Biochemistry*. 93 (1-2), 71–83.
- Miller, L.G. & Diep, B.A. (2008) Colonization, Fomites, and Virulence: Rethinking the pathogenesis of community-associated methicillin-resistant *Staphylococcus aureus* infection. *Clinical Infectious Diseases*. 46 (5), 752–760.
- Mishra, R.P.N., Mariotti, P., Fiaschi, L., Nosari, S., Maccari, S., Liberatori, S., Fontana, M.R., Pezzicoli, A., De Falco, M.G., Falugi, F., Altindis, E., Serruto, D., Grandi, G. & Bagnoli, F. (2012) *Staphylococcus aureus* FhuD2 is involved in the early phase of staphylococcal dissemination and generates protective immunity in mice. *Journal of Infectious Diseases*. 206 (7), 1041–1049.
- Mizuno, K., Whittaker, M.M., Bächinger, H.P. & Whittaker, J.W. (2004) Calorimetric studies on the tight binding metal interactions of *Escherichia coli* manganese superoxide dismutase. *Journal of Biological Chemistry*. 279 (26), 27339–27344.
- Monk, I.R., Shah, I.M., Xu, M., Tan, M.-W. & Foster, T.J. (2012) Transforming the untransformable: application of direct transformation to manipulate genetically *Staphylococcus aureus* and *Staphylococcus epidermidis*. *mBio*. 3 (2), e00277-11
- Morrissey, J.A., Cockayne, A., Brummell, K. & Williams, P. (2004) The staphylococcal ferritins are differentially regulated in response to iron and manganese and via PerR and Fur. *Infection and Immunity*. 72 (2), 972–979.
- Morrissey, J.A., Cockayne, A., Hill, P.J. & Williams, P. (2000) Molecular cloning and analysis of a putative siderophore ABC transporter from *Staphylococcus aureus*. *Infection and Immunity*. 68 (11), 6281–6288.
- Murshudov, G.N., Skubák, P., Lebedev, A.A., Pannu, N.S., Steiner, R.A., Nicholls, R.A., Winn, M.D., Long, F. & Vagin, A.A. (2011) REFMAC5 for the refinement of macromolecular crystal structures. *Acta Crystallographica Section D: Biological Crystallography*. 67 (4), 355–367.
- Nakashige, T.G., Zhang, B., Krebs, C. & Nolan, E.M. (2015) Human calprotectin is an iron-sequestering host-defense protein. *Nature Chemical Biology*. 11 (10), 765–771.
- Nakashige, T.G., Zygiel, E.M., Drennan, C.L. & Nolan, E.M. (2017) Nickel sequestration by the host-defense protein human calprotectin. *Journal of the American Chemical Society*. 139 (26), 8828–8836.
- Nathan, C. & Shiloh, M.U. (2000) Reactive oxygen and nitrogen intermediates in the relationship between mammalian hosts and microbial pathogens. *Proceedings of the National Academy of Sciences of the United States of America*. 97 (16), 8841–8848.
- Nemeth, E. (2002) Heparin, a putative mediator of anemia of inflammation, is a type II acute-phase protein. *Blood*. 101 (7), 2461–2463.

Nemeth, E. (2004) Hepcidin regulates cellular iron efflux by binding to ferroportin and inducing its internalization. *Science*. 306 (5704), 2090–2093.

Notredame, C., Higgins, D.G. & Heringa, J. (2000) T-Coffee: A novel method for fast and accurate multiple sequence alignment. *Journal of Molecular Biology*. 302 (1), 205–217.

O'Neill, A.J. (2010) *Staphylococcus aureus* SH1000 and 8325-4: comparative genome sequences of key laboratory strains in staphylococcal research. *Letters in Applied Microbiology*. 51(3), 358-361.

O'Riordan, K. & Lee, J.C. (2004) *Staphylococcus aureus* capsular polysaccharides. *Clinical Microbiology Reviews*. 17(1), 218-234.

Ogston, A. (1881) Report upon micro-organisms in surgical diseases. *British Medical Journal*. 1 (1054), 369.b2–375.

Okuma, K., Iwakawa, K., Turnidge, J.D., Grubb, W.B., Bell, J.M., O'Brien, F.G., Coombs, G.W., Pearman, J.W., Tenover, F.C., Kapi, M., Tiensasitorn, C., Ito, T. & Hiramatsu, K. (2002) Dissemination of new methicillin-resistant *Staphylococcus aureus* clones in the community. *Journal of Clinical Microbiology*. 40 (11), 4289–4294.

Osawa, M., Yamakura, F., Mihara, M., Okubo, Y., Yamada, K. & Hiraoka, B.Y. (2010) Conversion of the metal-specific activity of *Escherichia coli* Mn-SOD by site-directed mutagenesis of Gly165Thr. *Biochimica et Biophysica Acta*. 1804 (9), 1775–1779.

Ose, D. E., & Fridovich, I. (1979). Manganese-containing superoxide dismutase from *Escherichia coli*: reversible resolution and metal replacements. *Archives of Biochemistry and Biophysics*. 194(2), 360-364.

Ose, D.E. & Fridovich, I. (1976) Superoxide dismutase. Reversible removal of manganese and its substitution by cobalt, nickel or zinc. *Journal of Biological Chemistry*. 251 (4), 1217–1218.

Ose, D.E. & Fridovich, I. (1979) Manganese-containing superoxide dismutase from *Escherichia coli*: reversible resolution and metal replacements. *Archives of Biochemistry and Biophysics*. 194(2), 360-364.

Otto, M. (2010) Basis of virulence in community-associated methicillin-resistant *Staphylococcus aureus*. *Annual review of microbiology*. 64:143–162.

Otto, M. (2013) Community-associated MRSA: what makes them special? *International Journal of Medical Microbiology*, 303(6), 324-330.

Outten, C.E. & O'Halloran, T.V. (2001) Femtomolar sensitivity of metalloregulatory proteins controlling zinc homeostasis. *Science*. 292 (5526), 2488–2492.

Pagels, M., Fuchs, S., Pané-Farré, J., Kohler, C., Menschner, L., Hecker, M., McNamarra, P.J., Bauer, M.C., Wachenfeldt, von, C., Liebeke, M., Lalk, M., Sander, G., Eiff, Von, C., Proctor, R.A. &

- Engelmann, S. (2010) Redox sensing by a Rex-family repressor is involved in the regulation of anaerobic gene expression in *Staphylococcus aureus*. *Molecular Microbiology*. 76 (5), 1142–1161.
- Pal, C., Bengtsson-Palme, J., Kristiansson, E., & Larsson, D. G. J. (2015). Co-occurrence of resistance genes to antibiotics, biocides and metals reveals novel insights into their co-selection potential. *BMC Genomics*. 16(1), 964.
- Pal, C., Bengtsson-Palme, J., Kristiansson, E., & Larsson, D. G. J. (2016). The Structure and diversity of human, animal and environmental resistomes. *Microbiome*. 4(1), 54.
- Pané-Farré, J., Jonas, B., Förstner, K. & Engelmann, S. (2006) The σ B regulon in *Staphylococcus aureus* and its regulation. *International Journal of Medical Microbiology*. 296(4), 237-258.
- Parker M.W., Blake C.C. (1988) Iron- and manganese-containing superoxide dismutases can be distinguished by analysis of their primary structures. *FEBS Letters*. 229(2), 377-82.
- Peacock, S.J., de Silva, I. & Lowy, F.D. (2001) What determines nasal carriage of *Staphylococcus aureus*? *Trends in Microbiology*. 9 (12), 605–610.
- Peacock, S.J., Justice, A., Griffiths, D., de Silva, G.D.I., Kantzanou, M.N., Crook, D., Sleeman, K. & Day, N.P.J. (2003) Determinants of acquisition and carriage of *Staphylococcus aureus* in infancy. *Journal of Clinical Microbiology*. 41(12), 5718-5725.
- Peake, S.L., Peter, J.V., Chan, L., Wise, R.P., Butcher, A.R. & Grove, D.I. (2006) First report of septicemia caused by an obligately anaerobic *Staphylococcus aureus* infection in a human. *Journal of Clinical Microbiology*. 44 (6), 2311–2313.
- Pearson, W.R. (2013) Selecting the Right Similarity-Scoring Matrix. *Current Protocols in Bioinformatics*. 3-5.
- Pennella, M.A., Arunkumar, A.I. & Giedroc, D.P. (2006) Individual metal ligands play distinct functional roles in the zinc sensor *Staphylococcus aureus* CzrA. *Journal of Molecular Biology*. 356(5), 1124-1136.
- Perera, V. R., Newton, G. L., & Pogliano, K. (2015). Bacillithiol: a key protective thiol in *Staphylococcus aureus*. *Expert Review of Anti-Infective Therapy*, 13(9), 1089–1107.
- Pishchany, G., McCoy, A.L., Torres, V.J., Krause, J.C., Crowe, J.E., Fabry, M.E. & Skaar, E.P. (2010) Specificity for human hemoglobin enhances *Staphylococcus aureus* infection. *Cell Host and Microbe*. 8 (6), 544–550.
- Pletinckx, L.J., Verheghe, M., Crombé, F. & Dewulf, J. (2013) Evidence of possible methicillin-resistant *Staphylococcus aureus* ST398 spread between pigs and other animals and people residing on the same farm. *Preventive Veterinary Medicine*. 109(3), 293-303.
- Posada, A.C., Kolar, S.L., Dusi, R.G., Francois, P., Roberts, A.A., Hamilton, C.J., Liu, G.Y. & Cheung, A. (2014) Importance of bacillithiol in the oxidative stress response of *Staphylococcus aureus*. *Infection and Immunity*. 82(1), 316–332.

- Posey, J.E., Hardham, J.M., Norris, S.J. and Gherardini, F.C., 1999. Characterization of a manganese-dependent regulatory protein, TroR, from *Treponema pallidum*. Proceedings of the National Academy of Sciences. 96(19),10887-10892.
- Poyart, C., Berche, P. & Trieu-Cuot, P. (1995) Characterization of superoxide dismutase genes from gram-positive bacteria by polymerase chain reaction using degenerate primers. FEMS Microbiology Letters. 131(1), 41-45.
- Prajsnar, T.K., Hamilton, R., Garcia-Lara, J., McVicker, G., Williams, A., Boots, M., Foster, S.J. & Renshaw, S.A. (2012) A privileged intraphagocyte niche is responsible for disseminated infection of *Staphylococcus aureus* in a zebrafish model. Cellular Microbiology. 14(10), 1600-1619.
- Price, C.W., Fawcett, P., C  r  monie, H., Su, N., Murphy, C.K. & Youngman, P. (2001) Genome-wide analysis of the general stress response in *Bacillus subtilis*. Molecular Microbiology. 41 (4), 757–774.
- Purves, J., Thomas, J., Riboldi, G.P., Zapotoczna, M., Tarrant, E., Andrew, P.W., Londo  o, A., Planet, P.J., Geoghegan, J.A., Waldron, K.J. and Morrissey, J.A., 2018. A horizontally gene transferred copper resistance locus confers hyper-resistance to antibacterial copper toxicity and enables survival of community acquired methicillin resistant *Staphylococcus aureus* USA300 in macrophages. Environmental Microbiology. 20(4), 1576-1589
- Pynnonen, M., Stephenson, R. E., Schwartz, K., Hernandez, M., & Boles, B. R. (2011). Hemoglobin promotes *Staphylococcus aureus* nasal colonization. PLoS pathogens. 7(7), e1002104
- Quiles-Melero, I., Garc  a-Perea, A. & de Pablos, M. (2012) Resistance to linezolid in a methicillin-susceptible *Staphylococcus aureus* clinical isolate without previous exposure to oxazolidinones. International Journal of Medical Microbiology. 302(3), 145-147.
- Rachid, S., Ohlsen, K., Wallner, U. & Hacker, J. (2000) Alternative transcription factor ζ b is involved in regulation of biofilm expression in a *Staphylococcus aureus* mucosal isolate. Journal of Bacteriology. 182(23), 6824-6826.
- Rashid, G.M.M., Taylor, C.R., Liu, Y., Zhang, X., Rea, D., F  l  p, V. & Bugg, T.D.H. (2015) Identification of manganese superoxide dismutase from *Sphingobacterium* sp. T2 as a novel bacterial enzyme for lignin oxidation. ACS Chemical Biology. 10 (10), 2286–2294.
- Ray, M.D., Boundy, S. & Archer, G.L. (2016) Transfer of the methicillin resistance genomic island among staphylococci by conjugation. Molecular Microbiology. 100 (4), 675–685.
- Richardson, A.R., Dunman, P.M. & Fang, F.C. (2006) The nitrosative stress response of *Staphylococcus aureus* is required for resistance to innate immunity. Molecular Microbiology. 61 (4), 927–939.
- Rinke, C., Schwientek, P., Sczyrba, A., Ivanova, N.N., Anderson, I.J., Cheng, J.-F., Darling, A., Malfatti, S., Swan, B.K., Gies, E.A., Dodsworth, J.A., Hedlund, B.P., Tsiamis, G., Sievert, S.M., Liu,

- W.-T., Eisen, J.A., Hallam, S.J., Kyrpides, N.C., Stepanauskas, R., et al. (2013) Insights into the phylogeny and coding potential of microbial dark matter. *Nature*. 499 (7459), 431–437.
- Robinson, D.N.J. & Pohl, D.E. (2013) Zinc sensors in bacteria. *Encyclopedia of Metalloproteins*. 2499–2506.
- Robinson, D.R. & Jencks, W.P. (1963) Effect of denaturing agents of the urea-guanidinium class on the solubility of acetyltetraglycine ethyl ester and related compounds. *Journal of Biological Chemistry*. 238(4), 1558-1560.
- Ryu, S.Y., Jeong, K.S., Kang, B.N., Park, S.J., Yoon, W.K., Kim, S.H. & Kim, T.H. (2000) Modulation of transferrin synthesis, transferrin receptor expression, iNOS expression and NO production in mouse macrophages by cytokines, either alone or in combination. *Anticancer Research*. 20 (5A), 3331–3338.
- Sambrook, J. & Russell, D.W. (2001) *Molecular cloning: a laboratory manual* 3rd edition. Coldspring-Harbour Laboratory Press, UK.
- Sanz, R., Marín, I., Ruiz-Santa-Quiteria, J.A., Orden, J.A., Cid, D., Diez, R.M., Silhadi, K.S., Amils, R. & la Fuente, de, R. (2000) Catalase deficiency in *Staphylococcus aureus* subsp. *anaerobius* is associated with natural loss-of-function mutations within the structural gene. *Microbiology*. 146(2), 465–475.
- Scharn, C.R., Tenover, F.C. & Goering, R.V. (2013) Transduction of staphylococcal cassette chromosome mec elements between strains of *Staphylococcus aureus*. *Antimicrobial Agents and Chemotherapy*. 57 (11), 5233–5238.
- Schauber, J., & Gallo, R. L. (2008). Antimicrobial peptides and the skin immune defense system. *Journal of Allergy and Clinical Immunology*. 122(2), 261-266.
- Schleifer, K.-H. & Bell, J.A. (2015) *Staphylococcus*. 9(17). Chichester, UK: John Wiley & Sons, Ltd.
- Schwartz, A.L., Yikilmaz, E., Vance, C.K. & Vathyam, S. (2000) Mutational and spectroscopic studies of the significance of the active site glutamine to metal ion specificity in superoxide dismutase. *Journal of Inorganic Biochemistry*. 80(3), 247-256.
- Scientific Opinion of the Panel on Biological Hazards on a request from the European Commission on Assessment of the Public Health significance of methicillin resistant *Staphylococcus aureus* (MRSA) in animals and foods. *The EFSA Journal* (2009) 993, 1-73
- Sebulsky, M.T., Hohnstein, D., Hunter, M.D. & Heinrichs, D.E. (2000) Identification and characterization of a membrane permease involved in iron-hydroxamate transport in *Staphylococcus aureus*. *Journal of Bacteriology*. 182 (16), 4394.
- Seidl, K., Müller, S., Francois, P., Kriebitzsch, C., Schrenzel, J., Engelmann, S., Bischoff, M. & Berger-Bächi, B. (2009) Effect of a glucose impulse on the CcpA regulon in *Staphylococcus aureus*. *BMC Microbiology*. 9(1), 95.

- Senn, M.M., Giachino, P., Homerova, D., Steinhuber, A., Strassner, J., Kormanec, J., Flückiger, U., Berger-Bächli, B. & Bischoff, M. (2005) Molecular analysis and organization of the sigmaB operon in *Staphylococcus aureus*. *Journal of Bacteriology*. 187 (23), 8006–8019.
- Sheng, Y., Abreu, I.A., Cabelli, D.E., Maroney, M.J., Miller, A.-F., Teixeira, M. & Valentine, J.S. (2014) Superoxide dismutases and superoxide reductases. *Chemical Reviews*. 114 (7), 3854–3918.
- Sheng, Y., Butler Gralla, E., Schumacher, M., Cascio, D., Cabelli, D.E. & Valentine, J.S. (2012) Six-coordinate manganese (3+) in catalysis by yeast manganese superoxide dismutase. *Proceedings of the National Academy of Sciences*. 109 (36), 14314–14319.
- Sheng, Y., Stich, T.A., Barnese, K., Gralla, E.B., Cascio, D., Britt, R.D., Cabelli, D.E. & Valentine, J.S. (2011) Comparison of two yeast MnSODs: mitochondrial *Saccharomyces cerevisiae* versus cytosolic *Candida albicans*. *Journal of the American Chemical Society*. 133(51), 20878-20889.
- Sievert, D.M., Rudrik, J.T., Patel, J.B., McDonald, L.C., Wilkins, M.J. & Hageman, J.C. (2008) Vancomycin-resistant *Staphylococcus aureus* in the United States, 2002-2006. *Clinical Infectious Diseases*. 46 (5), 668–674.
- Singh, V.K., Xiong, A., Usgaard, T.R., Chakrabarti, S., Deora, R., Misra, T.K. & Jayaswal, R.K. (1999) ZntR is an autoregulatory protein and negatively regulates the chromosomal zinc resistance operon *znt* of *Staphylococcus aureus*. *Molecular Microbiology*. 33 (1), 200–207.
- Sitthisak, S., Knutsson, L., Webb, J.W. & Jayaswal, R.K. (2007) Molecular characterization of the copper transport system in *Staphylococcus aureus*. *Microbiology*. 153 (12), 4274–4283.
- Sjödin, M., Gätjens, J., Tabares, L.C., Thuéry, P., Pecoraro, V.L. & Un, S. (2008) Tuning the redox properties of manganese(II) and its implications to the electrochemistry of manganese and iron superoxide dismutases. *Inorganic Chemistry*. 47 (7), 2897–2908.
- Skaar, E.P. & Schneewind, O. (2004) Iron-regulated surface determinants (Isd) of *Staphylococcus aureus*: stealing iron from heme. *Microbes and Infection*, 6(4), 390-397.
- Slykhouse, T.O. & Fee, J.A. (1976) Physical and chemical studies on bacterial superoxide dismutases. Purification and some anion binding properties of the iron-containing protein of *Escherichia coli* B. *Journal of Biological Chemistry*. 251(18), 5472-5477.
- Smith, M.W. & Doolittle, R.F. (1992) A comparison of evolutionary rates of the two major kinds of superoxide dismutase. *Journal of Molecular Evolution*. 34 (2), 175–184.
- Smulevich, G., Mauro, J.M., Fishel, L.A. & English, A.M. (1988) Heme pocket interactions in cytochrome c peroxidase studied by site-directed mutagenesis and resonance Raman spectroscopy. *Biochemistry*, 27(15), 5477-5485.
- Soe-Lin, S., Sheftel, A.D., Wasyluk, B. & Ponka, P. (2008) Nramp1 equips macrophages for efficient iron recycling. *Experimental Hematology*, 36(8), 929-937.

- Speziali, C.D., Dale, S.E., Henderson, J.A., Vinés, E.D. & Heinrichs, D.E. (2006) Requirement of *Staphylococcus aureus* ATP-binding cassette-ATPase FhuC for iron-restricted growth and evidence that it functions with more than one iron transporter. *Journal of Bacteriology*. 188 (6), 2048–2055.
- Sreerama, N. & Woody, R.W. (2000) Estimation of protein secondary structure from circular dichroism spectra: comparison of CONTIN, SELCON, and CDSSTR methods with an expanded reference set. *Analytical Biochemistry*. 287 (2), 252–260.
- Stallings, W.C., Metzger, A.L., Pattridge, K.A., Fee, J.A. & Ludwig, M.L. (1991) Structure-function relationships in iron and manganese superoxide dismutases. *Free Radical Research Communications*. 12-13 Pt 1259–268.
- Stapels, D.A.C., Ramyar, K.X., Bischoff, M., Köckritz-Blickwede, von, M., Milder, F.J., Ruyken, M., Eisenbeis, J., McWhorter, W.J., Herrmann, M., Van Kessel, K.P.M., Geisbrecht, B.V. & Rooijackers, S.H.M. (2014) *Staphylococcus aureus* secretes a unique class of neutrophil serine protease inhibitors. *Proceedings of the National Academy of Sciences*. 111 (36), 13187–13192.
- Stefani, S., Chung, D. R., Lindsay, J. A., Friedrich, A. W., Kearns, A. M., Westh, H., & MacKenzie, F. M. (2012). Meticillin-resistant *Staphylococcus aureus* (MRSA): global epidemiology and harmonisation of typing methods. *International Journal Of Antimicrobial Agents*. 39(4), 273-282.
- Sun, G. & Budde, R.J. (1999) Substitution studies of the second divalent metal cation requirement of protein tyrosine kinase CSK. *Biochemistry*. 38 (17), 5659–5665.
- Surmann, K., Michalik, S., Hildebrandt, P., Gierok, P., Depke, M., Brinkmann, L., Bernhardt, J., Salazar, M.G., Sun, Z., Shteynberg, D., Kusebauch, U., Moritz, R.L., Wollscheid, B., Lalk, M., Völker, U. & Schmidt, F. (2014) Comparative proteome analysis reveals conserved and specific adaptation patterns of *Staphylococcus aureus* after internalization by different types of human non-professional phagocytic host cells. *Frontiers in Microbiology*. 5, 392.
- Suttisansanee, U., Lau, K., Lagishetty, S., Rao, K.N., Swaminathan, S., Sauder, J.M., Burley, S.K. & Honek, J.F. (2011) Structural variation in bacterial glyoxalase I enzymes. *Journal of Biological Chemistry*. 286 (44), 38367–38374.
- Tabares, L. C., Bittel, C., Carrillo, N., Bortolotti, A., & Cortez, N. (2003). The single superoxide dismutase of *Rhodobacter capsulatus* is a cambialistic, manganese-containing enzyme. *Journal of Bacteriology*, 185(10), 3223-3227.
- Tabares, L.C., Cortez, N. & Un, S. (2007) Role of tyrosine-34 in the anion binding equilibria in manganese(II) superoxide dismutases. *Biochemistry*. 46 (32), 9320–9327.
- Tabares, L.C., Gätjens, J. & Un, S. (2010) Understanding the influence of the protein environment on the Mn(II) centers in superoxide dismutases using High-Field Electron Paramagnetic Resonance. *Biochimica et Biophysica Acta*. 1804 (2), 308–317.

- Tachikawa, H. (2014) Electron detachment dynamics of O₂ – (H₂O): direct *ab initio* molecular dynamics (AIMD) approach. RSC Advances. 4 (1), 516–522.
- Tally, F.P., Goldin, B.R., Jacobus, N.V. & Gorbach, S.L. (1977) Superoxide dismutase in anaerobic bacteria of clinical significance. Infection and Immunity. 16 (1), 20–25.
- Teale, F.W. & Weber, G. (1957) Ultraviolet fluorescence of the aromatic amino acids. The Biochemical Journal. 65 (3), 476–482.
- Thakker, M., Park, J.S., Carey, V. & Lee, J.C. (1998) *Staphylococcus aureus* serotype 5 capsular polysaccharide is antiphagocytic and enhances bacterial virulence in a murine bacteremia model. Infection and Immunity. 66 (11), 5183–5189.
- Tottey, S., Waldron, K.J., Firbank, S.J., Reale, B., Bessant, C., Sato, K., Cheek, T.R., Gray, J., Banfield, M.J., Dennison, C. & Robinson, N.J. (2008) Protein-folding location can regulate manganese-binding versus copper- or zinc-binding. Nature. 455 (7216), 1138–1142.
- Touati, D. (2000). Iron and oxidative stress in bacteria. Archives of Biochemistry and Biophysics. 373(1), 1-6.
- Tu, W.Y., Pohl, S., Gray, J., Robinson, N.J., Harwood, C.R. & Waldron, K.J. (2012) Cellular iron distribution in *Bacillus anthracis*. Journal of Bacteriology. 194 (5), 932–940.
- Tuchscher, L., Heitmann, V., Hussain, M., Viemann, D., Roth, J., Eiff, Von, C., Peters, G., Becker, K. & Löffler, B. (2010) *Staphylococcus aureus* small-colony variants are adapted phenotypes for intracellular persistence. Journal of Infectious Diseases. 202 (7), 1031–1040.
- Tzagolo, H. & Novick, R. (1977) Geometry of cell division in *Staphylococcus aureus*. Journal of Bacteriology. 129, 343–350
- Ulrich, M., Bastian, M., Cramton, S.E., Ziegler, K., Pragman, A.A., Bragonzi, A., Memmi, G., Wolz, C., Schlievert, P.M., Cheung, A. & Döring, G. (2007) The staphylococcal respiratory response regulator SrrAB induces ica gene transcription and polysaccharide intercellular adhesin expression, protecting *Staphylococcus aureus* from neutrophil killing under anaerobic growth conditions. Molecular Microbiology. 65 (5), 1276–1287.
- Un, S., Tabares, L.C., Cortez, N. & Hiraoka, B.Y. (2004) Manganese (II) zero-field interaction in cambialistic and manganese superoxide dismutases and its relationship to the structure of the metal binding site. Journal of the American Chemical Society, 126(9), 2720-2726.
- Valderas, M.W. & Hart, M.E. (2001) Identification and characterization of a second superoxide dismutase gene (*sodM*) from *Staphylococcus aureus*. Journal of Bacteriology. 183 (11), 3399–3407.
- Valderas, M.W., Gatson, J.W., Wreyford, N. & Hart, M.E. (2002) The superoxide dismutase gene *sodM* is unique to *Staphylococcus aureus*: absence of *sodM* in coagulase-negative staphylococci. Journal of Bacteriology. 184 (9), 2465–2472.

- Valente, A.M., Jain, R., Scheurer, M., Fowler, V.G., Corey, G.R., Bengur, A.R., Sanders, S. & Li, J.S. (2005) Frequency of infective endocarditis among infants and children with *Staphylococcus aureus* bacteremia. *Pediatrics*. 115 (1), e15–e19.
- van Cleef, B.A.G.L., Graveland, H., Haenen, A.P.J., van de Giessen, A.W., Heederik, D., Wagenaar, J.A. & Kluytmans, J.A.J.W. (2011) Persistence of livestock-associated methicillin-resistant *Staphylococcus aureus* in field workers after short-term occupational exposure to pigs and veal calves. *Journal of Clinical Microbiology*. 49 (3), 1030–1033.
- van Cleef, B.A.G.L., Monnet, D.L., Voss, A., Krziwanek, K., Allerberger, F., Struelens, M., Zemlickova, H., Skov, R.L., Vuopio-Varkila, J., Cuny, C., Friedrich, A.W., Spiliopoulou, I., Pászti, J., Hardardottir, H., Rossney, A., Pan, A., Pantosti, A., Borg, M., Grundmann, H., et al. (2011) Livestock-associated methicillin-resistant *Staphylococcus aureus* in humans in Europe. *Emerging Infectious Diseases*. 17 (3), 502–505.
- van Rijen, M.M.L., Bosch, T., Verkade, E.J.M., Schouls, L., Kluytmans, J.A.J.W. & CAM Study Group (2014) Livestock-associated MRSA carriage in patients without direct contact with livestock. *PLOS ONE*. 9 (6), e100294.
- Vance, C. K., & Miller, A. F. (1998). A simple proposal that can explain the inactivity of metal-substituted superoxide dismutases. *Journal of the American Chemical Society*, 120(3), 461-467.
- Vivian, J.T. & Callis, P.R. (2001) Mechanisms of tryptophan fluorescence shifts in proteins. *Biophysical Journal*. 80 (5), 2093–2109.
- Voyich, J.M., Braughton, K.R., Sturdevant, D.E., Whitney, A.R., Saïd-Salim, B., Porcella, S.F., Long, R.D., Dorward, D.W., Gardner, D.J., Kreiswirth, B.N., Musser, J.M. & DeLeo, F.R. (2005) Insights into mechanisms used by *Staphylococcus aureus* to avoid destruction by human neutrophils. *Journal of Immunology*. 175 (6), 3907–3919.
- Vyoral, D. & Petrák, J. (2005) Hcpidin: a direct link between iron metabolism and immunity. *The International Journal of biochemistry and Cell Biology*. 37(9), 1768-1773.
- Wakeman, C.A. & Skaar, E.P. (2012) Metalloregulation of Gram-positive pathogen physiology. *Current Opinion in Microbiology*. 15 (2), 169–174.
- Waldron, D.E. & Lindsay, J.A. (2006) Sau1: a novel lineage-specific type I restriction-modification system that blocks horizontal gene transfer into *Staphylococcus aureus* and between *S. aureus* isolates of different lineages. *Journal of Bacteriology*. 188 (15), 5578–5585.
- Waldron, K.J. & Robinson, N.J. (2009) How do bacterial cells ensure that metalloproteins get the correct metal? *Nature*. 7 (1), 25–35.
- Waldron, K.J., Rutherford, J.C., Ford, D. & Robinson, N.J. (2009) Metalloproteins and metal sensing. *Nature*. 460 (7257), 823–830.
- Waldron, K.J., Tottey, S. & Yanagisawa, S. (2007) A periplasmic iron-binding protein contributes toward inward copper supply. *Journal of Biological Chemistry*, 282(6), 3837-3846.

- Wang R., Braughton K. R., Kretschmer D., Bach T. H., Queck S. Y., Li M., Kennedy A. D., Dorward D. W., Klebanoff S. J., Peschel A., DeLeo F. R., Otto M. (2007) Identification of novel cytolytic peptides as key virulence determinants for community-associated MRSA. *Nat. Med.* 13, 1510–1514
- Wassenberg, M.W.M., Bootsma, M.C.J., Troelstra, A., Kluytmans, J.A.J.W. & Bonten, M.J.M. (2011) Transmissibility of livestock-associated methicillin-resistant *Staphylococcus aureus* (ST398) in Dutch hospitals. *Clinical Microbiology and Infection.* 17 (2), 316–319.
- Waterhouse, A.M., Procter, J.B., Martin, D.M.A., Clamp, M. & Barton, G.J. (2009) Jalview Version 2-a multiple sequence alignment editor and analysis workbench. *Bioinformatics.* 25 (9), 1189–1191.
- Watlauer, D.B., Malik, S.K. & Stoller, L. (1964) Nonpolar group participation in the denaturation of proteins by urea and guanidinium salts. Model compound studies. *Journal of the American Chemical Society*, 86(3), 508-514.
- Weber, H., Engelmann, S., Becher, D. & Hecker, M. (2004) Oxidative stress triggers thiol oxidation in the glyceraldehyde-3-phosphate dehydrogenase of *Staphylococcus aureus*. *Molecular Microbiology.* 52 (1), 133–140.
- Weems, J.J. (2001) The many faces of *Staphylococcus aureus* infection. Recognizing and managing its life-threatening manifestations. *Postgraduate Medicine.* 110 (4), 24–36.
- Weinberg, E.D. (1978) Iron and infection. *Microbiological reviews.* 42 (1), 45–66.
- Wendlandt, S., Schwarz, S. & Silley, P. (2013) Methicillin-resistant *Staphylococcus aureus*: A food-borne pathogen? *Annual Review of Food Science and Technology.* 4 (1), 117–139.
- Wertheim, H., Vos, M.C., Ott, A., van Belkum, A. & Voss, A. (2004) Risk and outcome of nosocomial *Staphylococcus aureus* bacteraemia in nasal carriers versus non-carriers. *Lancet*, 364(9435), 703-705.
- Wertheim, H.F.L., Melles, D.C., Vos, M.C., van Leeuwen, W., van Belkum, A., Verbrugh, H.A. & Nouwen, J.L. (2005) The role of nasal carriage in *Staphylococcus aureus* infections. *The Lancet Infectious Diseases.* 5 (12), 751–762.
- Wessling-Resnick, M. (2015) Nramp1 and other transporters involved in metal withholding during infection. *Journal of Biological Chemistry*, 290(31), 18984-18990.
- White, C., Lee, J., Kambe, T., Fritsche, K. & Petris, M.J. (2009) A role for the ATP7A copper-transporting ATPase in macrophage bactericidal activity. *Journal of Biological Chemistry.* 284 (49), 33949–33956.
- Whitmore, L. & Wallace, B.A. (2004) DICHROWEB, an online server for protein secondary structure analyses from circular dichroism spectroscopic data. *Nucleic acids research.* 32, W668–W673.

- Whittaker, J. W., & Whittaker, M. M. (1991). Active site spectral studies on manganese superoxide dismutase. *Journal of the American Chemical Society*, 113(15), 5528-5540.
- Whittaker, J.W. (2003) The irony of manganese superoxide dismutase. *Biochemical Society Transactions*. 31 (6), 1318–1321.
- Whittaker, M. M., Lerch, T. F., Kirillova, O., Chapman, M. S., & Whittaker, J. W. (2011). Subunit dissociation and metal binding by *Escherichia coli* apo-manganese superoxide dismutase. *Archives of Biochemistry and Biophysics*, 505(2), 213-225.
- Whittaker, M.M. & Whittaker, J.W. (1996) Low-temperature thermochromism marks a change in coordination for the metal ion in manganese superoxide dismutase. *Biochemistry*, 35(21), 6762-6770.
- Whittaker, M.M. & Whittaker, J.W. (1997) Mutagenesis of a proton linkage pathway in *Escherichia coli* manganese superoxide dismutase. *Biochemistry*. 36 (29), 8923–8931.
- Whittaker, M.M. & Whittaker, J.W. (1998) A glutamate bridge is essential for dimer stability and metal selectivity in manganese superoxide dismutase. *The Journal of Biological Chemistry*. 273 (35), 22188–22193.
- Whittaker, M.M. & Whittaker, J.W. (1999) Thermally triggered metal binding by recombinant *Thermus thermophilus* manganese superoxide dismutase, expressed as the apo-enzyme. *The Journal of Biological Chemistry*. 274 (49), 34751–34757.
- Whittaker, M.M. & Whittaker, J.W. (2008) Conformationally gated metal uptake by apomanganese superoxide dismutase. *Biochemistry*, 47(44), 11625-11636.
- Whittaker, M.M., Mizuno, K., Bächinger, H.P. & Whittaker, J.W. (2006) Kinetic analysis of the metal binding mechanism of *Escherichia coli* manganese superoxide dismutase. *Biophysical Journal*. 90 (2), 598–607.
- Wielders, C., Vriens, M.R. & Brisse, S. (2001) Evidence for in-vivo transfer of *mecA* DNA between strains of *Staphylococcus aureus*. *The Lancet*, 357(9269), 1674-1675.
- Williams, T.A., Szöllösi, G.J., Spang, A., Foster, P.G., Heaps, S.E., Boussau, B., Ettema, T.J.G. & Embley, T.M. (2017) Integrative modeling of gene and genome evolution roots the archaeal tree of life. *Proceedings of the National Academy of Sciences*. 114 (23), E4602–E4611.
- Winn, M.D., Ballard, C.C., Cowtan, K.D., Dodson, E.J., Emsley, P., Evans, P.R., Keegan, R.M., Krissinel, E.B., Leslie, A.G.W., McCoy, A., McNicholas, S.J., Murshudov, G.N., Pannu, N.S., Potterton, E.A., Powell, H.R., Read, R.J., Vagin, A. & Wilson, K.S. (2011) Overview of the CCP4 suite and current developments. *Acta Crystallographica Section D: Biological Crystallography*. 67 (4), 235–242.
- Winterbourn, C.C. & Kettle, A.J. (2013) Redox reactions and microbial killing in the neutrophil phagosome. *Antioxidants & Redox Signaling*. 18 (6), 642–660.

- Wintjens, R., Gilis, D. & Rooman, M. (2008) Mn/Fe superoxide dismutase interaction fingerprints and prediction of oligomerization and metal cofactor from sequence. *Proteins: Structure, Function, and Bioinformatics*, 70(4), 1564-1577.
- Wintjens, R., Noël, C., May, A.C.W., Gerbod, D., Dufernez, F., Capron, M., Viscogliosi, E. & Rooman, M. (2004) Specificity and Phenetic Relationships of Iron- and Manganese-containing Superoxide Dismutases on the Basis of Structure and Sequence Comparisons. *The Journal of Biological Chemistry*. 279 (10), 9248–9254.
- Witte, W. (2009) Community-acquired methicillin-resistant *Staphylococcus aureus*: what do we need to know? *Clinical Microbiology and Infection*. 1517–25.
- Witte, W., Strommenger, B., Stanek, C., & Cuny, C. (2007). Methicillin-resistant *Staphylococcus aureus* ST398 in humans and animals, Central Europe. *Emerging Infectious Diseases*, 13(2), 255.
- Wolf, C., Hochgräfe, F., Kusch, H., Albrecht, D., Hecker, M. & Engelmann, S. (2008) Proteomic analysis of antioxidant strategies of *Staphylococcus aureus*: diverse responses to different oxidants. *Proteomics*. 8 (15), 3139–3153.
- Wolfe-Simon, F., Grzebyk, D., Schofield, O. & Falkowski, P.G. (2005) The role and evolution of superoxide dismutases in algae. *Journal of Phycology*. 41 (3), 453–465.
- Wulf, M. & Voss, A. (2008) MRSA in livestock animals—an epidemic waiting to happen? *Clinical Microbiology and Infection*. 14 (6), 519–521.
- Xiong, A., Singh, V.K., Cabrera, G. & Jayaswal, R.K. (2000) Molecular characterization of the ferric-uptake regulator, Fur, from *Staphylococcus aureus*. *Microbiology*, 146: 659–68.
- Xu, S. X., & McCormick, J. K. (2012). Staphylococcal superantigens in colonization and disease. *Frontiers in Cellular and Infection Microbiology*. 2, 52.
- Yamakura, F. & Suzuki, K. (1980) Cadmium, Chromium, and Manganese replacement for iron in iron-superoxide dismutase from *Pseudomonas ovalis*. *The Journal of Biochemistry*. 88(1), 191-196.
- Yamakura, F., Sugio, S., Hiraoka, B.Y., Ohmori, D. & Yokota, T. (2003) Pronounced conversion of the metal-specific activity of superoxide dismutase from *Porphyromonas gingivalis* by the mutation of a single amino acid (Gly155Thr) located apart from the active site. *Biochemistry*. 42 (36), 10790–10799.
- Yamano, S. & Maruyama, T. (1999) An azide-insensitive superoxide dismutase from a hyperthermophilic archaeon, *Sulfolobus solfataricus*. *Journal of Biochemistry*. 125 (1), 186–193.
- Yamano, S., Sako, Y., Nomura, N., & Maruyama, T. (1999). A cambialistic SOD in a strictly aerobic hyperthermophilic archaeon, *Aeropyrum pernix*. *The Journal of Biochemistry*, 126(1), 218-225.
- Yikilmaz, E., Rodgers, D. W., & Miller, A. F. (2006). The crucial importance of chemistry in the structure– function link: manipulating hydrogen bonding in iron-containing superoxide dismutase. *Biochemistry*, 45(4), 1151-1161.

- Yikilmaz, E., Xie, J., Brunold, T.C. & Miller, A.-F. (2002) Hydrogen-bond-mediated tuning of the redox potential of the non-heme Fe site of superoxide dismutase. *Journal of the American Chemical Society*. 124 (14), 3482–3483.
- Yocum, C.F. & Pecoraro, V.L. (1999) Recent advances in the understanding of the biological chemistry of manganese. *Current Opinion in Chemical Biology*. 3 (2), 182–187.
- Yost, F. J., & Fridovich, I. (1973). An iron-containing superoxide dismutase from *Escherichia coli*. *Journal of Biological Chemistry*, 248(14), 4905-4908.
- Yui, S., Nakatani, Y. & Mikami, M. (2003) Calprotectin (S100A8/S100A9), an inflammatory protein complex from neutrophils with a broad apoptosis-inducing activity. *Biological & Pharmaceutical Bulletin*. 26 (6), 753–760.
- Zheng, H., Chordia, M.D., Cooper, D.R. & Chruszcz, M. (2014) Validation of metal-binding sites in macromolecular structures with the CheckMyMetal web server. *Nature protocols*. 9(1), 156.
- Zhu, Y., Nandakumar, R., Sadykov, M.R., Madayiputhiya, N., Luong, T.T., Gaupp, R., Lee, C.Y. & Somerville, G.A. (2011) RpiR homologues may link *Staphylococcus aureus* RNAIII synthesis and pentose phosphate pathway regulation. *Journal of Bacteriology*. 193 (22), 6187–6196.